University of Strathclyde

Department of Naval Architecture, Ocean and Marine Engineering

Buckling Analysis of Structures with Corrosion under Insulation

Daniel Richard Hugh Mancini

Thesis submitted in fulfilment of the requirements for the degree of

Master of Philosophy

Glasgow, U.K.

September 2019

Declaration

This thesis is the result of the author's original research. It has been composed by the author and has not been previously submitted for examination which has led to the award of a degree.

The copyright of this thesis belongs to the author under the terms of the United Kingdom Copyright Acts as qualified by University of Strathclyde Regulation 3.50. Due acknowledgement must always be made of the use of any material contained in, or derived from, this thesis.

Signed: _____   Date: _____

Acknowledgements

I wish to express my deepest gratitude to my project supervisors Dr Erkan Oterkus and Dr Selda Oterkus for their endless support, guidance and enthusiasm. As a complete novice in the field of research, I could not have wished for more patient and encouraging supervisors.

I am grateful to the members of the Peridynamics Research Centre for their advice and for making my time as part of the group so enjoyable. Particular thanks must be made to Mr William Dickie, Mr Andrzej Czerwonka and Mr Zhenghao Yang for their expert knowledge and assistance at various times throughout the project.

Finally, and most importantly, I am truly thankful to my wife Sarah for her love, support and patience and that of both our families.

Abstract

The primary motivation behind this piece of research is the lack of information relating to the effect of the insulation and jacketing material's mechanical properties on the overall buckling strength of a steel structure. Very little research has been completed that focuses on the effect of different materials on the overall buckling value at varying stages of corrosion. It is expected that this thesis will act as the starting point for further research into the issue in the future. More detailed and accurate information relating to the mechanical properties of the insulation and jacketing is required to allow for more effective computational modelling of the problem.

Corrosion and corrosion under insulation are both topics that have been researched over a long period of time and yet there are still instances where the effects of corrosion have caused issues and problems from minor to catastrophic levels over this time. These incidents have led to the loss of human life, irreparable damage to the environment as well as costly repairs and shutdown times, not to mention reputation damage to the companies involved in such incidents.

Modelling the problem of corrosion under insulation to determine the effect of the insulation system on the buckling value result was performed in four stages. The author's style of coding using the ANSYS Mechanical APDL programme required initial validation. This was completed through comparison of the written code in both 2-D and 3-D formats against an already published version. Once the author's style of coding was validated and considered acceptable for further computational work the next stage involved a mesh convergence study. Two plate configurations with differing levels of corrosion damage were modelled and underwent buckling analysis at four varying levels of mesh coarseness to determine the best compromise between accurate results and acceptable computation time.

Once the preliminary computational work was completed the next stage involved modelling a steel plate with five levels of corrosion that also had an insulation system composed of one of six insulation materials and one of two protective jacketing materials. These plate and insulation system configurations were then subjected to axial buckling to determine the effect of the thickness of each component of the insulation system on the buckling value. The final stage involved modelling a hollow slender pipe system with the most common insulation systems to determine the effects of the materials on the new configuration.

As hypothesised the buckling value decreased as the corrosion damage of the steel components increased in severity. The effect of increasing the thickness of the insulation systems increased the buckling value as expected and these results are explained through application of the Euler Column Critical Load Formula.

Table of Contents

List of Figures

List of Tables

List of ANSYS Mechanical APDL Codes

Abbreviations and Nomenclature

DOP	Degree of Pitting
InterNACHI	International Association of Certified Home Inspectors
NACE	National Association of Corrosion Engineers
PP	Polypropylene
a	Plate Length (m)
b	Plate Breadth (m)
n	Number of Pits
$A_p i$	Surface Area of ith Pit (m^2)
d	Diameter of Pits (m)
$d_{r\,(i)}$	Diameter of Pit i (m)
W	Mass Loss (g)
D	Density of the Specimen (g/cm^3)
A	Area of the Specimen (cm^2)
T	Exposure Time (hr)
E	Young's Modulus (GPa) or (Pa)
v	Poisson's Ratio
P_{Cr}	Euler's Critical Load (N)
I	Minimum area moment of inertia of the cross-section of the column (m^4)
K	Column effective length factor
L	Unsupported length of the column (m)

e^-	Electron
H^+	Hydrogen Ion (Proton)
OH^-	Hydroxide Ion
H_2O	Water
O_2	Oxygen
Cl^-	Chloride Ion
Na^+	Sodium Ion
Fe	Iron
Fe^{2+}	Iron (II)
Fe_2O_3	Iron (III) Oxide
$Fe(OH)_2$	Iron (II) Hydroxide
$Fe(OH)_3$	Iron (III) Oxide-Hydroxide
SO_4^-	Sulphate
Mg^+	Magnesium
Ca^{2+}	Calcium
K^+	Potassium
HCO_3^-	Bicarbonate
(s)	Solid
(l)	Liquid
(g)	Gas
(aq)	Aqueous

Chapter One: Introduction

Chapter One is divided into four sections; where the piece of research conducted is introduced. The background and motivations for the research are explored along with the objectives of what is hoped to be achieved by the end of the project.

There has been a small amount of research directly related to this field and the impact of this research is discussed and the effect it has had on the direction this project has taken is presented. Finally, the first chapter will be completed with a short introduction to the structure of the thesis to assist with navigation.

1.1 Background

There are two main process types of corrosion; dry corrosion which is a chemical reaction and wet corrosion which is an electrochemical reaction. The type of reaction is determined by the corrosive environment in which the metal is found. Corrosion is essentially the deterioration of the metal's mechanical properties through the loss of the metal's structure.

Noble metals, such as gold, platinum and copper are usually found in nature in their natural pure form and are much less likely to suffer from corrosion as they have such low tendencies to react to the environment. This is in direct contrast to non-noble metals such as aluminium, zinc and iron which are usually found in metallic ores in nature and are highly reactive to their environment so are susceptible to corrosion processes.

To extract the metal from the ore large amounts of energy is required and this results in a thermodynamically unstable metal that tends to want to return to its unexcited state. The task for corrosion engineers is to prevent this from occurring. More details on this phenomenon can found in section three of Chapter One.

There are a number of mechanisms of corrosion but they fall under two main categories; localised corrosion and uniform or general corrosion. Localised corrosion is of greater concern to corrosion engineers as the effect are highly unpredictable. In some circumstances, it may not even be known that there is an issue, especially if the corrosion taking place is hidden under insulation and jacketing. This environment can promote the rate of corrosion exponentially and is discussed in further detail in section four of Chapter One.

There are three important reasons why corrosion mechanisms and processes require more study and why more assistance is required to increase the level and efficiency of the current efforts to hinder and prevent the effects of corrosion:

- Health and safety
- Reduction in costs associated with issues
- Protecting the environment

Corrosion and corrosion under insulation are both topics that have been researched over a long period of time and yet there are still instances where the effects of corrosion have caused issues and problems from minor to catastrophic levels over this time. These incidents have led to the loss of human life, irreparable damage to the environment as well as costly repairs and shutdown times not to mention reputation damage to the companies involved in such incidents.

It can be argued that the cost to prevent corrosion occurring in the first place is surely less than the cost of repairing all the damage caused, financial and reputational, if and when an incident occurs. The problem is not one experienced only in the oil and gas industry so it is the responsibility of all industries to work together with research to find an effective solution to this worldwide problem.

1.2   Motivation and Objectives

The primary motivation behind this piece of research is the lack of information relating to the effect of the insulation and jacketing material's mechanical properties on the overall buckling strength of a steel component. Very little research has been completed that focuses on the effect of different materials on the overall buckling value at varying stages of corrosion. It is expected that this thesis will act as the starting point for further research into the issue in the future. More detailed and accurate information relating to the mechanical properties of the insulation and jacketing is required to allow for more effective modelling of the problem.

At the time of writing, no model existed to computationally model corrosion damage with an external insulation and jacketing system though models did exist that focused on the strength of a corroded steel component under various load types. These papers are discussed in more detail shortly in this section. As mentioned, this project is only in the very early phases and with more research, it will be possible to generate more effective and accurate models that will allow corrosion engineers to better predict and tackle the problem of corrosion under insulation.

The research conducted in this thesis has four main objectives:

1. Create a 2-D and 3-D ANSYS mechanical APDL code that models a steel plate where the centre has been subjected to five levels of corrosion. The first level is no corrosion at all and the plate is fully intact, the next three levels are the progression in depth of a pit from one-quarter of the depth of the plate through one half of the depth to three-quarters depth of a pit. The final level is where the model has fully corroded and a full depth hole has been created in the centre of the plate. The plate will be fully constrained at the left-hand nodes and the buckling value will be determined.

2. Model each of the corrosion levels of the plate described above with same constraints and determine the difference in buckling value when the model includes six different insulation materials at ten different thicknesses and two protective jacketing materials at five different thicknesses.

3. Create a 2-D model of a steel pipe with the five levels of corrosion described above and determine the buckling value of each configuration.

4. Model the effects of the most common insulation and jacketing thickness options on the buckling value of the steel pipe at the five levels of corrosion.

1.3   Literature Review

The effect corrosion has on structures and the potentially disastrous failures that may be caused due to the process continuing unabated has affected a number of industries for a considerable time and these situations do not appear to be becoming a less common occurrence. Corrosion has therefore been of great interest to a number of research institutions and a number of papers have been produced over a long period of time.

One area of study that has received a considerable amount of attention involves the researching of the effects of a plate element that has been subjected to corrosion processes. This results in both uniform thinning of the plate element as well as localised areas of corrosion attack that result in pitting. Much of the research in the 1980s focussed mainly on uniform corrosion processes and the effect of this corrosion type on plate elements. Hart et al. (1986) and Soares (1988) chose to utilise simplified linear structure models in place of more complex options to measure the continued uniform corrosion progress over a period of time.

Soares and Garbatov (1999) proposed a non-linear model to simulate uniform corrosion damage to further build on the study performed by Soares in 1988. In this 1999 study, the plates were also subjected to a compressive load which allowed the authors to examine the variation in plate collapse strength over time due to the increased levels of uniform corrosion exhibited and therefore the thinning of the plate over the period of time. Teixeira and Soares (2008) again built on the earlier work by introducing a random spatial distribution of the corrosion thickness. This was proposed to replace the previous theory of uniform thickness loss due to general corrosion and presented a more real-world alternative.

Frankel et al. (1987) effectively described the formation and evolution of pitting morphologies under metastable conditions in stainless steel and the levels of interest in the field of corrosion have remained pretty constant. Daidola et al. (1996) produced a report for the Ship Structure Committee as it was recognised that pitting corrosion was having a highly detrimental effect on the shipping industry. A new way to evaluate the strength of pitted plate panels was required as at the time the evaluation method of the time was highly subjective and was based upon the personal judgement of a single evaluator. Any borderline cases were always considered conservatively and this led to the potential for unnecessary repairs to be carried out, which would be considered less urgent and would, therefore, put the vessel out of commission. Daidola et al. (1997) developed a mathematical model of the pitted plate and this model would allow the user to calculate the residual thickness of the plate after factoring in a number of variables. These parameters included the depth of the deepest present pit, the variation between the

maximum and minimum data value sets of all the pits and the total number of pits present. The authors created a decision-making tool to calculate the measure of residual strength to ensure there was no longer any variation due to human consideration.

Rajeev et al. (2000) describe how pitting corrosion ought to be considered to have a special place within the eight most common types of corrosion as it should be considered the most dangerous. This is especially the case when the metal has been continuously subjected to an electrolyte solution as these conditions increase the proliferation of pitting corrosion.

Two papers published by Paik et al. (2003; 2004) presenting the effect varying levels of pit corrosion deterioration had on the effect of the ultimate compressive and ultimate shear strength of plate elements that have been subjected to pit corrosion wastage. The degree of pitting (DOP) and the geometric properties were the variables altered in the papers and the changing strength values were presented. The main purpose of these studies was to use the results to assist in the design of damage tolerant plate structures that have deteriorated due to pitting corrosion.

These papers provided a number of details regarding the geometric properties of the steel plates used in the study and many of these properties were used in this project. Table 1.1 provides the details of the geometric properties used in this project as recorded by Paik et al. (2003; 2004).

Table 1.1 Steel Plate Geometric Properties (Paik et al., 2003; 2004)

Geometric or Material Property	Value
Plate Width (m)	0.8
Plate Length (m)	0.8
Plate Thickness* (m)	0.01
The Shape of the Corrosion Pit	Circular
The Depth of the Pit	0.25, 0.5 and 0.75 x Thickness of the Plate
Young's Modulus (E) (GPa)	205.8
Poisson's Ratio (v)	0.3

*One of the recommended future actions would be to continue the collection of computational data to include additional steel plate thicknesses of 0.015m and 0.02m.

The equation for the degree of pitting (DOP) intensity is shown in Figure 1.1 along with a working example made up in Microsoft Excel to showcase two separate examples of the theory in practice. The studies explained that the equation can be used to assess the scale of the breakdown of the plate structure due to pitting corrosion. It is defined as the ratio between the percentages of the corroded surface area to the original surface area.

DOP Calculator

$$DOP = \left[\frac{1}{(ab)}\right]\sum_{i=1}^{n} A_{p}i \ x \ 100(\%)$$

a = plate length
b = plate breadth
n = number of pits
Ap^i = surface area of ith pit
d = diameter of pits

If the pit is circular:

$$A_{p}i = \left[\frac{\pi d_{r(i)}^2}{4}\right]$$

a =	0.8	**DOP (%) =**	**3.14**		
b =	0.8				
n =	64				
d =	0.02	DOP (%) =	3.1415926535898		

Add in Information above

Workings:	1/area =	1.562500000000
	pi =	3.141592653590
	d2 =	0.000400000000
	Ap^i =	0.000314159265
	Sum of Pits =	0.020106192983
	Sum of Parts =	0.031415926536

$$DOP = \left[\frac{1}{(ab)}\right]\sum_{i=1}^{n} A_{p}i \ x \ 100(\%)$$

a = plate length
b = plate breadth
n = number of pits
Ap^i = surface area of ith pit
d = diameter of pits

If the pit is circular:

$$A_{p}i = \left[\frac{\pi d_{r(i)}^2}{4}\right]$$

a =	0.8	**DOP (%) =**	**9.82**		
b =	0.8				
n =	32				
d =	0.05	DOP (%) =	9.8174770424681		

Add in Information above

Workings:	1/area =	1.562500000000
	pi =	3.141592653590
	d2 =	0.002500000000
	Ap^i =	0.001963495408
	Sum of Pits =	0.062831853072
	Sum of Parts =	0.098174770425

Figure 1.1 Example of Degree of Pitting (DOP) Intensity Calculator in Excel

The scope of the project had considered using the calculator to provide an accurate degree of pitting (DOP) intensity percentage should a comparison of plates with multiple various pits numbers and diameters be conducted. This is recommended as a future action to be taken to gather further information for more accurate overall conclusions.

The conclusions from the two papers were that the simplest way to model a plate that had experienced uniform corrosion would be to simply produce the same model but alter the thickness of the intact uncorroded plate to take into account the total loss of this experienced due to equal uniform corrosion across the full surface of the plate.

The studies also showed that the degree of pitting (DOP) intensity had an impact on the ultimate strength of the plate where the most highly corroded area of the plate governed the ultimate strength when the plate was placed under axial compressive loads.

One way the two papers previously discussed differs from the current project is in the way the steel plate elements are constrained. In the two papers, Paik et al. (2003; 2004) simply supported the plate at all four of the edges. In this project, all of the nodes on the left-hand side of steel plate were fully constrained and a compressive load was subjected to the plate on the right-hand side to determine the Eigenvalue buckling value.

Zhang et al. (2016) produced a paper again looking at the ultimate strength of a structural plate that had been subjected to pitting corrosion under combined loading. The paper looked into how the results differed depending on the shape of the pits. Paik et al. (2003; 2004) focused specifically on spherical pits, as did this project, whereas Zhang et al. (2016) also considered cylindrical and cone-shaped pits in their analysis.

The reason this project focused solely on circular shape pits was due to the fact was felt that it would be more important to model data at varying insulation and jacketing thicknesses, that had not been completed before, rather than repeating work that had been completed recently. However, it should be noted that a recommendation for future work would be to complete the collection of data by including models of differing pit shape.

Zhang et al. (2016) also concluded that the ultimate strength of the plate related to the thickness of the plate minus the overall loss of thickness due to corrosion. They also noted that it is possible to simply real-world pit configuration into a finite element model with acceptable accuracy as long as the pit distribution and volume loss are modelled correctly. The modelling option for both shell and solid elements both produced conducive results.

1.4   Structure of the Thesis

This thesis is compiled from a total of eleven chapters. The main topics from each chapter are detailed below.

> Chapter One introduces the piece of research; the background and the motivation behind the piece of research is explained. The main objectives of the piece of research are stated and the current literature relating to the thesis is explored and reviewed.

> Chapter Two aims to give a general introduction to the oil and gas industry as a whole before exploring the corrosion phenomena experienced in various sectors within the offshore sector.

> Chapter Three introduces the phenomenon of corrosion and the processes by which the various forms of corrosion mechanism attack the surfaces of metals. The chemistry that drives these reactions is explored before the various classes of corrosion are introduced and described.

> Chapter Four explores the process of corrosion under insulation which is of great interest to this project. The fundamentals governing the process of corrosion under insulation is introduced before the mechanism is presented and discussed in greater detail.

> Chapter Five introduces the concept of the insulation system and explores in more detail the materials used in this project.

> Chapter Six serves as a brief introduction to the finite element method and also the ANSYS Mechanical APDL programme which is one of a number of software options commercially available to perform finite element analysis mathematical techniques.

> Chapter Seven details the procedure followed to validate the author's coding style through comparison with a published example.

> Chapter Eight completes the validation work where a mesh convergence study is performed on both the 2-D and 3-D models to deduce the best balance between accurate results and computation time.

Chapter Nine presents the procedures and the results generated from the computational work determining the effect of the different insulation and protective jacketing materials would have on the expected buckling value of a metal plate subjected to a load.

Chapter Ten presents the procedures and the results generated from the computational work determining what effect mineral wool insulation with two jacketing systems would have on the expected buckling value of metal pipe subjected to a load.

Chapter Eleven provides a review of the objectives of the piece of research and whether the objectives have been met. A summary of the major findings is also presented whilst providing information regarding any gaps in the research and advises of any future work that would be recommended. The novelty of the piece of research and the potential contribution to the field is also presented as well as any final remarks regarding the project.

Chapter Two: Corrosion in the Oil and Gas Industry

The aim of this section is to give a general introduction to the industry as a whole before exploring the corrosion phenomena experienced in various sectors within the oil and gas industry. The demand for oil and gas and the importance of the industry generally has been noted for a considerable time and at various stages, engineers are battling against corrosion to continue the supply of this worldwide demand. Understanding the processes of the various mechanisms of corrosion is imperative if engineers are to develop long-lasting defences to decrease the cost of repairs and instances of failure due to this preventable issue.

2.1   The Oil and Gas Industry

Oil and gas are two of the earth's most abundant energy sources, and they both come from hydrocarbon reserves that occur naturally within the earth. These hydrocarbons were formed over millions of years as the organic remains of various plants and animals were compressed at very high pressures and temperatures for long periods of time under the earth's crust. Depending on the composition of the organic matter and the environment in which the fossil fuel was formed either a solid, known as coal, a liquid, known as crude oil, or a natural gas fuel source was created. When the temperature is "lower" more crude oil is created than natural gas which explains why wells that are much deeper into the earth would be expected to yield a higher percentage of natural gases (Papavinasam, 2014).

Over two hundred years ago the first oil was drilled and since then civilisation has depended heavily on this source of energy, whether it be from fuels derived from crude oil or natural gas. Since oil's discovery, man has also harnessed other fuel sources from the earth and the atmosphere to continue to meet our demands. Other sources include coal and nuclear as well as renewable resources such as solar, wind and tidal. Throughout this period of advancement, the importance of oil and gas sources has remained and are still expected to for a number of decades. Figure 2.1 is taken from the World Energy Council's "World Energy Resources Report" (2016) and shows the changing landscape over a period of 15 years. As can be seen, the demand for oil as a primary fuel source has seen it remain as the largest percentage consumed at 32.9% at the time of publishing. Natural gas follows closely behind with a demand of 23.85%.
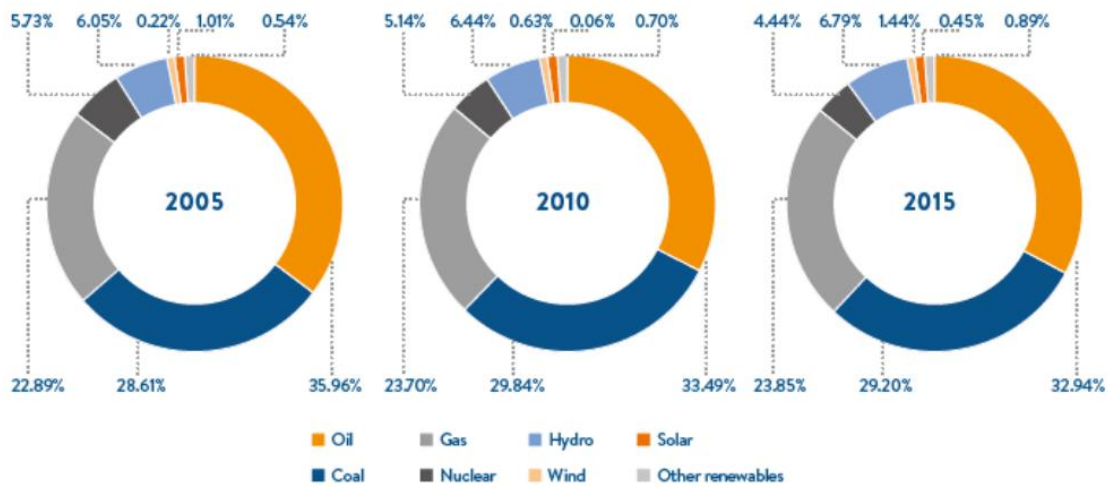
Figure 2.1 Comparative Primary Energy Consumption between 2005 and 2015

(World Energy Council, 2016)

The International Oil Agency (2018) publishes a market report detailing the world supply for oil at any one time and the previous 4 years data is also available. At the time of the writing, the world demand for oil was 98.45 million barrels per day. This was an increase from the 93.52 million barrels per day in the third quarter of 2014 which was the earliest graphical data available. The graphical data showed a generally steady increase in the demand for oil over the period with occasional dips as expected which can be seen in Figure 2.2 (International Energy Agency, 2018). To coincide with the data detailing the world demand for oil the International Oil Agency also publishes a market report detailing the world supply of oil which is shown in Figure 2.3 (International Energy Agency, 2018). Over this same period, the supply of oil increased from 94.16 million barrels per day in the third quarter of 2014 to 99.03 million barrels at the time of writing. It can be seen from Figure 2.3 (International Energy Agency, 2018) that the supply of oil followed much the same pattern as that of demand. Data published by the OPEC Statistical Bulletin (2018) and shown in Figures 2.4 and 2.5, shows the proven world crude oil and natural gas reserves by continent and gives an indication of the location of the reserves are that have met this increasing demand over the last 60 years.
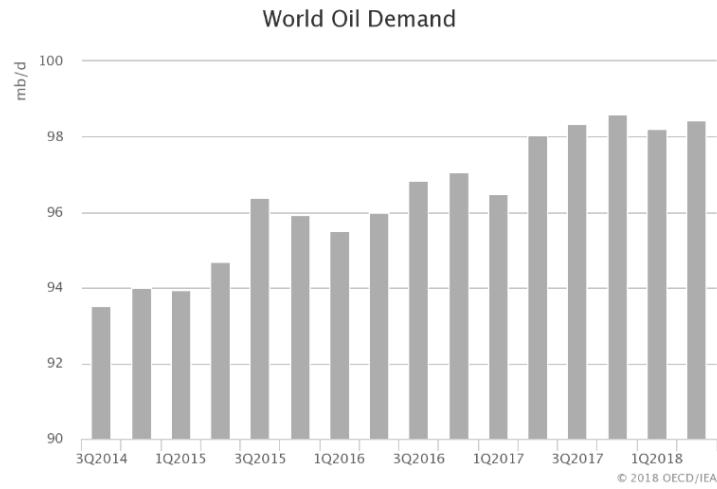
Figure 2.2 World Oil Demand (International Energy Agency, 2018)
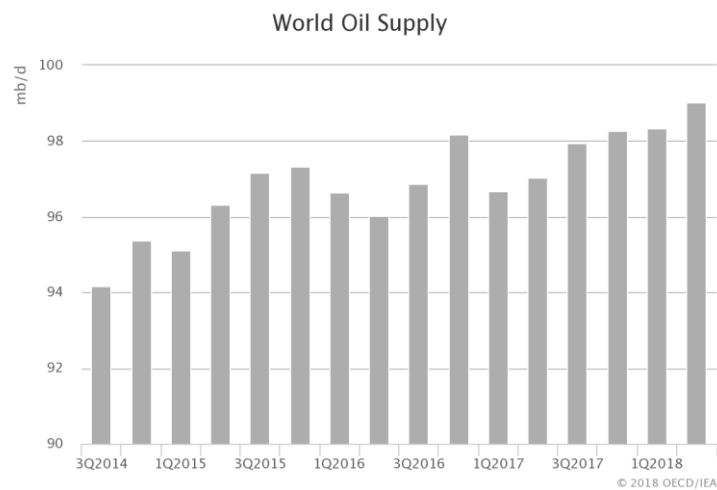
Figure 2.3 World Oil Supply (International Energy Agency, 2018)
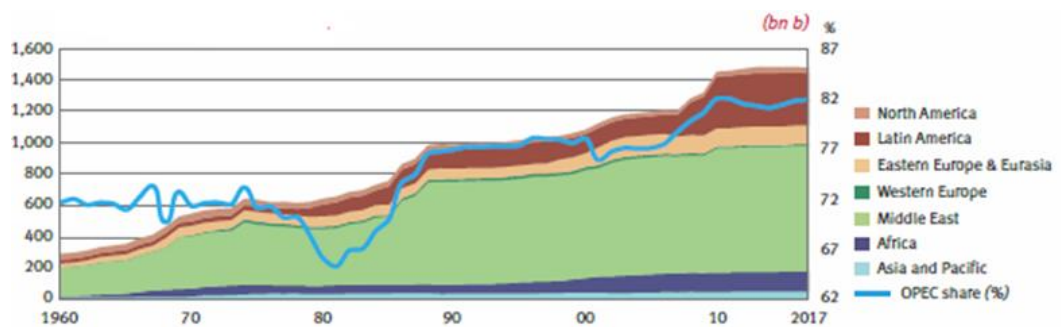
Figure 2.4 World Proven Crude Oil Reserves (OPEC Statistical Bulletin, 2018)
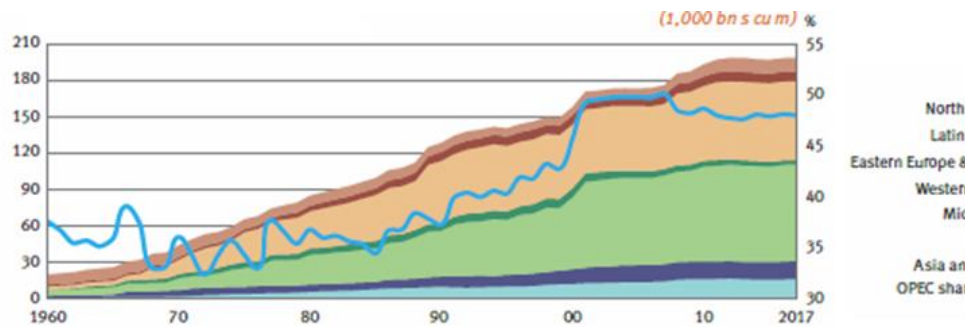
Figure 2.5 World Proven Natural Gas Reserves (OPEC Statistical Bulletin, 2018)

In their natural form, these petroleum products are of little commercial use to consumers and must undergo a number of complex refining process to produce marketable products. The progress from exploration and drilling where the crude product is extracted from the earth to the point where it is distributed to the consumer is represented simply in Figure 2.6 (Resource Dynamics LLC, 2018).

The initial phase is to collect and analyse seismic data and reservoir technology to locate potential crude fuel reserves which will then be drilled to extract the fuel source. At the extraction site, whether on land or at sea, the crude oil is cleaned and separated ready for transport to refineries. When the crude oil initially comes to the surface it is a hot heavily contaminated blend of saltwater, drilling fluids, solid particles from the earth, microorganisms and a mixture of the crude oil and gases such as carbon dioxide and sulphur. These components must be separated in settling tanks prior to transport (Devold, 2013).

The crude oil once settled is transported either by pipelines, for shorter distances, or tanker truck or sea tanker if the distance is much greater to a refinery. These refineries are usually located near oil consumer markets. The crude oil is then stored until required by the refinery for processing into the various fractions for use to make up the finished products which are then stored again before being sold to retailers. Of the fractions that are separated and sold approximately 90% are a fuel in their own right such as petrol, kerosene, aviation fuel and liquefied petroleum gas. The remaining approximately 10% is made up of non-fuel products such as bitumen, solvents, waxes and petrochemicals. The petrochemicals that are produced include ethylene and propylene which are sold to chemical plants to manufacture other chemicals and plastics (Devold, 2013).
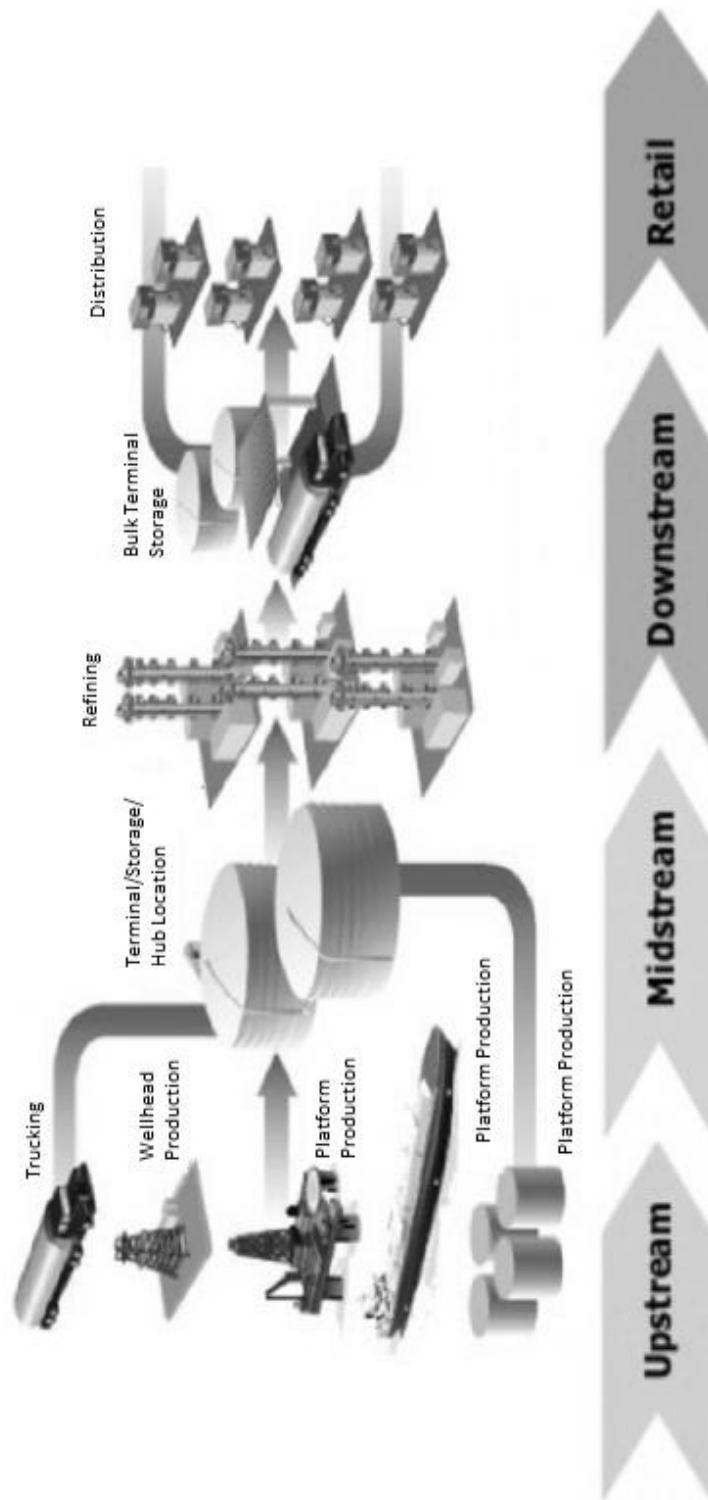
Figure 2.6 Representation of the Oil and Gas Processing Stream (Resource Dynamics LLC, 2018)

2.2   Corrosion of Offshore Structures and Equipment

Since drilling operations commenced in offshore locations oil and gas exploration companies have developed a number of different structure types that allow them to driller deeper and deeper to exploit reserves all around the globe. In this section, the various drilling platform types and offshore production facilities that are used around the world are briefly introduced.

Put simply, an offshore drilling and production platform can be broken down to two constituent areas; the platform itself, which is a manufactured structure of either reinforced concrete or steel, and the topside facilities. These topside facilities are supported on the different platform types as seen in Figures 2.7 (Devold, 2013) and 2.8 (Devold, 2013). These two structure types and an alternative called a floating production, storage and offloading vessel, shown in Figure 2.9 (Devold, 2013), will be discussed in more detail shortly.

The steel platform type can either rest on the seabed or float while being effectively anchored, depending on the drilling application and the water depth of the location. The reinforced concrete platform type always rests on the seabed. It is also quite common for this platform to have "built-in" storage tanks for storing the oil before depositing to other vessels for transport onshore. The topside facilities mentioned previously are the location for of all the oil production processing stations from the drilling facilities to the processing facilities where the oil is prepared for storage or transport. The offshore worker's sleeping and recreational quarters can also be found here as well as all of the instrumentation systems, electrical systems and control centre where the offshore installation manager manages the production services of the platform as well as ensuring the safety of all personnel. The decision on the type and size of the offshore structure that will be used is normally determined by two factors; the type of hydrocarbon that is being harvested and the maximum depth of the reservoir relative to the platform above. The main effect of the hydrocarbon to be harvested is the type of processing and storage facilities on the platform as each hydrocarbon type has different processing requirements (Devold, 2013).

As mentioned previously there are three main classes of structure used for the extraction and processing of oil and gas reserves offshore. These main classes will be explored briefly:

- Steel structured platform: one of the most common classes of structure found around the globe. When used in shallow water, of up to 100 metres, it can be common to see a number of these platforms operating together where each platform is independent of the others and is responsible for a specific process within the overall production. Each platform is connected by a gangway bridge. Figure 2.7 is an example of this type of complex. The tubular steel framework for the underwater portion of the platform is often assembled and then towed to the site by barge and then submerged and anchored to the seabed (Devold, 2013).

- Gravity base platform: the concrete for these types of structure were poured on land and then towed out to their location. These types of structure often have oil storage tanks within the concrete legs and the air contained within these legs when poured allow for it to float to its resting spot before lowering to the seabed. These types of platform are often used to extract from reservoirs in deeper locations of 100 metres to 500 metres (Devold, 2013).

- Floating production, storage and offloading vessel: This type of vessel is advantageous as it contains all the equipment associated with a stationary platform on a movable vessel with no requirement for external infrastructure. The vessel is able to drill for hydrocarbon sources using subsea wellheads and can then process and store this hydrocarbon source as well as other products from other structures before transferring by pipe for transport to the refineries by smaller tanker (Devold, 2013).

Figure 2.7 Steel Platform Supporting Topside Facilities (Devold, 2013)

Figure 2.8 Concrete Platform Supporting Topside Facilities (Devold, 2013)

Figure 2.9 Floating Production, Storage and Offloading Vessel (Devold, 2013)

The offshore environment can be one of the most hostile and unpredictable operating environments on earth. Platforms can be operating in tropical conditions at one point of the year and then may be subjected to hurricane-like conditions at another; as in the Gulf of Mexico. In other places, such as the North Sea, there may well be sub-zero temperatures and continuous freezing precipitation for long periods of time. In both areas, oil platforms can be subjected to wind gusts and high waves due to swell and are designed to withstand these and other inhospitable weather conditions.

One of the largest problems is that these conditions can be the perfect precursor to corrosion in general and corrosion under insulation in specific circumstances of the insulation and jacketing of components is not sufficient. Figure 2.10 (Chandrasekaran & Jain, 2017) shows the three zones that an offshore structure can be separated into with respect to corrosion. Figure 2.10 also shows the corrosion types expected within each of these zones.

These three zones from the top down are defined as:

- The atmospheric zone: this is where the deck modules, for example, the living quarters, and derricks, which are lifting devices, are located. This zone is located the furthest distance from the water level and is therefore never in direct contact with water. It is however subjected to exposure to solar radiation, wind, precipitation and sea spray. So though limited in comparison to the lower zones this area does experience a level of corrosion. This zone is often protected from corrosion processes through the use of various protective barrier layers such as chlorinated rubber, epoxy and specialist coatings (Chandrasekaran & Jain, 2017).

- The splash zone: this zone is sometimes referred to as the tidal zone as it is the zone closest to the water level without being submerged. The highest level of corrosive processes occurs in this area due to the continuous wetting and drying due to sea well caused by tide changes, wind and wave fluctuations. Often protective coatings and claddings are utilised here to prevent higher levels of corrosion occurring (Chandrasekaran & Jain, 2017).

- The immersed zone: this zone is constantly submerged under the waterline and can also include an area which is below the mud line, commonly known as the seabed. Due to the lower concentration of oxygen the levels of corrosion in this area is much lower. Corrosion in this area is usually governed by the microorganisms in the water and the oxygen diffusion rate through rusted layers, because of this the most common protection utilised in this area is cathodic protection. Cathodic protection is where an electrochemical cell is created with the metal of the structure acting as a cathode. The anode is made of a sacrificial metal which corrodes more readily and therefore protects the metal structure (Chandrasekaran & Jain, 2017).
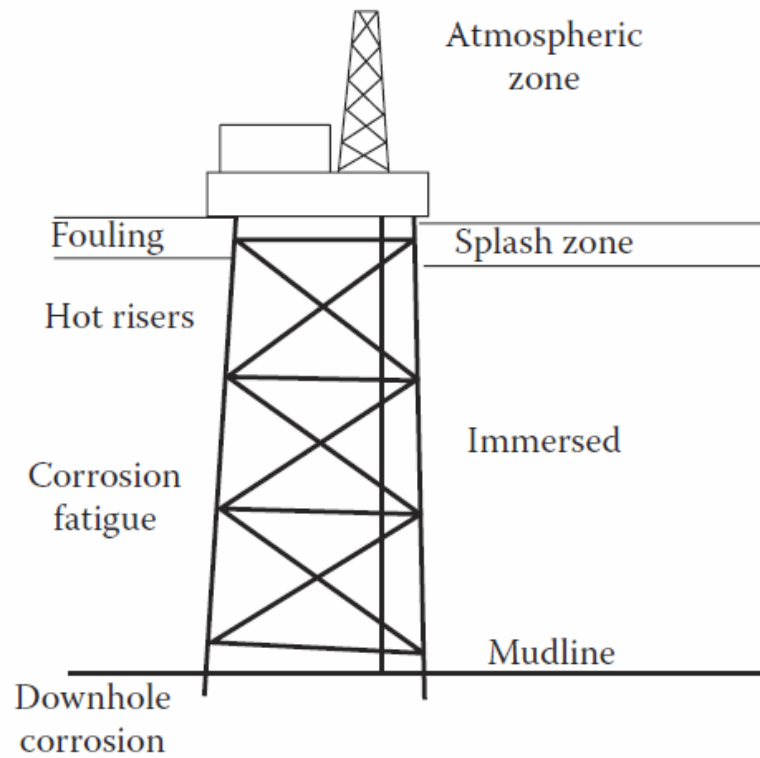
Figure 2.10 Typical Corrosion Zones of an Offshore Platform and Type of Corrosion Expected

(Chandrasekaran & Jain, 2017)

University of Strathclyde
Daniel Richard Hugh Mancini
Department of Naval Architecture, Ocean and Marine Engineering
Chapter Two: Corrosion in the Oil and Gas Industry

2.3 Corrosion of Topside Facilities

The main focus of this project is to computationally model the impact insulating and jacketing materials have on the buckling strength of a corroded offshore structural component. For this reason, the main focus will be on that of the topside structures as they are the only ones that would more realistically be insulated and jacketed to protect against corrosion. There are a number of factors considered when selecting insulating and jacketing materials and these are addressed in section five of Chapter One, where the introduction to insulation and jacketing materials is located.

The topside facilities of a platform are responsible for the extraction, processing, storage and offloading of hydrocarbon fuel sources for transport to oil refineries or processing plants for natural gas. Many of these systems require insulating to protect personnel from dangerously hot surfaces and to control the temperature to ensure the systems are operating at optimum system temperatures and are not losing or gaining heat from the external atmosphere. The vast majority of these structures are of steel construction and are therefore liable to be at risk from corrosion. In the next three sections, the main process function areas that are commonly insulated for protection will be addressed in a little more detail.

2.3.1 Processing Systems

The main role of the processing systems is to remove the unwanted impurities and seawater from the crude oil and natural gas mixture. Then the crude oil and natural gas mixture also need to be separated into a number of different components before transporting these resulting products onshore. The gas impurities and seawater are usually located in the reservoir along with the desired products. They are actually very useful in the first instance as they are required to ensure the desired products are able to break through to the topside processing systems (Papavinasam, 2014).

In an oil processing network, high temperatures are required to remove the undesired water from the emulsion with crude oil. To protect these systems and reduce the opportunity for heat loss to the atmosphere these vessels are insulated. Due to the high operating temperatures and the inevitable ingress of water from the elements, this produces the perfect conditions for the phenomena of corrosion of the metal surface the under insulation. Corrosion under insulation is of great importance to this project and to the industry as a whole and will be discussed in more detail in Chapter Four (Papavinasam, 2014).

In a gas processing network, there is a zone that relies on the principles of fluid dynamics and pressure change to separate a mixture of oil, gas and water into their individual parts. Within the vessel, the decrease in pressure ensures the dissolved gas fraction can be separated through the top leaving the oil and water mixture below. This mixture then settles into two layers of different specific gravities and can be syphoned off to two separate holding tanks (Papavinasam, 2014). Though not necessarily insulated these vessels are still susceptible to corrosion processes and may be protected in other ways.

Heat exchangers are another part of the processing network that can be highly susceptible to corrosion processes. They are required to facilitate the separation of oil from water and to regenerate glycol which is used in gas dehydration systems. Consideration is taken when selecting the metal material heat exchangers are manufactured from depending on the environment that they are to be used in. Heat exchangers are often treated with coatings and claddings in an attempt to protect them when they are located in environments where the incidence of corrosion is of greater risk (Mather, 2000).

One particularly challenging area when attempting to insulate and protect processing equipment is the fact there can often be a number of attachments and supports of awkward geometry and configuration. Ensuring that these vessels and parts are properly insulated is not often the difficult part. Ensuring that the protective jacketing is weathertight and that all seals are joined correctly so as to keep the insulation dry is where the real issue lies. Failure to complete this correctly will result in water ingress and will result in favourable corrosion conditions.

2.3.2   Storage Systems

Storage systems are commonly a collection of vessels operating at atmospheric pressure whose role is to act a temporary container for holding processed oil, water and condensate products. Metering systems ensure that products contained within storage vessels remain between acceptable limits and pump product in or out depending on the requirement. Some of these products are stored under hot conditions and require insulating to protect personnel from the heat and to reduce heat loss to the atmosphere. In this instance, rigid systems are often used as the vessels are of a configuration that is relatively simple to manipulate the insulation with very few awkward areas to manoeuvre. Care needs to be taken to ensure the joints are sufficiently secured otherwise water ingress and condensation can accumulate at the bottom of the vessel and can potentially corrode the securing rig (Mather, 2000).

2.3.3   Piping Systems

As with the other production facilities in the oil and gas industry, all of which are subjected to great amounts of wear, corrosion and stress, piping systems may require to be the most durable. The design of a piping system must consider the potentially abrasive, thermal and corrosive loads that will travel through it throughout its lifespan.

The piping system will be subjected to the abrasive wear of particles travelling internally the length of the pipework to the processing areas. When this is combined with the variable temperature range of the products carried within the piping from extremely low temperatures to extremely high temperatures and corrosive nature of some of these products the requirements for the durability of the pipe internally comes into question when designing. This is before the consideration for protecting the external of the pipes is considered as well. This project will focus solely on the external parameters affecting the piping system.

Piping systems are the most commonly insulated and jacketed system on an offshore facility will be the piping systems. They are an integral part of the entire system and are responsible for the linking of all of the other zones from the start of the process to the final act of transferring the hydrocarbon products onto a tanker destined for the refineries.

One of the most important considerations when insulating and jacketing pipework will be the fact there can be a number of protrusions from the pipe. These can include but are not limited to support clamps, monitoring devices and rod hangers. Figure 2.11 (NACE International, 2016) gives an illustration of a potential water entry point in a supported pipework setup. Due to the non-uniform nature of these protrusions caulks and sealants are often used to insulate as they can mould around these areas effectively. They must be monitored as they can be highly susceptible to damage through extreme weather conditions or unexpected mechanical abuse like vibrations (NACE International, 2016).

In the area where there is an expanse of pipeline connecting two zones then the types of material used within this project can be used. They will be discussed further in section five of Chapter One, where the introduction to insulation and jacketing materials is located. Proper installation of the jacketing system is extremely important to ensure the integrity of the piping system as an error here can lead to potentially very expensive repairs or possible failure. Particular care should be taken when pipes are in close proximity to other structures due to the lack of space on an offshore platform. Often the jacketing layer is discontinued and worked around the structure. If not completed and sealed correctly a potential avenue for water ingress is created.
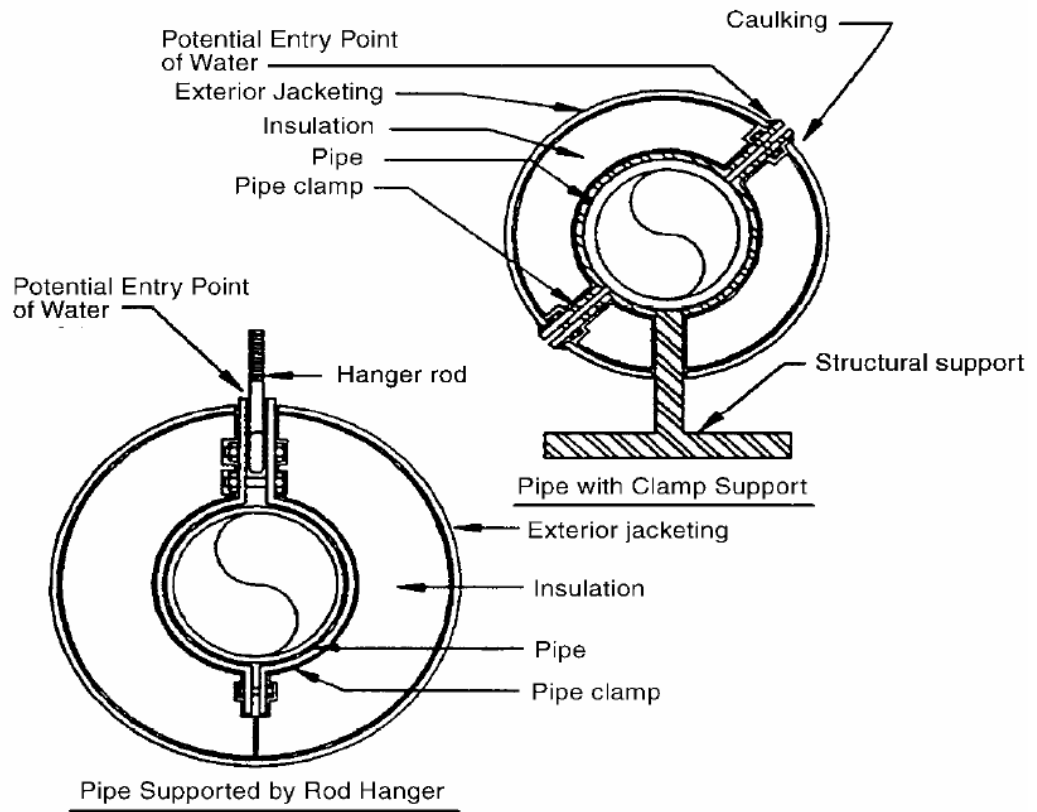
Figure 2.11 Potential Entry Point of Water on Jacketed Pipe Systems (NACE International, 2016)

Chapter Three: Corrosion

The aim of this section is to give a general introduction to the phenomenon of corrosion and the processes by which the various forms of corrosion mechanism attack the surfaces of metals. The chemistry that drives these reactions is explored before the various classes of corrosion are introduced and described. Understanding the processes of the various mechanisms of corrosion is imperative if engineers are to develop long-lasting defences to decrease the cost of repairs and instances of failure due to this preventable issue.

3.1   Fundamentals of Corrosion

The natural process by which a metallic material deteriorates through an electrochemical or chemical reaction due to the surrounding environment is known as corrosion. Although all environments are technically corrosive there are certain conditions which result in a faster rate of corrosion, these can include (Roberge, 2000):

- The presence of freshwater and saltwater
- The presence of gases such as sulphur dioxide, hydrogen sulphide and chlorine
- The presence of high levels of moisture or pollutants in the air

Steel is a widely used construction material in the oil and gas industry and as it is an alloy of iron, carbon and other elements it can be susceptible to corrosion through an electrochemical process attacking the iron. The term aqueous corrosion can be used to describe a number of mechanisms of corrosion which all share four distinct components (Edwards, 2013). Should one of these components not be present then no corrosion will take place:

- An anode – the location where corrosion occurs and rust is formed
- A cathode – the location of oxygen reduction or hydrogen creation depending on the conditions
- The presence of a conductive electrolyte made up of anions and cations – in this case, it is water
- A metallic path for the transport of electrons

Figure 3.1 illustrates a simplified version of the mechanism described above. Please note the presence of water is implied (Edwards, 2013).
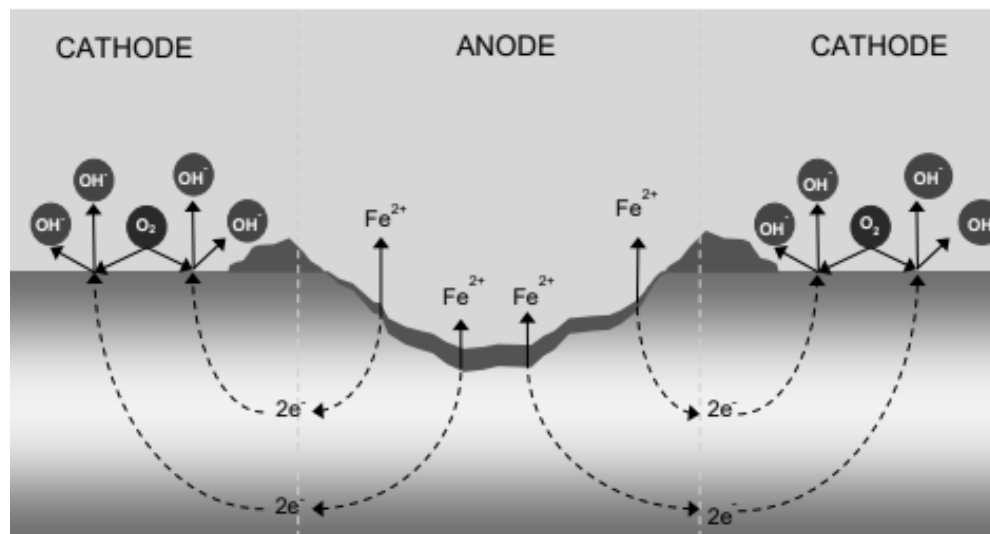
Figure 3.1 Simplified Schematic of the Corrosion Process (Edwards, 2013)

The reactions occurring at these sites will be discussed in more detail and the specific equations will be presented where relevant. Equation (3.1) details the reaction occurring at the anode when the steel is dissolved when in solution. This reaction does not change regardless of the conditions in which the steel is present. The conditions under which the steel is dissolving gives rise to the specific reactions detailed in Equations (3.2), (3.3) and (3.4). In each circumstance to confirm the corrosion of iron proceeds the electrons that have been released in Equation (3.1) must be consumed thus ensuring the electrochemical systems remains in equilibrium. This second cathodic reaction occurs at exactly the same time as the anodic reaction and is subject to the conditions by which the system is dissolving the iron (Edwards, 2013). When a metal material is used corrosion will always be a major concern due to the fact that a metal's natural state is the oxidised state. After a metal has been mined and processed, they no longer remain in this natural state and instead reside at a more excited level. Due to this, a metal will always want to revert back to its natural state. If the environment is oxygen and moisture-rich the metal will essentially want to corrode as this will allow it to return its lower energy state. During this corrosion process, the accumulated energy will be released as the metal converts to its corrosion products (Popov, 2015). Table 3.1 depicts the standard potential series for a number of metals some of which are used in construction processes and their tendency to corrode (Popov, 2015).

$$Fe(s) \rightarrow Fe^{2+}(aq) + 2e^- \qquad\qquad (3.1)$$

Table 3.1 Standard Potential Series for Metals and their Tendency to Corrode (Popov, 2015)

Nobility of Metal	Metal	Electrode Potential (V)	Tendency to Corrode
Non-Noble	Aluminium	-1.66	Greatest
	Zinc	-0.76	
	Iron	-0.44	
	Tin	-0.14	
	Hydrogen	0	
	Copper	0.34	
	Platinum	1.20	
Noble	Gold	1.50	Least

Under oxygenated neutral or alkaline conditions Equation (3.2) details the cathodic reaction occurring. If the conditions were either acidic and/or at low levels of oxygenation then the cathodic reaction would be expressed by Equation (3.3). If the reaction was to occur under acidic conditions Equation (3.4) would explain this. A redox reaction is a term used to describe two simultaneous reactions occurring. This name is used as it describes both parts of the reaction; "red-" for the gain of electrons, or reduction, and "-ox" for the loss of electrons or "oxidation". It can be seen that the electrons "lost" by the metal in Equation (3.1) are gained by the reaction occurring at the cathode in Equations (3.2), (3.3) or (3.4) depending on the environmental conditions (Edwards, 2013).

$$O_2(g) + 2H_2O(l) + 4e^- \rightarrow 4OH^- \qquad (3.2)$$

$$2H_3O^+ + 2e^- \rightarrow H_2O(l) + H_2(g) \qquad (3.3)$$

$$O_2(g) + 4H^+ + 4e^- \rightarrow 2H_2O(l) \qquad (3.4)$$
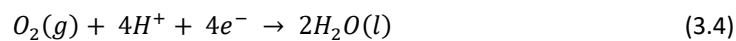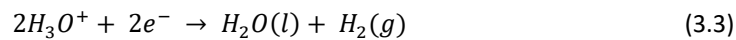
Equation (3.5) shows that when Equation (3.1) and Equation (3.2) combine, a balanced equation is created that proves that corrosion can only occur when each part of the half equation exists. In theory, it is possible for the corrosion mechanism to cease action and for the entire steel component to be fully consumed. In this scenario, the corroded Fe^{2+} ions would remain suspended in solution and this leads to a potentially very dangerous conclusion. If there had been no scheduled routine inspection of the steel component it is possible that no indication of corrosive action until total failure occurs. Fortunately, this is a relatively unlikely scenario. Often iron will precipitate out of the solution and will present as hydrated ferric oxide, or rust. Though this is not necessarily a desirable situation it does at least alert personnel to the corrosion issue and will allow them time to remedy the problem (Edwards, 2013). The three common reactions for the formation of rust are shown in Equations (3.6), (3.7) and (3.8).

$$2Fe(s) + O_2(g) + 2H_2O(l) \rightarrow 2Fe^{2+}(aq) + 4OH^- \qquad (3.5)$$

$$2Fe^{2+}(aq) + 4OH^- \rightarrow 2Fe(OH)_2 \qquad (3.6)$$

$$4Fe(OH)_2 + O_2 + 2H_2O \rightarrow 4Fe(OH)_3 \qquad (3.7)$$

$$4Fe(OH)_3 \rightarrow 4Fe_2O_3.H_2O + 2H_2O \qquad (3.8)$$
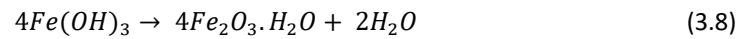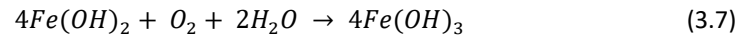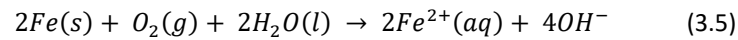
As noted, it is unlikely that the reactions at the anode and cathode are ever likely to cease entirely there is an option for corrosion engineers to slow down and therefore control the corrosion processes taking place at these locations. Protective coatings are well documented as a protective layer over the metal structure to prevent the ingress of moisture and exposure to oxygen and can, therefore, reduce the rate of corrosion.

The severity of the offshore environment was discussed previously and due to the common use of carbon and stainless steel, it is no surprise that a number of oil and gas structures are at severe risk of corrosion. This is especially the case offshore in the case of offshore platforms and rig topside facilities as there is also the marine environment to account for as well. This combination of factors leads to many exploration companies accounting large sums of their operating budget to effectively monitor and repair their working structures as a potential failure will be considerably costlier than the continued resolution of issues.

Equation (3.9) depicts the corrosion rate equation, which is often used to indicate the capacity of a material's resistance to corrosion in a specific environment. It is possible to quantify the corrosion rate in a number of different ways including grams lost per square inch per hour, the percentage weight loss or the number of milligrams lost per square centimetre each day. The most common usage, however, of millimetres per year as depicted in Equation (3.9), calculates the weight lost during a corrosion test (ASTM International, 2017). NACE Standard RP0775-2005 (2005) details the relative severity of annual corrosion rates of carbon steel and this has been presented in Table 3.2 to give an indication of acceptable levels of corrosion expected.

$$\frac{mm}{Year} = \frac{87.6 \ x \ 10^4 \ x \ W}{D \ x \ A \ x \ T} \tag{3.9}$$

where:

87.6   Conversion factor to produce mm/year*

W   Mass loss (g)

D   Density of the specimen (g/cm^3)

A   Area of the specimen (cm^2)

T   Exposure time (hr)

*There are alternative choices depending on the measurement and timescale required.

Table 3.2 Annual Carbon Steel Corrosion Rates and their Relative Severity

(NACE Standard, 2005)

Corrosion Rate (mm/year)	Severity	Relative Corrosion Resistance
<0.025	Low	Outstanding
0.025 − 0.12	Moderate	Good
0.13 − 0.25	High	Fair
>0.25	Severe	Unacceptable

3.2   Classifications of Corrosion

Metals that have undergone the process of corrosion can appear in a number of different visual forms, the overall look will depend on a number of variables such as the metal material type, the type of corrosive environment, whether any stresses were exerted on the metal during the corrosive period and a number of other variables. When deciding on the classification of corrosive action generally this is confirmed by visual inspection as the appearance of the resulting metal after an attack is often considered the most important factor. Many of the different corrosion types share similar mechanisms or characteristics and can be grouped together for easier classification.

There are two classifications used to describe corrosion; uniform, or general, corrosion and localised corrosion. Uniform corrosion is much easier to predict as it takes place over the entire surface of the material, whereas, localised corrosion only occurs in a selective area of the material. Figure 3.2 (Oxyplast UK Ltd, 2018) depicts a number of forms of corrosion of which the eight most common forms experienced in the oil and gas industry will be described individually and include:

- Uniform Corrosion
- Pitting Corrosion
- Crevice Corrosion
- Stress Corrosion Cracking
- Intergranular Corrosion
- Galvanic Corrosion
- Selective Leaching
- Hydrogen Embrittlement
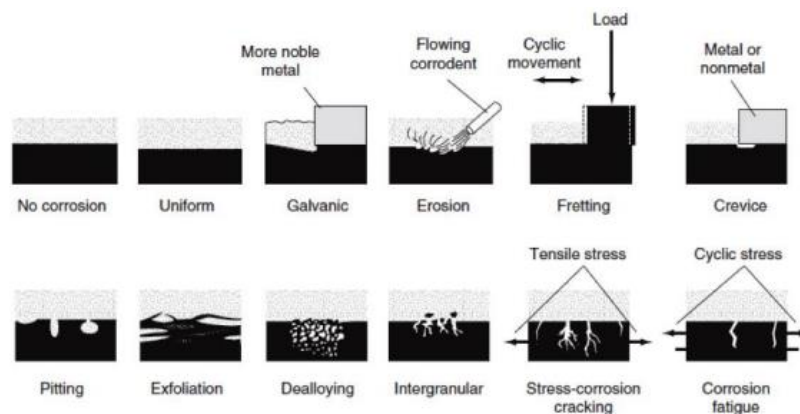
Figure 3.2 Various Classifications of Corrosion (Oxyplast UK Ltd, 2018)

3.2.1   Uniform Corrosion

General corrosion, which can also be termed as generalised corrosion, is categorised as either an electrochemical or chemical reaction that advances in a regular manner over the majority of the entire exposed metal surface. This results in considerable uniform thinning of the metal which eventually leads to the failure of the system due to the decreased overall strength. This type of corrosion does not usually attack within a localised area and is the most common type experienced worldwide. Despite this type of corrosion occurring most commonly it is relatively simple to monitor and remedy as required.

An example of a situation where this type of corrosion can be expected would be a carbon steel structure that has been subjected to continuous atmospheric elements over a long period of time. The corroding metal acts as both the anode and cathode in this classification of corrosion (Papavinasam, 2014). Figure 3.3 (Chemblinks Blogspot, 2018) provides an example of a pipe that has been subjected to uniform corrosion.

Figure 3.3 Example of Uniform Corrosion (Chemblinks Blogspot, 2018)

3.2.2   Pitting Corrosion

In direct comparison to uniform corrosion, pitting corrosion is a classification of the localised corrosion mechanism. This type of corrosion attacks in specific locations in much more concentrated doses and therefore will have larger corrosion rates spike in these areas when compared to the overall structure. The expression "pit" usually denotes a small mark on the surface of the corroded material that has the configuration of that of a hole forming. The initiation of these pits may be due to a number of scenarios such as the continuous dripping of water on a specific location or crevice corrosion, galvanic corrosion or the failure of a protective coating in a certain location. Often in the case of the galvanic reaction, the corroding area becomes anodic whereas the surrounding metal remains cathodic so the galvanic reaction remains localised as shown in Figure 3.4 (Substech, 2018). Seawater is well documented as a precursor to promote pitting of steel structures offshore due to the chlorine presence which prevents the metals ability to produce a passivating film (Papavinasam, 2014). Figure 3.5 (Steel Fabrication Services, 2018b) provides an example of a pipe that has been subjected to pitting corrosion.
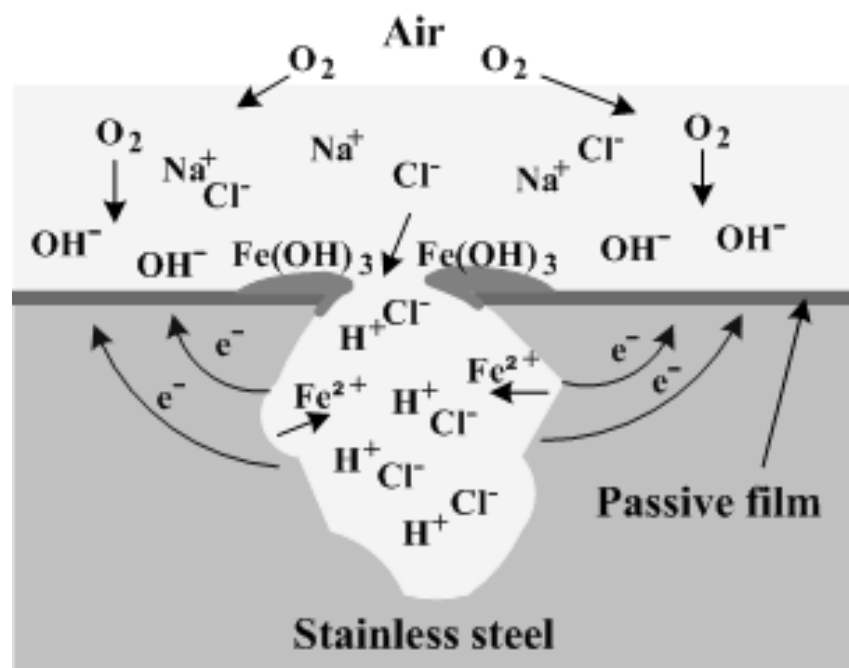
Figure 3.4 Pitting Corrosion Cell (Substech, 2018)

Figure 3.5 Example of Pitting Corrosion of Steel (Steel Fabrication Services, 2018b)

Often pitting corrosion occurs rapidly in a small area so is very difficult to detect and also can grow very quickly under the surface to produce a large cavity. Due to the formation of these deep under surface cavities pitting corrosion is considered a very dangerous form as it can easily cause unexpected failure due to minimal loss of material in strategic locations. The pit crevice can develop into a number of different morphologies as shown in Figure 3.6 (Popov, 2015). The holes themselves can either be deep or shallow but usually, they remain relatively small and hard to detect. The corrosive environment that material has been subjected to is usually the driving factor that determines the overall morphology of the resulting pit. The location of pits relative to one another can vary; on occasion, they may be closely bunched together or equally, they can be widely spaced, though they are well known to grow relative to the direction of gravity (Popov, 2015).
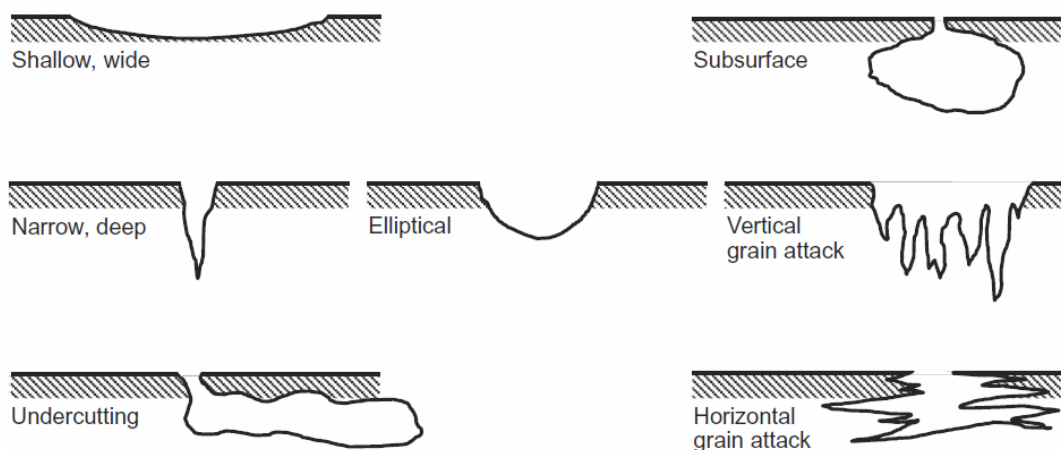
Figure 3.6 Examples of Pitting Morphologies (Popov, 2015)

Depending on the corrosive environment and the material subjected to corrosion it is possible that a number of months or even years may pass before any evidence of pitting corrosion is visible on the surface of the metal. Corrosion occurring by pitting is very difficult to model in a laboratory setting so it can be difficult to research. It is almost impossible to mimic the identical conditions experienced in nature to model this type of corrosion under controlled setting as a very minuscule variation may potentially produce large differences in morphologies and depths of pits created (Papavinasam, 2014).

3.2.3   Crevice Corrosion

This type of corrosion is very similar to pitting corrosion in the sense that it occurs intensely in a localised location. The main difference with regards to the location is that where pitting corrosion usually occurs within expanses of a material, crevice corrosion occurs within confined spaces such as in gaps and contact areas between parts, under seals and gaskets and within cracks and seams as it is often associated with a stagnant microenvironment as shown in Figure 3.7 (Steel Fabrication Services, 2018a). The four main mechanisms whereby crevice corrosion can initiate are (Popov, 2015):

- Moisture ingress into a crack, seam or defect in the metal
- Gaps between metal contacts, such as a loose nut on a bolt, allowing ingress of moisture
- Contaminant deposits over the surface of the metal, for example, dust, dirt or precipitated salts
- Contact between a porous non-metallic material, such as insulation, and the metal surface

Figure 3.7 Example of Crevice Corrosion (Steel Fabrication Services, 2018a)

Aluminium, stainless steel, magnesium and titanium are particularly prone to crevice corrosion as they are often protected by passive films which when breached then help create the microenvironment where crevice corrosion thrives. In the presence of seawater stainless steel crevices deteriorate from inside the crevice due to the fact the metal has been anodic within this area. The remaining area outside the crevice becomes cathodic resulting in a large ratio difference between the two areas which drives the corrosion mechanism. The process of crevice corrosion can develop over time to result in stress corrosion cracking (Popov, 2015).

3.2.4   Stress Corrosion Cracking

When metal structures are subjected to tensile stress or plastic strain very fine fractures can be created that potentially may travel very deep to the core of the metal structure. If a corrosive substance is able to travel through these fine fracture paths it is possible that stress corrosion cracking will occur as seen in Figure 3.8 (Southwest Research Institute, 2018). As these fractures are very fine there is very little loss of metal mass associated with this type of corrosion. Potential initiation sites include mechanical cracks or pits from alternative corrosion mechanisms, these discontinuations of the surface act as stress raisers and become the starting point of the fine fractures. Some pure metals appear to be resistant to this variety of corrosion but all alloys are susceptible to variable degrees as are certain polymers and ceramics. The end result of stress corrosion cracking appears to be the result of mechanical failure due to brittleness but it is, in reality, a corrosion mechanism (Papavinasam, 2014) (Popov, 2015).

There are a few main factors that can facilitate higher incidences of stress corrosion cracking (Papavinasam, 2014) (Popov, 2015):

- Higher temperatures

- Higher stress intensities of the metal

- A stronger concentration of the corrosive solution

- The metal's composition – alloys are more susceptible

- Metal structural damage – initiation site from fine cracks

- The presence of chlorine – leached from certain wetted insulation materials

Figure 3.8 Example of Stress Corrosion Cracking (Southwest Research Institute, 2018)

3.2.5   Hydrogen Induced Damage

The combined action of residual stress and the presence of hydrogen atoms can result in mechanical damage known as hydrogen-induced damage. Commonly this type of damage presents by either embrittlement, cracking or blistering of the metal surface depending on the metal composition. Hydrogen atoms are very small and have the ability to diffuse inside metal structures whereby they can initiate the mechanism by which the damage occurs. In an environment where hydrogen gas is produced, much of which escapes in the form of bubbles, a small proportion is adsorbed into the metal. These adsorbed atoms when inside can form into molecular hydrogen gas which can expand suddenly and destructively causing failure. The presence of the hydrogen atoms is a by-product from corrosion reactions in acidic conditions occurring nearby due to high temperature, moisture presence and the electrolysis process. As mentioned previously hydrogen damage usually takes the form of one of the following three presentations (Papavinasam, 2014):

- Hydrogen Blistering (Figure 3.9) (Maverick Inspection Ltd, 2018) – also referred to as soft zone cracking due to the blistering proliferation in softer metals, or softer zones within stronger metals, in corrosive environments. Usually, the blisters are relatively small, around 25mm in diameter, but can grow as large as 1.2 metres.

- Hydrogen Induced Cracking (Figure 3.10) (King Fahd University of Petroleum & Minerals, 2018) – occurs in carbon and alloy steels when the hydrogen atoms suddenly form molecular hydrogen gas inside a metal which pressurises the material and results in mechanical failure.

- Hydrogen Embrittlement (Figure 3.11) (System 22 Inc., 2018) – the metal becomes less ductile and less strong due to the hydrogen atoms disrupting the metal lattice. Iron, titanium and nickel are more prone to this type of attack and the action of embrittlement may be reversible if the metal is removed from the source and heated to high temperatures around 200°C.

Figure 3.9 Example of Hydrogen Blistering (Maverick Inspection Ltd, 2018)

Figure 3.10 Example of Hydrogen Induced Cracking

(King Fahd University of Petroleum & Minerals, 2018)
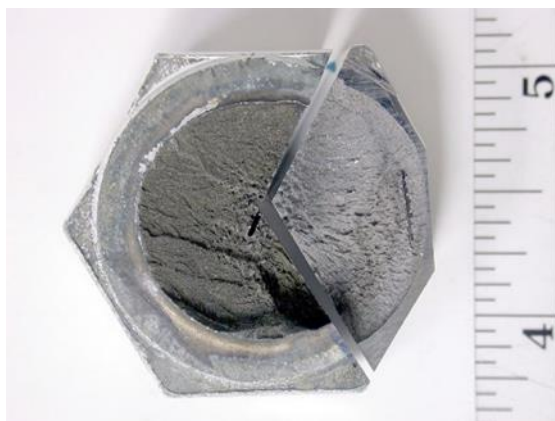
Figure 3.11 Example of Hydrogen Embrittlement (System 22 Inc., 2018)

3.2.6   Galvanic Corrosion

The best-known variant of electrochemical corrosion is that of galvanic or bimetallic corrosion. In this situation, two different metals are in contact within a conductive or corrosive environment. One of the metals will be less resistant to corrosion and will become the anode within an electrochemical, or galvanic, cell and will corrode. The resistant metal will, in turn, become the cathode and will appear almost unaffected by the environment as seen in Figure 3.12 (InterNACHI, 2018).

One factor that determines the speed of the corrosion process is the ratio of the anode area versus cathode area within the galvanic cell. The larger the cathode area subjected to the corrosive environment the more proportional the severity of the damage to the corroded metal. So, a large cathode and a small anode result in much more severe corrosion and more minor corrosion with a large anode and small cathode.

The intensity of galvanic corrosion can also be altered drastically by the volume of atmospheric moisture under which the corrosive environment is located. In an offshore location, for example, there would be much higher moisture levels present than a location inland and therefore would be subjected to more intense corrosion. The addition of the natural salts within this moisture-rich offshore environment also makes the medium even more conductive and therefore more corrosive when compared to similar humidity and temperature conditions at an inland location.

Figure 3.12 Example of Galvanic Corrosion (InterNACHI, 2018)

3.2.7   Intergranular Corrosion

When metal materials are magnified it can be seen that the microstructure of the metal is a combination of grain crystals which are divided by gaps known as grain boundaries. A magnified example of this can be seen in Figure 3.13 (Pace Technologies, 2018). Intergranular corrosion, as the name suggests, occurs mainly at the grain boundaries and the areas adjacent to them. This type of corrosion rarely affects the grain crystals themselves and one other characteristic of this corrosion type is that it can occur without a stress input. One of the most common precursors for the initiation of intergranular corrosion is the presence of impurities which result in the altered chemical composition of the boundaries differing radically from the grain crystal. When the concentrations of the impurities reach a critical level, these impurities react with other components present in grain boundary to produce new compounds. These additional compounds alter the chemical composition further causing a difference in electrical potential between the grain crystals and the grain boundaries which are the ideal conditions for the intergranular corrosion to commence. Technically this type of corrosion can be considered a special form of galvanic corrosion due to the presence of different electrical potentials. Depending on the differing impurities present the grain boundary can act as the anode, the cathode or may be neutral when compared to the grain crystal (Papavinasam, 2014).
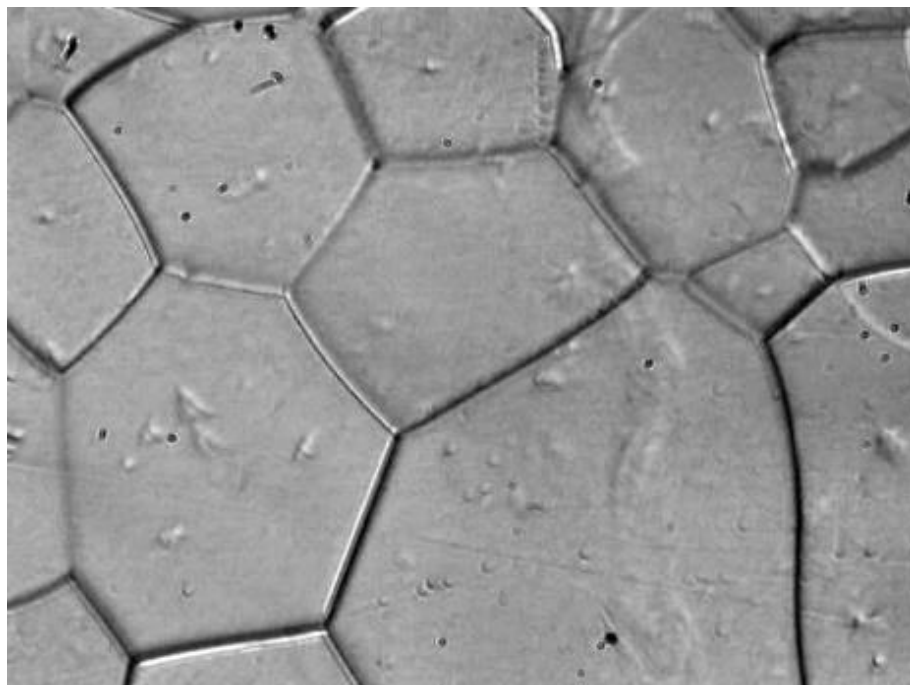
Figure 3.13 Magnified Microstructure of a Metal (Pace Technologies, 2018)

3.2.8 Selective Leaching

Selective leaching is sometimes referred to as dealloying or selective dissolution as the mechanism involves the deterioration or dissolving of one metal within an alloy whilst the other(s) remain undamaged. It is also a special variety of galvanic corrosion which occurs at the microscopic scale of the metal alloy microstructure. To give an example of the process a common situation is that of the dezincification of a brass pipe. Zinc is anodic when compared to copper so will leach out of the pipe under certain conditions and this action can be seen with the naked eye as the brass, which is yellow, converts back to red copper as seen in Figure 3.14 (Berkeley Research Company, 2018). Selective leaching in this manner can either occur in a localised area or may be uniform over the entire component. It should be noted that this mechanism does not occur in all alloys. Generally speaking, this type of corrosion develops over long periods of time as it is a very slow process that weakens the strength of the metal but it can be speeded up under the following conditions (Papavinasam, 2014):

- Higher temperatures
- Lower flow velocity
- Crevice or deposit presence
- Higher chlorine content in the corrosive solution

Figure 3.14 Selective Leaching of Brass (Berkeley Research Company, 2018)

Chapter Four: Corrosion under Insulation

The process of corrosion under insulation is of great interest in this project and is explored in this section. The fundamentals governing the process of corrosion under insulation is introduced before the mechanism is presented and discussed in greater detail. Understanding these processes and the factors that promote corrosion under insulation is of great importance to corrosion engineers if they are to develop long-lasting defences to decrease the cost of repairs and instances of failure due to this preventable issue.

4.1   Fundamentals of Corrosion under Insulation

The term corrosion under insulation refers to the deterioration by corrosion of the external surface of a structure such as a pipe or a vessel that has a layer of insulation and jacketing whose purpose was to primarily protect the structure from the atmospheric elements or to prevent system heat loss. The method by which this corrosion is often initiated is usually the ingress of water and contaminants through a defect in the protective jacketing which wets the insulation producing a contaminated corrosive liquid which effectively sits undetected in contact with the metal surface in near-perfect corrosion conditions for long periods of time. Unless there are extensive and routine inspection and maintenance regimes the likelihood of costly repairs and loss of production time due to shutdown are highly likely to occur (Papavinasam, 2014).

Corrosion under insulation is not a new phenomenon and it is not associated solely with the oil and gas industry. It is a common problem experienced worldwide by various other industries that rely on their infrastructure being protected against heat loss or environmental conditions such as the chemical processing industry. Failure to effectively mitigate the potential for leaks or failures due to corrosion may result in potentially highly damaging reputation, safety, health and environmental related issues (Winnik, 2016).

In a 2016 article in the International Association of Certified Practicing Engineers journal "Engineering Practice" (Kolmetz, 2016) the cost of corrosion to a number of industries was discussed. At the time of writing the approximate combined annual cost from corrosion-related issues to the utilities, infrastructure, production and manufacturing, transportation and government industries totalled almost one hundred and forty billion U.S. dollars in the USA alone. The oil and gas exploration and production industries are included within the production and manufacturing category of the report and Figure 4.1 (Kolmetz, 2016) illustrates the cost of corrosion to this industry relative to others within the category

according to the article. As many of the structures within the industry are insulated it can be expected that a sizable portion of the cost associated with corrosion will be related to corrosion under insulation. Another article from 2005 by Michael Lettich of the National Insulation Association (2005) states in a 2003 ExxonMobil study that with regards to the refining and chemicals industry between forty and sixty per cent of all piping maintenance costs relate to corrosion and that eighty-one per cent of leak incidents are attributed to piping systems where the diameter of the pipe is four inches or less.
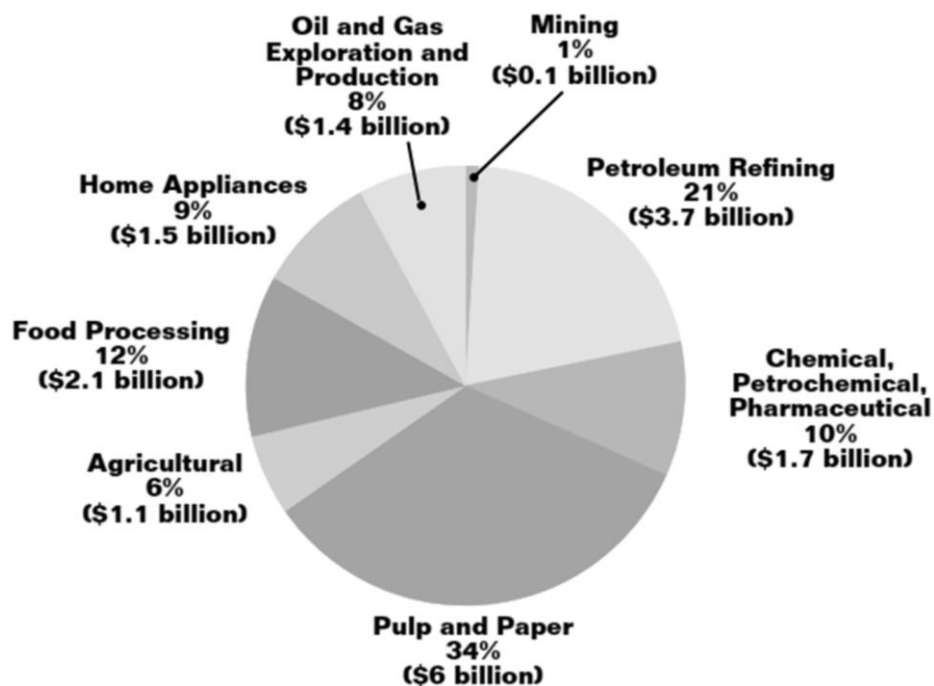
Figure 4.1 Annual Cost of Corrosion per Industry (Kolmetz, 2016)

When originally built most offshore platforms and pipelines were designed to have an operating life of approximately twenty to twenty-five years with the potential to extend this to an additional twenty years. Realistically, regardless of the care taken by engineers when designing systems corrosion under insulation will inevitably occur and will present a threat to the offshore structure, the personnel working on the structure and the surrounding environment. This is particularly the case when the structure has been in service for around ten years as this is the time when issues are expected to become prevalent (McIntyre, 2003). It is realistic to expect that through the passing of time the jacketing system in place to act as a water barrier loses the capacity to complete this task with one hundred per cent efficiency. As soon as the protective layer allows the ingress of water the insulation materials wet and this can result in corrosive contaminants reaching and remaining in contact with the metal structure for sustained periods along with additional water and oxygen resulting in severe undetected corrosion (Papavinasam, 2014).

Most piping and vessel systems have a standard operating temperature between -4°C and 175°C and this temperature zone is the ideal condition for the proliferation of corrosion mechanisms under insulation materials. That is not to say out with this temperature zone no corrosion can be expected but it is much more common and faster acting within the standard operating range. Also, as many of these structures are produced from either carbon or stainless steel the prevalence of failure information due to corrosion under insulation of these materials is more common. In the case of carbon steel, the most common corrosion mechanism taking place between the insulation and structure will be uniform or pitting corrosion and with stainless steel, it is most likely to be other localised corrosion or stress corrosion cracking due to their respective susceptibilities to each of the corrosion types (Winnik, 2016). These forms of corrosion and others were described in more detail in Chapter Three.

4.2   Mechanism of Corrosion under Insulation

The main reason why metal materials corrode that have been insulated is that once the water source has found a route to the metal structure underneath it can often go undetected until a routine maintenance check unearths the issue or the failure of the system results. The moisture and corrosive agents infiltrate the protective jacketing layer through a defective seal or damaged area and migrate through the insulation to the annular space between the structure and the insulation where corrosion processes are initiated. Often the metal structure under the insulation layer will be extremely hot and when the water contacts the hot metal it will evaporate and travel back through the insulation towards the colder external jacketing barrier. Here the evaporated water condenses and channels back towards the hot metal surface starting the cyclic nature of the evaporation/condensation cycle. If a protective coating was present on the metal surface with each passing of the cycle the coating would disintegrate until such a point that a zone will open to allow for the electrochemical corrosion processes to initiate. Every time the condensed water passes through the insulation material it degrades and leaches contaminants into the water which gradually build to concentrated levels. Another by-product of the degradation of the insulation layer will be the reduced efficiency of the insulation to prevent heat loss of the system. The rate of corrosion expected on the metal surface can be determined by the following conditions many of which are related to the type of insulation and jacketing used in the system (Winnik, 2016):

- Availability of oxygen – increase in the rate at higher concentrations
- Variety of the contaminants in the water – affects the metal's ability to create a passivating film
- The temperature of the system – hotter temperatures increase the rate
- Heat transfer properties of the metal – affects the evaporation/condensation cycle
- Wet/dry conditions on the metal surface – affects the electrochemical corrosion cell

Figure 4.2 (Winnik, 2016) shows a simple illustration of the action of hot corrosion under insulation described before.
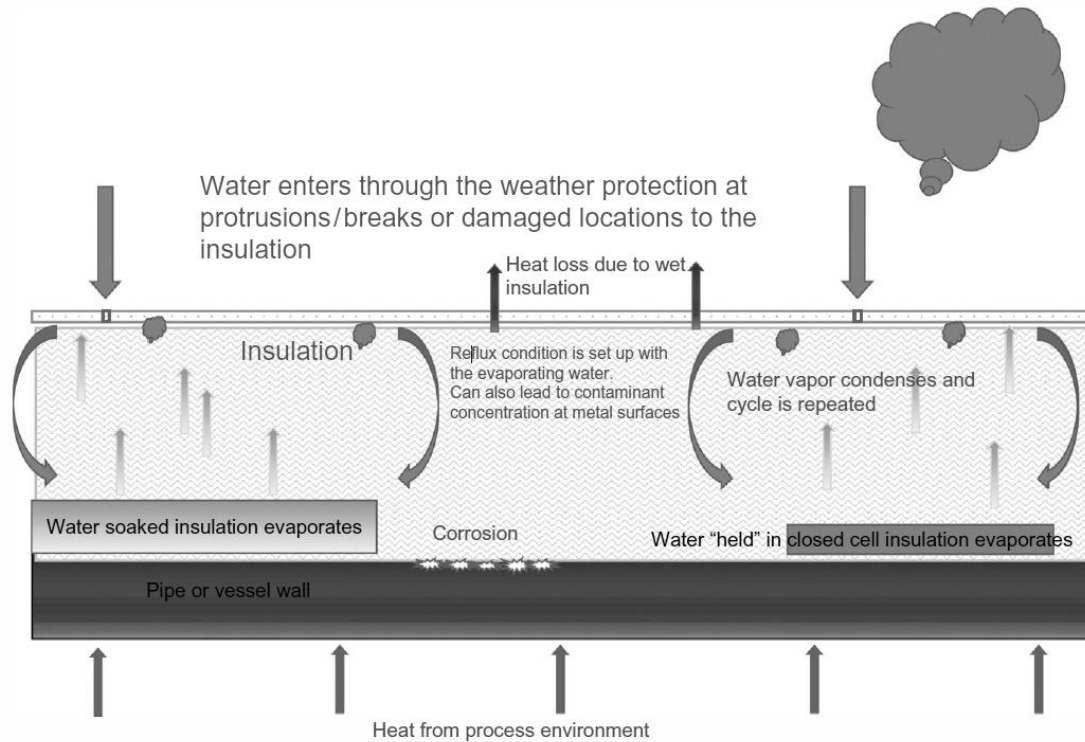
Figure 4.2 Hot Corrosion under Insulation in Action (Winnik, 2016)

In Chapter Three, the mechanism of corrosion was introduced and it was explained that essentially corrosion is a natural process where a metal is attempting to return to its natural unexcited state and this will occur if the four components of a corrosion cell are present. In a correctly functioning insulated system three of the four components are available; the anode, the cathode and the metallic pathway. The missing component is the electrolyte or water in any form, and because of this missing part, the metal would only corrode at an insignificant rate. The importance of the jacketing layer cannot be underestimated as it is the first and main line of defence preventing the ingress of water. With an effective maintenance routine, in theory, at least, it could be expected that the integrity of the protective layer would be maintained relatively easily. Though in reality, all of these materials degrade at varying rates due to a number of factors such as mechanical abuse, solar radiation, vibration and harsh environmental conditions. To expect maintenance personnel to be able to dedicate as much time as would be required to routinely inspect and maintain many hundreds of metres of the pipeline is simply impossible. Inevitably at some point during the lifespan of the protective layers water will ingress and the corrosion cycle will commence (McIntyre, 2003).

4.3   Factors that Promote Corrosion under Insulation

The main action required to prevent corrosion under insulation would simply be to keep the water source from permeating the protective jacket and actually reaching the surface of the metal. The ability for the insulation material to absorb water and hold it once it has breached the outer protective layers plays a pivotal role in determining the rate at which corrosion occurs. The insulation material can deteriorate as it gets wet and because of this it can no longer effectively absorb and store the water. This deterioration also results with the leaching of contaminants into the water. When the now corrosive water reaches the surface of the metal it will promote the action of corrosion. If it did not break down as quickly and managed to store large volumes of water it would impact the volume of water eventually reaching the metal surface (Papavinasam, 2014). At the time of writing, no insulation and jacketing system is able to fully maintain its integrity and protect the structure permanently. The next few sections will explore some of the factors that contribute to the effects of corrosion under insulation.

4.3.1   Effect of Insulation Materials

Selection of either the wrong type or insufficient amounts of insulation and jacketing materials can hasten the effects of corrosion. If the protective weatherproofing layer is not fit for purpose and allows the ingress of water and the insulation type has the capacity to store large volumes of absorbed water then the chances and rates of corrosion are likely to increase significantly. Selecting the correct material for the correct application can reduce the potential for corrosion processes to initiate. Though cost is always a consideration it is reasonable to assume the cost involved attempting to remedy a situation where water breach has occurred must surely be greater than completing the job to a satisfactory level in the first instance. In ideal circumstances, an insulation system that does not absorb large volumes of water and dries quickly in the event it does affords the most protective option against corrosion. Due to the long-expected lifetimes of use of most materials a level of deterioration is to be expected, so the selection of materials that leach fewer corrosive materials must also be considered (NACE International, 2016).

4.3.2   Effect of Equipment Design and Insulation Installation

Effective design of equipment relative to other structures and with the minimum number of necessary protrusions have a beneficial effect on the prevention of potential corrosion processes. Regular configurations are much easier to insulate and weatherproof so are less likely to have probable water entry points (Winnik, 2016).

This is an unrealistic expectation as almost all structures will require some awkward configuring of insulation but if this is performed correctly using the most suitable materials the likelihood of leaving no access points is possible. Continued inspection of these areas is necessary as they are the most likely to deteriorate over time (Winnik, 2016).

4.3.3   Effect of Mechanical Damage

In the absence of water, no corrosion would be expected to occur as there will be an incomplete electrochemical cell due to the electrolyte medium being missing. If the protective weatherproofing layer remains intact with no damage then the system will continue to be protected from the effects of corrosion. However, as soon as the protective layer becomes damaged and deteriorates in any way through any cause an easy access point has opened to allow water to enter the system. As soon as water enters the systems inevitably the processes of corrosion will commence and if left undetected may result in catastrophic failure (NACE International, 2016).

The damage can simply occur by mechanical abuse when maintenance personnel are required to walk over or scale an insulated pipe or vessel to access the location for routine inspection and work. Even a minuscule tear is enough of an opening to allow water to enter and to begin the process. Even if the effects of corrosion under insulation are identified and remedied in a timely manner unplanned shutdown, replacement material costs and loss of production time still have a detrimental effect on the company (Winnik, 2016).

4.3.4   Effect of Service Operating Temperature

The service temperature of a system is a key factor in determining the prevalence of corrosion under insulation. As mentioned earlier, the usual normal operating temperature range of piping and vessel systems is from -4°C to 175°C and this range is at the greatest risk especially when carbon steel materials are used. At very low temperatures where the water freezes there is less chance of corrosion as the water must be in a liquid form to act as an electrolyte and at especially high temperatures the water evaporates before it reaches the metal surface. It should be noted however that in cases where the weatherproof jacketing is very poorly maintained corrosion can still occur even at very high temperatures (NACE International, 2016). Figure 4.3 (NACE International, 2016) illustrates the rate of corrosion of steel in water in an open and closed system at varying temperatures. It shows that in an open system as the temperature increases up to 80°C, where the levels of dissolved oxygen begin depleting, there is an increase in corrosion rate up to the threshold at which it also starts to decrease. This differs in a closed system where there is a continuous even increase in corrosion rate as the temperature increases as no oxygen escapes and the levels don't drop.
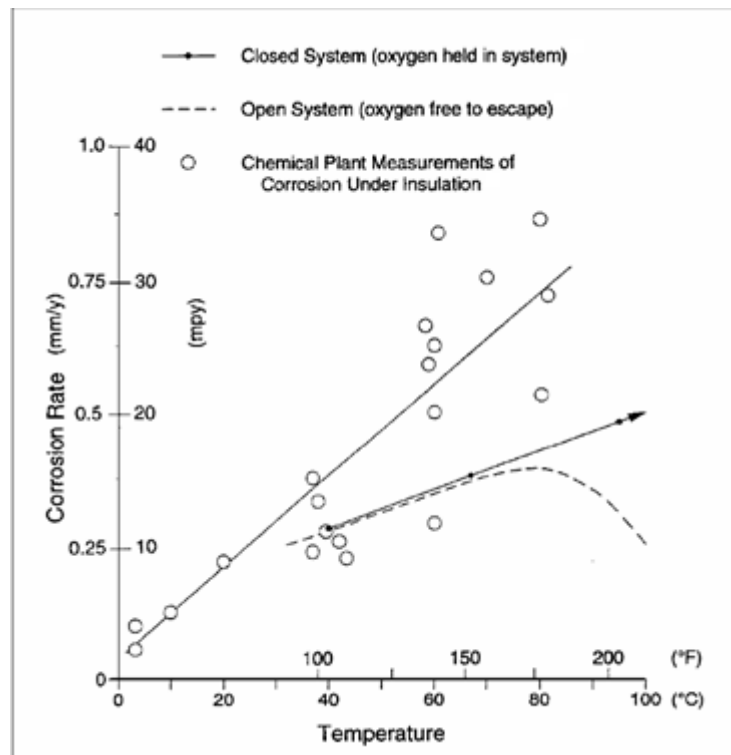
Figure 4.3 Effect of Temperature on Steel Corrosion in Water (NACE International, 2016)

4.3.5   Effect of Marine Environment

Offshore platforms and topside facilities are designed to withstand highly changeable and aggressive atmospheric and tidal conditions for sustained periods of time. Chloride ions and other ion salt components are highly soluble in water and exist in varying concentrations in seawater and the surrounding air. When the sea spray deposits the salt ions onto the metal structure's surface the electrical conductivity of the electrolyte increases and therefore the rate of corrosion also increases.

The chloride ions in the seawater are the component responsible for the salinity measurement with sodium chloride considered the most common chloride salt responsible in corrosion under insulation cases. Salinity is the measure of the saltiness of a body of water and is the weight in grams of dry salts dissolved in one kilogram of seawater. The concentrations of the various salt ions in oceans and seas are generally considered to be constant with a universally accepted average of 34.7 parts per thousand in oceans. Table 4.1 (Dhanak & Xiros, 2016) shows the varying salinity ranges in general regions and in specific locations an explains why the Atlantic Ocean has slightly saltier water than the Pacific Ocean due to the outflow of water from the Mediterranean Sea. The open oceans around the equator have higher levels of freshwater rainfall so in turn, have lower salinity readings in these respective areas (Dhanak & Xiros, 2016).

Table 4.1 Varying Ocean and Sea Salinity (Dhanak & Xiros, 2016)

Region or Location	Minimum Salinity Measurement (parts per thousand)	Maximum Salinity Measurement (parts per thousand)
River Estuaries	0	30
Polar Regions	0	30
Coastal Areas	30	34
Oceanic Average	N/A	34.7
Open Ocean	33	37
Mediterranean Sea	N/A	39
Red Sea	N/A	41

As mentioned, the proportions of the dissolved ion salts in seawater are considered constant, this means it is possible to obtain the respective concentrations of eight common ion salts if the salinity of the body of water is known. Table 4.2 breaks down the ion salt composition of a body of water with a salinity measurement of 34.4 parts per thousand (Dhanak & Xiros, 2016).

Table 4.2 Ion Salt Composition of a Body of Water with Known Salinity (Dhanak & Xiros, 2016)

Ion Salts	Weight (parts per thousand)
Chloride (Cl^-)	18.98
Sulphate (SO_4^-)	2.65
Magnesium (Mg^+)	1.272
Calcium (Ca^{2+})	0.4
Potassium (K^+)	0.38
Bicarbonate (HCO_3^-)	0.14
Bromine	0.067
Carbon	0.028

In an offshore environment, the amount of ion salt particles making contact with the metal surface will have a massive influence on the rate of corrosion experienced by the structure due to an ineffective insulation and jacketing system. The deposition and transport of the ion salts are predominantly through the actions of sea spray, rain and wind forces. Once the seawater travels through the insulation layer and makes contact with the hot metal surface the water component will evaporate and begin the evaporation/condensation cycle and the salt particulate will remain on the metal. Through the continued ingress of water and the cyclic nature of the system, the ion salt concentrations will quickly rise and will affect the rate of corrosion experienced. Due to this continued action and the continuous gradual increase in the ion salt levels, it is clear that even with an originally weak salt concentration in the water it will very rapidly accumulate to much larger levels (Winnik, 2016).

4.3.6   Effect of Pollutants in the Air

The presence and concentrations of certain pollutants in the air affects the rate of corrosion experienced under insulation materials. This is especially the case where there is any concentration of sulphur dioxide present as this can convert into sulphuric acid when combined with moisture in the atmosphere results in acid rain. When the protective jacketing layer has been breached the acid rain can enter and when combined with all the other components its presence can accelerate the rate of corrosion due to the lowering of the pH level. The burning of fossil fuels and general industrial activity are the main sources of sulphur dioxide and other contaminants such as hydrogen chlorides and nitrogen compounds like NO_x in the atmosphere. The presence of these other contaminants also increases the rate of corrosion. Hydrogen chloride in a gaseous form present in water is considered to have a more strongly acidic character than dissolved chlorine salt anions in water (Roberge, 2000).

4.3.7   Effect of pH

The chemical composition of the water can have a major effect on the rate of corrosion as highly acidic water solutions result in higher levels of uniform and pitting corrosion. The effect of the different pH values on the rate of annual corrosion of iron in the aerated water, which contains dissolved oxygen, at room temperature can be seen in Figure 4.4 (Integrated Publishing, 2018). It can be seen on the graph that between the pH values of four and ten the relative rate of corrosion remains the same and therefore can be considered independent of the actual pH value. The rate of corrosion is predominantly governed by the rate at which the dissolved oxygen reacts with atomic hydrogen, which results in the depolarization of the surface of the metal allowing the reduction reaction to continue. When the conditions become more acidic the ferrous oxide that is formed is highly soluble and is unable to deposit on the metal surface to create a protective film. The lack of protective film ensures the metal surface remains in constant contact with the acidic solution driving the rate of corrosion at a more rapid pace. At lower pH levels hydrogen is produced at high enough levels that the depolarization of oxygen does not solely govern the rate of corrosion alone but is now a combination of the two factors. At higher pH levels a protective ferric oxide film forms as the ferrous oxide reacts with the dissolved oxygen and decreases the rate of corrosion. At higher water temperatures this protective film effect is not noted (El-Sherik, 2017).
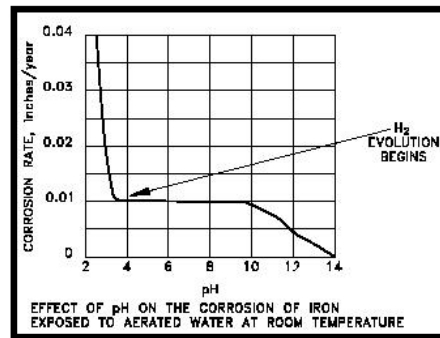
Figure 4.4 Effect of pH on the Corrosion Rate of Iron in Room Temperature Aerated Water

(Integrated Publishing, 2018)

Clean unpolluted rainwater usually has a pH around 5.6 an in areas with issues relating to acid rain the pH can drop to as low as 3.0 and the effect of acid rain can magnify the rate of corrosion due to the lowering of the pH. The deterioration of certain insulation materials and some sealants and caulks also result in the lowering of the pH as the contaminants leach of the materials and into the water and can potentially lower the pH even further. This effect is tempered slightly with the introduction of seawater spray which neutralises the acidic environment slightly as it usually has a pH of approximately 8.2. This effect is most likely nullified overall due to the introduction of salt ions which alter the rate of corrosion as discussed earlier (Dhanak & Xiros, 2016).

4.3.8 Effect of Environmental Conditions

Atmospheric conditions including temperature, relative humidity and levels of precipitation all have an effect on the rates of corrosion experienced. Depending on the specific conditions faced in a location corrosion engineers will select the best possible combination of insulation and protection materials to combat the effects of the environment (Popov, 2015).

Increased levels of humidity mean that there are higher levels of moisture in the air which can potentially transport contaminants to the corrosion site. When the humidity is at a critical level it also prevents the potential for evaporation to occur, effectively blanketing the site and ensuring corrosion processes continue without interruption. The wetting cycle is prolonged should the external atmospheric temperature not rise above the dew point as no additional evaporation will occur. As the temperature rises the levels of relative humidity also decrease and at temperatures around 15°C above the dew point the rate of corrosion essentially ceases (Popov, 2015). Figure 4.5 (Winnik, 2016) gives an indication of the varying temperature and humidity conditions throughout the year in three locations corrosion engineers must battle against to attempt to prevent corrosion under insulation.
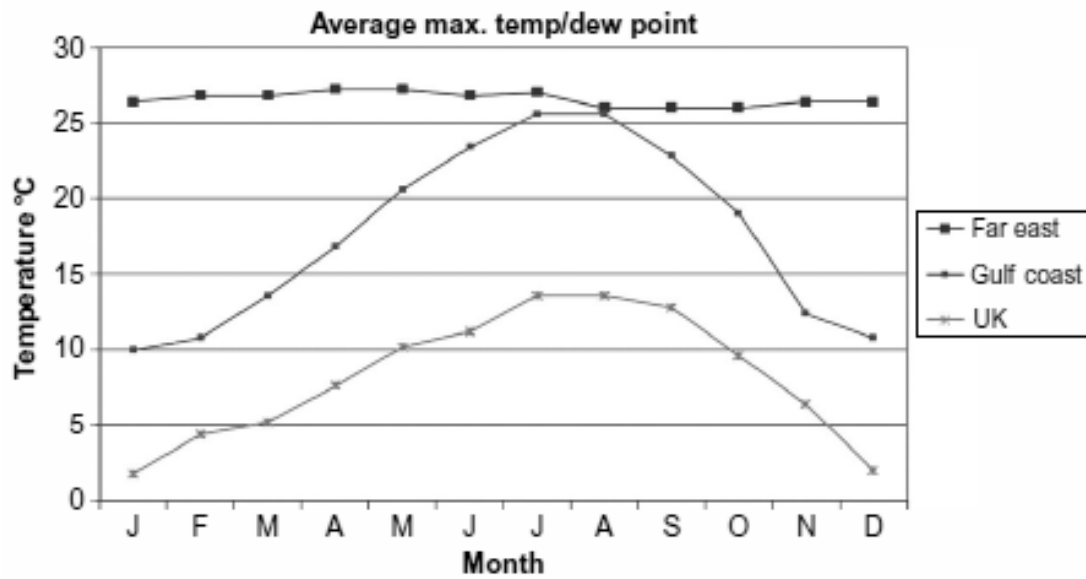
Figure 4.5 Influence of Annual Temperature and De Point Variation in Different Regions

(Winnik, 2016)

Prolonged precipitation in any form results in additional volumes of available water to begin the corrosion cycle. Periods were there are storm conditions and high winds may be responsible for damage and deterioration of the protective layers allowing for the ingress of water and contaminants, this can also be the case if there is severely cold weather which can cause expansion of trapped water due to icing (Popov, 2015).

4.4   Locations Susceptible to Corrosion under Insulation

One method by which corrosion engineers are focussing their efforts on the war against corrosion is by attempting to identify the likeliest areas where of corrosion under insulation may proliferate and remedying the issue before the ingress of water occurs and the corrosion cycle begins. An effective programme for monitoring corrosion must have a proactive element to prevent rather than solely resolve issues once they have initiated. Certain equipment and specific areas on an offshore platform, for example, may be at a higher risk of corrosion than other locations so should receive special consideration when developing a programme to combat the effects of corrosion. The following list details some areas that can be considered at a higher risk (Roberge, 2000) (Mather, 2000) (Singh, 2017):

- Steel piping systems operating between -4°C and 175°C – ideal conditions for the initiation of corrosion under insulation as discussed earlier in the section

- Equipment and piping systems that are subjected to vibrations – may damage the protective jacketing system

- Irregularly shaped systems – difficult to insulate efficiently and there may be gaps in the seals as they are difficult to close properly

- Equipment and piping systems with numerous protrusions and attachments – the insulation system will have numerous discontinuations and may not be correctly sealed and the protrusions create a temperature difference bridge between the hot pipe and cold support

- Vertical piping runs that turn and becomes horizontal runs – water may accumulate at the bottom on turns

- Exposed areas with insufficient waterproofing – likely to be unfit for purposes and deteriorate at a faster rate

- Corrosion inspection areas – incorrect sealing of plugs may contribute to water ingress

- Missing or damaged jacketing systems and sealants

- Systems insulated with wicking type insulation materials – these materials such mineral wool once wetted can retain large volumes of water

- Termination or joint sections of insulation – may be subjected to more mechanical abuse and will deteriorate at a faster rate

Chapter Five: Insulation Systems

The purpose of this chapter is to briefly introduce the concept of the insulation system and to explore in more detail the materials used in this project. Each insulation material has its own set of mechanical properties and each is most suited to a certain environment. These parameters will be discussed briefly and the mechanical properties used in the project will be provided.

5.1   Introduction to Insulation Systems

In its most general form, an insulation system is a material or group of materials whose main purpose is to prevent the transfer of heat from a hot area to a colder area. For example, a hot gas/liquid mix travelling inside a pipe which is submerged in the ocean. In the case of this project, an insulation system is simply an insulation material covered by a protective jacket affecting the buckling of steel structure component in perfectly dry conditions. In reality, there are a number of other considerations when designing a system such as protective coatings. For simplicity, these are not taken into account but are discussed below.

Some of the main considerations for the building of an effective insulation system are as follows:

- Reduction of heat loss – reduce the amount of money wasted when energy is not conserved and efforts have to be made to return the system to the optimum conditions
- Resistance to moisture – decrease in the efficiency of heat loss reduction system if wet
- Prevention of condensation – condensation onto the outer surface of a metal component with a layer of insulation on top is the perfect condition for the mechanism of corrosion under insulation
- Compressive Strength – the system may be expected to support a load or may be subject to mechanical abuse such as foot traffic
- Consideration of cost – ensure that the correct thickness and grade of insulation materials are used for the intended purpose

There are additional auxiliary considerations such as:

- Protection of Personnel – prevent contact burns if a hot or cold system
- Fireproofing – some materials have the ability to withstand fire exposure whereas others may actually spread the flames or produce smoke
- Removability and reusability – ability to perform routine maintenance easily and without waste
- Availability – generally lower cost

There has been an increase in the efficiency of insulation systems due to the development of more modern materials which have these heat conservation design concepts in mind. The oil and gas industry, however, does have a number of older structures in place with older insulation systems still in use. These older systems are of more interest in a sense as they are more susceptible to damage and then fail due to corrosion under insulation and other mechanisms.

Each of the six insulation materials and two protective jacketing materials will now be discussed in more detail.

5.2   Insulation Materials

There are a large variety of insulation materials available for engineers to select from depending on the intended application. Each material has its own set of characteristics with the associated advantages and disadvantages taken into account when being selected for use. Within the context of this project the main concern with regards to an insulation material's characteristics are the two mechanical properties of the Young's Modulus, which measures the stiffness of a solid material, and the Poisson's ratio, which is a measure of the ratio between the proportional decrease in the lateral measurement of a material when compared to the proportional increase in the same material when it has been stretched elastically. These characteristics are not commonly of great primary importance to engineers during the design of systems so it was quite challenging to find more than one reference of an accurate measurement for each property. Generally, engineers are interested in the properties relating to heat loss prevention, water absorption and the economic considerations of the material. For the purposes of diligence, these conditions were described earlier and there are a large number of sources where this type of data can be located.

As this project was primarily focussed on the impact of the insulation material on the buckling strength these additional properties were not of primary interest and were therefore not taken into account when designing the computational models. According to the Corrosion under Insulation Guidelines (2016), the six insulation materials discussed in the next sections are some of the most commonly used within the industry. A general description of each of the insulation materials will be presented along with a table highlighting some of the material's main characteristics and the mechanical properties relevant to the project.

Each of the insulation materials has its own recommended minimum and maximum layer thickness. To simplify for the purposes of comparison each of these six insulation materials were modelled where the thickness ranged from 0.01 metres up to 0.1 metres in 0.01 metre increments. It is possible in this situation that values that were generated could be either considerably higher or lower than what would be expected in real-world conditions. It was felt that keeping the parameters the same was important so as to view the effect of insulation layer thickness variation on the overall buckling strength.

5.2.1   Mineral Wool

Mineral wool is a generic name attributed to a group of fibrous materials that have been formed by the extruding of a mineral in a molten state into a fibrous form which is then mixed with organic binders. These types of insulation materials are suitable for use in ambient to high-temperature conditions (Winnik, 2016). The exact optimum temperature ranges vary depending on the base material of the fibre wool, for example, glass, rock or silicon slag. The material composition of the wool fibres can also affect the rate of water absorption and there are also certain composition combinations that will actually break down in the presence of heat and water (NACE International, 2016). Once the material has broken down it has the potential to become a vehicle for wicking moisture and corrosive solutions towards the metal underneath. For the purposes of the project the material properties data used was for that of silicon wool and is shown in Table 5.1 (American Elements, 2018) (Winnik, 2016).

Table 5.1 Material Property Data for Mineral Wool Insulation

(American Elements, 2018) (Winnik, 2016)

Young's Modulus (E) (Pa)	Poisson's Ratio (v)	Additional Notes
5.1E10	0.064	Optimum service range of 20 to 650ºC pH between 7 and 10.5

5.2.2   Fibreglass

Fibreglass is composed of layers of bound glass wool fibres; this formation technique results in a number of air and gas pockets within the material's composition. This makes fibreglass an effective insulation material as these pockets can either trap heat inside or outside of the insulation depending on the requirement. This is a very commonly utilised insulation material within domestic homes due to this quality where it can trap heat in winter and let it out in the summer. The large availability of the material ensures that it is a relatively low-cost option but it can cause irritation when being worked with. One of the largest disadvantages of the material is that it is hygroscopic and readily absorbs water so it can be problematic if there are defects with an outer protective coating. The material property data for fibreglass insulation is shown in Table 5.2 (Katz & Milewski, 1987) (Nayyar, 2000).

Table 5.2 Material Property Data for Fibreglass Insulation (Katz & Milewski, 1987) (Nayyar, 2000)

Young's Modulus (E) (Pa)	Poisson's Ratio (v)	Additional Notes
7.2E10	0.22	Optimum service range of -5 to 454ºC

5.2.3   Expanded Perlite

Expanded perlite is a product made from the perlite mineral, which is a glassy volcanic rock formed during the hydration of obsidian. Whilst the perlite is being manufactured it is expanded by heating the water contained within the grains to produce pressurised steam. Sodium silicates are then added as binders and the resulting expanded perlite product has low density and high porosity due to the numerous air cells held in place by the vitrified perlite. It is possible to decrease the perlite's affinity to absorb water through the introduction of water-resistant additives (Watson, 2005). The material property data for expanded perlite insulation is shown in Table 5.3 (Allameh-Haery, Kisi, Pineda, Suwal, & Fiedler, 2017) (Nayyar, 2000).

Table 5.3 Material Property Data for Expanded Perlite Insulation

(Allameh-Haery, Kisi, Pineda, Suwal, & Fiedler, 2017) (Nayyar, 2000)

Young's Modulus (E) (Pa)	Poisson's Ratio (v)	Additional Notes
7.563E10	0.182	Optimum service range of 121 to 538°C

5.2.4   Syntactic Polypropylene

Syntactic polypropylene manufacture results in a similar product physically to expanded perlite in the sense that it is a composite material where a metal, ceramic matrix or in this case thermoplastic polymer polypropylene is filled with hollow spheres. In the case of expanded perlite, it is non-hollow spheres. This manufacturing process results in a lower density and therefore also a higher specific strength. The introduction of the air pockets is what results in this material having a lower coefficient of thermal expansion and is, therefore, a good choice for insulation purposes (Shutov, 1986). These air pockets also increase the buoyancy which as mentioned previously is an important consideration when selecting insulation materials. The material property data for syntactic polypropylene insulation is shown in Table 5.4 (Bouchonneau et al., 2007) (Socotherm, 2018).

Please note that syntactic polypropylene is a layer within a system normally utilised in deepwater locations. Usually, there are two relatively thin layers of solid polypropylene on each side of the syntactic polypropylene. This syntactic polypropylene layer acts as the thermal insulator within the system which the polypropylene layers acting as protective coatings (Socotherm, 2018). The Young's Modulus and Poisson's ratio for solid polypropylene is similar to syntactic polypropylene (Bouchonneau et al., 2007) so for the purposes of simplifying the procedure, these two layers have effectively been incorporated into the thickness of the syntactic polypropylene layer.

Table 5.4 Material Property Data for Syntactic Polypropylene Insulation

(Bouchonneau et al., 2007) (Socotherm, 2018)

Young's Modulus (E) (Pa)	Poisson's Ratio (v)	Additional Notes
1.0812E9	0.32	Optimum service range up to 150°C at sea depths of up to 3000 metres

5.2.5   Calcium Silicate

Calcium silicate insulation is available either preformed or it can be cut from large blocks. The material is rigid with a well-opened internal structure and does not contain any asbestos. It is manufactured by mixing cement, silica and lime which is then reinforced with either organic or inorganic fibres. The mixture undergoes an autoclaving process where the mixture is subjected to high pressure and high temperature and cures to a very durable material with a high compressive strength. The material is lightweight due to its open structure and can therefore potentially absorb large volumes of water under specific operating conditions (Winnik, 2016). The NACE Standard Practice 0198-2016 (2016) advises that this material is better utilised in lower temperature environments of approximately 150°C when applied in an outdoor location. The material property data for calcium silicate insulation is shown in Table 5.5 (Vermelfoort & Ng'andu, 2005) (Winnik, 2016) (Process Insulation, 1987).

Table 5.5 Material Property Data for Calcium Silicate Insulation

(Vermelfoort & Ng'andu, 2005) (Winnik, 2016) (Process Insulation, 1987)

Young's Modulus (E) (Pa)	Poisson's Ratio (v)	Additional Notes
4E9	0.12	Optimum service range of -150 to 730°C pH between 9 and 10

5.2.6   Cellular Glass

Cellular glass is available either in rigid blocks or in preformed coverings for pipes. The product is manufactured using no binder agents under molten conditions. This forms a closed cell structure which ensures the material does not absorb moisture or water at any rate under any condition. It is susceptible to water ingress at joint locations or cracks so care should be taken to ensure the security of these areas (NACE International, 2016). Consideration should be taken that although generally, cellular glass has good overall strength it can be brittle in certain circumstances when installing. The thermal conductivity value is higher as the product is made of glass. Despite these disadvantages, cellular glass is still often used offshore as it exhibits certain additional features discussed previously (Turner & Doty, 2007). The material property data for cellular glass insulation is shown in Table 5.6 (Winnik, 2016) (NACE International, 2016).

Table 5.6 Material Property Data for Cellular Glass Insulation

(Winnik, 2016) (NACE International, 2016)

Young's Modulus (E) (Pa)	Poisson's Ratio (v)	Additional Notes
8E8	0.3	Optimum service range of -25 to 200°C pH between 7 and 10.5

5.3   Jacketing Materials

Earlier the importance of protecting the insulation material from weather exposure and mechanical abuse was discussed. Jacketing systems play the main role in this line of defence. Should the outer jacketing layer be breached the potential for wetting of the inner insulation layer is almost inevitable. This can over time result in corrosion of the metal component that is being protected and ultimately may lead to mechanical failure. Special care should be taken during the installation stages to ensure all joints are effectively sealed and that there are no gaps or tears that would allow water ingress. Generally, the choice of the jacketing system will be made on the basis of the application, the cost and the availability of materials.

There are two types of the jacketing system which are classified as metallic or non-metallic. Metallic systems can include aluminium, steel or coated metal systems. This project focused solely on an aluminium system, due to its lower cost compared to steel, to give a general overview of the protection afforded by metal systems. Non-metallic systems can include plastics such as polycarbonate (Pojtanabuntoeng, Ehsani, Kinsella, & Brameld, 2017) and also more recently there has been a move towards UV-cured, fibre-reinforced materials (Winnik, 2016). This is due to the fact they are believed to be stronger against mechanical abuse, more resistant to UV radiation and have a higher melting point (Winnik, 2016). This project focused solely on polycarbonate jacketing to give a general overview of the protection afforded by not-metallic systems. It should be noted, however, that due to the issues mentioned earlier polycarbonate tubes are not recommended for external use (Winnik, 2016) but the relevant information was not readily available for the UV-cured, fibre-reinforced materials. It was felt that the mechanical properties of polycarbonate would give a sufficient indication of the expectations of the more appropriate material.

The two jacketing materials have their own recommended minimum and maximum layer thickness. These layer thicknesses did not overlap at any point so entirely different values were used during the modelling phase. For the aluminium layer, the thickness ranged from 0.0005 metres up to 0.0015 metres in 0.00025 metre increments. This value for the aluminium layer was chosen as the Corrosion under Insulation guidelines (2016) advised the thickness for varying metal configurations would be within this range. Therefore, as with the insulation layers, it is possible in this situation that values that were generated could be either considerably higher or lower than what would be expected in the real-world conditions as is the case with the thickness of the polycarbonate layer. The polycarbonate layer thickness ranged from 0.002 metres to 0.1 metres in 0.002 metre increments. The data for this was taken from work performed by Pojtanabuntoeng et al. (2017). Again, the value used in the paper was within the overall range chosen

for the modelling phase. Although the parameters for the thickness of the jacketing differed it was believed that they represented acceptable potential real-world conditions to view the effect of jacketing layer thickness variation on the overall buckling strength.

5.3.1   Aluminium Jacketing

Aluminium jacketing can be found in a number of different thickness and sizes. Aluminium jacketing can be attached by a number of means including straps or screws. There is the option to have the sheeting with a smooth finish or it can be corrugated and there is also the option to have it with an additional moisture barrier attached or unbacked (Winnik, 2016). This barrier can also be useful if the insulation layer underneath leaches corrosive components when wetted as it will protect the aluminium sheeting from further disintegration (Watson, 2005). As mentioned previously this is one of the most commonly used metallic jacketing materials primarily due to its lower cost. The material property data for the aluminium jacketing is shown in Table 5.7 (The Engineering Toolbox, 2018a; 2018b).

Table 5.7 Material Property Data for Aluminium Jacketing (The Engineering Toolbox, 2018a; 2018b)

Young's Modulus (E) (Pa)	Poisson's Ratio (v)
6.9E10	0.334

5.3.2   Polycarbonate Jacketing

Polycarbonate is one of many thermoplastic jacketing materials used in the oil and gas industry. Other options include polyvinyl chloride and polyvinyl fluoride tubing (NACE International, 2016). Despite the disadvantages discussed previously with regards to plastic jacketing there are a few general characteristics of thermoplastics which make them a useful material. They are easily mouldable and can be thermoformed so this makes them a good material for easy use and adaptability. Polycarbonate is a very durable product with a high impact resistance, it is however very susceptible to scratching and is therefore occasionally coated to protect against this. Should the polycarbonate jacket be subjected to either too high a temperature or a damaged by mechanical abuse and damaged they can be easily and quickly replaced because they are a relatively cheap option. The material property data for the polycarbonate jacketing is shown in Table 5.8 (Goodfellow, 2018).

Table 5.8 Material Property Data for Polycarbonate Jacketing (Goodfellow, 2018)

Young's Modulus (E) (Pa)	Poisson's Ratio (v)
2.4E9	0.37

Chapter Six: The Finite Element Method

This section will serve as a brief introduction to the finite element method and also the ANSYS Mechanical APDL programme which is one of a number of software options commercially available to perform finite element analysis mathematical techniques.

The concept of the finite element method was first described in 1956 by Turner et al. and involved the solving of equations by hand. In the 1980s a number of commercial software packages became available which boosted the ability for engineers to quickly and accurately solve much more complex equations.

6.1   Fundamentals of the Finite Element Method

The finite element method is a mathematical technique in which a number of partial differential equations are created by a computer programme and are then solved. These equations would be either very difficult and time-consuming or impossible to complete by analytical methods. The differential equations together describe the displacement field of a structure, or domain, where the behaviour of the full displacement field of the element cannot be forecast with the use of closed equations and in its full state. The system must be subdivided into smaller sections, or finite elements, where the solution of each of these subdomains is either already known or can be closely approximated (Logan, 2012).

One stipulation is that the geometry of the system must be fully defined and this is achieved through the use of nodes and elements. Nodes are prescribed points in space which can either be on the lines denoting the boundaries of the structure or within the structure internal space itself. The displacement field is approximated by polynomials which are created through mathematical functions related to the known nodes. In turn, they effectively generate data to fill in the gaps. For the data to be generated accurately each node has a set of degrees of freedom relating to itself, as defined but the user, such as displacement data and temperature data. Elements are formed when these individual nodes are connected and their function is to define the mathematical interactions of each of the degrees of freedom relating to the nodes (Logan, 2012). Figure 6.1 (Stochastic Simulation and Lagrangian Dynamics, 2018) depicts some of the options available for element types in one, two and three dimensions.
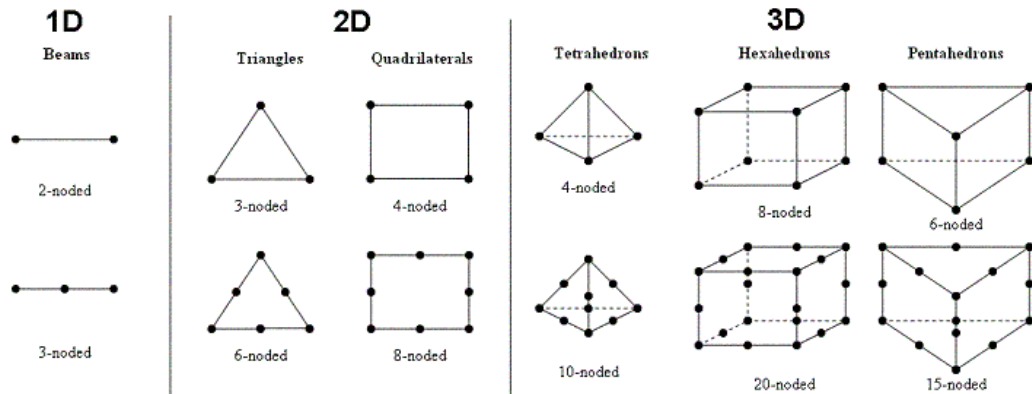
Figure 6.1 Types of Finite Elements in Three Varying Dimensions

(Stochastic Simulation and Lagrangian Dynamics, 2018)

Figure 6.2 (Madenci & Guven, 2015) is a reworking of an illustration from Madenci's book the Finite Element Method and Applications in Engineering using ANSYS. It has been altered slightly with the addition of colouring and numbering to draw attention to the details discussed in relation to the division of a complex shaped domain into a number of smaller subdomains. The nodes have been coloured red and the three finite elements have been coloured and numbered separately.
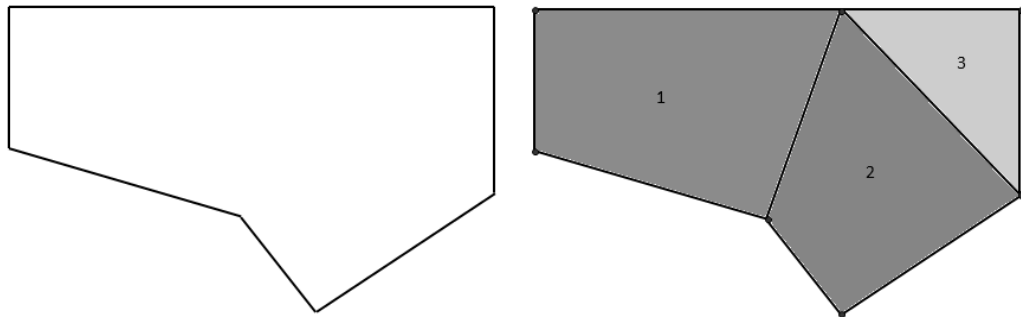
Figure 6.2 Division of a Complex Shaped Domain into Three Subdomains (Elements)

(Madenci & Guven, 2015)

In certain circumstances, the relationship between individual degrees of freedom is known and in others, these interactions can be estimated by numerical integration over each of the elements. Combining all of the equations generated for all of the individual elements generates an overall representation of the entire system being analysed. Relevant information defining the behaviour of the entire system can be generated by solving all of the generated equations (Madenci & Guven, 2015).

6.2   Advantages and Disadvantages of the Finite Element Method

As with any concept, there are a number of advantages and disadvantages associated with its use. The finite element method can and has been applied to numerous different types of structural and non-structural problems. Some of the advantages that have made it very popular include (Logan, 2012):

- The ability to model a wide variety of engineering problems – structural problems, heat transfer, fluid mechanics etc.

- The ability to model complex and irregular geometries simply

- Can handle problems with complex loading

- Can analyse models made of different materials – element equations solved individually

- Can solve problems with various numbers of boundary condition and varying types

- Option to vary element size depending on the problem and the degree of accuracy of the solution versus computation time

- The concept can easily commutate nonlinear behaviour and large deformations

Despite all of the advantages of the concept, there are also a few disadvantages (Madenci & Guven, 2015):

- Finite element results are approximate – a number of factors such as the type and number of elements as well as the adopted assumptions alter the accuracy of the result

- The experience of the user affects the accuracy – it is an engineering programme, not an engineer, therefore any inputted errors or any information not entirely suited for the application will still generate results and it is up to the user to confirm the accuracy

- The concept contains inherent errors – the system makes a number of assumptions and approximates certain values of the data as it is impossible to divide the system up into an infinite number of subdomains to generate results with perfect accuracy

6.3   Finite Element Analysis Procedure

Finite element analysis is the name given to the practical use of the finite element method and is made up of ten basic steps. There is the option to omit certain steps and utilise the computer programme's default options if a simple problem is being solved. It should also be noted that it is not necessary to follow these steps in this exact order. Certain steps must be completed in sequence as they lead onto other steps but others can be completed in any order depending on the preferences of the user (Madenci & Guven, 2015). Figure 6.3 (Madenci & Guven, 2015) has been created to illustrate the most common sequence of events and each step will be discussed briefly. The first four steps, in blue, are performed in the pre-processor section of the ANSYS Mechanical APDL programme. The next four steps, in green, are performed in the solution processor section with the final two, in orange, performed in one of the two postprocessor sections depending on the requirement (Madenci & Guven, 2015).
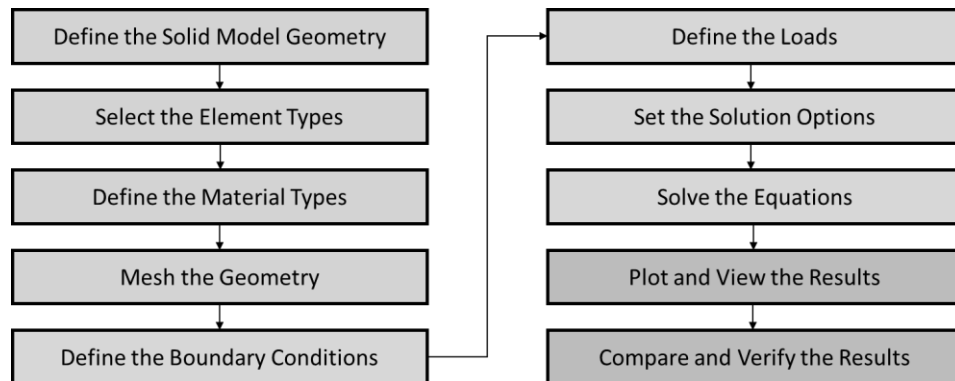
Figure 6.3 Finite Element Analysis Procedure (Madenci & Guven, 2015)

Step 1 – Create the structure of the model to be solved

Step 2 – Select the element type best suited to modelling the physical problem

Step 3 – Define the relevant mechanical and physical data for the materials used in the model

Step 4 – Discretise the model into the individual nodes and finite elements, the finer the mesh the longer the computation time but the more accurate the model

Step 5 – Provide the data for the support conditions and set several nodal values to known values

Step 6 – Set the values for the external uniform or concentrated forces or moments that will be exerted on the model

Step 7 – Set any specific solve requirements relating to the results needed

Step 8 – Computationally solve the simultaneous algebraic equations

Step 9 – Manipulate the raw data to reproduce the results in the required format

Step 10 – Comparison with data acquired by other means is necessary to confirm the accuracy of the results

6.4   Introduction to ANSYS Mechanical APDL

ANSYS Mechanical APDL is a computer programme that is often used to perform and solve finite element analysis problems. In this project, it is used to calculate the difference in buckling values of a corroded structure when that structure has a layer of insulation and protective jacketing at various thicknesses and where there is no additional layering at all.

This section includes a very brief introduction to the ANSYS Mechanical APDL software product input options and in later chapters more of the specific functions will be described and explored in the context of the requirements of the project. It should be noted that although the ANSYS Mechanical APDL can appear overwhelming at first there are a number of resources available online and in textbook format.

Combining these resources with experience using the programme will give novice users a much better understanding of the programme itself and the finite element method as a whole. This section only serves as a very basic introduction to the programme.

6.5   Inputting Information into ANSYS Mechanical APDL

There are four methods by which the user can issue commands to ANSYS to input information or numerical data which is required to solve a problem; the ANSYS command prompt, the graphical user interface or by uploading batch and input files. The choice of which is used is based upon personal preference though new users often gain a better understanding of the system initially using the graphical user interface before graduating onto the command prompt option. Using the command prompt option is much quicker once a level of understanding has been reached and allows for easier and quicker remedying of any errors. The batch file input option was not used in this project so only the other three methods are looked at individually in the next sections.

6.5.1   Graphical User Interface

The graphical user interface allows the user to interact with the programme through a collection of windows, taskbars and buttons. When ANSYS first starts up there are two windows that open, the smaller window is the output window which displays all the actions that have occurred in ANSYS in a text format. The larger window is the graphical user interface which contains all the elements described earlier and can be seen in Figure 6.4 (Madenci & Guven, 2015).
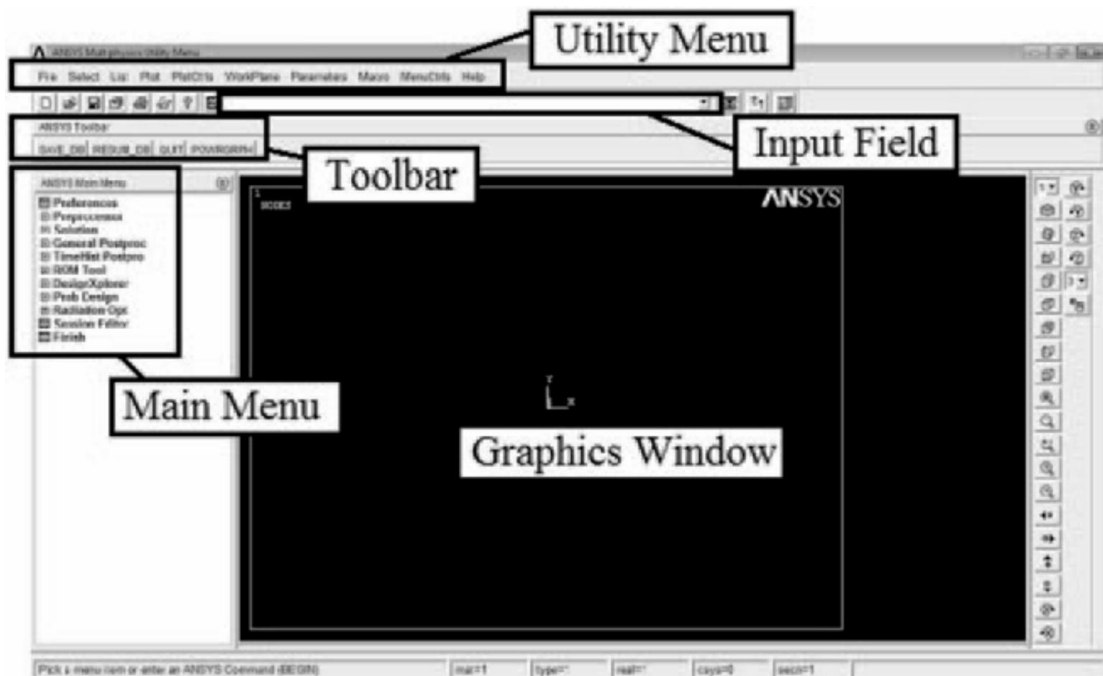
Figure 6.4 Graphical User Interface of ANSYS Mechanical APDL (Madenci & Guven, 2015)

Users select from the main menu and submenus the information they wish to input and then using the mouse and keyboard either select the tick boxes or type in the required information as needed. An example of one of the procedures that may occur will be the inputting of linear material properties for a material. Figures 6.5 and 6.6 detail in written and pictorial format the options to click and the information that needs to be typed into the graphical user interface to provide the following data: material number one (1) with Young's modulus value of 2.058E11 and a Poisson's ratio of 0.3. In the next section, the entering of the same data will be explained through the command prompt option.
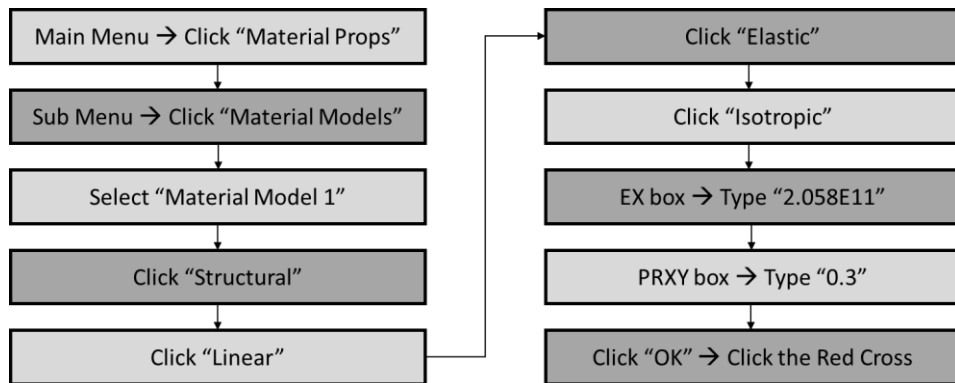
Figure 6.5 Written Form of Graphical User Interface Information Input
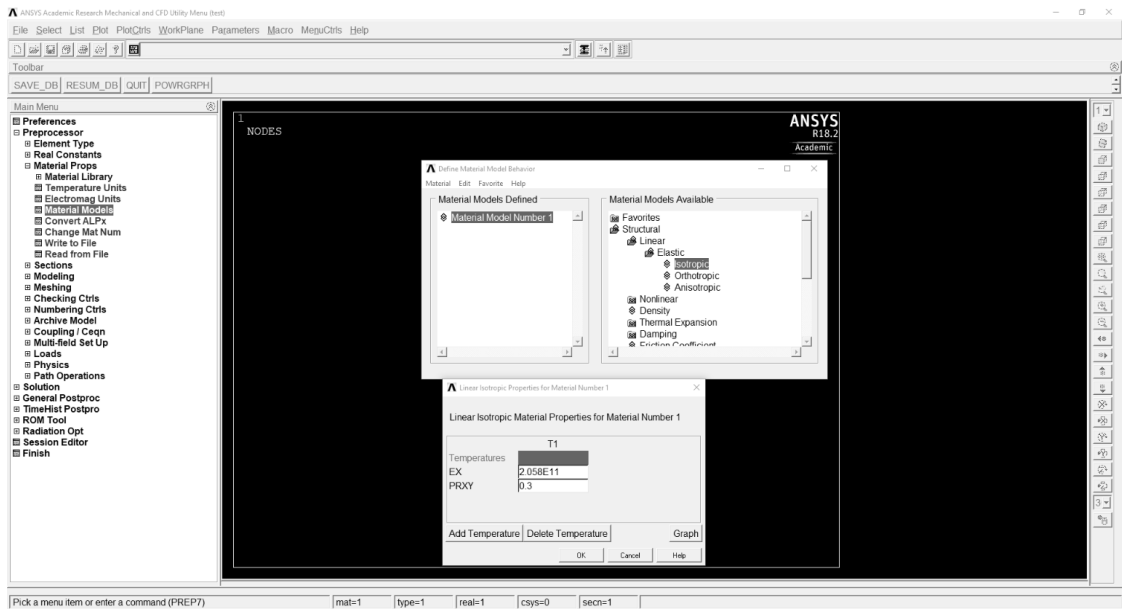
Figure 6.6 Pictorial Form of Graphical User Interface Information Input

Please note that the command prompt option can be used in conjunction with the graphical user interface if needed.

6.5.2   Command Prompt

The command language used contains alphanumeric strings that provide the necessary information or instruction to the system. Each command is made from a combination of an ANSYS verb and the related argument, this verb along with the arguments that follow inform the system of the information to input or the action that is to occur.

An example of a command and its argument is shown in Figure 6.7 taken from one of the code protocols written for the practical element of this project. In the example shown the "MP" denotes the command verb, which in this case relates to the specification of linear material properties. Following the ANSYS verb the argument details what material properties are to be attributed, to which material and the value of the property. In the first line, the material property being attributed is Young's modulus (EX), it is being attributed to material number one ("1") and the value is "2.058E11". The unit used has been given in a previous line and is pascals. The second line attributes a value of "0.3" to material number one for the Poisson's ratio (PRXY). Each of the fields needs to be separated by a comma and the enter key must be pressed after each command to enter the details into the software.

MP,EX,1,2.058E11

MP,PRXY,1,0.3

Figure 6.7 Example of an ANSYS Command Prompt

The style of the commands whether in upper or lower case is personal preference and has no effect on the outcome. This is also the case when inputting numerical data; inputting "1E2" is the same as "1.0E2" or "100". Commands that contain blank spaces are ignored so can be used to provide all the relevant input data specific to a problem but use the default settings for certain parts of the input. ANSYS will flag any warnings or errors to the user and they will be required to clear all the commands, correct these errors and input all of the commands again to generate the information.

6.5.3   Input Files

Input files are essentially a collection of commands written line by line on a plain text document and then the full document is uploaded to the programme whilst in the interactive mode used by the other two input options. It means that a document containing numerous command prompts does not have to be individually entered line by line. The use of an exclamation point (!) before any writing denotes the information is a comment and informs ANSYS to disregard anything to the right of the exclamation point on that line. These comments can be utilised by new users to describe the action of the command prompt for learning purposes or to explain actions to readers. Figure 6.8 illustrates the example of inputting the material data used previously.

```
!Define Material Data
MP,EX,1,2.058E11
MP,PRXY,1,0.3
```

Figure 6.8 Example of a Section of an Input File

Chapter Seven: Validation of Coding Style

Each user of the ANSYS mechanical APDL software programme develops their own style of coding based on their experience level and their personal preferences. The author of this thesis had no experience in the use of ANSYS Mechanical APDL before undertaking this piece of research and it was felt that a useful technique to help develop their coding style would be to compare and contrast their style of coding and the results generated with a published example.

The University of Strathclyde uses Madenci's (2015) book "The Finite Element Method and Application in Engineering using ANSYS" in some of their teaching classes. It was felt that an example from this book would be a good starting point for the author to develop their style using the example from the book as a template.

The plan for the project was to focus on non-linear deformation analyses so an appropriate example was selected from the book. Initially, the author produced a copy of the example from the book to present in this chapter and then created their version of the problem which will be broken down and described before the results from each version are compared. The example in the Madenci (2015) book is a 2-D problem, the author created a 2-D example for comparison and then created a 3-D version to further validate the code. In later chapters, 2-D and 3-D models were created to ensure validation of the results generated.

For the purposes of the thoroughness, the example in the book was also completed with a small variation. In the book, the problem had a maximum applied load of forty thousand Newtons. To complete this comparison of coding it was decided to also create the two code variations to include a maximum load of forty Newtons instead of the forty thousand Newtons. In doing this it ensured the code would also function for regular linear analysis as well as for large deformation non-linear analysis.

Further validation of the coding style was completed through the development of a modified version of the Madenci (2015) example. In this example, changes were made to the geometric and material properties of the plate and the nodes on the right-hand side of the plate were coupled. These modifications reflect the future plate configurations that will be modelled in later chapters and also serve as additional validation of the coding style.

7.1   Large Deformation Analysis of a Plate using 2-D Shell Elements

As mentioned, the problem from the book has the maximum load given as forty thousand Newtons. This version will be presented first and then followed by an additional example with a maximum load of forty Newtons.

The following excerpt is taken directly from the Madenci (2015) book along with Figure 7.1 to illustrate the problem. The code titled "Exact Coding from Madenci Book: 40 kN Load" is exactly as given in the book but rewritten in a similar style to the author for easier contrast and comparison. Please note the figure has been renumbered from the original text to the appropriate numbering in the thesis.

"Consider the cantilever plate with a transverse force at one corner shown in Figure 7.1. The plate has length, width and thickness of 40, 30 and 0.4 metres, respectively. Its elastic modulus is 120 MPa, and the Poisson's ratio is 0.3. The maximum applied load of 40 kN is reached in five equal increments. The non-linear geometry option is used in the ANSYS solution. This is achieved by writing load step files for each increment and obtaining the solution from these files (LSSOLVE command). The goal is to find the displacement components as the applied load increases, at points A and B shown in Figure 7.1".
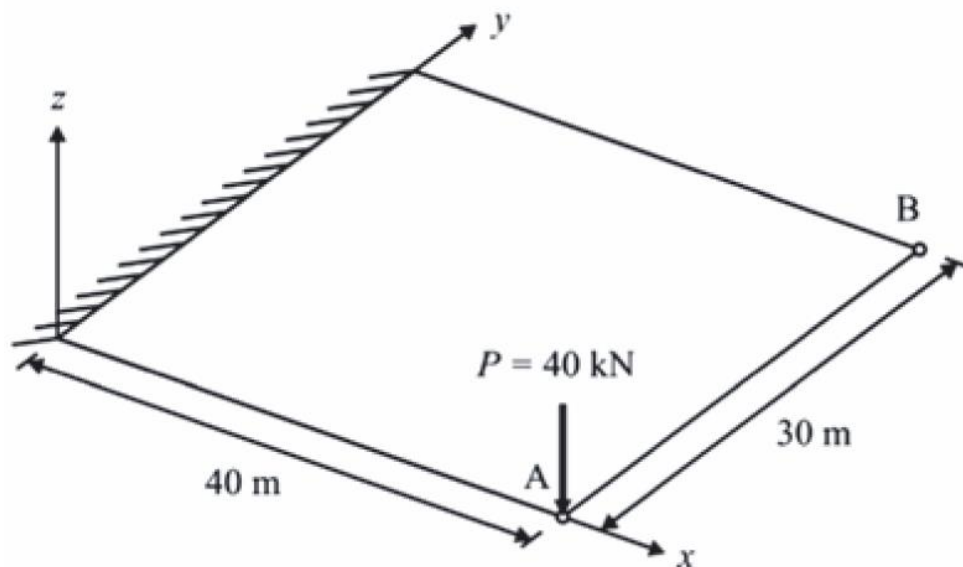
Figure 7.1 Cantilever Plate with a Transverse Force at One Corner (Madenci, 2015)

7.1.1 Madenci's 2-D Coding Style

The Madenci code was recreated using the exact information from the book and can be found in Appendix A as code A.1. It was modified slightly from the book to conform to a similar coding style to the author for easier comparison. The left-hand column contains the coding information for the ANSYS programme and the right-hand column contains the description of each action for the benefit of the author to explain their actions.

Instead of reproducing an almost exact replica of the code for the example where the maximum load is forty Newtons rather than forty thousand Newtons the author thought it would be more sensible to highlight the changes between the two codes.

In Code A.1, when the load value is forty Newtons, the portion of the code required to inform ANSYS that the non-linear geometry functions are needed to produce a result can be deleted. In the example where the maximum load is only forty Newtons, there are no large deformations so it is an unnecessary step and can be omitted.

Further explanation of any of the aspects of the Madenci (2015) code can be found in the book for any required clarification.

7.1.2   Author's 2-D Coding Style

The code designed by the author shall now be presented and each section shall be described individually before the complete code is presented in Appendix A as Code A.2. As with the Madenci code presented in section 7.1.1, where the information differs between the two maximum loads this will be highlighted to the reader. The differences between the Madenci code and author's code will also be highlighted and compared. Please note that the Madenci code utilises an alternative version of the coding language, where the main command only contains the first four letters. An example would be where the Madenci code reads "SECT,1,SHELL" as opposed to the author code reading "SECTYPE,1,SHELL". These are exactly the same and have no effect on the programme.

The code written by the author only contains one difference at the beginning of the code. The units used are determined to be SI units, this was primarily done to prevent confusion for any reader.

In the material properties section, all of the information is the same. The first line denotes that the element type used will be a SHELL181 element and that it has been given the arbitrary element number one. In this example, there is only one element, but later there will be examples with more than one element and each type would be given its own local arbitrary local element type number. The next two lines define the material properties for the material: "EX" denotes the Young's Modulus value and "PRXY" denotes the Poisson's ratio value. The type of section is defined as a shell configuration and the thickness is defined as well as the material type.

The geometry of the structure is detailed in a different way to the Madenci code but produces the same shape. The code is written in a longer form as later when the geometries become more complex the same style could be used to illustrate the data in a written format for the reader. The keypoints are created and joined together by lines. The four lines are selected to confirm the full rectangular area of the structure. The code advises ANSYS to divide each of the lines a given number of times before applying a mapped mesh to the structure.

The function of the following section is to apply the same action as the Madenci example where there is an equal application of one-fifth of the load at five separate time points. Rather than individually specifying the load step the underlined lines of code replace the need for these multiple commands. Altering the numbers within the "NSUBST" command line would result in different load step options. The first number denotes the total number of sub-steps with the following two numbers denoting the maximum and the minimum number of sub-steps respectively if the auto-stepping function is used.

ANSYS Mechanical APDL can determine the best combination of sub-steps and timings if the user requires this option. By ensuring the three numbers are the same it prevents ANSYS from altering the sub-steps frequency and ensures, in this case, that the load is added in five equal increments. In later examples, the loading patterns are much more complex and would involve too many lines of code to write the required loading increment steps as done by Madenci.

The two code variations have a couple of lines that are the same, and they are there to ensure the relevant data collected is stored and that there is a maximum number of equilibrium iterations allowed at each sub-step.

The analysis type is specified as static and as with the Madenci example; the non-linear geometry function has been turned on in this section and is seen in Code A.2. If the load was the forty Newtons then this part of the code would be omitted as before.

The relevant boundary conditions were then applied to constrain the model. When compared to the Madenci code each variable is specified individually in the author's code. As before, the reason for this is due to the future complexity of the computational models. Having the option to alter each individual boundary condition option was an important consideration.

The portion of the code regarding degrees-of-freedom for displacements are "UX", "UY" and "UZ" and for rotations, it is "ROTX", "ROTY" and "ROTZ". The last letter denotes the direction of the degree-of-freedom. The "D" command offered the greatest accuracy when selecting the nodes to constrain so is used in these early simpler examples as well as the latter more complex problems.

The first two lines of code select the nodes in the areas defined; all nodes in the x-direction between (0-0.0001) and (0+0.0001) are selected. From this collection of nodes, an additional selection is made; this is the nodes between the locations of (0-0.0001) and (30+0.0001) in the y-direction. It can be seen in Figure 7.1 the selection made from this piece of coding.

The final section of the author's code describes the load location point, in the same style as before, and the maximum value of the load applied to the model and informs ANSYS to solve the model. Due to the earlier coding informing ANSYS of the relevant sub-steps only a single value of the maximum load is now required.

In later chapters, any new sections of code not seen in the previous examples will be highlighted and their function will be described. Coding information that has been presented in this section will not be described in future sections. The full version of the author's code discussed in this section is presented in Appendix A as Code A.2 where the total load applied is forty thousand Newtons. As before the code can be simply altered to represent the maximum loading of forty Newtons.

7.1.3   2-D Post Processor Coding

To generate the results data for the two different 2-D coding styles the displacements values at two different points are needed. Referring to Figure 7.1 it can be seen that point A is the location of the node at which the load is applied. Point B is in the same coordinate with regards to the x-axis location of point A and is plus thirty with regards to the y-axis coordinate location of point A. Point A is (40,0) and point B is (40,30) with respect to the origin.

The displacement data of points A and point B in the x, y and z directions are needed to compare the two coding styles and if the results generated match then it is acceptable to validate the authors coding style in a 2-D shell model.

To use the code the node number at that position in numeral format must be entered. For example, if the identifying node number at point A was "2" and the node number at point B was "22" then the respective sections of code would be as shown in Code A.3 in Appendix A.

Displacement values were collected in the x, y and y directions at points A and B and tables of raw displacement data were compiled for each of the four model types:

- Madenci Coding with a forty Newton load applied
- Author Coding with a forty Newton load applied
- Madenci Coding with a forty thousand Newton load applied
- Author Coding with a forty thousand Newton load applied

7.1.4   Results and Discussion of the 2-D Coding Validation

The tables of raw displacement data were then converted into graphical representations for easier comparison. The raw data tables can be found in Appendix A and the graphs are presented in this chapter.

Table A.1 and Figure 7.2 present the data for the Madenci 2-D Code with a forty Newton load applied.

Table A.2 and Figure 7.2 present the data for the Author 2-D Code with a forty Newton load applied.

Table A.3 and Figure 7.3 present the data for the Madenci 2-D Code with a forty thousand Newton load applied.

Table A.4 and Figure 7.3 present the data for the Author 2-D Code with a forty thousand Newton load applied.

When the graphical results of the rewritten Madenci code, shown in Figure 7.3, were compared to the results in the book it was decided that the results were comparably similar and it was agreed that the rewritten code acceptably mimicked the original code in the book (Madenci, 2015).

After reviewing and comparing the results for the different coding styles in the two loading applications it was concluded that the results were comparably similar to validate the use of the author's coding style. Comparison of the raw data tables as well as the graphical representations provided no discernible deviation from the expected result.
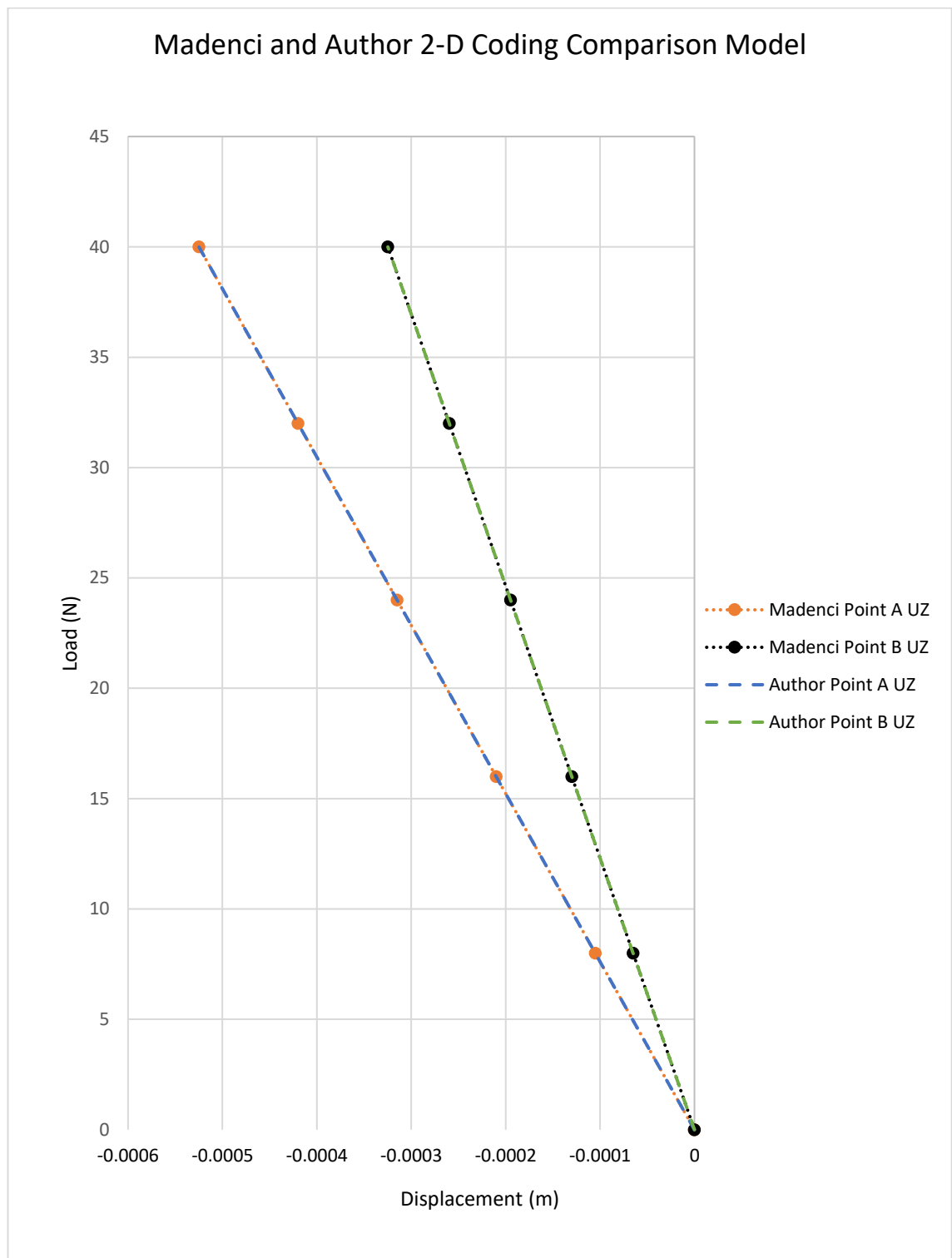
Figure 7.2 Displacement Data Graph for the Madenci and Author 2-D Codes

with Forty Newton Load Applied
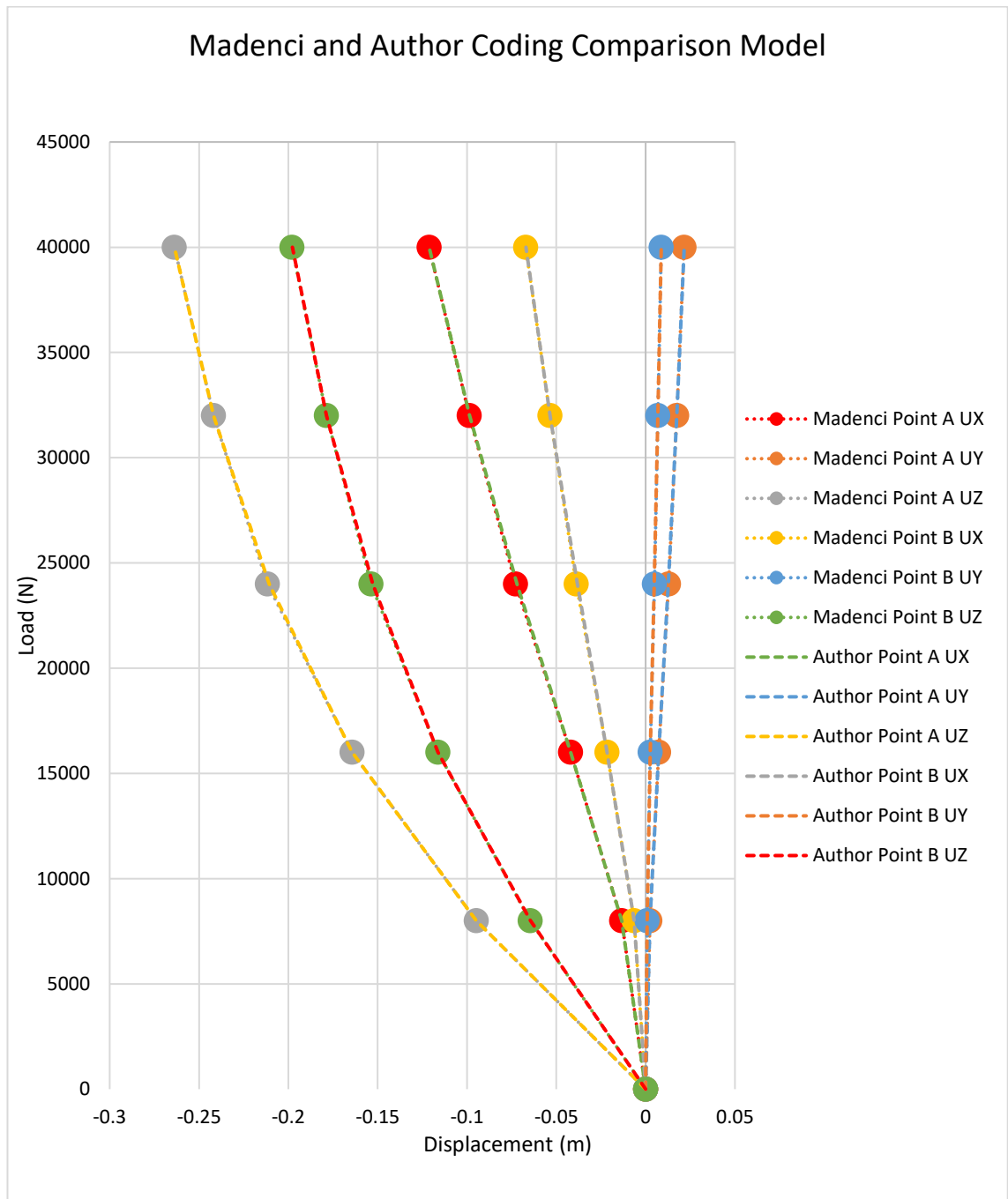
Figure 7.3 Displacement Data Graph for the Madenci and Author 2-D Codes

with Forty Thousand Newton Load Applied

7.2   Large Deformation Analysis of a Plate using 3-D Solid Elements

The next stage required the creation of a 3-D version of the code using solid elements to validate the author's style with regards to 3-D solid coding. In later chapters, the use of 3-D solid models is required to validate the results generated by 2-D shell element models when the models are subjected to different corrosion degradation configurations. 2-D models are much quicker to analyse through ANSYS so it was important to ensure that these models accurately depicted the conditions they were subjected to. A 3-D model allows for easier visualisation of the physical problem compared to a 2-D model.

There are two options for 3-D solid modelling; which are SOLID185 and SOLID186. These two element types differ in the number of nodes they each have, SOLID185 has eight nodes in 3-D space and SOLID186 has twenty nodes in 3-D space. Figure 7.4 (SHARCNET,2018a) shows a visual representation of the SOLID185 element and Figure 7.5 (SHARCNET, 2018b) shows a visual representation of the SOLID186 element.

Two versions of the 3-D code were created to see if there was any discernible difference with the results depending on the element type used. The number of line divisions was also increased to see if the fineness of the mesh had any effect on the results produced (only in the forty thousand Newton loading model). In theory, a finer mesh produces a more accurate result but the time required for analysis is much greater. A balancing act to determine the most accurate result versus the time required to produce this result is important. When the 3-D code is broken down the alterations to the coding will be highlighted at the relevant points as before. The three alterations explored in the 3-D validation model were:

- The maximum loadings - forty Newtons and forty thousand Newtons
- The element type – SOLID185 and SOLID186
- The number of line divisions – twenty in the original coarser mesh and forty in the finer mesh
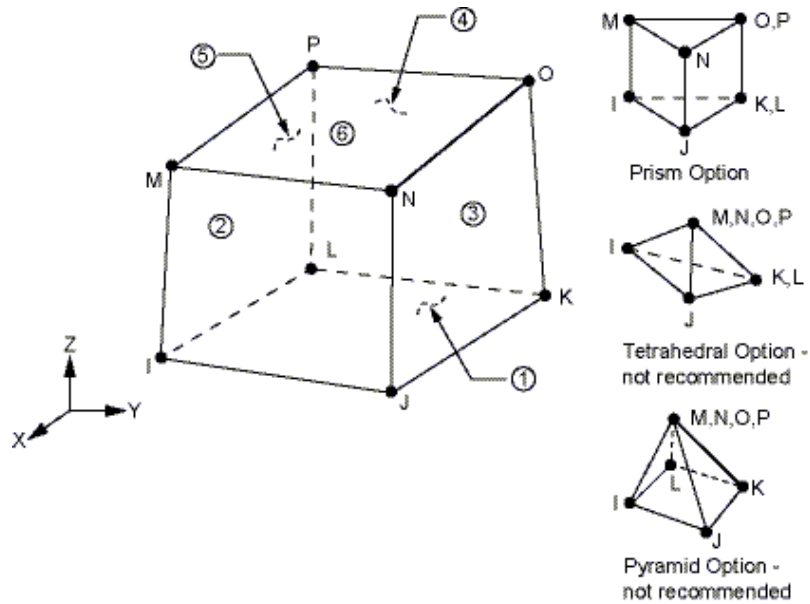
Figure 7.4 SOLID185 Element with Eight Nodes (SHARCNET,2018a)
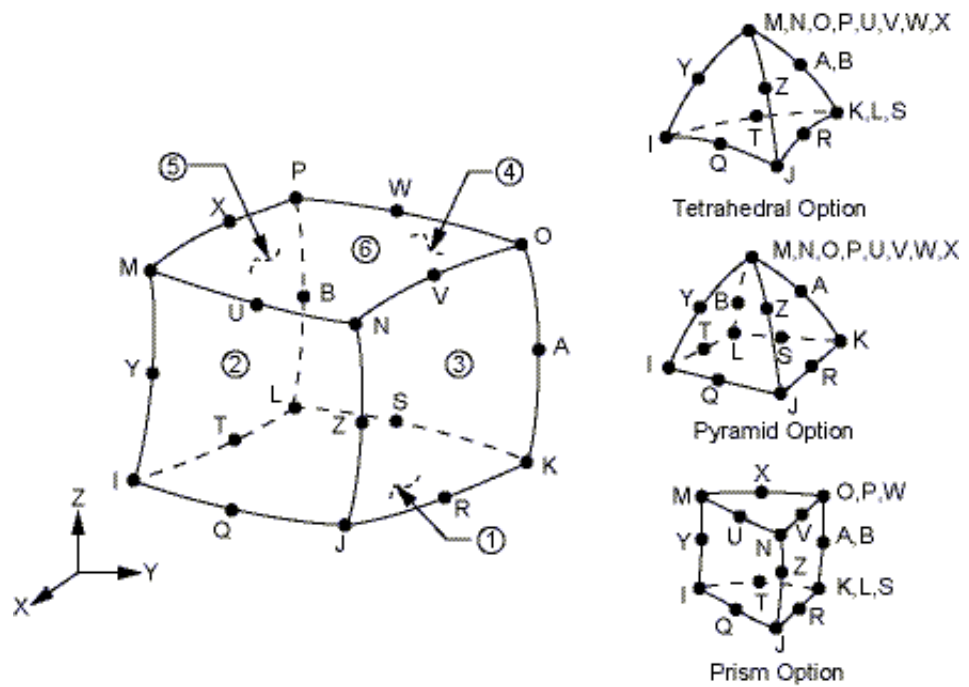
Figure 7.5 SOLID186 Element with Twenty Nodes (SHARCNET,2018b)

7.2.1   Author's 3-D Coding Style

The 3-D code designed by the author shall now be presented and each new section shall be described individually before the complete code is presented in Appendix A as Code A.4. As with the author's 2-D code presented in section 7.1.2, where the information differs between the two maximum loads, the element types and the line divisions this will be highlighted to the reader. The differences between the author's 2-D code and 3-D code will also be highlighted and compared.

As before the title would vary depending on the maximum load applied, this would be altered to read "/TITLE,Author Coding from Madenci Book: 40N Load". The part of the code relating to the element type would be changed to take into account the alternative element type and would read "ET,1,SOLID186" instead.

The material properties portion of the code is as before but the geometry sections are altered slightly with the inclusion of the z-direction coordinates and a line of code at the bottom of the section instructing the model to be extruded to create a volume and therefore exist in 3-D.

The divisions of the lines are slightly different than before as there are now many more and there are also lines defining the thickness. The lines defining the length and width are selected separately from the thickness lines and are divided appropriately. To model the finer mesh variation the number of line divisions would be changed from the number "20" to "40".

The thickness lines were divided into four sections. The reason for this was a consideration for later more complex models that include pits at three different depths. By creating the early code with this consideration, it would make later complex codes easier to create and they would also share as much commonality as possible with these early models. As before the last part of the code advises ANSYS to model with a volume mapped mesh as it is now a 3-D model.

There are no changes to the section advising ANSYS of the load and time stepping static analysis. Additional information is required to advise ANSYS of the boundary conditions relating to the z-direction. Please note that in a 3-D model there are no degrees of freedom related to the rotations so these are omitted from the code. As before, a portion of the code can be altered to read "F,ALL,FZ,-40" for the forty Newton maximum loading condition.

7.2.2 3-D Post Processor Coding

The coding style originally presented in section 7.1.3 is utilised to collect the relevant displacement values in the x, y and z directions at points A and B and tables of raw displacement data were compiled for each of the six model types:

- 3-D Coding with a forty Newton load applied to a SOLID185 element type model
- 3-D Coding with a forty Newton load applied to a SOLID186 element type model
- 3-D Coding with a forty thousand Newton load applied to a SOLID185 element type model
- 3-D Coding with a forty thousand Newton load applied to a SOLID186 element type model
- 3-D Coding with a forty thousand Newton load applied to a SOLID185 element type model with a finer mapped meshing
- 3-D Coding with a forty thousand Newton load applied to a SOLID186 element type model with a finer mapped meshing

7.2.3 Results and Discussion of the 3-D Coding Validation

The tables of raw displacement data were then converted into graphical representations for easier comparison. As before, the raw data tables can be found in Appendix A and the graphs are presented in this chapter.

Table A.5 and Figure 7.6 present the data for the 3-D code with a forty Newton load applied to a SOLID185 element type model.

Table A.6 and Figure 7.6 present the data for the 3-D code with a forty Newton load applied to a SOLID186 element type model.

Table A.7 and Figure 7.7 present the data for the 3-D code with a forty thousand Newton load applied to a SOLID185 element type model.

Table A.8 and Figure 7.7 present the data for the 3-D code with a forty thousand Newton load applied to a SOLID186 element type model.

Table A.9 and Figure 7.8 present the data for the 3-D code with a forty thousand Newton load applied to a SOLID185 element type model with a finer mapped meshing.

Table A.10 and Figure 7.8 present the data for the 3-D code with a forty thousand Newton load applied to a SOLID186 element type model with a finer mapped meshing.

It can be seen in graphical data depicting the three SOLID185 models, Figures 7.6, 7.7 and 7.8; the results generated do not match closely enough with the 2-D models generated in section 7.1.3. The reason for this is believed to be the lower number of nodes on a SOLID185 element. Essentially due to the lower number of nodes, many more approximations are made by the ANSYS programme and because of this the accuracy of the result is lost. For this reason, no 3-D models from this point will use the SOLID185 element type. It should be noted that the lost accuracy may only be in an issue when the "bending" capability of the model is important. It is possible that if the problem involved the structure being "pulled" then a model with SOLID185 elements may be acceptable.

The 3-D models created using the SOLID186 element, Figures 7.6, 7.7 and 7.8, do exhibit similar results to the 2-D models generated in section 7.1.3. It was concluded that the results were comparably similar to validate the use of the author's 3-D coding style. Figure 7.9 confirms the validation of the 3-D where the load applied is forty Newtons. The forty thousand Newton load 3-D validation is depicted in Figure 7.10.

The finer mesh in the SOLID186 did not increase the level of accuracy to a considerably noticeable degree to necessarily warrant the additional analysis time. It was decided that the best course of action would be to perform a mesh convergence study for both the 2-D SHELL181 and 3-D SOLID186 models with more complex geometries to ascertain the best combination of mapped mesh coarseness versus computation time and this data is presented in Chapter Eight.
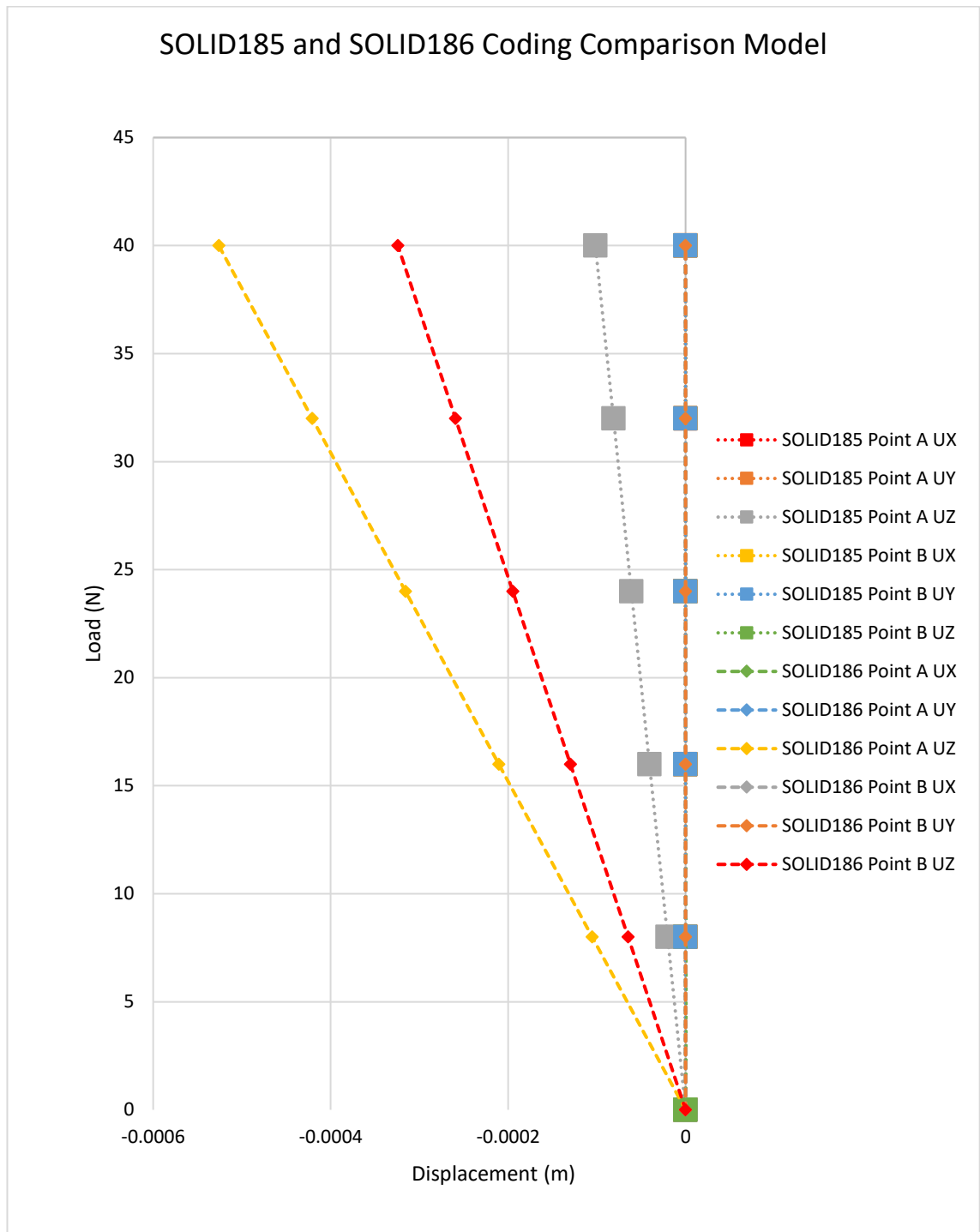
Figure 7.6 Displacement Data Graph for 3-D Code with a Forty Newton Load Applied to a SOLID185 and SOLID186 Element Type Model
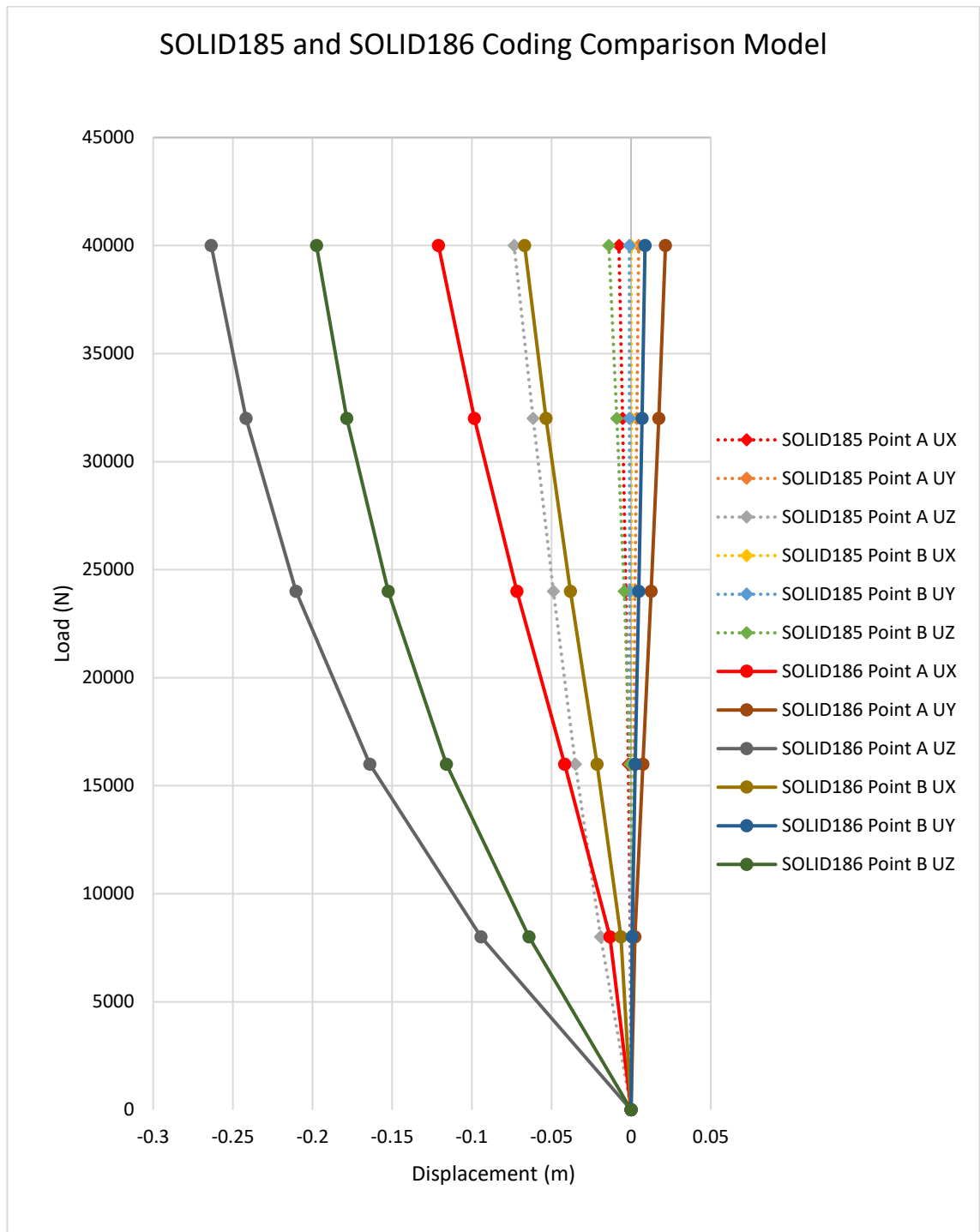
Figure 7.7 Displacement Data Graph for 3-D Code with a Forty Thousand Newton Load Applied to a SOLID185 and SOLID186 Element Type Model
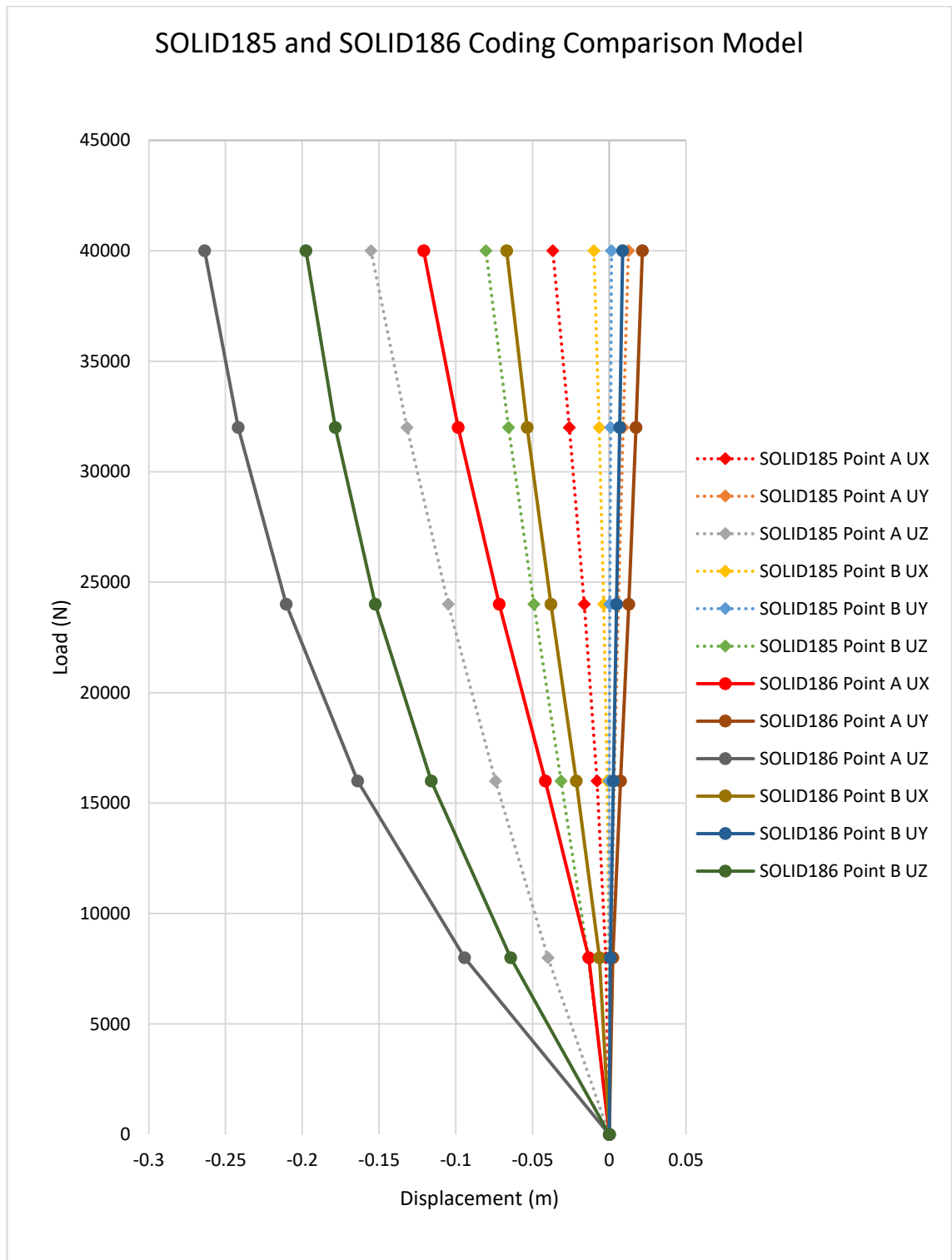
Figure 7.8 Displacement Data Graph for 3-D Code with a Forty Thousand Newton Load Applied to a SOLID185 and SOLID186 Element Type Model with a Finer Mapped Mesh
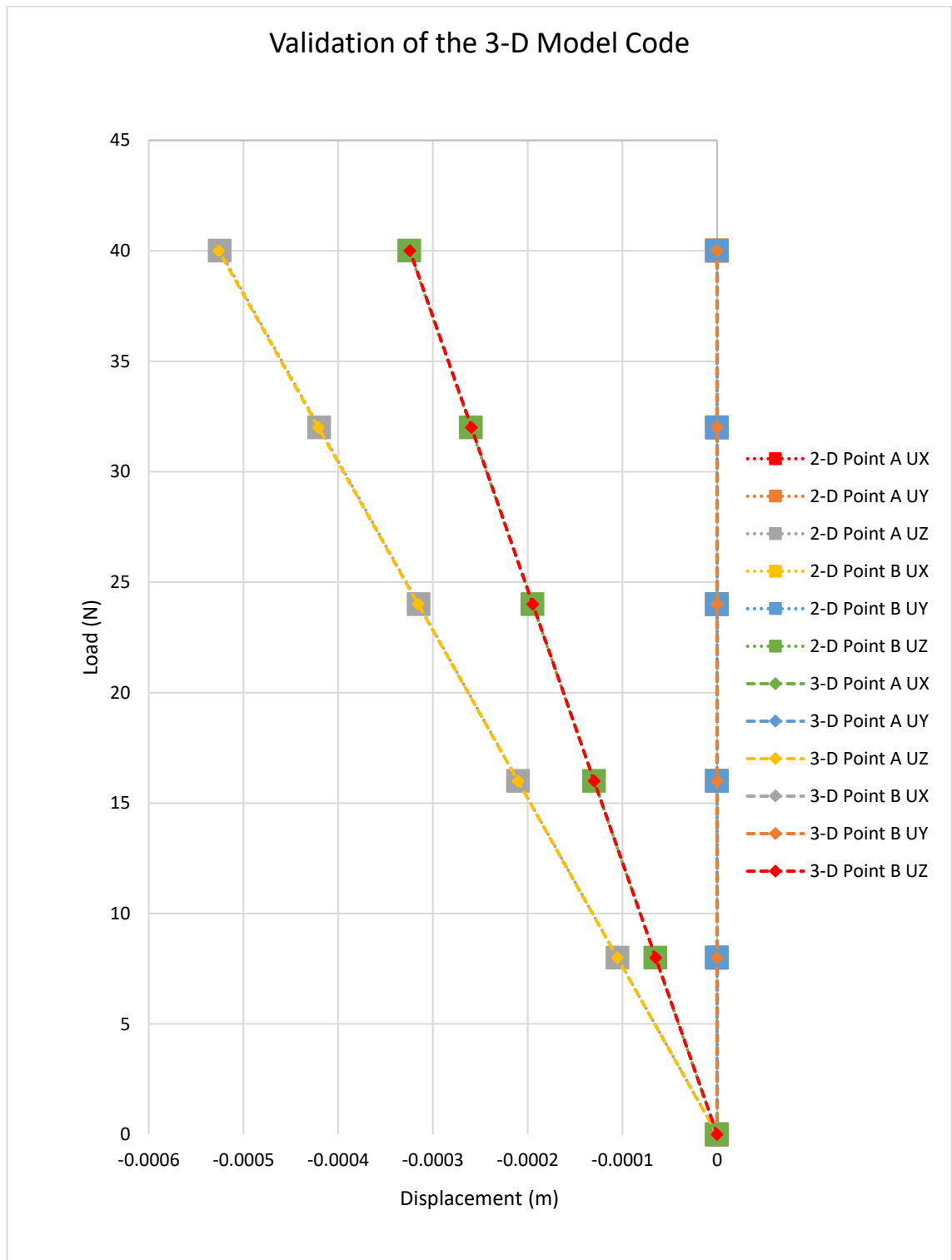
Figure 7.9 Displacement Data Graph to Confirm the Validation of the 3-D Code

with Forty Newton Load Applied
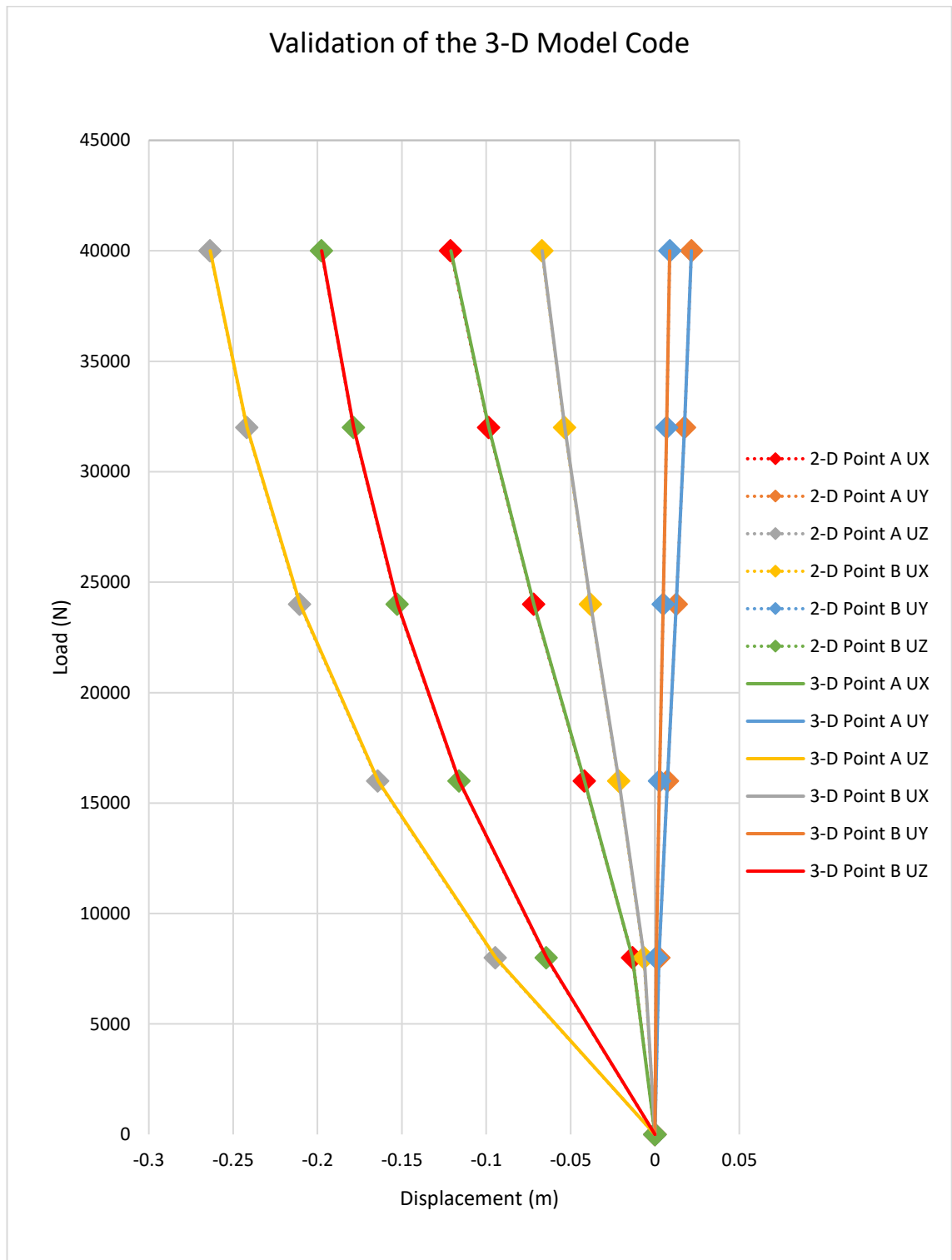
Figure 7.10 Displacement Data Graph to Confirm the Validation of the 3-D Code

with Forty Thousand Newton Load Applied

7.3   Further Model Validation

In sections 7.1 and 7.2, the author's 2-D and 3-D buckling models have been compared to each other as well as to a published example to confirm the validity and accuracy of the author's style. In this section, the plate geometries and the material properties discussed in Chapter One for the steel plate have replaced the Madenci (2015) published model data. The data from Chapter One that is relevant to these validation procedures have been presented in Table 7.1 (Paik et al., 2003; 2004).

Table 7.1 Steel Plate Geometric and Material Properties (Paik et al., 2003; 2004)

Geometric or Material Property	Value
Plate Width (m)	0.8
Plate Length (m)	0.8
Plate Thickness (m)	0.01
Young's Modulus (E) (GPa)	205.8
Poisson's Ratio (v)	0.3

The model is still fully constrained as before but this time the nodes between points A and B have been coupled to ensure the model behaves as is expected in future computational work where the load is applied in the x-direction rather than the z-direction. In the following validation procedures, it is expected that the displacement measurements at point B should exactly mimic that of point A. Figure 7.11 is a modified version of Figure 7.1 taken from the Madenci (2015) publication to illustrate the model used in this final validation section.
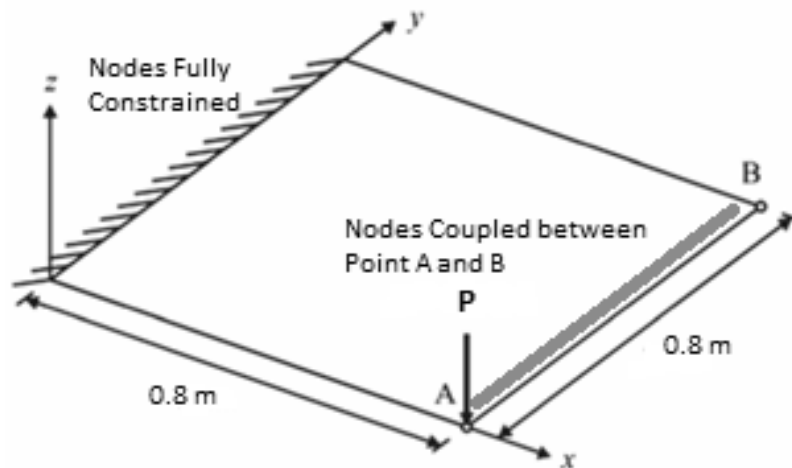
Figure 7.11 Further Validation Model Illustration (Madenci, 2015)

The author decided to create and compute two further models to fully validate the 2-D and 3-D models to be used in the main results chapters of this project. The Madenci (2015) example and subsequent author code variations discussed in sections 7.1 and 7.2 modelled the non-linear buckling of the plate. This analysis type will be repeated two more times with the new model shown in Figure 7.11, once for the SHELL181 element and once for the SOLID186 element type and will be presented in this section of the chapter.

The two models presented in this section will have an arbitrary maximum load of forty thousand Newtons applied on both occasions as before. It is felt that the codes for these two models do not need much further explanation as they are very similar to the models explored previously. The two differences that can be highlighted are the new coding option for creating the geometry where a block option is used instead of the keypoint, line and area functions as before and also the code to include the coupling of the nodes. Please note that the load stepping has also been altered from the previous examples.

In the 2-D example, the "BLC4" command is used, along with a different style of line division where it is the element size that is specified rather than the line size. In the 3-D example, the "Block" command is used and includes the z coordinate to produce the model in 3-D without the need for a second command line. Here due to the complexity, the line size command is used again as before afterwards. In both models the line command to couple the nodes are very similar, the only difference is the additional line relating to the z-axis node selection in the 3-D model.

The full code variations are shown in Appendix A with Code A.5 denoting the 2-D code and 3-D code shown in Code A.6. and the post-processor code introduced in section 7.1.3 is used to generate the displacement data values in the x, y and z directions at points A and B. Tables of raw displacement data were compiled for the two model types:

- 2-D Coding with an arbitrary forty thousand Newton load applied
- 3-D Coding with an arbitrary forty thousand Newton load applied

The tables of raw displacement data were then converted into graphical representations for easier comparison. The raw data tables can be found in Appendix A and the graphs are presented in this chapter.

- Table A.11 and Figure 7.12 present the data for the 2-D code with an arbitrary forty thousand Newton load applied
- Table A.12 and Figure 7.12 present the data for the 3-D code with an arbitrary forty thousand Newton load applied

The graphical representations of the 2-D and 3-D models created with the altered validation conditions shown in Figure 7.12 exhibit similar results to each other. It was concluded that the results were comparably similar to validate the use of the author's coding style and that the next stage can begin, whereby a mesh convergence study is completed.
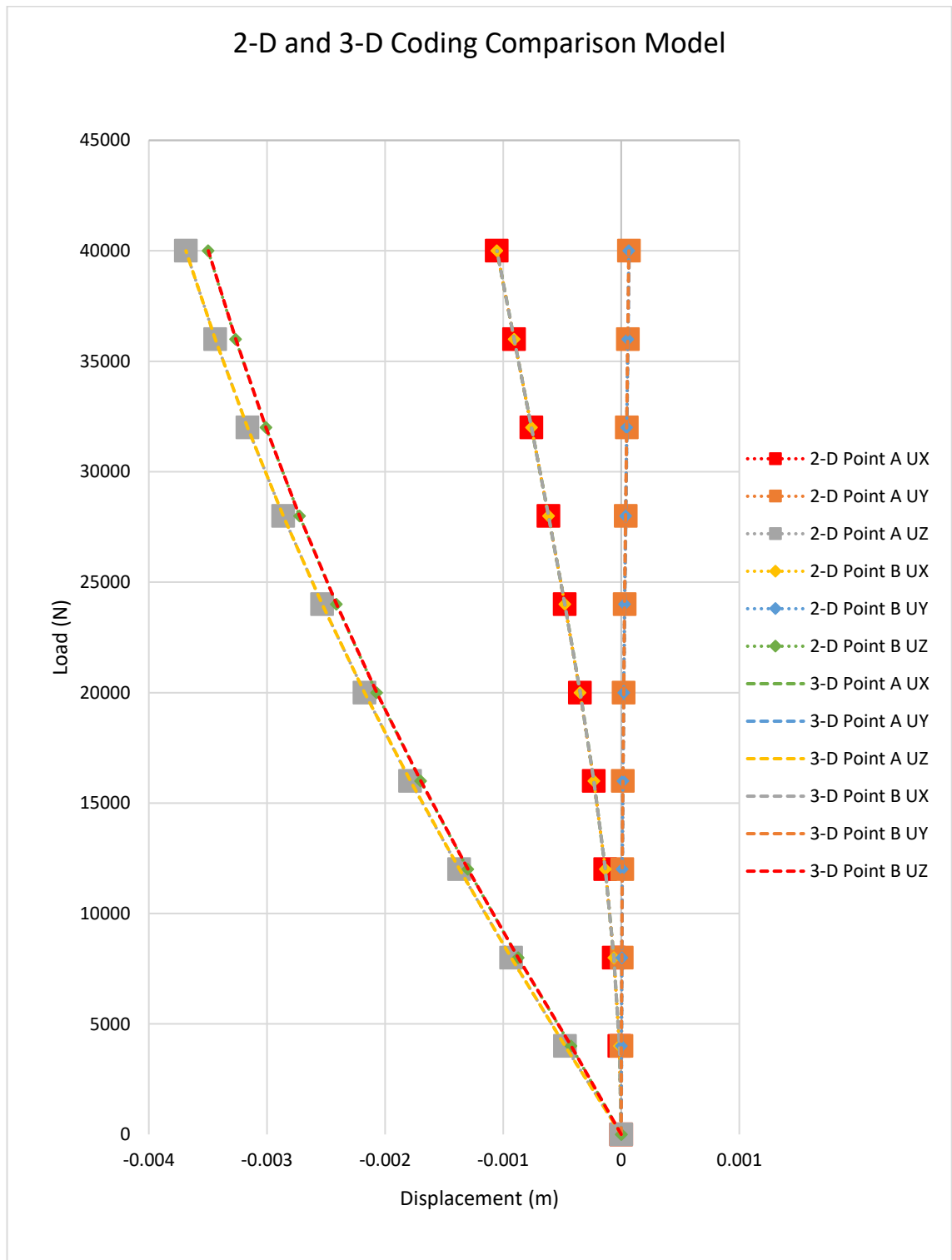
Figure 7.12 Displacement Data Graph for 2-D and 3-D Code with an Arbitrary Forty Thousand Newton Load Applied

Chapter Eight: Mesh Convergence Study

The final piece of validation work involved the completion of a mesh convergence study for a fully intact plate and a plate with a hole in 2-D and 3-D. It is well known that as a mesh is made finer the solution produced is more accurate but to generate this more accurate result a longer computation time is required. Therefore, by performing a mesh convergence study it was possible to deduce the best balance between accurate results and computation time. To complete the convergence study for this project the finest mesh was analysed first and was made incrementally coarser until the fourth and final iteration had approximately one quarter the number of the elements of the finest mesh.

The SHELL181 element type was used for the 2-D analysis and from the validation work completed in Chapter Seven it was decided that the SOLID186 element type would be used for the 3-D model. Figures 8.1 and 8.2 show the two plate configurations used in the convergence study and the position where the load is applied. The geometric and material properties of the plates are as in Chapter One and are presented in Table 8.1 (Paik et al., 2003; 2004).
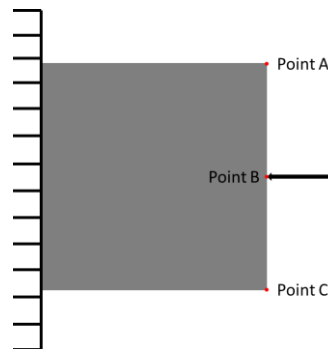
Figure 8.1 Intact Plate Configuration
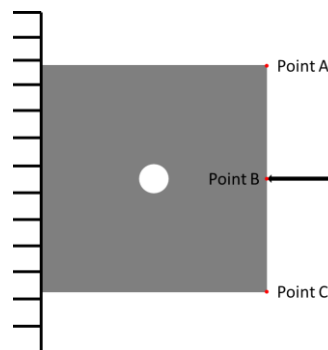
Figure 8.2 Plate with a Hole Configuration

Table 8.1 Steel Plate Geometric and Material Properties (Paik et al., 2003; 2004)

Geometric or Material Property	Value
Plate Width (m)	0.8
Plate Length (m)	0.8
Plate Thickness (m)	0.01
Shape of Hole	Circular
Diameter of Hole (m)	0.1
Young's Modulus (E) (GPa)	205.8
Poisson's Ratio (v)	0.3

For each plate configuration and mesh coarseness, the Eigenvalue buckling was deduced and in the appropriate section, the results are shared. Using the Eigenvalue result the next stage was to simulate a non-linear analysis run where the Eigenvalue buckling load was incrementally added in 10 individual step points.

As before, in Chapter Seven, the nodes on the right-hand side had been coupled to ensure the displacement was the equal at the three measured points A, B and C. The nodes on the left-hand side were again fully constrained and the load was applied to the centre node on the right-hand side of the plate denoted as point B in Figures 8.1 and 8.2.

In sections 8.1 and 8.2, the shell convergence study will be documented and the solid convergence study will be documented in sections 8.3 and 8.4. The first part of each section will focus on the fully intact plate and the results before considering the plate with a hole configuration. As in the previous chapter, any new lines of coding will be introduced with the full version of the respective code presented in Appendix B.

8.1 Intact Shell Convergence Study

The purpose of an Eigenvalue buckling analysis is to produce an estimated Eigenvalue buckling result which can then be used in the non-linear analysis code to produce a node displacement result. In the previous chapter, the maximum load value was an arbitrary value, by completing an Eigenvalue buckling analysis a much more accurately predicted result is produced that relates exactly to the model under inspection. The result produced by the Eigenvalue analysis is applied to a non-linear analysis at 110% of the load predicted in the appropriate load direction with a 0.5% load applied in a transverse direction to initiate the buckling mechanism.

The first stage is to create the conditions to predict the Eigenvalue buckling value. Taking the example of the finest mesh configuration; the first part of the code is effectively exactly as seen before and the 2-D model is created with the appropriate geometric and material properties. The boundary conditions and node coupling matched the styles used before.

The loading portion of the code and the analysis options of the code differ from what has been introduced previously. The load applied is one Newton and through the analysis options selected by the user ANSYS essentially continually increases the load by one newton until the buckling point is reached and the model fails.

To generate the Eigenvalue buckling result, a deflected shape model is generated that the user can use to validate the buckling mechanism along with a text box detailing the Eigenvalue buckling value. The code written in full for the 2-D intact plate using a SHELL181 element type with a very fine mesh is presented in Appendix B as Code B.1.

8.1.1   Mesh Fineness Variation for the 2-D Intact Plate

As mentioned, the fineness of the mesh is the only property altered in the convergence study. For the 2-D fully intact SHELL181 model this requires an alteration to only one line of the code relating to the mesh element size to produce the four various options

As well as changing the title of the code the value inserted into the code is altered to one of the four following options depending on the mesh fineness required:

- Very fine mesh   = 0.02
- Fine mesh   = 0.027
- Coarse mesh   = 0.04
- Very coarse mesh   = 0.08

The results of the Eigenvalue buckling at each mesh fineness is presented in Table 8.2. The results are very comparable so when the total load of 110% and a transverse load of 0.5% were calculated for the non-linear analysis the results for each meshing fineness was the same at -61550 N and 308 N, respectively.

Table 8.2 Eigenvalue Buckling Results for the 2-D Intact Plate

Mesh Type	Eigenvalue Buckling Result (N)
Very Fine Mesh	55937
Fine Mesh	55952
Coarse Mesh	55990
Very Coarse Mesh	56184

8.1.2 Non-Linear Analysis for the 2-D Intact Plate

As discussed in section 7.1 the only alteration to the non-linear analysis coding styles presented in the previous chapter is the style of the maximum loading and the addition of the transverse load to initiate buckling.

The full code for the non-linear analysis of the fully intact 2-D plate with a very fine mesh is shown as Code B.2 in Appendix B; please note as before the element size must be altered as per section 8.1.1 depending on the fineness of the mesh required.

The post-processor used in the convergence studies is very similar to the one used in the previous chapter. The only difference is the addition of a section of coding to generate the displacement values for the additional point C that was not present before. Please note point B has moved from the top edge of the right-hand side of the plate to the centre loading point with point C in the old location. The post-processor requires the insertion of the specific node numbers to replace the respective parts of the code as was the case in the previous chapter. The full post processor code is presented as Code B.3 in Appendix B.

8.1.3 Results for the 2-D Intact Plate

The four levels of mesh fineness will be presented in this section where each has a table denoting the displacement values at each time step at each point. A load-deflection graph for each level of mesh fineness is also presented which shows the accuracy of the predicted buckling value to the failure point as expected. If the Eigenvalue buckling value predicted is accurate the graph will show a sudden dip at this load point as the model has buckled and failed. The table discussed will be presented in Appendix B and the figures will be presented in the relevant chapter sub-section.

Three graphs will also be presented to better illustrate the data presented in the table. These graphs show the displacement at each point, A, B and C, at each time step relative to the load applied at each time step. If the coupling applied to the model has been successful each of the three graphs will be identical.

8.1.3.1 Very Fine Mesh Results

Table B.1 presents the data collected from the non-linear analysis and can be found in Appendix B. The load-deflection graph generated from this data is presented in Figure 8.3. The individual graphs for the node displacement values generated at points A, B and C are shown in Figures 8.4, 8.5 and 8.6, respectively.
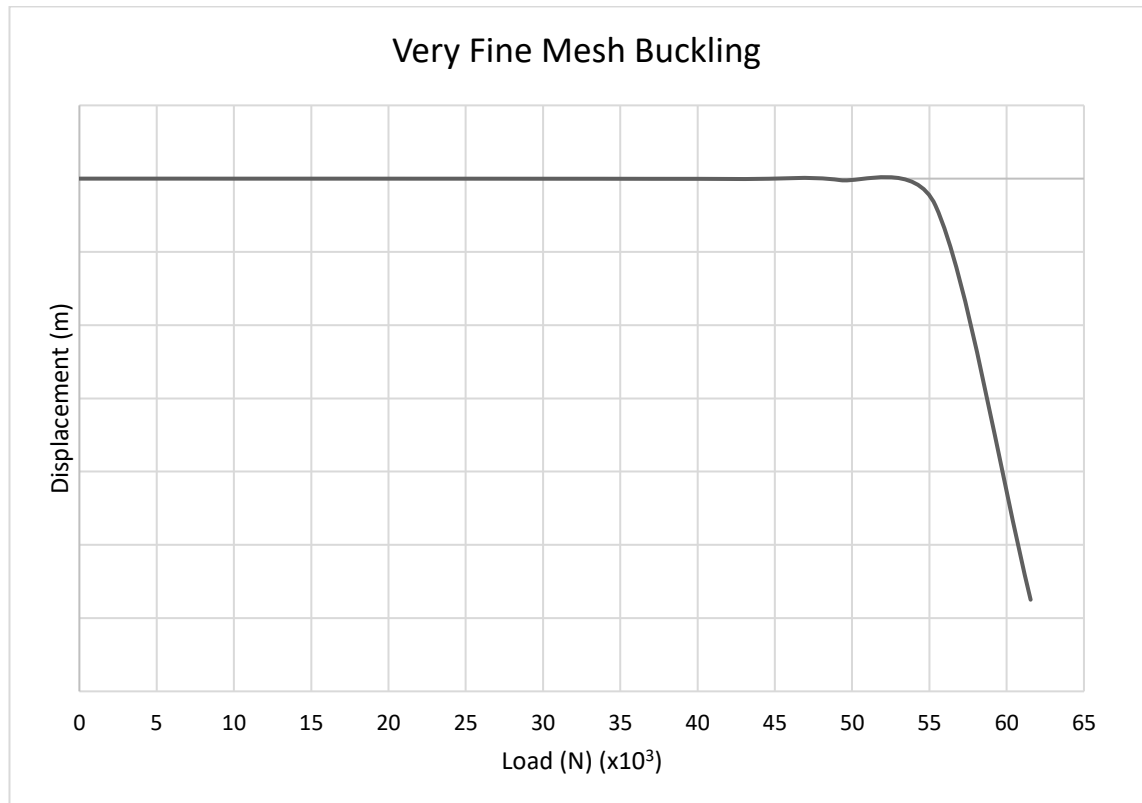
Figure 8.3 Load – Deflection Graph for an Intact Shell Plate with a Very Fine Mesh
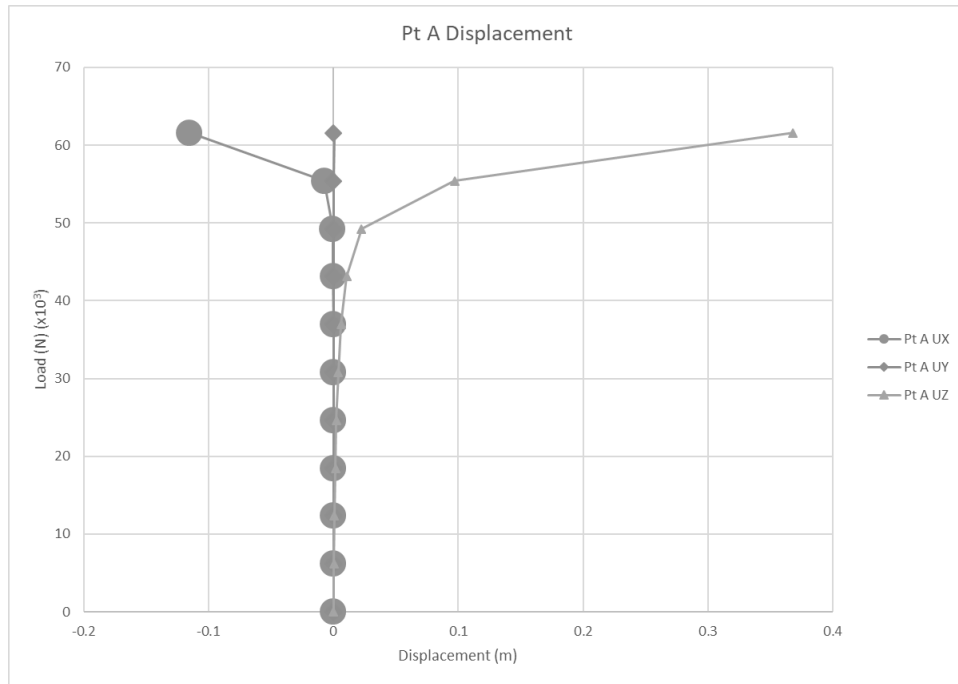
Figure 8.4 Intact Shell Plate with a Very Fine Mesh Node Displacement at Point A
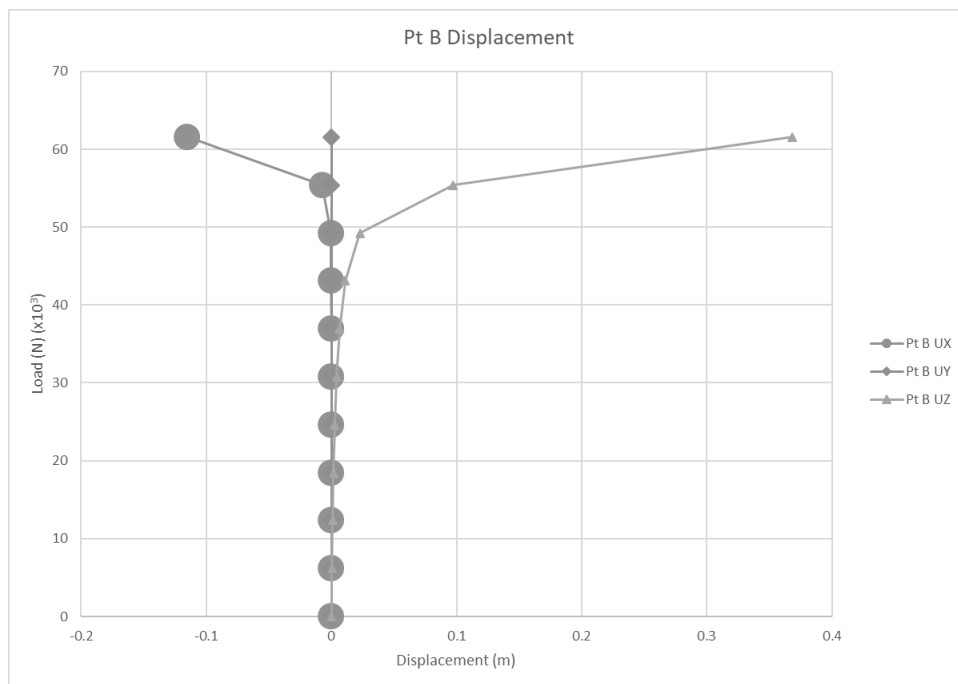
Figure 8.5 Intact Shell Plate with a Very Fine Mesh Node Displacement at Point B
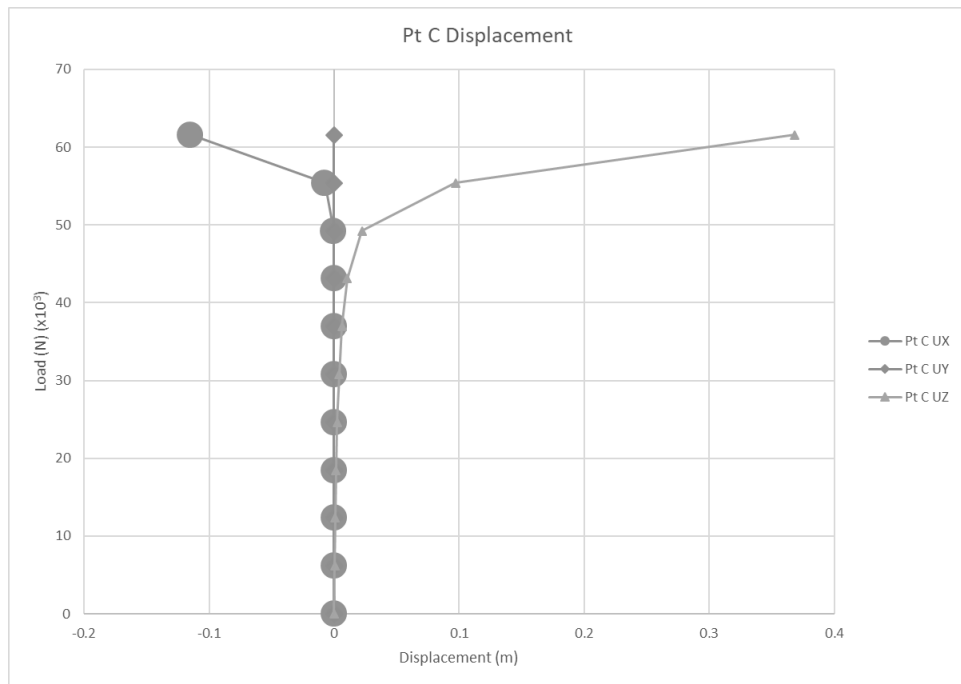
Figure 8.6 Intact Shell Plate with a Very Fine Mesh Node Displacement at Point C

8.1.3.2   Fine Mesh Results

Table B.2 presents the data collected from the non-linear analysis and can be found in Appendix B. The load-deflection graph generated from this data is presented in Figure 8.7. The individual graphs for the displacement values generated at points A, B and C are shown in Figures 8.8, 8.9 and 8.10, respectively.
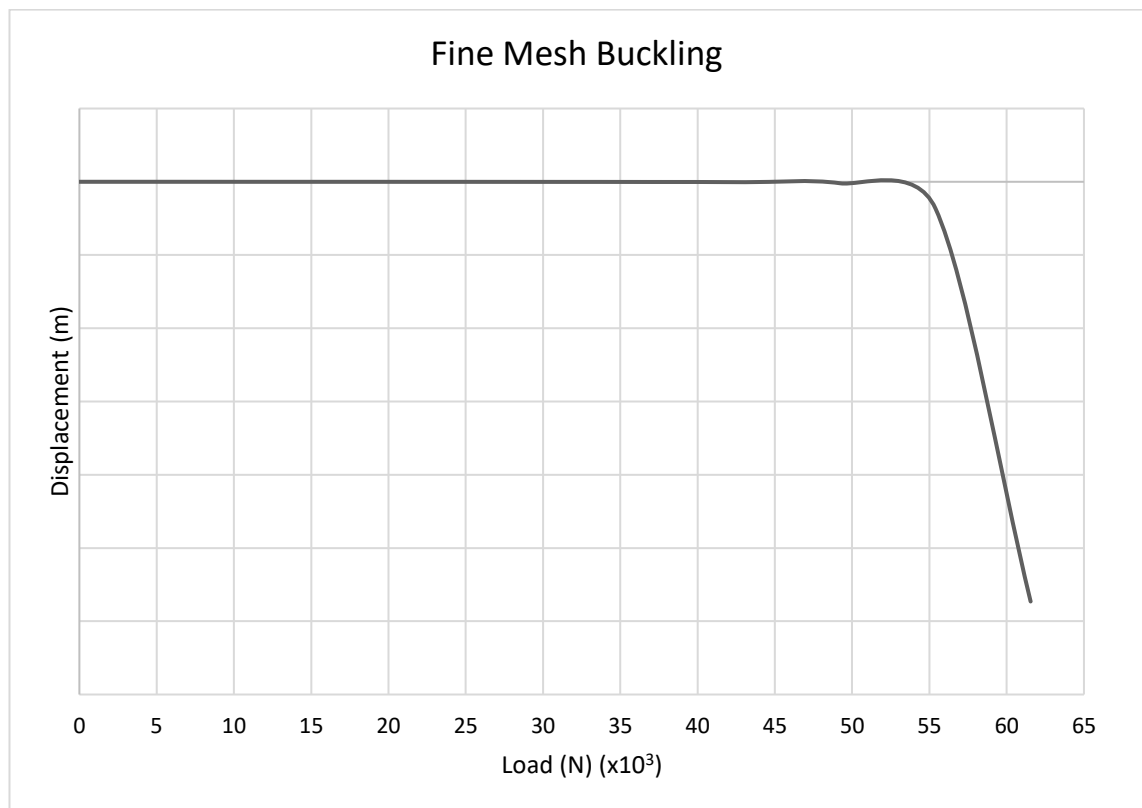
Figure 8.7 Load – Deflection Graph for an Intact Shell Plate with a Fine Mesh
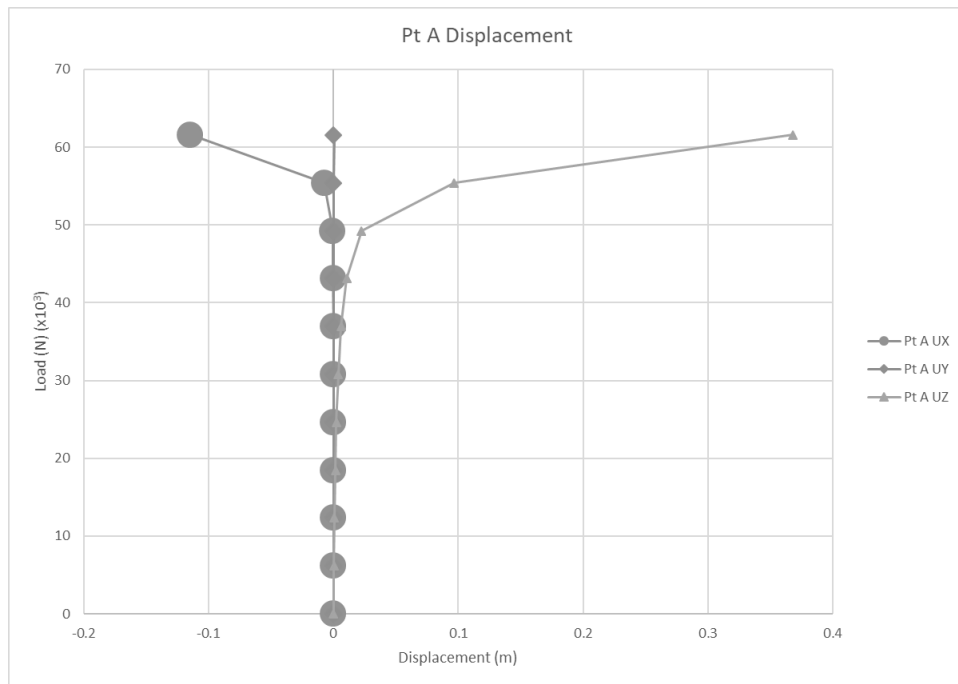
Figure 8.8 Intact Shell Plate with a Fine Mesh Node Displacement at Point A
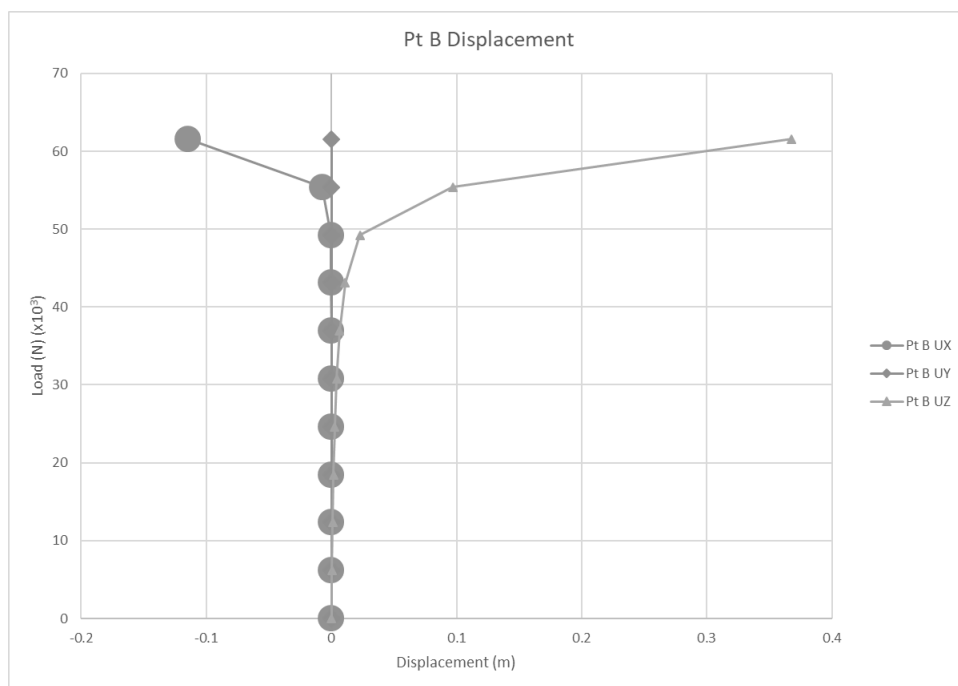
Figure 8.9 Intact Shell Plate with a Fine Mesh Node Displacement at Point B
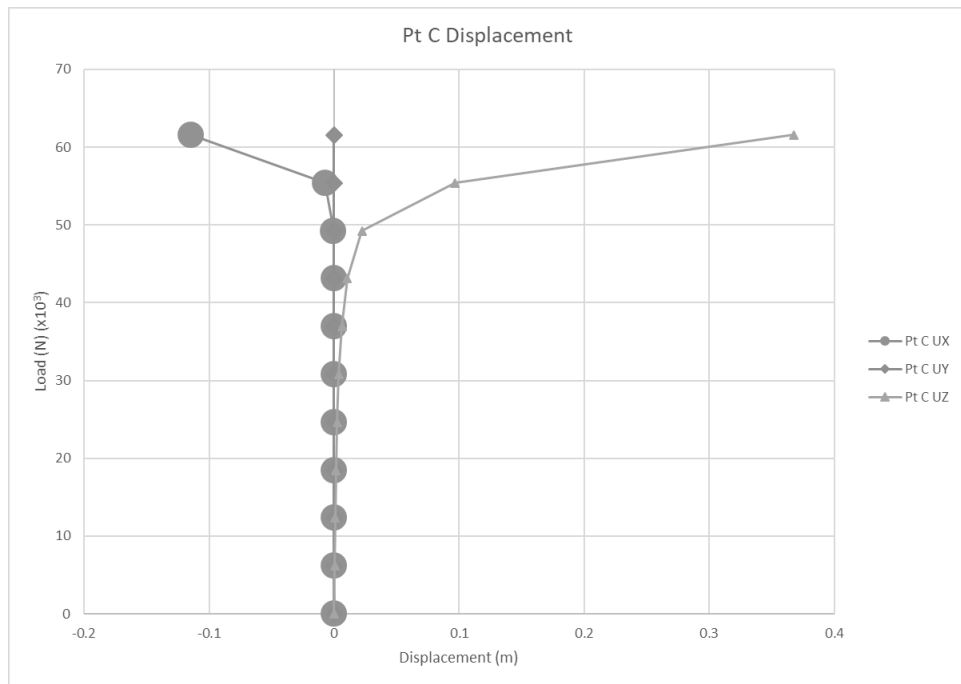
Figure 8.10 Intact Shell Plate with a Fine Mesh Node Displacement at Point C

8.1.3.3 Coarse Mesh Results

Table B.3 presents the data collected from the non-linear analysis and can be found in Appendix B. The load-deflection graph generated from this data is presented in Figure 8.11. The individual graphs for the displacement values generated at points A, B and C are shown in Figures 8.12, 8.13 and 8.14, respectively.
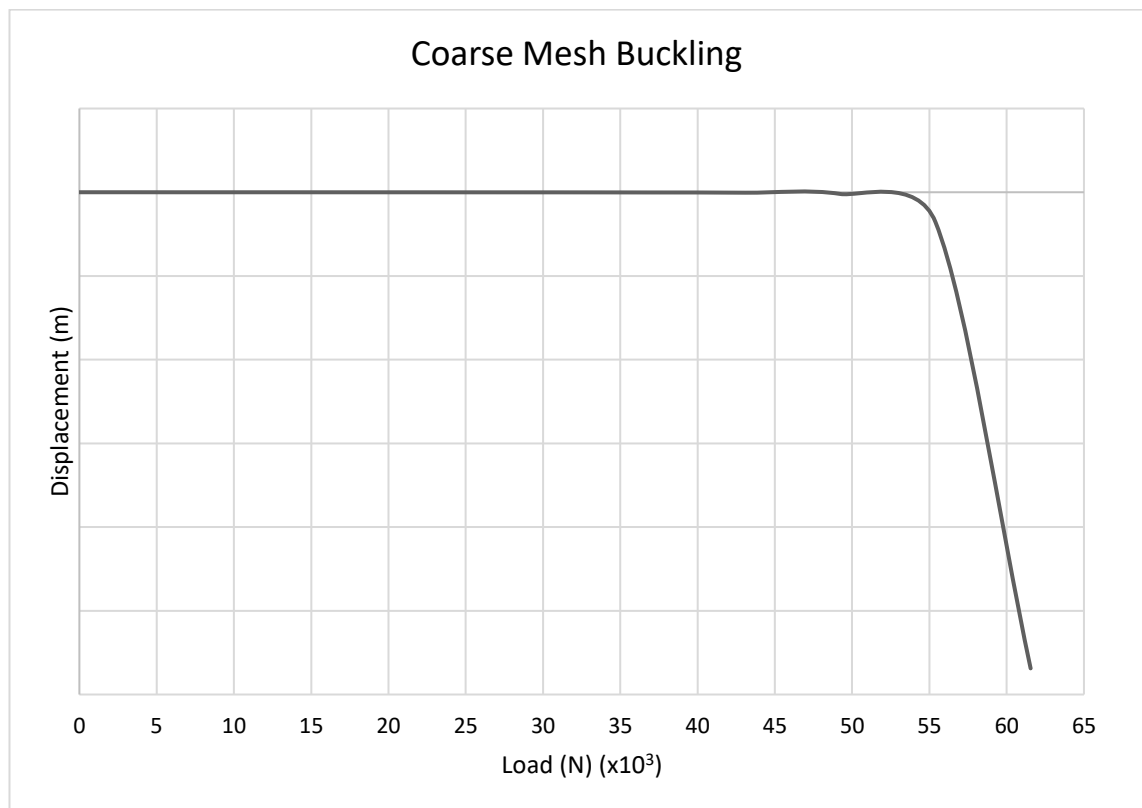
Figure 8.11 Load – Deflection Graph for an Intact Shell Plate with a Coarse Mesh
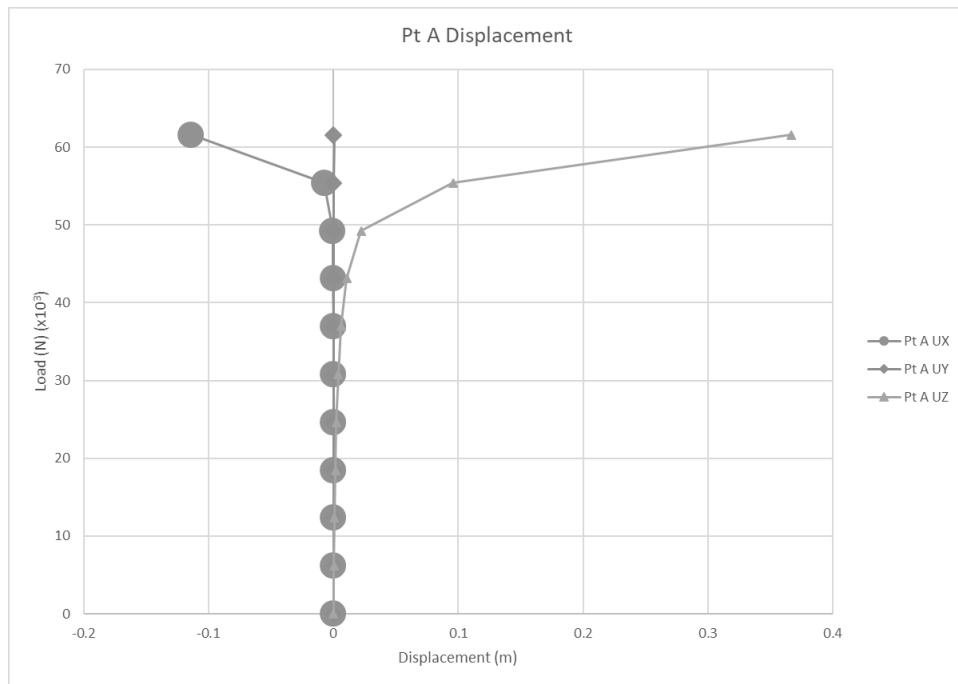
Figure 8.12 Intact Shell Plate with a Coarse Mesh Node Displacement at Point A
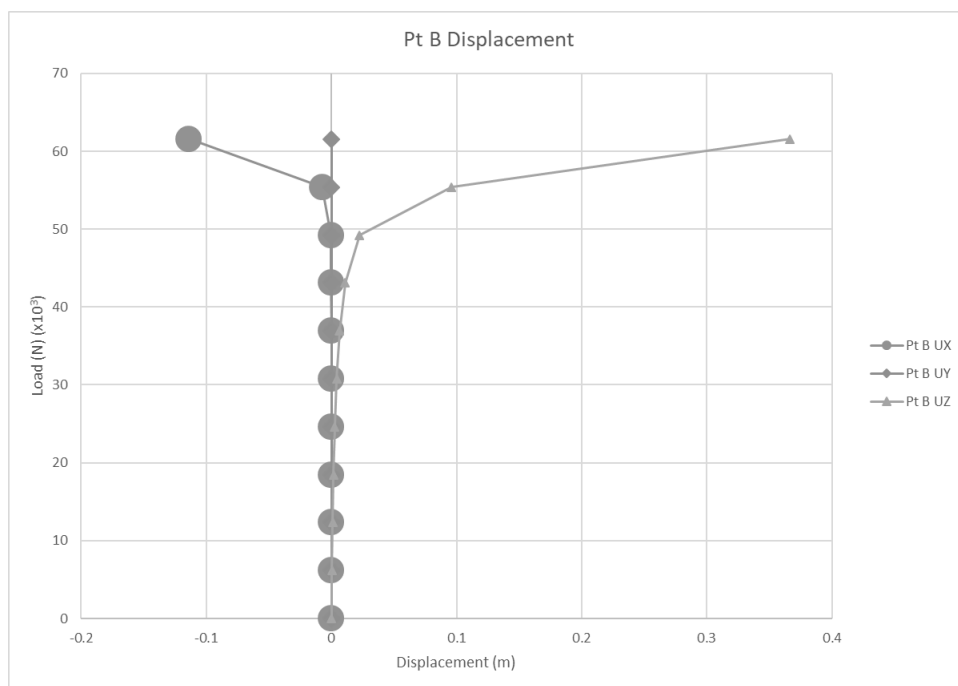
Figure 8.13 Intact Shell Plate with a Coarse Mesh Node Displacement at Point B
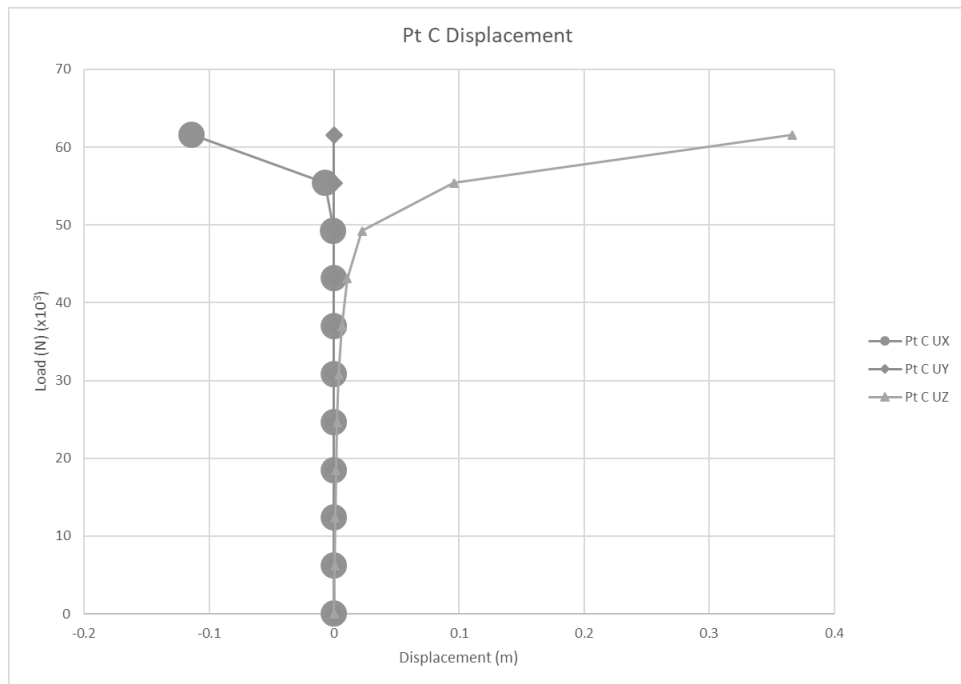
Figure 8.14 Intact Shell Plate with a Coarse Mesh Node Displacement at Point C

8.1.3.4   Very Coarse Mesh Results

Table B.4 presents the data collected from the non-linear analysis and can be found in Appendix B. The load-deflection graph generated from this data is presented in Figure 8.15. The individual graphs for the displacement values generated at points A, B and C are shown in Figures 8.16, 8.17 and 8.18, respectively.
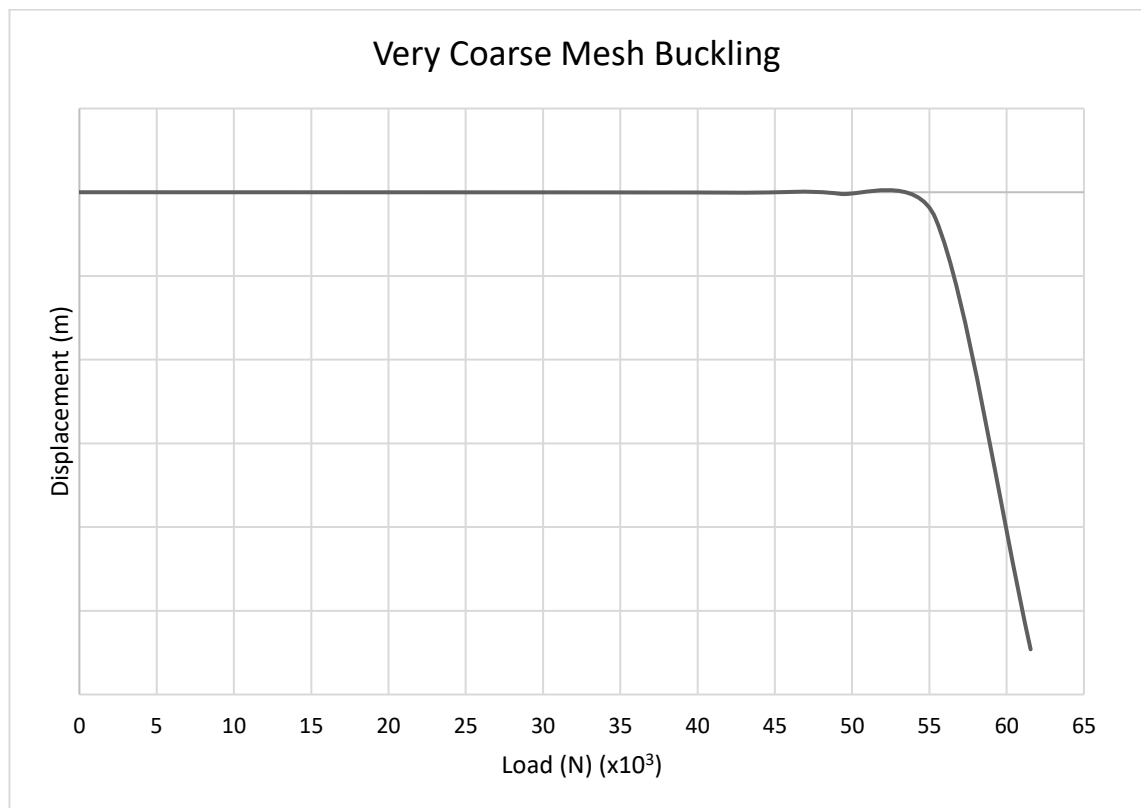
Figure 8.15 Load – Deflection Graph for an Intact Shell Plate with a Very Coarse Mesh
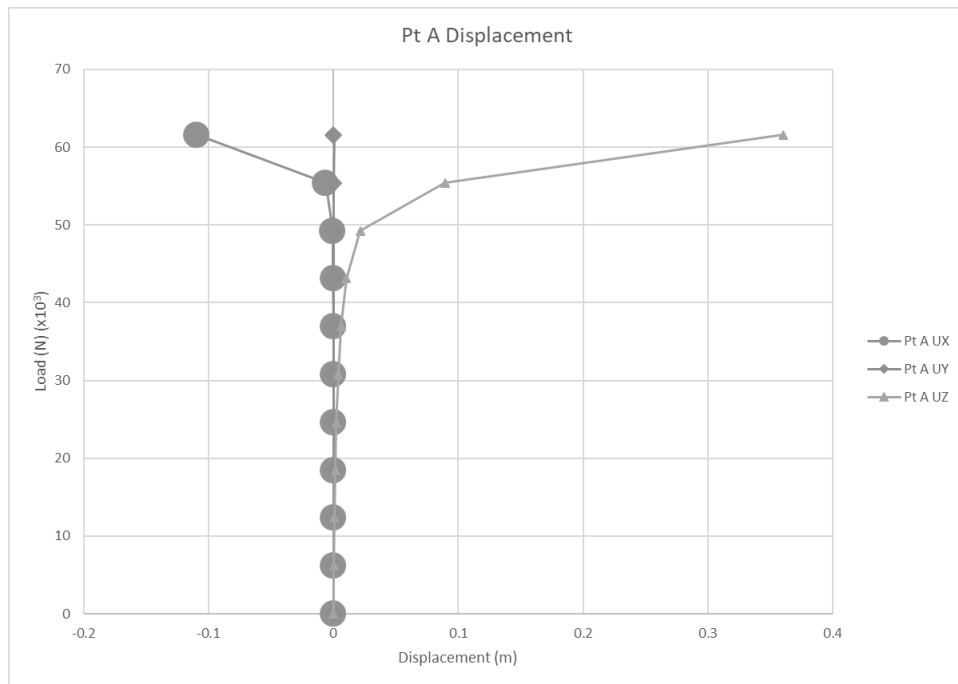
Figure 8.16 Intact Shell Plate with a Very Coarse Mesh Node Displacement at Point A
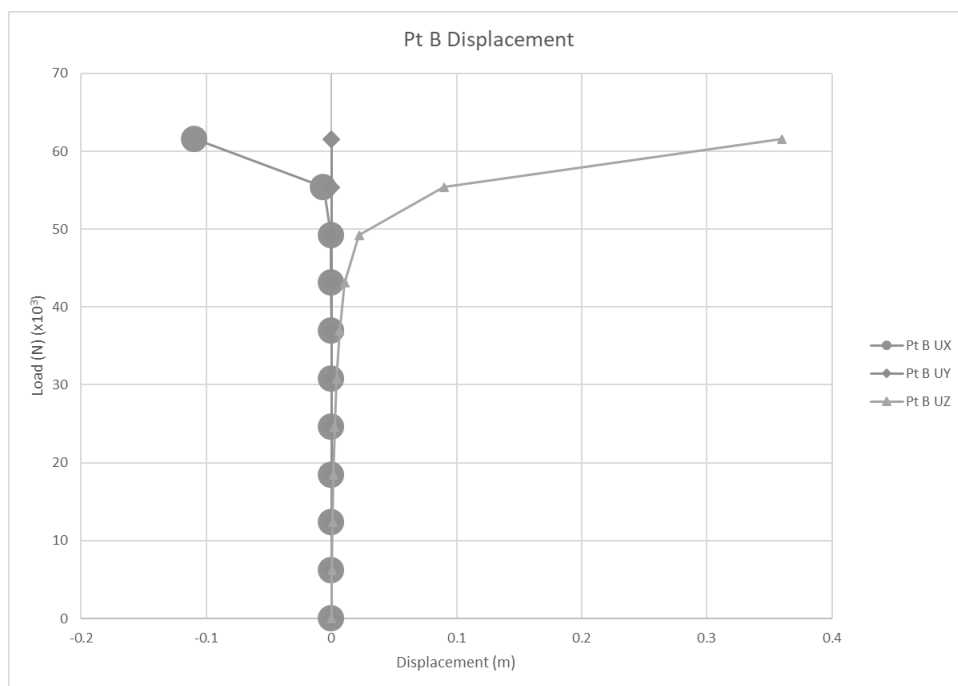
Figure 8.17 Intact Shell Plate with a Very Coarse Mesh Node Displacement at Point B
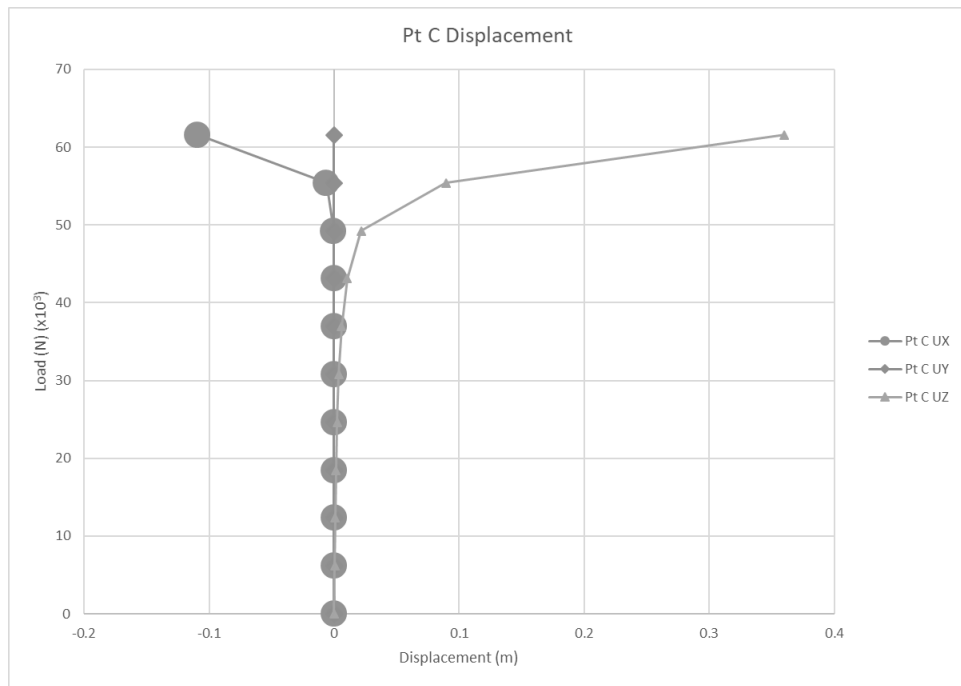
Figure 8.18 Intact Shell Plate with a Very Coarse Mesh Node Displacement at Point C

8.2   Plate with a Hole Shell Convergence Study

In section 8.1 the reasons and the procedure for producing an Eigenvalue buckling value were discussed so in this section only the variations in the written code will be discussed before focussing on how the variation in meshing fineness is applied. The variations in the code for the non-linear analysis will then be introduced before the results are presented.

The geometrical configuration of a plate with a hole is much more complex than the intact model so the code uses the keypoint, line and area creation style seen previously to allow for finer detailing. The fifth keypoint becomes the centre of a circular area that is created and then removed to produce a hole in the centre of the plate.

The lines that are formed when this circle is created must be merged to produce a smaller number of lines as ANSYS has a limitation with regards to the number of lines that can be used to create an area. Without combining the lines on the circumference of the circle then there would be too many to allow ANSYS to create the individual areas.

As seen in Chapter Seven, for the solid example, the individual lines are divided into a given number to allow for the mapped meshing to be applied. The remaining portion of the code is similar to the 2-D shell mesh convergence example from section 8.1. The full code for the 2-D shell plate with a hole including the post-processor step to produce the visual check and the actual Eigenvalue buckling result is presented in Appendix B as Code B.4.

8.2.1   Mesh Fineness Variation for the 2-D Plate with a Hole

As mentioned, the fineness of the mesh is the only property altered in the convergence study. For the 2-D plate with a hole SHELL181 model, this requires alterations to three lines of the code to produce the four various options. The sites of the variations are in the sections detailing the line size of the "Outer Line Divisions", "Inner Line Divisions and Spacing" and the "Circle Divisions" sections of Code B.4.

As well as changing the title of the code the inserted values of the code as detailed above are altered to one of the four following combinations of options depending on the mesh fineness required:

- Very fine mesh   = 40 – 50 – 20
- Fine mesh   = 30 – 37 – 15
- Coarse mesh   = 20 – 25 – 10
- Very coarse mesh   = 10 – 12 – 5

The results of the Eigenvalue buckling at each mesh fineness is presented in Table 8.3. The results are very comparable so when the total load of 110% and a transverse load of 0.5% were calculated for the non-linear analysis the results for each meshing fineness was the same at -55750 N and 278 N, respectively.

Table 8.3 Eigenvalue Buckling Results for the 2-D Plate with a Hole

Mesh Type	Eigenvalue Buckling Result (N)
Very Fine Mesh	50667
Fine Mesh	50667
Coarse Mesh	50703
Very Coarse Mesh	50831

8.2.2   Non-Linear Analysis for the 2-D Plate with a Hole

The code for the non-linear analysis of the 2-D plate with a hole does not contain any lines of code not seen previously so it is presented in full with a very fine mesh in Appendix B as Code B.5; please note as before the line sizes must be altered as per section 8.2.1 depending on the fineness of the mesh.

The post-processor code is exactly as before, please see Code B.3 in Appendix B for the full code.

8.2.3   Results for the 2-D Plate with a Hole

The four levels of mesh fineness will be presented in this section where each has a table denoting the displacement values at each time step at each point. A load-deflection graph for each level of mesh fineness is also presented which shows the accuracy of the predicted buckling value to the failure point as expected. If the Eigenvalue buckling value predicted is accurate the graph will show a sudden dip at this load point as the model has buckled and failed. The table discussed will be presented in Appendix B and the figures will be presented in the relevant chapter sub-section.

Three graphs will also be presented to better illustrate the data presented in the table. These graphs show the displacement at each point, A, B and C, at each time step relative to the load applied at each time step. If the coupling applied to the model has been successful each of the three graphs will be identical.

8.2.3.1   Very Fine Mesh Results

Table B.5 presents the data collected from the non-linear analysis and can be found in Appendix B. The load-deflection graph generated from this data is presented in Figure 8.18. The individual graphs for the node displacement values generated at points A, B and C are shown in Figures 8.19, 8.20 and 8.21, respectively.
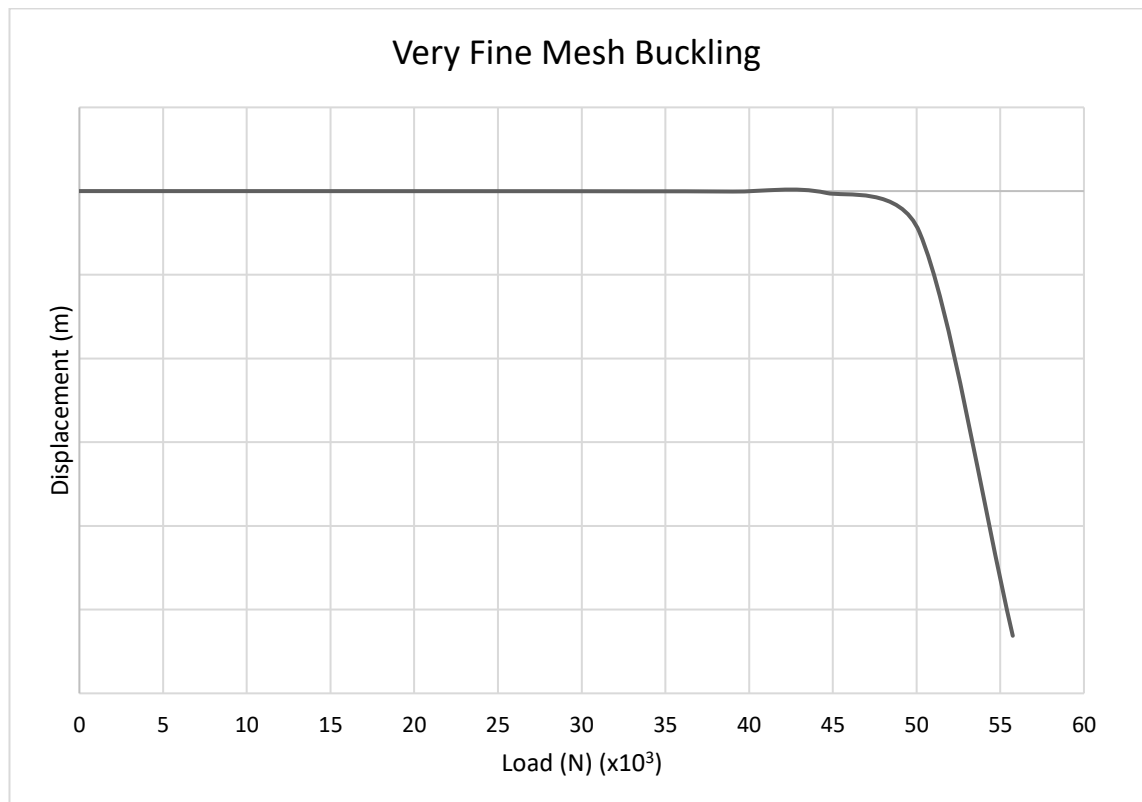
Figure 8.18 Load – Deflection Graph for a Shell Plate with a Hole and a Very Fine Mesh
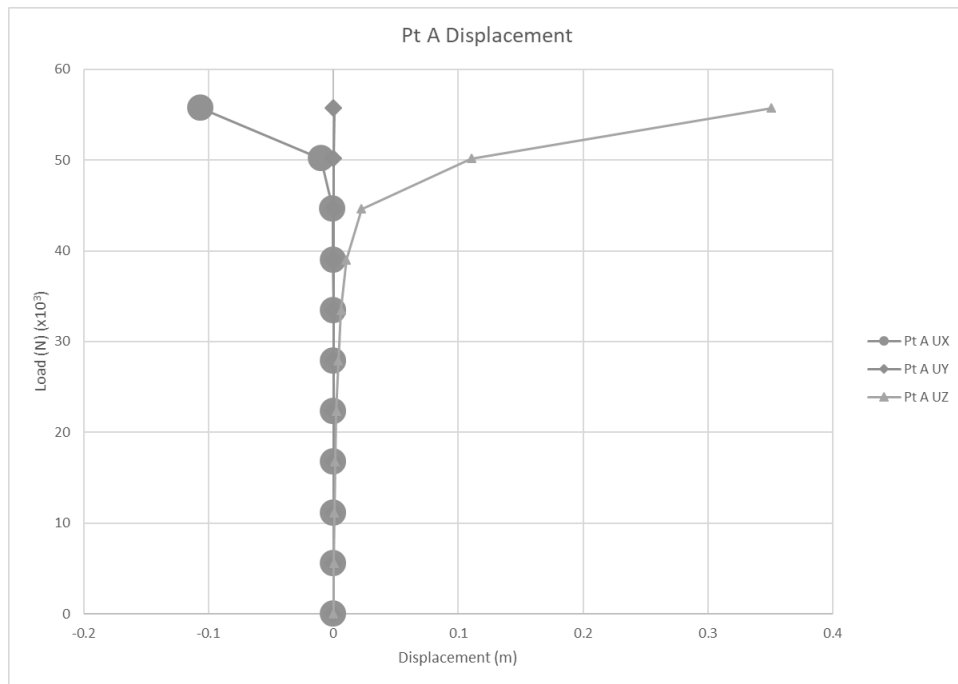
Figure 8.19 Shell Plate with a Hole and a Very Fine Mesh Node Displacement at Point A
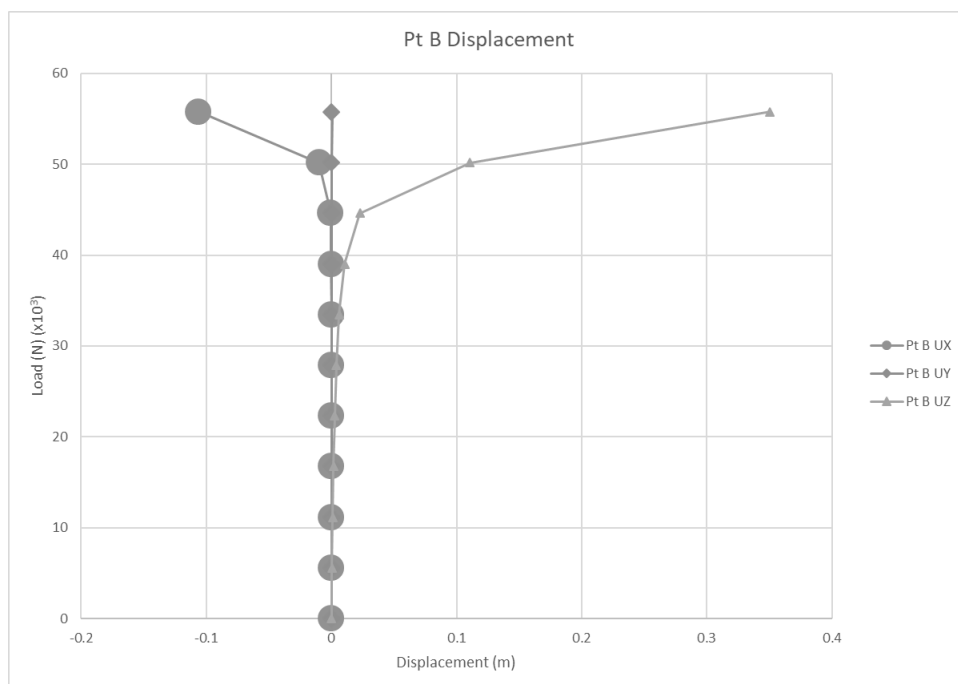
Figure 8.20 Shell Plate with a Hole and a Very Fine Mesh Node Displacement at Point B
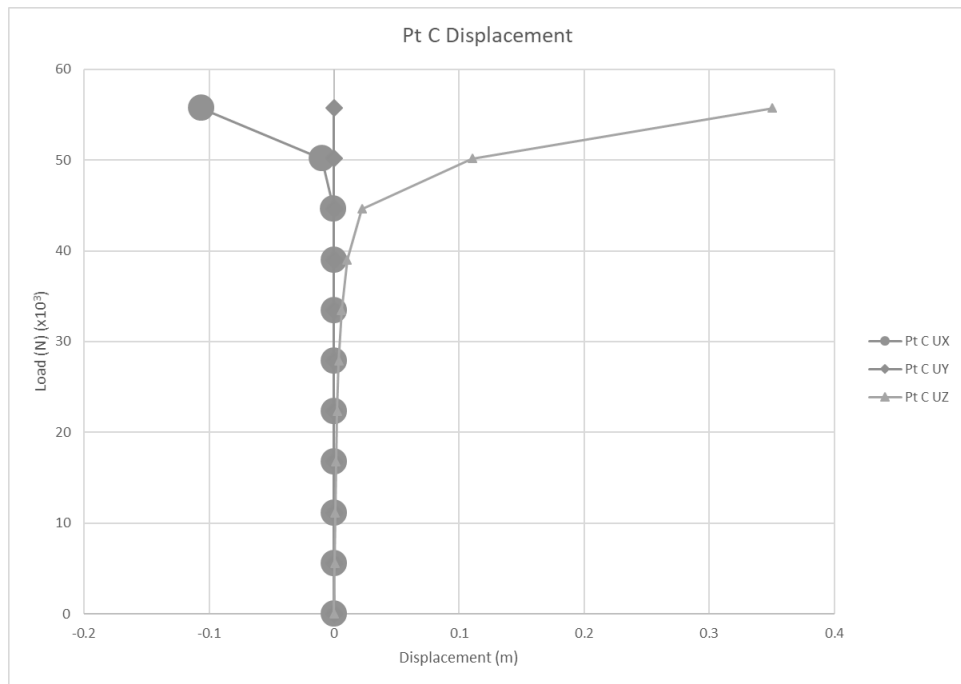
Figure 8.21 Shell Plate with a Hole and a Very Fine Mesh Node Displacement at Point C

8.2.3.2   Fine Mesh Results

Table B.6 presents the data collected from the non-linear analysis and can be found in Appendix B. The load-deflection graph generated from this data is presented in Figure 8.22. The individual graphs for the displacement values generated at points A, B and C are shown in Figures 8.23, 8.24 and 8.25, respectively.
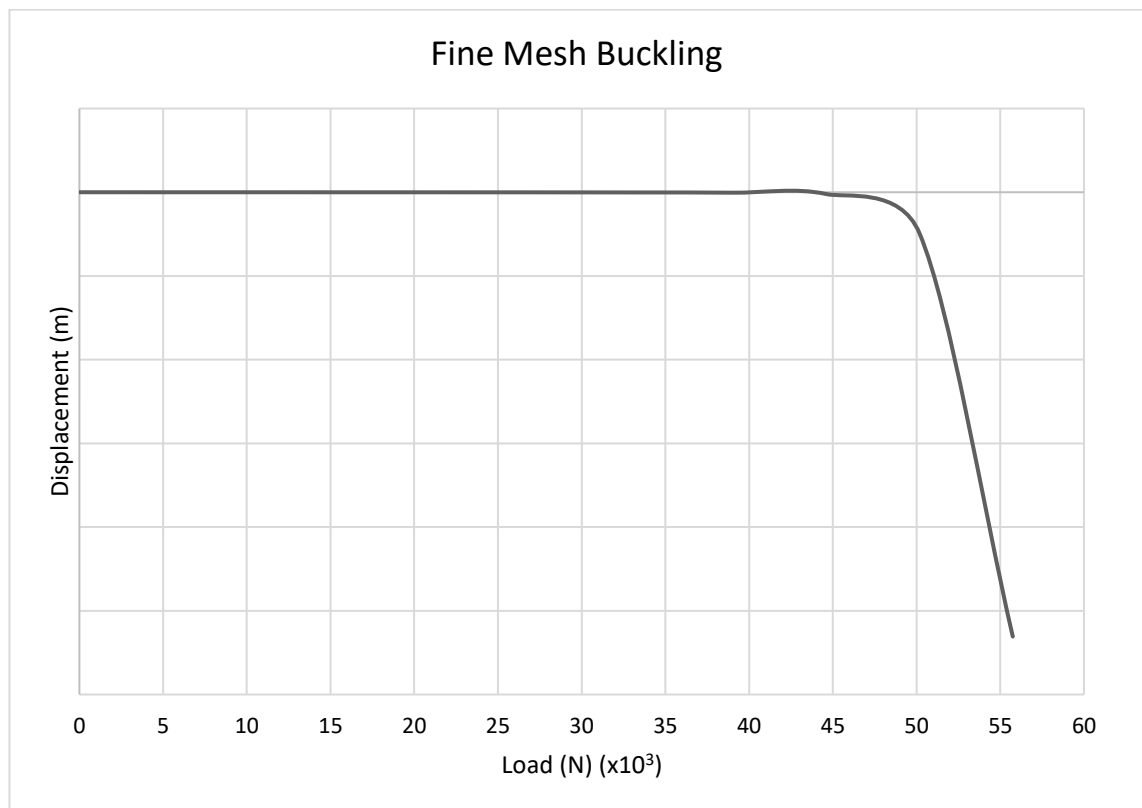
Figure 8.22 Load – Deflection Graph for a Shell Plate with a Hole and a Fine Mesh
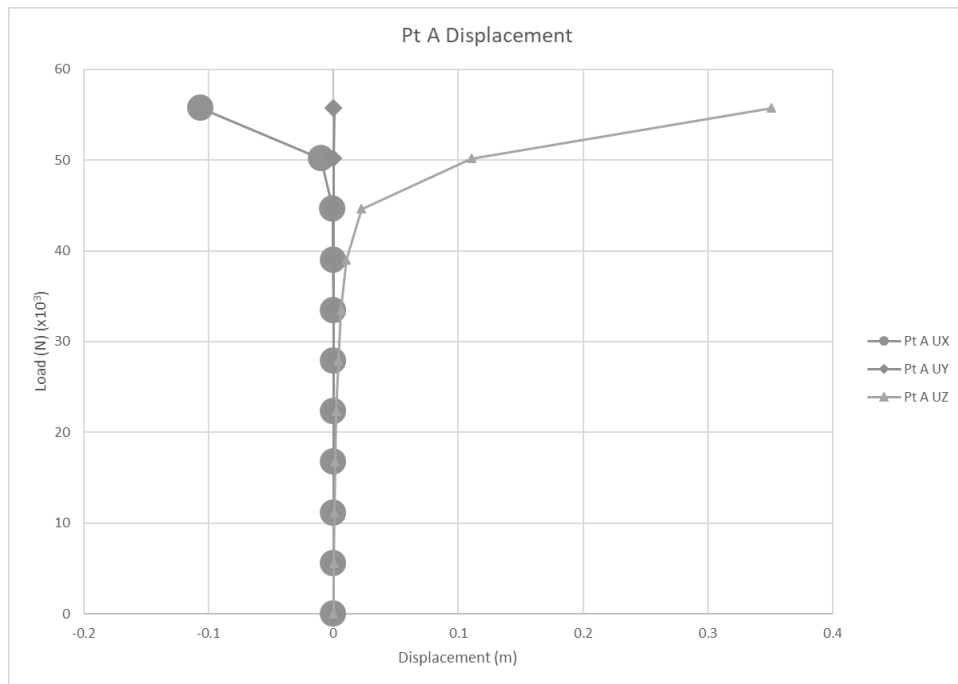
Figure 8.23 Shell Plate with a Hole and a Fine Mesh Node Displacement at Point A
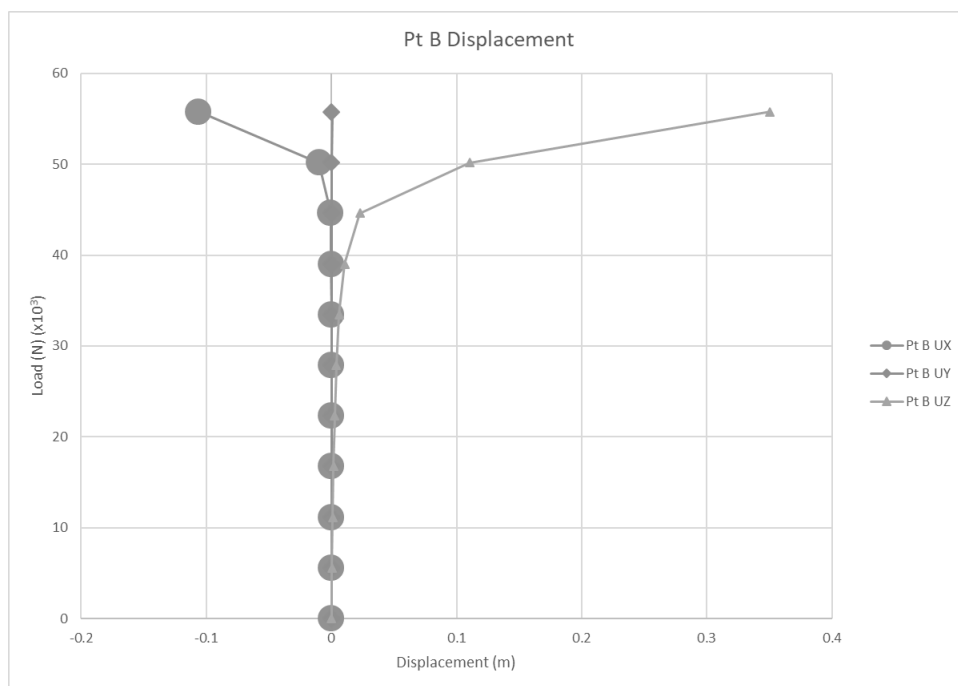
Figure 8.24 Shell Plate with a Hole and a Fine Mesh Node Displacement at Point B
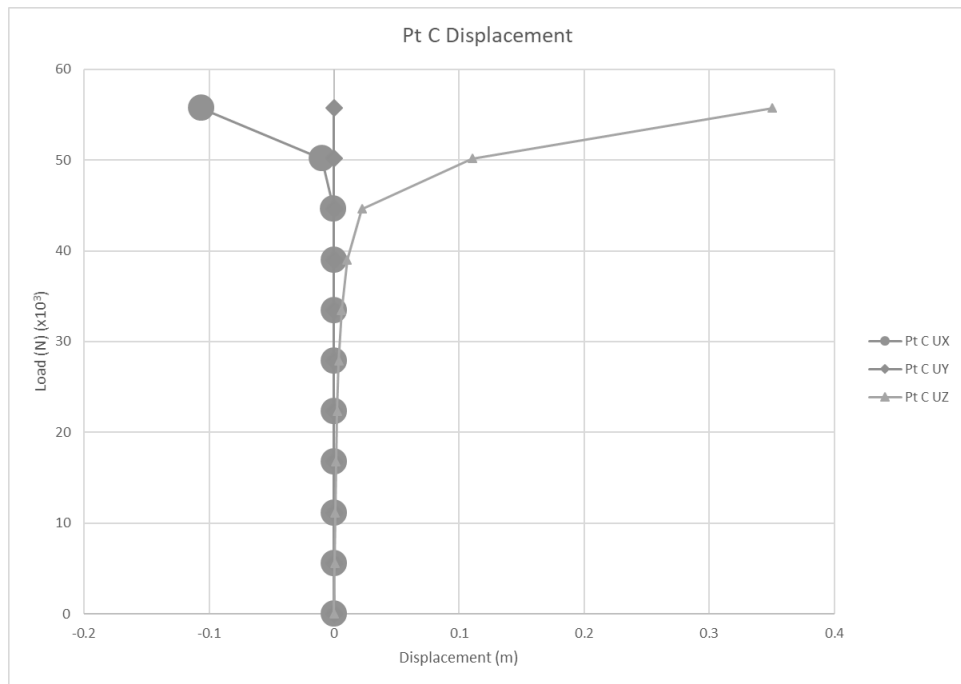
Figure 8.25 Shell Plate with a Hole and a Fine Mesh Node Displacement at Point C

8.2.3.3   Coarse Mesh Results

Table B.7 presents the data collected from the non-linear analysis and can be found in Appendix B. The load-deflection graph generated from this data is presented in Figure 8.26. The individual graphs for the displacement values generated at points A, B and C are shown in Figures 8.27, 8.28 and 8.29, respectively.
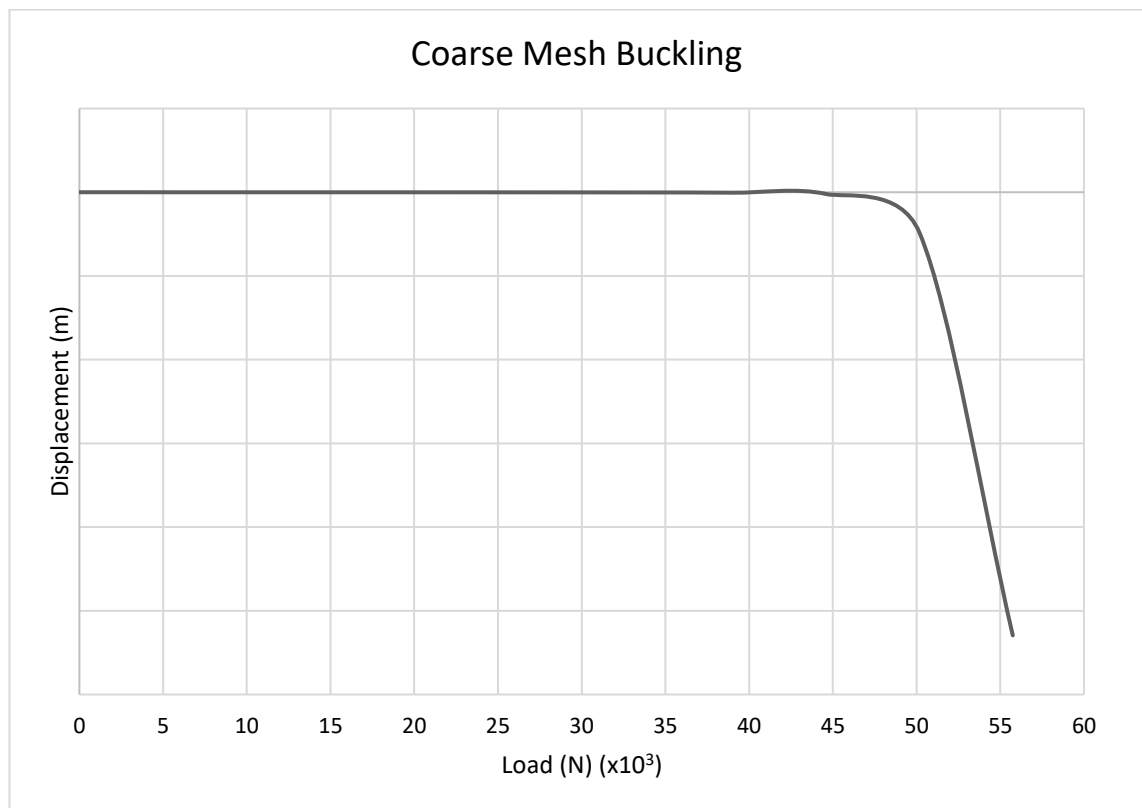
Figure 8.26 Load – Deflection Graph for a Shell Plate with a Hole and a Coarse Mesh
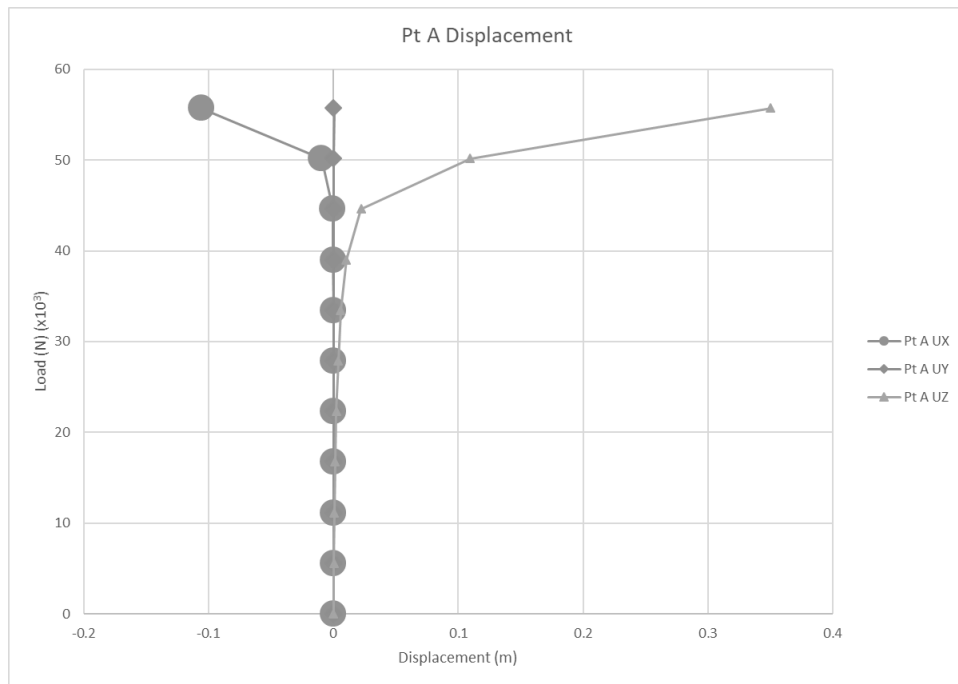
Figure 8.27 Shell Plate with a Hole and a Coarse Mesh Node Displacement at Point A
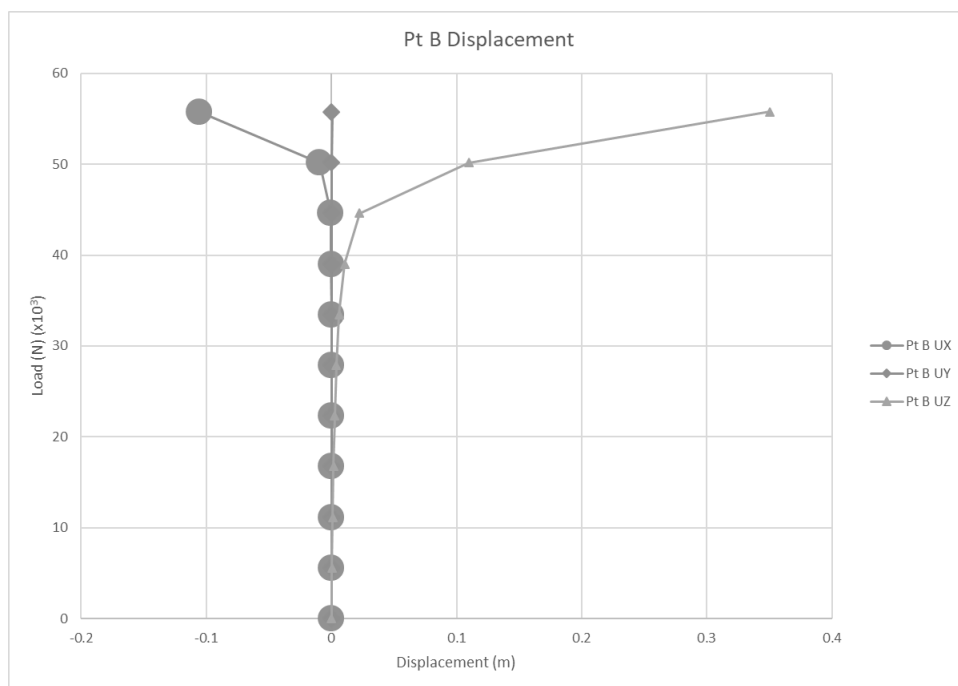
Figure 8.28 Shell Plate with a Hole and a Coarse Mesh Node Displacement at Point B
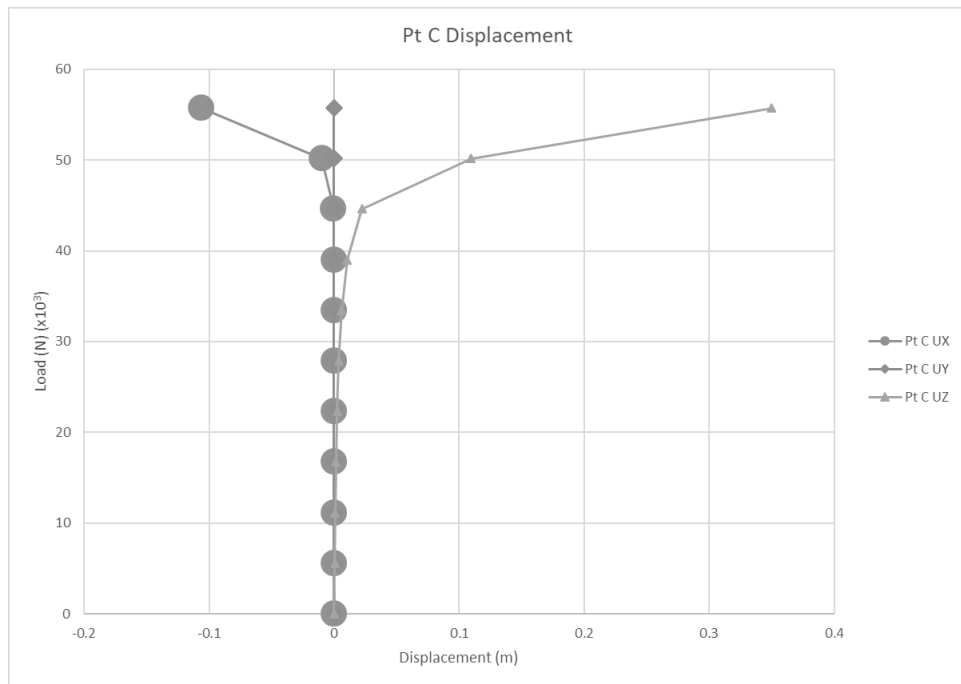
Figure 8.29 Shell Plate with a Hole and a Coarse Mesh Node Displacement at Point C

8.2.3.4   Very Coarse Mesh Results

Table B.8 presents the data collected from the non-linear analysis and can be found in Appendix B. The load-deflection graph generated from this data is presented in Figure 8.30. The individual graphs for the displacement values generated at points A, B and C are shown in Figures 8.31, 8.32 and 8.33, respectively.
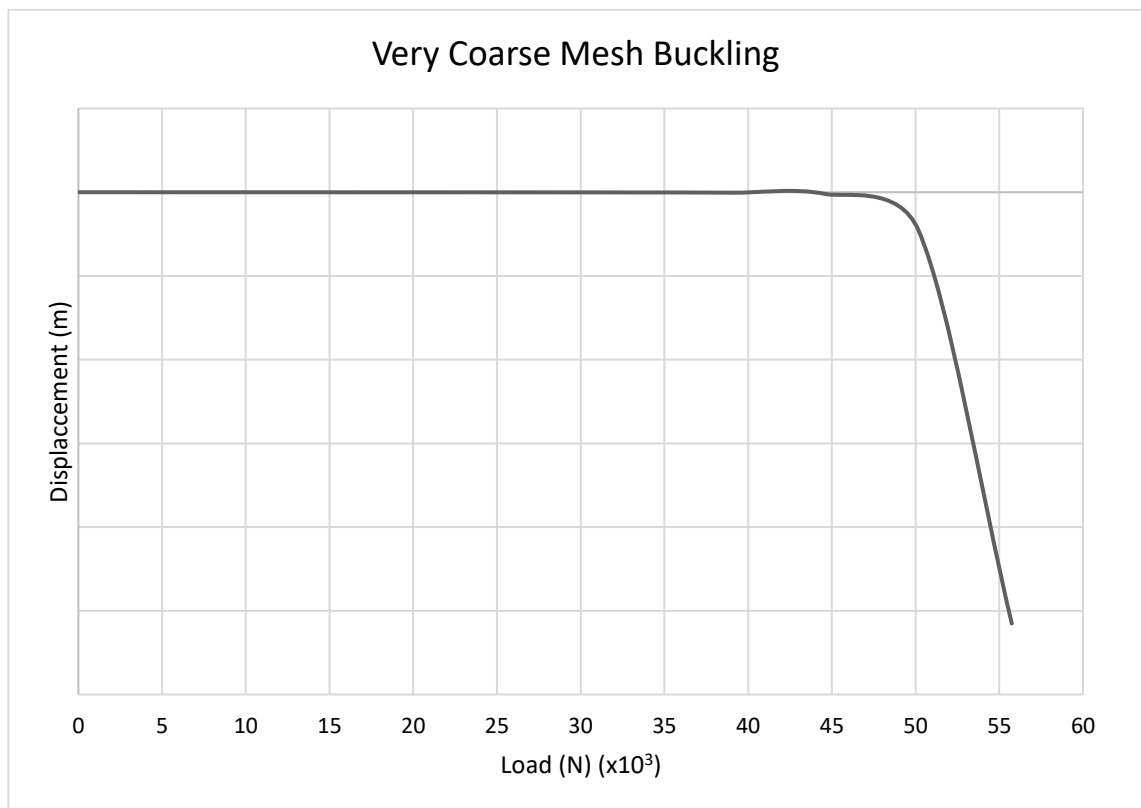
Figure 8.30 Load – Deflection Graph for a Shell Plate with a Hole and a Very Coarse Mesh
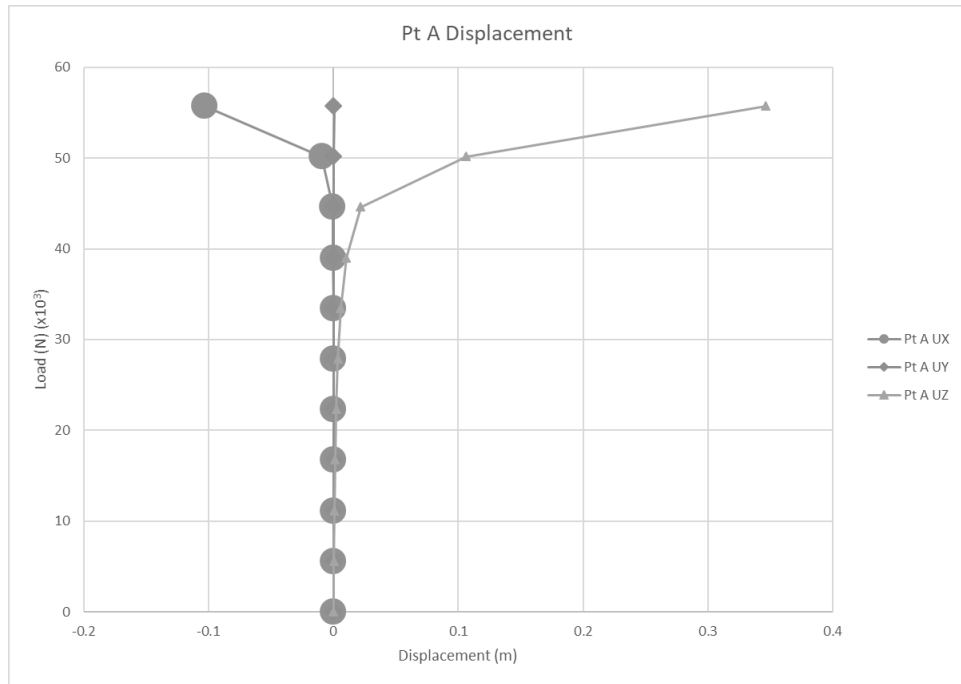
Figure 8.31 Shell Plate with a Hole and a Very Coarse Mesh Node Displacement at Point A
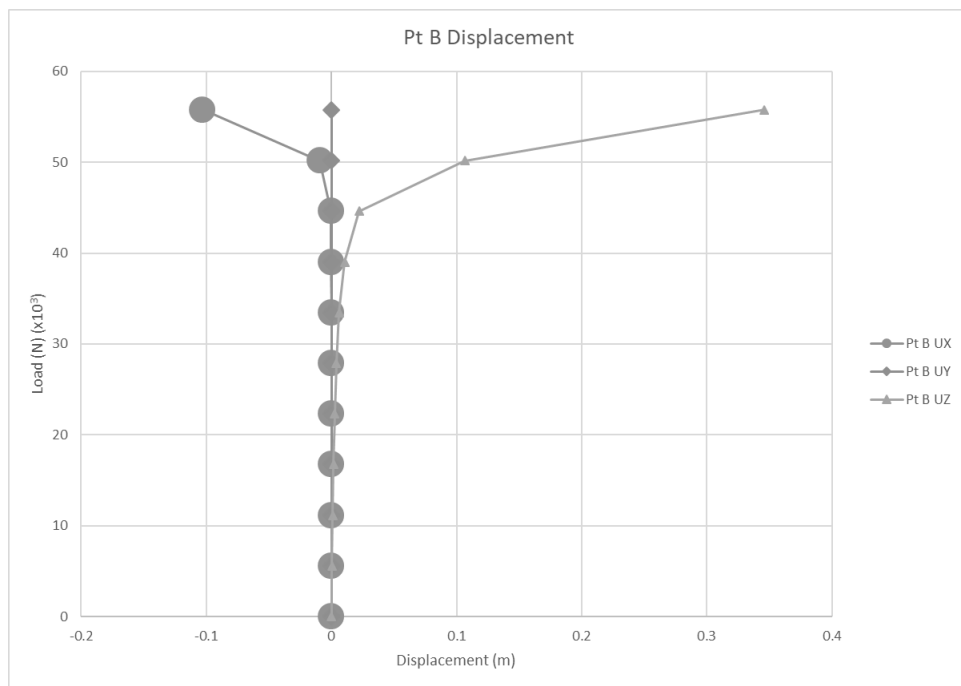
Figure 8.32 Shell Plate with a Hole and a Very Coarse Mesh Node Displacement at Point B
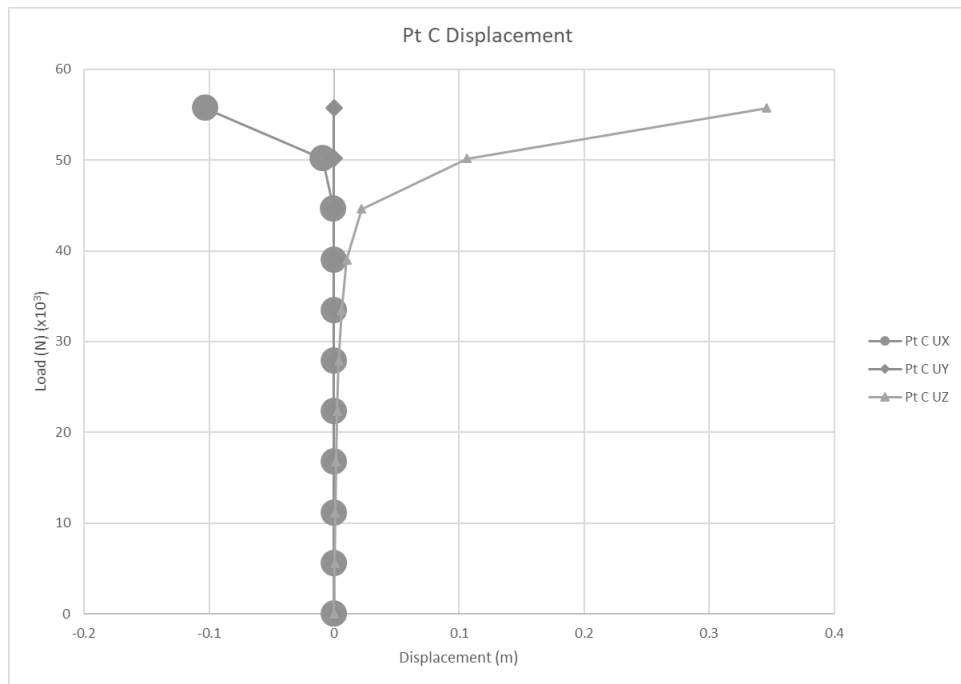
Figure 8.33 Shell Plate with a Hole and a Very Coarse Mesh Node Displacement at Point C

8.3   Intact Solid Convergence Study

In section 8.1 the reasons and the procedure for producing an Eigenvalue buckling value were discussed. In this section, there are no new lines of the written code that need to be discussed so the Eigenvalue buckling code will be presented in full before focussing on how the variation in meshing fineness is applied. There are also no new variations in the code for the non-linear analysis, so again, it will be presented in full before the results are shown.

The full Eigenvalue buckling code is shown in Code B.6 in Appendix B for the intact 3-D solid plate with a very fine mesh including the post-processor step to produce the visual check and the actual Eigenvalue buckling result.

8.3.1   Mesh Fineness Variation for the Intact 3-D Plate

As mentioned, the fineness of the mesh is the only property altered in the convergence study. For the fully intact 3-D SOLID186 model this requires an alteration to a single line of the code to produce the four various options.

As well as changing the title of the code the inserted value of the code highlighted above is altered to one of the four following options depending on the mesh fineness required:

- Very fine mesh   = 40
- Fine mesh   = 30
- Coarse mesh   = 20
- Very coarse mesh   = 10

The results of the Eigenvalue buckling at each mesh fineness is presented in Table 8.4. The results are very comparable so when the total load of 110% and a transverse load of 0.5% were calculated for the non-linear analysis the results for each meshing fineness was the same at -61550 N and 308 N, respectively.

Table 8.4 Eigenvalue Buckling Results for the Intact 3-D Plate

Mesh Type	Eigenvalue Buckling Result (N)
Very Fine Mesh	55942
Fine Mesh	55945
Coarse Mesh	55953
Very Coarse Mesh	55984

8.3.2 Non-Linear Analysis for the Intact 3-D Plate

The code for the non-linear analysis of the Intact 3-D plate does not contain any lines of code not seen previously so it is presented in full as Code B.7 on Appendix B with a very fine mesh; please note as before the line sizes must be altered as per section 8.3.1 depending on the fineness of the mesh.

The post-processor code is exactly as before, please see Code B.3 in Appendix B for the full code.

8.3.3 Results for the Intact 3-D Plate

The four levels of mesh fineness will be presented in this section where each has a table denoting the displacement values at each time step at each point. A load-deflection graph for each level of mesh fineness is also presented which shows the accuracy of the predicted buckling value to the failure point as expected. If the Eigenvalue buckling value predicted is accurate the graph will show a sudden dip at this load point as the model has buckled and failed. The table discussed will be presented in Appendix B and the figures will be presented in the relevant chapter sub-section.

Three graphs will also be presented to better illustrate the data presented in the table. These graphs show the displacement at each point, A, B and C, at each time step relative to the load applied at each time step. If the coupling applied to the model has been successful each of the three graphs will be identical.

8.3.3.1   Very Fine Mesh Results

Table B.9 presents the data collected from the non-linear analysis and can be found in Appendix B. The load-deflection graph generated from this data is presented in Figure 8.34. The individual graphs for the node displacement values generated at points A, B and C are shown in Figures 8.35, 8.36 and 8.37, respectively.
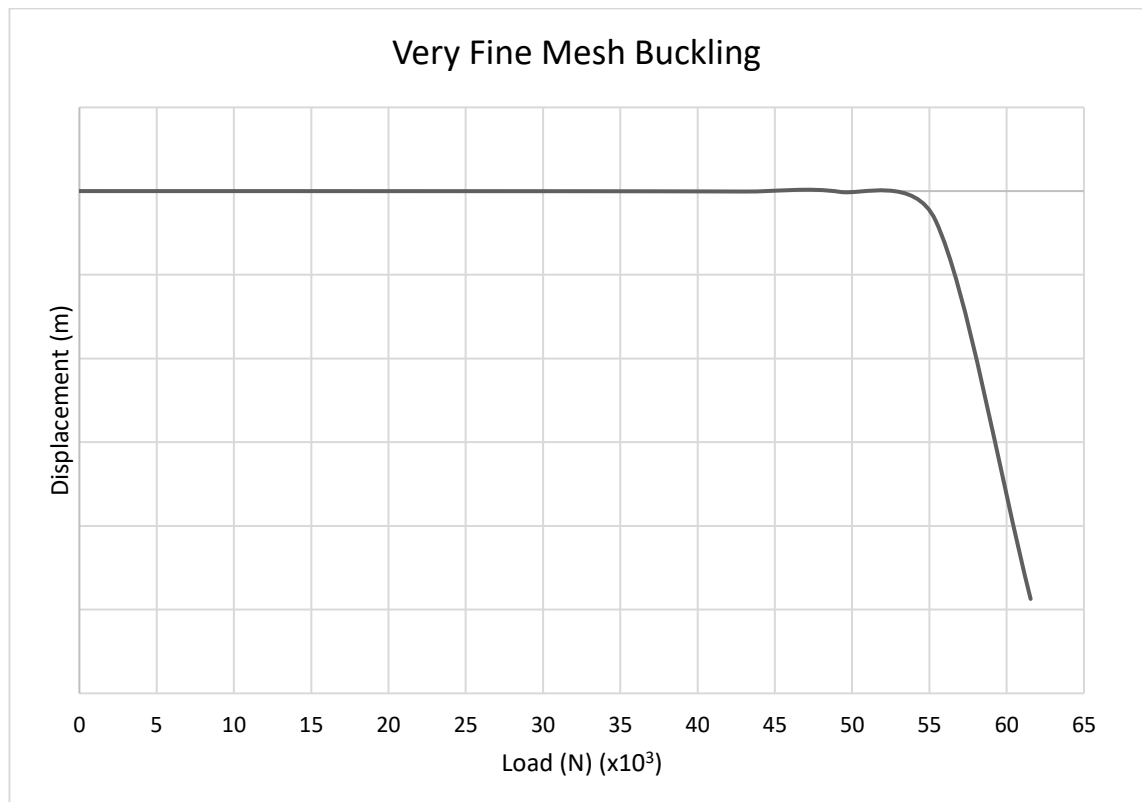
Figure 8.34 Load – Deflection Graph for an Intact Solid Plate with a Very Fine Mesh
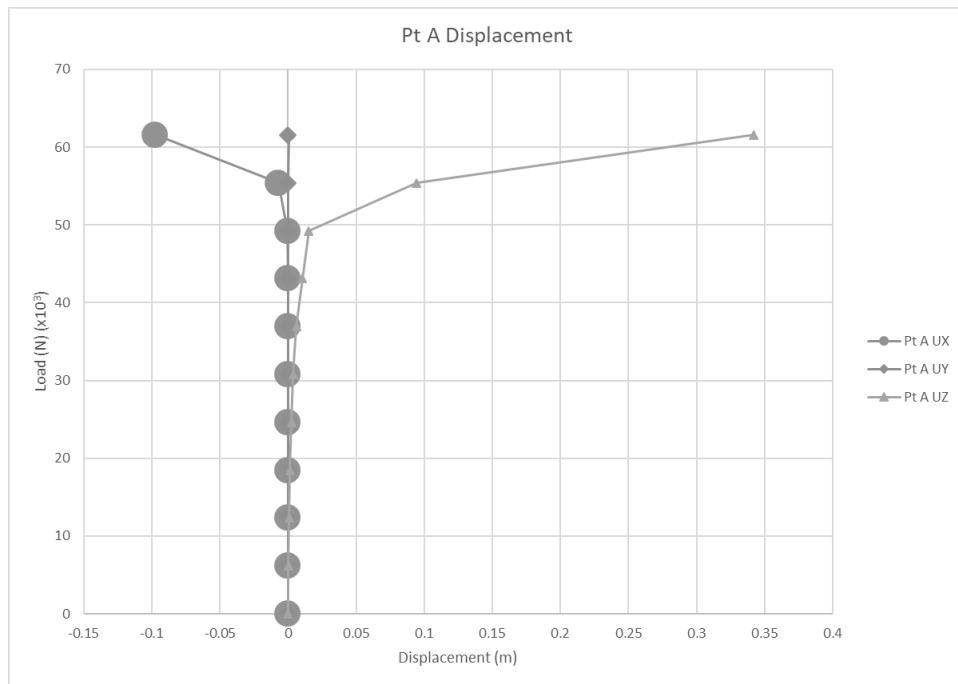
Figure 8.35 Intact Solid Plate with a Very Fine Mesh Node Displacement at Point A
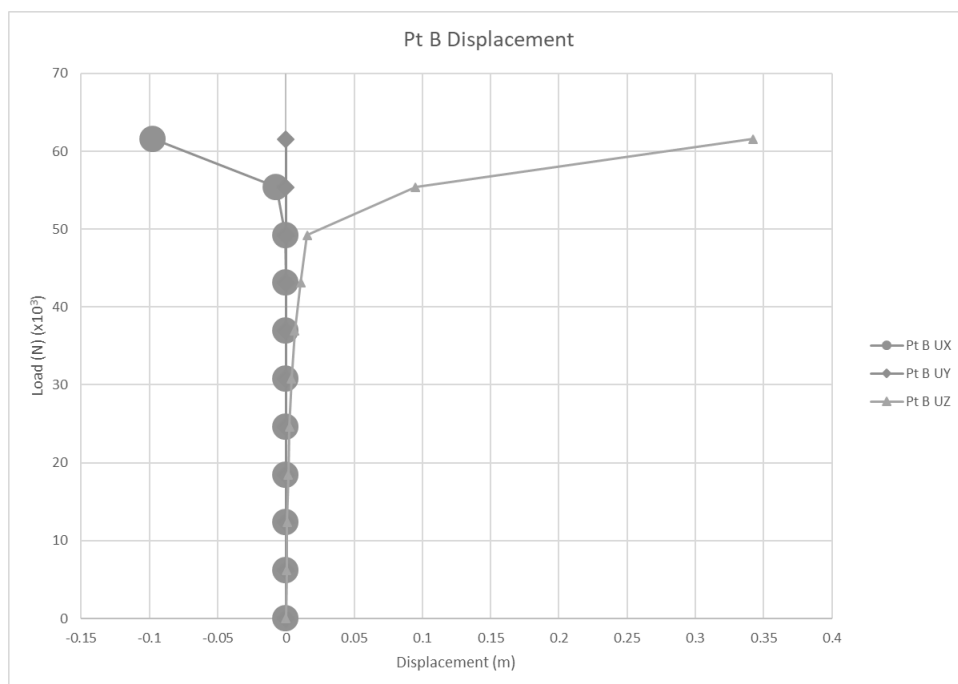
Figure 8.36 Intact Solid Plate with a Very Fine Mesh Node Displacement at Point B
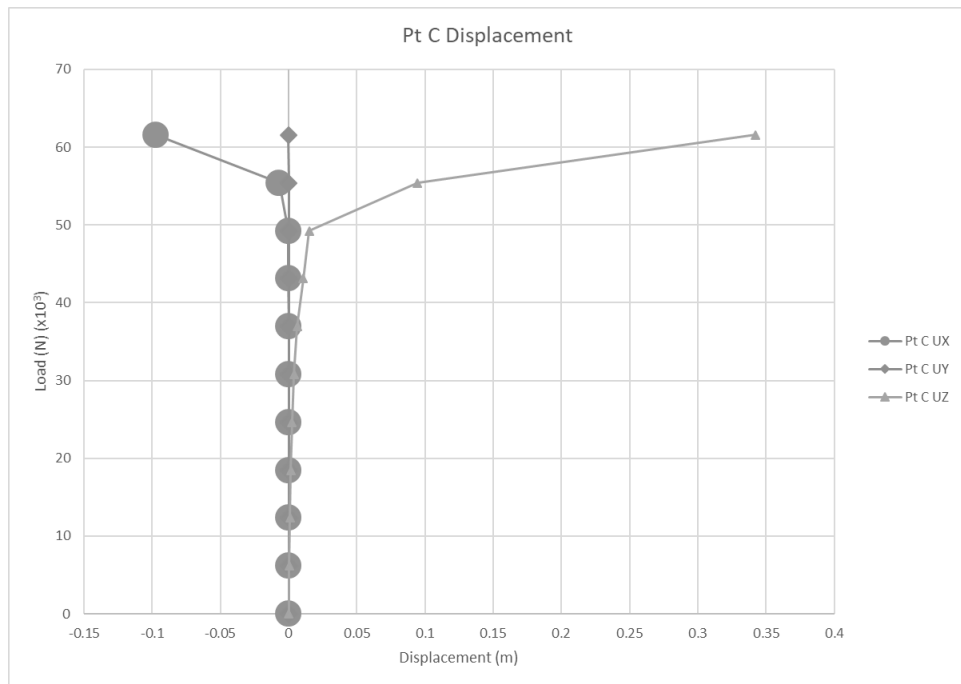
Figure 8.37 Intact Solid Plate with a Very Fine Mesh Node Displacement at Point C

8.3.3.2   Fine Mesh Results

Table B.10 presents the data collected from the non-linear analysis and can be found in Appendix B. The load-deflection graph generated from this data is presented in Figure 8.38. The individual graphs for the displacement values generated at points A, B and C are shown in Figures 8.39, 8.40 and 8.41, respectively.
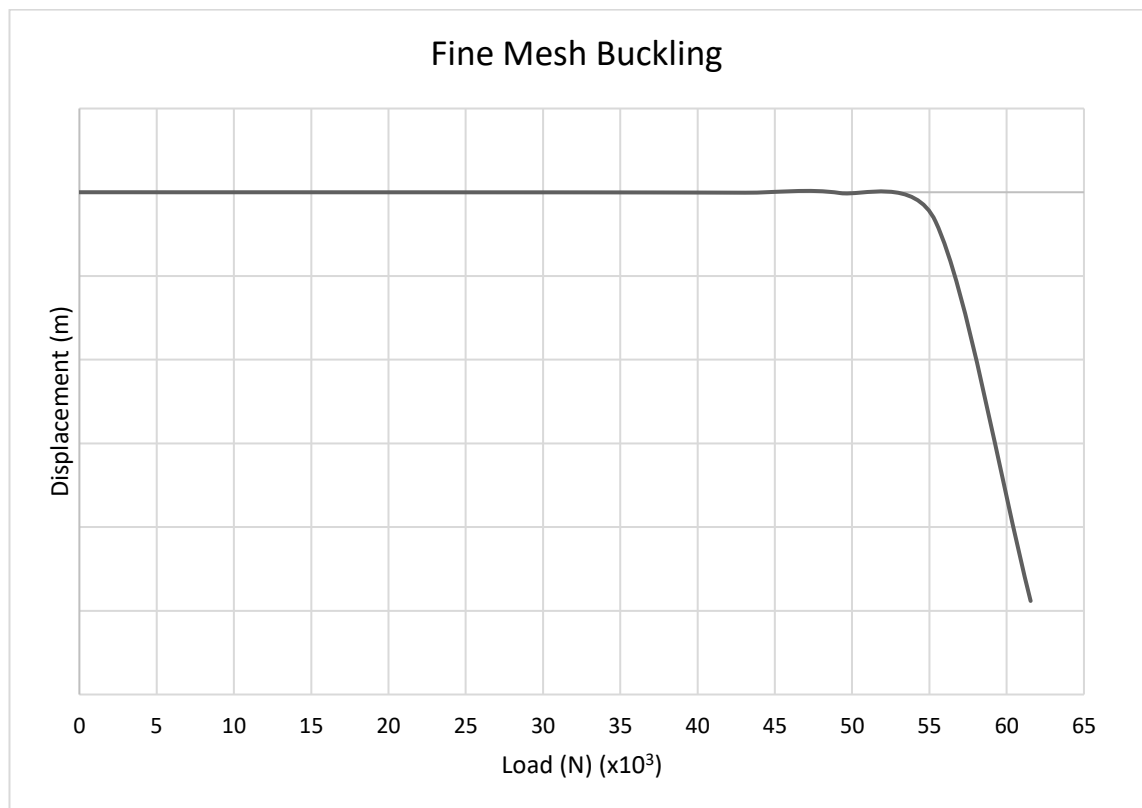
Figure 8.38 Load – Deflection Graph for an Intact Solid Plate with a Fine Mesh
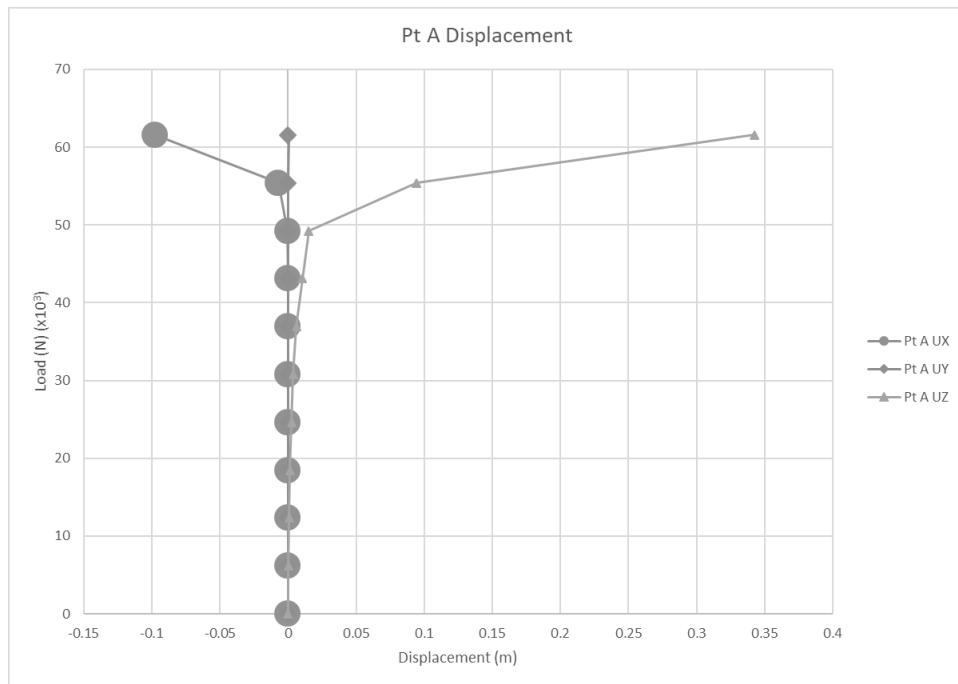
Figure 8.39 Intact Solid Plate with a Fine Mesh Node Displacement at Point A
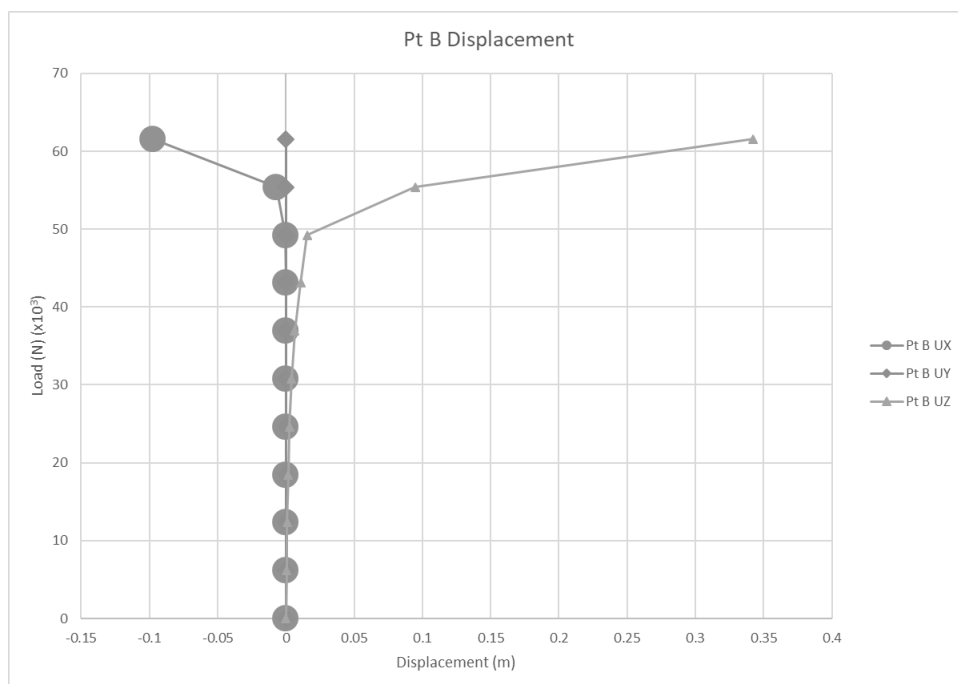
Figure 8.40 Intact Solid Plate with a Fine Mesh Node Displacement at Point B
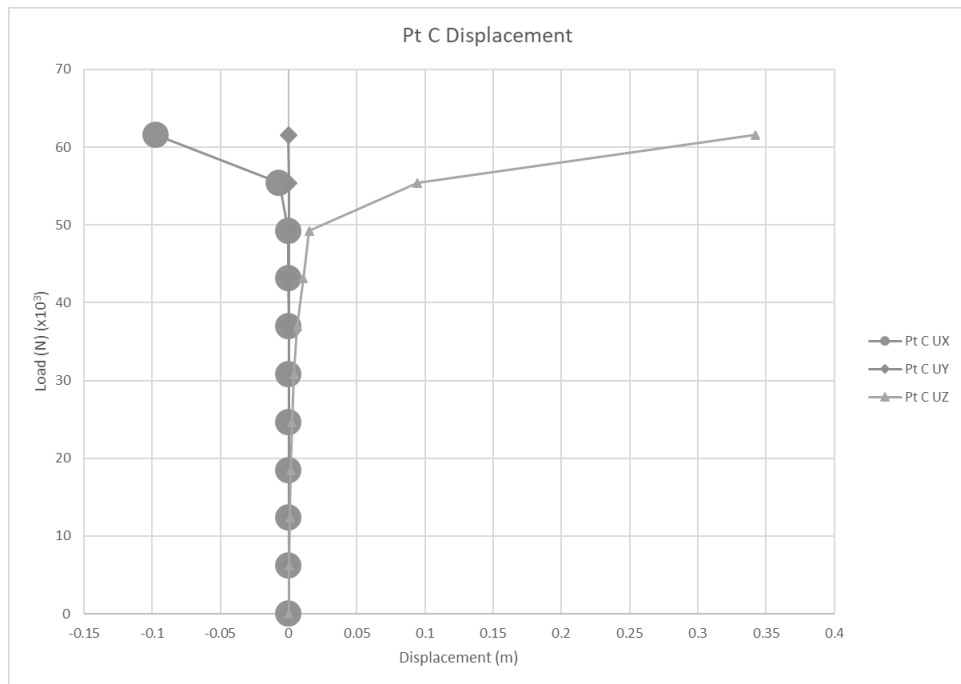
Figure 8.41 Intact Solid Plate with a Fine Mesh Node Displacement at Point C

8.3.3.3   Coarse Mesh Results

Table B.11 presents the data collected from the non-linear analysis and can be found in Appendix B. The load-deflection graph generated from this data is presented in Figure 8.42. The individual graphs for the displacement values generated at points A, B and C are shown in Figures 8.43, 8.44 and 8.45, respectively.
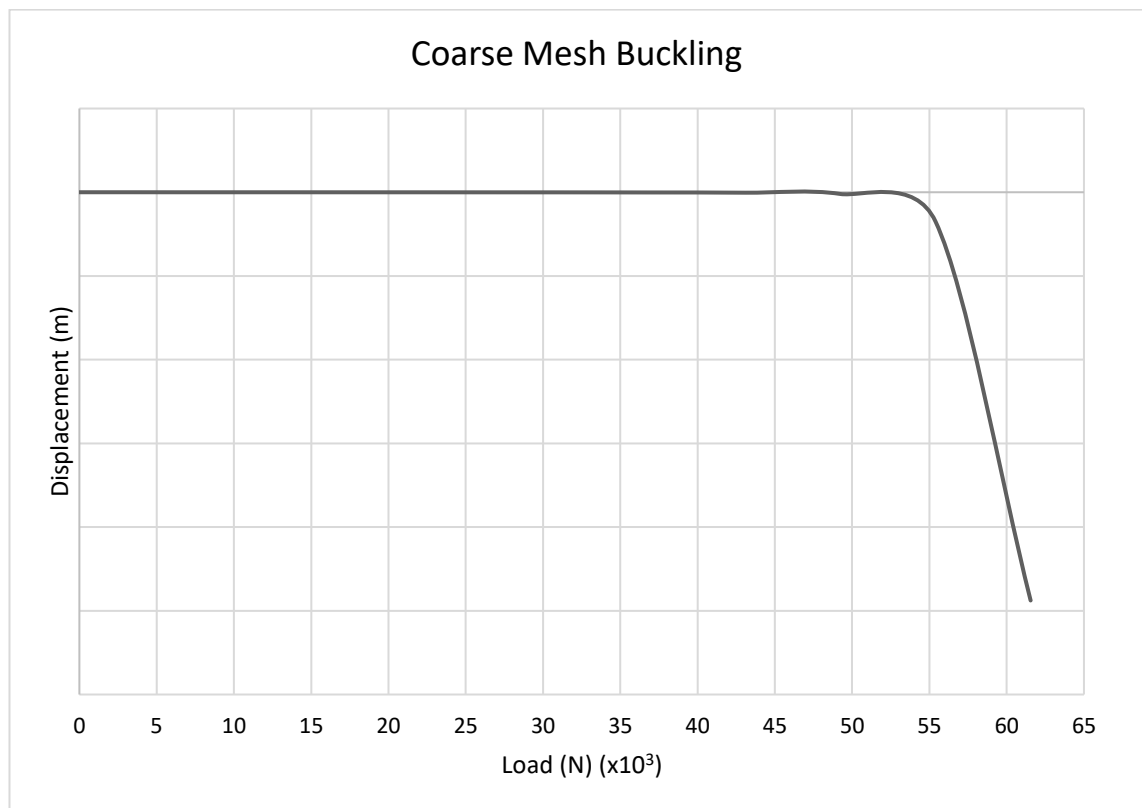
Figure 8.42 Load – Deflection Graph for an Intact Solid Plate with a Coarse Mesh
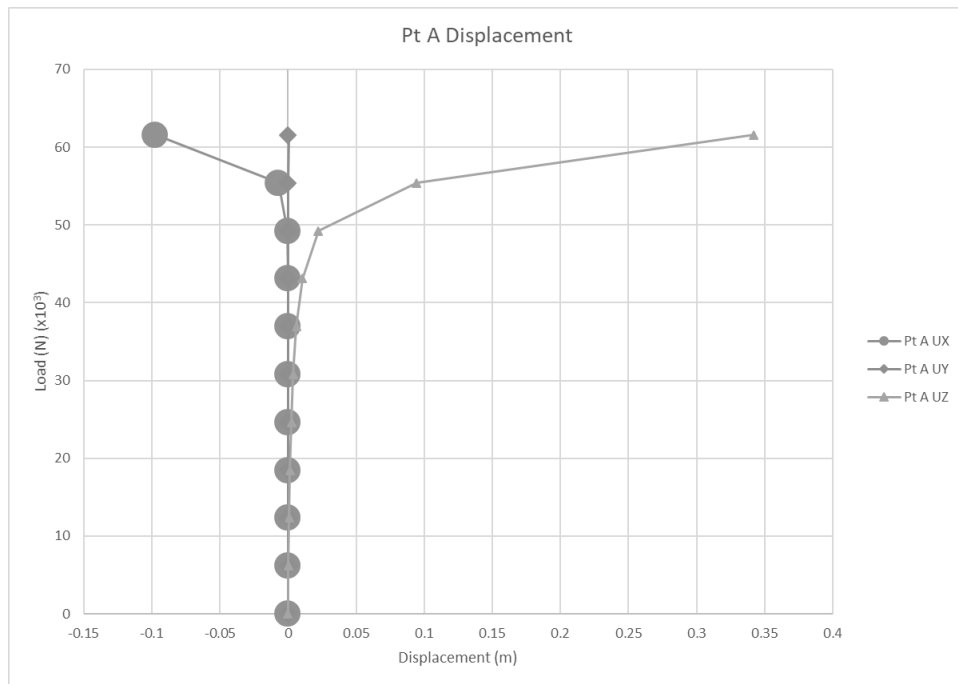
Figure 8.43 Intact Solid Plate with a Coarse Mesh Node Displacement at Point A
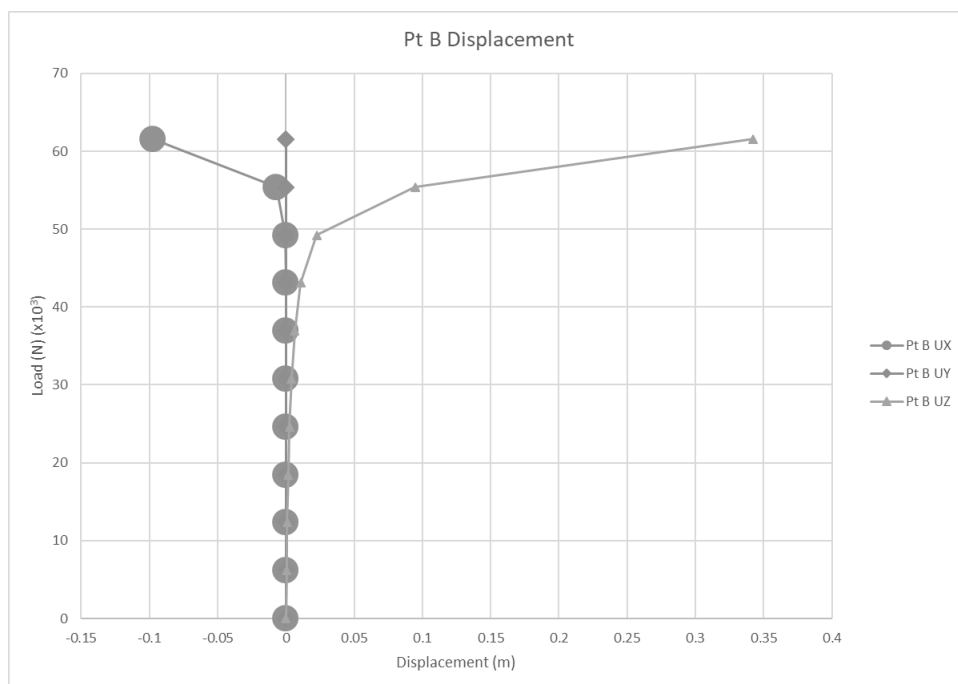
Figure 8.44 Intact Solid Plate with a Coarse Mesh Node Displacement at Point B
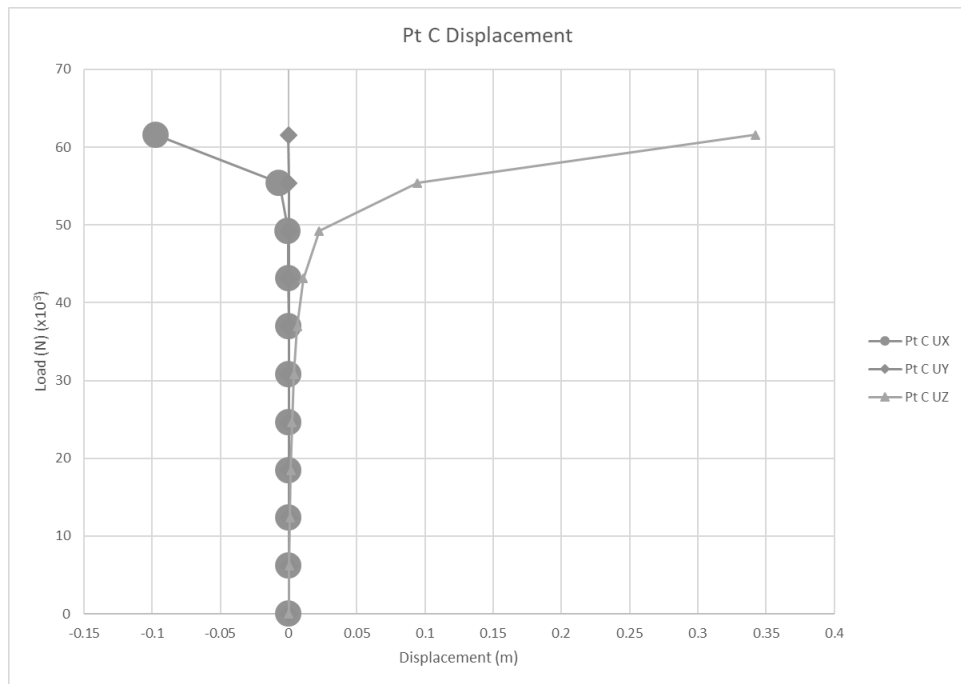
Figure 8.45 Intact Solid Plate with a Coarse Mesh Node Displacement at Point C

8.3.3.4   Very Coarse Mesh Results

Table B.12 presents the data collected from the non-linear analysis and can be found in Appendix B. The load-deflection graph generated from this data is presented in Figure 8.46. The individual graphs for the displacement values generated at points A, B and C are shown in Figures 8.47, 8.48 and 8.49, respectively.
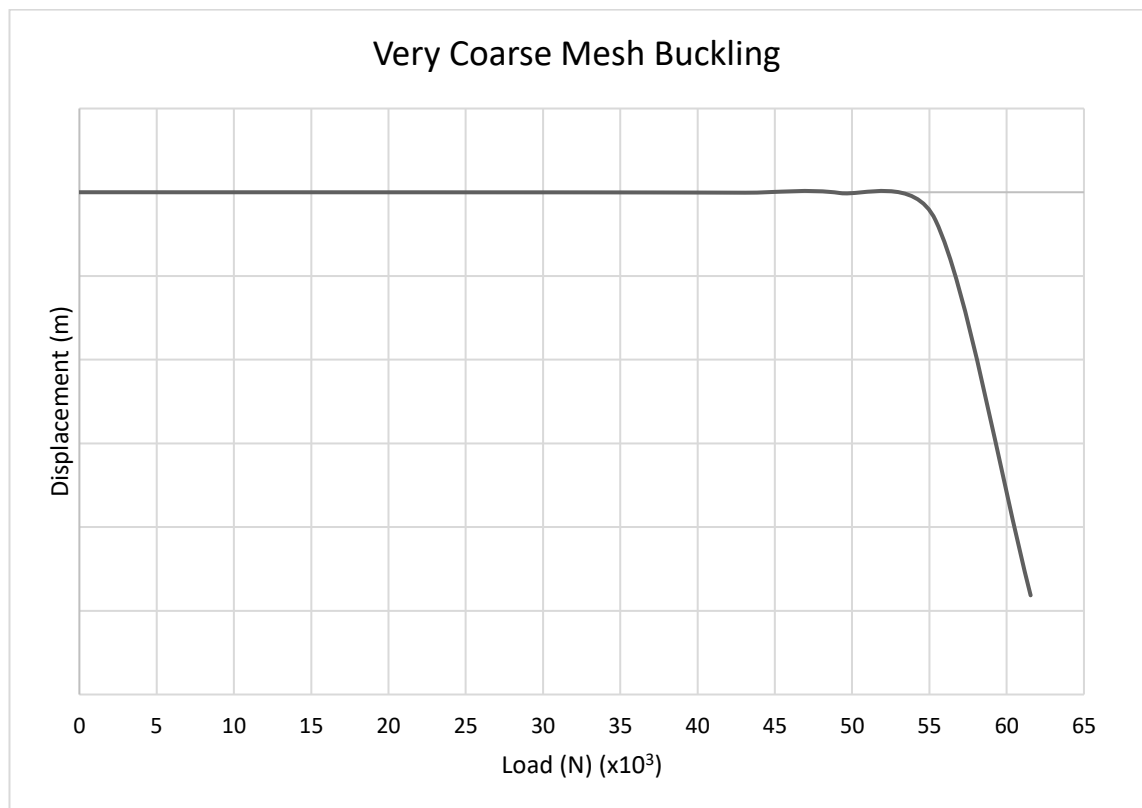
Figure 8.46 Load – Deflection Graph for an Intact Solid Plate with a Very Coarse Mesh
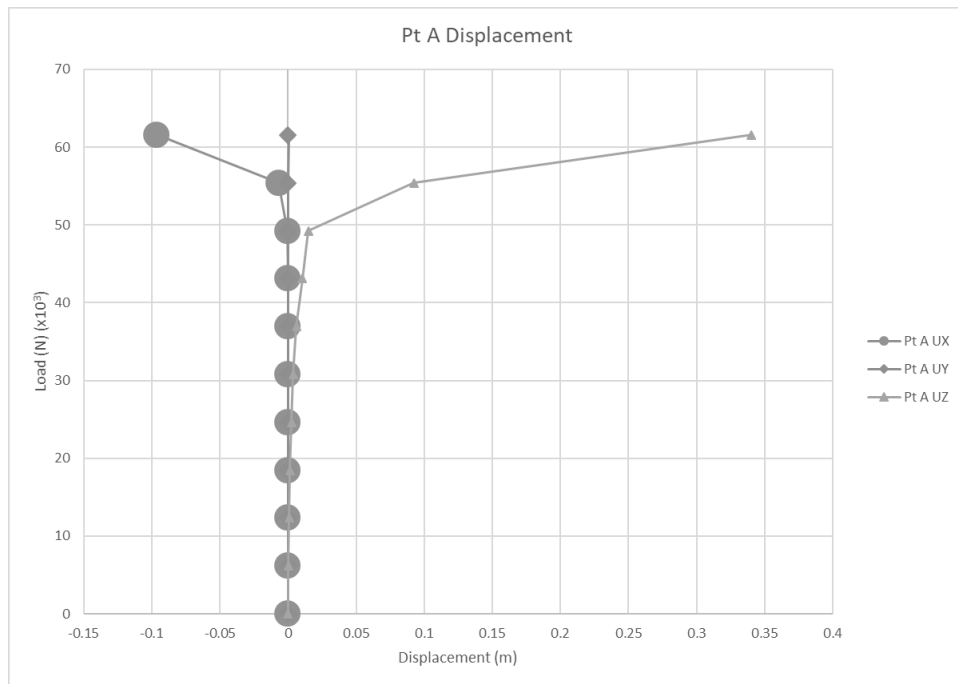
Figure 8.47 Intact Solid Plate with a Very Coarse Mesh Node Displacement at Point A
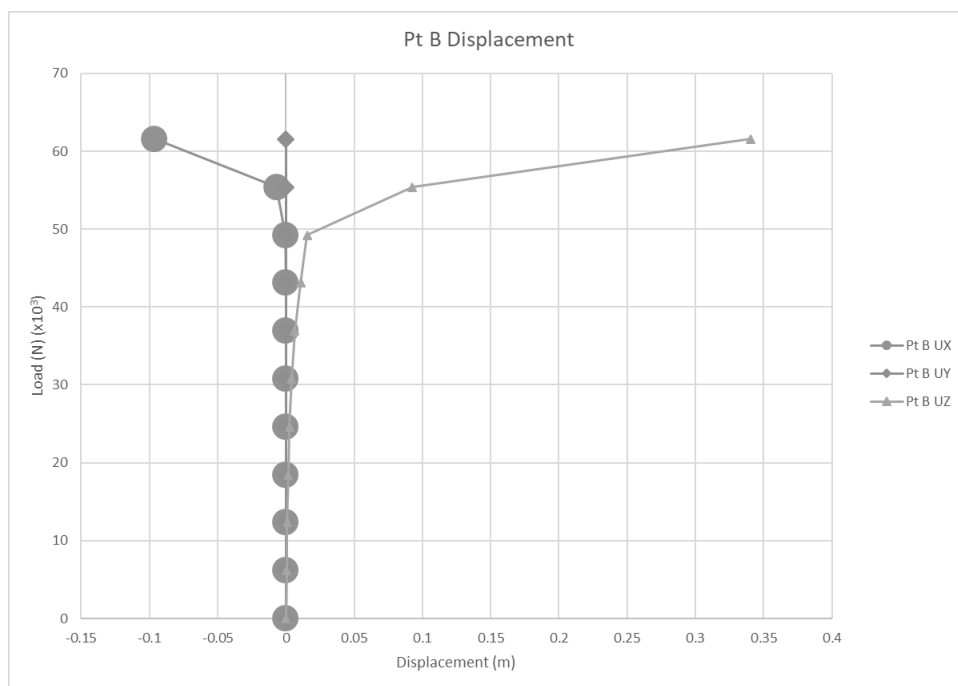
Figure 8.48 Intact Solid Plate with a Very Coarse Mesh Node Displacement at Point B
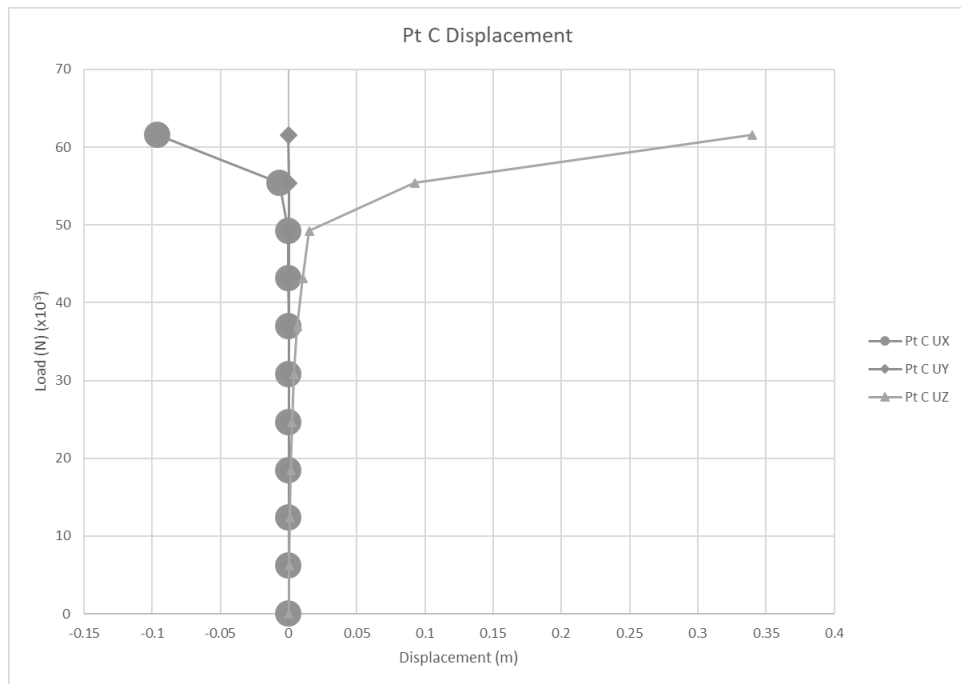
Figure 8.49 Intact Solid Plate with a Very Coarse Mesh Node Displacement at Point C

8.4   Plate with a Hole Solid Convergence Study

In section 8.1 the reasons and the procedure for producing an Eigenvalue buckling value were discussed. In this section, there are no new lines of the written code that need to be discussed so the Eigenvalue buckling code will be presented in full before focussing on how the variation in meshing fineness is applied. There are also no new variations in the code for the non-linear analysis, so again, it will be presented in full before the results are shown.

The full Eigenvalue buckling code is shown in Appendix B as Code B.8 for the 3-D solid plate with a hole with a very fine mesh including the post-processor step to produce the visual check and the actual Eigenvalue buckling result.

8.4.1   Mesh Fineness Variation for the 3-D Plate with a Hole

As mentioned, the fineness of the mesh is the only property altered in the convergence study. For the 3-D plate with a hole SOLID186 model, this requires alterations to three lines of the code to produce the four various options. The sites of the variations are in the sections detailing the line size of the "Outer Line Divisions", "Inner Line Divisions and Spacing" and the "Circle Divisions" section of Code B.8.

As well as changing the title of the code the inserted values of the code as detailed above are altered to one of the four following combinations of options depending on the mesh fineness required:

- Very fine mesh   = 40 – 50 – 20
- Fine mesh   = 30 – 37 – 15
- Coarse mesh   = 20 – 25 – 10
- Very coarse mesh   = 10 – 12 – 5

The results of the Eigenvalue buckling at each mesh fineness is presented in Table 8.5. The results are very comparable so when the total load of 110% and a transverse load of 0.5% were calculated for the non-linear analysis the results for each meshing fineness was the same at -55750 N and 278 N, respectively.

Table 8.5 Eigenvalue Buckling Results for the 3-D Plate with a Hole

Mesh Type	Eigenvalue Buckling Result (N)
Very Fine Mesh	50669
Fine Mesh	50672
Coarse Mesh	50677
Very Coarse Mesh	50718

8.4.2   Non-Linear Analysis for the 3-D Plate with a Hole

The code for the non-linear analysis of the 3-D plate with a hole does not contain any lines of code not seen previously so it is presented in full as Code B.9 in Appendix B with the option for a very fine mesh; please note as before the line sizes must be altered as per section 8.4.1 depending on the fineness of the mesh.

The post-processor code is exactly as before, please see Code B.3 in Appendix B for the full code.

8.4.3   Results for the 3-D Plate with a Hole

The four levels of mesh fineness will be presented in this section where each has a table denoting the displacement values at each time step at each point. A load-deflection graph for each level of mesh fineness is also presented which shows the accuracy of the predicted buckling value to the failure point as expected. If the Eigenvalue buckling value predicted is accurate the graph will show a sudden dip at this load point as the model has buckled and failed. The table discussed will be presented in Appendix B and the figures will be presented in the relevant chapter sub-section.

Three graphs will also be presented to better illustrate the data presented in the table. These graphs show the displacement at each point, A, B and C, at each time step relative to the load applied at each time step. If the coupling applied to the model has been successful each of the three graphs will be identical.

8.4.3.1   Very Fine Mesh Results

Table B.13 presents the data collected from the non-linear analysis and can be found in Appendix B. The load-deflection graph generated from this data is presented in Figure 8.50. The individual graphs for the node displacement values generated at points A, B and C are shown in Figures 8.51, 8.52 and 8.53, respectively.
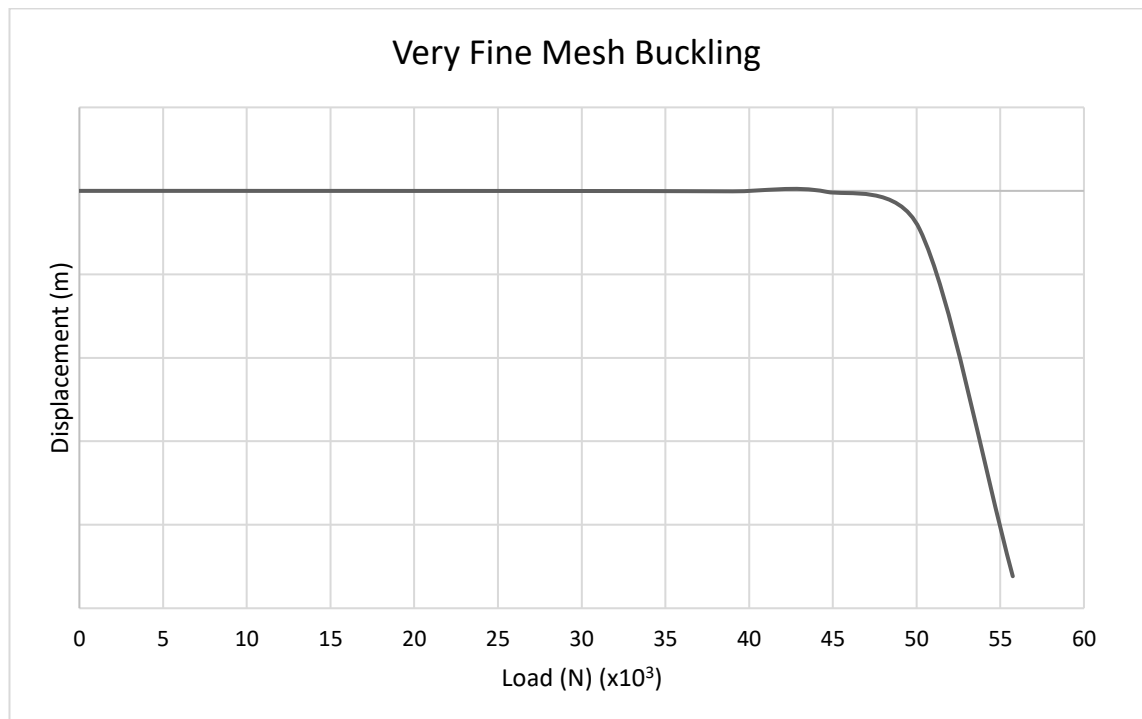
Figure 8.50 Load – Deflection Graph for a Solid Plate with a Hole and a Very Fine Mesh
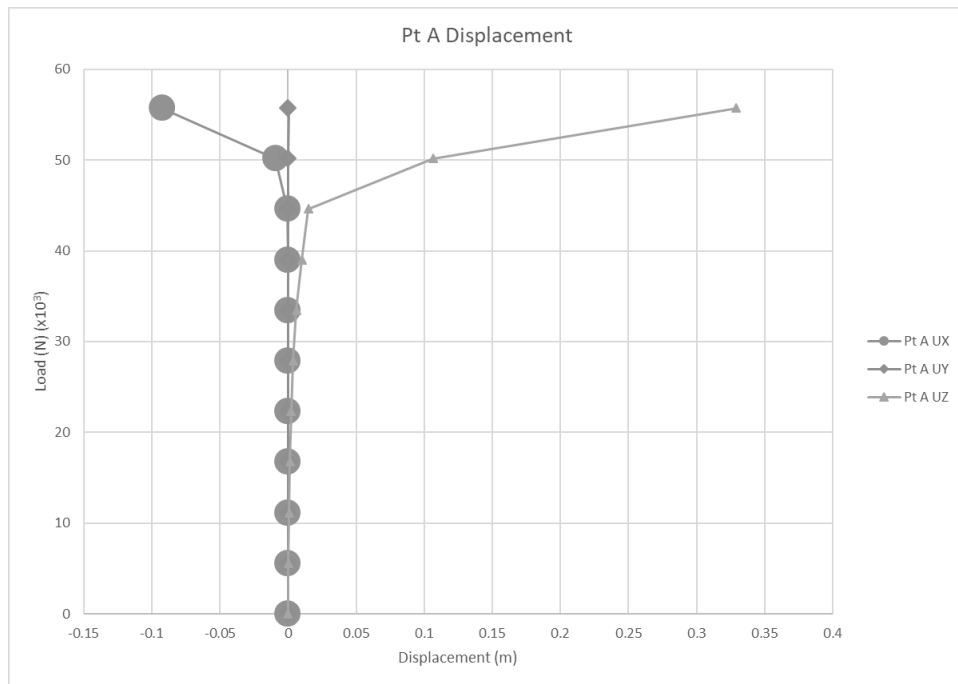
Figure 8.51 Solid Plate with a Hole and a Very Fine Mesh Node Displacement at Point A
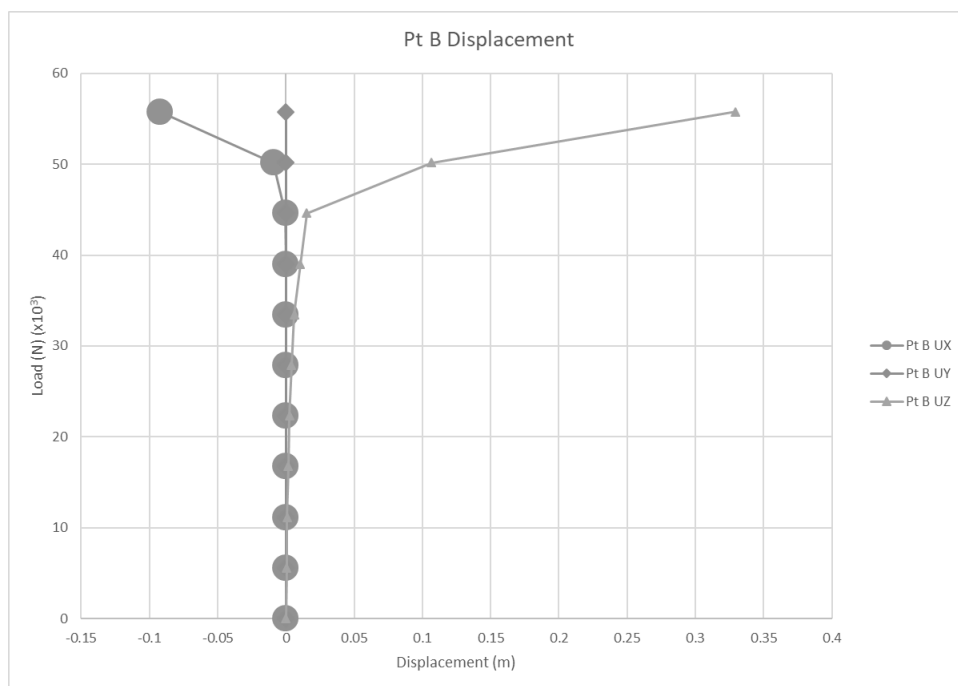
Figure 8.52 Solid Plate with a Hole and a Very Fine Mesh Node Displacement at Point B
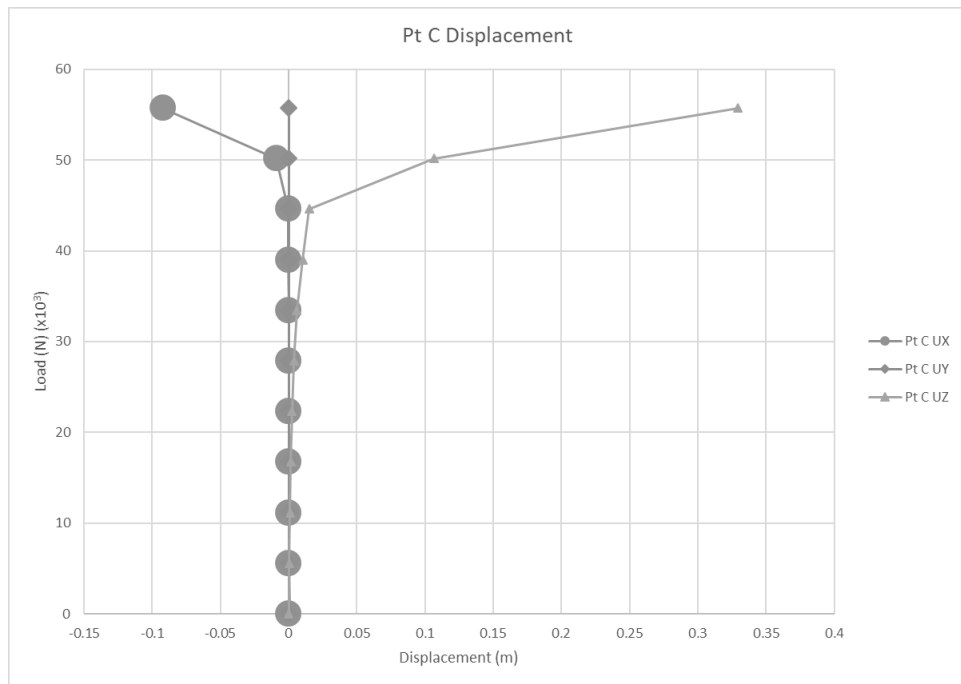
Figure 8.53 Solid Plate with a Hole and a Very Fine Mesh Node Displacement at Point C

8.4.3.2   Fine Mesh Results

Table B.14 presents the data collected from the non-linear analysis and can be found in Appendix B. The load-deflection graph generated from this data is presented in Figure 8.54. The individual graphs for the displacement values generated at points A, B and C are shown in Figures 8.55, 8.56 and 8.57, respectively.
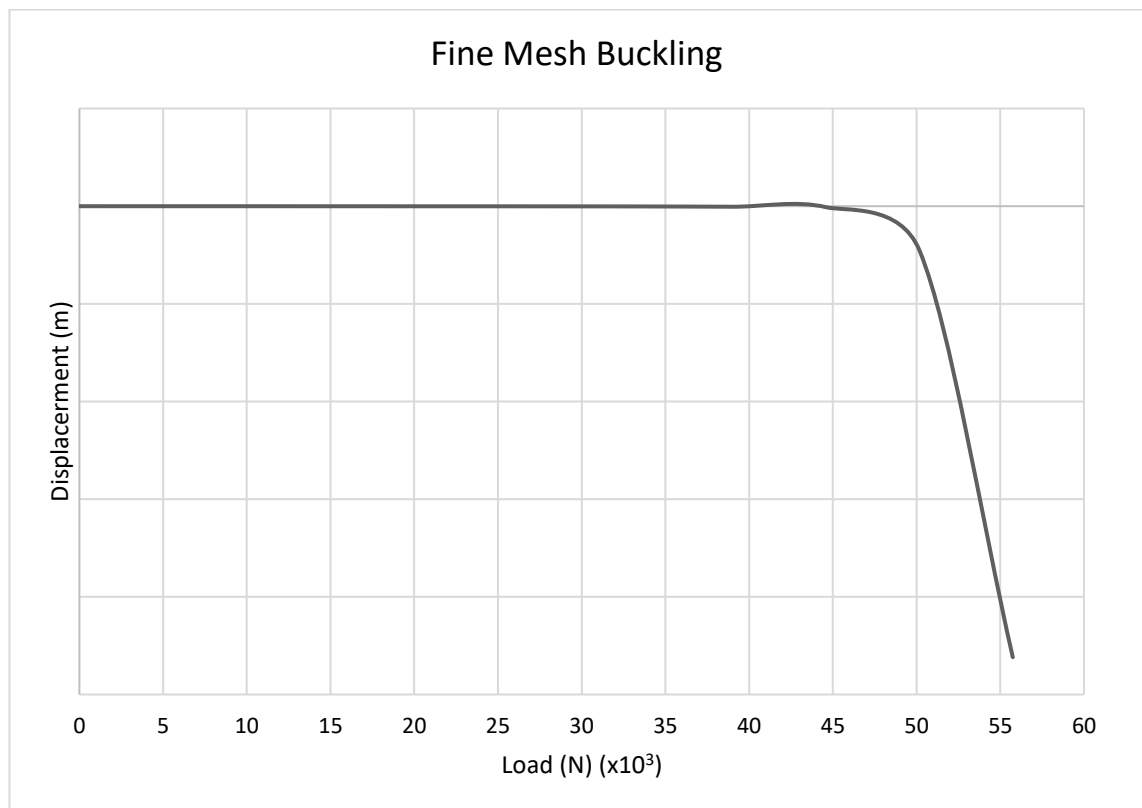
Figure 8.54 Load – Deflection Graph for a Solid Plate with a Hole and a Fine Mesh
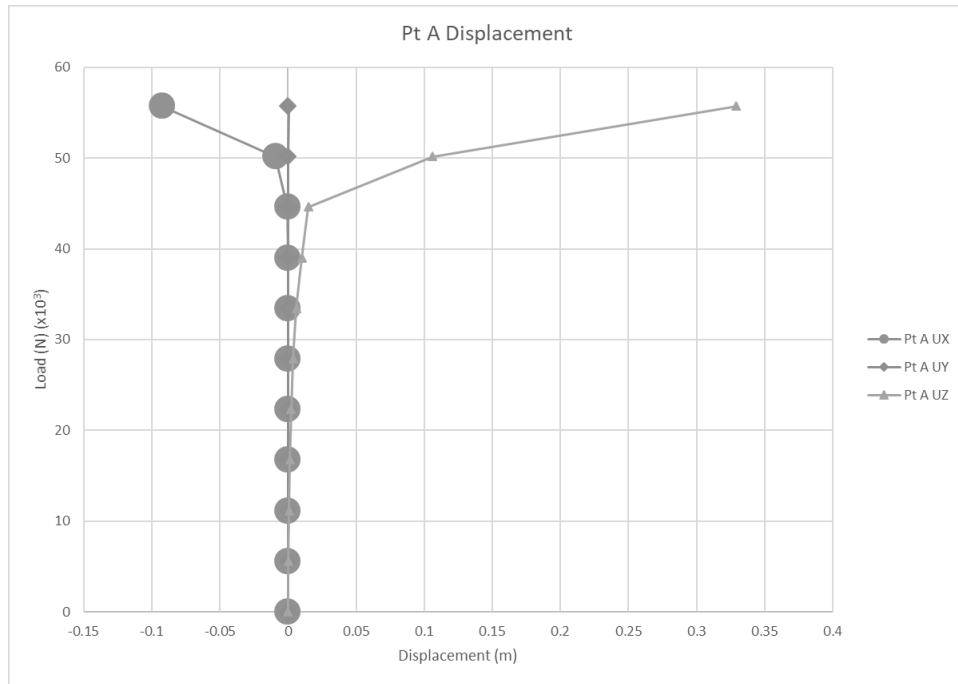
Figure 8.55 Solid Plate with a Hole and a Fine Mesh Node Displacement at Point A
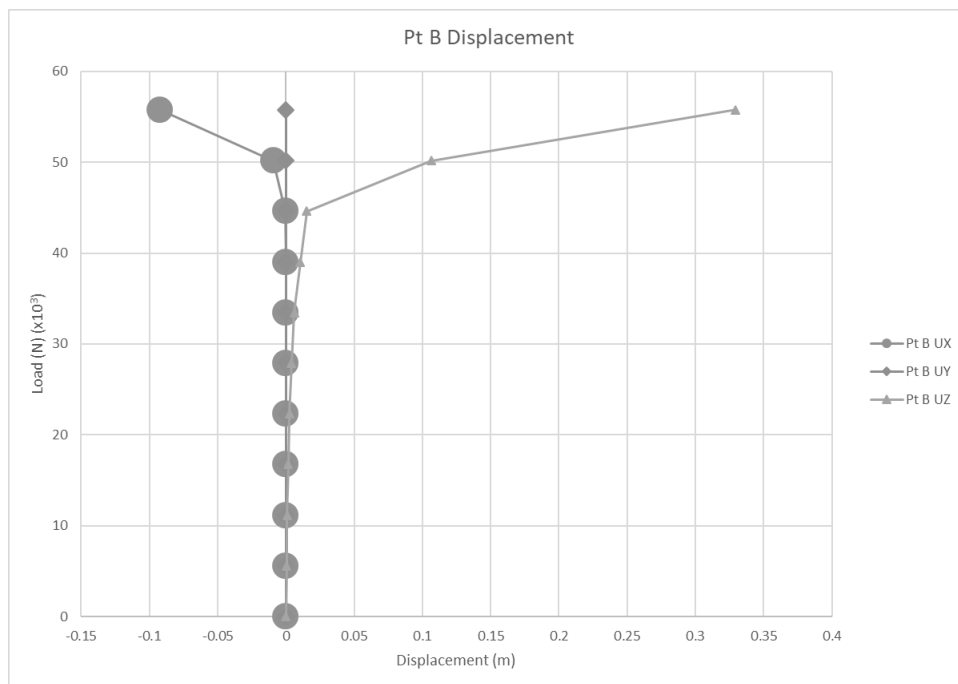
Figure 8.56 Solid Plate with a Hole and a Fine Mesh Node Displacement at Point B
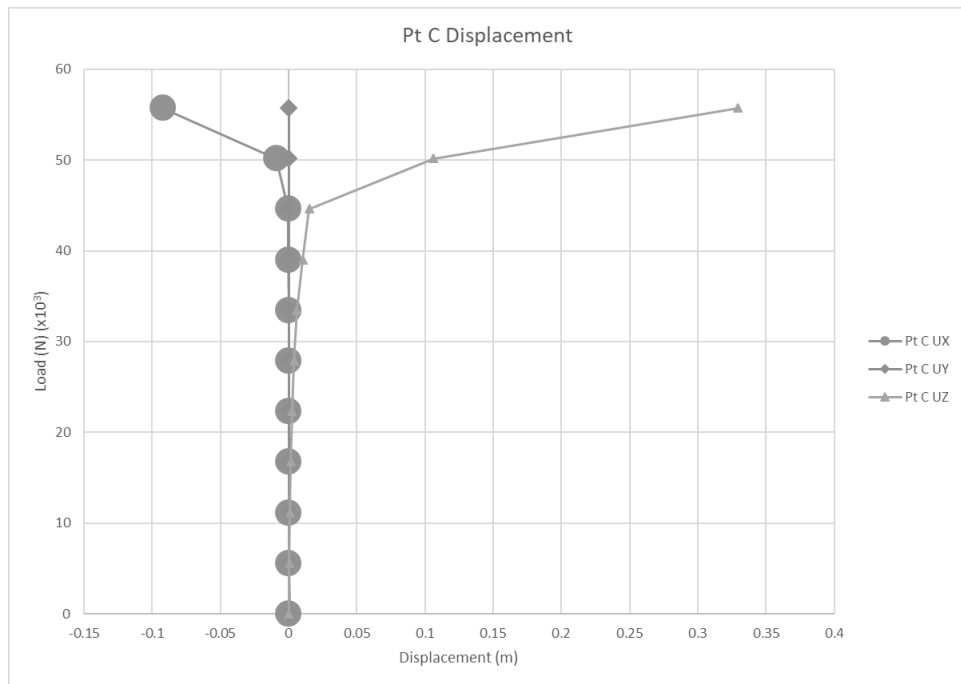
Figure 8.57 Solid Plate with a Hole and a Fine Mesh Node Displacement at Point C

8.4.3.3   Coarse Mesh Results

Table B.15 presents the data collected from the non-linear analysis and can be found in Appendix B. The load-deflection graph generated from this data is presented in Figure 8.58. The individual graphs for the displacement values generated at points A, B and C are shown in Figures 8.59, 8.60 and 8.61, respectively.
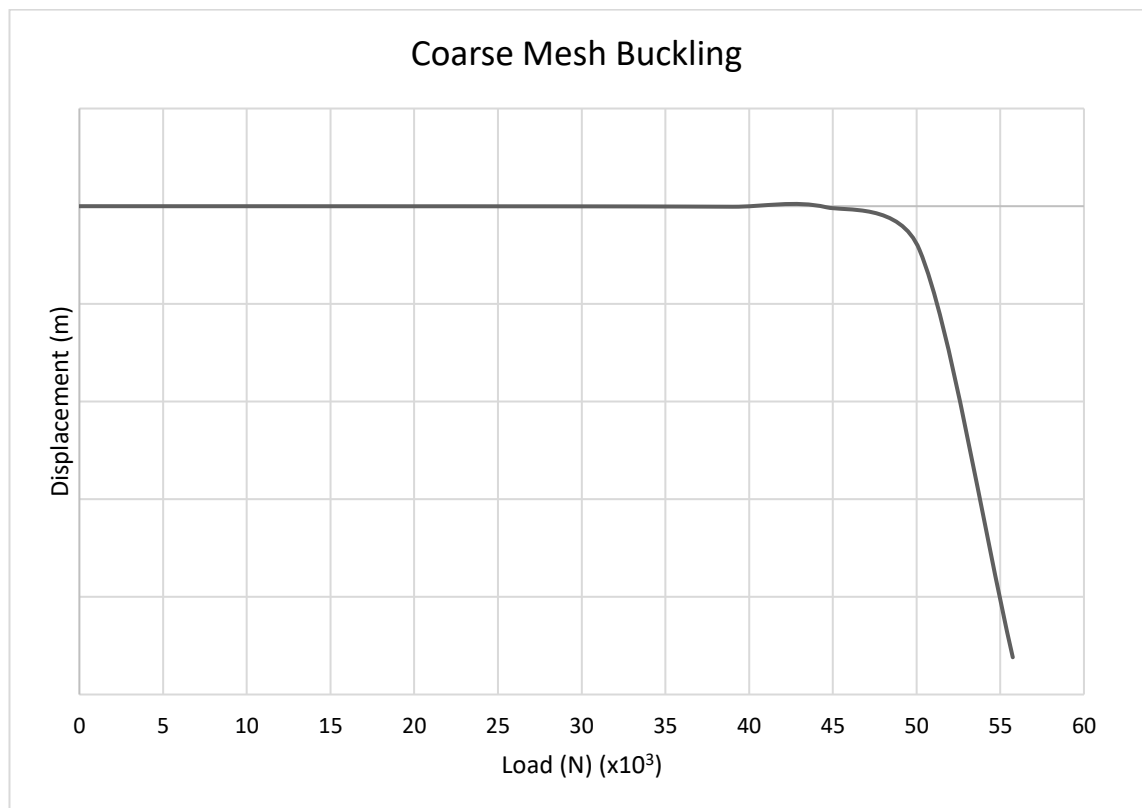
Figure 8.58 Load – Deflection Graph for a Solid Plate with a Hole and a Coarse Mesh
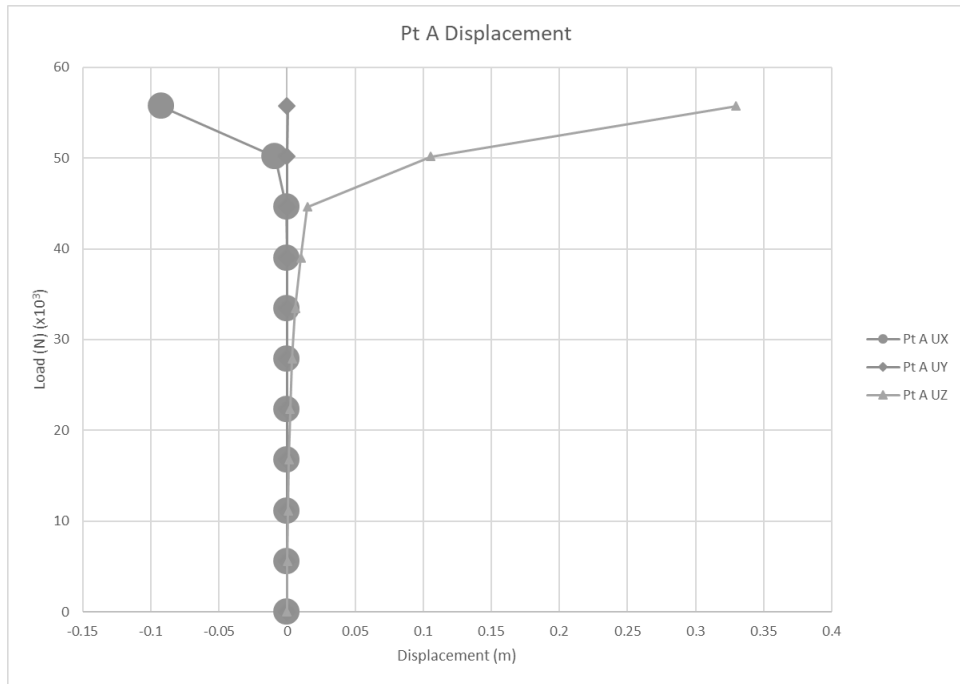
Figure 8.59 Solid Plate with a Hole and a Coarse Mesh Node Displacement at Point A
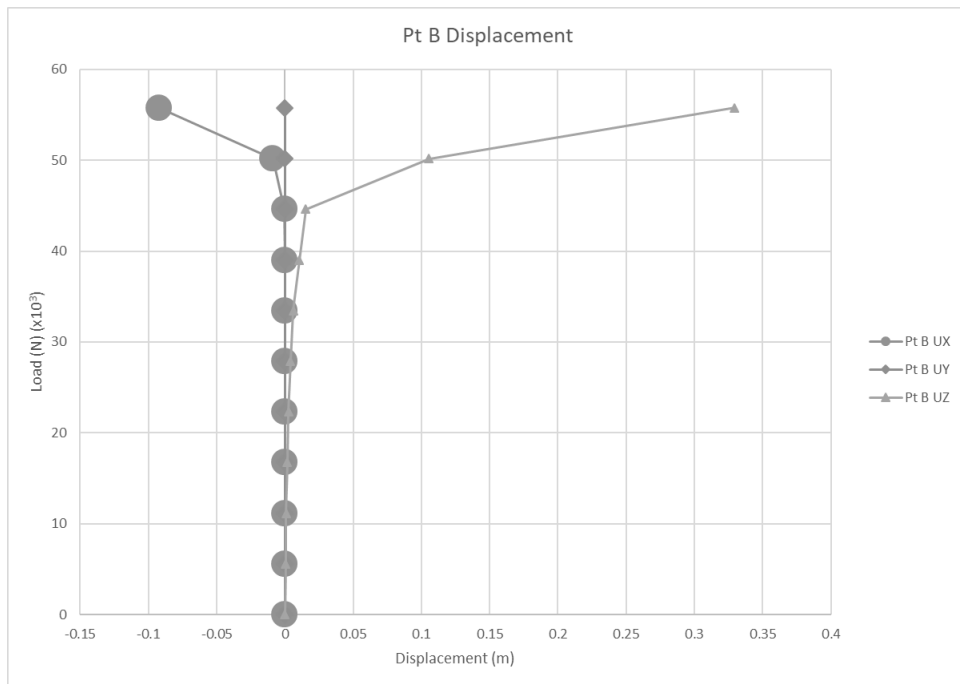
Figure 8.60 Solid Plate with a Hole and a Coarse Mesh Node Displacement at Point B
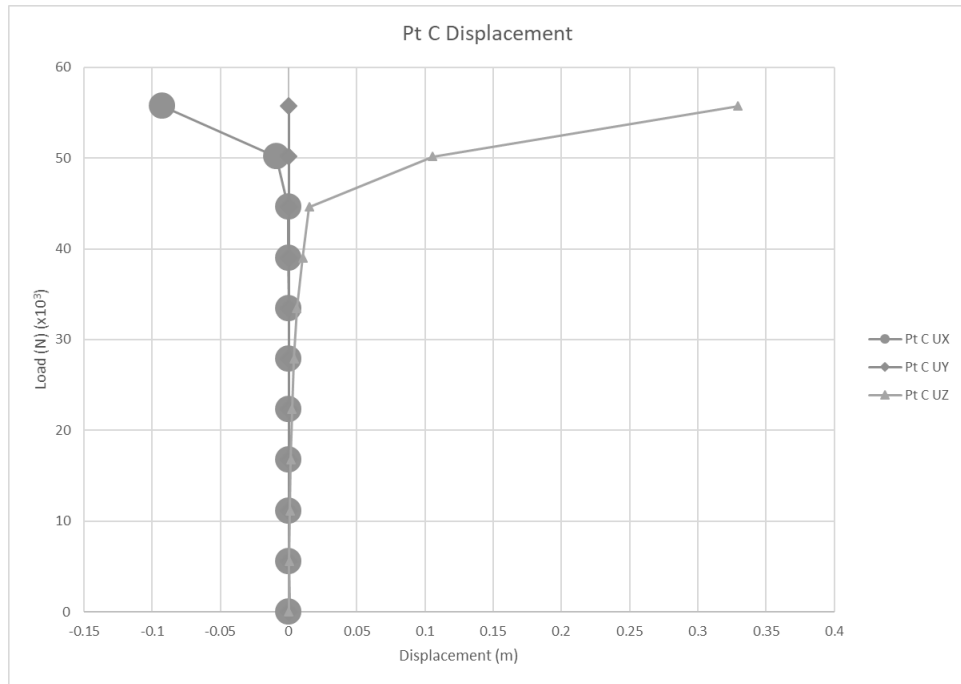
Figure 8.61 Solid Plate with a Hole and a Coarse Mesh Node Displacement at Point C

8.4.3.4   Very Coarse Mesh Results

Table B.16 presents the data collected from the non-linear analysis and can be found in Appendix B. The load-deflection graph generated from this data is presented in Figure 8.62. The individual graphs for the displacement values generated at points A, B and C are shown in Figures 8.63, 8.64 and 8.65, respectively.
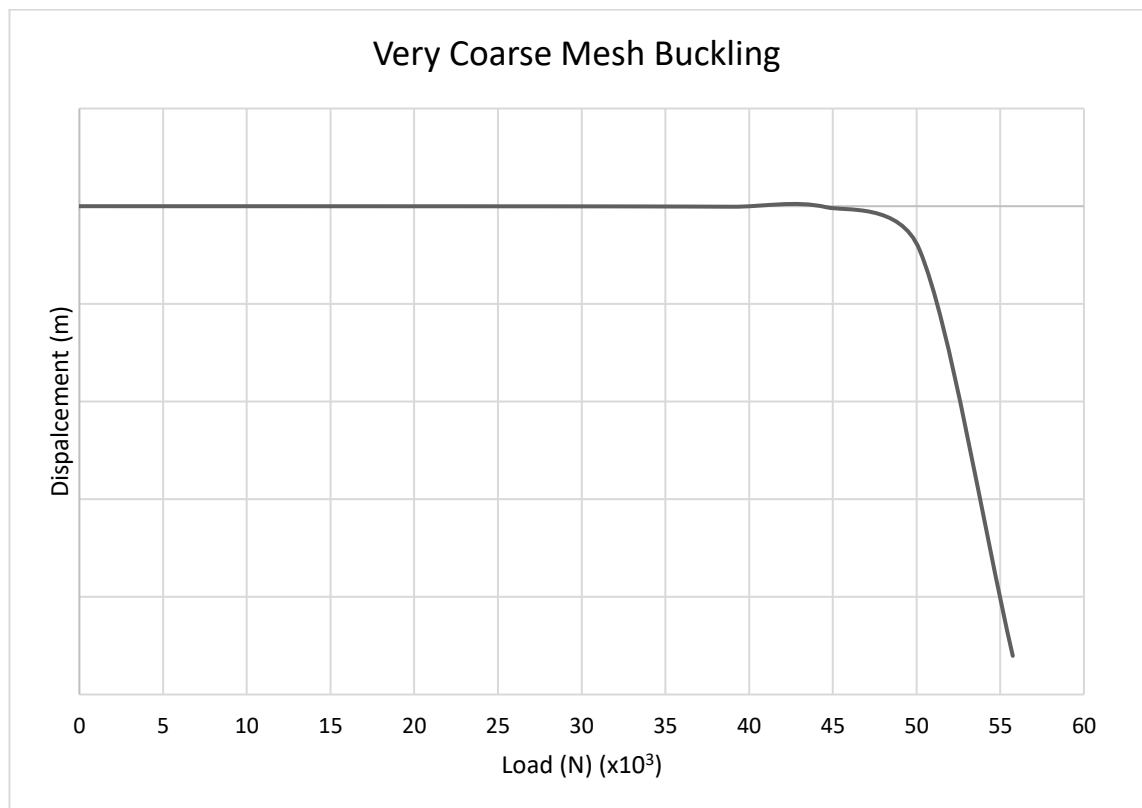
Figure 8.62 Load – Deflection Graph for a Solid Plate with a Hole and a Very Coarse Mesh
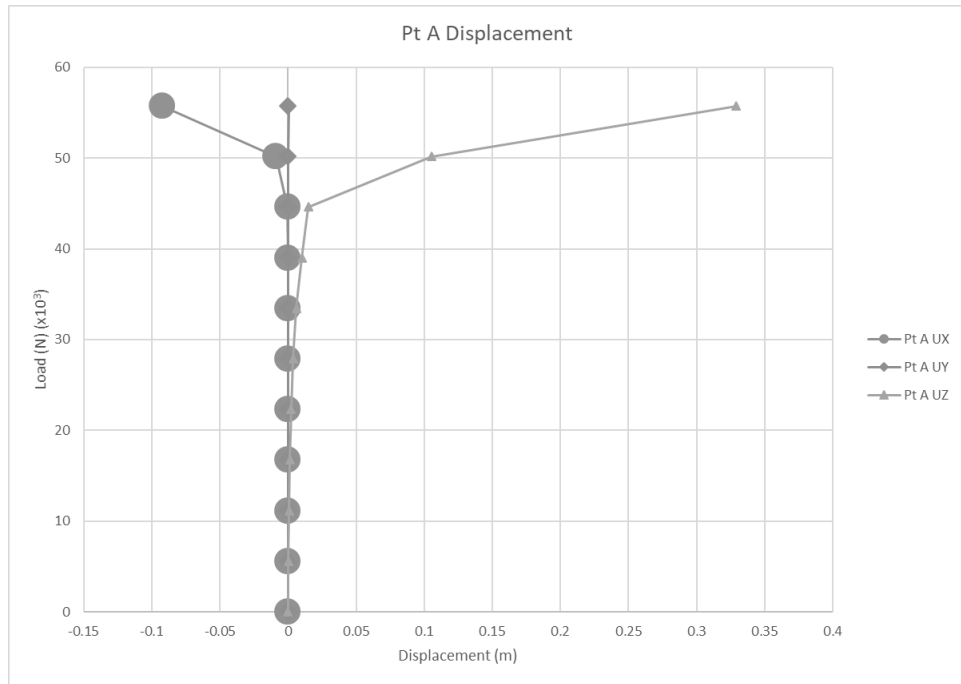
Figure 8.63 Solid Plate with a Hole and a Very Coarse Mesh Node Displacement at Point A
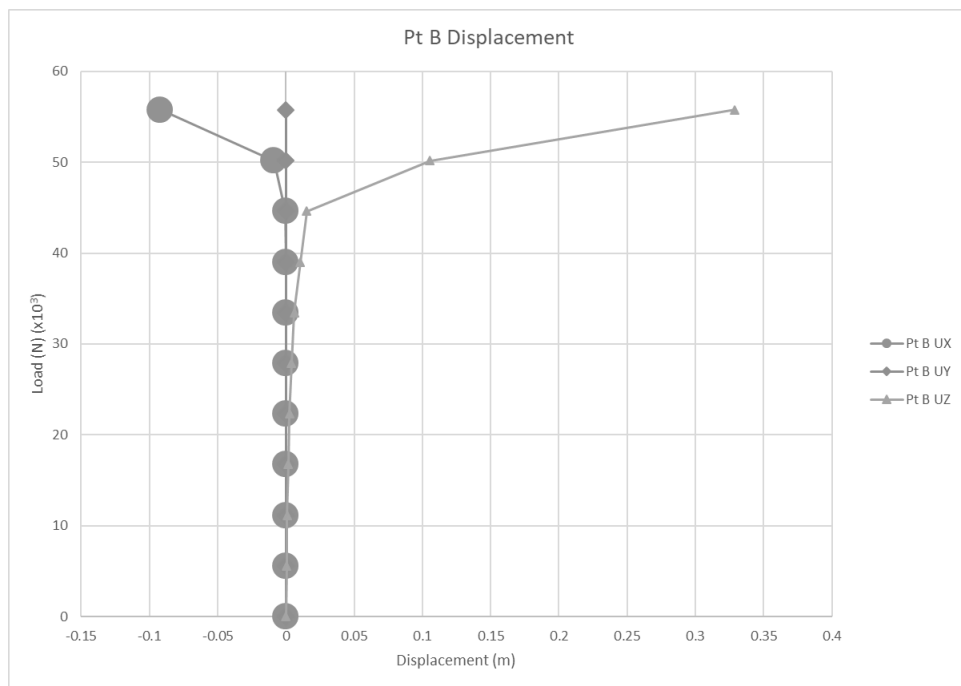
Figure 8.64 Solid Plate with a Hole and a Very Coarse Mesh Node Displacement at Point B
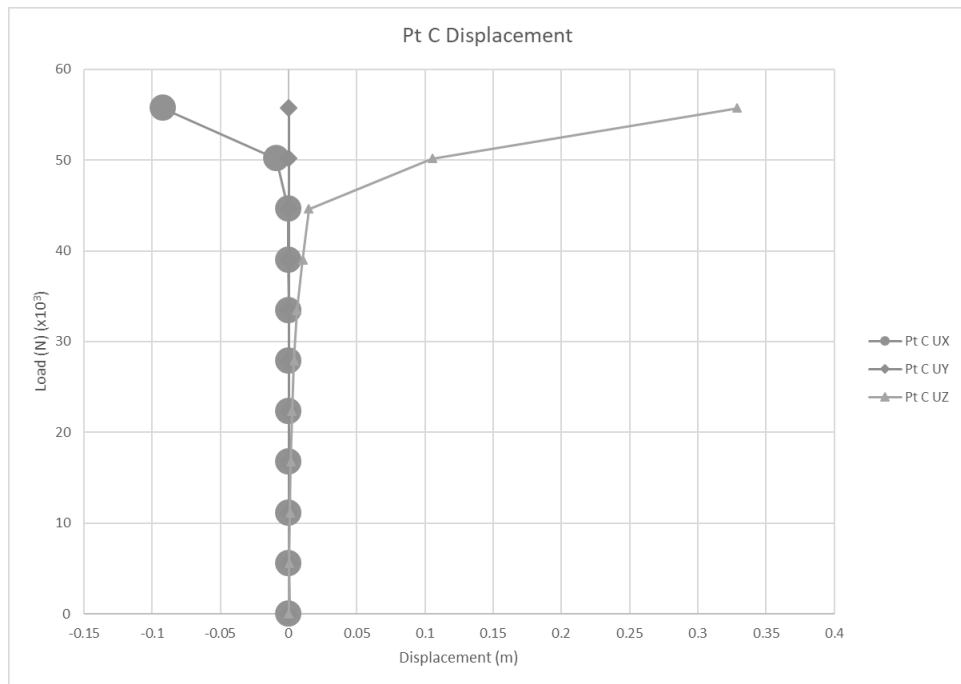
Figure 8.65 Solid Plate with a Hole and a Very Coarse Mesh Node Displacement at Point C

8.5   Result of the Mesh Convergence Study

As can be seen from the results of the mesh convergence study the effect of the coarseness of the mesh has very little impact on the Eigenvalue buckling and the non-linear analysis displacement results generated. It would be recommended to use as fine a mesh as possible that still has an acceptable computation time.

For the 2-D analysis, the fineness of the mesh makes little difference to the overall computation time so the finest mesh is advised for accuracy. In the next chapter, it will be seen that the line division values introduced in this chapter required altering. This was due to the ANSYS programme requiring specific values to ensure the elements in different areas had equal numbers of nodes and could line up correctly. The values are not vastly different but this change should be noted.

The 3-D analysis does incur a slightly longer computation time at finer mesh coarseness's. The minimal increase in the accuracy at these finer mesh levels does not necessarily deem the use of the finer mesh as the most viable option. The 3-D configurations are generally used only as a method of validation for the 2-D models. For this reason, it may be considered acceptable to 3-D model with a finer mesh as in reality there shall be minimal computational runs performed as a validation technique.

It can be seen in the four load-deflection graphs that the point at which the data line suddenly drops is relatively close to the value expected from the Eigenvalue buckling analysis. Therefore, the accuracy of the written code and graphical data is considered sound.

Tables 8.6 and 8.7 summarise the numerical results obtained in the mesh convergence study for each of the plate configurations.

Table 8.6 Summary of the Results of the Mesh Convergence Study for an Intact Plate

Plate Configuration	Mesh Type	2-D Model Eigenvalue Buckling Result (N)	3-D Model Eigenvalue Buckling Result (N)
Intact	Very Fine Mesh	55937	55942
	Fine Mesh	55952	55945
	Coarse Mesh	55990	55953
	Very Coarse Mesh	56184	55984

Table 8.7 Summary of the Results of the Mesh Convergence Study for a Plate with a Hole

Plate Configuration	Mesh Type	2-D Model Eigenvalue Buckling Result (N)	3-D Model Eigenvalue Buckling Result (N)
Plate with a Hole	Very Fine Mesh	50667	50669
	Fine Mesh	50667	50672
	Coarse Mesh	50703	50677
	Very Coarse Mesh	50831	50718

It can be seen that the Eigenvalue buckling data generated by the 2-D and the 3-D models for each plate configuration at the various mesh coarseness levels closely mimic each other which further validates the accuracy of both models and their fitness for use.

The results generated are very similar in buckling value, however, had the results been considerably further apart in magnitude then further analysis of the written codes would be required as either one or both of the models would be considered unsuitable at presenting the relevant details pertaining to the problem for ANSYS to solve.

Comparison of the graphs depicting the node displacement at each of the three points measured in the four models also confirms visually that the coding models are accurate and are effectively presenting the data requested.

Chapter Nine: Insulated Plate Buckling

One of the main objectives of this piece of research was to determine the effect different insulation and protective jacketing materials would have on the expected buckling value of a metal plate subjected to a load. This chapter presents the method developed to research this problem and presents the results from the computational work.

There are five different pit degradation configurations of the steel plate studied in this chapter:

- Fully Intact Plate
- Quarter Depth Pit
- Half Depth Pit
- Three-Quarter Depth Pit
- Plate with a Hole

There are also six different insulation materials configured to insulate the system and as a by-product alter the buckling value:

- Calcium Silicate
- Cellular Glass
- Expanded Perlite
- Fibreglass
- Mineral Wool
- Syntactic Polypropylene

Two protective outer coating materials were also researched:

- Aluminium
- Polycarbonate

The chapter has been separated into three sections each focussing on a different part of the problem. In section 9.1 the code will be introduced along with the alternate sections of code to configure the various plate degradations and insulation system material properties. The geometric and material properties will also be presented in tables in section 9.1.

In section 9.2 the numerical results for the mineral wool insulation material will be presented where an aluminium protective jacket was used. As the results of the other five insulation materials with an aluminium jacket follow a similar pattern of buckling result the raw data tables can be found in Appendix D. The reason mineral wool was chosen to be represented in the main chapter was because it is the most common insulation type currently in use in the real world.

The final section, 9.3, will show the numerical results when a polycarbonate protective jacket was used with the mineral wool insulation. The remaining insulation material raw data tables will also be found in Appendix D.

The raw data tables for the mineral wool with the two protective jacketing options will show the exact values gathered through the Eigenvalue buckling code in ANSYS and these will be found in Appendix C. In the results section of this chapter graphs will be presented to show the effect on the buckling value due to the increasing jacketing and insulation thickness on each of the plate degradation types. There will also graphs comparing and contrasting the effect each plate degradation configuration has at each insulation and jacketing thickness.

9.1   Setup for the Insulated Plate Buckling

As mentioned in the introduction there are five configurations of the steel plate with varying levels of pit deterioration. The fully intact plate has been subjected to no corrosion damage, through deterioration equal to a quarter of the thickness of the plate, to half the thickness, then three-quarters and finally where the corrosion has fully deteriorated a section of the plate leaving a circular hole. Figures 9.1, 9.2 and 9.3 depict the levels of deterioration and also indicate the point at which the load is applied. The nodes along the side where the load is applied are coupled to ensure they displace equally. The boundary conditions associated with the plate are that all the nodes on the side of the plate opposite to the load point are fully constrained and the remaining sides are fully free. These conditions are exactly the same as those presented in Chapter Eight for continuity. Table 9.1 presents the geometric and material properties relating to the steel plate and Table 9.2 provides the material properties for each of the six insulation materials and two protective jacketing materials used in this study.
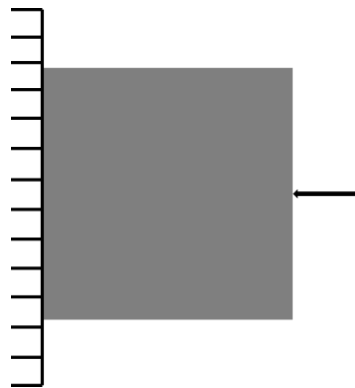
Figure 9.1 Intact Plate Configuration
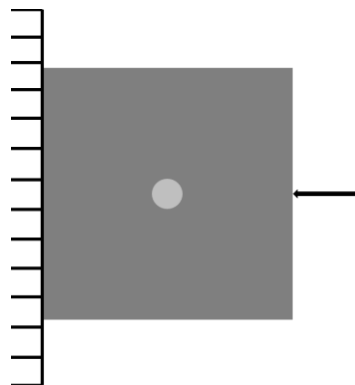
Figure 9.2 Plate Depicting the Three Varying Pit Depths Configuration
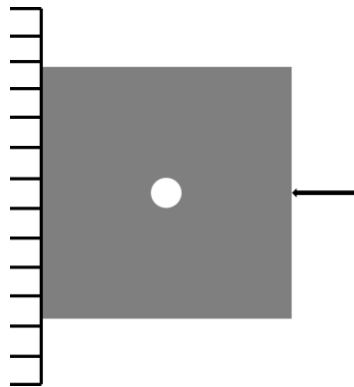
Figure 9.3 Plate with a Hole Configuration

Table 9.1 Steel Plate Geometric and Material Properties

Geometric or Material Property	Value
Plate Width (m)	0.8
Plate Length (m)	0.8
Plate Thickness (m)	0.01
The Shape of the Pit or Hole	Circular
The Diameter of the Pit or Hole (m)	0.1
Young's Modulus (E) (GPa)	205.8
Poisson's Ratio (v)	0.3

Table 9.2 Insulation and Jacketing Material Properties

Material	Young's Modulus (E) (Pa)	Poisson's Ratio (v)
Calcium Silicate	4E9	0.12
Cellular Glass	8E8	0.3
Expanded Perlite	7.563E10	0.182
Fibreglass	7.2E10	0.22
Mineral Wool	5.1E10	0.064
Syntactic Polypropylene	1.0812E9	0.32
Aluminium	6.9E10	0.334
Polycarbonate	2.4E9	0.37

9.1.1   Validation of the Written Code

In previous chapters, 3-D variations of the code were created to model the problem and have then been used to validate the results provided by ANSYS. In this chapter, the method to validate the code was simpler and quicker than in previous chapters as the buckling results for a fully intact plate and a plate with a hole using 2-D shell elements were already documented. In the next sub-section, the modifications to the written codes used to configure each of the plate degradation types and the various insulation system configurations will be presented.

To validate these codes the information regarding the shell thickness was altered so that the sum would equal 0.01 metres as is the plate thickness in the study. With this consideration along with the insulation system properties being altered to provide the information as if there was a hole in the plate or the hole was in fact solid steel allowed for the validation of the model. Figures 9.4 and 9.5 present this idea; the view is from the side of the plate and it has been divided into four equal levels, each level represents one-quarter of the thickness of the plate. The eight outer quadrants are shaded grey to show that they are steel and in Figure 9.4 this is also the case as each of the four levels within the pit area have been modelled as steel. In Figure 9.5 they are white as each of the four levels within the pit area have been modelled as if there is a material with a very small Young's modulus value, computationally this is the equivalent to a hole. Please note these figures are not to scale to allow for easier comprehension of the idea.
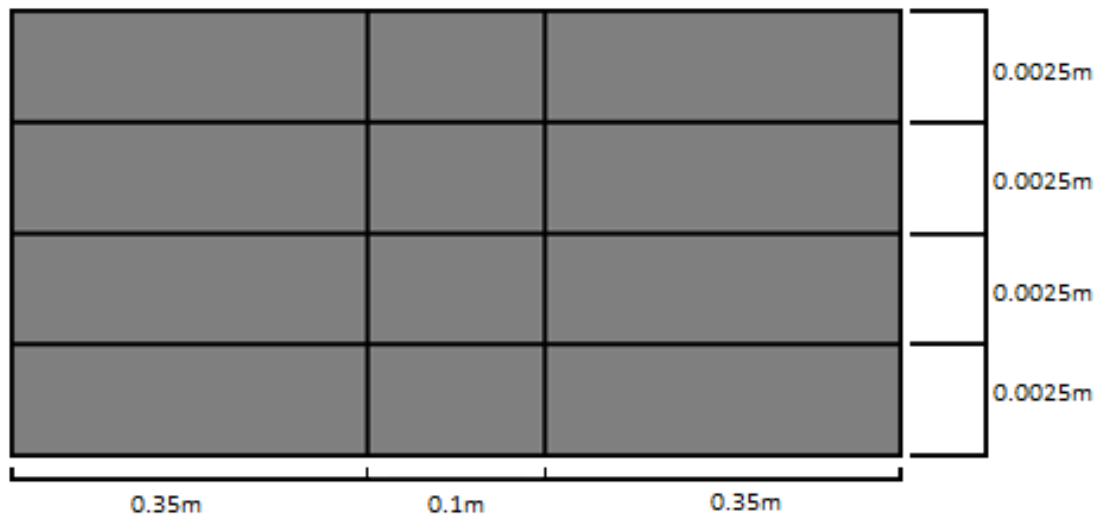
Figure 9.4 Intact Plate Model Validation
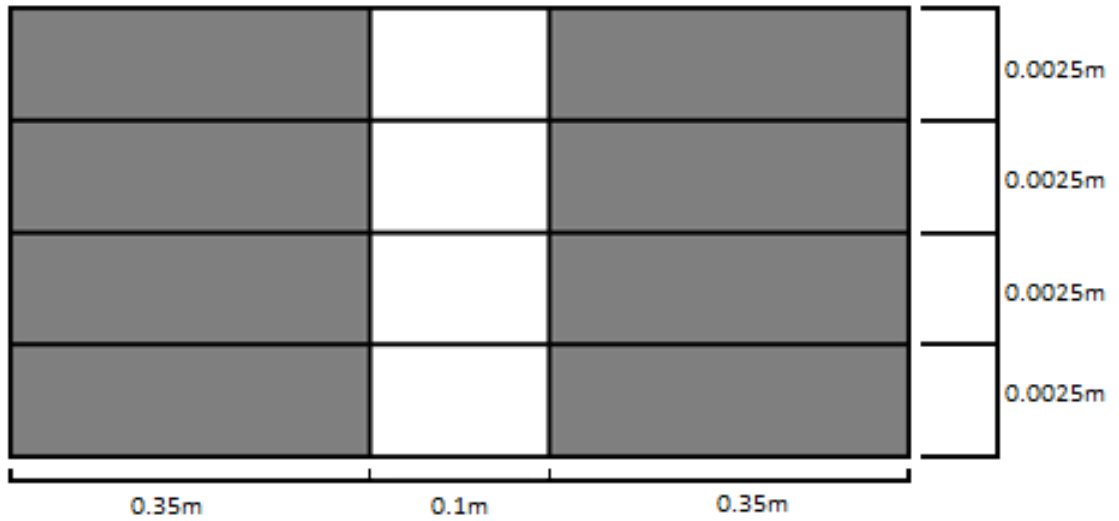
Figure 9.5 Plate with a Hole Model Validation

Using Figures 9.4 and 9.5 as a template to present the theory for this chapter; Figure 9.6 is a representation of a steel plate with a pit equal to three-quarters of the thickness of the plate. The plate has been insulated using a material that is twice the thickness of the plate (0.02 metres) and has a protective material layer that is equal to 40% of the thickness as the plate (0.004 metres). This is an example of one of the many configurations that will be explored later. As before the void is coloured white with steel depicted as grey. The insulation material, mineral wool in this example, is in blue and the protective coating, which is aluminium, is coloured green.
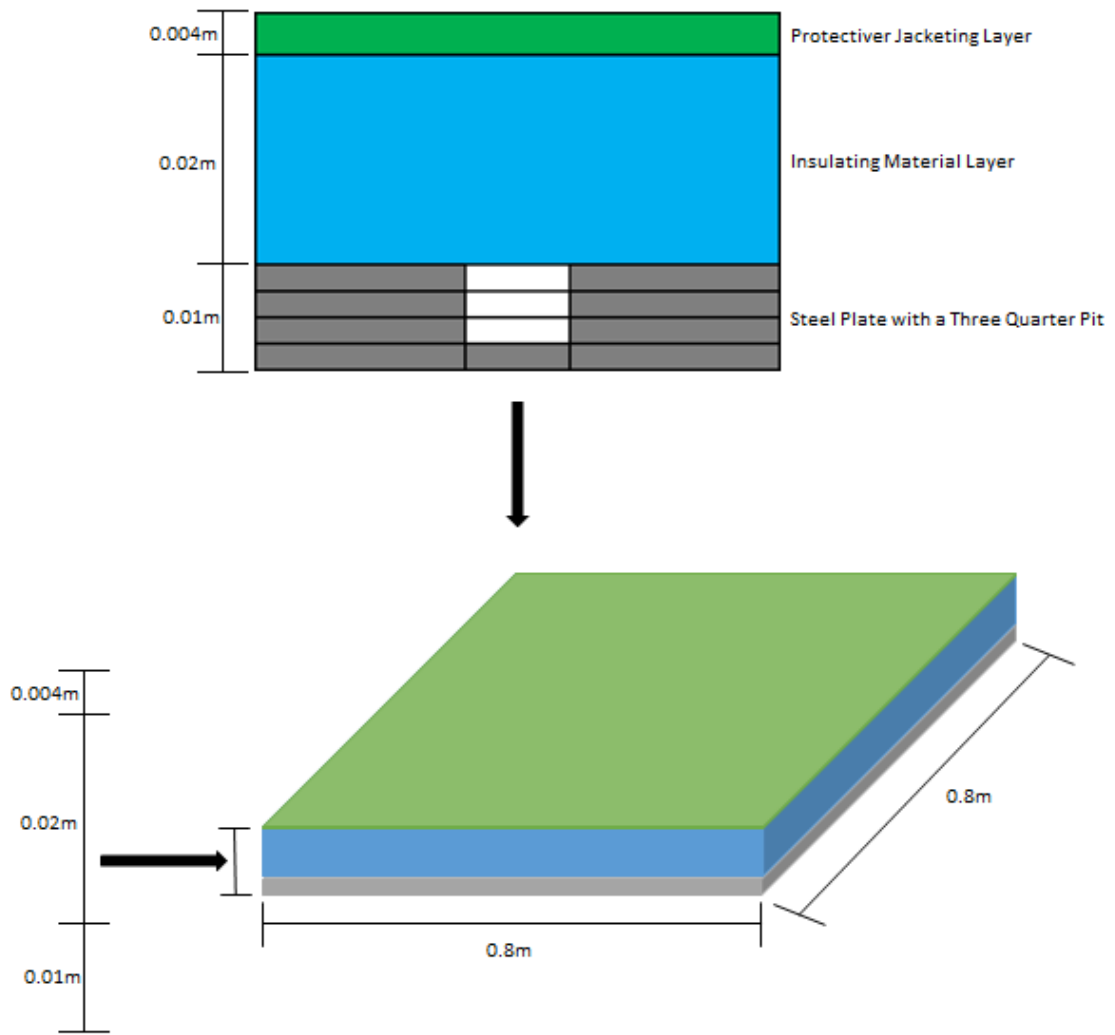
Figure 9.6 Visual Representation of the Theory for the Chapter

9.1.2 Variations in the Code

The code for the example depicted in Figure 9.6 is shown as Code C.1 in Appendix C as a starting point and from there the sections that are altered to model the desired combination of materials and pit configurations will be introduced. As before any new pieces of coding language not previously seen will also be introduced.

The material properties for the insulation and protective jacketing materials are altered depending on the desired materials using the data in Table 9.2. The Young's modulus for the insulation material is inserted into the relevant position with the Poisson's ratio of the insulation material entered into the position below. The jacketing material's Young's modulus is entered with the Poisson's ratio in the section at the bottom. Material one denotes the steel components with material two as the void section of the pit or hole. Material three is the insulation material with the jacketing material indicated by material four.

"SECTYPE,1,SHELL" is the name given to the section of the steel plate that is always present and always remains the same thickness of 0.01 metres. There is no part of this shell section that has the material properties of the void as it is not present. This explains why the coding section shown below omits material two in the "Outer Plate Shell Section ID" and also why the "0.01" in the second line of the code is hard written, it also always remains the same.

Part of the code varies depending on the thickness of the insulation, from a minimum of 0.01 to a maximum of 0.1 regardless of the jacketing material present but both numbers must always be the same. The part in denoting the thickness of the protective jacketing materials and the maximum and minimum differ depending on the material used but again both numbers must be the same. When the material used is aluminium the range is from 0.0005 to 0.0015 and for polycarbonate, it varies from 0.002 to 0.01.

"SECTYPE,2,SHELL" is the part of the code relating to the pit section of the steel plate that is always present but the composition of this section varies depending on the level of pit deterioration that is to be modelled. Table 9.3 details the possible combinations available depending on the pit composition.

Table 9.3 Coding Options to Model Degradation Configuration

Degradation Type	Material One (m) (Steel) (Shaded)	Material Two (m) (Void) (Underlined)
Intact Plate	0.01	Omitted
Quarter Depth Pit	0.0075	0.0025
Half Depth Pit	0.005	0.005
Three-Quarter Depth Pit	0.0025	0.0075
Plate with a Hole	Omitted	0.01

There is only one new section of code to introduce that has not been present in earlier models. The purpose of the code is to inform ANSYS that there are two parts to the model with differing shell configurations. Automatically ANSYS considers the full model to consist of the shell configuration that is denoted as "SECTYPE,1,SHELL", the code informs ANSYS that there is a second configuration and also which areas, in this case, are to be regarded as this second shell configuration, "SECTYPE,2,SHELL".

Figure 9.7 presents an example of the buckling mode shape generated by the ANSYS Mechanical APDL programme using one of the plate configurations discussed in this chapter. It can be seen in the figure that both the original shape (uncoloured area) and the deformed shape (grey area) can be presented together for comparison as viewed from above.
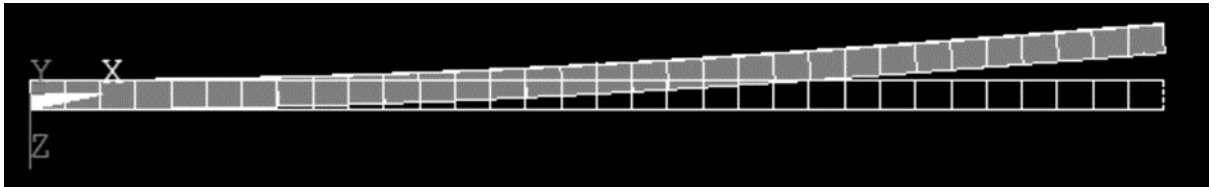
Figure 9.7 Example of the Buckling Mode Shape of an Insulated Plate

9.2   Aluminium Protective Jacketing

In this section, the results from the Eigenvalue buckling analysis will be presented for the mineral wool insulation material where the system has an aluminium protective jacketing. The plate was configured at each of the five degradation levels discussed previously.

A table presenting the raw buckling data in its entirety for the mineral wool insulation system can be found as Table C.1 in Appendix C. A number of graphs will be produced and shown in this section from the data in Table C.1 to represent these results and to illustrate the following variables:

- Effect of increasing jacketing thickness
- Effect of increasing insulation thickness
- Comparison of buckling values at each insulation thickness depending on the plate degradation
- Comparison of buckling values at each jacketing thickness depending on the plate degradation

The geometric and material properties of the plate have remained constant and these details can be found in Table 9.1. The material properties for each of the six insulation and two jacketing materials are provided in Table 9.2. Please pay close attention to the axes values as they may change drastically so as to give the best overall indication of the piece of information described.

Figures 9.8 to 9.12 depict the effect of the increase in jacketing thickness on each of the five plate degradation configurations. It can be seen at the bottom of each graph there is a plot that spans the full width, this plot denotes the buckling value of the plate configuration where there is no insulation system providing additional strength. The jacketing thickness increases from 0.0005 metres as a minimum up to 0.0015 metres at the largest thickness.

In the case of the plate with a hole this value is 50667 N, with a three-quarter depth pit it is 53141 N, a half depth pit equals 53246 N, a quarter depth pit is 54135 N and finally a fully intact plate equals 55937 N. As would be expected the buckling value increases as the level of degradation of the plate decreases. The degradations cause the plate to lose some of its inherent structural strength.

The expectation with regards to the addition of an insulation system would be that the buckling strength of the plate would increase which is exactly as the results show. As the thickness of the protective coating increases, there is a minor increase in the buckling strength value when compared to the more significant increase in buckling strength value noted as the insulation thickness is increased.

Figures 9.13 to 9.17 depict the effect of increasing the thickness of the insulation on each of the plate degradation configurations. These latter figures show a much larger relative rise in the buckling value where the insulation thickness increases at each jacketing thickness. The minimum insulation thickness measured is 0.01 metres ranging up to 0.1 metres at the largest value. As before, it can be seen at the bottom of each graph there is a plot that spans the full width, this plot denotes the buckling value of the plate configuration where there is no insulation system providing additional strength.

As an example, when looking at Figure 9.8, it can be seen that with an insulation thickness of 0.1 metres the buckling value where the jacketing thickness is 0.0005 metres is 209,610 N. At the same insulation thickness but after increasing the thickness of the jacketing to the maximum of 0.0015 metres the new buckling value is 251,790 N. The only parameter that has changed is the thickness of the protective jacketing and with that, the buckling value has increased as expected.

This increase is relatively modest when compared to another example when looking a Figure 9.13, which will depict the increase in buckling through an increase in insulation thickness. Where the jacketing thickness is 0.0005 metres and the insulation thickness is 0.01 metres the buckling value is 209,610 N as before. If instead of increasing the jacketing thickness the insulation thickness is increased only one level up to 0.02 metres the new buckling value is 666,710 N.

If the insulation thickness were to be increased to the maximum value of 0.1 metres the new buckling value would be 26,739,000 N. These numbers are clearly only theoretical as it is highly unlikely that any system would ever be insulated in this way but it was felt that it would be sensible to continue up to these system configurations as a way of testing the written model codes to see if there was a point at which they lost their viability.

In the next chapter, the Euler Formula will be used as a method to validate the results. This formula, shown in Equation (10.1) of Chapter Ten, can also be used to explain the large values generated in the plate results here. As the thickness of the insulated plate increases the moment of inertia also increases which means that the system is considered to be much stiffer. So, although this chapter deals with plates rather than columns the theory still holds as the plate could be considered to be a column that has been split lengthwise and then flattened. This formula will be explained in more detail in the next chapter.

In Appendix D it can be seen that despite the varying material properties and therefore the overall measured buckling values the patterns remain similar. The effect of increasing the thickness of the jacketing does increase the buckling value but to a much lesser degree than increasing the thickness of the insulation.

Figure 9.8 Effect of Increasing Jacketing Thickness – Plate with a Hole
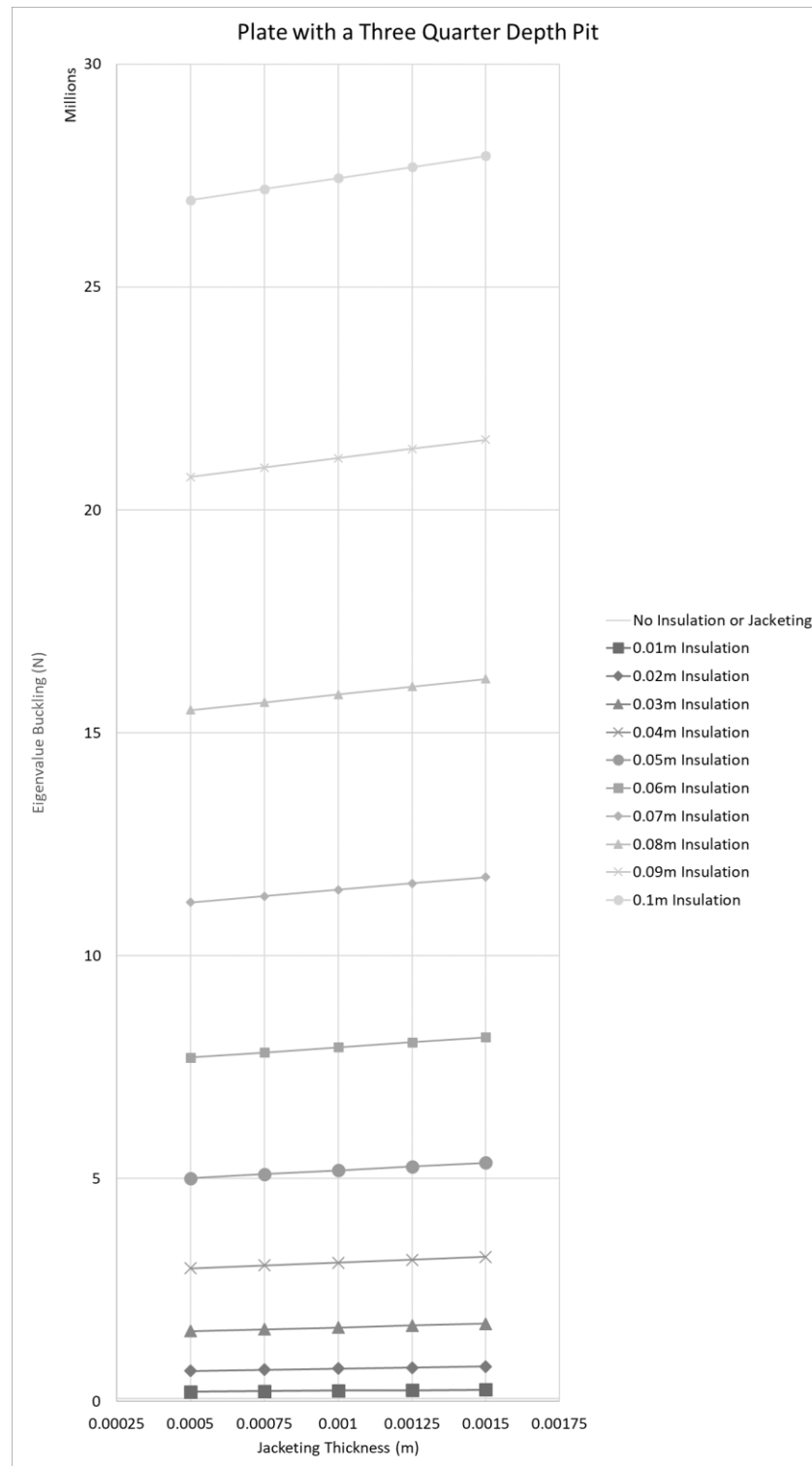
Figure 9.9 Effect of Increasing Jacketing Thickness – Plate with a Three-Quarter Depth Pit
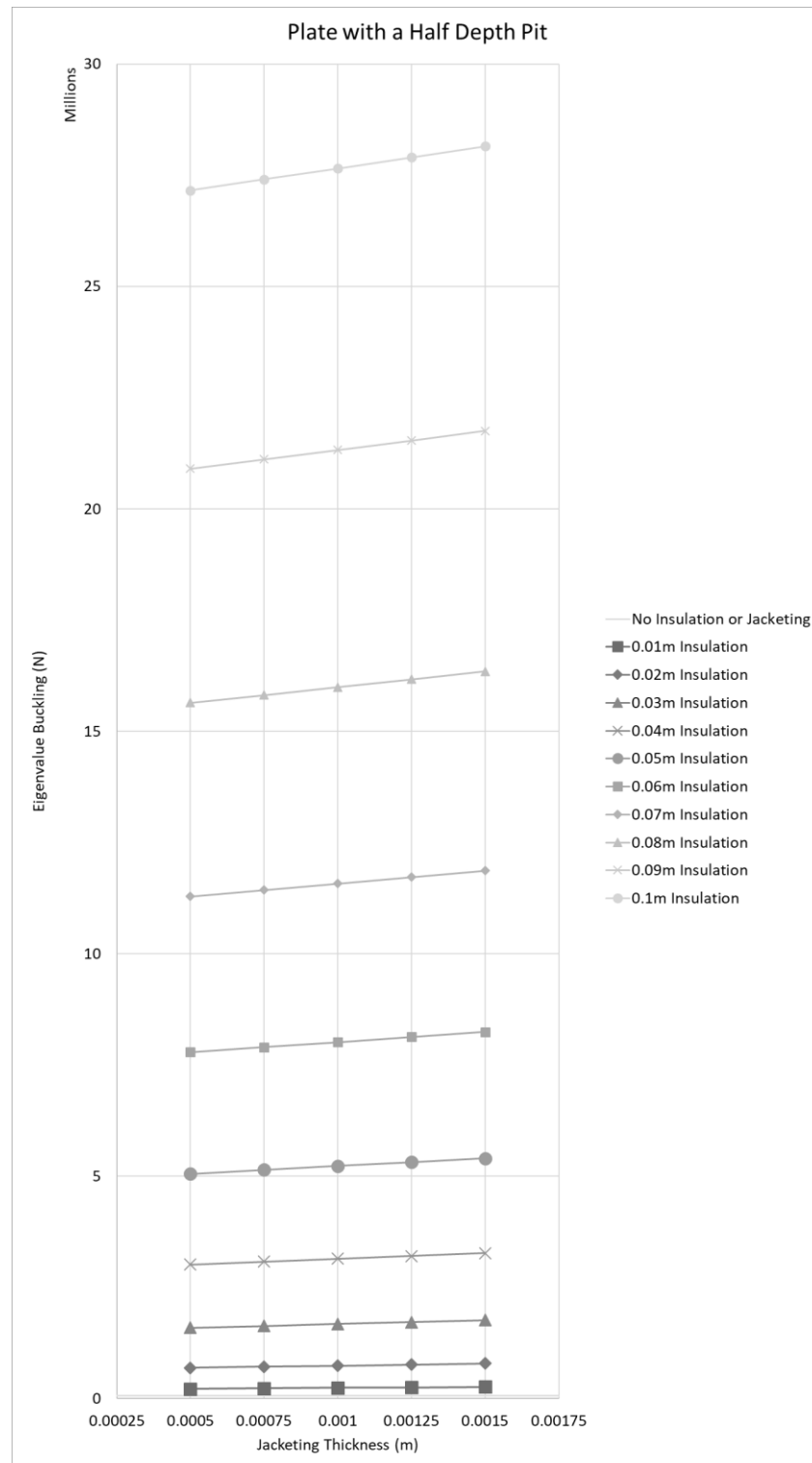
Figure 9.10 Effect of Increasing Jacketing Thickness – Plate with a Half Depth Pit
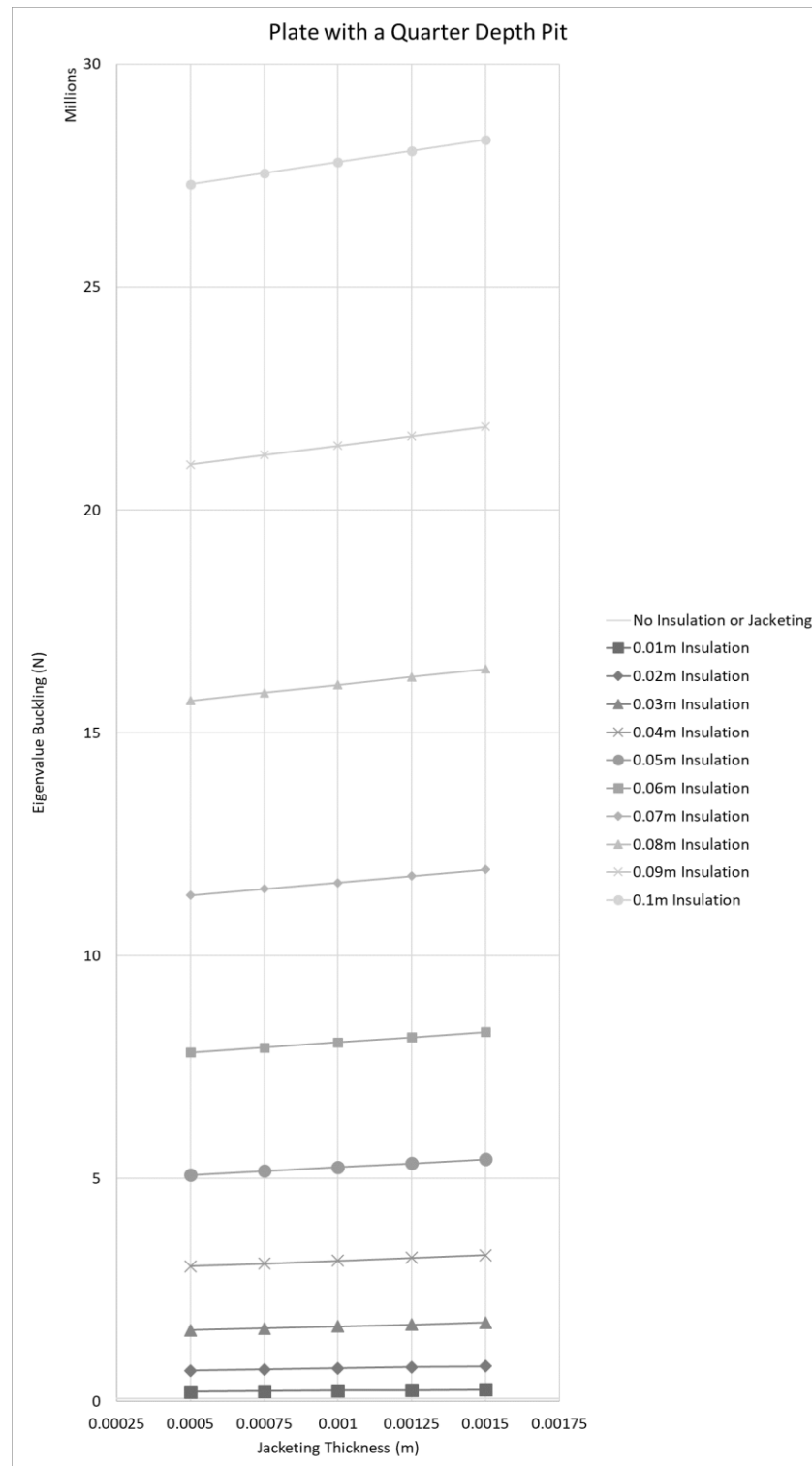
Figure 9.11 Effect of Increasing Jacketing Thickness – Plate with a Quarter Depth Pit
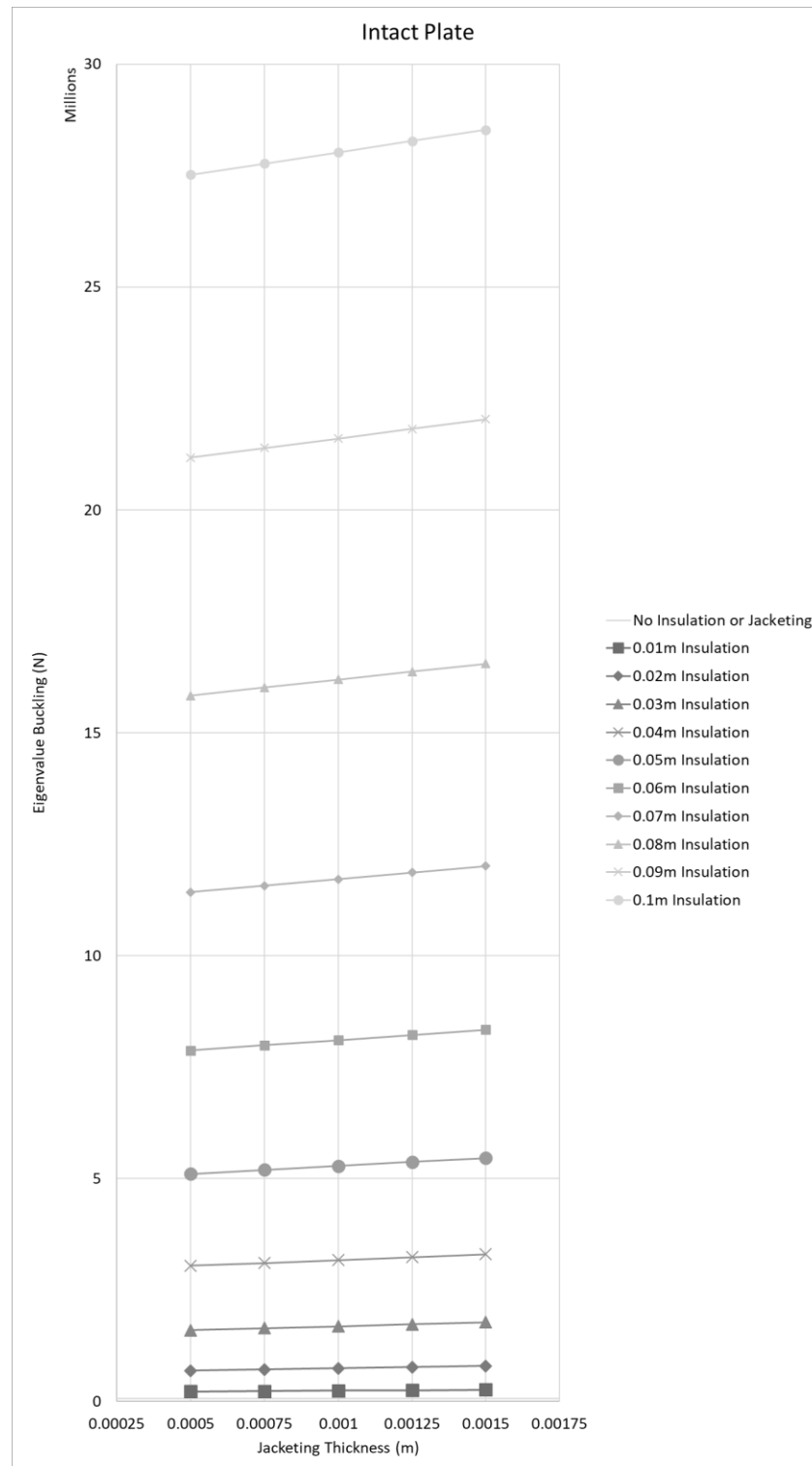
Figure 9.12 Effect of Increasing Jacketing Thickness – Intact Plate
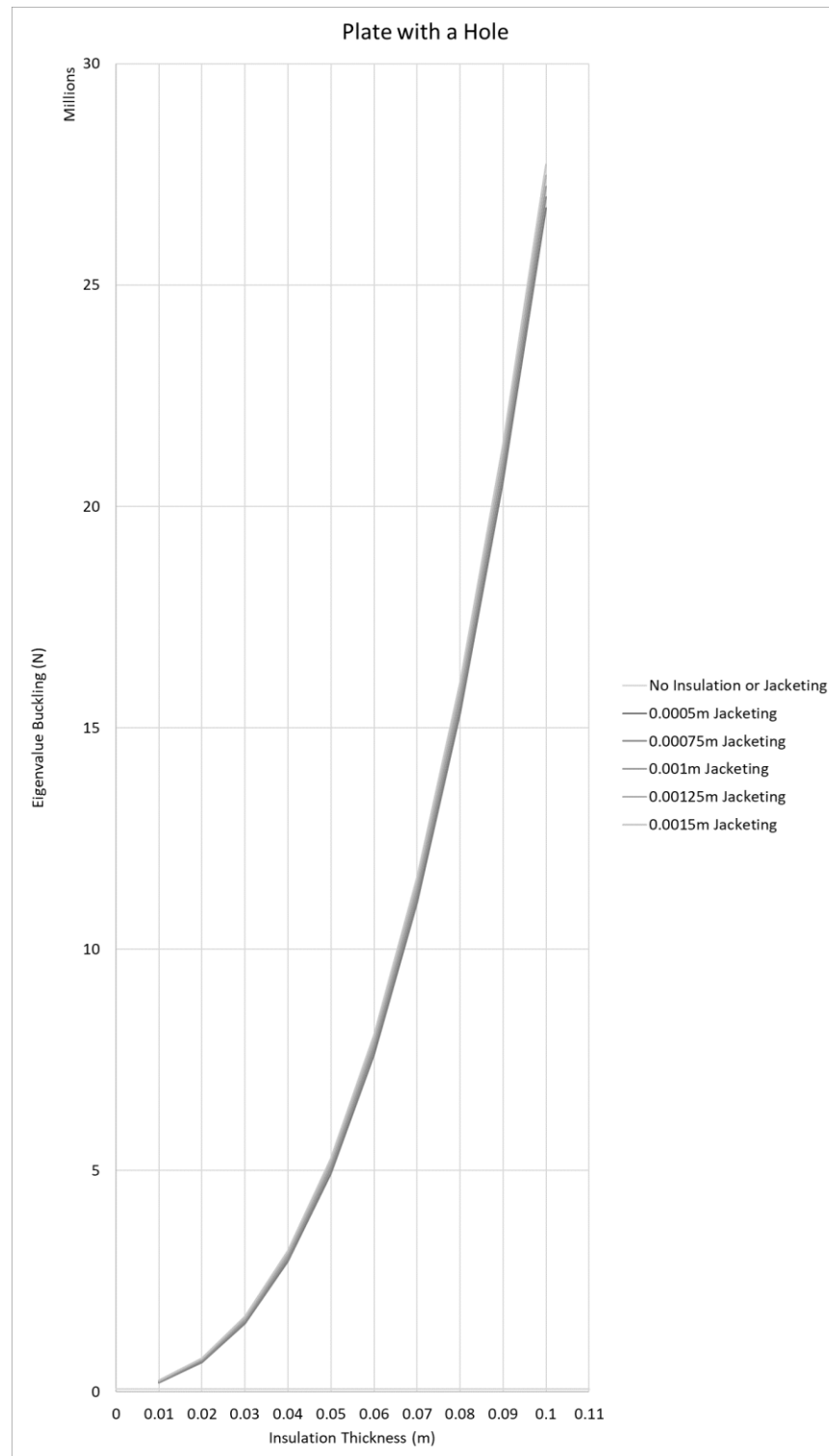
Figure 9.13 Effect of Increasing Insulation Thickness – Plate with a Hole
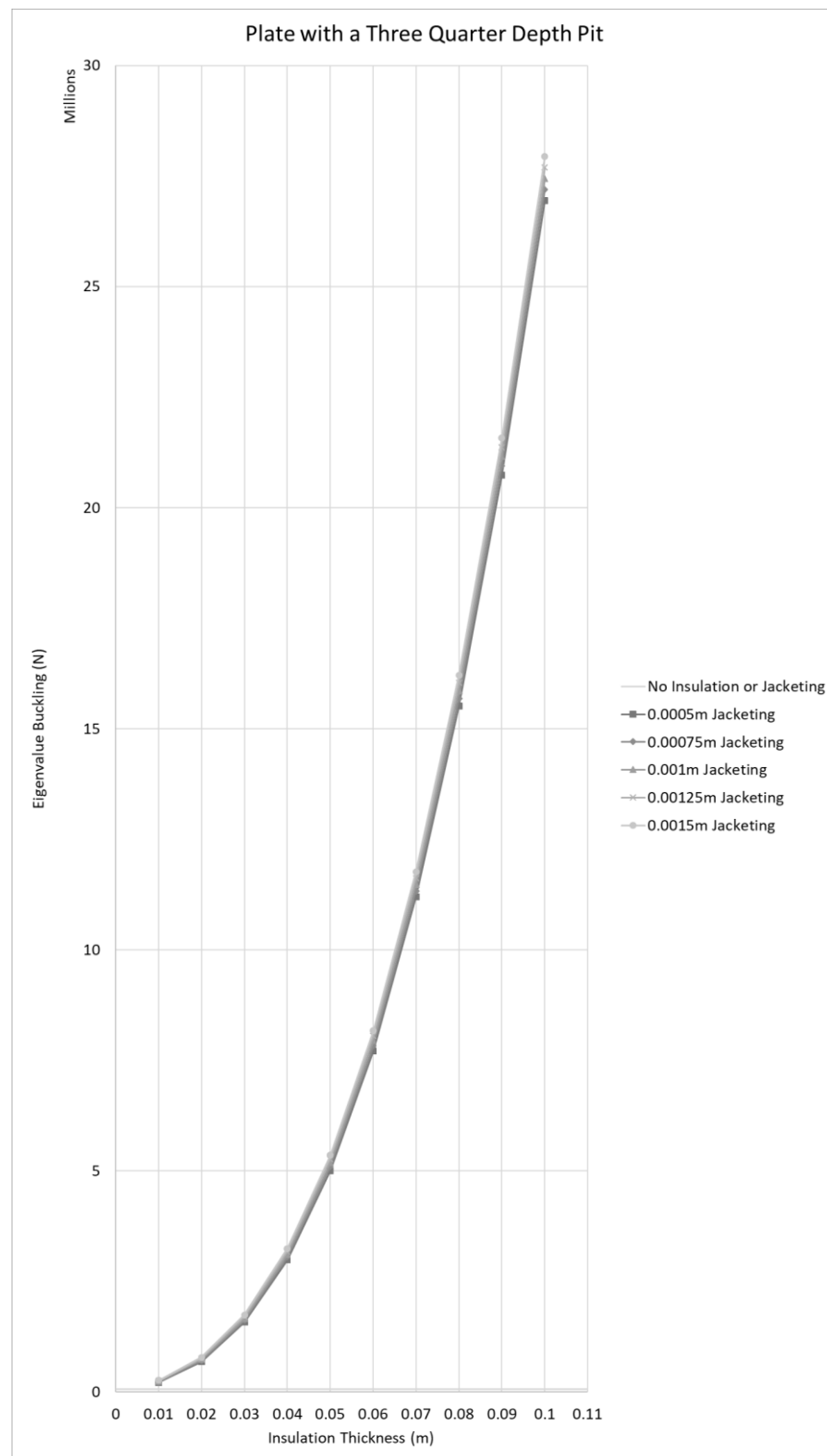
Figure 9.14 Effect of Increasing Insulation Thickness – Plate with a Three-Quarter Depth Pit
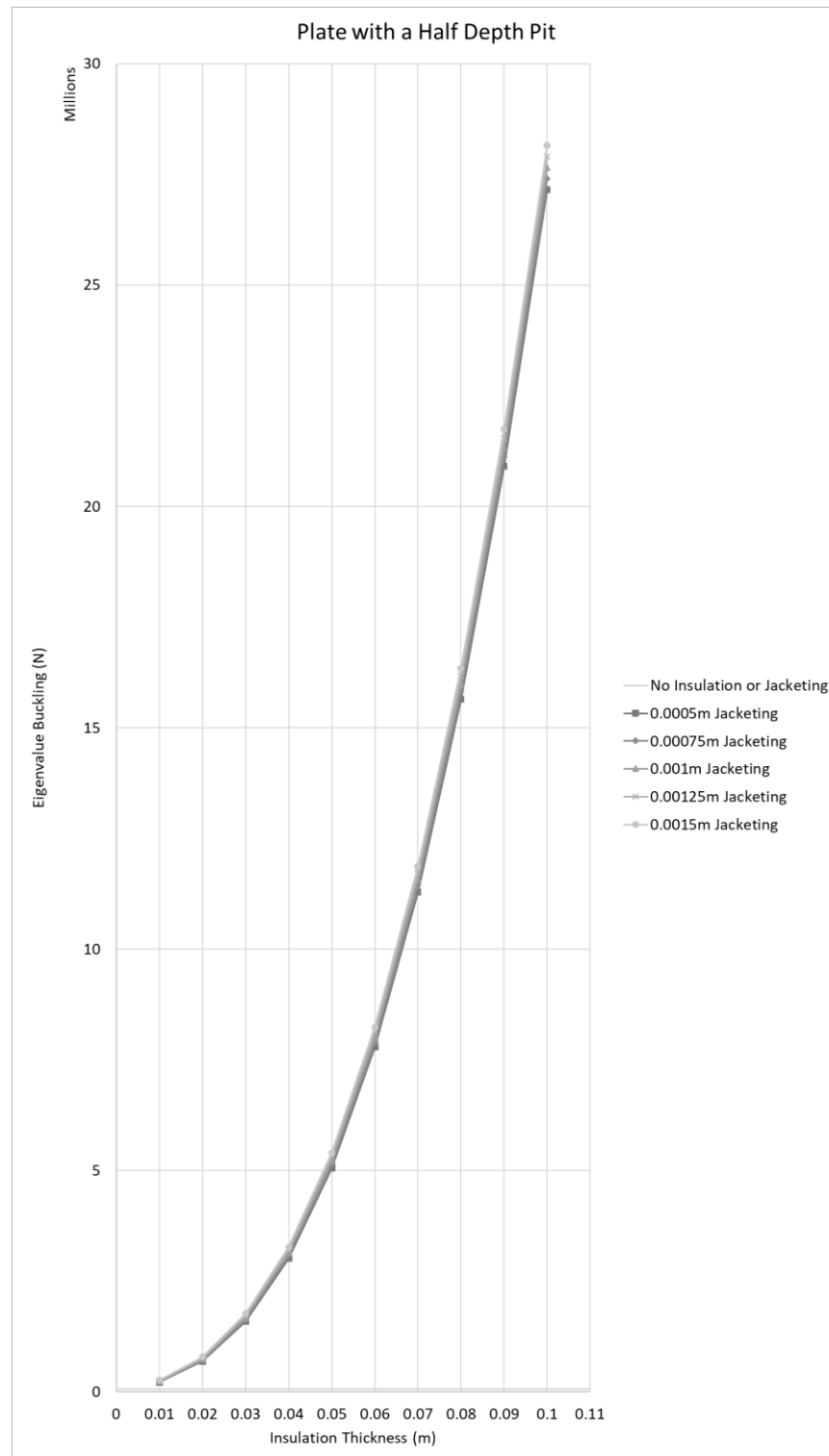
Figure 9.15 Effect of Increasing Insulation Thickness – Plate with a Half Depth Pit
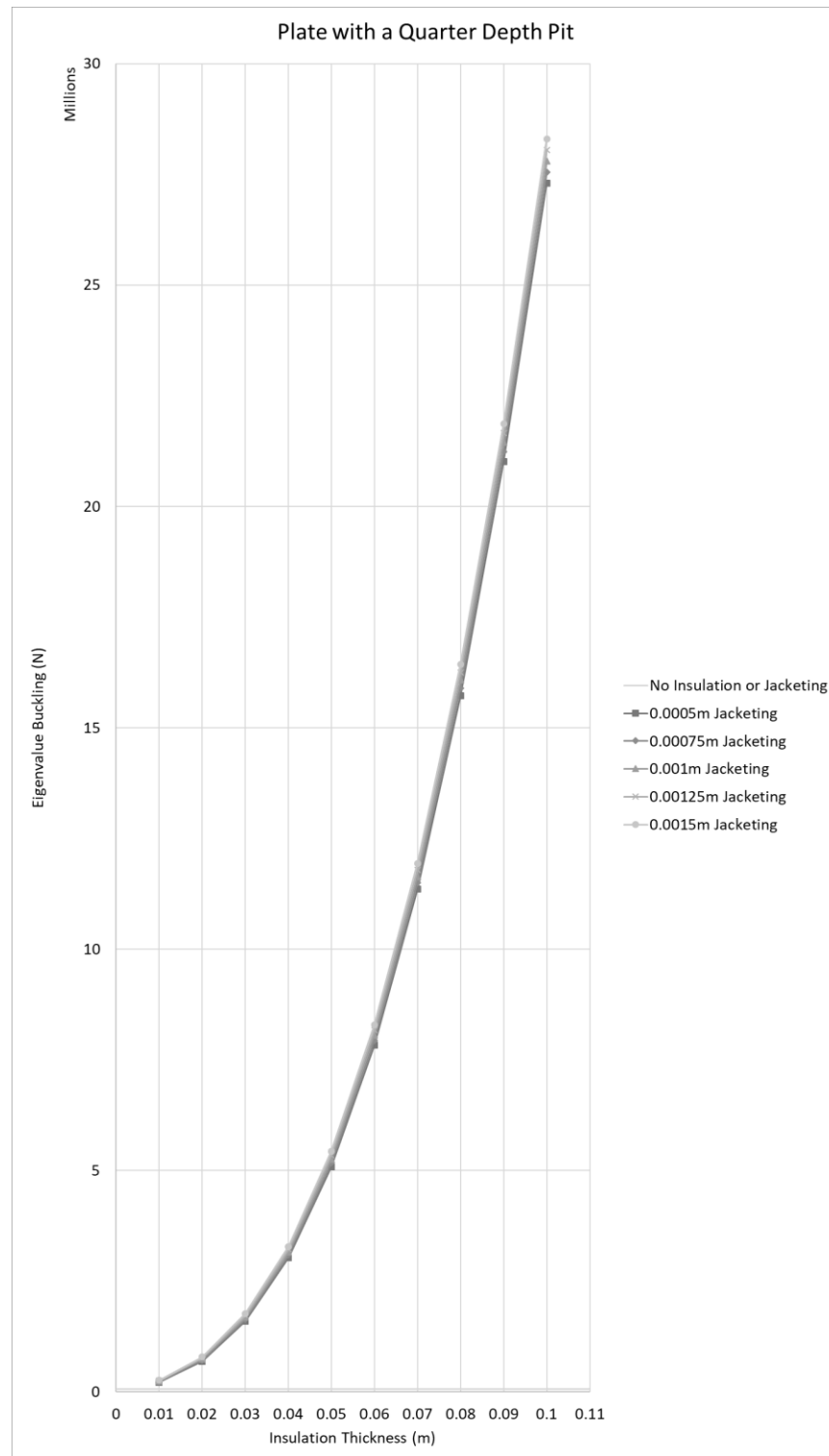
Figure 9.16 Effect of Increasing Insulation Thickness – Plate with a Quarter Depth Pit
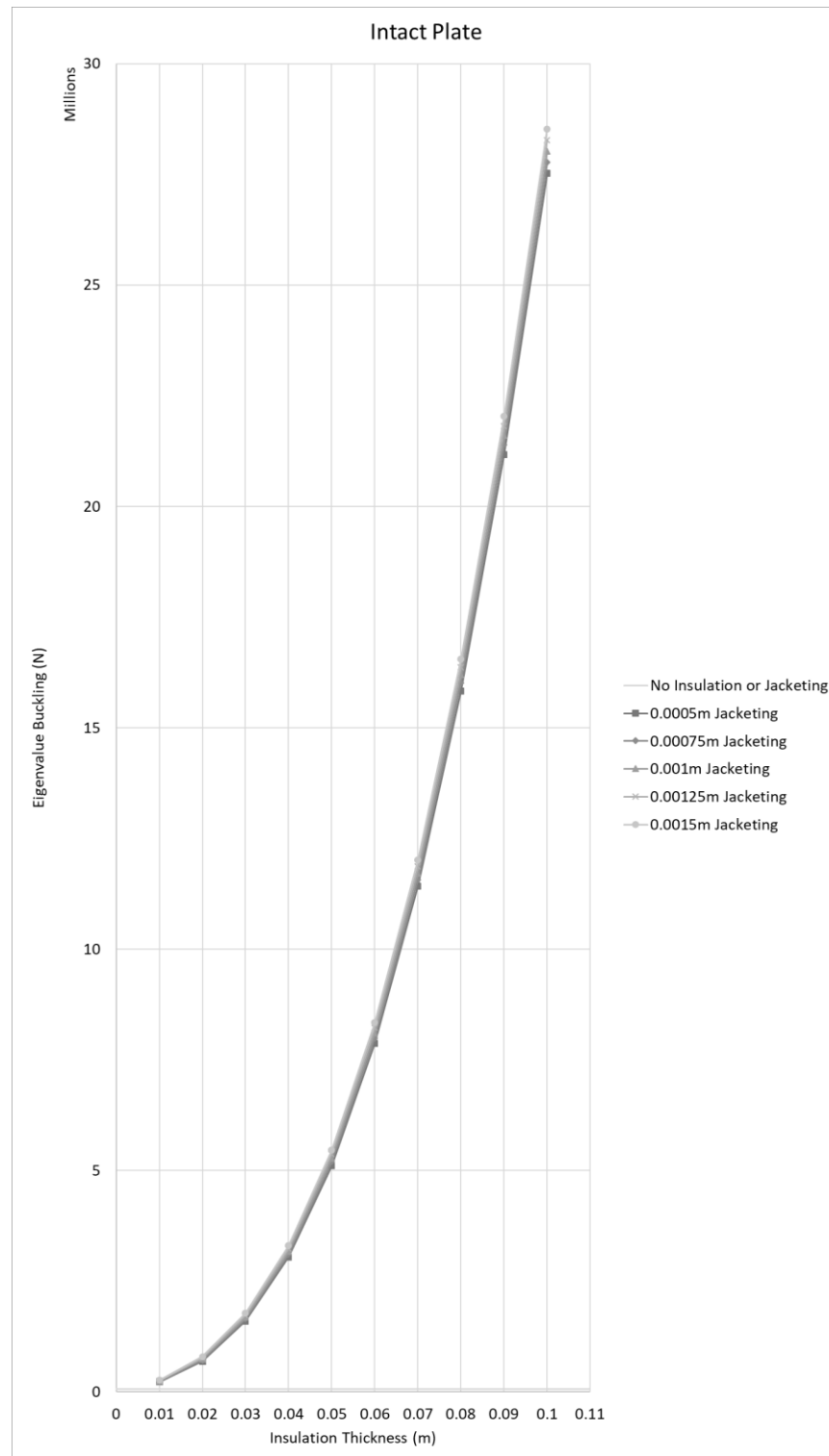
Figure 9.17 Effect of Insulation Jacketing Thickness – Intact Plate

Figures 9.18 to 9.27 allow for the opportunity to compare the buckling values of each of the five plate configurations at each of the ten insulation thicknesses. The effect of the level of degradation is quite apparent at each of the insulation thicknesses. As would be expected the plate with the hole having the highest level of corrosion effect has the lowest buckling values at each respective point when compared to the highest values as seen in the fully intact plate.

It is interesting to note that it appears when comparing each of the figures that as the insulation thickness increases the relative difference in buckling values between each plate configuration also increases. That is to say that in Figure 9.18 the values for the intact plate and the three plates with pit degradations are quite closely bunched together with the plate with a hole slightly separated.

In Figure 9.27 this is no longer the case as each of the five configurations are now quite evenly spaced. Clearly, the effect of the much larger buckling values will have had some effect on this as the numbers on the y-axis will be considerably larger but in relative terms, it would still be expected that the bunching pattern remains.
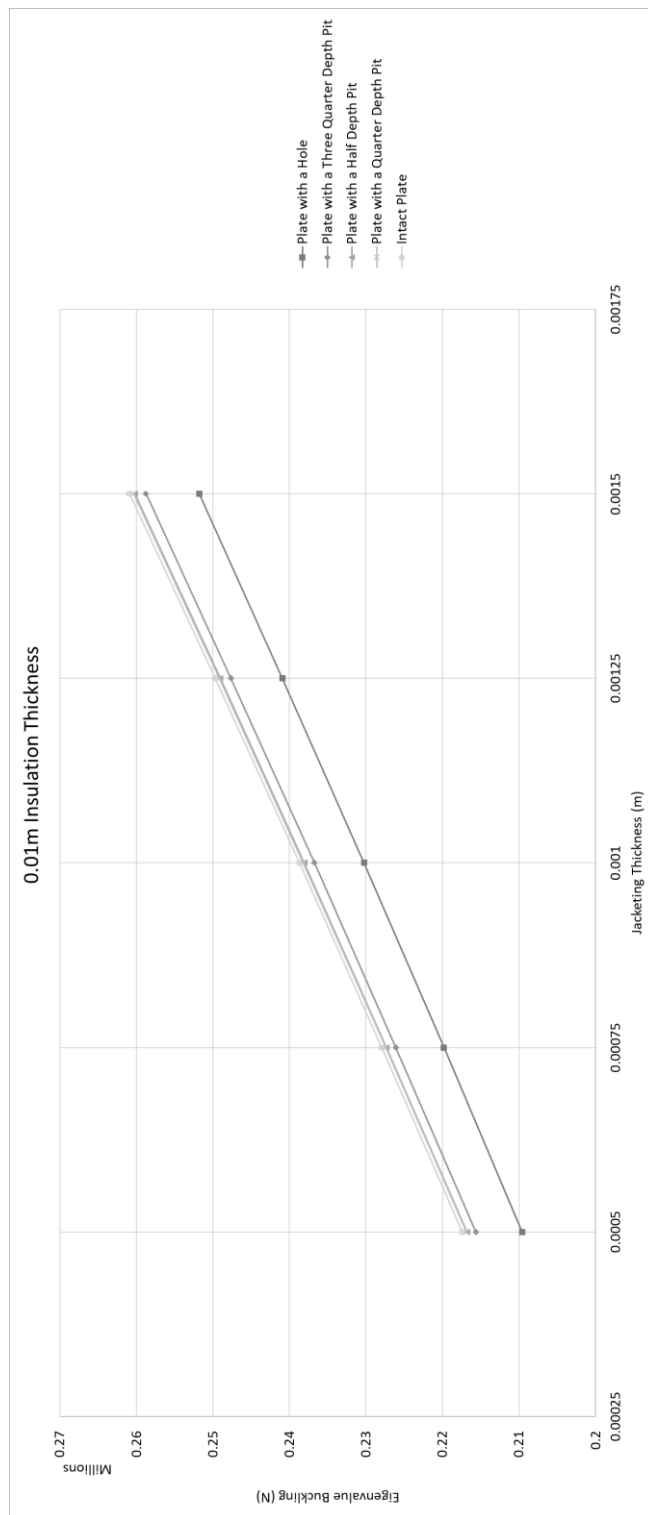
Figure 9.18 Effect of Plate Degradation on Buckling with 0.01 m Insulation Thickness
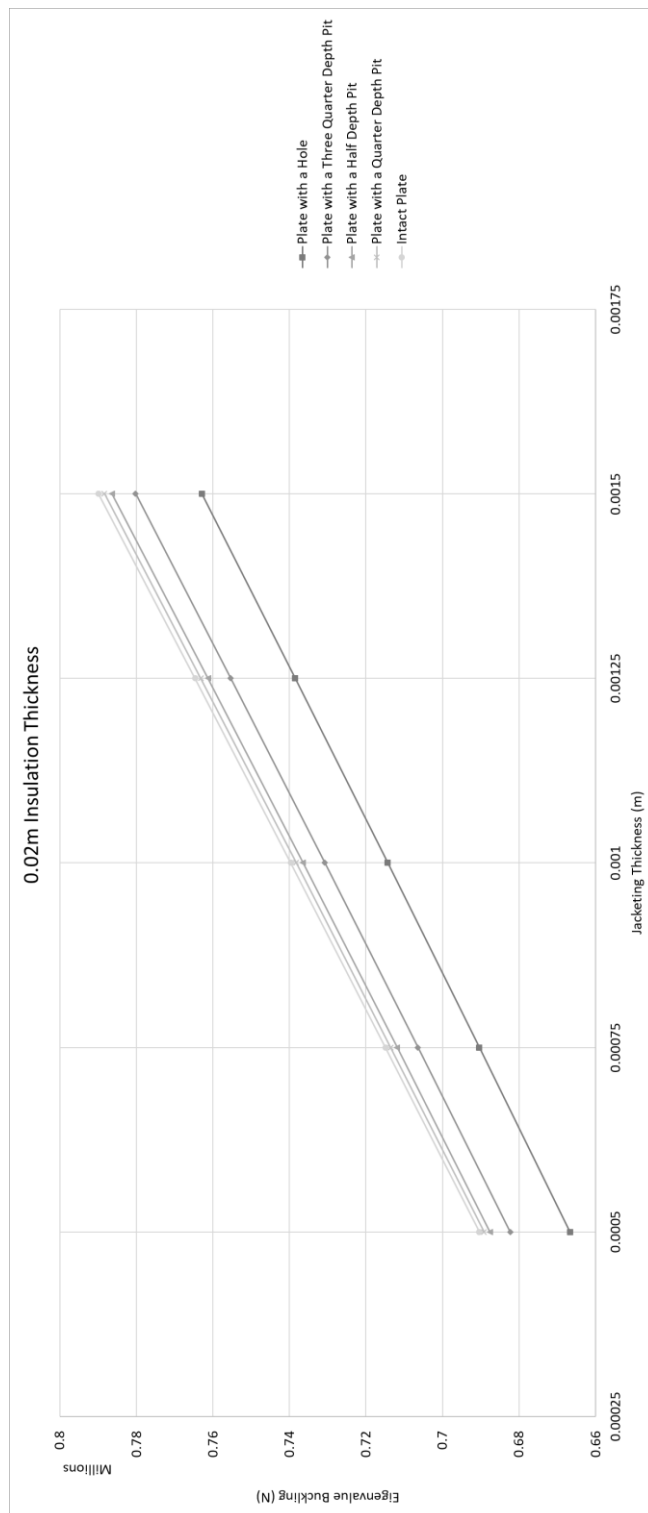
Figure 9.19 Effect of Plate Degradation on Buckling with 0.02 m Insulation Thickness
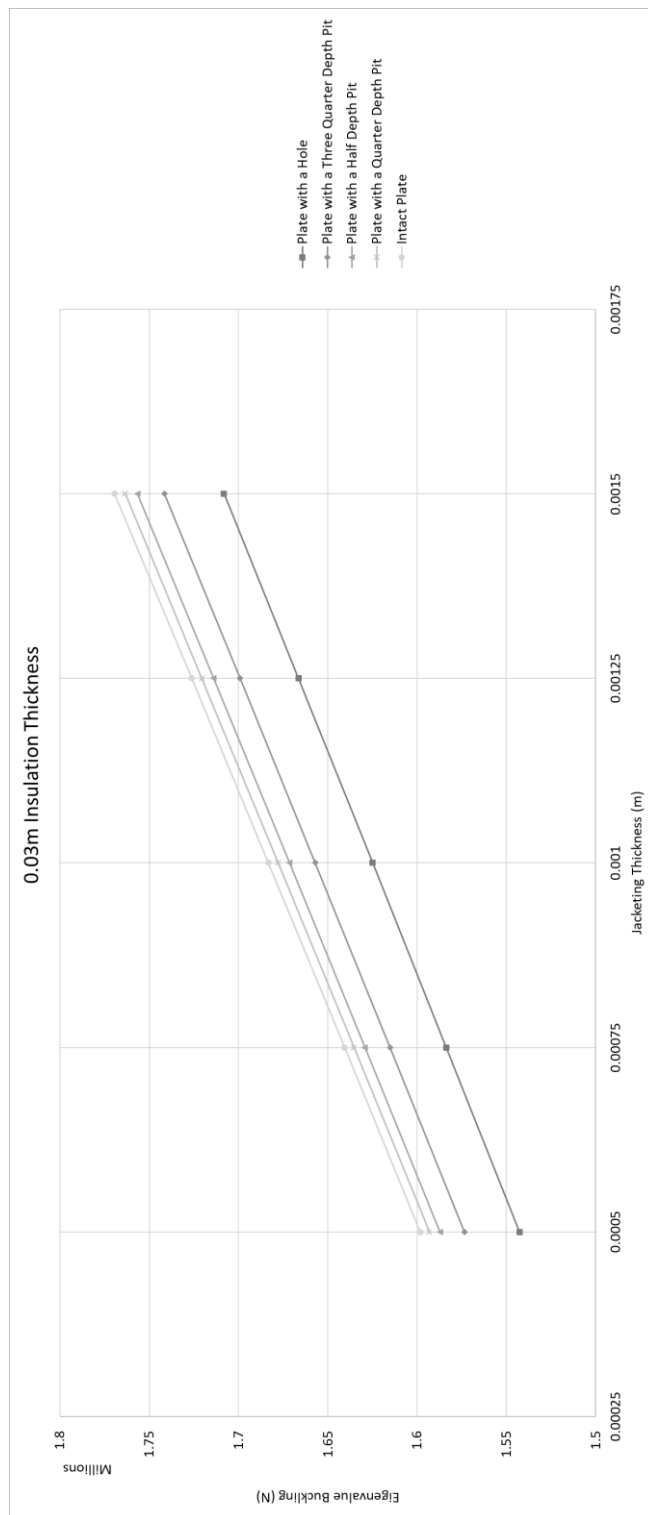
Figure 9.20 Effect of Plate Degradation on Buckling with 0.03 m Insulation Thickness
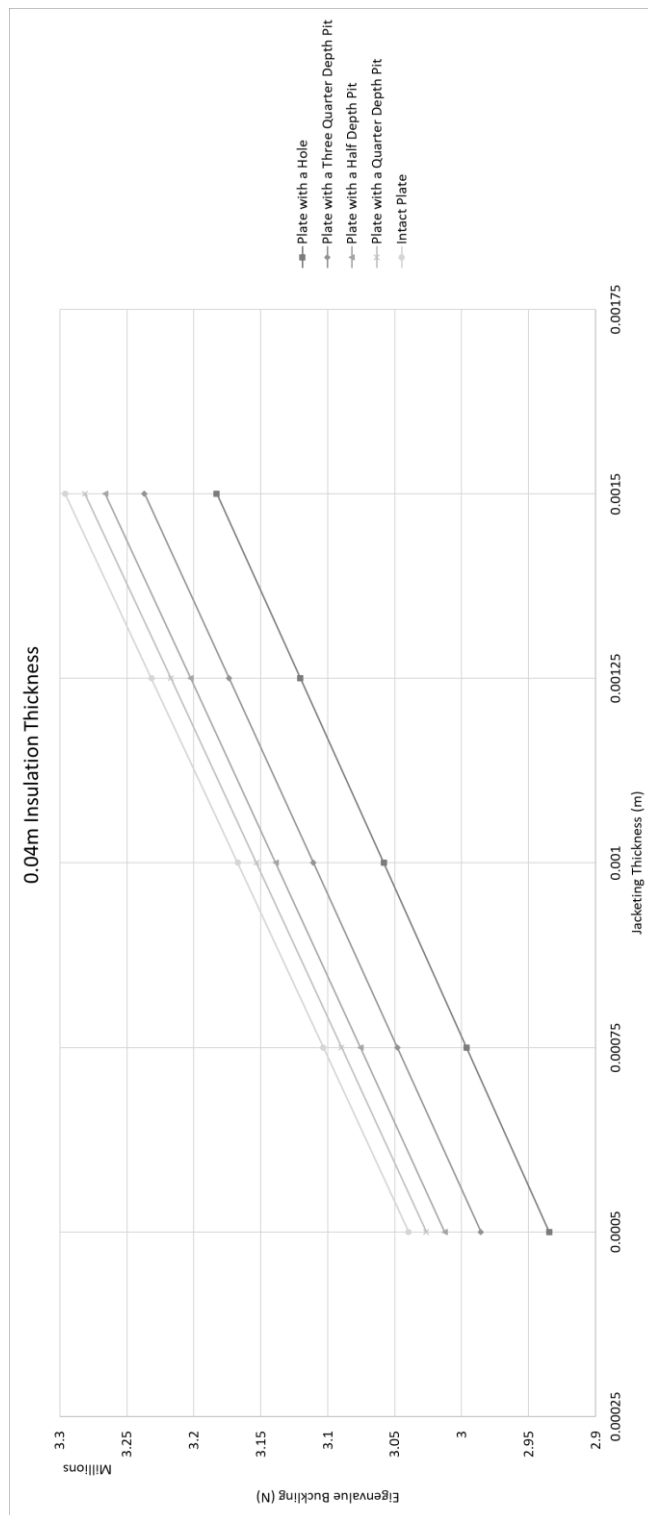
Figure 9.21 Effect of Plate Degradation on Buckling with 0.04 m Insulation Thickness
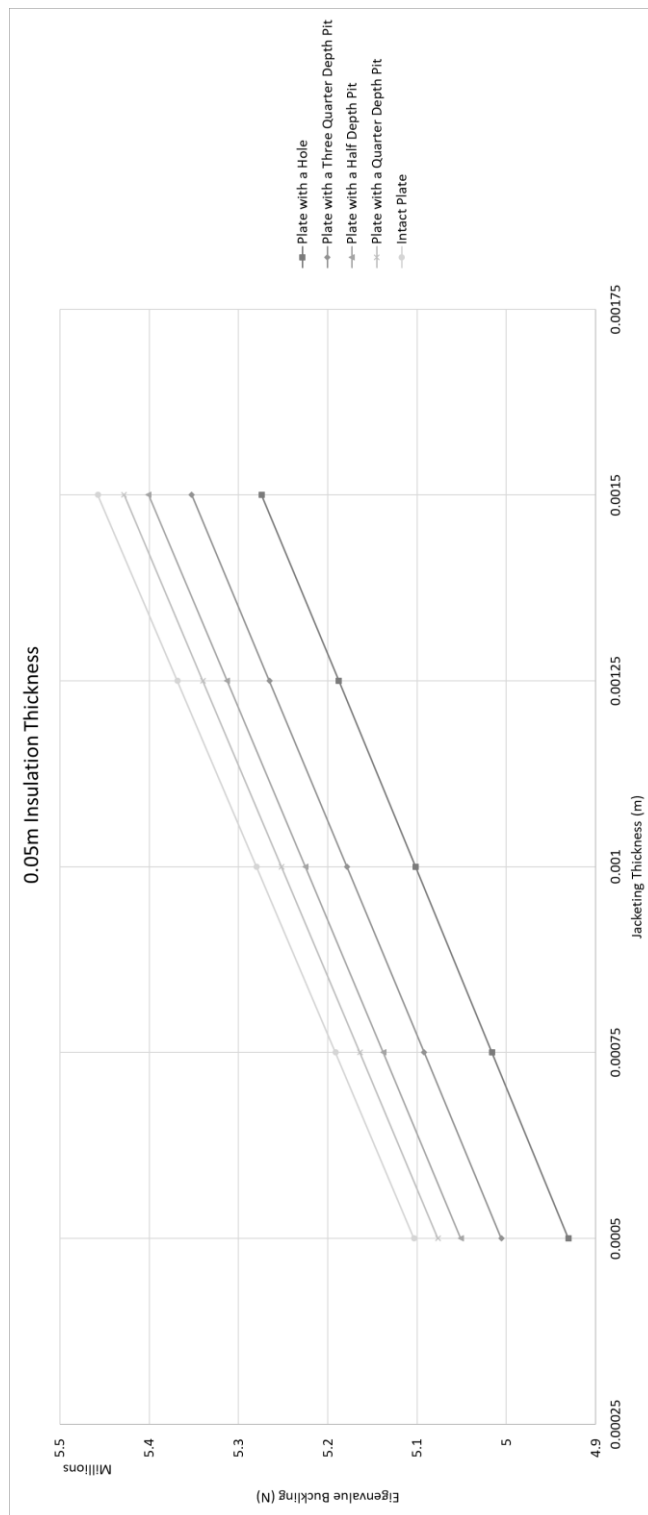
Figure 9.22 Effect of Plate Degradation on Buckling with 0.05 m Insulation Thickness
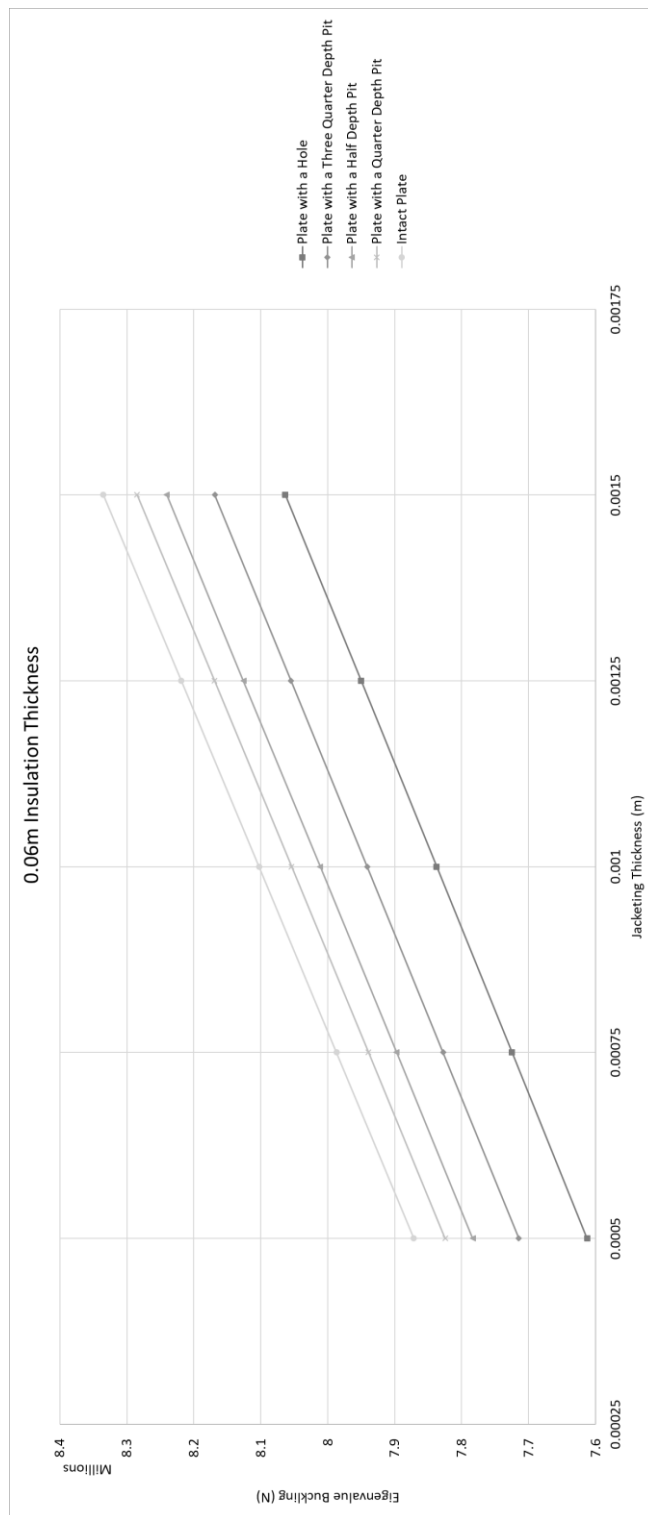
Figure 9.23 Effect of Plate Degradation on Buckling with 0.06 m Insulation Thickness
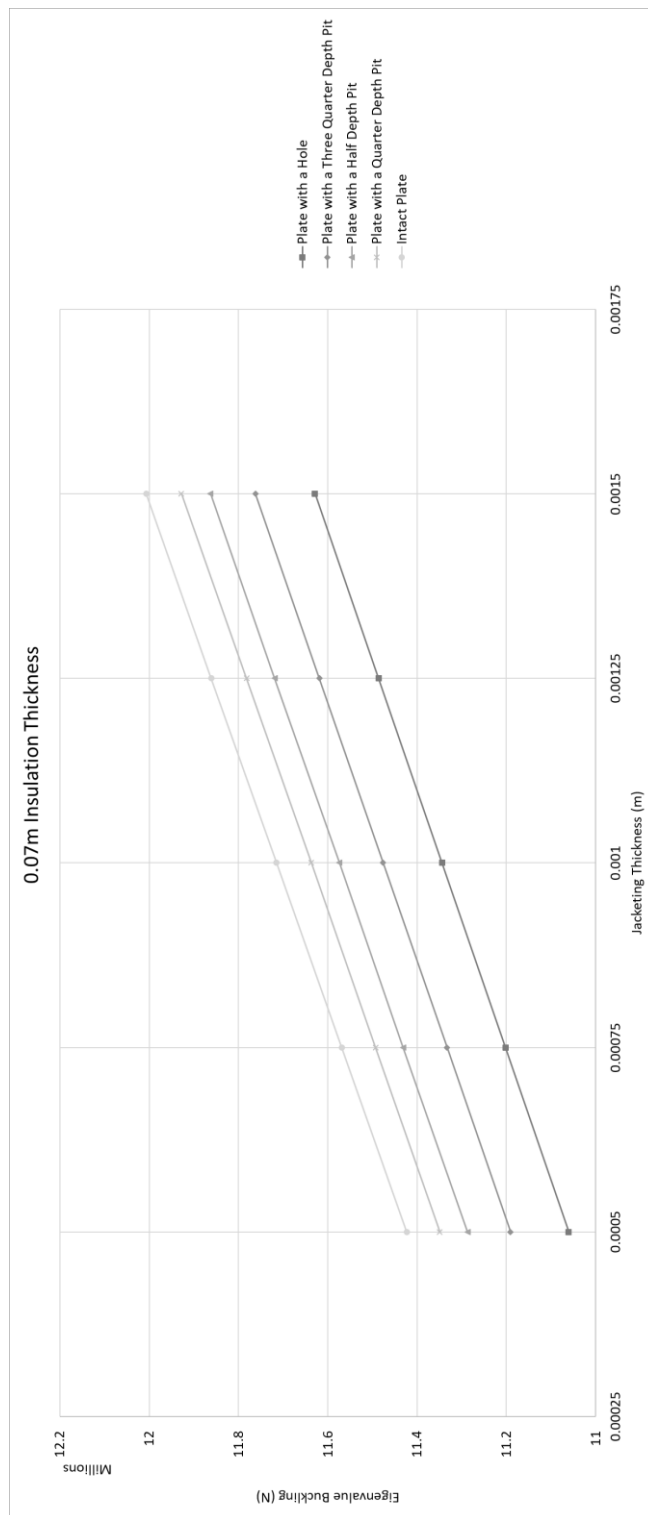
Figure 9.24 Effect of Plate Degradation on Buckling with 0.07 m Insulation Thickness
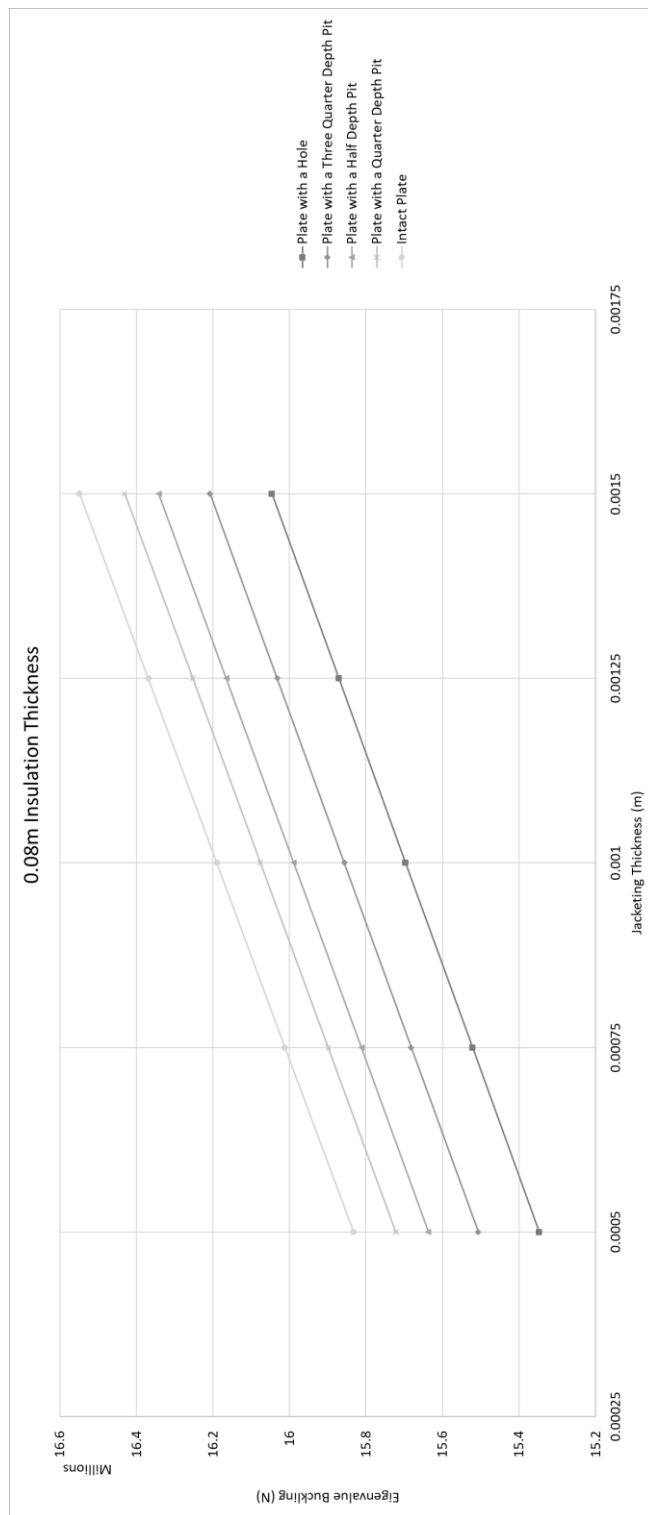
Figure 9.25 Effect of Plate Degradation on Buckling with 0.08 m Insulation Thickness
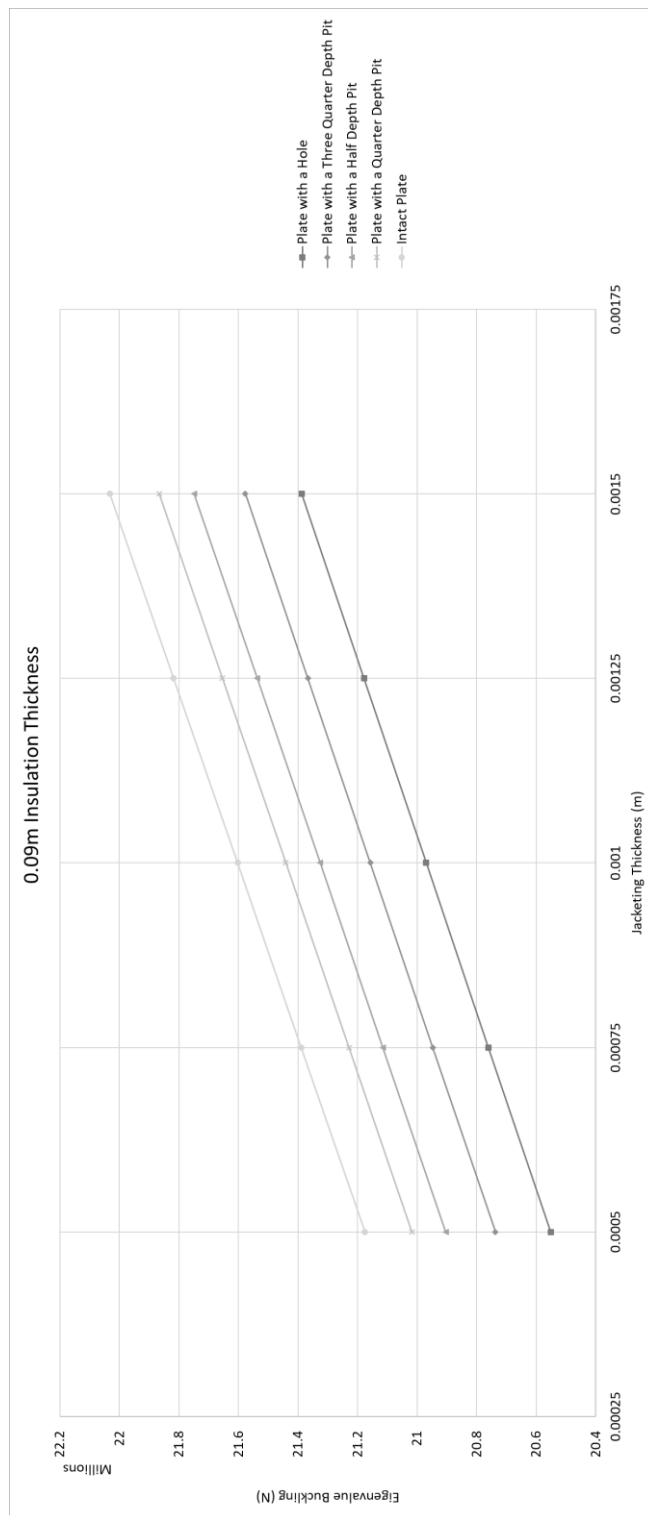
Figure 9.26 Effect of Plate Degradation on Buckling with 0.09 m Insulation Thickness
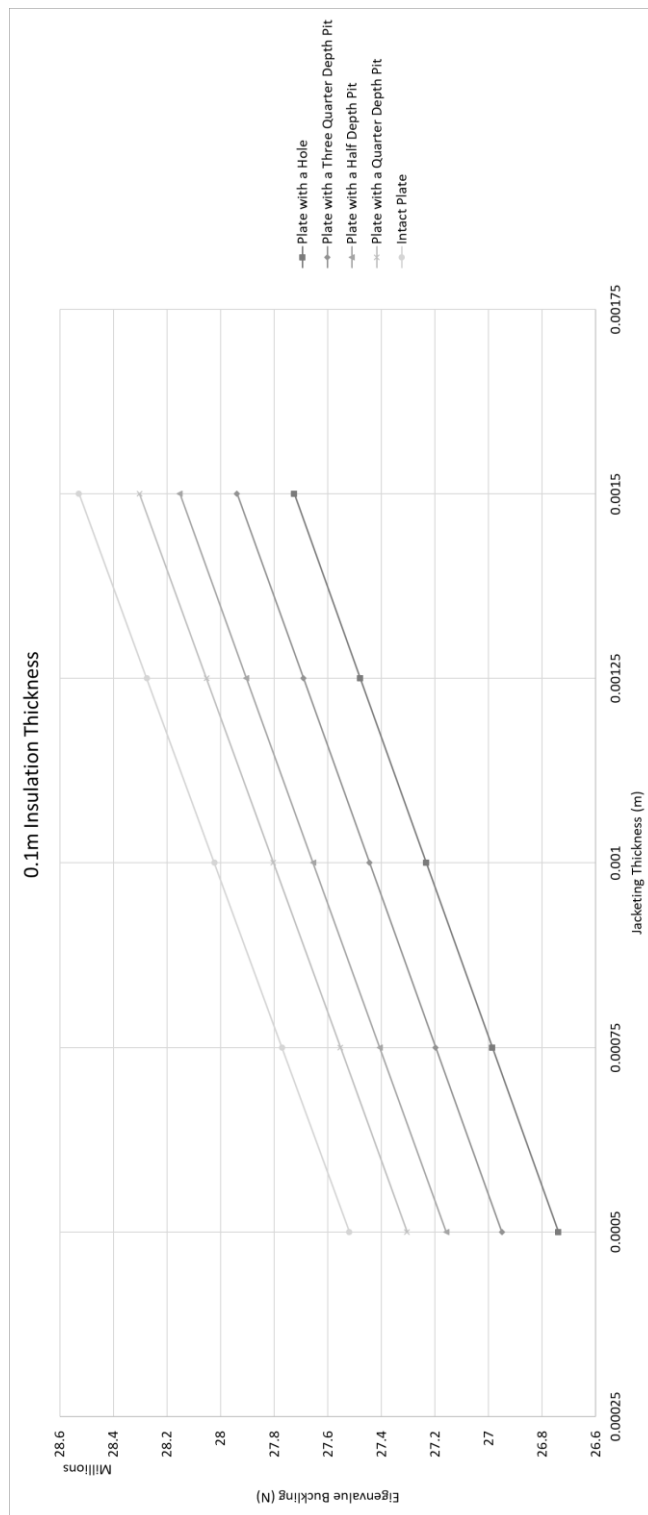
Figure 9.27 Effect of Plate Degradation on Buckling with 0.1 m Insulation Thickness

9.3 Polycarbonate Protective Jacketing

In this section, the results from the Eigenvalue buckling analysis will be presented for the mineral wool insulation material where the system has a polycarbonate protective jacketing. The plate was configured at each of the five degradation levels discussed previously.

A table presenting the raw buckling data in its entirety for the mineral wool insulation system can be found as Table C.2 in Appendix C. A number of graphs will be produced and shown in this section from the data in Table C.2 to represent these results and to illustrate the following variables:

- Effect of increasing jacketing thickness
- Effect of increasing insulation thickness
- Comparison of buckling values at each insulation thickness depending on the plate degradation
- Comparison of buckling values at each jacketing thickness depending on the plate degradation

The geometric and material properties of the plate have remained constant and these details can be found in Table 9.1. The material properties for each of the six insulation and two jacketing materials are provided in Table 9.2. Please pay close attention to the axes values as they may change drastically so as to give the best overall indication of the piece of information described.

Figures 9.28 to 9.32 depict the effect of the increase in jacketing thickness on each of the five plate degradation configurations. It can be seen at the bottom of each graph there is a plot that spans the full width, this plot denotes the buckling value of the plate configuration where there is no insulation system providing additional strength. The jacketing thickness increases from 0.002 metres as a minimum up to 0.01 metres at the largest thickness.

In the case of the plate with a hole this value is 50667 N, with a three-quarter depth pit it is 53141 N, a half depth pit equals 53246 N, a quarter depth pit is 54135 N and finally a fully intact plate equals 55937 N. As would be expected the buckling value increases as the level of degradation of the plate decreases. The degradations cause the plate to lose some of its inherent structural strength.

The expectation with regards to the addition of an insulation system would be that the buckling strength of the plate would increase which is exactly as the results show. Whether that be the increase in the thickness of the insulation or an increase in the thickness of the protective coating. As the thickness of the protective coating increases, there is a minor increase in the buckling value when comparing the values at a single insulation thickness.

Figures 9.33 to 9.37 depict the effect of increasing the thickness of the insulation on each of the plate degradation configurations. These latter figures show a much larger relative rise in the buckling value where the insulation thickness increases at each jacketing thickness. The minimum insulation thickness measured is 0.01 metres ranging up to 0.1 metres at the largest value. As before, it can be seen at the bottom of each graph there is a plot that spans the full width, this plot denotes the buckling value of the plate configuration where there is no insulation system providing additional strength.

As an example, when looking at Figure 9.33, it can be seen that with an insulation thickness of 0.1 metres the buckling value where the jacketing thickness is 0.002 metres is 200,320 N. At the same insulation thickness but after increasing the thickness of the jacketing to the maximum of 0.01 metres the new buckling value is 223,990 N. The only parameter that has changed is the thickness of the protective jacketing and with that, the buckling value has increased as expected.

This increase is relatively modest when compared to another example when looking a Figure 9.37, which will depict the increase in buckling through an increase in insulation thickness. Where the jacketing thickness is 0.002 metres and the insulation thickness is 0.01 metres the buckling value is 200,320 N as before. If instead of increasing the jacketing thickness the insulation thickness is increased only one level up to 0.02 metres the new buckling value is 649,560 N.

If the insulation thickness were to be increased to the maximum value of 0.1 metres the new buckling value would be 27,091,000 N. These numbers are clearly only theoretical as it is highly unlikely that any system would ever be insulated in this way but it was felt that it would be sensible to continue up to these system configurations as a way of testing the written model codes to see if there was a point at which they lost their viability.

In the next chapter, the Euler Formula will be used as a method to validate the results. This formula, shown in Equation (10.1) of Chapter Ten, can also be used to explain the large values generated in the plate results here. As the thickness of the insulated plate increases the moment of inertia also increases which means that the system is considered to be much stiffer. So, although this chapter deals with plates rather than columns the theory still holds as the plate could be considered to be a column that has been split lengthwise and then flattened. This formula will be explained in more detail in the next chapter.

In Appendix D it can be seen that despite the varying material properties and therefore the overall measured buckling values the patterns remain similar. The effect of increasing the thickness of the jacketing does increase the buckling value but to a much lesser degree than increasing the thickness of the insulation.

Figure 9.28 Effect of Increasing Jacketing Thickness – Plate with a Hole
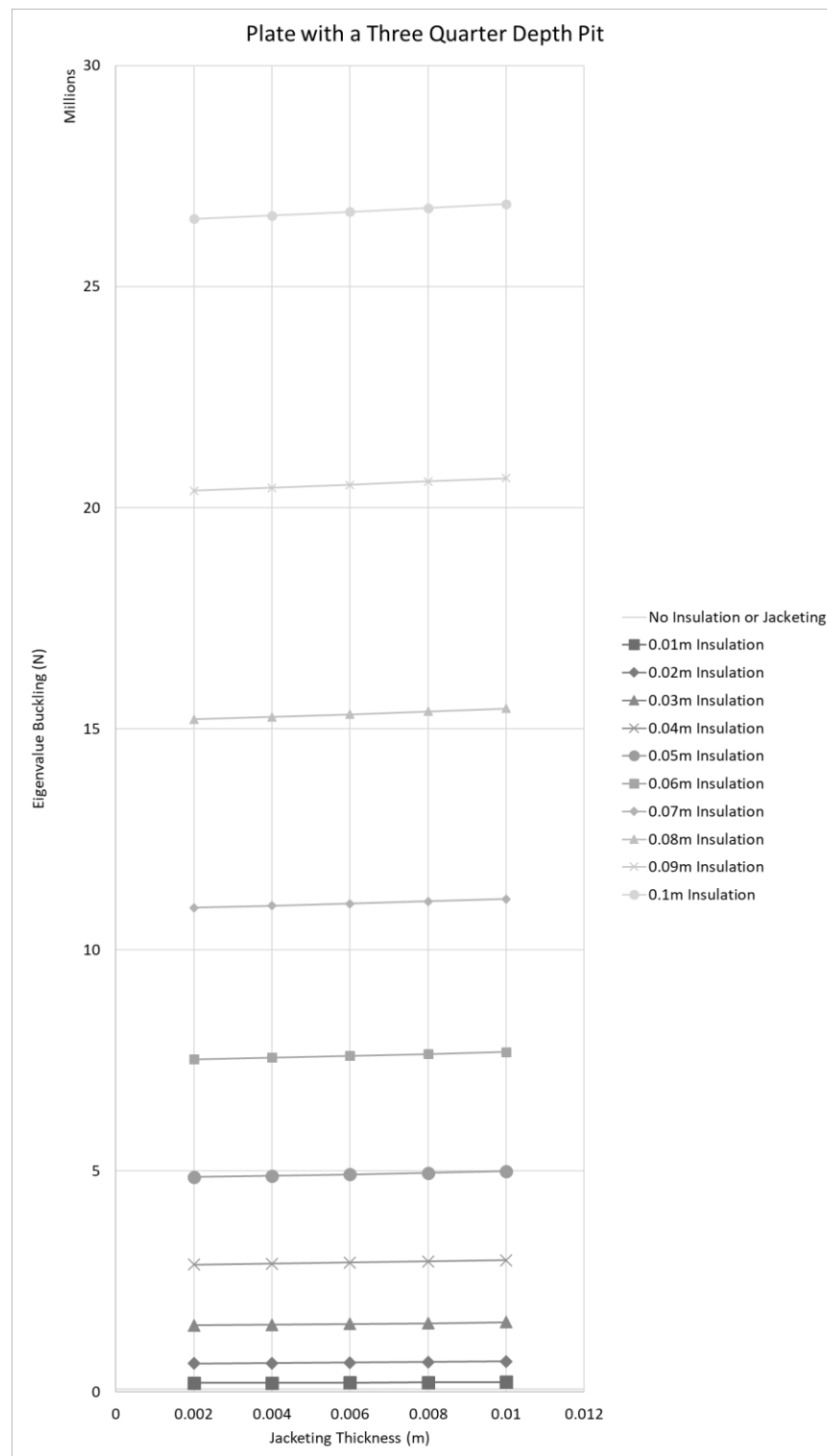
Figure 9.29 Effect of Increasing Jacketing Thickness – Plate with a Three-Quarter Depth Pit
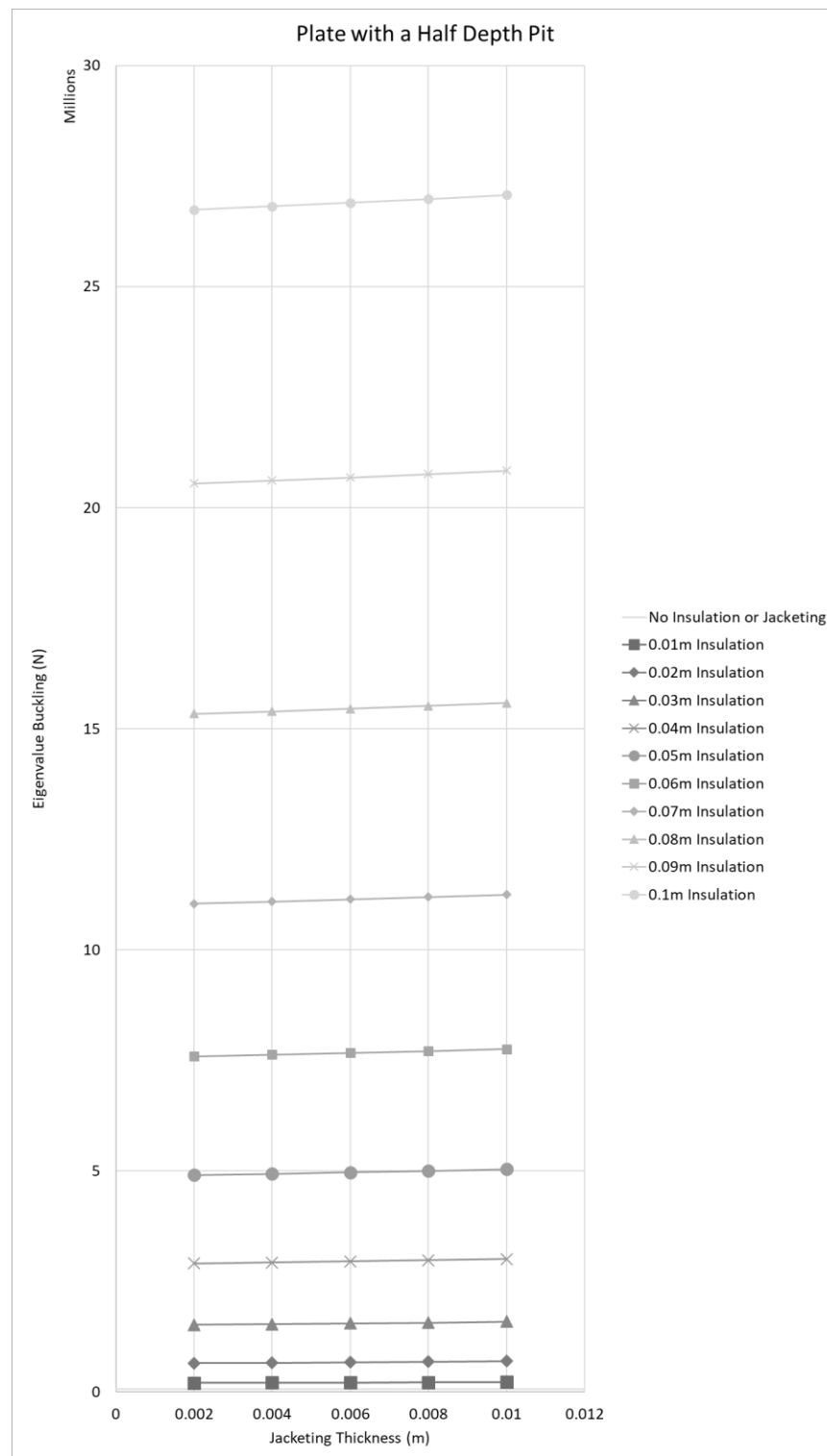
Figure 9.30 Effect of Increasing Jacketing Thickness – Plate with a Half Depth Pit
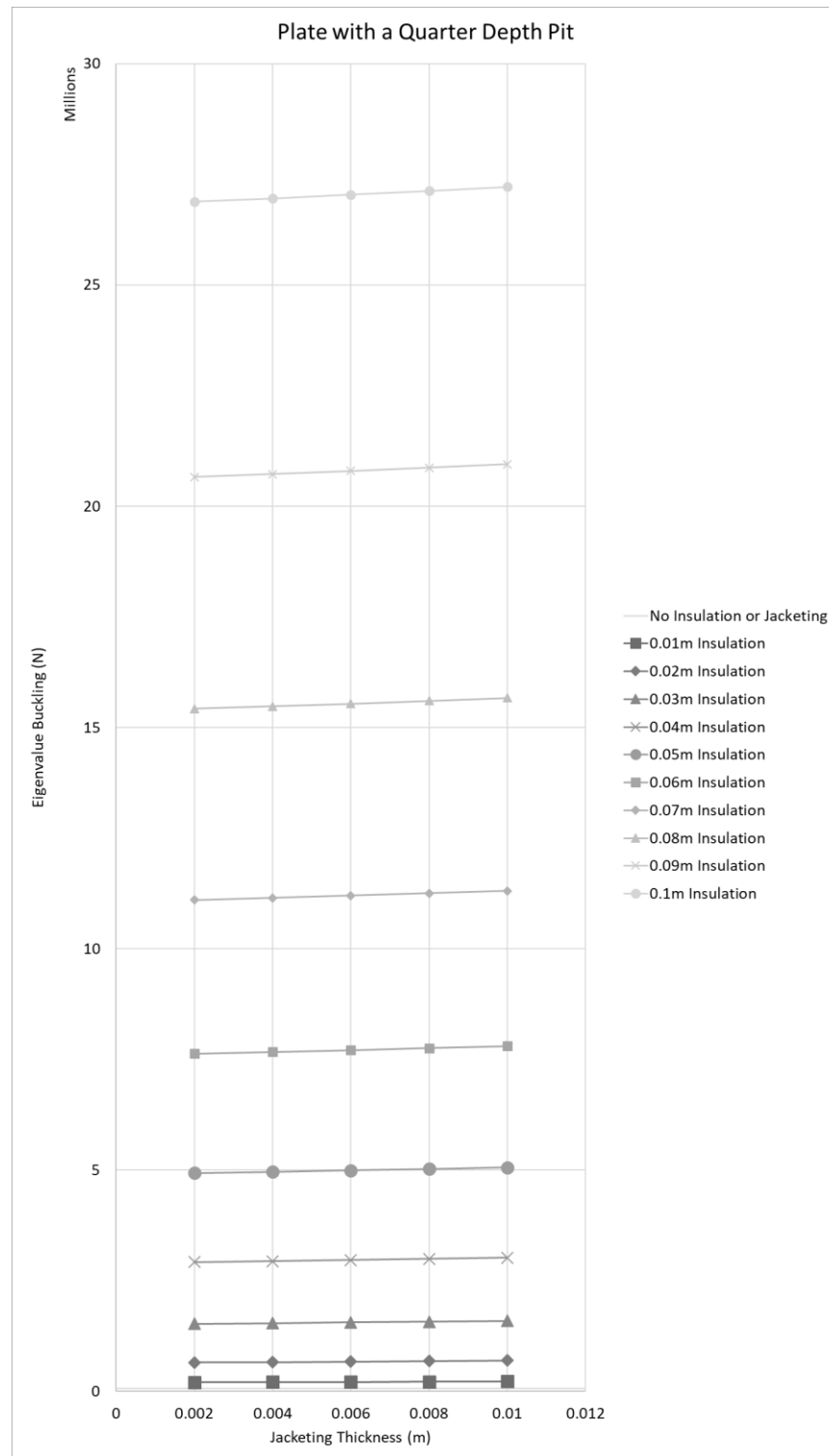
Figure 9.31 Effect of Increasing Jacketing Thickness – Plate with a Quarter Depth Pit
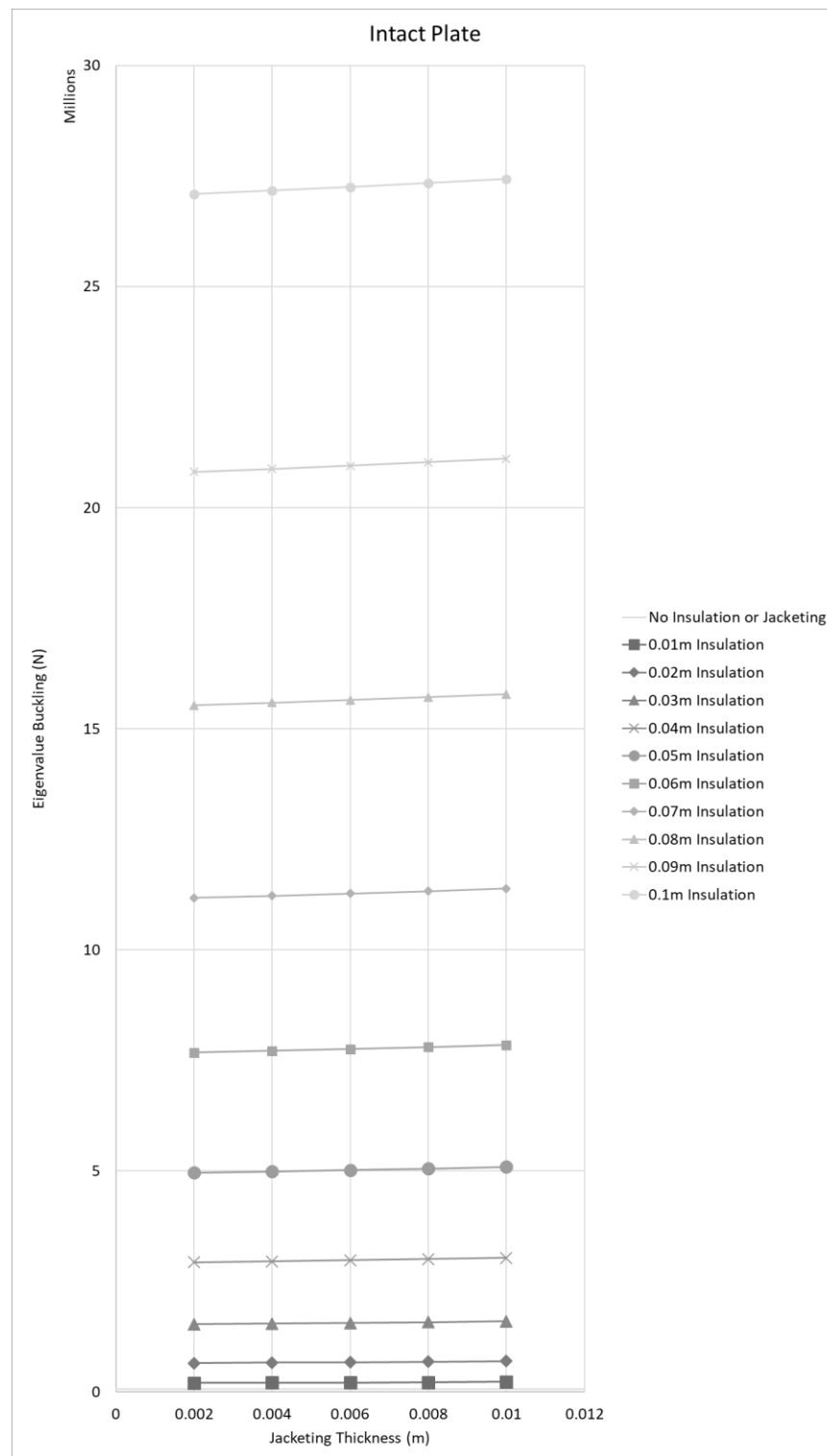
Figure 9.32 Effect of Increasing Jacketing Thickness – Intact Plate
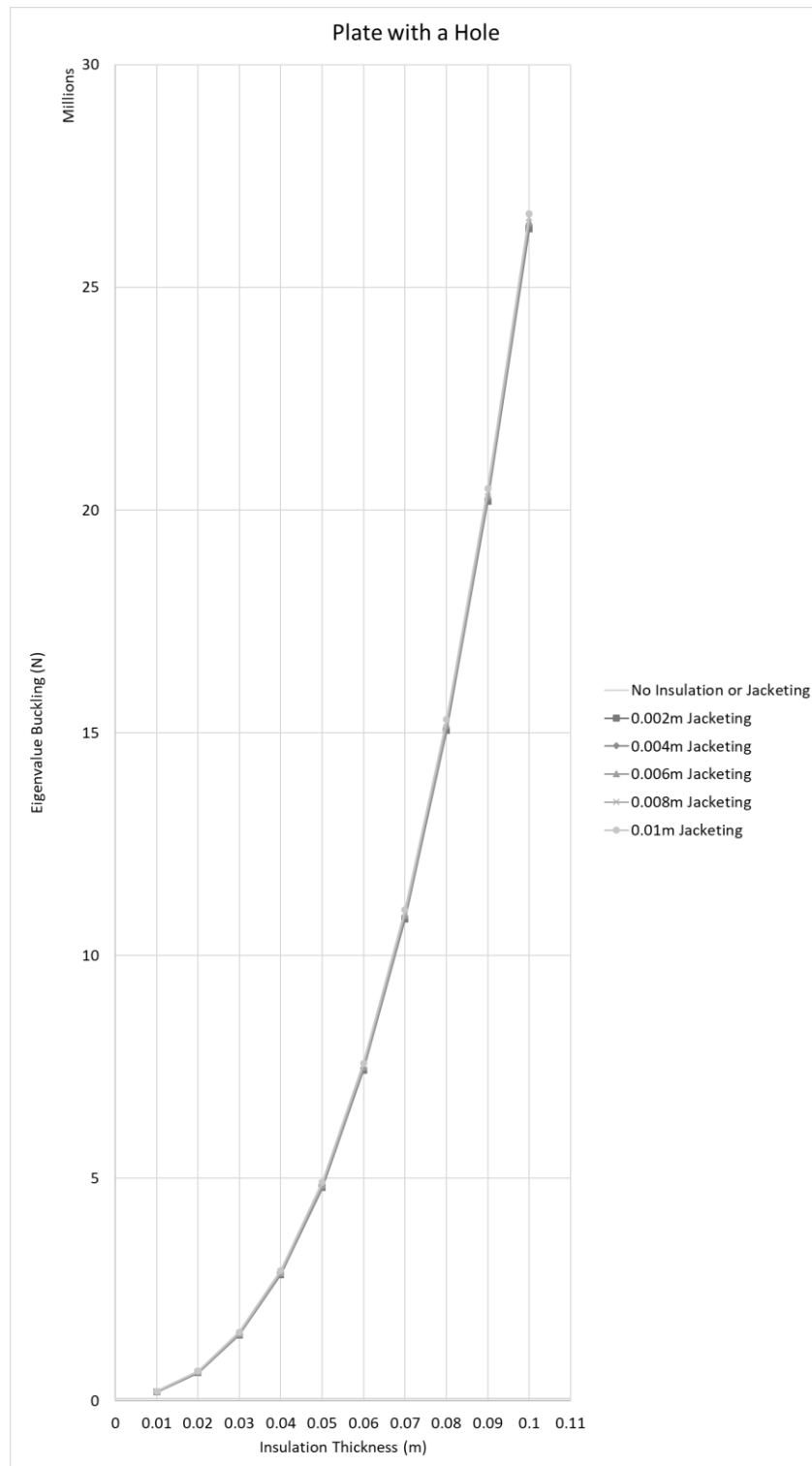
Figure 9.33 Effect of Increasing Insulation Thickness – Plate with a Hole
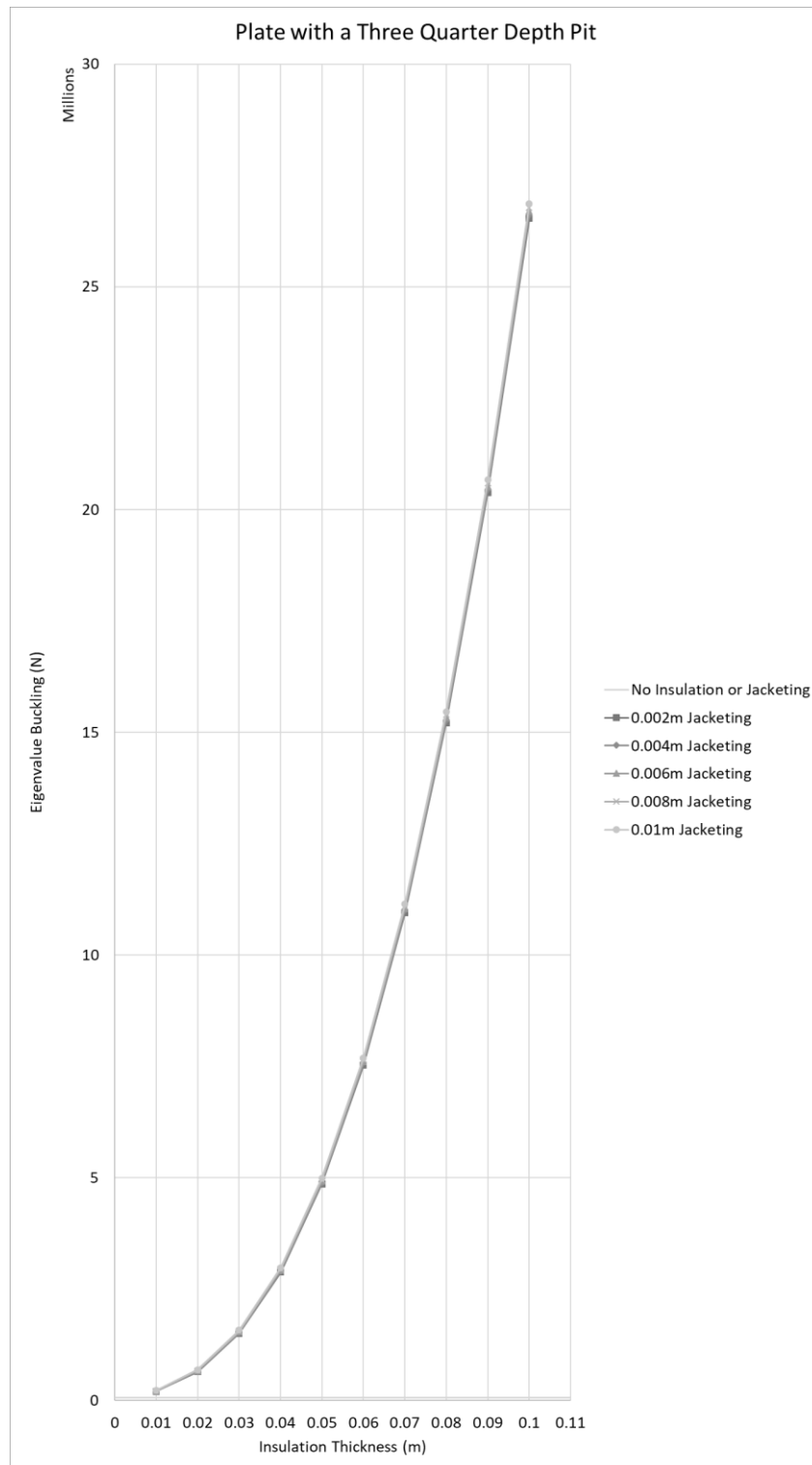
Figure 9.34 Effect of Increasing Insulation Thickness – Plate with a Three-Quarter Depth Pit
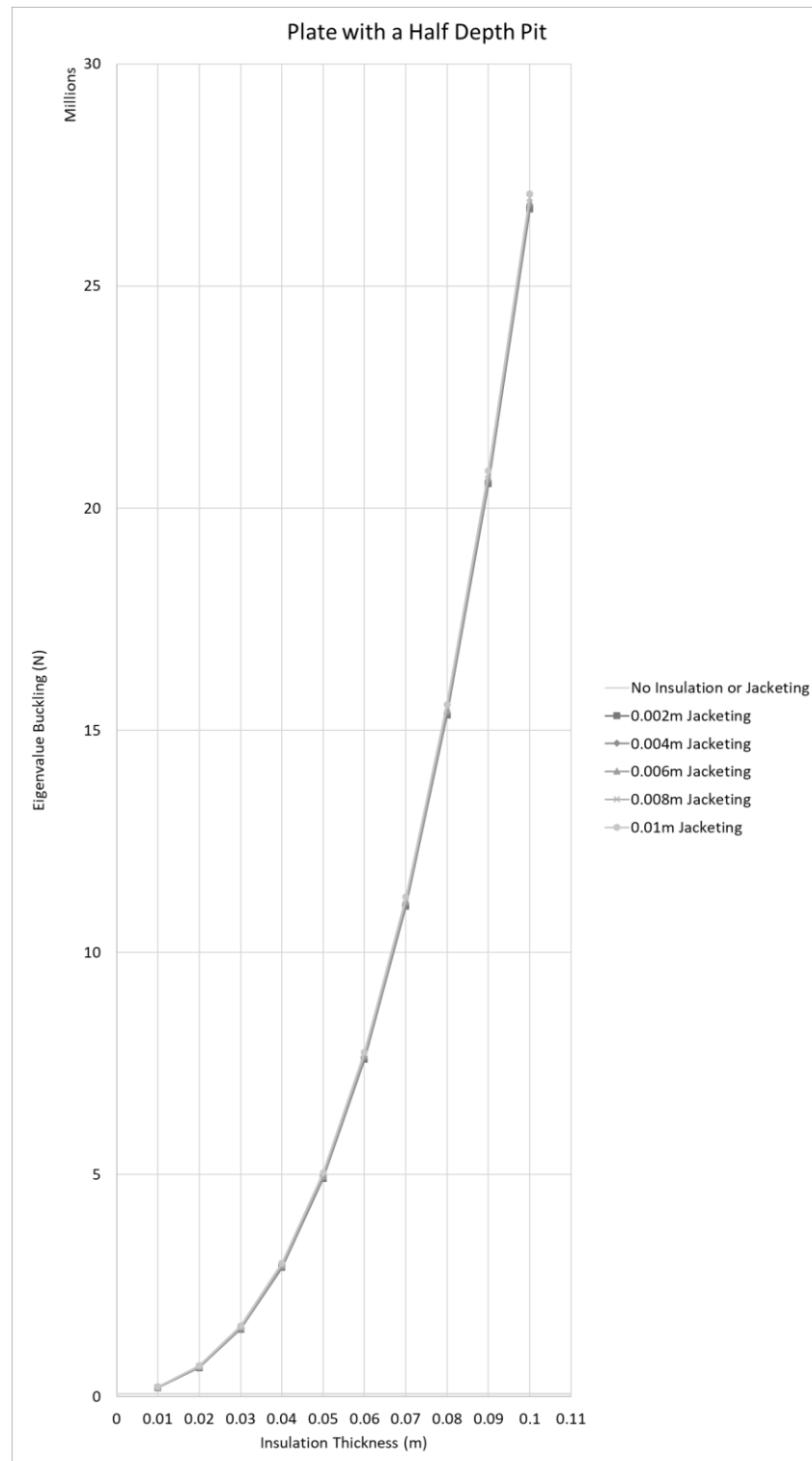
Figure 9.35 Effect of Increasing Insulation Thickness – Plate with a Half Depth Pit
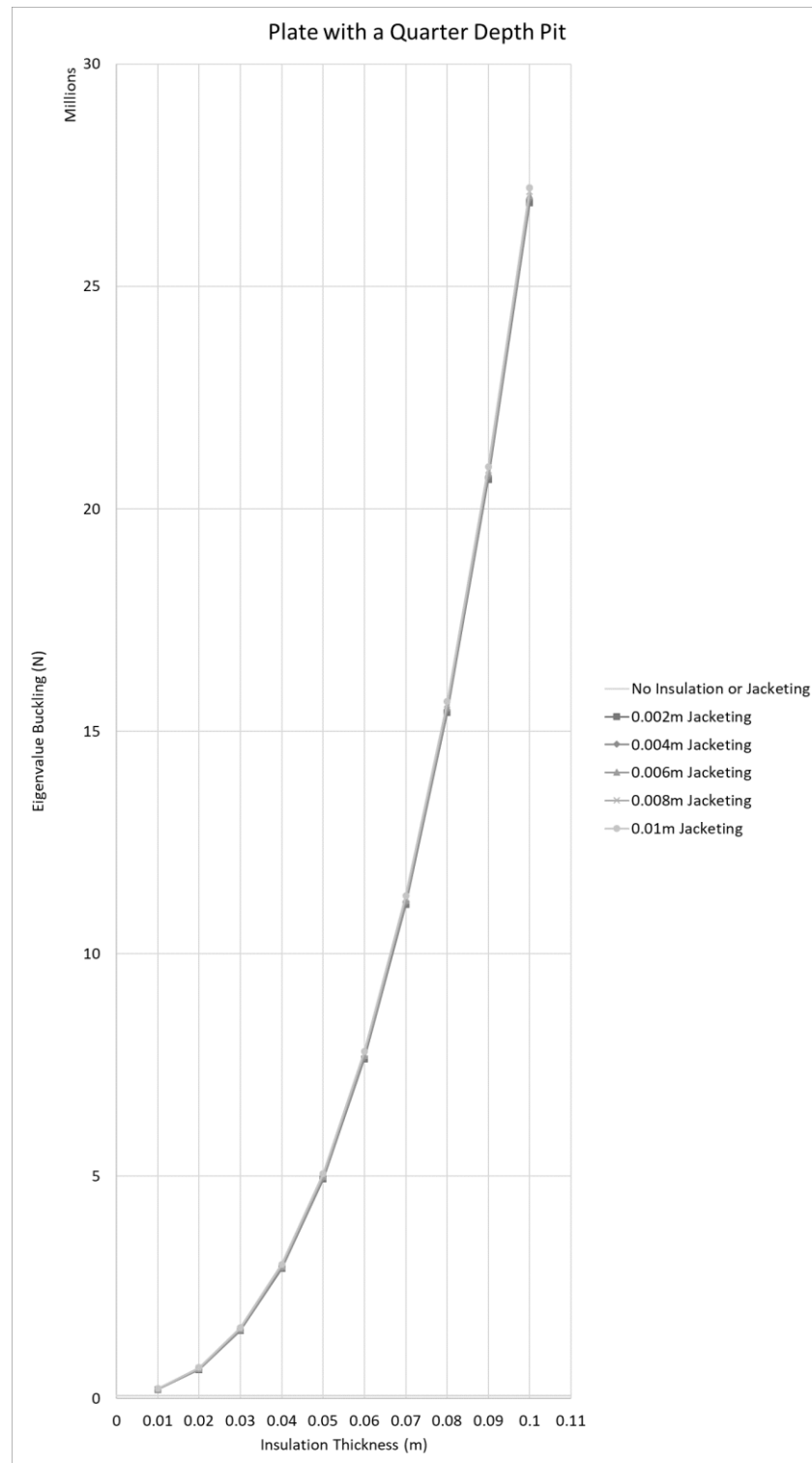
Figure 9.36 Effect of Increasing Insulation Thickness – Plate with a Quarter Depth Pit
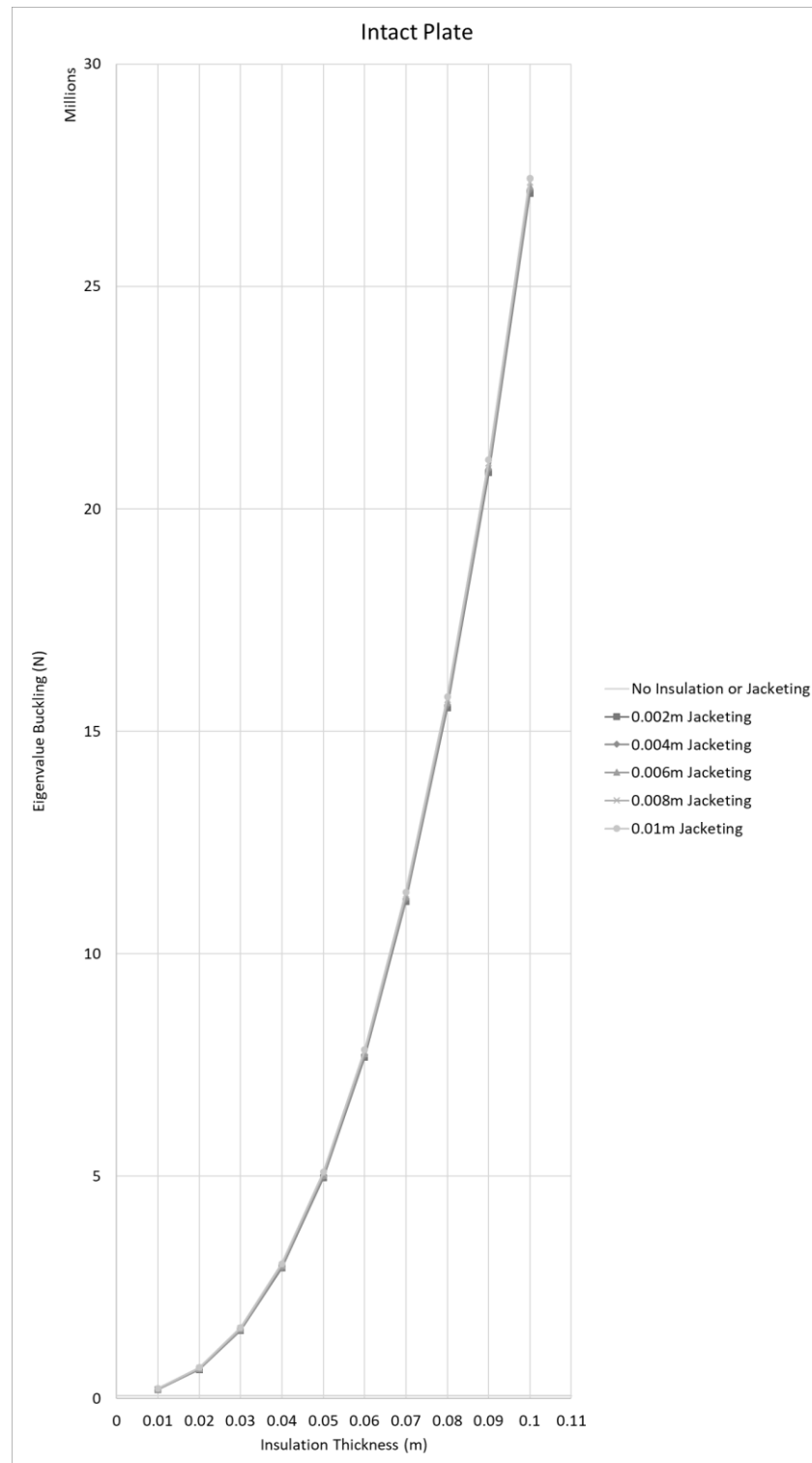
Figure 9.37 Effect of Insulation Jacketing Thickness – Intact Plate

Figures 9.38 to 9.47 allow for the opportunity to compare the buckling values of each of the five plate configurations at each of the ten insulation thicknesses. The effect of the level of degradation is quite apparent at each of the insulation thicknesses. As would be expected the plate with the hole having the highest level of corrosion effect has the lowest buckling values at each respective point when compared to the highest values as seen in the fully intact plate.

It is interesting to note, as was the case in section 9.2, that it appears when comparing each of the figures that as the insulation thickness increases the relative difference in buckling values between each plate configuration also increases. That is to say that in Figure 9.38 the values for the intact plate and the three plates with pit degradations are quite closely bunched together with the plate with a hole slightly separated.

In Figure 9.47 this is no longer the case as each of the five configurations are now quite evenly spaced. Clearly, the effect of the much larger buckling values will have had some effect on this as the numbers on the y-axis will be considerably larger but in relative terms, it would still be expected that the bunching pattern remains.

There is no real major difference in the effect and the patterns seen with regards to the protective jacketing used. As would be expected the actual buckling values do differ between jacketing types as expected because they have different material properties.

The case is the same when comparing the data in Appendix D, the patterns all remain largely the same with minor fluctuations but the magnitudes of the values can differ drastically due to the varying material properties of the insulation materials.
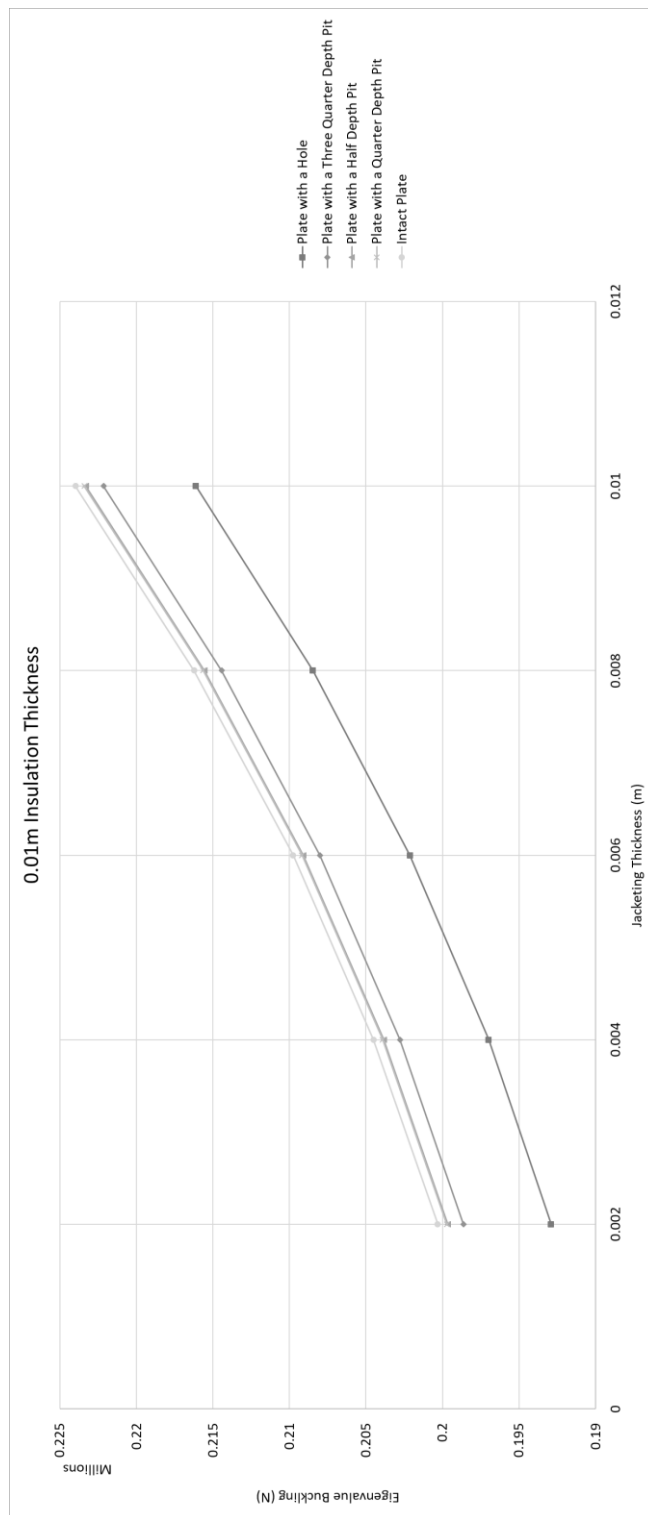
Figure 9.38 Effect of Plate Degradation on Buckling with 0.01 m Insulation Thickness
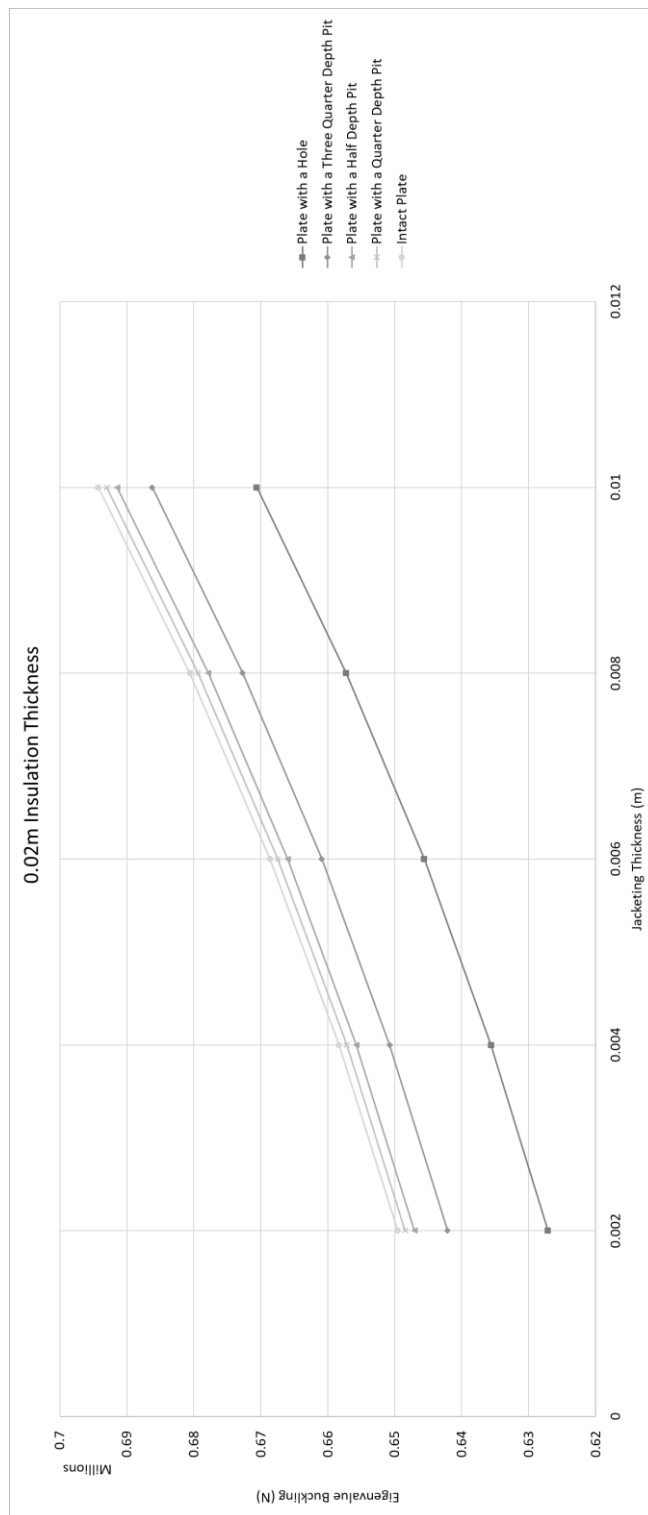
Figure 9.39 Effect of Plate Degradation on Buckling with 0.02 m Insulation Thickness
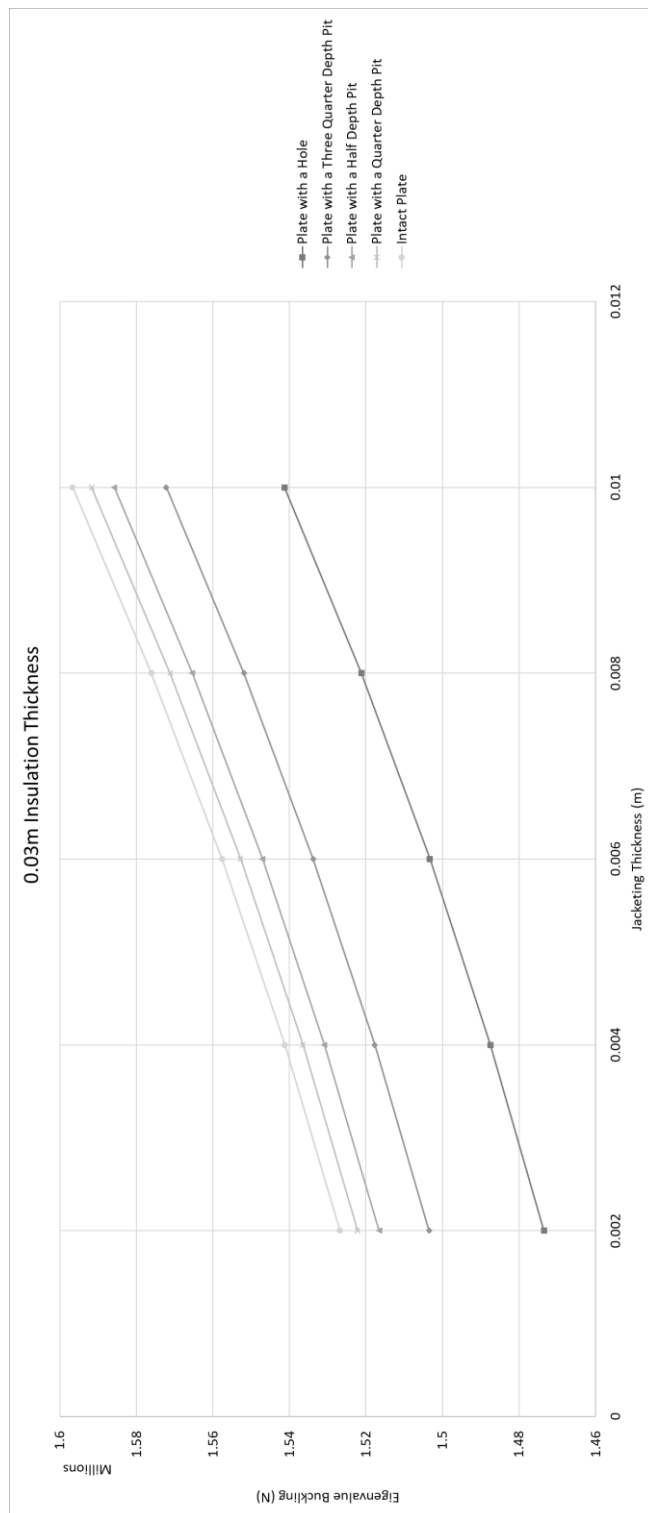
Figure 9.40 Effect of Plate Degradation on Buckling with 0.03 m Insulation Thickness
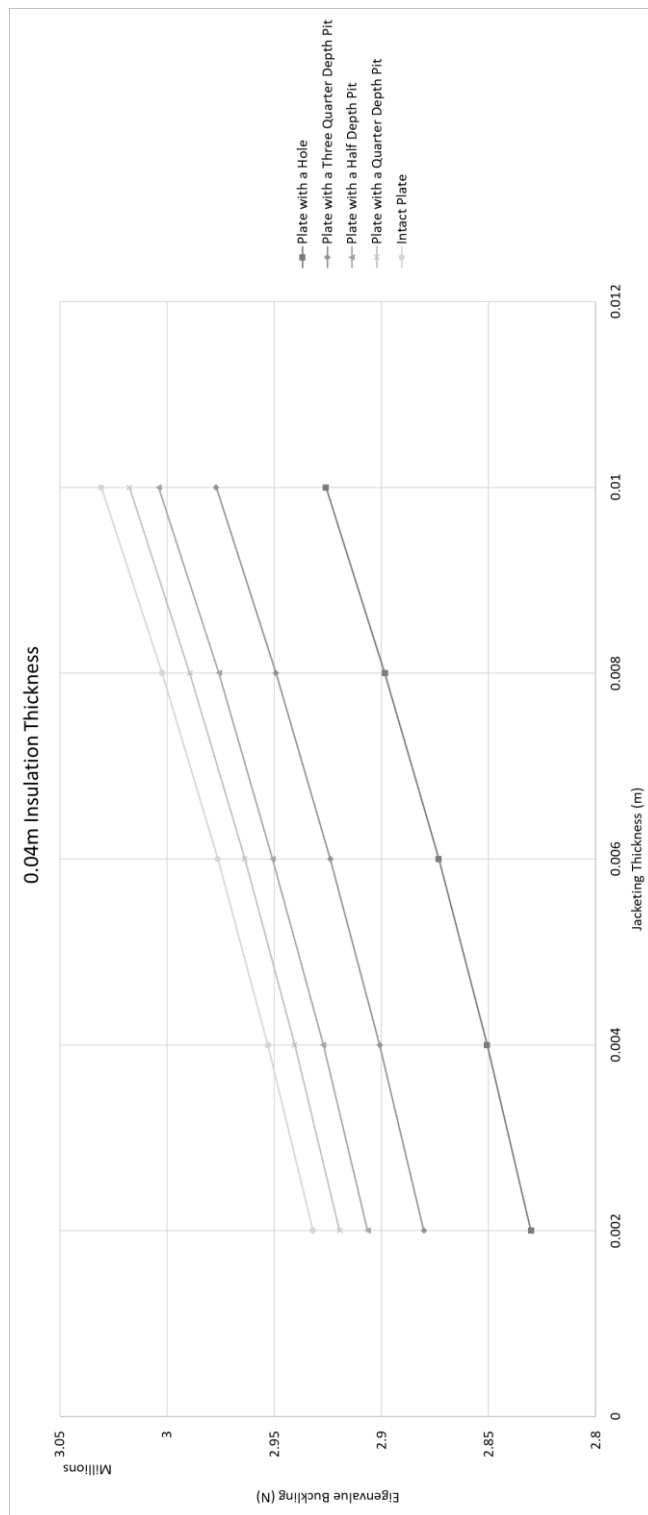
Figure 9.41 Effect of Plate Degradation on Buckling with 0.04 m Insulation Thickness
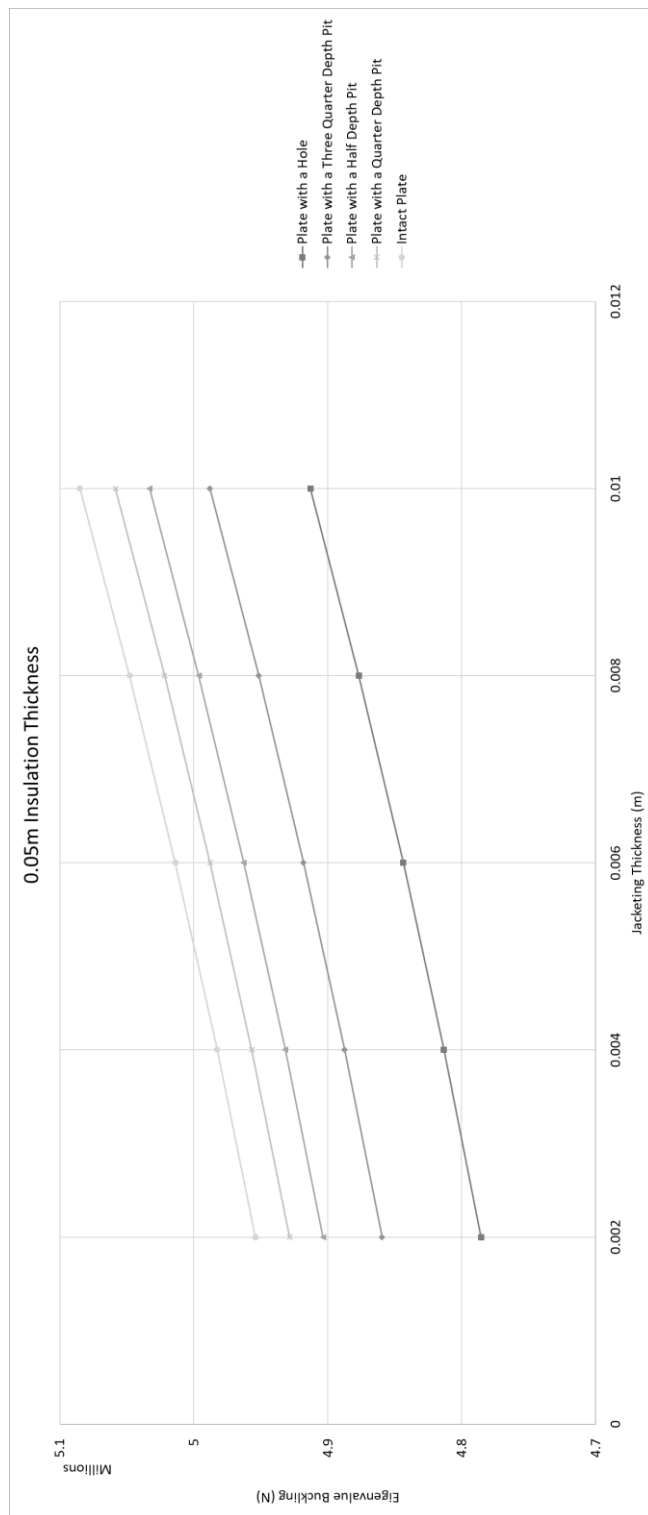
Figure 9.42 Effect of Plate Degradation on Buckling with 0.05 m Insulation Thickness
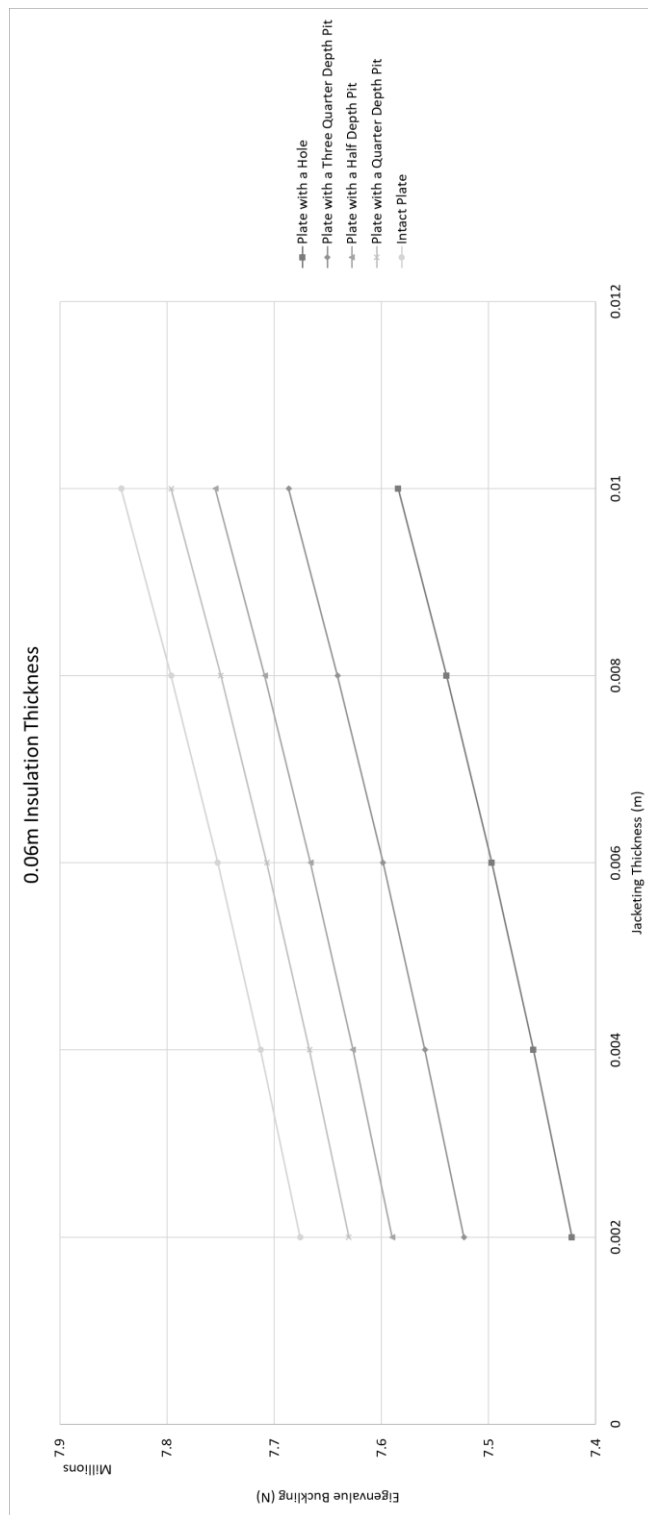
Figure 9.43 Effect of Plate Degradation on Buckling with 0.06 m Insulation Thickness
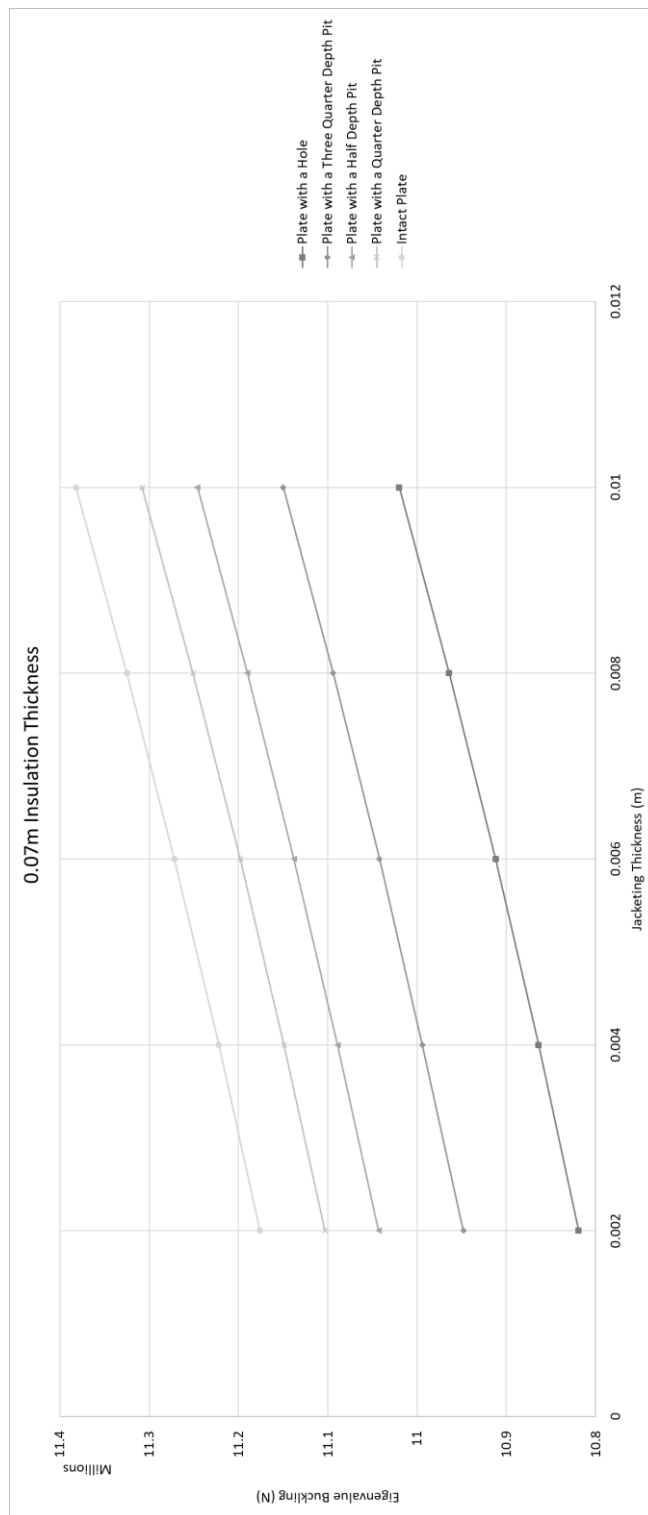
Figure 9.44 Effect of Plate Degradation on Buckling with 0.07 m Insulation Thickness
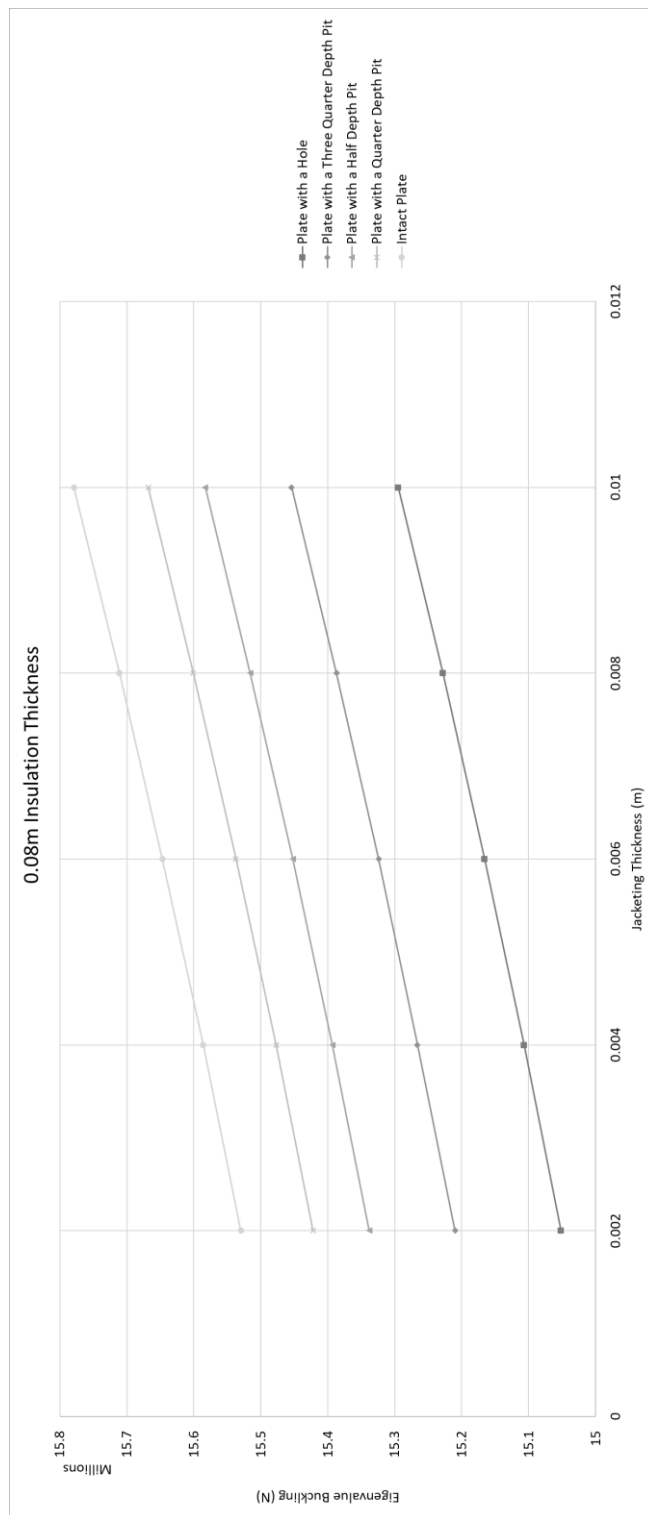
Figure 9.45 Effect of Plate Degradation on Buckling with 0.08 m Insulation Thickness
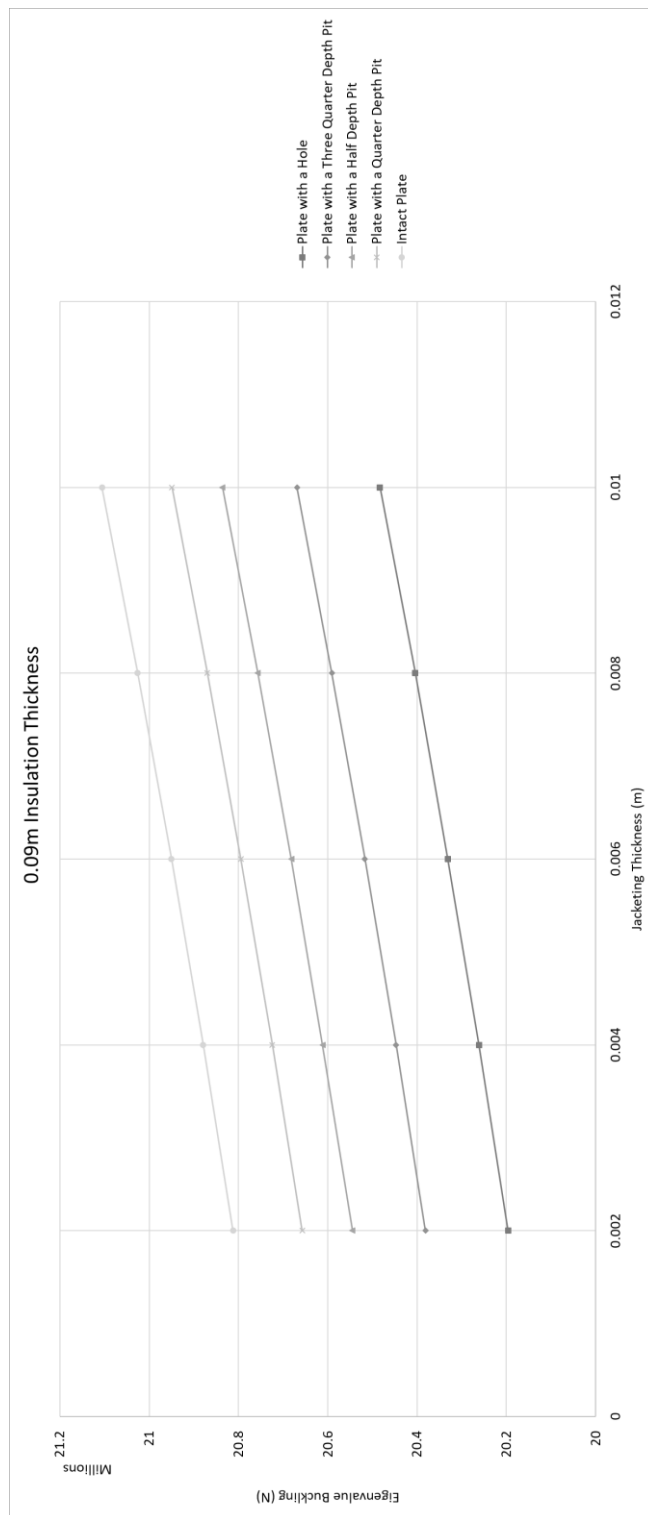
Figure 9.46 Effect of Plate Degradation on Buckling with 0.09 m Insulation Thickness
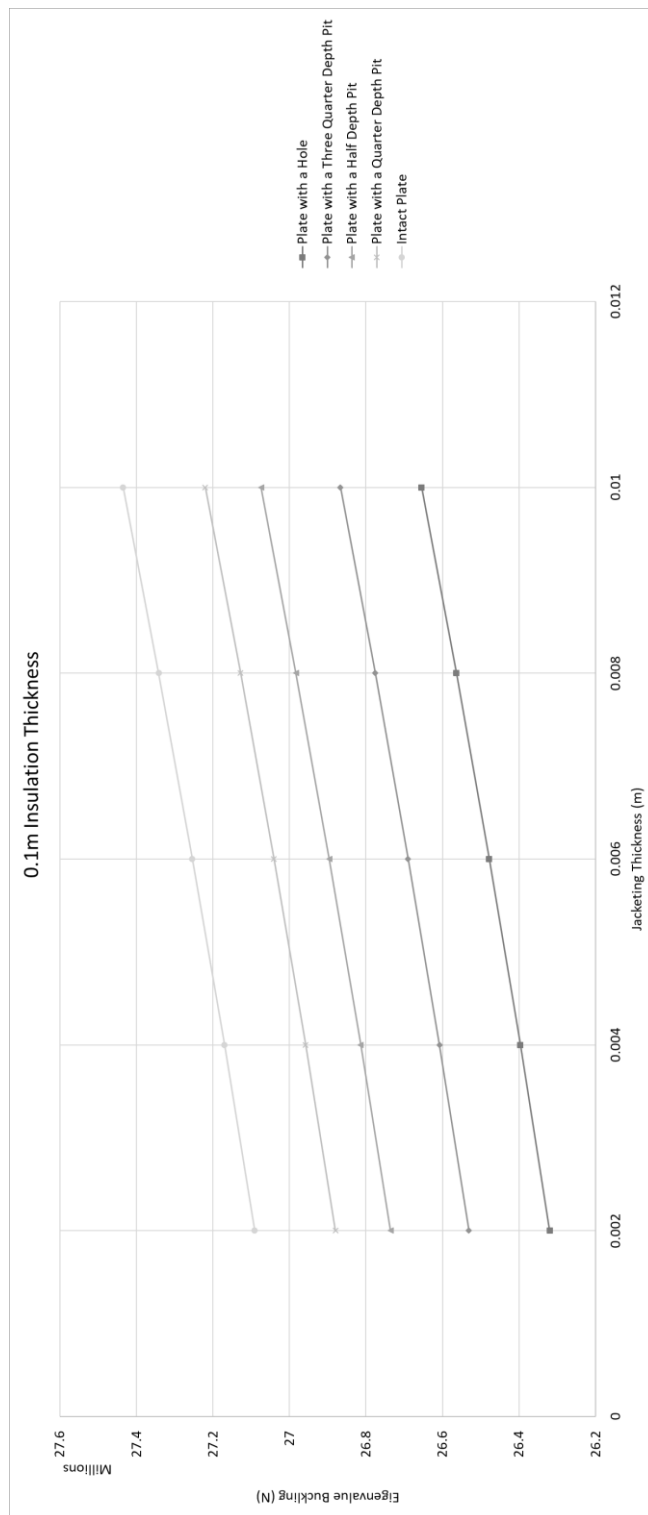
Figure 9.47 Effect of Plate Degradation on Buckling with 0.1 m Insulation Thickness

Chapter Ten: Insulated Pipe Buckling

In the previous chapter, one of the main objectives of this piece of research was presented. This chapter presents another main objective of the project; here the modelling of a 2-D pipe is performed and the effect that the variation of the corrosion damage pit configuration has on the generated buckling value is shown. As before there are five different pit degradation configurations; Fully intact pipe, quarter depth pits, half-depth pits, three-quarter depth pits and pipe with holes

In Chapter Nine, the results of the buckling values with the various insulation systems were presented. In this chapter, only two insulation systems are presented. In both cases, the insulation material is mineral wool and the two jacketing materials are as before; aluminium and polycarbonate. The results presented in the previous chapter establish the variation in the magnitude of the result as attributed to each of the insulation system configurations.

It was felt that the repetition of the analysis of the pipe with each of these various systems was not an efficient use of time and resources. Therefore, as mineral wool is the most commonly used insulation material it was prudent to complete the analysis solely use this material and the two protective coatings to establish the buckling pattern of a steel pipe. From these results it would be possible to extrapolate, if required, to generate approximate results for the other insulation systems.

The chapter has been separated into three sections each focussing on a different part of the problem. In section 10.1 the code will be introduced along with the alternate lines of code to configure the various pipe configurations, corrosion damage and the insulation system material properties. The geometric and material properties will also be presented in tables in section 10.1.

In section 10.2 the results for the mineral wool insulation material will be presented where an aluminium protective jacket was used. The final section, 10.3, will show the results when a polycarbonate protective jacket was used with the mineral wool insulation.

The raw data tables for the results from sections 10.2 and 10.3 will be found in Appendix E, which will also contain any full versions of the code used to model the pipe buckling problem. In the results section of this chapter, graphs will be presented to show the effect on the buckling value due to the increasing jacketing and insulation thickness on each of the pipe degradation types. There will also be graphs that compare the effect each of the corrosion damage configurations has at each of the varying insulation and jacketing thicknesses.

10.1   Setup for the Insulated Pipe Buckling

As mentioned in the introduction there are five configurations of the steel pipe with varying levels of pit deterioration. The fully intact pipe has been subjected to no corrosion damage, through deterioration equal to a quarter of the thickness of the pipe, to half the thickness, then three-quarters and finally where the corrosion has fully deteriorated a section of the pipe leaving a circular hole.

In previous chapters, the damage due to corrosion has occurred in a single place in the centre of the geometric system. For this chapter, it was decided to add in some additional complexity to the model. As the system is a pipe it was decided that the corrosion damage would take place in the central section of the pipe and instead of a single degradation site there would be four equally sized and spaced sites around the circumference of the model in this central section. Figure 10.1 depicts these corrosion sites in relation to the full model and also indicates dimensions associated with the geometry. The boundary conditions associated with the pipe are that all the nodes on the end of the pipe opposite to the load point are fully constrained and the remaining nodes throughout the pipe are fully free. Unlike before where the nodes were coupled to ensure equal displacement in this configuration the load is divided equally between the nodes as a load at the centre point would not be feasible as the pipe is hollow. In this chapter the codes presented initially will be where the corrosion sites are fully corroded holes.
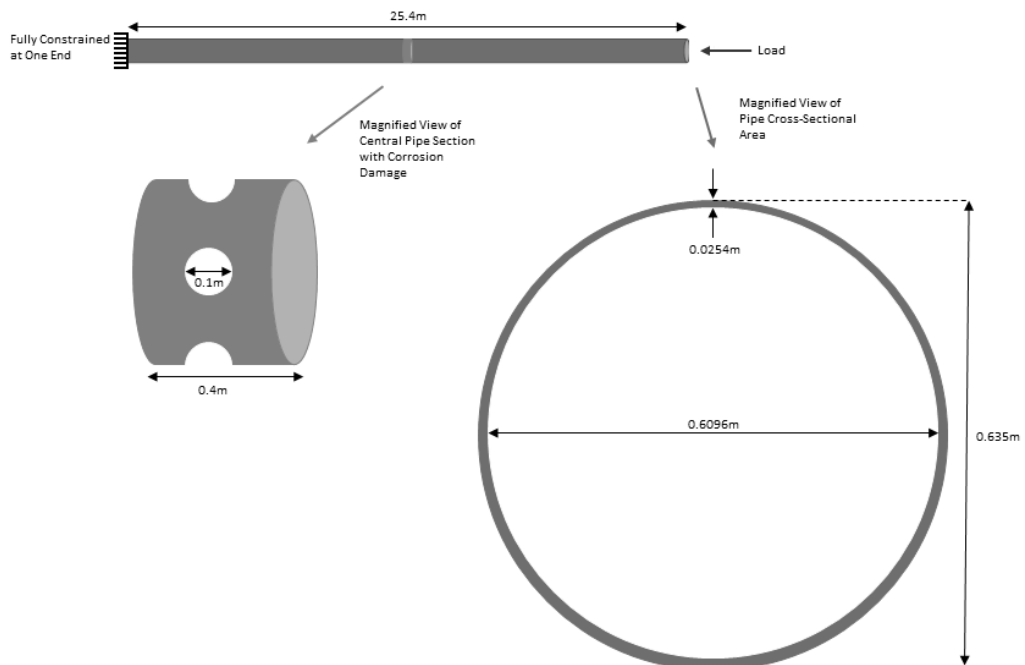
Figure 10.1 Pipe Configuration

Table 10.1 presents the geometric and material properties relating to the steel pipe setup and Table 10.2 provides the material properties for the mineral wool; insulation materials and two protective jacketing materials used in this chapter. Please note that some of the geometric and material property values vary when compared to those used in previous chapters.

Table 10.1 Steel Pipe Geometric and Material Properties

Geometric or Material Property	Value
Total Pipe Length (m)	25.4
Central Section of Pipe Length (m)	0.4
The Inner Radius of the Pipe (m)	0.6096
The Outer Radius of the Pipe (m)	0.635
The Thickness of the Pipe (m)	0.0254
The Shape of the Pit or Hole	Circular
The Diameter of the Pit or Hole (m)	0.1
Young's Modulus (E) (Pa)	2E11
Poisson's Ratio (v)	0.3

Table 10.2 Insulation and Jacketing Material Properties

Material	Young's Modulus (E) (Pa)	Poisson's Ratio (v)
Mineral Wool	5.1E10	0.064
Aluminium	6.9E10	0.334
Polycarbonate	2.4E9	0.37

10.1.1 Validation of the Written Code

In previous chapters, 3-D variations of the code were created to model the problem and have then been used to validate the results provided by ANSYS. In this chapter, instead of creating a 3-D code a variation of the 2-D code which does not include the separate central section, where the corrosion degradations are present, was created to validate the 2-D model. These two models were both run in ANSYS and as can be seen in Table 10.3 the results generated are suitably similar to validate the code. A copy of the full version of the validation code can found in Appendix E as Code E.1. There are some new pieces of coding language in the validation, these will be discussed further in section 10.1.2.

As a second level of validation, it was decided that it would be interesting to use the Euler Column Critical Load Formula (Beer & Johnston, 2014), shown by Equation 10.1, to generate a buckling value for comparison and validation purposes and this result is also presented in Table 10.3. Again the results generated by the hand calculation are very similar to both of the ANSYS results.

Table 10.3 Generation of Intact Pipe Buckling Value through Various Methods

Buckling Result Method	Buckling Result (N)
Solid Pipe with Areas for Holes/Pits Model	14,672,000
Solid Pipe Validation Model	14,668,000
Hand Calculation	14,679,000

$$P_{Cr} = \frac{\pi^2 \, x \, E \, x \, I}{(K \, x \, L)^2}$$

(10.1)

where:

P$_{Cr}$ Euler's Critical Load (N)

E   Young's Modulus (Pa)

I   Minimum area moment of inertia of the cross-section of the column (m^4)

K   Column effective length factor – accounting for the end conditions – in this case, "2"

L   Unsupported length of the column (m)

10.1.2 Variations in the Code

The code for the insulated example depicted in Figure 10.1 is shown as Code E.2 in Appendix E as a starting point and from there the sections that are altered to model the desired combination of materials and pit configurations will be introduced. As before, any new pieces of coding language not previously seen will also be introduced.

As seen previously, the material properties for the insulation and protective jacketing materials are altered depending on the desired materials. Using the data in Table 10.2 the relevant data is inputted to replace the information shown in the example below.

The first part of the code is where the jacketing material's Young's modulus is entered with the Poisson's ratio in the line underneath. The other information is now hardcoded as there is only insulation type used. Material one denotes the steel components with material two as the void section of the pit or hole. Material three is the insulation material with the jacketing material indicated by material four.

"SECTYPE,1,SHELL" is the name given to the section of the steel pipe that is always present and always remains the same thickness of 0.0254 metres. This is the two large areas at either side of the central section as well as the areas of the central section that do not make up the corrosion degradation areas. There is no part of this shell section that has the material properties of the void as it is not present. This explains why the coding section shown below omits material two in the "Pipe Shell Section ID" and also why the "0.0254" in the second line of the code is hard written, it also always remains the same.

Part of the code varies depending on the thickness of the insulation, from a minimum of 0.01 to a maximum of 0.1 regardless of the jacketing material present but both numbers must always be the same. The part denoting the thickness of the protective jacketing materials and the maximum and minimum differ depending on the material used but again both numbers must be the same. When the material used is aluminium the range is from 0.0005 to 0.0015 and for polycarbonate, it varies from 0.002 to 0.01.

"SECTYPE,2,SHELL" is the part of the code relating to the pit section of the steel pipe that is always present but the composition of this section varies depending on the level of pit deterioration that is to be modelled. Table 10.4 details the possible combinations available depending on the pit composition.

Table 10.4 Coding Options to Model Degradation Configuration

Degradation Type	Material One (m) (Steel) (Shaded)	Material Two (m) (Void) (Underlined)
Intact Pipe	0.0254	Omitted
Quarter Depth Pit	0.01905	0.00635
Half Depth Pit	0.0127	0.0127
Three-Quarter Depth Pit	0.00635	0.01905
Pipe with a Hole	Omitted	0.0254

The same piece of coding as presented in Chapter Nine is used to inform ANSYS of the two different shell configurations and to which areas to attribute each set of values.

As seen previously the method of using keypoints to create the geometry was considered the best option in this situation. In the first instance the central area where the corrosion degradation was created first. The silhouette of the end of the hollow column was created with keypoints before being connected with arc lines. These arc lines were then divided into two shorter lines of equal length which would produce more area panels when the model was extruded to create the full area.

These actions were repeated two more times in different working planes to create the corrosion degradation areas. Basically, two solid cylinders were created and were then deleted in such a way that the area where these two cylinders made contact with the original hollow column as they passed through would remain as a separate area from the original column. These circular areas became the location of the degradation sites and using the section of code described earlier they could be selected and be given the attribute of shell type two.

Once the central section has been completed the method to produce a hollow column is repeated on either end to produce the full length of the pipe. The areas are glued to ensure the model performs as expected before the boundary conditions and the load is applied. In this example, the number of nodes where the load is to be applied is calculated and the load is divided by this number. It was not possible to use the same loading styles as used with the plate as the load is applied to the centre where there would be a void in this example.

Figure 10.2 presents an example of the buckling mode shape generated by the ANSYS Mechanical APDL programme using one of the pipe configurations discussed in this chapter. It can be seen in the figure that both the original shape (bottom section) and the deformed shape (top section) can be presented together for comparison.
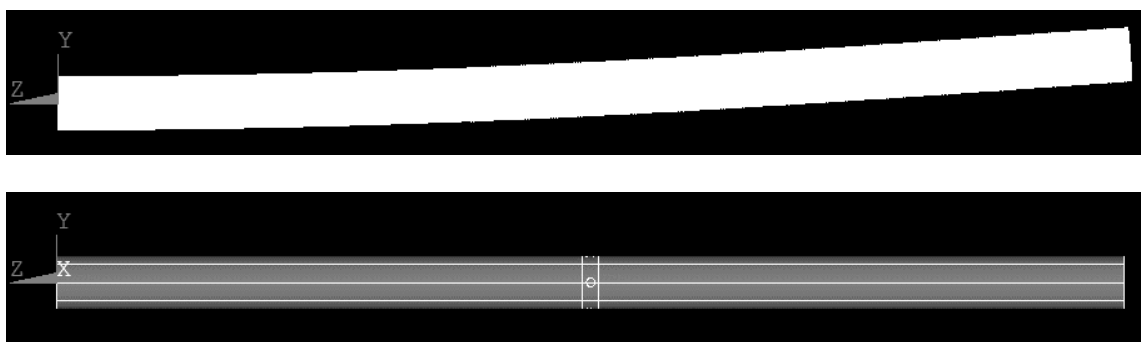
Figure 10.2 Example of the Buckling Mode Shape of an Insulated Pipe

10.2   Aluminium Protective Jacketing

In this section, the results from the Eigenvalue buckling analysis will be presented for the mineral wool insulation material where the system has an aluminium protective jacketing. The pipe was configured at each of the five degradation levels discussed previously.

A table presenting the raw buckling data in its entirety for the mineral wool insulation system can be found as Table E.1 in Appendix E. A number of graphs will be produced and shown in this section from the data in Table E.1 to represent these results and to illustrate the following variables:

- Effect of increasing jacketing thickness
- Effect of increasing insulation thickness
- Comparison of buckling values at each insulation thickness depending on the pipe degradation
- Comparison of buckling values at each jacketing thickness depending on the pipe degradation

The geometric and material properties of the pipe system have remained constant and these details can be found in Table 10.1. The material properties for each of the mineral wool insulation and two jacketing materials are provided in Table 10.2. Please pay close attention to the axes values as they may change drastically so as to give the best overall indication of the piece of information described.

Figures 10.3 to 10.7 depict the effect of the increase in jacketing thickness on each of the five pipe degradation configurations. It can be seen at the bottom of each graph there is a plot that spans the full width, this plot denotes the buckling value of the pipe configuration where there is no insulation system providing additional strength. The jacketing thickness increases from 0.0005 metres as a minimum up to 0.0015 metres at the largest thickness.

In the case of the pipe with holes, this value is 14,588,000 N, with three-quarter depth pits it is 14,627,000 N, half-depth pits equal 14,651,000 N, quarter depth pits are 14,665,000 N and finally a fully intact pipe equals 14,672,000 N. As would be expected the buckling value increases as the level of degradation of the pipe decreases. The degradations cause the pipe to lose some of its inherent structural strength. This information is exactly the same as exhibited with the plate example in Chapter Nine. In the case of the pipe, the magnitude of the difference between the pipe with the holes and the fully intact pipe is considerably smaller than the same examples with the plate. It appears that the differences between the mechanical properties and the geometric properties appear to have a more pronounced effect within the plate example.

The expectation with regards to the addition of an insulation system would be that the buckling strength of the pipe would increase which is exactly as the results show. Whether that be the increase in the thickness of the insulation or an increase in the thickness of the protective coating. As the thickness of the protective coating increases, there is a minor increase in the buckling value when comparing the values at a single insulation thickness. With the pipe examples, these variations are quite small but can be clearly seen in graphical format.

Figures 10.8 to 10.12 depict the effect of increasing the thickness of the insulation on each of the pipe degradation configurations. These latter figures show a much larger relative rise in the buckling value where the insulation thickness increases at each jacketing thickness. The minimum insulation thickness measured is 0.01 metres ranging up to 0.1 metres at the largest value. As before, it can be seen at the bottom of each graph there is a plot that spans the full width, this plot denotes the buckling value of the pipe configuration where there is no insulation system providing additional strength.

As an example, when looking at Figure 10.3, it can be seen that with an insulation thickness of 0.1 metres the buckling value where the jacketing thickness is 0.0005 metres is 16,126,000 N. At the same insulation thickness but after increasing the thickness of the jacketing to the maximum of 0.0015 metres the new buckling value is 16,317,000 N. The only parameter that has changed is the thickness of the protective jacketing and with that, the buckling value has increased as expected.

This increase is relatively modest when compared to another example when looking a Figure 10.8, which will depict the increase in buckling through an increase in insulation thickness. Where the jacketing thickness is 0.0005 metres and the insulation thickness is 0.01 metres the buckling value is 16,126,000 N as before. If instead of increasing the jacketing thickness the insulation thickness is increased only one level up to 0.02 metres the new buckling value is 17,546,000 N.

These results are very similar to the results seen in the previous chapter with regards to the relationship. Clearly, the results in this chapter are considerably smaller in relative terms but the relationship remains the same. As before, the Euler Column Critical Load Formula explains the relationship. The formula produces results more realistically expected as it is dealing with an actual columnar form which affects the results rather than the flat plate from the previous chapter. It is also interesting to note that the results have a more linear character than the plate results due to the more realistic values involved.

Also, the fact that the pipe example deals with a considerably slenderer example, i.e. the length relative to the thickness is considerably more. This was not the case in the plate example which may further explain the generation of more theoretical results. The plate example would not usually be considered in isolation but would be part of a larger network, its purpose was to provide a comparison tool to the pipe example which is of greater interest overall.

Figure 10.3 Effect of Increasing Jacketing Thickness – Pipe with Holes
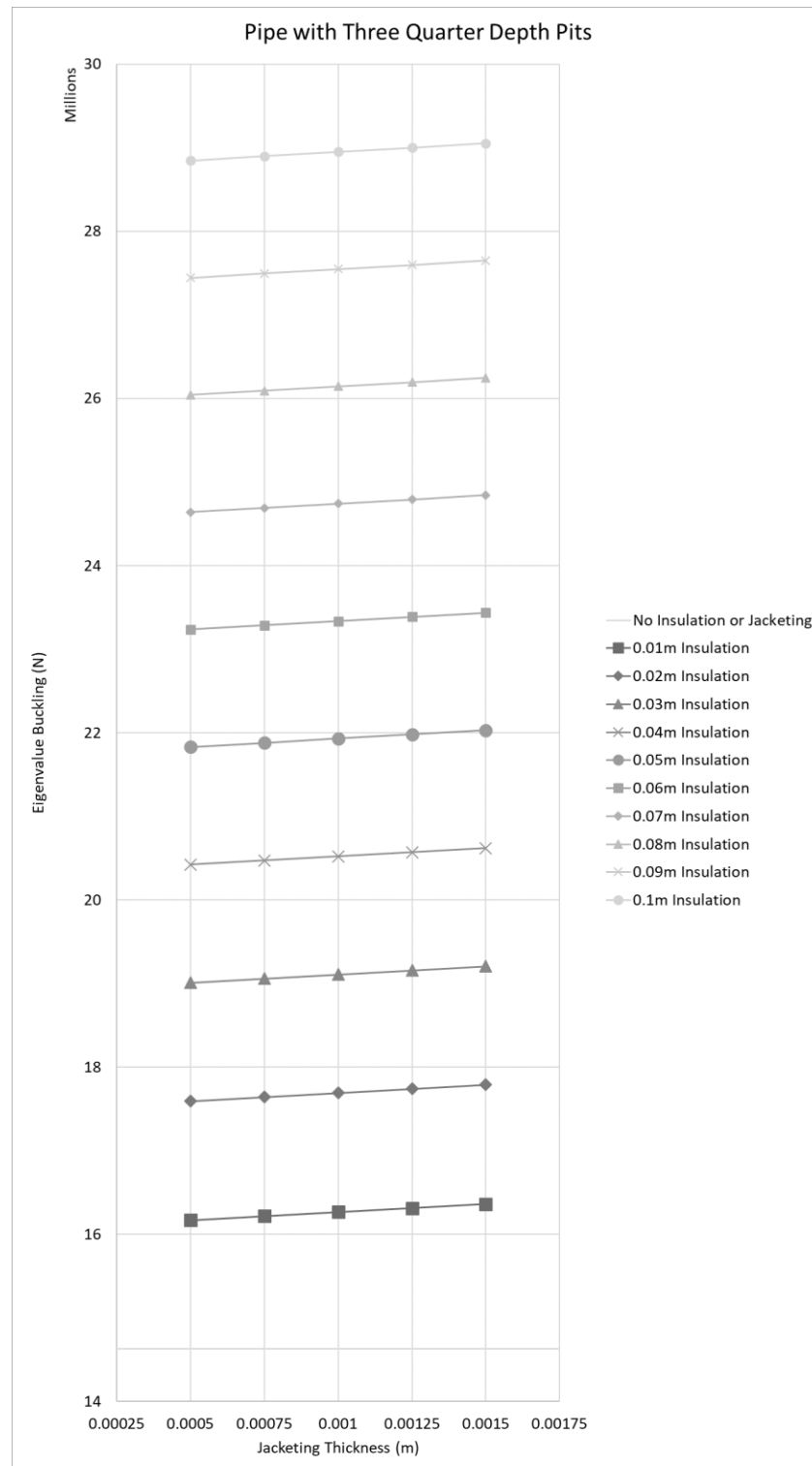
Figure 10.4 Effect of Increasing Jacketing Thickness – Pipe with Three-Quarter Depth Pits
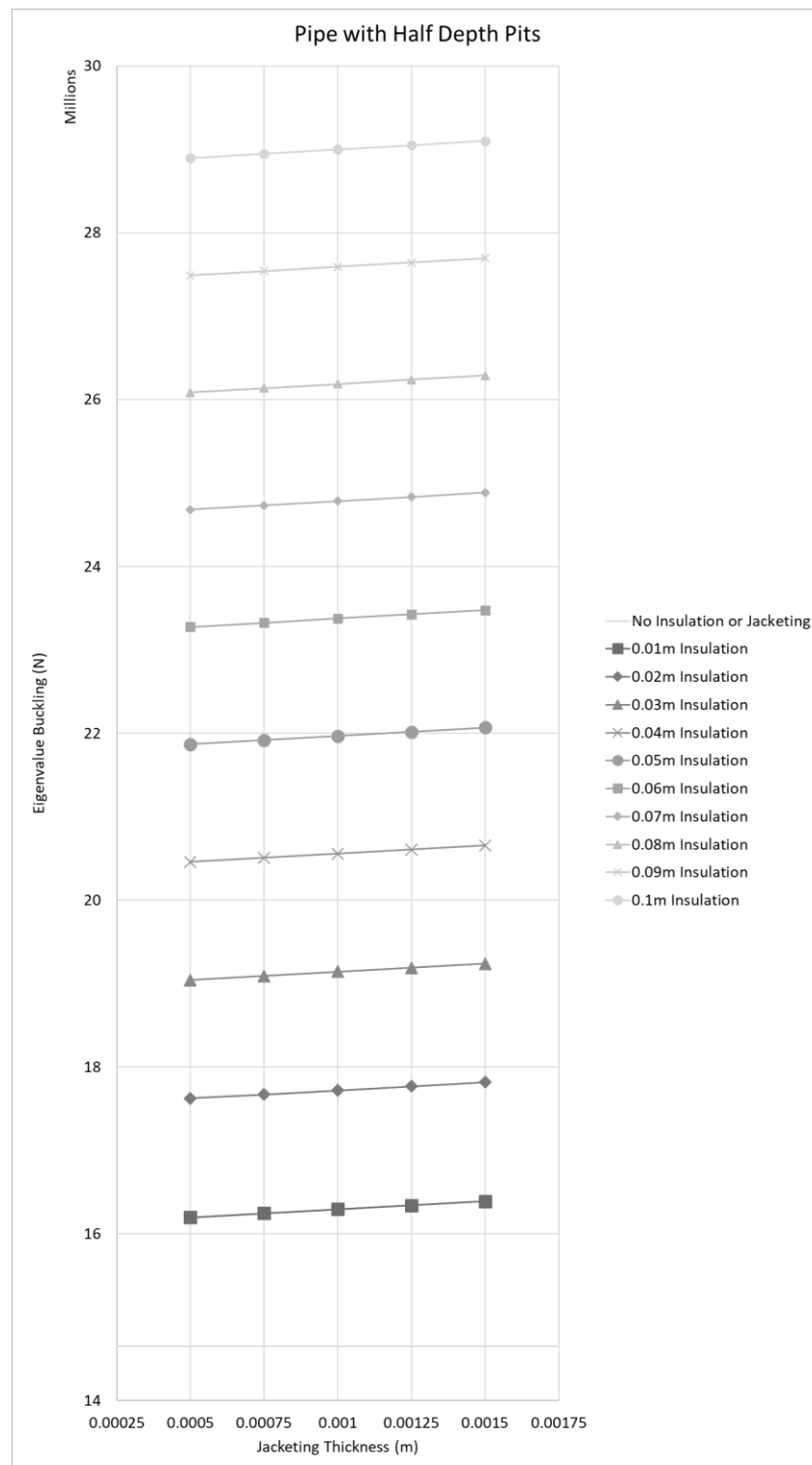
Figure 10.5 Effect of Increasing Jacketing Thickness – Pipe with Half Depth Pits
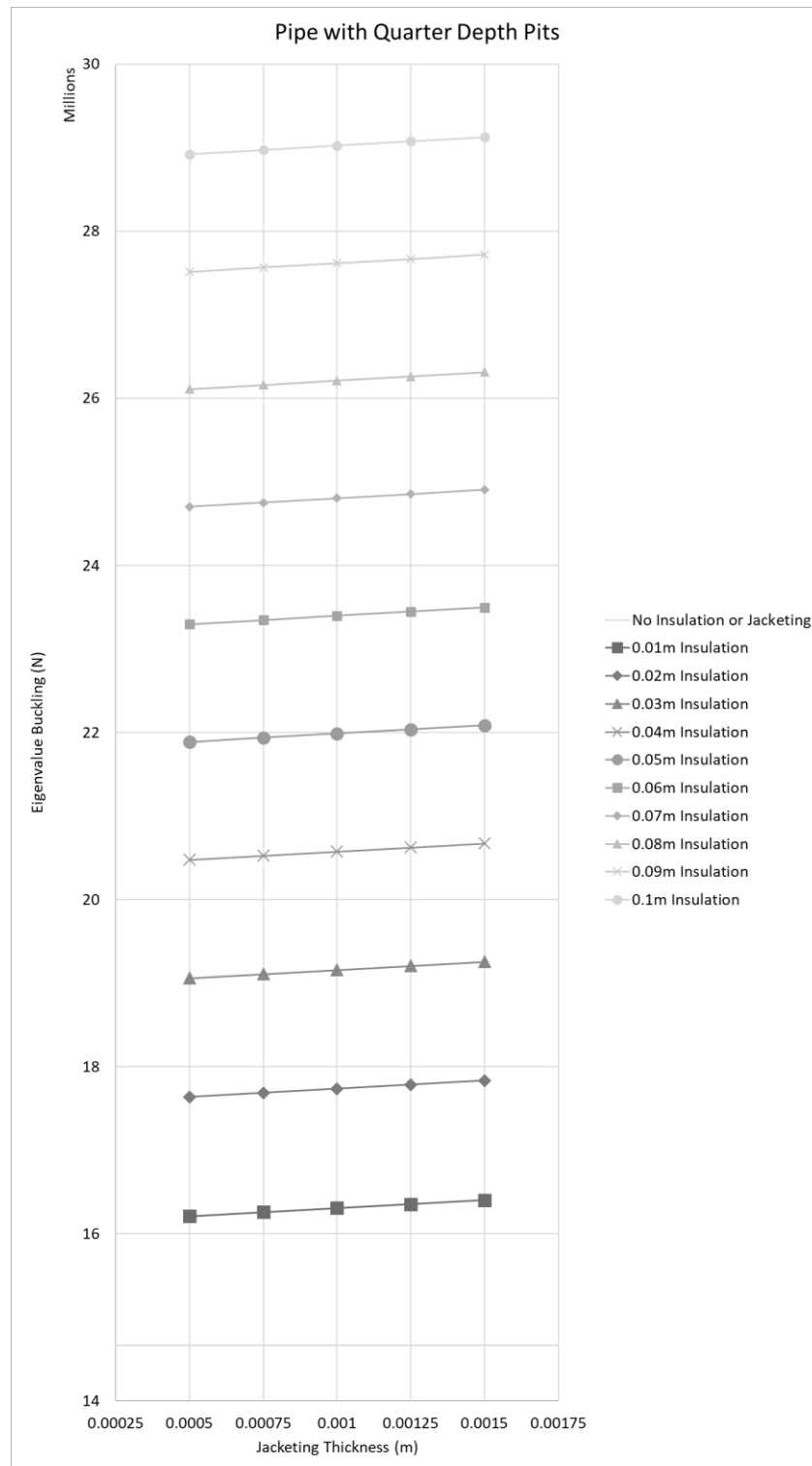
Figure 10.6 Effect of Increasing Jacketing Thickness – Pipe with Quarter Depth Pits
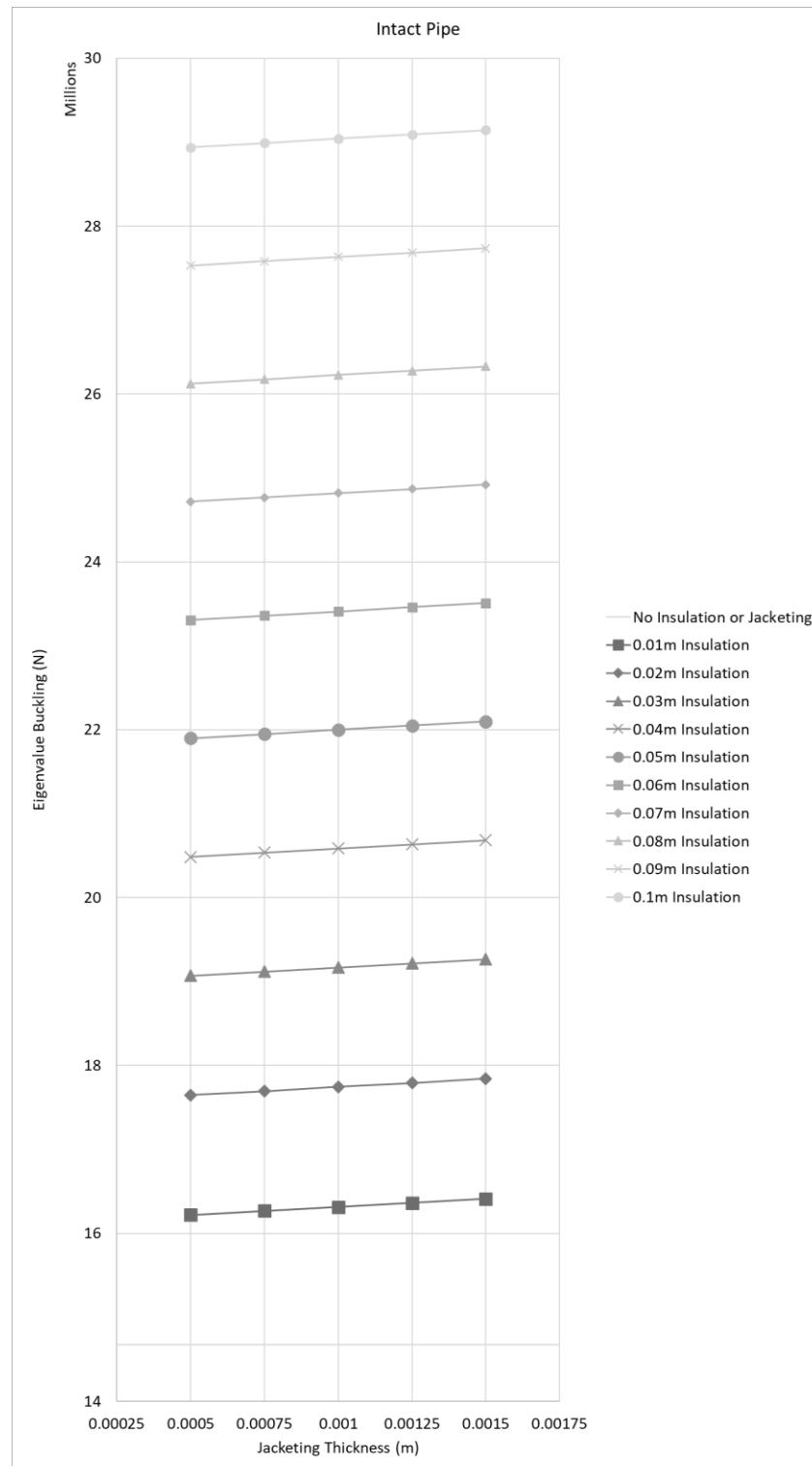
Figure 10.7 Effect of Increasing Jacketing Thickness – Intact Pipe
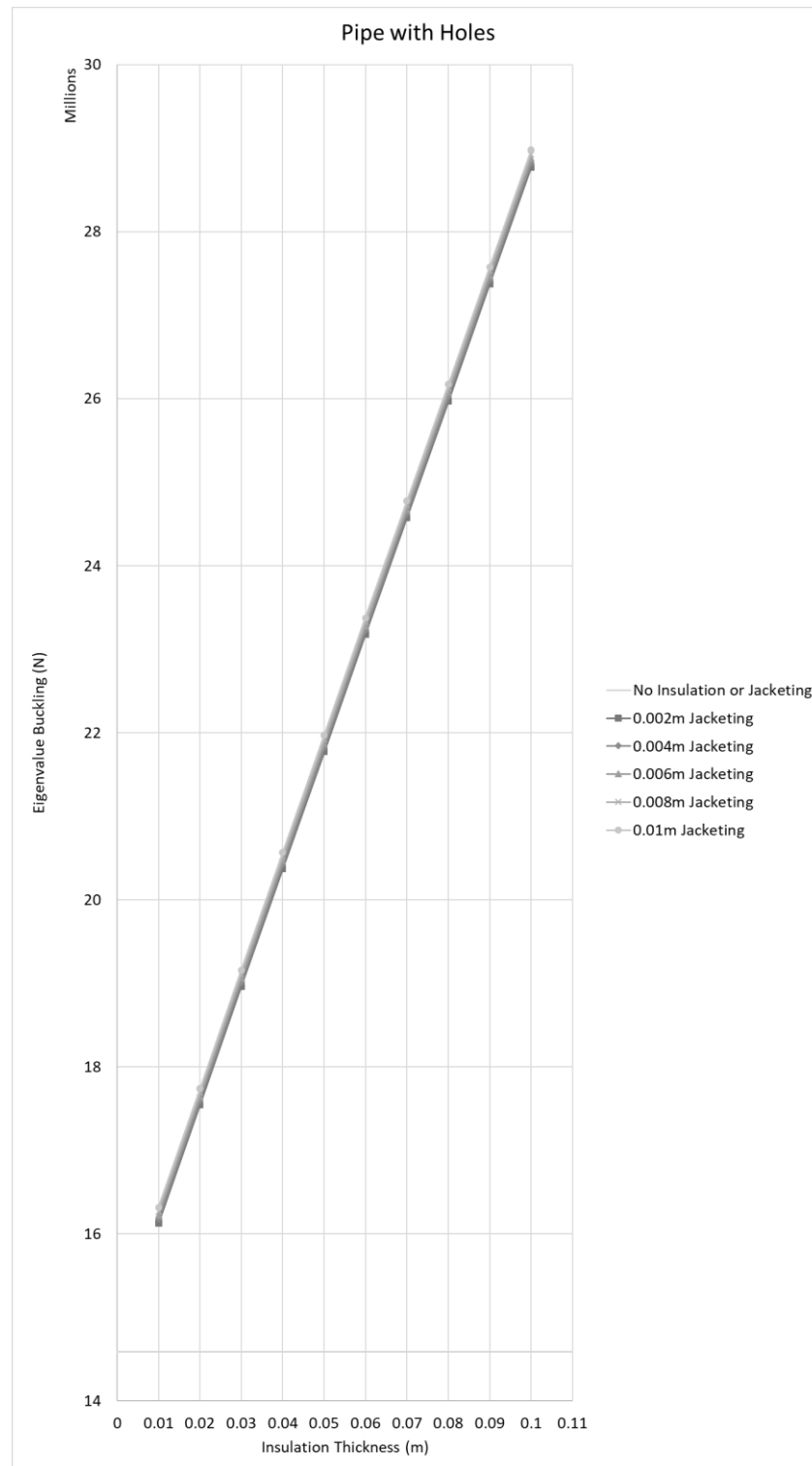
Figure 10.8 Effect of Increasing Insulation Thickness – Pipe with Holes
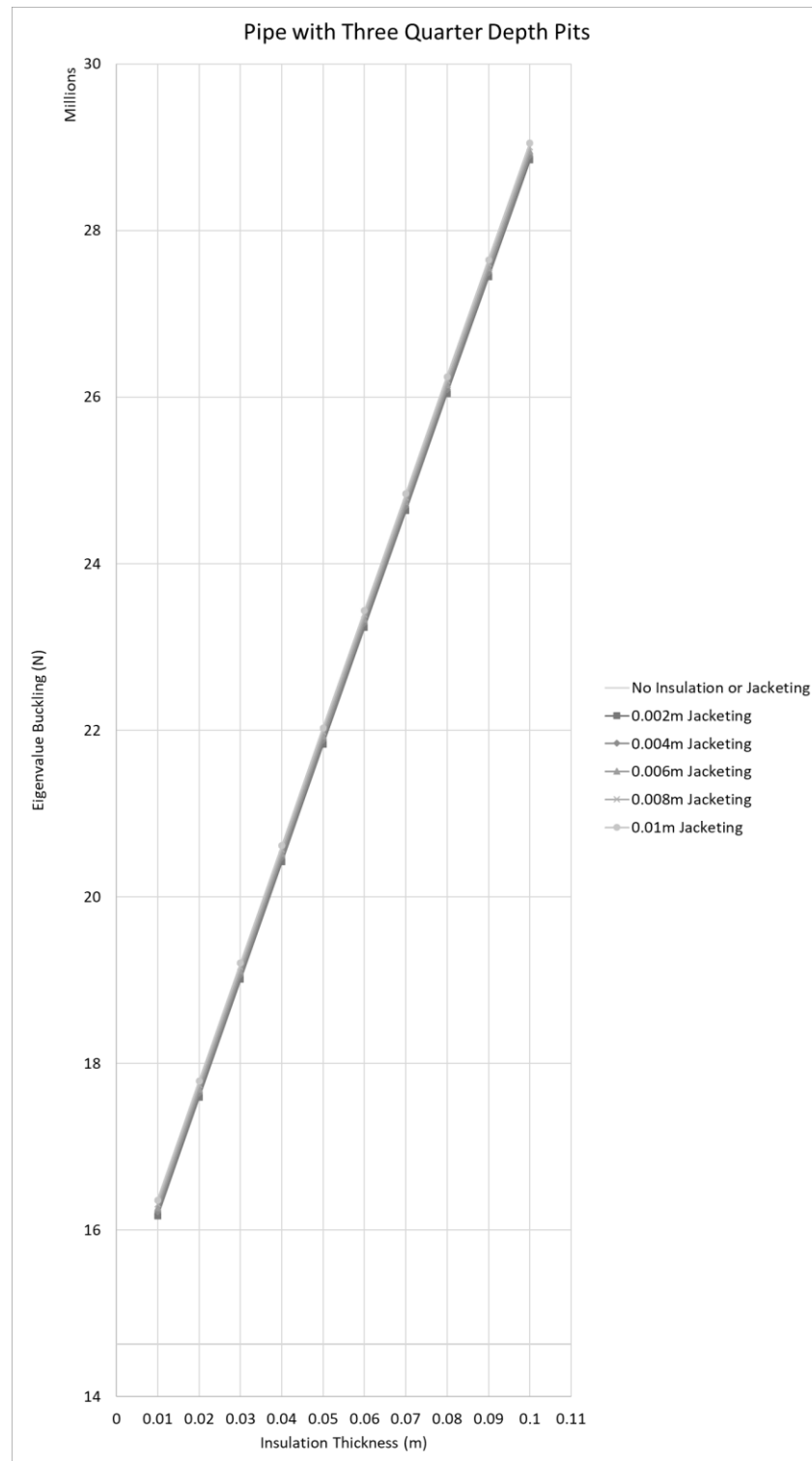
Figure 10.9 Effect of Increasing Insulation Thickness – Pipe with Three-Quarter Depth Pits
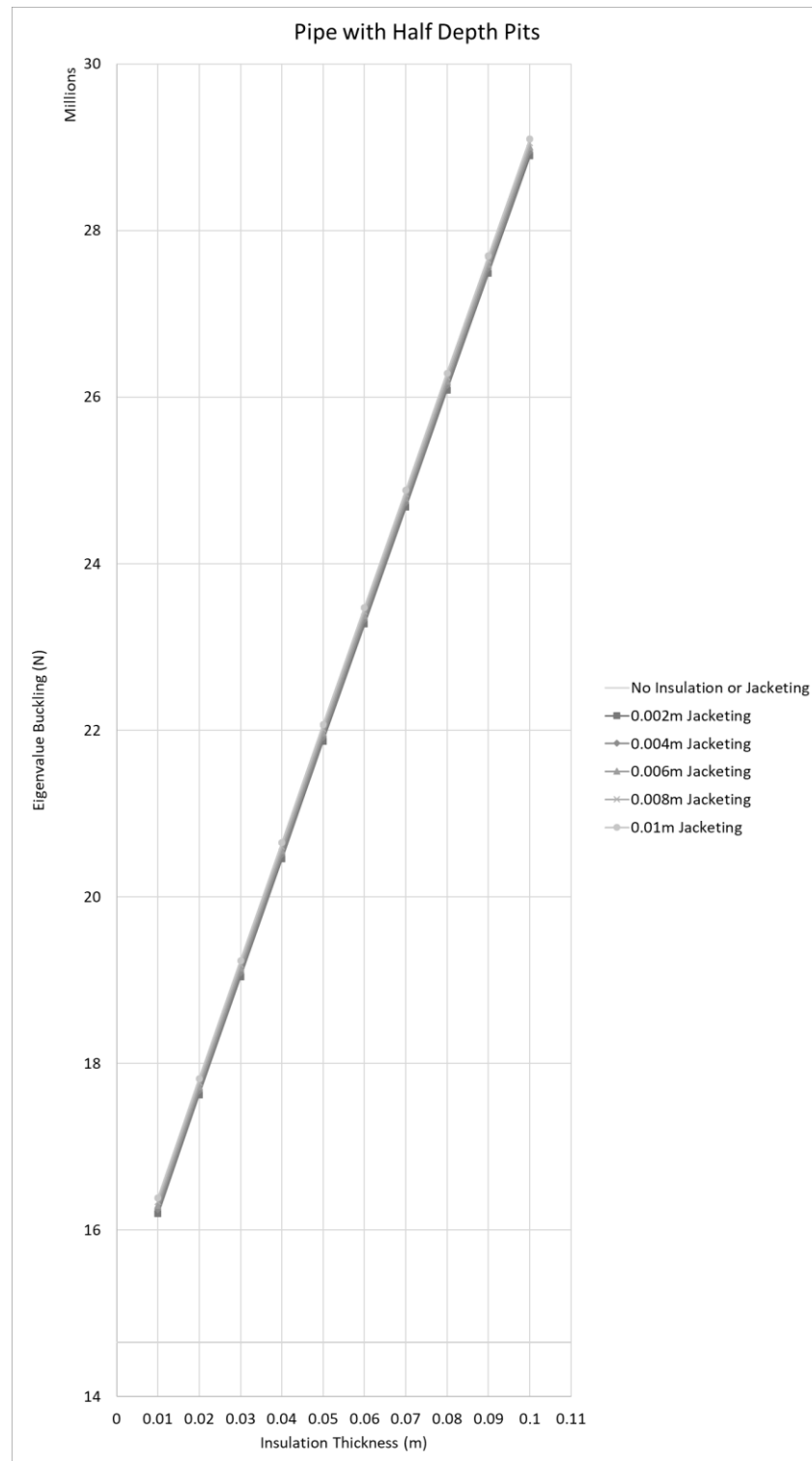
Figure 10.10 Effect of Increasing Insulation Thickness – Pipe with Half Depth Pits
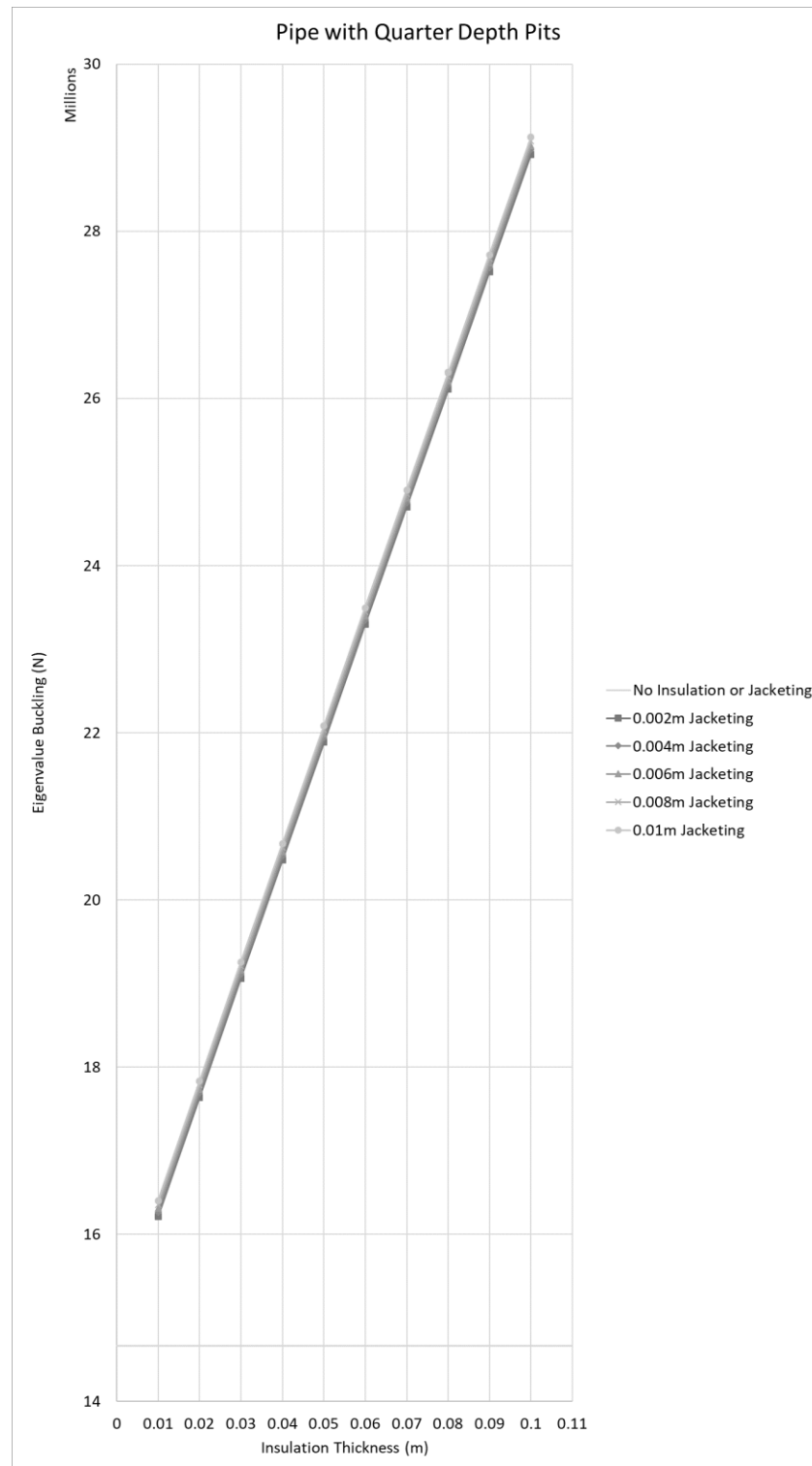
Figure 10.11 Effect of Increasing Insulation Thickness – Pipe with Quarter Depth Pits
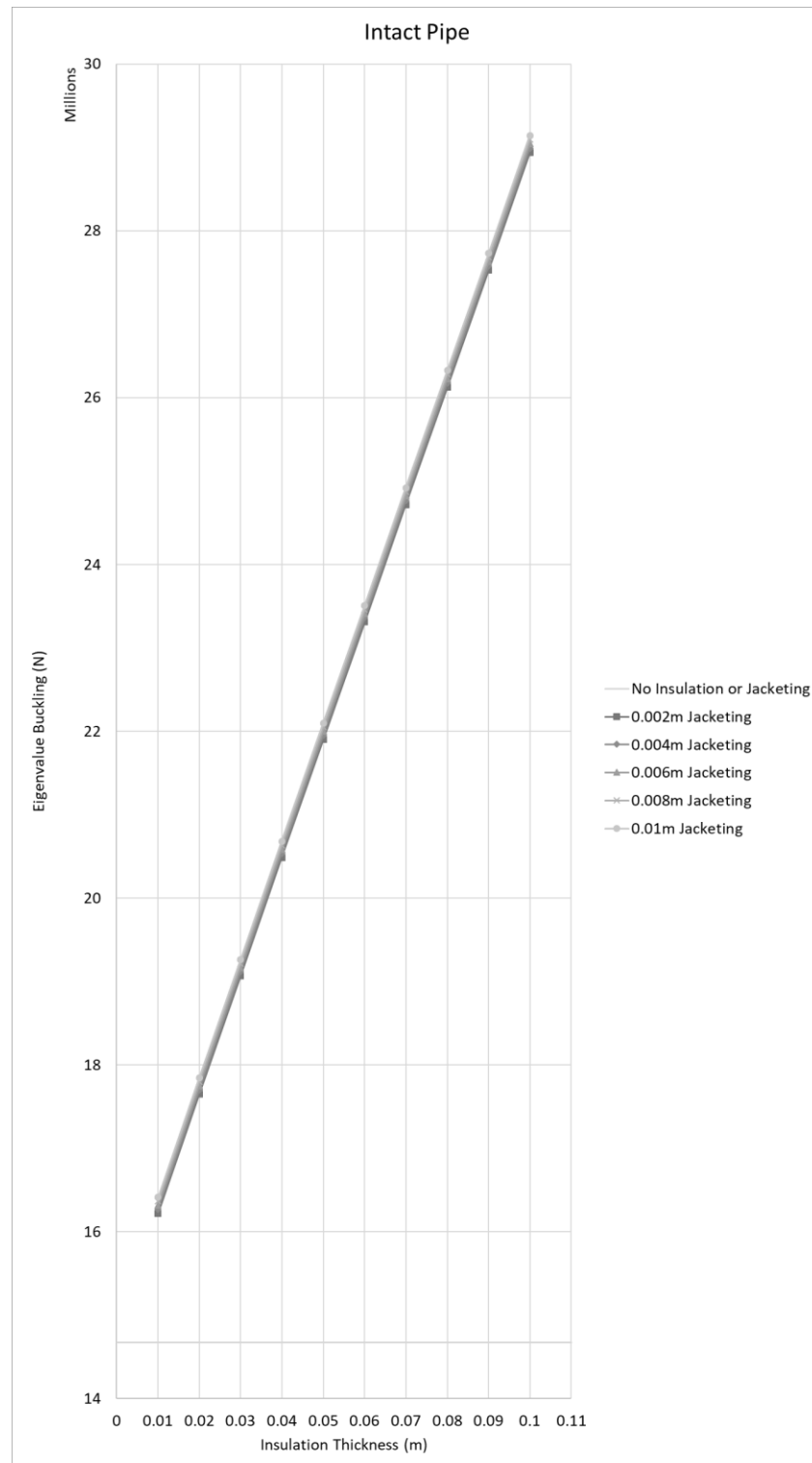
Figure 10.12 Effect of Insulation Jacketing Thickness – Intact Pipe

Figures 10.13 to 10.22 allow for the opportunity to compare the buckling values of each of the five pipe configurations at each of the ten insulation thicknesses. The effect of the level of degradation is quite apparent at each of the insulation thicknesses. As would be expected the pipe with the holes having the highest level of corrosion effect has the lowest buckling values at each respective point when compared to the highest values as seen in the fully intact pipe.

It is interesting to note that it appears when comparing each of the figures that as the insulation thickness increases the relative difference in buckling values between each pipe configuration remains fairly constant with a possible slight increase in the values as the insulation thickness increases. That is to say that in Figure 10.13 the values for the intact pipe and the three pipes with pit degradations are quite closely bunched together with the pipe with the holes slightly separated. In Figure 10.22 this formation is still present with a possible slight increase in the spacing between the plate configurations accounting for the relative increase in value.
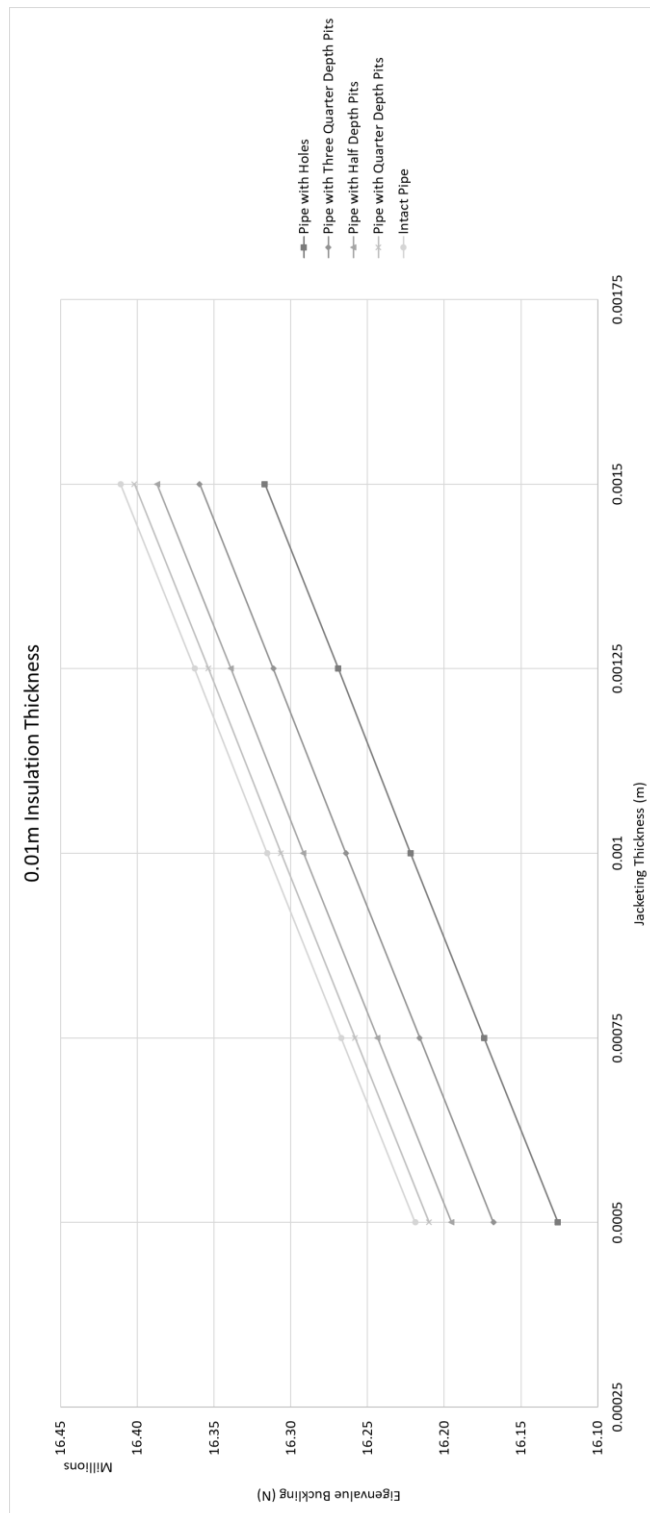
Figure 10.13 Effect of Pipe Degradation on Buckling with 0.01 m Insulation Thickness
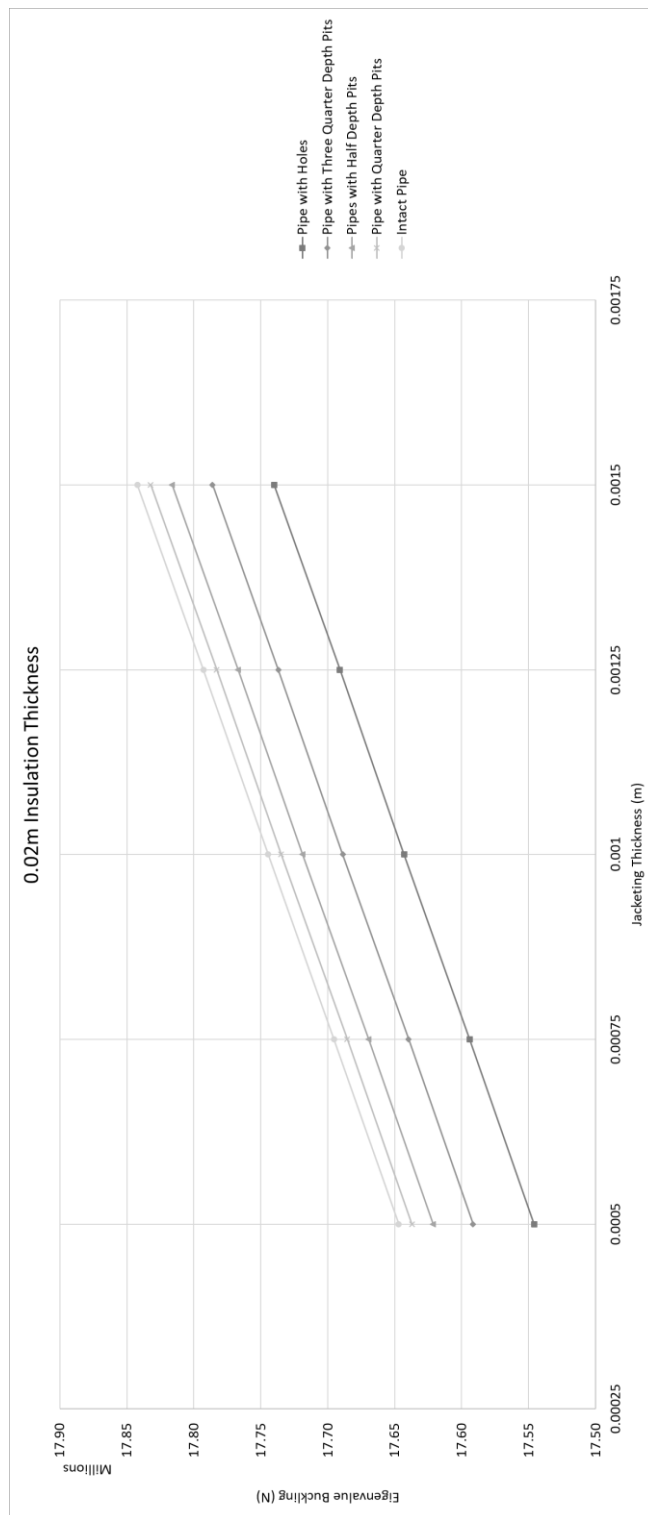
Figure 10.14 Effect of Pipe Degradation on Buckling with 0.02 m Insulation Thickness
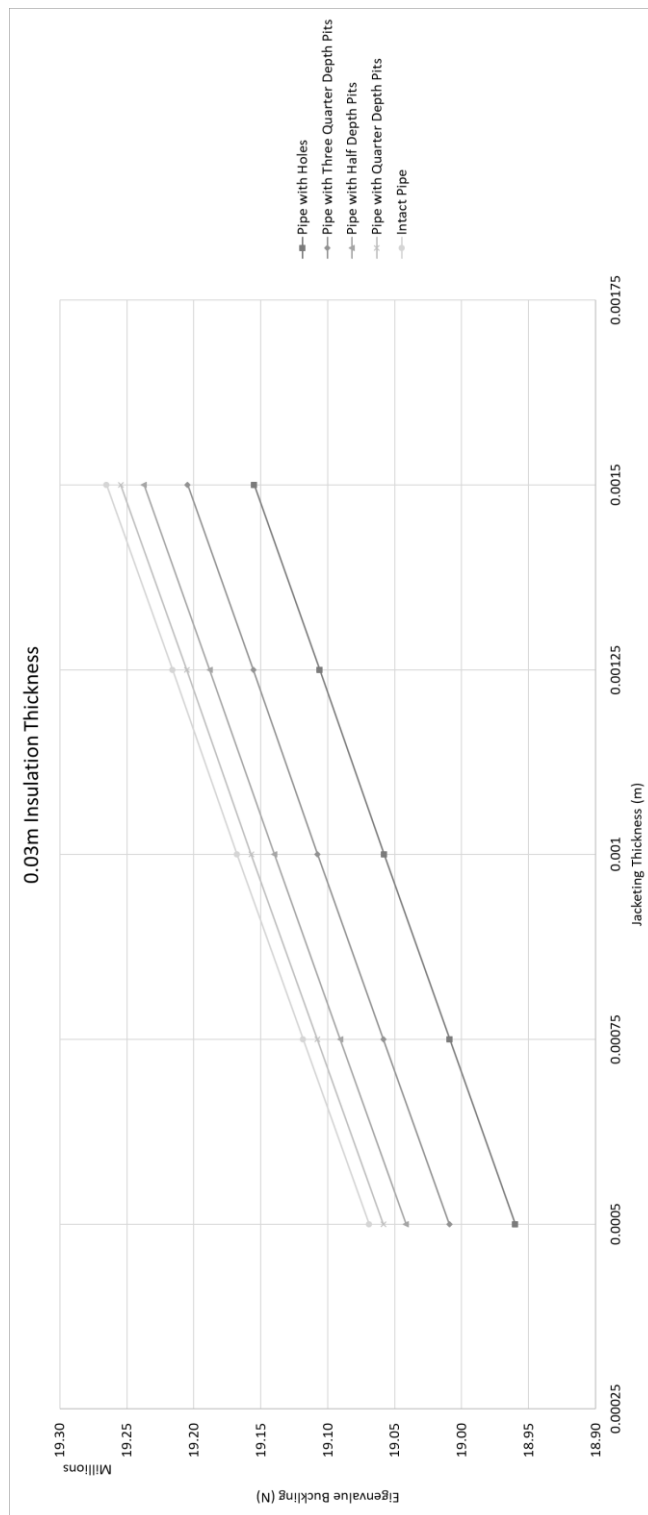
Figure 10.15 Effect of Pipe Degradation on Buckling with 0.03 m Insulation Thickness
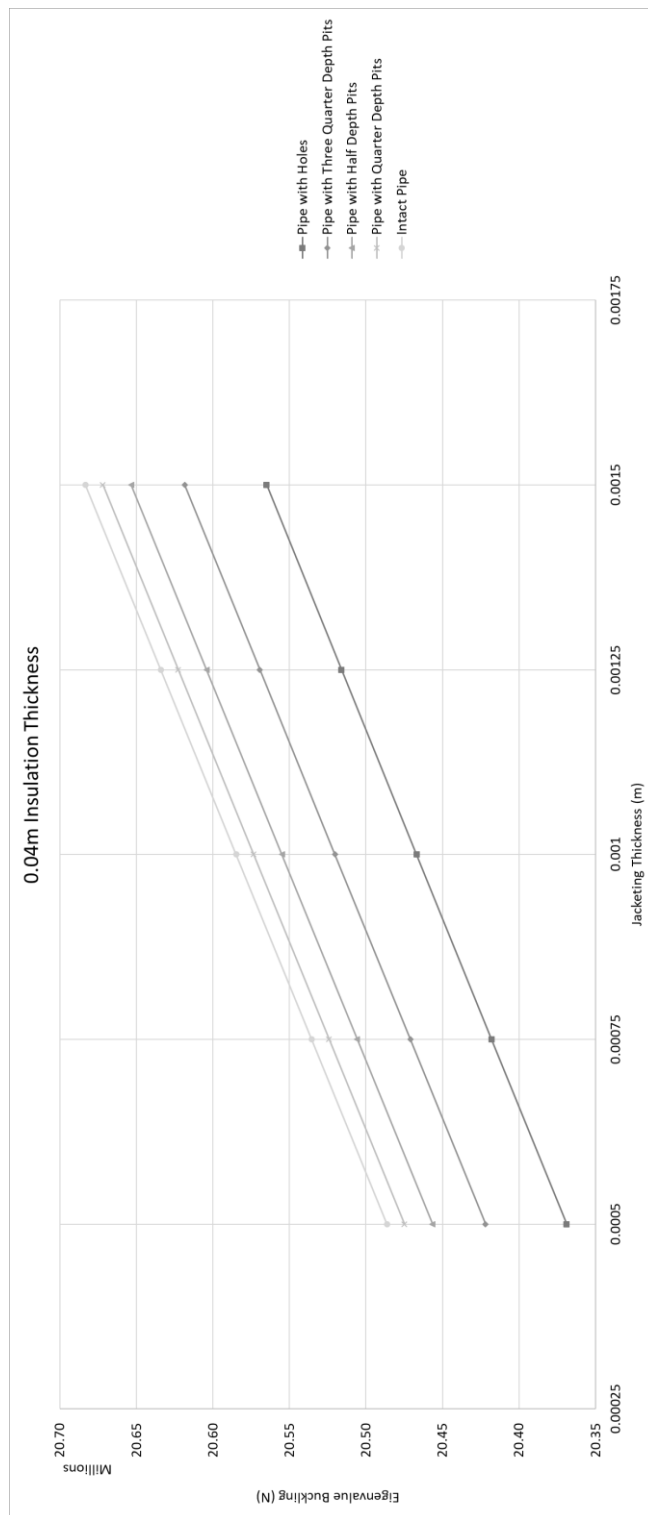
Figure 10.16 Effect of Pipe Degradation on Buckling with 0.04 m Insulation Thickness
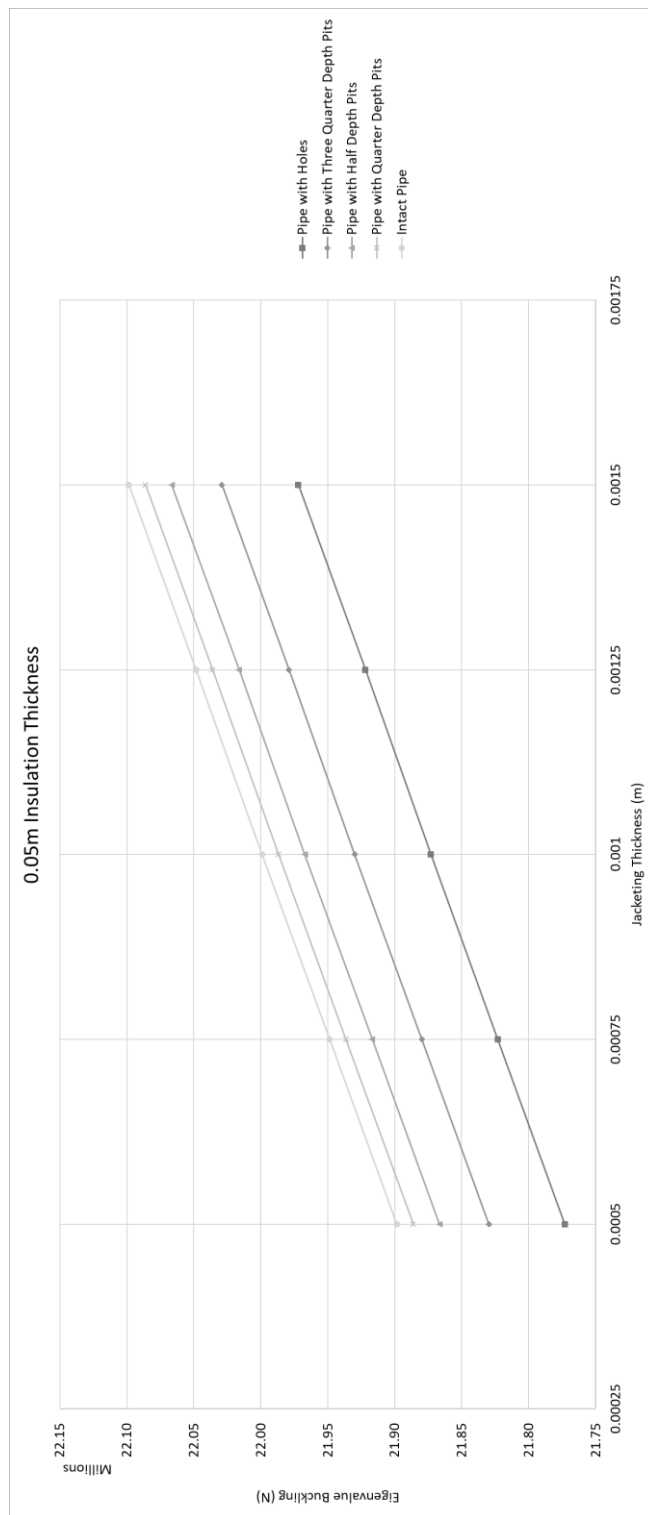
Figure 10.17 Effect of Pipe Degradation on Buckling with 0.05 m Insulation Thickness
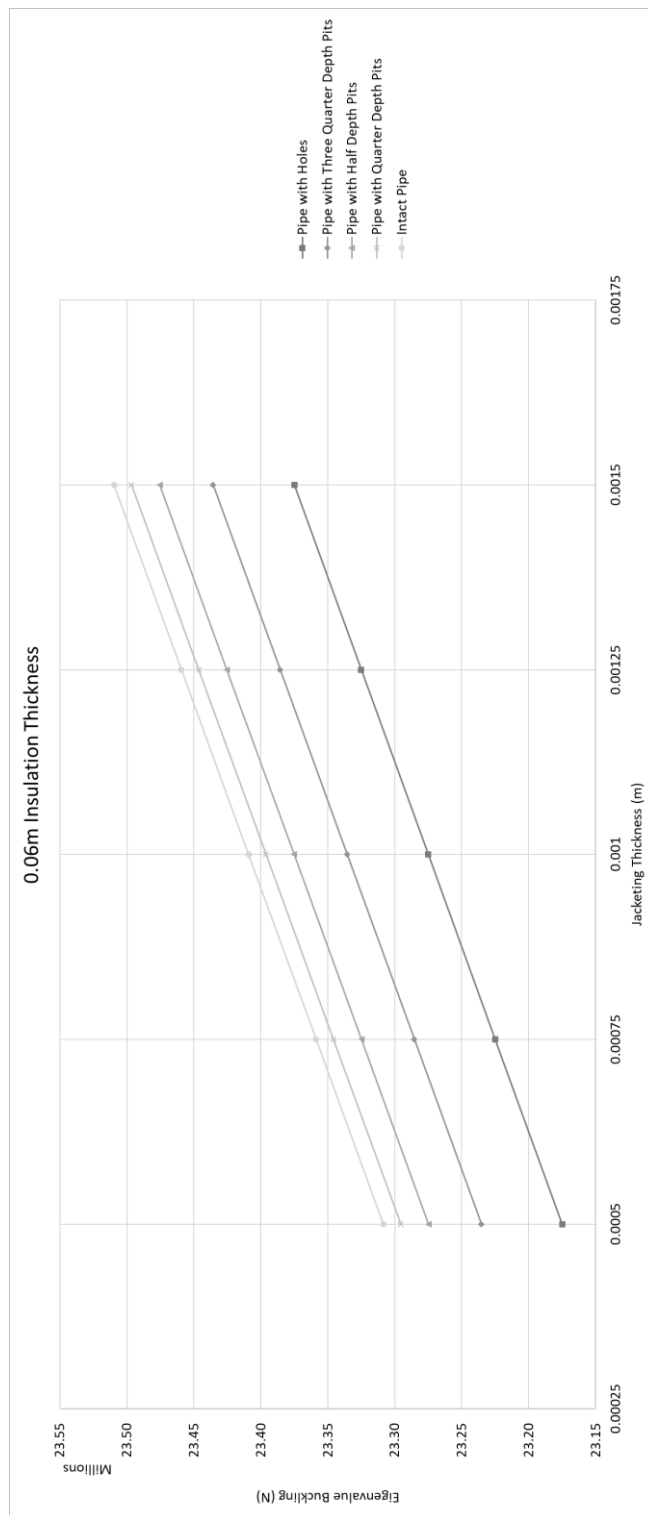
Figure 10.18 Effect of Pipe Degradation on Buckling with 0.06 m Insulation Thickness
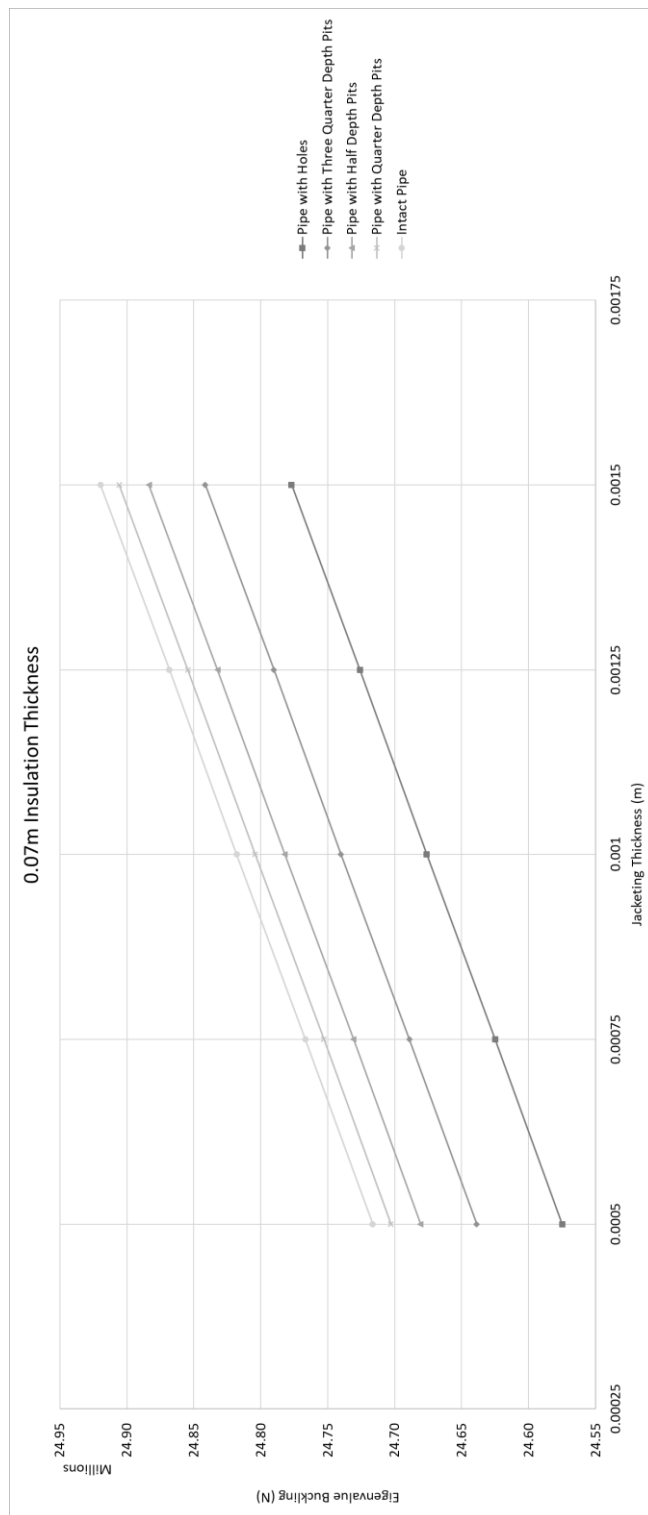
Figure 10.19 Effect of Pipe Degradation on Buckling with 0.07 m Insulation Thickness
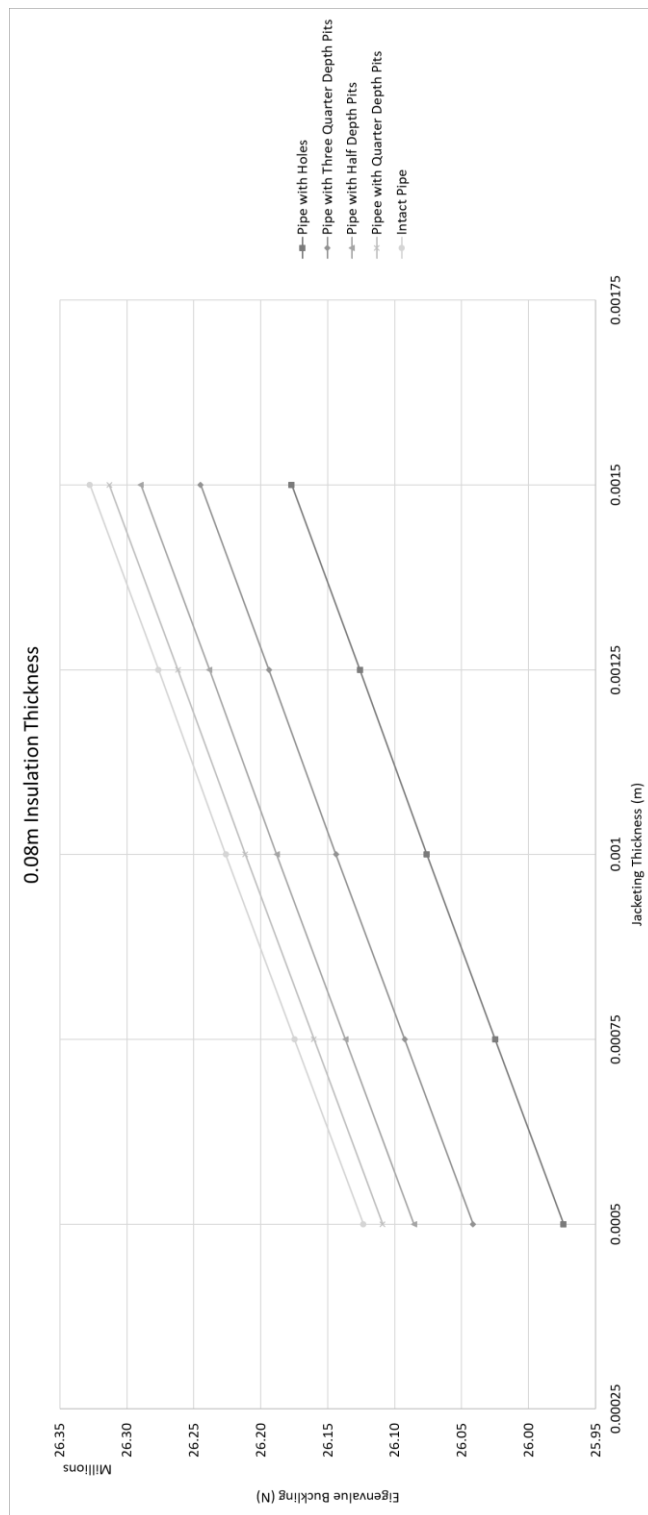
Figure 10.20 Effect of Pipe Degradation on Buckling with 0.08 m Insulation Thickness
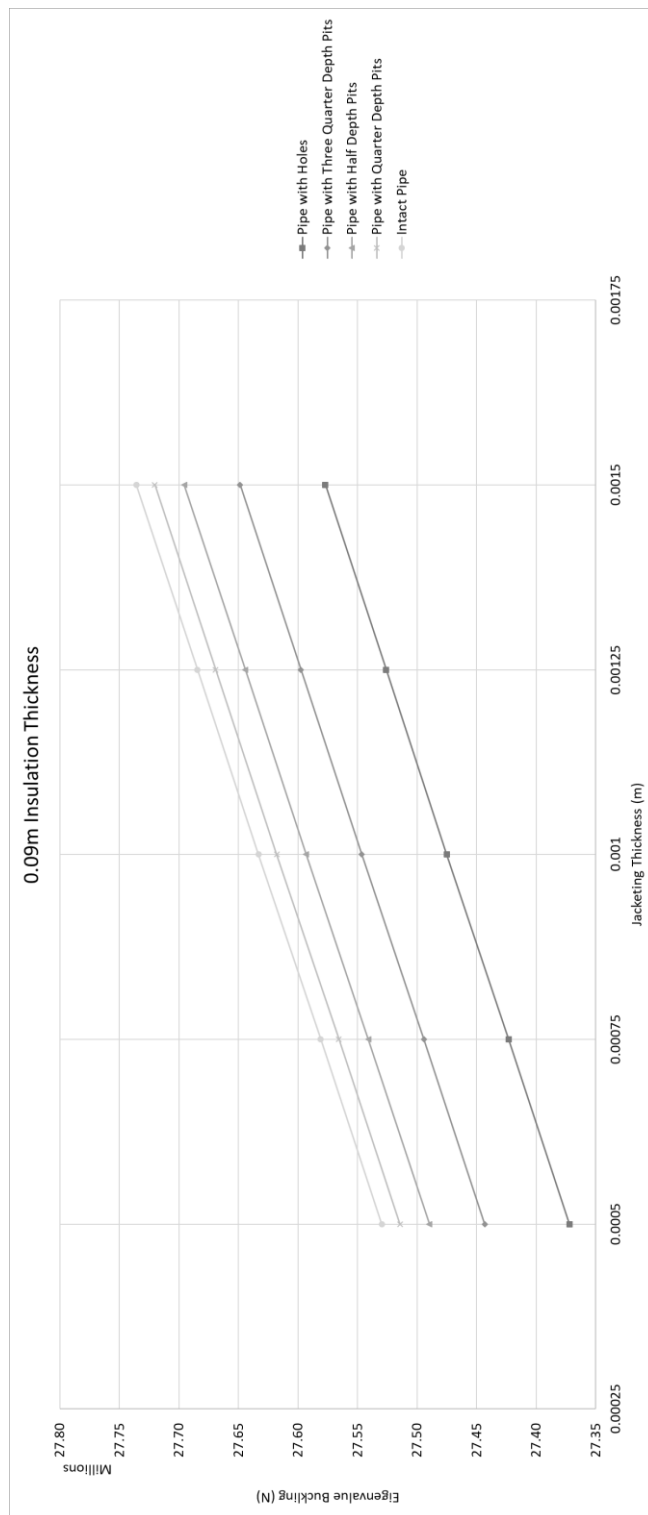
Figure 10.21 Effect of Pipe Degradation on Buckling with 0.09 m Insulation Thickness
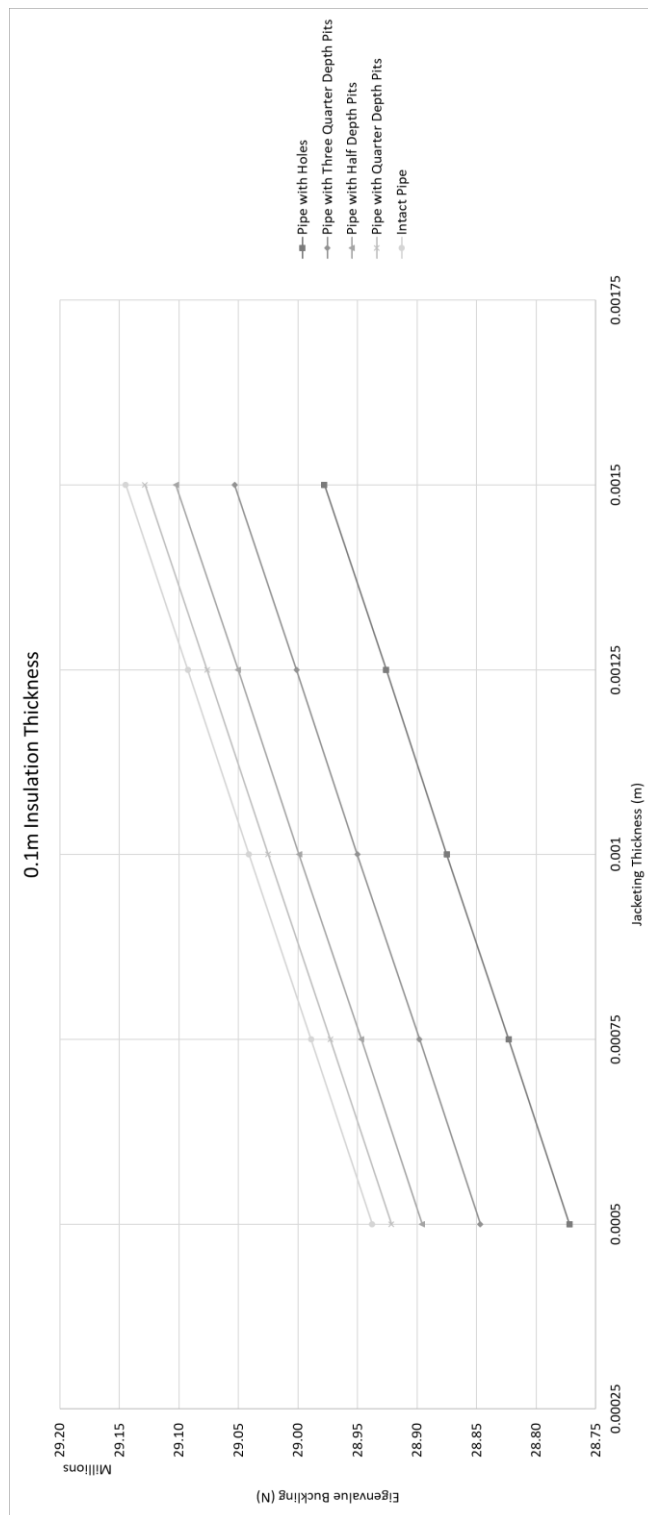
Figure 10.22 Effect of Pipe Degradation on Buckling with 0.1 m Insulation Thickness

10.3   Polycarbonate Protective Jacketing

In this section, the results from the Eigenvalue buckling analysis will be presented for the mineral wool insulation material where the system has a polycarbonate protective jacketing. The pipe was configured at each of the five degradation levels discussed previously.

A table presenting the raw buckling data in its entirety for the mineral wool insulation system can be found as Table E.2 in Appendix E. A number of graphs will be produced and shown in this section from the data in Table E.2 to represent these results and to illustrate the following variables:

- Effect of increasing jacketing thickness
- Effect of increasing insulation thickness
- Comparison of buckling values at each insulation thickness depending on the pipe degradation
- Comparison of buckling values at each jacketing thickness depending on the pipe degradation

The geometric and material properties of the pipe system have remained constant and these details can be found in Table 10.1. The material properties for each of the mineral wool insulation and two jacketing materials are provided in Table 10.2. Please pay close attention to the axes values as they may change drastically so as to give the best overall indication of the piece of information described.

Figures 10.23 to 10.27 depict the effect of the increase in jacketing thickness on each of the five pipe degradation configurations. It can be seen at the bottom of each graph there is a plot that spans the full width, this plot denotes the buckling value of the pipe configuration where there is no insulation system providing additional strength. The jacketing thickness increases from 0.0005 metres as a minimum up to 0.0015 metres at the largest thickness.

In the case of the pipe with holes, this value is 14,588,000 N, with three-quarter depth pits it is 14,627,000 N, half-depth pits equal 14,651,000 N, quarter depth pits are 14,665,000 N and finally a fully intact pipe equals 14,672,000 N. As would be expected the buckling value increases as the level of degradation of the pipe decreases. The degradations cause the pipe to lose some of its inherent structural strength. This information is exactly the same as exhibited with the plate example in Chapter Nine. In the case of the pipe, the magnitude of the difference between the pipe with the holes and the fully intact pipe is considerably smaller than the same examples with the plate. It appears that the differences between the mechanical properties and the geometric properties appear to have a more pronounced effect within the plate example.

The expectation with regards to the addition of an insulation system would be that the buckling strength of the pipe would increase which is exactly as the results show. Whether that be the increase in the thickness of the insulation or an increase in the thickness of the protective coating. As the thickness of the protective coating increases, there is a minor increase in the buckling value when comparing the values at a single insulation thickness. With the pipe examples, these variations are quite small but can be clearly seen in graphical format.

Figures 10.28 to 10.32 depict the effect of increasing the thickness of the insulation on each of the pipe degradation configurations. These latter figures show a much larger relative rise in the buckling value where the insulation thickness increases at each jacketing thickness. The minimum insulation thickness measured is 0.01 metres ranging up to 0.1 metres at the largest value. As before, it can be seen at the bottom of each graph there is a plot that spans the full width, this plot denotes the buckling value of the pipe configuration where there is no insulation system providing additional strength.

As an example, when looking at Figure 10.23, it can be seen that with an insulation thickness of 0.1 metres the buckling value where the jacketing thickness is 0.0005 metres is 16,003,000 N. At the same insulation thickness but after increasing the thickness of the jacketing to the maximum of 0.0015 metres the new buckling value is 16,192,000 N. The only parameter that has changed is the thickness of the protective jacketing and with that, the buckling value has increased as expected.

This increase is relatively modest when compared to another example when looking at Figure 10.28, which will depict the increase in buckling through an increase in insulation thickness. Where the jacketing thickness is 0.0005 metres and the insulation thickness is 0.01 metres the buckling value is 16,003,000 N as before. If instead of increasing the jacketing thickness the insulation thickness is increased only one level up to 0.02 metres the new buckling value is 17,412,000 N.

These results are very similar to the results seen in the previous chapter with regards to the relationship. Clearly, the results in this chapter are considerably smaller in relative terms but the relationship remains the same. As before, the Euler Column Critical Load Formula explains the relationship. The formula produces results more realistically expected as it is dealing with an actual columnar form which affects the results rather than the flat plate from the previous chapter. It is also interesting to note that the results have a more linear character than the plate results due to the more realistic values involved.

Also, the fact that the pipe example deals with a considerably slenderer example, i.e. the length relative to the thickness is considerably more. This was not the case in the plate example which may further explain the generation of more theoretical results. The plate example would not usually be considered in isolation but would be part of a larger network, its purpose was to provide a comparison tool to the pipe example which is of greater interest overall.

Figure 10.23 Effect of Increasing Jacketing Thickness – Pipe with Holes
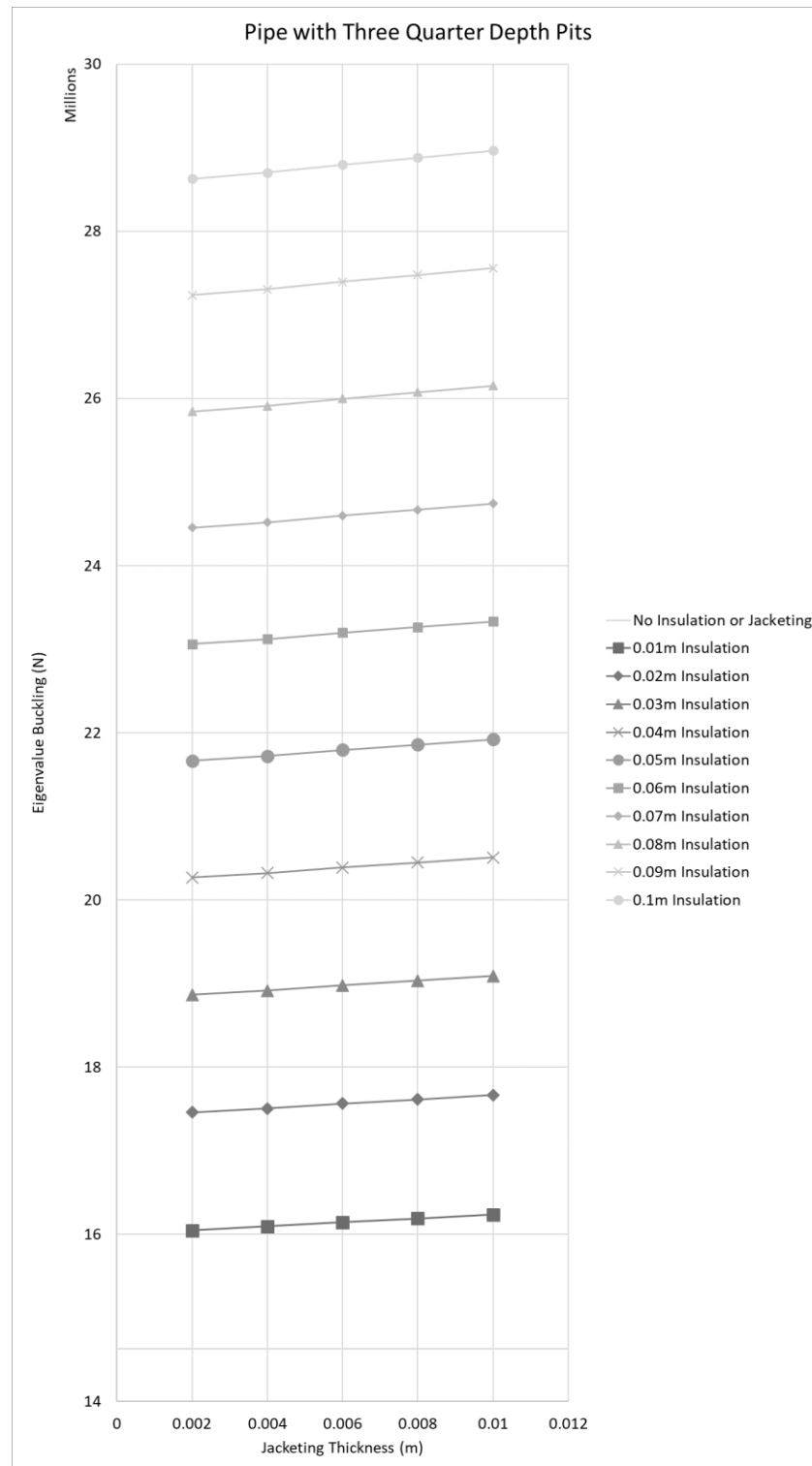
Figure 10.24 Effect of Increasing Jacketing Thickness – Pipe with Three-Quarter Depth Pits
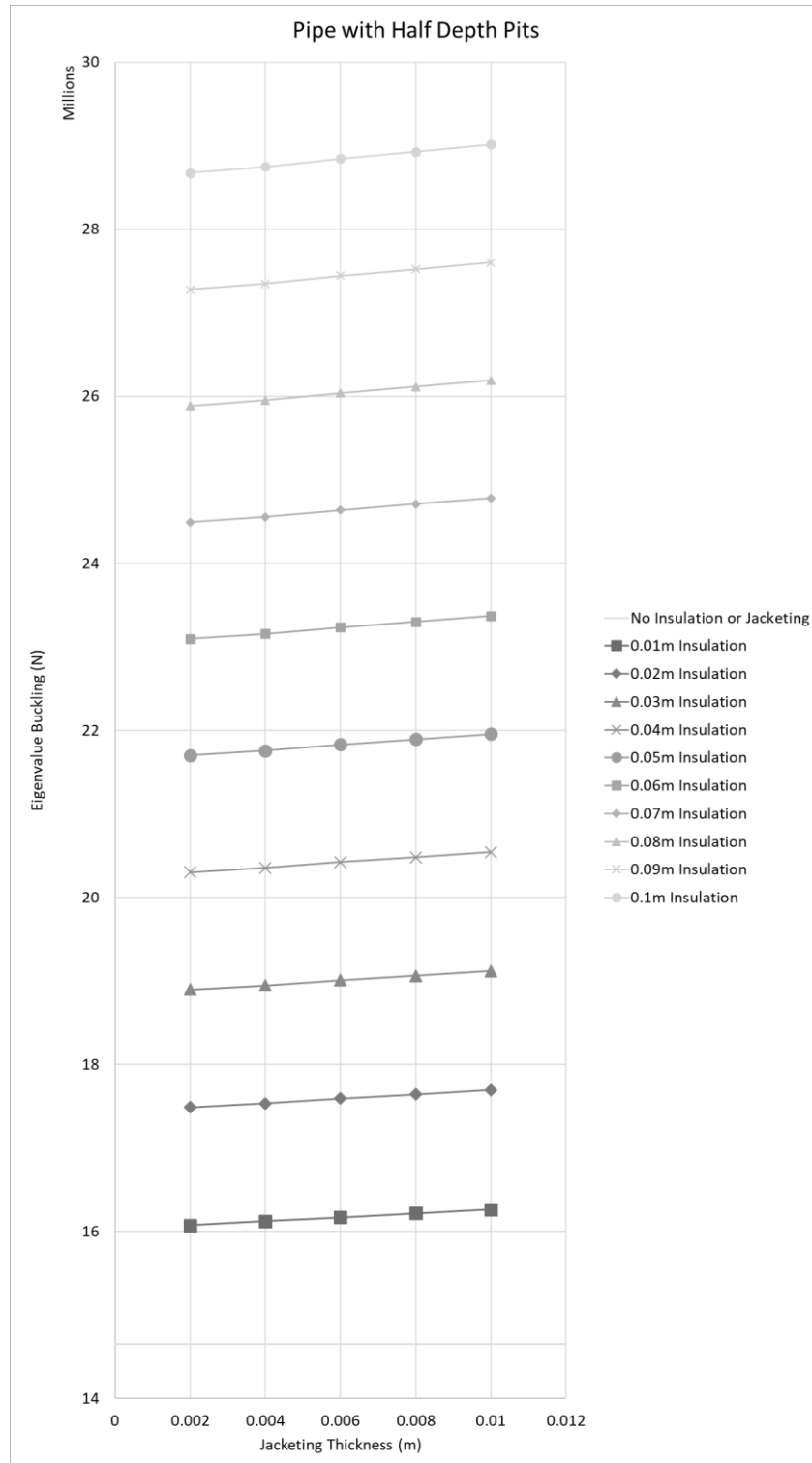
Figure 10.25 Effect of Increasing Jacketing Thickness – Pipe with Half Depth Pits
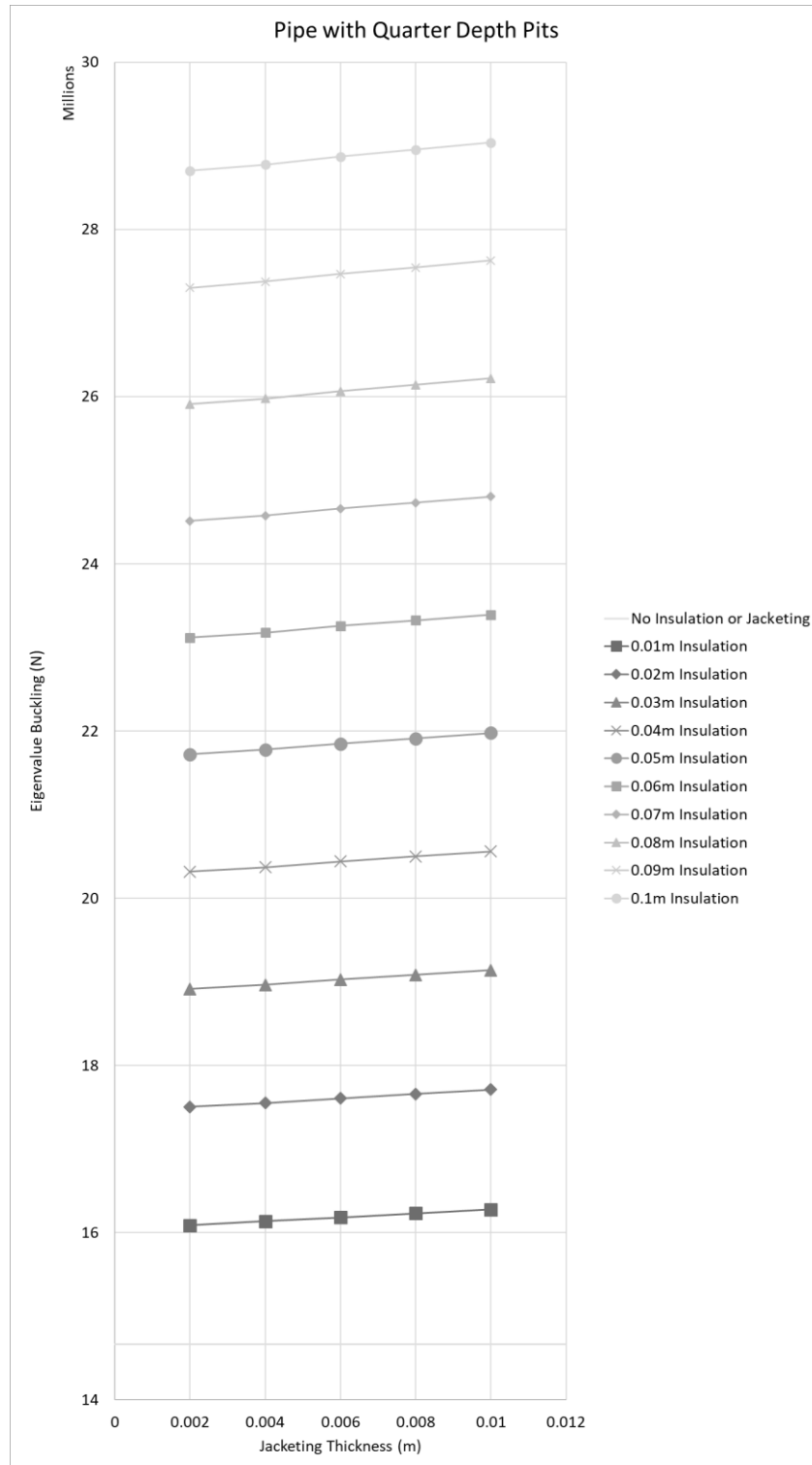
Figure 10.26 Effect of Increasing Jacketing Thickness – Pipe with Quarter Depth Pits
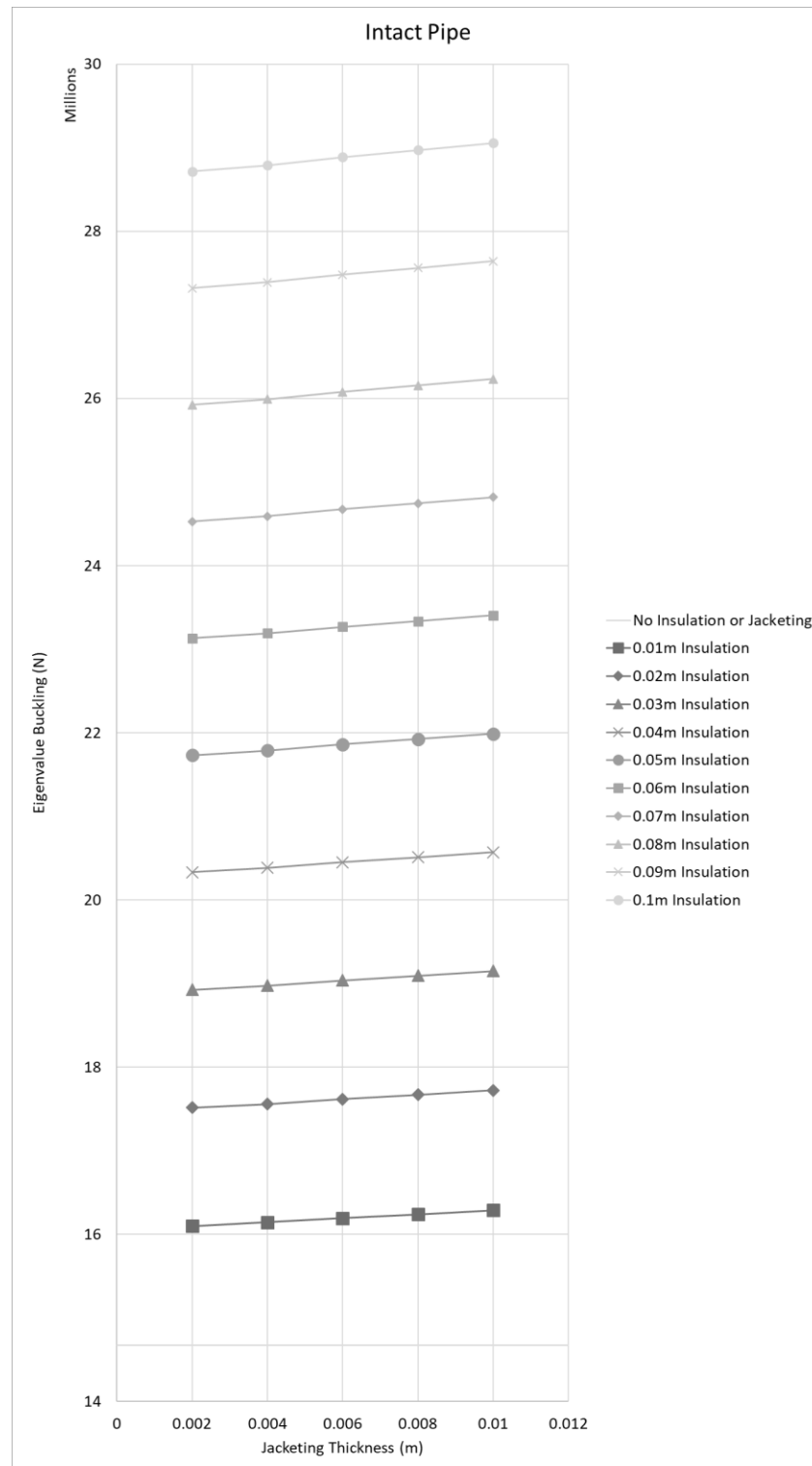
Figure 10.27 Effect of Increasing Jacketing Thickness – Intact Pipe
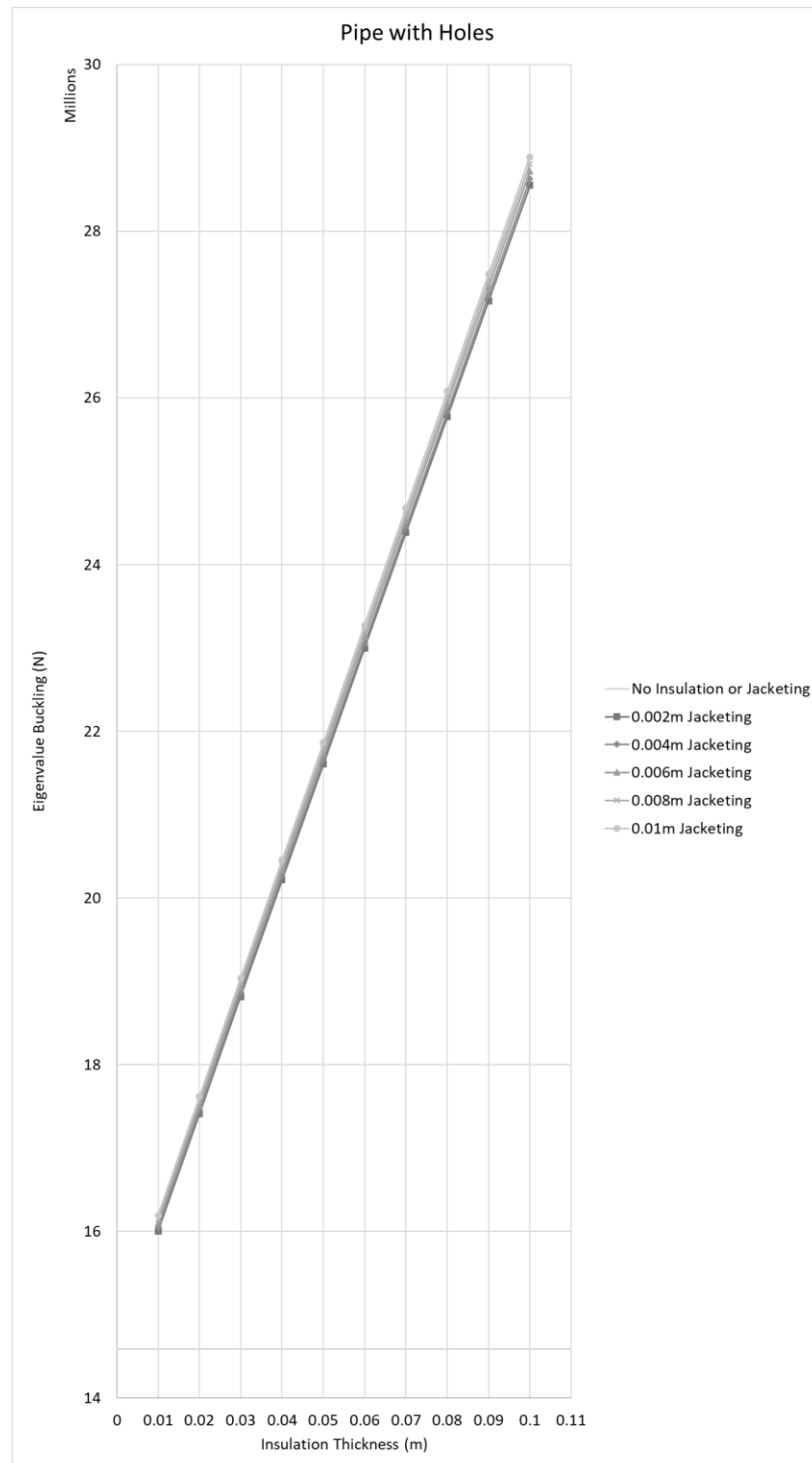
Figure 10.28 Effect of Increasing Insulation Thickness – Pipe with Holes
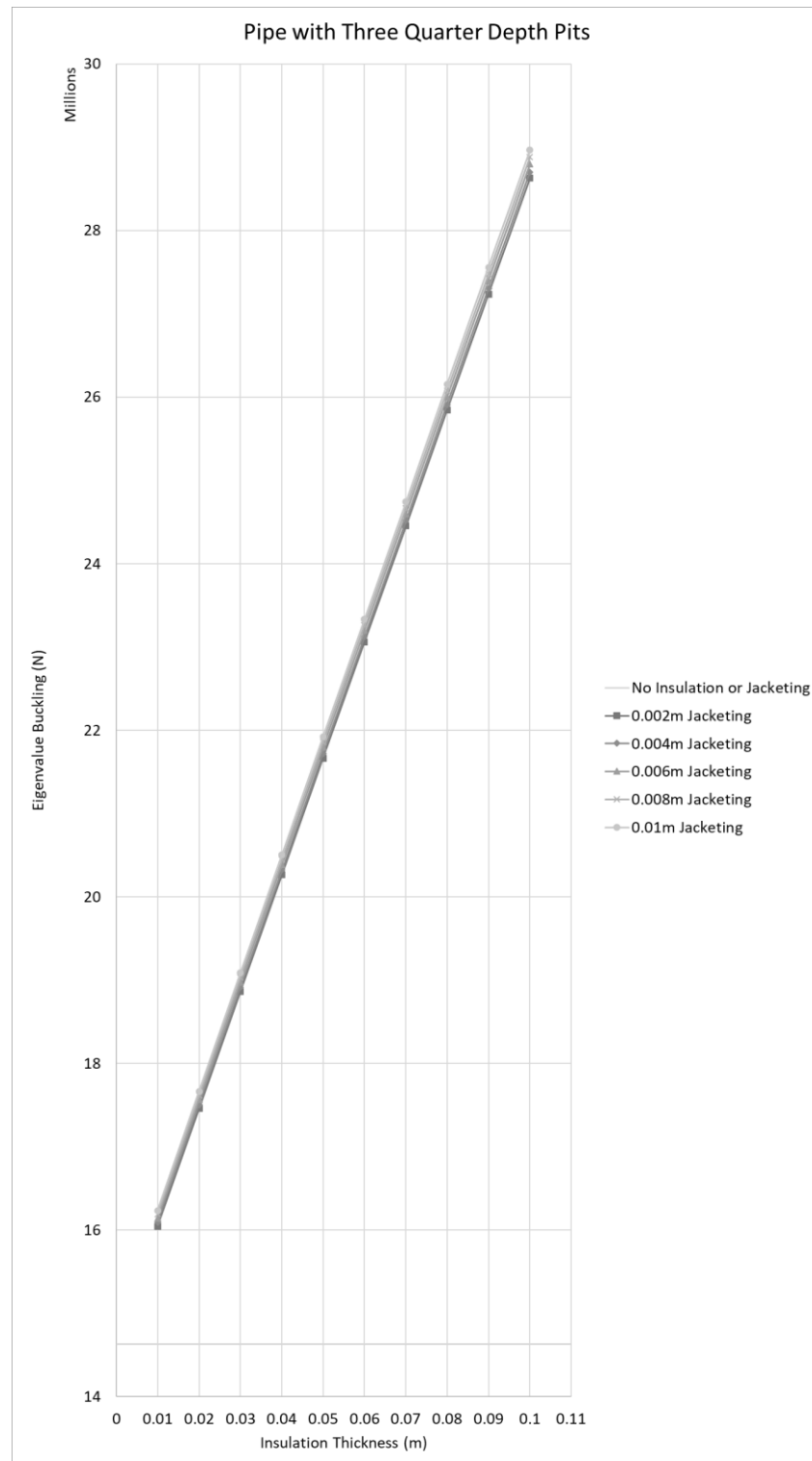
Figure 10.29 Effect of Increasing Insulation Thickness – Pipe with Three-Quarter Depth Pits
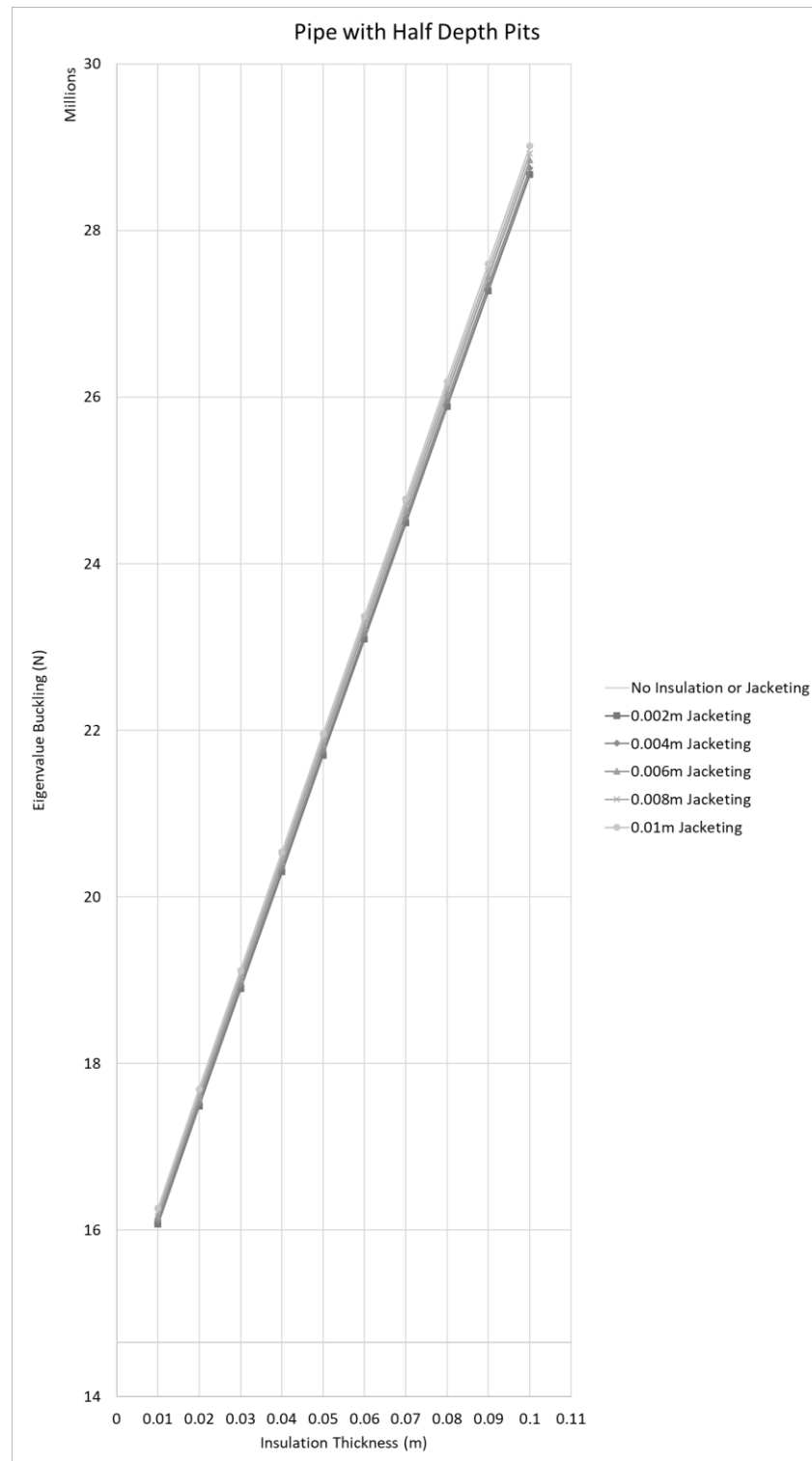
Figure 10.30 Effect of Increasing Insulation Thickness – Pipe with Half Depth Pits
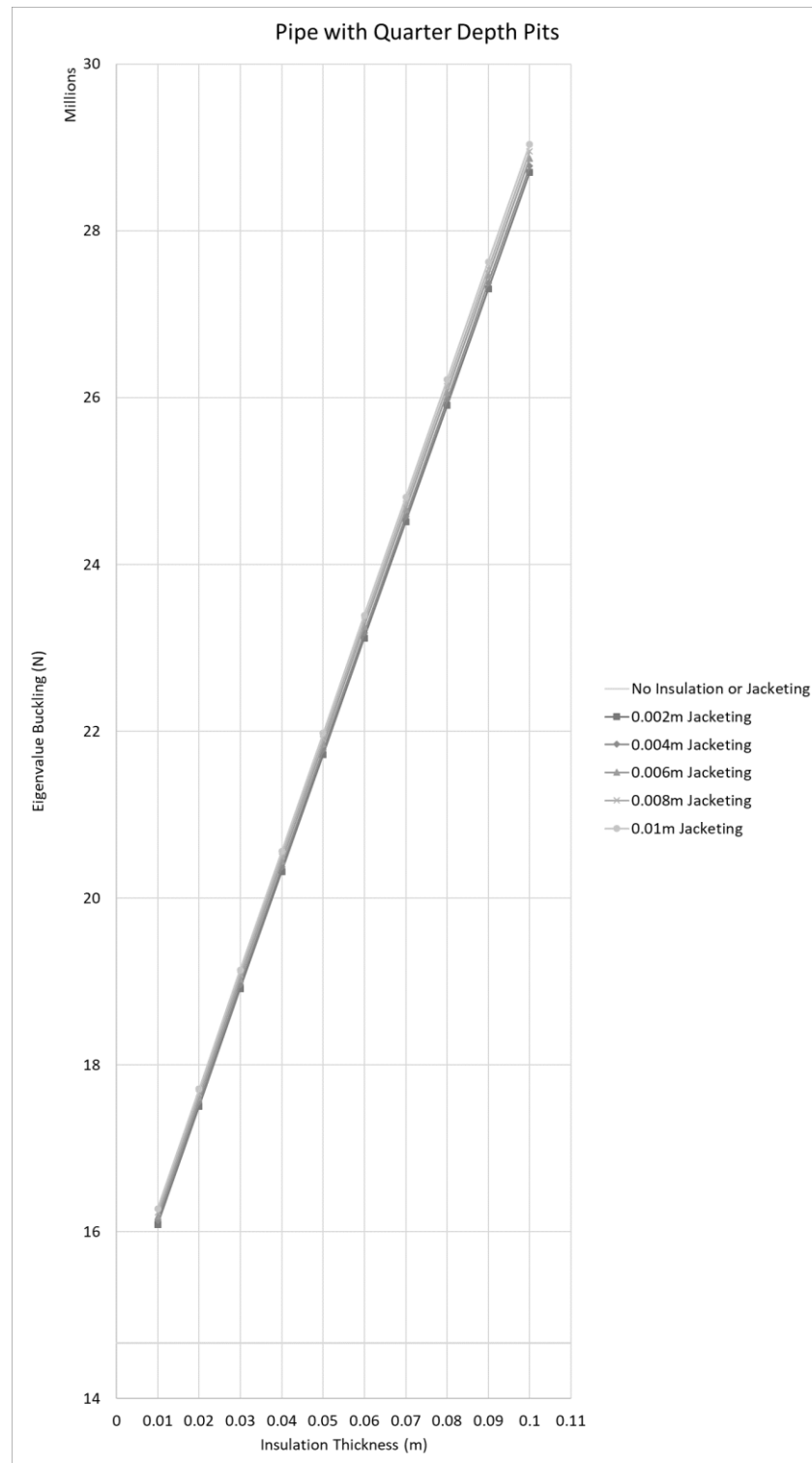
Figure 10.31 Effect of Increasing Insulation Thickness – Pipe with Quarter Depth Pits
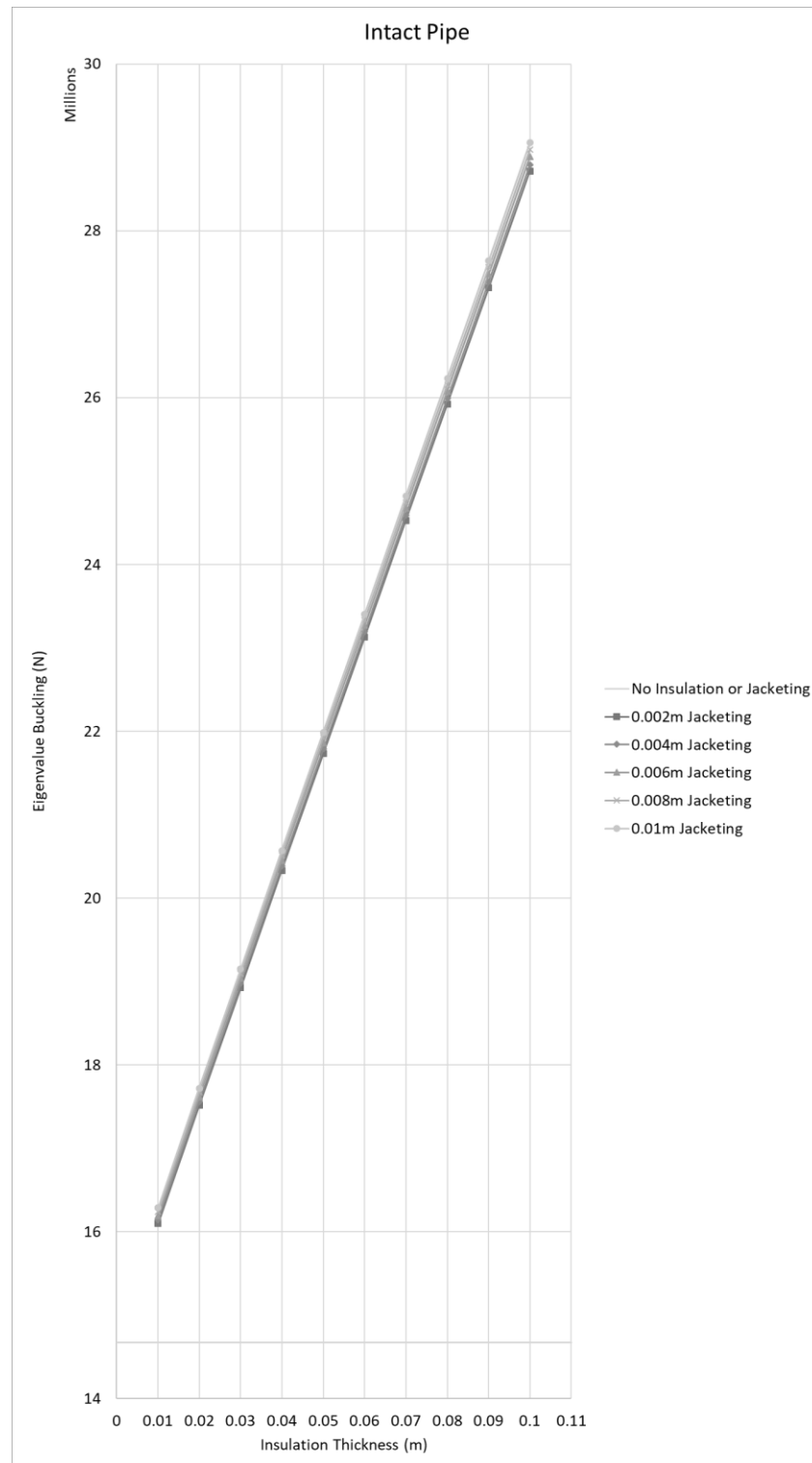
Figure 10.32 Effect of Insulation Jacketing Thickness – Intact Pipe

Figures 10.33 to 10.42 allow for the opportunity to compare the buckling values of each of the five pipe configurations at each of the ten insulation thicknesses. The effect of the level of degradation is quite apparent at each of the insulation thicknesses. As would be expected the pipe with the holes having the highest level of corrosion effect has the lowest buckling values at each respective point when compared to the highest values as seen in the fully intact pipe.

It is interesting to note that it appears when comparing each of the figures that as the insulation thickness increases the relative difference in buckling values between each pipe configuration remains fairly constant with a possible slight increase in the values as the insulation thickness increases. That is to say that in Figure 10.33 the values for the intact pipe and the three pipes with pit degradations are quite closely bunched together with the pipe with the holes slightly separated. In Figure 10.42 this formation is still present with a possible slight increase in the spacing between the plate configurations accounting for the relative increase in value. Another interesting point to note is that it can be seen that these graphs appear to have a less linear shape than those noted before. However, this has no particular overall effect on the results.
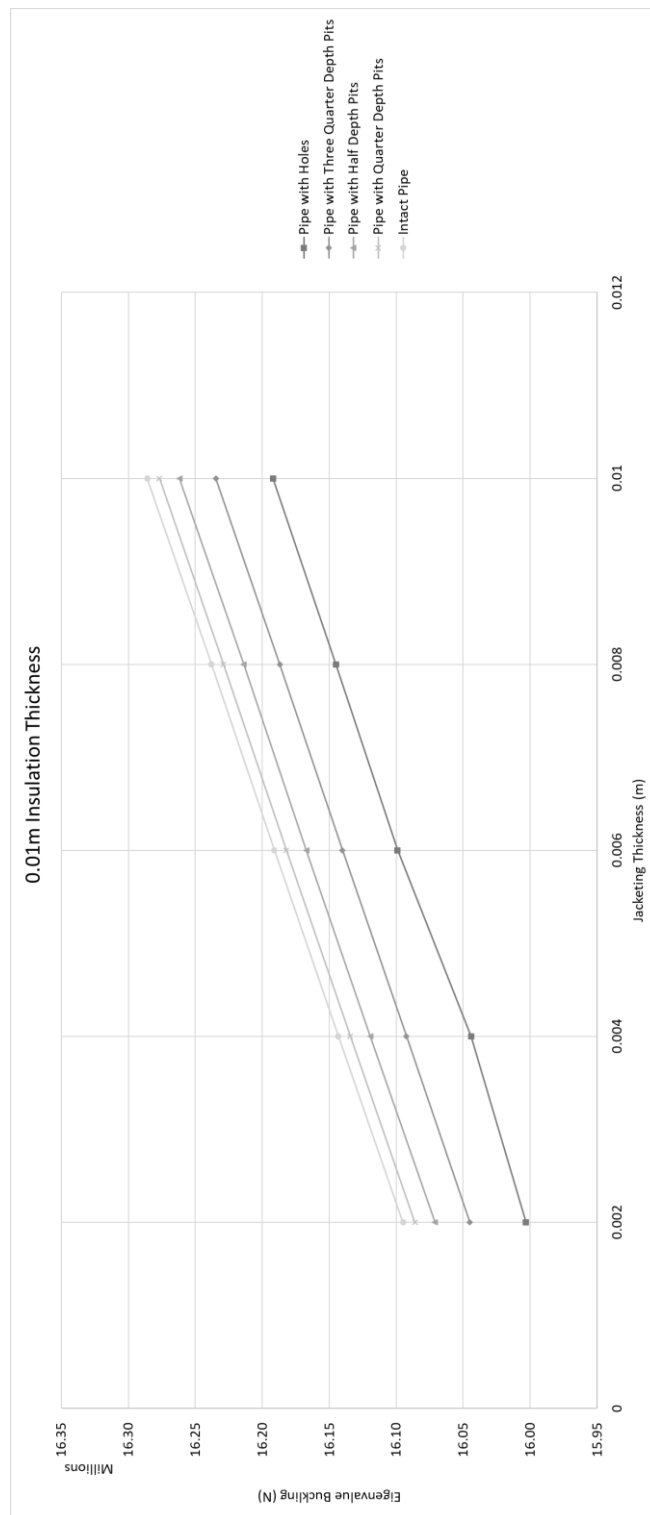
Figure 10.33 Effect of Pipe Degradation on Buckling with 0.01 m Insulation Thickness
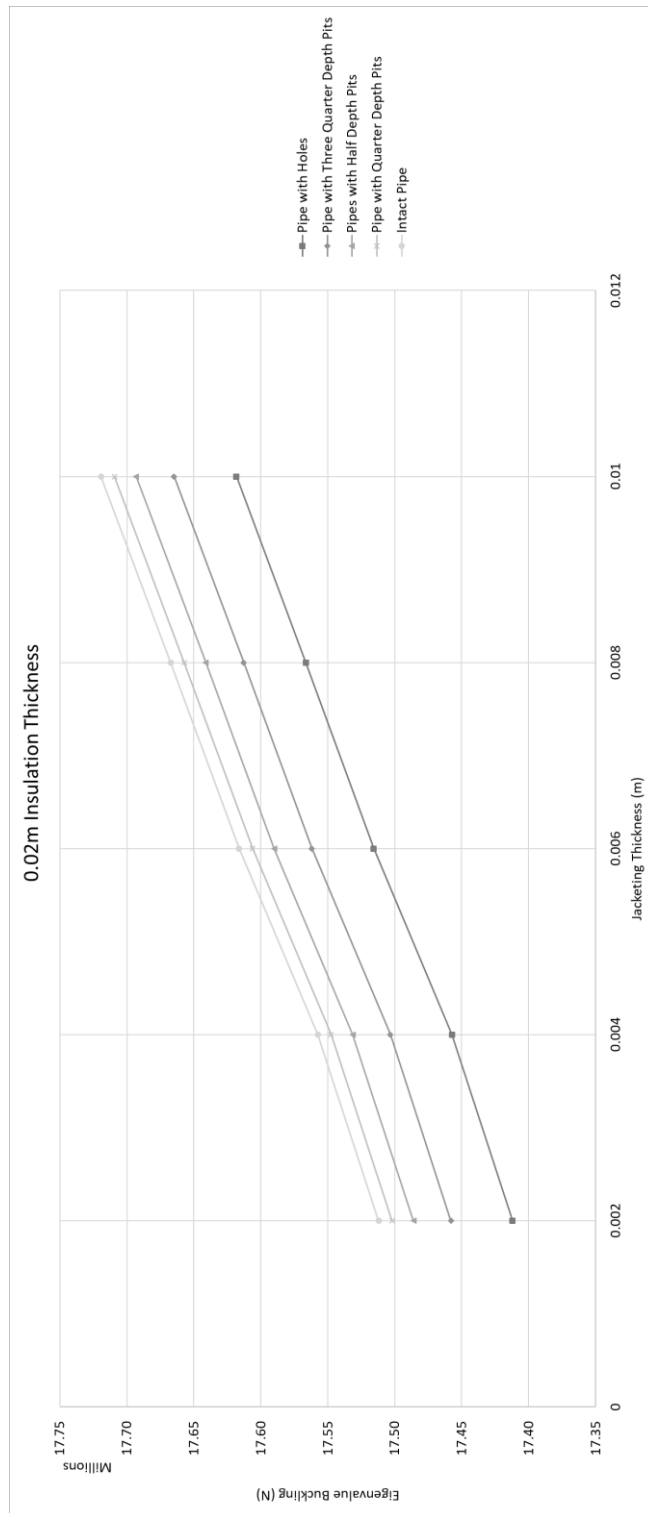
Figure 10.34 Effect of Pipe Degradation on Buckling with 0.02 m Insulation Thickness
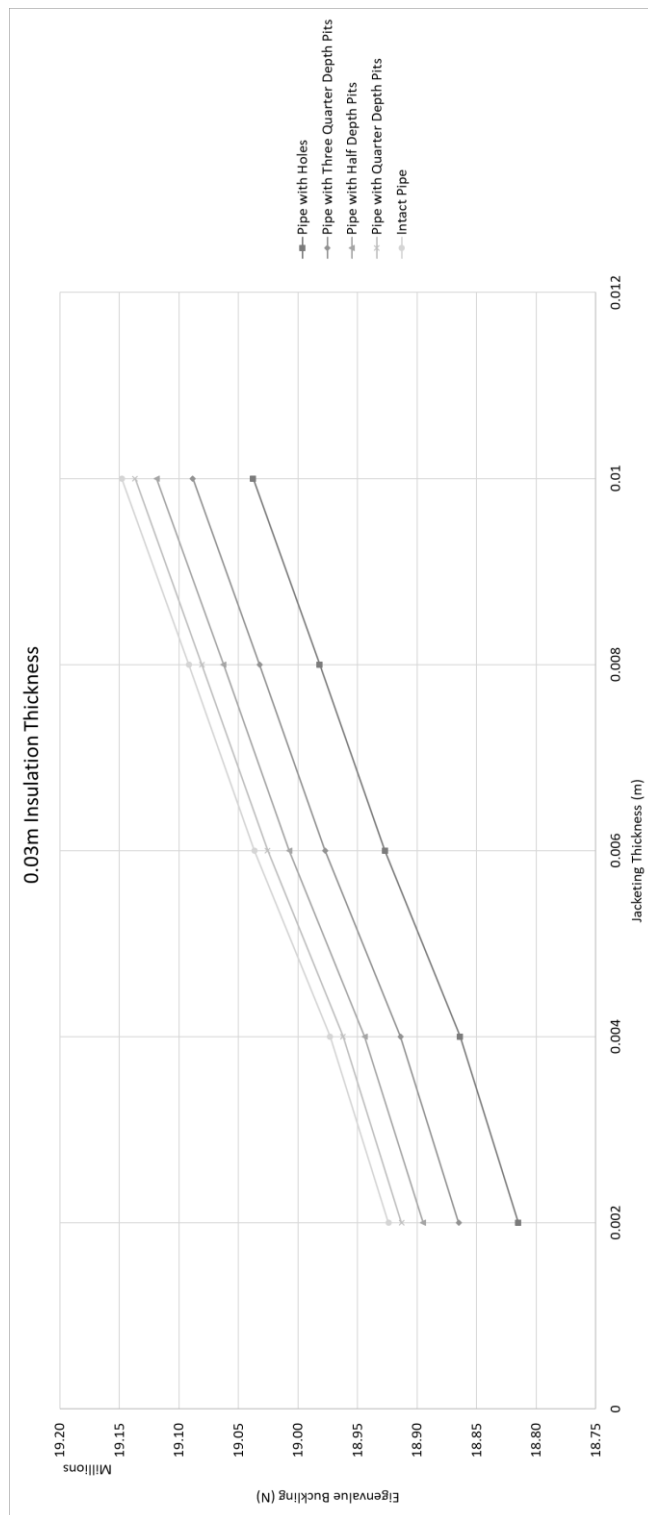
Figure 10.35 Effect of Pipe Degradation on Buckling with 0.03 m Insulation Thickness
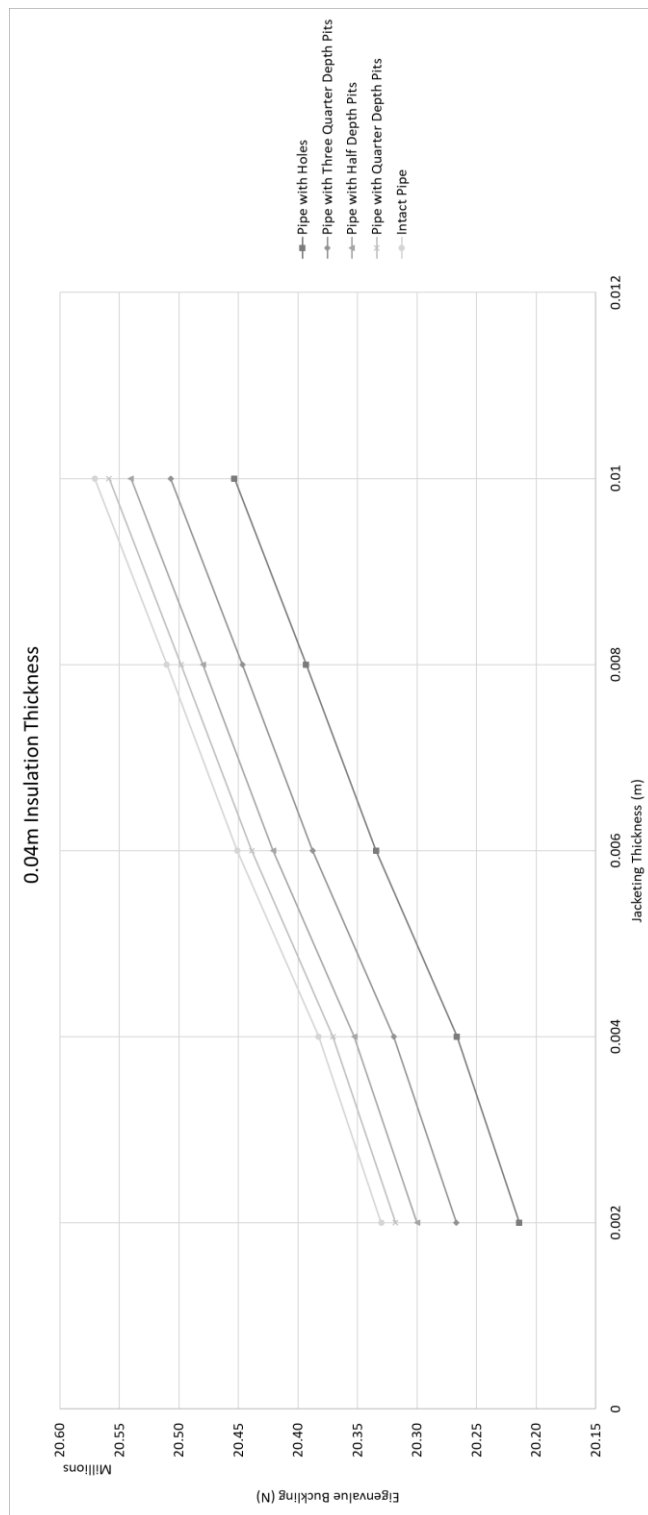
Figure 10.36 Effect of Pipe Degradation on Buckling with 0.04 m Insulation Thickness
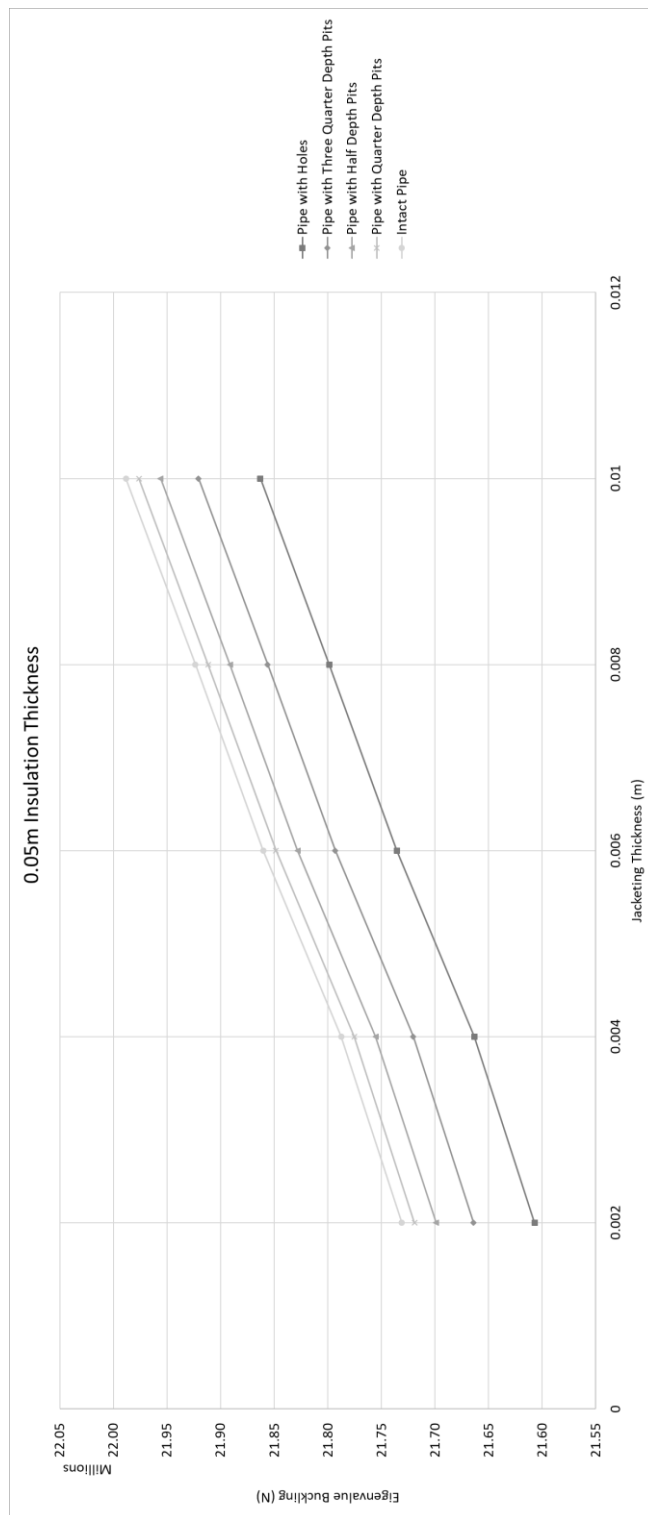
Figure 10.37 Effect of Pipe Degradation on Buckling with 0.05 m Insulation Thickness
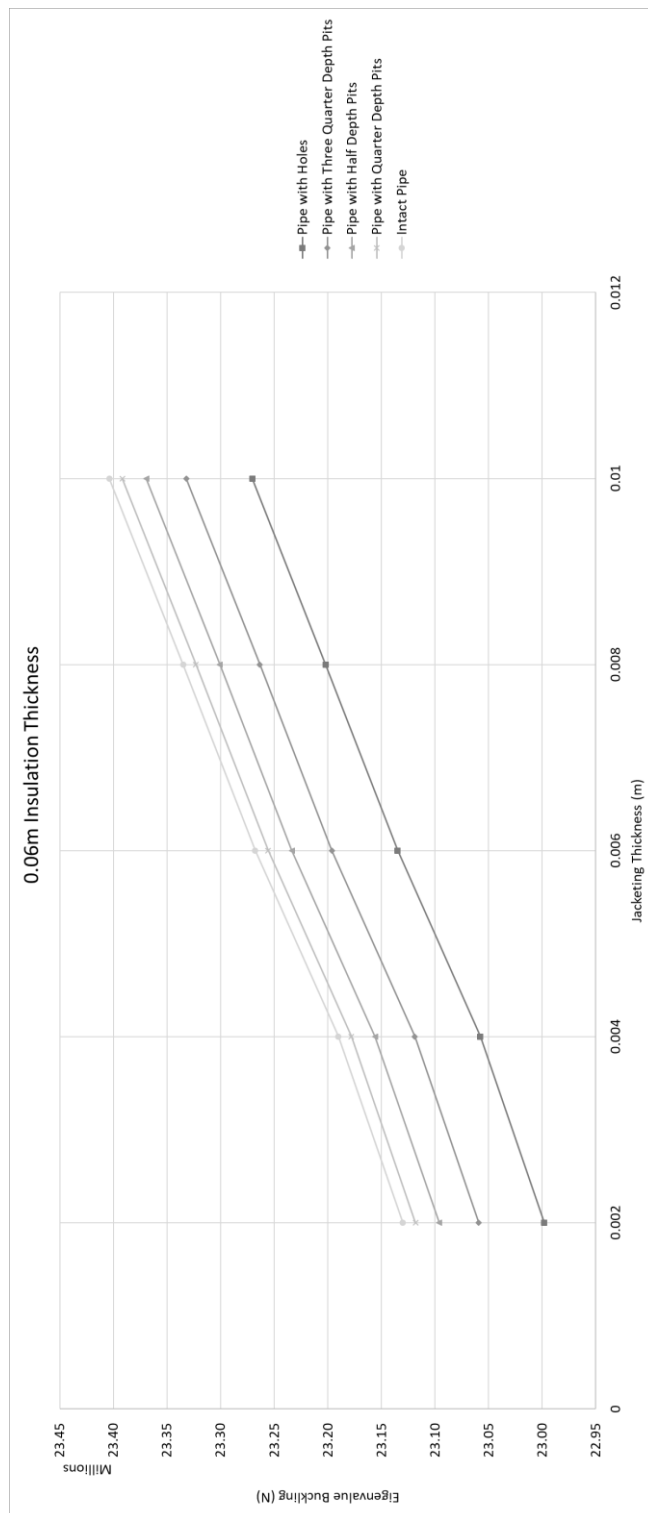
Figure 10.38 Effect of Pipe Degradation on Buckling with 0.06 m Insulation Thickness
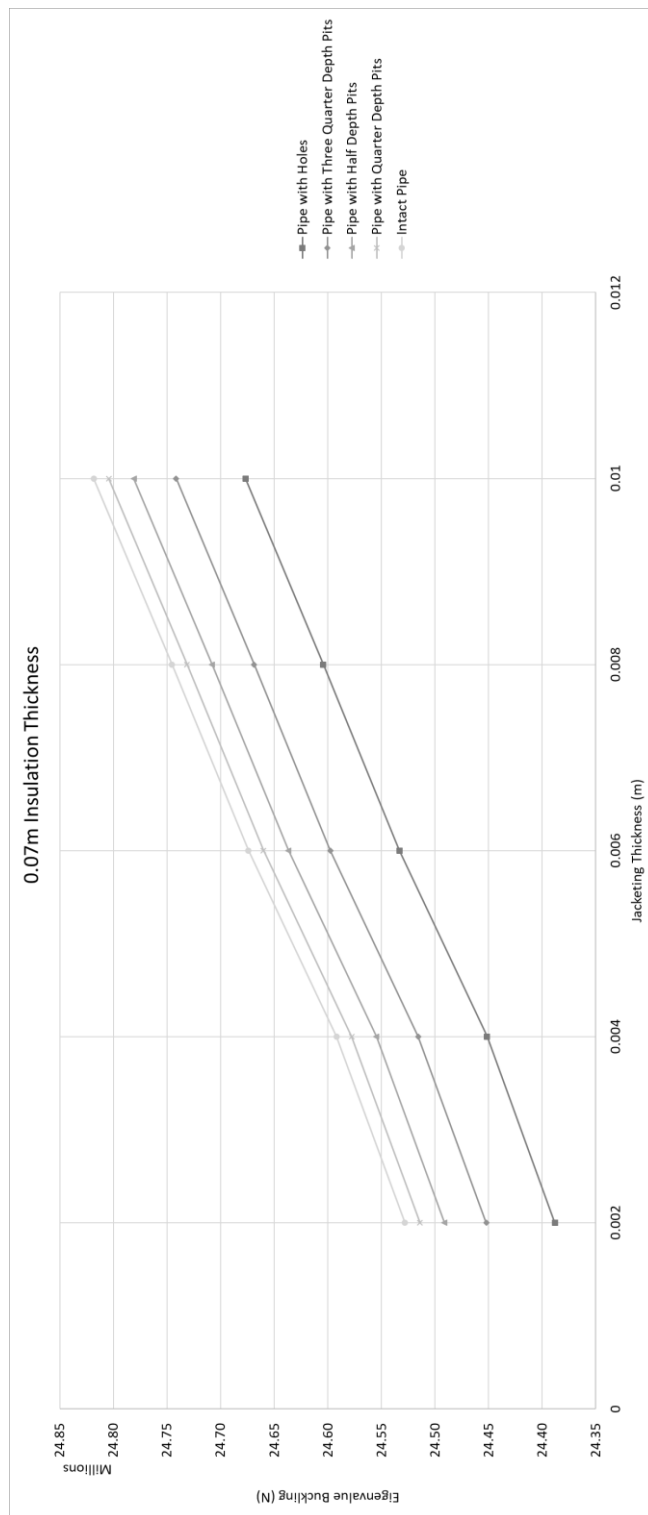
Figure 10.39 Effect of Pipe Degradation on Buckling with 0.07 m Insulation Thickness
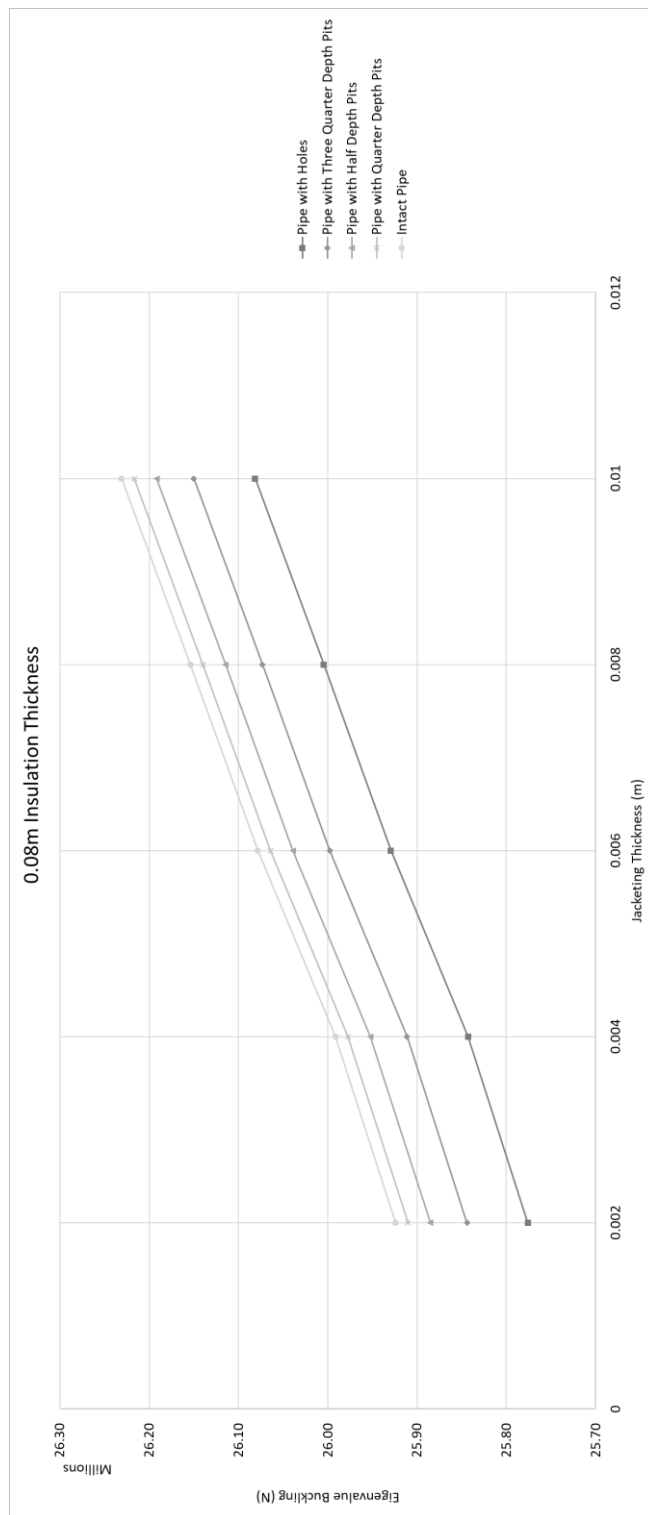
Figure 10.40 Effect of Pipe Degradation on Buckling with 0.08 m Insulation Thickness
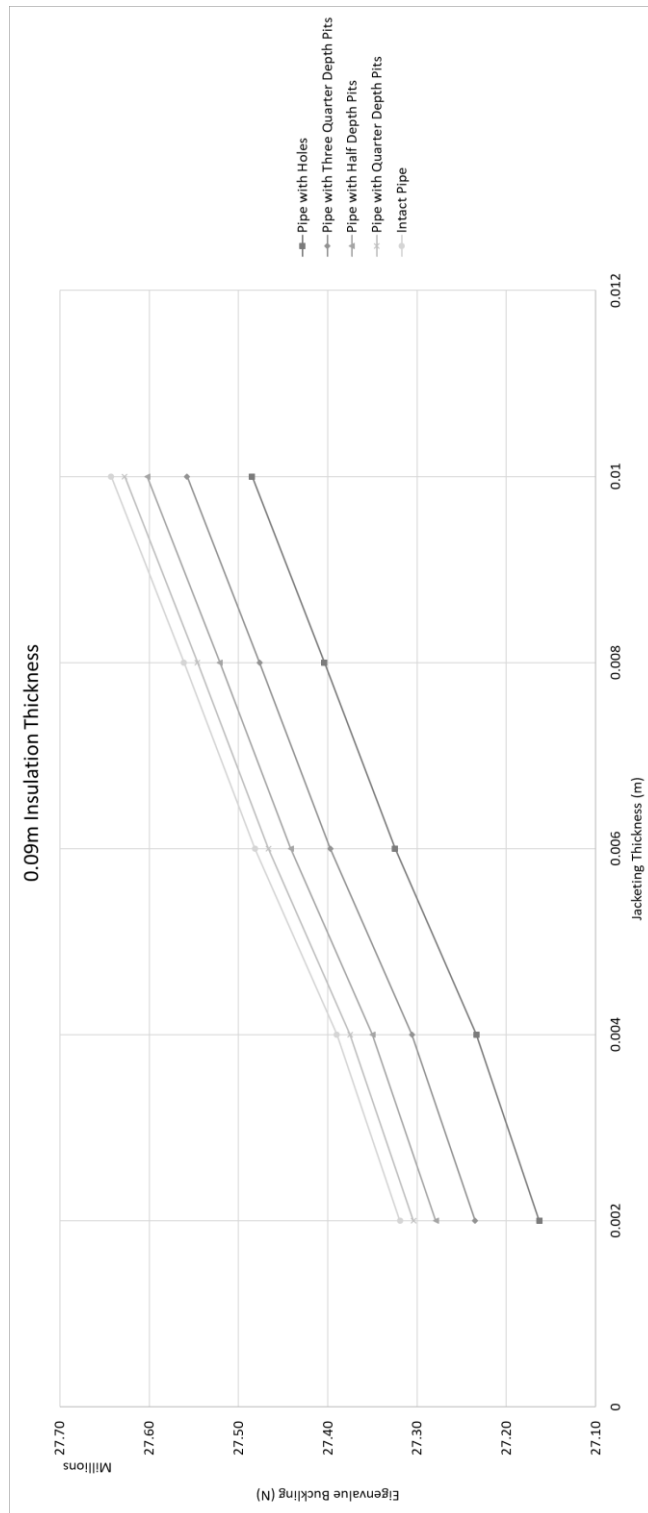
Figure 10.41 Effect of Pipe Degradation on Buckling with 0.09 m Insulation Thickness
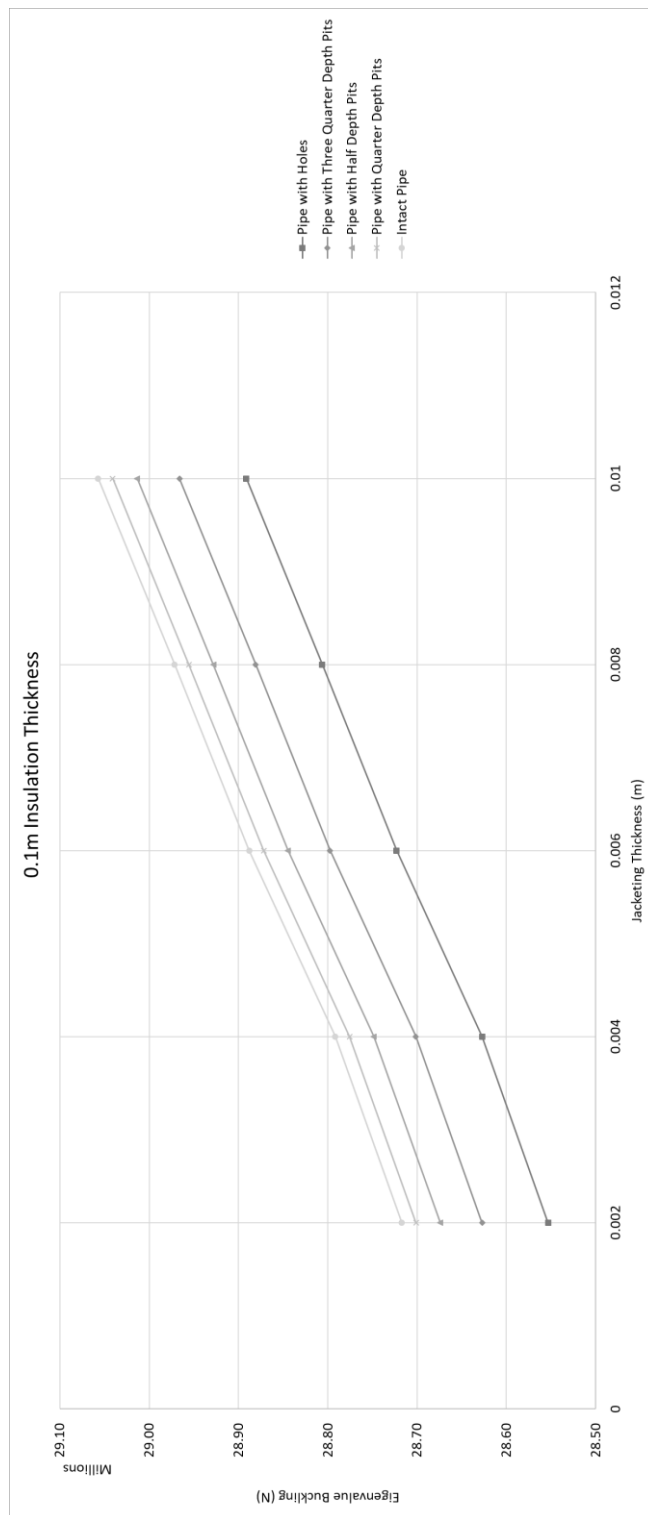
Figure 10.42 Effect of Pipe Degradation on Buckling with 0.1 m Insulation Thickness

Chapter Eleven: Conclusions

Chapter Eleven is dived into five sections. In the first section, the list of objectives that were set out in Chapter One are reviewed and whether these objectives have been met. A short summary of the main findings of the piece of research is then presented before the author's view of any gaps in the research are presented. As discussed previously there has been very little research completed in this field so any potential future work the author believes may benefit the research will be presented. The fourth and fifth sections of the chapter will discuss the novelty of the piece of research and any contributions it has made to the field and any final remarks regarding the project.

11.1   Review of the Objectives

The main goal of this piece of research was to unite the fields of corrosion chemistry and structure mechanics to successfully model corrosion damaged steel components with an insulation system that has been subjected to a buckling load. The effect on the buckling load attributed to the mechanical properties of the insulation system was of particular interest.

At the time of writing, no model existed to computationally model corrosion damage with an external insulation and jacketing system though models did exist that focus on the strength of a corroded steel component under various load types.

The numbered points below relate to the objectives set out in Chapter One section 1.2 and are a summary of the main objectives and whether they have been achieved:

1. Create a 2-D and 3-D ANSYS mechanical APDL code that models a steel plate where the centre has been subjected to five levels of corrosion – results from Chapters Seven and Eight present the preliminary work undertaken to produce the 2-D and 3-D models with the varying degrees of corrosion damage. The boundary constraint and loading conditions are provided and explained along with the author's reasoning for producing the models in the way they are presented. Step-by-step directions describing any new lines of coding are provided were necessary and their reasoning and use are explained where relevant.

2. Model each of the corrosion levels of the plate with various insulation systems and determine the effect of each system on the buckling results - the buckling results of the plate models with the varying levels of corrosion damage with the various insulation system configurations are presented in Chapter Nine and Appendices C and D.

3. Create a 2-D model of a steel pipe with the five levels of corrosion - the 2-D pipe model with the five levels of corrosion damage and the respective buckling values is presented in Chapter Ten and Appendix E.

4. Model the effects of the most common insulation and jacketing thickness options on the buckling value of the steel pipe - Chapter Ten and Appendix E also present the values determined when the pipe model has a mineral wool insulation system with both aluminium and polycarbonate protective jacketing.

11.2   Summary of the Findings

This section shall present a brief summary of the main four chapter's results and the impact of these findings on the course taken during the project. The first two sub-sections shall focus on the preliminary work to set up the working parameters for the computational work. The next two sub-sections will focus on the results generated due to the effect of the insulation system materials.

11.2.1 Validation of the Coding

The main purpose of the chapter was to validate the coding style of the author to ensure that the results in future chapters would be considered accurate and acceptable. To do this the first stage was to reproduce a published 2-D example and then run and compare the results to a version created by the author. A linear and non-linear version was run and graphs were produced to illustrate the displacement of two points on the geometry of the example. The displacement graphs matched sufficiently to validate the author's 2-D coding style.

The second stage was to validate the author's 3-D coding style. This was required as it would allow the author to self-validate the results in future chapters. The same published example was used as the template from which to model the 3-D validation example. It was found that during this part of the project the option of the SOLID185 ANSYS element was unsuitable for use as the lack of nodes mean there were too many approximations made and this resulted in a highly inaccurate result. The SOLID186 element did produce accurate results and these results matched the 2-D published model and the author's 2-D model sufficiently.

The final validation section involved altering the geometry data, material data, boundary conditions and loading conditions of the model to better reflect the conditions that would be used in the main computational sections. In this set of validation work, the displacements at two points were again measured and illustrated graphically. The results for the 2-D and 3-D model again matched allowing the author to validate the computational models and move on the second preliminary section which would be the mesh convergence study.

11.2.2 Mesh Convergence Study

The second piece of preliminary work was to complete a mesh convergence study to determine the best compromise between a suitable model computation time and accurate results. The two models used were the fully intact plate and the plate with the hole. Other than these two different plate configurations all the remaining variables were exactly the same other than the meshing coarseness. The same material properties were used and the loading and boundary conditions were kept the same.

The displacement values at three separate nodes were measured and the graphical data was presented to show that the displacement distance at each node was the same regardless of the meshing variance. Load-displacement plots were also generated to show that the buckling value was within the expected range as determined by the ANSYS results.

The variation between the finest and the coarsest mesh had very little impact on the buckling value generated during the non-linear analysis for both plate configurations. It was therefore advised to use the finest mesh possible that did not impact computation time unfavourably.

The load-deflection graphs confirmed the validity of the models used as all the plots suddenly dropped in the vicinity of the expected buckling point. There was virtually no difference in the results generated by both the 2-D and 3-D models for each of the respective configurations which further validated the results generated by each of the model codes.

11.2.3 Insulated Plate Buckling

The purpose of this chapter was to create a number of ANSYS models which subjected a steel plate with five levels of corrosion damage in the centre of the plate to a buckling load to generate a result where no insulation system was present. Once these initial configurations were documented the effect of varying the insulation and protective jacketing material and their respective thicknesses were then also processed. The steel plate geometries and material data remained constant with the variation in the thicknesses and the composition of the insulation system materials. In total six insulation materials were processed at ten thicknesses and the two protective jacketing materials were processed at five different thicknesses.

The increase in the buckling value due to the variance in the insulation systems were graphically represented. With no insulation present, the buckling value increased as the level of corrosion in the plate decreased as was expected. This pattern continued as the thickness of the insulation layer and/or the protective layer increased. It was noted that an increase of a single increment in the insulation layer thickness corresponded to a considerably larger increase in the buckling value of the plate as compared to an increase in the thickness of the protective layer at a single insulation thickness.

The results generated in this section at the thicker end of the insulation scale were considered to be only theoretical and not a realistic representation of reality. The Euler column critical load formula was used as an explanation of the results generated. As the thickness of the insulated plate increases the moment of inertia also increases which means that the system is considered to be much stiffer. So, although this chapter dealt with plates rather than columns the theory still holds as the plate could be considered to be a column that has been split lengthwise and then flattened.

The raw data for each insulation system configuration could be used in the future to approximate the effect to the magnitude of the buckling value of each system. It was felt that the repetition of the analysis of the pipe with each of these various systems was not an efficient use of time and resources. So, for the purposes of this project, the insulated pipe buckling chapter only focussed on the most common insulation material in use.

11.2.4 Insulated Pipe Buckling

The purpose of this chapter was to create a number of ANSYS models which subjected a hollow slender steel pipe with five levels of corrosion damage in a central section of the pipe to a buckling load to generate a result where no insulation system was present. Once these initial configurations were documented the effect of varying the insulation material and the protective jacketing materials and their respective thicknesses were then also processed. The steel pipe geometries and material data remained constant with the variation in the thicknesses and the composition of the insulation system materials. A single insulation material was processed at ten thicknesses and the two protective jacketing materials were processed at five different thicknesses.

As completed before in the plate configuration, the increase in the buckling value due to the variance in the insulation systems were graphically represented. With no insulation present, the buckling value increased as the level of corrosion in the pipe decreased as was expected. This pattern continued as the thickness of the insulation layer and/or the protective layer increased. It was noted that an increase of a single increment in the insulation layer thickness corresponded to a considerably larger increase in the buckling value of the pipe as compared to an increase in the thickness of the protective layer at a single insulation thickness.

These results are very similar to the results seen in the previous chapter with regards to the relationship. Clearly, the results in this chapter are considerably smaller in relative terms but the relationship remains the same. As before, the Euler column critical load formula explains the relationship. The formula produces results more realistically expected as it is dealing with an actual columnar form which affects the results rather than the flat plate from the previous chapter. It is also interesting to note that the results have a more linear character than the plate results due to the more realistic values involved.

Also, the fact that the pipe example deals with a considerably slenderer example, i.e. the length relative to the thickness is considerably more. This was not the case in the plate example which may further explain the generation of more theoretical results. The plate example would not usually be considered in isolation but would be part of a larger network, its purpose was to provide a comparison tool to the pipe example which is of greater interest overall.

11.3   Gaps in the Research and Recommended Future Work

The author of this thesis had virtually no knowledge in the field of research at the outset. The first few months of the project were spent building up a general core knowledge of structural mechanics and finite element method. It is assumed therefore that in some circumstances the actions taken in this piece of research have been simplified and assumptions have been made to prevent overly complex situations, especially as this is an introductory piece of research into the field. This piece of research was always assumed to be an initial early phase investigation to open up possible future research avenues.

Examples of simplifications or assumptions made during the project include:

- The fully constrained model was the only boundary condition option explored – previous research described in Chapter One used simply supported boundary conditions
- Void in plates and pipe were given a Young's modulus value of "1" and Poisson' ratio of "0.3" – these were assumed to be acceptable as the Young's modulus was very small when compared to the other material values so would in effect be essentially zero
- Generic Young's Modulus and Poisson's ratio values for steel components – various other options available
- There are very few sources of relevant material properties for the insulation system materials – unable to provide two sources for validation
- Circular shaped pits the only option modelled – other shaped pits are possible
- The corrosion degradation on the plate was centrally located
- Insulation systems only include insulation material and protective jacketing – though this is possible in reality many systems include additional components which may have affected results
- Pipe buckling only subjected to axial load – in reality, there would be internal pressures within the pipe as well
- The location of the four corrosion degradations in the pipe were in a single central section location
- Pipe model was hollow and slender to allow Euler's column critical load formula to be used as a validation technique

As mentioned previously there has been practically no research into the effect of the insulation system's mechanical properties on the overall buckling values exhibited by the components. Therefore, the opportunity to compare results is impossible, the author has however attempted where possible to validate the initial condition results with no insulation system present by more than a single means. The author maintains that they have a strong confidence with regards to these results and believes that with further investigation by other research groups a better picture of the overall effect of the insulation system can be produced.

There are numerous avenues appropriate for future work in this field of research as very little has been completed to this point. It would be advised that research focussing on the determination of the material properties relating to the insulation systems would be of great importance in the first instance as currently there is very little available source data. There are also numerous other insulation and protective jacketing materials used in various industries that were not presented in this piece of research.

There are numerous plate and pipe geometric and material configurations that are possible to be explored, the initial research built upon the small amount of previous work in the field. The plate data was taken from previous research and the insulation system data was added to this as a level of novelty to further the initial research presented.

The shape and distribution of the pit and holes is another area of interest for future work. In this piece of research, only single circular pits or holes were modelled in the plate and four circular pits or holes in the pipe model. The number and distribution of these degradations may have a substantive impact on the results gathered. There are options to model pits of varying diameter and shape in either regular or random distributions. As with the options available for the plate and pipe configuration, there are so many options available regarding the pits or holes, with shape, depth, location and distribution variation opening so many potential avenues.

11.4   Novelty and Contribution to the Field

Pitting corrosion, generally, negatively affects a huge number of structures of various industries. It has been well documented to be one of the most common mechanisms of corrosion and has the potential to be very dangerous with catastrophic failures possible. Especially in circumstances where the processes of corrosion have been hidden due to insulation systems. These systems once breached often perpetuate the problems associated with corrosion and can impact the rate of corrosion greatly leading to very costly repair procedures if companies are lucky and capture the issue before failure. Should the system fail then there are many more negative considerations to consider. The prevention of a highly damaging incident in terms of financial, reputational and environmental concerns prove the importance and relevance of a study such as the project presented in this thesis. Any means by which corrosion engineers can prevent the actions of corrosion processes is of paramount importance. The likelihood of the full prevention in all scenarios are not necessarily wholly realistic so an understanding the effects of the materials currently used in the systems already in place may assist in the formulation of systems in the future. The best way to prevent issues in the future is to modify the actions taken in the present.

The models created by the author depicting the five levels of corrosion damage have been presented in full in the appendices and it is hoped that future researchers may use these documents as a starting point to create more complex and accurate versions. At the time of writing, there were very few full examples available to the author to assist with the creation of these models. The experience and knowledge of the author's two supervisors and fellow research group students were extremely important in the preparation of these models.

As seen in the literature review there has been some work completed looking at the effect on the buckling of a plate under simply supported conditions. These examples did not include any effect on the buckling value due to the insulation system materials used. It is therefore believed that this study may represent the first foray into the effect of these materials on the buckling values. As recommended in the section regarding future work there is an important requirement to attain more accurate mechanical data for the insulation types as currently this information is not readily available and there are no sources available to corroborate the values expressed.

One of the goals of the study was to combine the author's previous chemistry and chemical engineering knowledge with that of structural mechanics and finite element analysis to help effect change to a real-world issue. This idea perfectly illustrates the situation in the real world where experts of different disciplines need to work together to eradicate these dangers associated with corrosion processes.

11.5   Final Remarks

The results from this project support the idea that the insulation material and protective jacketing material used to protect the system primarily from heat loss may as a by-product have a considerable effect on the buckling values of a steel plate and a steel pipe system.

These systems may be undergoing corrosion under insulation with no visible issues present; the effect that each stage of the corrosion process has, from the fully intact plate to the fully corroded hole, on this buckling value was also shown.

This project should act as a starting point for further research into this field of study which at this point has received no real research input. Further research is urgently required to ensure this hidden phenomenon does not continue undetected with the potential to cause catastrophic damage. Any means by which corrosion engineers can alleviate the risk must be thoroughly explored.

Appendix A: Additional Information from Chapter Seven

/TITLE,2-D Coding from Madenci Book: 40kN Load	!Title
/PREP7	!Enter Preprocessor
ET,1,181	!Element Type
MP,EX,1,1.2E8	!Define Material Data
MP,NUXY,1,0.3	
SECT,1,SHELL	!Define Shell Section ID
SECDATA,0.4,1	
K,1,0	!Create Keypoints for Geometry
K,2,40	
K,3,40,30	
K,4,0,30	
A,1,2,3,4	!Create Area
LESIZE,ALL,,,20	!Define Line Divisions
MSHKEY,1	!Apply Mapped Meshing
AMESH,ALL	
FINISH	!Finish Preprocessor
/SOLU	!Enter Solution
ANTYPE,STATIC	!Type of Analysis
NLGEOM,ON	!Turn on Non-Linear Geometry
NEQIT,1000	!Specify Max Number of Equilibrium Iterations
OUTRES,ALL,ALL	!Control Data Written to Database
NSEL,S,LOC,X,0	!Apply Boundary Conditions
D,ALL,ALL	
ALLSEL	
NSEL,S,LOC,X,40	!Apply 1st Force of 8kN in the Negative Direction
NSEL,R,LOC,Y,0	
F,ALL,FZ,-8000	
ALLSEL	
LSWRITE	!Write Load Step File 1
NSEL,S,LOC,X,40	!Apply 2nd Force of 16kN in the Negative Direction
NSEL,R,LOC,Y,0	
F,ALL,FZ,-16000	
ALLSEL	
LSWRITE	!Write Load Step File 2
NSEL,S,LOC,X,40	!Apply 3rd Force of 24kN in the Negative Direction
NSEL,R,LOC,Y,0	
F,ALL,FZ,-24000	
ALLSEL	
LSWRITE	!Write Load Step File 3
NSEL,S,LOC,X,40	!Apply 4th Force of 32kN in the Negative Direction
NSEL,R,LOC,Y,0	
F,ALL,FZ,-32000	
ALLSEL	
LSWRITE	!Write Load Step File 4
NSEL,S,LOC,X,40	!Apply 5th Force of 40kN in the Negative Direction
NSEL,R,LOC,Y,0	
F,ALL,FZ,-40000	
ALLSEL	
LSWRITE	!Write Load Step File 5
LSSOLVE,1,5,1	!Solve from Load Step Files
FINISH	!Finish Solution

Code A.1 Recreated Full Version of the 2-D Madenci Code from the Book

/TITLE,Author 2-D Coding: 40kN Load	!Title
/UNITS,SI	!Determine Units
/PREP7	!Enter Preprocessor
ET,1,SHELL181	!Element Type
MP,EX,1,1.2E8	!Define Material Data
MP,PRXY,1,0.3	
SECTYPE,1,SHELL	!Define Shell Section ID
SECDATA,0.4,1	
K,1,0,0	!Create Keypoints for Geometry
K,2,40,0	
K,3,40,30	
K,4,0,30	
L,1,2	!Create Lines
L,2,3	
L,3,4	
L,4,1	
AL,1,2,3,4	!Create Area
LESIZE,ALL,,,20	!Define Line Divisions
MSHKEY,1	!Apply Mapped Meshing
AMESH,ALL	
/SOLU	!Enter Solution
ANTYPE,STATIC	!Type of Analysis
NLGEOM,ON	!Turn on Non-Linear Geometry
OUTRES,ALL,ALL	!Control Data Written to Database
NSUBST,5,5,5	!Determine Number of Sub-Steps
AUTOTS,ON	!Turn on Automatic Time Stepping
LNSRCH,ON	!Activate Line Search
NEQIT,1000	!Specify Max Number of Equilibrium Iterations
NSEL,S,LOC,X,0-0.0001,0+0.0001	!Define Boundary Conditions
NSEL,R,LOC,Y,0-0.0001,30+0.0001	
D,ALL,UX,0	
D,ALL,UY,0	
D,ALL,UZ,0	
D,ALL,ROTX,0	
D,ALL,ROTY,0	
D,ALL,ROTZ,0	
ALLSEL	
NSEL,S,LOC,X,40-0.0001,40+0.0001	!Apply Load in z Direction
NSEL,R,LOC,Y,0-0.0001,0+0.0001	
F,ALL,FZ,-40000	
ALLSEL	
SOLVE	!Solve

Code A.2 Author's Full 2-D Version of the Madenci Code

FINISH	!Finish Solve
/POST26	!Enter Post-Processor
NUMVAR,200	!Specify Number of Allowed Variables
SOLU,191,NCMIT	!Specify Solution Summary Data per Substep
STORE,MERGE	!Store Data in Database
FILLDATA,191,,,,1,1	!Fills a Variable by a Ramp Function
REALVAR,191,191	!Forms a Variable using only the Real Part
NSOL,2,2,U,X,POINT_A_UX	!Specify Nodal Data to be Stored
STORE,MERGE	!Store Data in Database
NSOL,3,2,U,Y,POINT_A_UY	!Specify Nodal Data to be Stored
STORE,MERGE	!Store Data in Database
NSOL,4,2,U,Z,POINT_A_UZ	!Specify Nodal Data to be Stored
STORE,MERGE	!Store Data in Database
NSOL,5,22,U,X,POINT_B_UX	!Specify Nodal Data to be Stored
STORE,MERGE	!Store Data in Database
NSOL,6,22,U,Y,POINT_B_UY	!Specify Nodal Data to be Stored
STORE,MERGE	!Store Data in Database
NSOL,7,22,U,Z,POINT_B_UZ	!Specify Nodal Data to be Stored
STORE,MERGE	!Store Data in Database
PRVAR,2,3,4,5,6,7	!Display Nodal Data

Code A.3 Full Version of the 2-D Post Processor Code

/TITLE,Author 3-D Coding: 40kN Load	!Title
/UNITS,SI	!Determine Units
/PREP7	!Enter Preprocessor
ET,1,SOLID185	!Element Type
MP,EX,1,1.2E8	!Define Material Data
MP,PRXY,1,0.3	
K,1,0,0,0	!Create Keypoints for Geometry
K,2,40,0,0	
K,3,40,30,0	
K,4,0,30,0	
L,1,2	!Create Lines
L,2,3	
L,3,4	
L,4,1	
AL,1,2,3,4	!Create Area
VEXT,ALL,,,0,0,-0.4	!Extrude to Create Volume
LSEL,S,LINE,,1,,,0	!Define Length and Width Line Divisions
LSEL,A,LINE,,2,,,0	
LSEL,A,LINE,,3,,,0	
LSEL,A,LINE,,4,,,0	
LSEL,A,LINE,,5,,,0	
LSEL,A,LINE,,6,,,0	
LSEL,A,LINE,,7,,,0	
LSEL,A,LINE,,8,,,0	
LESIZE,ALL,,,20,,,,,1	
ALLSEL	
LSEL,S,LINE,,9,,,0	!Define Thickness Line Divisions
LSEL,A,LINE,,10,,,0	
LSEL,A,LINE,,11,,,0	
LSEL,A,LINE,,12,,,0	
LESIZE,ALL,,,4,,,,,1	
ALLSEL	
MSHKEY,1	!Apply Mapped Meshing
VMESH,ALL	
/SOLU	!Enter Solution
ANTYPE,STATIC	!Type of Analysis
NLGEOM,ON	!Turn on Non-Linear Geometry
OUTRES,ALL,ALL	!Control Data Written to Database
NSUBST,5,5,5	!Determine Number of Sub-Steps
AUTOTS,ON	!Turn on Automatic Time Stepping
LNSRCH,ON	!Activate Line Search
NEQIT,1000	!Specify Max Number of Equilibrium Iterations
NSEL,S,LOC,X,0-0.0001,0+0.0001	!Define Boundary Conditions
NSEL,R,LOC,Y,0-0.0001,30+0.0001	
NSEL,R,LOC,Z,-0.4-0.0001,0+0.0001	
D,ALL,UX,0	
D,ALL,UY,0	
D,ALL,UZ,0	
ALLSEL	
NSEL,S,LOC,X,40-0.0001,40+0.0001	!Apply Load in z Direction
NSEL,R,LOC,Y,0-0.0001,0+0.0001	
NSEL,R,LOC,Z,-0.2-0.0001,-0.2+0.0001	
F,ALL,FZ,-40000	
ALLSEL	
SOLVE	!Solve

Code A.4 Author's Full 3-D Version of the Madenci Code using the SOLID185 Element

/TITLE,Non-Linear Buckling of a 2D Shell Element	!Title
/UNITS,SI	!Determine Units
/PREP7	!Enter Preprocessor
ET,1,SHELL181	!Element Type
MP,EX,1,2.058E11	!Define Material Data
MP,PRXY,1,0.3	
SECTYPE,1,SHELL	!Define Shell Section ID
SECDATA,0.01	
BLC4,0,0,0.8,0.8	!Create Geometry
ESIZE,0.02	!Define Element Size
MSHKEY,1	!Apply Mapped Meshing
AMESH,ALL	
/SOLU	!Enter Solution
ANTYPE,STATIC	!Type of Analysis
NLGEOM,ON	!Turn on Non-Linear Geometry
OUTRES,ALL,ALL	!Control Data Written to Database
NSUBST,10,10,10	!Determine Number of Sub-Steps
AUTOTS,ON	!Turn on Automatic Time Stepping
LNSRCH,ON	!Activate Line Search
NEQIT,1000	!Specify Max Number of Equilibrium Iterations
NSEL,S,LOC,X,0-0.0001,0+0.0001	!Define Boundary Conditions
NSEL,R,LOC,Y,0-0.0001,0.8+0.0001	
D,ALL,UX,0	
D,ALL,UY,0	
D,ALL,UZ,0	
D,ALL,ROTX,0	
D,ALL,ROTY,0	
D,ALL,ROTZ,0	
ALLSEL	
NSEL,S,LOC,X,0.8-0.0001,0.8+0.0001	!Couple Nodes
CP,NEXT,UX,ALL	
ALLSEL	
NSEL,S,LOC,X,0.8-0.0001,0.8+0.0001	!Apply 40kN Load in z Direction
NSEL,R,LOC,Y,0-0.0001,0+0.0001	
F,ALL,FZ,-40000	
ALLSEL	
SOLVE	!Solve

Code A.5 Full 2-D Version of the Code for Further Model Validation

/TITLE,Non-Linear Buckling of a 3D Solid Element	!Title
/UNITS,SI	!Determine Units
/PREP7	!Preprocessor
ET,1,SOLID186	!Element Type
MP,EX,1,2.058E11	!Define Material Data
MP,PRXY,1,0.3	
BLOCK,0,0.8,0,0.8,0,-0.01	!Create Geometry
LSEL,S,LINE,,1,,,0	!Define Outer Line Divisions
LSEL,A,LINE,,2,,,0	
LSEL,A,LINE,,3,,,0	
LSEL,A,LINE,,4,,,0	
LSEL,A,LINE,,5,,,0	
LSEL,A,LINE,,6,,,0	
LSEL,A,LINE,,7,,,0	
LSEL,A,LINE,,8,,,0	
LESIZE,ALL,,,40,,,,,1	
ALLSEL	
LSEL,S,LINE,,9,,,0	!Define Short Internal Line Divisions
LSEL,A,LINE,,10,,,0	
LSEL,A,LINE,,11,,,0	
LSEL,A,LINE,,12,,,0	
LESIZE,ALL,,,4,,,,,1	
ALLSEL	
MSHKEY,1	!Apply Mapping Meshing
VMESH,ALL	
/SOLU	!Enter Solution
ANTYPE,STATIC	!Type of Analysis
NLGEOM,ON	!Turn on Non-Linear Geometry
OUTRES,ALL,ALL	!Control Data Written to Database
NSUBST,10,10,10	!Determine Number of Sub-Steps
AUTOTS,ON	!Turn on Automatic Time Stepping
LNSRCH,ON	!Activate Line Search
NEQIT,1000	!Specify Max Number of Equilibrium Iterations
NSEL,S,LOC,X,0-0.0001,0+0.0001	!Define Boundary Conditions
NSEL,R,LOC,Y,0-0.0001,0.8+0.0001	
NSEL,R,LOC,Z,-0.01-0.0001,0+0.0001	
D,ALL,UX,0	
D,ALL,UY,0	
D,ALL,UZ,0	
ALLSEL	
NSEL,S,LOC,X,0.8-0.0001,0.8+0.0001	!Couple Nodes
NSEL,R,LOC,Z,-0.005-0.0001,-0.005+0.0001	
CP,NEXT,UX,ALL	
ALLSEL	
NSEL,S,LOC,X,0.8-0.0001,0.8+0.0001	!Apply 40kN Load in z Direction
NSEL,R,LOC,Y,0-0.0001,0+0.0001	
NSEL,R,LOC,Z,-0.005-0.0001,-0.005+0.0001	
F,ALL,FZ,-40000	
ALLSEL	
SOLVE	!Solve

Code A.6 Full 3-D Version of the Code for Further Model Validation

Table A.1 Raw Data for Madenci 2-D Code with Forty Newton Load Applied

		Madenci Coding 40N Load					
Max Load (N)	40	Displacement (m)					
		Point A			Point B		
Time	Load (N)	UX	UY	UZ	UX	UY	UZ
0	0	0	0	0	0	0	0
0.2	8	0	0	-1.05E-02	0	0	-6.50E-03
0.4	16	0	0	-2.10E-02	0	0	-1.30E-02
0.6	24	0	0	-3.15E-02	0	0	-1.95E-02
0.8	32	0	0	-4.20E-02	0	0	-2.60E-02
1	40	0	0	-5.25E-02	0	0	-3.25E-02

Table A.2 Raw Data for Author 2-D Code with Forty Newton Load Applied

		Author 2-D Coding 40N Load					
Max Load (N)	40	Displacement (m)					
		Point A			Point B		
Time	Load (N)	UX	UY	UZ	UX	UY	UZ
0	0	0	0	0	0	0	0
0.2	8	0	0	-1.05E-02	0	0	-6.50E-03
0.4	16	0	0	-2.10E-02	0	0	-1.30E-02
0.6	24	0	0	-3.15E-02	0	0	-1.95E-02
0.8	32	0	0	-4.20E-02	0	0	-2.60E-02
1	40	0	0	-5.25E-02	0	0	-3.25E-02

Table A.3 Raw Data for Madenci 2-D Code with Forty Thousand Newton Load Applied

		Madenci Coding 40kN Load					
Max Load (N)	40000	Displacement (m)					
		Point A			Point B		
Time	Load (N)	UX	UY	UZ	UX	UY	UZ
0	0	0	0	0	0	0	0
0.2	8000	-1.33655	0.24058	-9.46958	-0.64575	0.07824	-6.44848
0.4	16000	-4.19031	0.73837	-16.42790	-2.15148	0.26678	-11.61850
0.6	24000	-7.27729	1.28052	-21.17000	-3.87324	0.49154	-15.36820
0.8	32000	-9.86235	1.74803	-24.19270	-5.35589	0.69038	-17.86860
1	40000	-12.12060	2.15410	-26.37640	-6.71151	0.87603	-19.79090

Table A.4 Raw Data for Author 2-D Code with Forty Thousand Newton Load Applied

		Author 2-D Coding 40kN Load					
Max Load (N)	40000	Displacement (m)					
		Point A			Point B		
Time	Load (N)	UX	UY	UZ	UX	UY	UZ
0	0	0	0	0	0	0	0
0.2	8000	-1.33566	0.24046	-9.46658	-0.64521	0.07817	-6.44592
0.4	16000	-4.19132	0.73846	-16.42960	-2.15222	0.26687	-11.62030
0.6	24000	-7.19801	1.26885	-21.07230	-3.82011	0.48357	-15.27560
0.8	32000	-9.86123	1.74753	-24.19150	-5.35569	0.69024	-17.86840
1	40000	-12.11830	2.16127	-26.37620	-6.69833	0.87679	-19.77230

Table A.5 Raw Data for 3-D Code with a Forty Newton Load Applied to

a SOLID185 Element Type Model

		Solid185 Coding 40N Load					
Max Load	40	Displacement (m)					
		Point A			Point B		
Time	Load (N)	UX	UY	UZ	UX	UY	UZ
0	0	0	0	0	0	0	0
0.2	8	3.30E-16	7.06E-16	-2.03E-03	-2.14E-16	5.39E-16	2.33E-04
0.4	16	6.61E-16	1.41E-15	-4.07E-03	-4.28E-16	1.08E-15	4.65E-04
0.6	24	9.89E-16	2.11E-15	-6.10E-03	-6.42E-16	1.62E-15	6.98E-04
0.8	32	1.32E-15	2.83E-15	-8.13E-03	-8.56E-16	2.15E-15	9.31E-04
1	40	1.65E-15	3.52E-15	-1.02E-02	-1.07E-15	2.69E-15	1.16E-03

Table A.6 Raw Data for 3-D Code with a Forty Newton Load Applied to

a SOLID186 Element Type Model

		Solid186 Coding 40N Load					
Max Load	40	Displacement (m)					
		Point A			Point B		
Time	Load (N)	UX	UY	UZ	UX	UY	UZ
0	0	0	0	0	0	0	0
0.2	8	5.54E-14	1.22E-13	-1.05E-02	-5.51E-14	1.51E-13	-6.49E-03
0.4	16	1.11E-13	2.43E-13	-2.10E-02	-1.10E-13	3.02E-13	-1.30E-02
0.6	24	1.66E-13	3.65E-13	-3.16E-02	-1.65E-13	4.53E-13	-1.95E-02
0.8	32	2.22E-13	4.86E-13	-4.21E-02	-2.20E-13	6.04E-13	-2.59E-02
1	40	2.77E-13	6.08E-13	-5.26E-02	-2.75E-13	7.55E-13	-3.24E-02

Table A.7 Raw Data for 3-D Code with a Forty Thousand Newton Load Applied to a SOLID185 Element Type Model

		Solid185 Coding 40kN Load					
Max Load	40000	Displacement (m)					
		Point A			Point B		
Time	Load (N)	UX	UY	UZ	UX	UY	UZ
0	0	0	0	0	0	0	0
0.2	8000	-4.83E-02	4.50E-02	-1.91E+00	5.24E-03	-2.04E-02	1.18E-01
0.4	16000	-1.65E-01	1.36E-01	-3.49E+00	1.46E-02	-5.22E-02	-6.85E-02
0.6	24000	-3.28E-01	2.42E-01	-4.88E+00	2.03E-02	-7.81E-02	-4.34E-01
0.8	32000	-5.28E-01	3.57E-01	-6.15E+00	1.85E-02	-9.67E-02	-8.89E-01
1	40000	-7.63E-01	4.79E-01	-7.34E+00	7.26E-03	-1.09E-01	-1.39E+00

Table A.8 Raw Data for 3-D Code with a Forty Thousand Newton Load Applied to a SOLID186 Element Type Model

		Solid186 Coding 40kN Load					
Max Load	40000	Displacement (m)					
		Point A			Point B		
Time	Load (N)	UX	UY	UZ	UX	UY	UZ
0	0	0	0	0	0	0	0
0.2	8000	-1.32335	0.23873	-9.42654	-0.63867	0.07733	-6.41504
0.4	16000	-4.17052	0.73537	-16.39420	-2.14197	0.26559	-11.59480
0.6	24000	-7.16675	1.26524	-21.03450	-3.80240	0.48165	-15.24310
0.8	32000	-9.84089	1.74587	-24.17240	-5.34501	0.68951	-17.85170
1	40000	-12.08880	2.15852	-26.35270	-6.68117	0.87528	-19.74950

Table A.9 Raw Data for 3-D Code with a Forty Thousand Newton Load Applied to a SOLID185 Element Type Model with a Finer Mapped Mesh

		Solid185 Coding 40kN Load					
Max Load	40000	Displacement (m)					
		Point A			Point B		
Time	Load (N)	UX	UY	UZ	UX	UY	UZ
0	0	0	0	0	0	0	0
0.2	8000	-0.22584	0.10289	-3.99055	-0.02239	-0.01062	-1.35862
0.4	16000	-0.79772	0.31279	-7.41804	-0.14100	0.00037	-3.14069
0.6	24000	-1.62532	0.59153	-10.49440	-0.36185	0.03522	-4.91655
0.8	32000	-2.60767	0.90941	-13.18080	-0.65729	0.08593	-6.55248
1	40000	-3.67774	1.24833	-15.52000	-1.00376	0.14724	-8.03745

Table A.10 Raw Data for 3-D Code with a Forty Thousand Newton Load Applied to a SOLID186 Element

Type Model with a Finer Mapped Mesh

		Solid186 Coding 40kN Load					
Max Load	40000	Displacement (m)					
		Point A			Point B		
Time	Load (N)	UX	UY	UZ	UX	UY	UZ
0	0	0	0	0	0	0	0
0.2	8000	-1.32400	0.23896	-9.42989	-0.63903	0.07741	-6.41718
0.4	16000	-4.17135	0.73588	-16.39780	-2.14259	0.26575	-11.59710
0.6	24000	-7.16881	1.26638	-21.04020	-3.80380	0.48204	-15.24650
0.8	32000	-9.83941	1.74693	-24.17500	-5.34409	0.68967	-17.85150
1	40000	-12.09200	2.16049	-26.36010	-6.68379	0.87601	-19.75400

Table A.11 Raw Data for 2-D Code with an Arbitrary Forty Thousand Newton Load Applied

		Shell 40kN Load					
Max Load	40000	Displacement (m)					
		Point A			Point B		
Time	Load (N)	UX	UY	UZ	UX	UY	UZ
0.0	0	0	0	0	0	0	0
0.1	4000	-1.51E-03	2.39E-04	-4.76E-02	-1.51E-03	1.86E-04	-4.25E-02
0.2	8000	-6.14E-03	5.30E-04	-9.32E-02	-6.14E-03	4.65E-04	-8.74E-02
0.3	12000	-1.35E-02	9.60E-04	-0.137057	-1.35E-02	8.80E-04	-0.129868
0.4	16000	-2.32E-02	1.52E-03	-0.178586	-2.32E-02	1.42E-03	-0.169849
0.5	20000	-3.48E-02	2.20E-03	-0.21739	-3.48E-02	2.07E-03	-0.207019
0.6	24000	-4.77E-02	2.98E-03	-0.253276	-4.77E-02	2.82E-03	-0.241229
0.7	28000	-6.15E-02	3.83E-03	-0.286175	-6.15E-02	3.65E-03	-0.272431
0.8	32000	-7.59E-02	4.75E-03	-0.31629	-7.59E-02	4.53E-03	-0.300841
0.9	36000	-9.06E-02	5.72E-03	-0.343685	-9.06E-02	5.46E-03	-0.326534
1.0	40000	-0.105275	6.73E-03	-0.368587	-0.105275	6.43E-03	-0.349739

Table A.12 Raw Data for 3-D Code with an Arbitrary Forty Thousand Newton Load Applied

		Solid 40kN Load					
Max Load	40000	Displacement (m)					
		Point A			Point B		
Time	Load (N)	UX	UY	UZ	UX	UY	UZ
0.0	0	0	0	0	0	0	0
0.1	4000	-1.50E-03	2.40E-04	-4.76E-02	-1.50E-03	1.86E-04	-4.24E-02
0.2	8000	-6.13E-03	5.33E-04	-9.32E-02	-6.13E-03	4.65E-04	-8.72E-02
0.3	12000	-1.35E-02	9.64E-04	-0.136923	-1.35E-02	8.79E-04	-0.129643
0.4	16000	-2.32E-02	1.53E-03	-0.17848	-2.32E-02	1.42E-03	-0.169642
0.5	20000	-3.48E-02	2.21E-03	-0.21736	-3.48E-02	2.08E-03	-0.206882
0.6	24000	-4.77E-02	2.99E-03	-0.253261	-4.77E-02	2.83E-03	-0.241099
0.7	28000	-6.15E-02	3.85E-03	-0.286206	-6.15E-02	3.65E-03	-0.272337
0.8	32000	-7.59E-02	4.78E-03	-0.316287	-7.59E-02	4.54E-03	-0.300705
0.9	36000	-9.05E-02	5.75E-03	-0.343669	-9.05E-02	5.47E-03	-0.326375
1.0	40000	-0.105194	6.77E-03	-0.36856	-0.105194	6.44E-03	-0.349561

Appendix B: Additional Information from Chapter Eight

/TITLE,Very Fine Mesh	!Title
/UNITS,SI	!Determine Units
/PREP7	!Enter Preprocessor
ET,1,SHELL181	!Element Type
MP,EX,1,2.058E11	!Define Material Data
MP,PRXY,1,0.3	
SECTYPE,1,SHELL	!Define Shell Section ID
SECDATA,0.01	
BLC4,0,0,0.8,0.8	!Create Geometry
ESIZE,0.02	!Define Element Size
MSHKEY,1	!Apply Mapped Meshing
AMESH,ALL	
NSEL,S,LOC,X,0-0.0001,0+0.0001	!Define Boundary Conditions
NSEL,R,LOC,Y,0-0.0001,0.8+0.0001	
D,ALL,UX,0	
D,ALL,UY,0	
D,ALL,UZ,0	
D,ALL,ROTX,0	
D,ALL,ROTY,0	
D,ALL,ROTZ,0	
ALLSEL	
NSEL,S,LOC,X,0.8-0.0001,0.8+0.0001	!Couple Nodes
CP,NEXT,UX,ALL	
ALLSEL	
NSEL,S,LOC,X,0.8-0.0001,0.8+0.0001	!Apply Load in x Direction
NSEL,R,LOC,Y,0.4-0.0001,0.4+0.0001	
F,ALL,FX,-1	
ALLSEL	
/SOLU	!Enter Solution
ANTYPE,STATIC	!Type of Analysis
PSTRES,ON	!Include Prestress Effect Calculations
SOLVE	!Solve
FINISH	!Finish First Solve
/SOLU	!Enter Solution
ANTYPE,BUCKLE	!Change Type of Analysis
BUCOPT,LANB,1	!Apply Bucking Analysis Options
SOLVE	!Solve
FINISH	!Finish Second Solve
/SOLU	!Enter Solution
EXPASS,ON	!Perform Expansion Pass
MXPAND,1	!Specify Number of Modes to Expand
SOLVE	!Solve
FINISH	!Finish Third Solve
/POST1	!Enter Post-Processor
SET,LIST	!List Eigenvalue Solution – Buckling Strength
SET,LAST	!Read Data for Desired Mode
PLDISP,2	!Plot Deflected Shape vs Original

Code B.1 Intact 2-D Plate Eigenvalue Buckling Code with a Very Fine Mesh

/TITLEVery Fine Mesh	!Title
/UNITS,SI	!Determine Units
/PREP7	!Enter Preprocessor
ET,1,SHELL181	!Element Type
MP,EX,1,2.058E11	!Define Material Data
MP,PRXY,1,0.3	
SECTYPE,1,SHELL	!Define Shell Section ID
SECDATA,0.01	
BLC4,0,0,0.8,0.8	!Create Geometry
ESIZE,0.02	!Define Element Size
MSHKEY,1	!Apply Mapped Meshing
AMESH,ALL	
/SOLU	!Enter Solution
ANTYPE,STATIC	!Type of Analysis
NLGEOM,ON	!Turn on Non-Linear Geometry
OUTRES,ALL,ALL	!Control Data Written to Database
NSUBST,10,10,10	!Determine Number of Sub-Steps
AUTOTS,ON	!Turn on Automatic Time Stepping
LNSRCH,ON	!Activate Line Search
NEQIT,1000	!Specify Max Number of Equilibrium Iterations
NSEL,S,LOC,X,0-0.0001,0+0.0001	!Define Boundary Conditions
NSEL,R,LOC,Y,0-0.0001,0.8+0.0001	
D,ALL,UX,0	
D,ALL,UY,0	
D,ALL,UZ,0	
D,ALL,ROTX,0	
D,ALL,ROTY,0	
D,ALL,ROTZ,0	
ALLSEL	
NSEL,S,LOC,X,0.8-0.0001,0.8+0.0001	!Couple Nodes
CP,NEXT,UX,ALL	
ALLSEL	
NSEL,S,LOC,X,0.8-0.0001,0.8+0.0001	!Apply Approx 110% of Predicted Load in x Direction
NSEL,R,LOC,Y,0.4-0.0001,0.4+0.0001	
F,ALL,FX,-61550	
ALLSEL	
NSEL,S,LOC,X,0.8-0.0001,0.8+0.0001	!Apply 0.5% Load in z Direction to Initiate Buckling
NSEL,R,LOC,Y,0.4-0.0001,0.4+0.0001	
F,ALL,FZ,308	
ALLSEL	
SOLVE	!Solve

Code B.2 Intact 2-D Plate Non-Linear Buckling Code with a Very Fine Mesh

FINISH	!Finish Solve
/POST26	!Enter Post-Processor
NUMVAR,200	!Specify Number of Allowed Variables
SOLU,191,NCMIT	!Specify Solution Summary Data per Substep
STORE,MERGE	
FILLDATA,191,,,,1,1	!Fills a Variable by a Ramp Function
REALVAR,191,191	!Forms a Variable using only the Real Part
NSOL,2,###,U,X,POINT_A_UX	!Specify Nodal Data to be Stored
STORE,MERGE	
NSOL,3,###,U,Y,POINT_A_UY	!Specify Nodal Data to be Stored
STORE,MERGE	
NSOL,4,###,U,Z,POINT_A_UZ	!Specify Nodal Data to be Stored
STORE,MERGE	
NSOL,5,###,U,X,POINT_B_UX	!Specify Nodal Data to be Stored
STORE,MERGE	
NSOL,6,###,U,Y,POINT_B_UY	!Specify Nodal Data to be Stored
STORE,MERGE	
NSOL,7,###,U,Z,POINT_B_UZ	!Specify Nodal Data to be Stored
STORE,MERGE	
NSOL,8,###,U,X,POINT_C_UX	!Specify Nodal Data to be Stored
STORE,MERGE	
NSOL,9,###,U,Y,POINT_C_UY	!Specify Nodal Data to be Stored
STORE,MERGE	
NSOL,10,###,U,Z,POINT_C_UZ	!Specify Nodal Data to be Stored
STORE,MERGE	
PRVAR,2,3,4	!Display Nodal Data
PRVAR,5,6,7	
PRVAR,8,9,10	

Code B.3 Full Version of the Mesh Convergence Study Post-Processor Code

/TITLE,Very Fine Mesh	!Title
/UNITS,SI	!Determine Units
/PREP7	!Enter Preprocessor
ET,1,SHELL181	!Element Type
MP,EX,1,2.058E11	!Define Material Data
MP,PRXY,1,0.3	
SECTYPE,1,SHELL	!Define Shell Section ID
SECDATA,0.01	
K,1,0,0,0	!Create Keypoints for Geometry
K,2,0.8,0,0	
K,3,0.8,0.8,0	
K,4,0,0.8,0	
K,5,0.4,0.4,0	
L,1,2	!Create Lines
L,2,3	
L,3,4	
L,4,1	
L,1,5	
L,2,5	
L,3,5	
L,4,5	
AL,1,5,6	!Create Triangular Areas
AL,2,6,7	
AL,3,7,8	
AL,4,5,8	
CM,GROUP1,AREA	!Group Areas
CYL4,0.4,0.4,0.1	!Create Circle
ASBA,GROUP1,5	!Generate the Hole
LCOMB,15,16,0	!Merge Lines on Hole
LCOMB,18,19,0	
LCOMB,21,22,0	
LCOMB,23,24,0	
LSEL,S,LINE,,1,,,0	!Define Outer Line Divisions
LSEL,A,LINE,,2,,,0	
LSEL,A,LINE,,3,,,0	
LSEL,A,LINE,,4,,,0	
LESIZE,ALL,,,40,,,,,1	
ALLSEL	
LSEL,S,LINE,,13,,,0	!Define Inner Line Divisions and Spacing
LSEL,A,LINE,,14,,,0	
LSEL,A,LINE,,17,,,0	
LSEL,A,LINE,,20,,,0	
LESIZE,ALL,,,50,1/8,,,,,1	
ALLSEL	
LSEL,S,LINE,,15,,,0	!Define Circle Divisions
LSEL,A,LINE,,18,,,0	
LSEL,A,LINE,,21,,,0	
LSEL,A,LINE,,23,,,0	
LESIZE,ALL,,,20,,,,,1	
ALLSEL	
MSHKEY,1	!Apply Mapped Meshing
AMESH,ALL	
NSEL,S,LOC,X,0-0.0001,0+0.0001	!Define Boundary Conditions
NSEL,R,LOC,Y,0-0.0001,0.8+0.0001	
D,ALL,UX,0	
D,ALL,UY,0	
D,ALL,UZ,0	
D,ALL,ROTX,0	
D,ALL,ROTY,0	

D,ALL,ROTZ,0	
ALLSEL	
NSEL,S,LOC,X,0.8-0.0001,0.8+0.0001	!Couple Nodes
CP,NEXT,UX,ALL	
ALLSEL	
NSEL,S,LOC,X,0.8-0.0001,0.8+0.0001	!Apply Load in x Direction
NSEL,R,LOC,Y,0.4-0.0001,0.4+0.0001	
F,ALL,FX,-1	
ALLSEL	
/SOLU	!Enter Solution
ANTYPE,STATIC	!Type of Analysis
PSTRES,ON	!Include Prestress Effect Calculations
SOLVE	!Solve
FINISH	!Finish First Solve
/SOLU	!Enter Solution
ANTYPE,BUCKLE	!Change Type of Analysis
BUCOPT,LANB,1	!Apply Bucking Analysis Options
SOLVE	!Solve
FINISH	!Finish Second Solve
/SOLU	!Enter Solution
EXPASS,ON	!Perform Expansion Pass
MXPAND,1	!Specify Number of Modes to Expand
SOLVE	!Solve
FINISH	!Finish Third Solve
/POST1	!Enter Post-Processor
SET,LIST	!List Eigenvalue Solution – Buckling Strength
SET,LAST	!Read Data for Desired Mode
PLDISP,2	!Plot Deflected Shape vs Original

Code B.4 2-D Plate with a Hole Eigenvalue Buckling Code with a Very Fine Mesh

/TITLE,Very Fine Mesh	!Title
/UNITS,SI	!Determine Units
/PREP7	!Enter Preprocessor
ET,1,SHELL181	!Element Type
MP,EX,1,2.058E11	!Define Material Data
MP,PRXY,1,0.3	
SECTYPE,1,SHELL	!Define Shell Section ID
SECDATA,0.01	
K,1,0,0,0	!Create Keypoints for Geometry
K,2,0.8,0,0	
K,3,0.8,0.8,0	
K,4,0,0.8,0	
K,5,0.4,0.4,0	
L,1,2	!Create Lines
L,2,3	
L,3,4	
L,4,1	
L,1,5	
L,2,5	
L,3,5	
L,4,5	
AL,1,5,6	!Create Triangular Areas
AL,2,6,7	
AL,3,7,8	
AL,4,5,8	
CM,GROUP1,AREA	!Group Areas
CYL4,0.4,0.4,0.1	!Create Circle
ASBA,GROUP1,5	!Generate the Hole
LCOMB,15,16,0	!Merge Lines on Hole
LCOMB,18,19,0	
LCOMB,21,22,0	
LCOMB,23,24,0	
LSEL,S,LINE,,1,,,0	!Define Outer Line Divisions
LSEL,A,LINE,,2,,,0	
LSEL,A,LINE,,3,,,0	
LSEL,A,LINE,,4,,,0	
LESIZE,ALL,,,40,,,,,1	
ALLSEL	
LSEL,S,LINE,,13,,,0	!Define Inner Line Divisions and Spacing
LSEL,A,LINE,,14,,,0	
LSEL,A,LINE,,17,,,0	
LSEL,A,LINE,,20,,,0	
LESIZE,ALL,,,50,1/8,,,,,1	
ALLSEL	
LSEL,S,LINE,,15,,,0	!Define Circle Divisions
LSEL,A,LINE,,18,,,0	
LSEL,A,LINE,,21,,,0	
LSEL,A,LINE,,23,,,0	
LESIZE,ALL,,,20,,,,,1	
ALLSEL	
MSHKEY,1	!Apply Mapped Meshing
AMESH,ALL	
/SOLU	!Enter Solution
ANTYPE,STATIC	!Type of Analysis
NLGEOM,ON	!Turn on Non-Linear Geometry
OUTRES,ALL,ALL	!Control Data Written to Database
NSUBST,10,10,10	!Determine Number of Sub-Steps
AUTOTS,ON	!Turn on Automatic Time Stepping
LNSRCH,ON	!Activate Line Search

NEQIT,1000	!Specify Max Number of Equilibrium Iterations
NSEL,S,LOC,X,0-0.0001,0+0.0001	!Define Boundary Conditions
NSEL,R,LOC,Y,0-0.0001,0.8+0.0001	
D,ALL,UX,0	
D,ALL,UY,0	
D,ALL,UZ,0	
D,ALL,ROTX,0	
D,ALL,ROTY,0	
D,ALL,ROTZ,0	
ALLSEL	
NSEL,S,LOC,X,0.8-0.0001,0.8+0.0001	!Couple Nodes
CP,NEXT,UX,ALL	
ALLSEL	
NSEL,S,LOC,X,0.8-0.0001,0.8+0.0001	!Apply Approx 110% of Predicted Load in x Direction
NSEL,R,LOC,Y,0.4-0.0001,0.4+0.0001	
F,ALL,FX,-55750	
ALLSEL	
NSEL,S,LOC,X,0.8-0.0001,0.8+0.0001	!Apply 0.5% Load in z Direction to Initiate Buckling
NSEL,R,LOC,Y,0.4-0.0001,0.4+0.0001	
F,ALL,FZ,278	
ALLSEL	
SOLVE	!Solve

Code B.5 2-D Plate with a Hole Non-Linear Buckling Code with a Very Fine Mesh

/TITLE,Very Fine Mesh	!Title
/UNITS,SI	!Determine Units
/PREP7	!Preprocessor
ET,1,SOLID186	!Element Type
MP,EX,1,2.058E11	!Define Material Data
MP,PRXY,1,0.3	
BLOCK,0,0.8,0,0.8,0,-0.01	!Create Geometry
LSEL,S,LINE,,1,,,0	!Define Outer Line Divisions
LSEL,A,LINE,,2,,,0	
LSEL,A,LINE,,3,,,0	
LSEL,A,LINE,,4,,,0	
LSEL,A,LINE,,5,,,0	
LSEL,A,LINE,,6,,,0	
LSEL,A,LINE,,7,,,0	
LSEL,A,LINE,,8,,,0	
LESIZE,ALL,,,40,,,,,1	
ALLSEL	
LSEL,S,LINE,,9,,,0	!Define Short Internal Line Divisions
LSEL,A,LINE,,10,,,0	
LSEL,A,LINE,,11,,,0	
LSEL,A,LINE,,12,,,0	
LESIZE,ALL,,,4,,,,,1	
ALLSEL	
MSHKEY,1	!Apply Mapping Meshing
VMESH,ALL	
NSEL,S,LOC,X,0-0.0001,0+0.0001	!Define Boundary Conditions
NSEL,R,LOC,Y,0-0.0001,0.8+0.0001	
NSEL,R,LOC,Z,-0.01-0.0001,0+0.0001	
D,ALL,UX,0	
D,ALL,UY,0	
D,ALL,UZ,0	
ALLSEL	
NSEL,S,LOC,X,0.8-0.0001,0.8+0.0001	!Couple Nodes
NSEL,R,LOC,Z,-0.005-0.0001,-0.005+0.0001	
CP,NEXT,UX,ALL	
ALLSEL	
NSEL,S,LOC,X,0.8-0.0001,0.8+0.0001	!Apply Load in x Direction
NSEL,R,LOC,Y,0.4-0.0001,0.4+0.0001	
NSEL,R,LOC,Z,-0.005-0.0001,-0.005+0.0001	
F,ALL,FX,-1	
ALLSEL	
/SOLU	!Enter Solution
ANTYPE,STATIC	!Type of Analysis
PSTRES,ON	!Include Prestress Effect Calculations
SOLVE	!Solve
FINISH	!Finish First Solution
/SOLU	!Enter Solution
ANTYPE,BUCKLE	!Change Type of Analysis
BUCOPT,LANB,1	!Apply Bucking Analysis Options
SOLVE	!Solve
FINISH	!Finish Second Solution
/SOLU	!Enter Solution
EXPASS,ON	!Perform Expansion Pass
MXPAND,1	!Specify Number of Modes to Expand
SOLVE	!Solve
FINISH	!Finish Third Solve
/POST1	!Enter Post-Processor
SET,LIST	!List Eigenvalue Solution – Buckling Strength
SET,LAST	!Read Data for Desired Mode

PLDISP,2	!Plot Deflected Shape vs Original

Code B.6 Intact 3-D Plate Eigenvalue Buckling Code with a Very Fine Mesh

Code	Comment
/TITLE,Very Fine Mesh	!Title
/UNITS,SI	!Determine Units
/PREP7	!Preprocessor
ET,1,SOLID186	!Element Type
MP,EX,1,2.058E11	!Define Material Data
MP,PRXY,1,0.3	
BLOCK,0,0.8,0,0.8,0,-0.01	!Create Geometry
LSEL,S,LINE,,1,,,0	!Define Outer Line Divisions
LSEL,A,LINE,,2,,,0	
LSEL,A,LINE,,3,,,0	
LSEL,A,LINE,,4,,,0	
LSEL,A,LINE,,5,,,0	
LSEL,A,LINE,,6,,,0	
LSEL,A,LINE,,7,,,0	
LSEL,A,LINE,,8,,,0	
LESIZE,ALL,,,40,,,,1	
ALLSEL	
LSEL,S,LINE,,9,,,0	!Define Short Internal Line Divisions
LSEL,A,LINE,,10,,,0	
LSEL,A,LINE,,11,,,0	
LSEL,A,LINE,,12,,,0	
LESIZE,ALL,,,4,,,,1	
ALLSEL	
MSHKEY,1	!Apply Mapping Meshing
VMESH,ALL	
/SOLU	!Enter Solution
ANTYPE,STATIC	!Type of Analysis
NLGEOM,ON	!Turn on Non-Linear Geometry
OUTRES,ALL,ALL	!Control Data Written to Database
NSUBST,10,10,10	!Determine Number of Sub-Steps
AUTOTS,ON	!Turn on Automatic Time Stepping
LNSRCH,ON	!Activate Line Search
NEQIT,1000	!Specify Max Number of Equilibrium Iterations
NSEL,S,LOC,X,0-0.0001,0+0.0001	!Define Boundary Conditions
NSEL,R,LOC,Y,0-0.0001,0.8+0.0001	
NSEL,R,LOC,Z,-0.01-0.0001,0+0.0001	
D,ALL,UX,0	
D,ALL,UY,0	
D,ALL,UZ,0	
ALLSEL	
NSEL,S,LOC,X,0.8-0.0001,0.8+0.0001	!Couple Nodes
NSEL,R,LOC,Z,-0.005-0.0001,-0.005+0.0001	
CP,NEXT,UX,ALL	
ALLSEL	
NSEL,S,LOC,X,0.8-0.0001,0.8+0.0001	!Apply Approx 110% of Predicted Load in x Direction
NSEL,R,LOC,Y,0.4-0.0001,0.4+0.0001	
NSEL,R,LOC,Z,-0.005-0.0001,-0.005+0.0001	
F,ALL,FX,-61550	
ALLSEL	
NSEL,S,LOC,X,0.8-0.0001,0.8+0.0001	!Apply 0.5% Load in z Direction to Initiate Buckling
NSEL,R,LOC,Y,0.4-0.0001,0.4+0.0001	
NSEL,R,LOC,Z,-0.005-0.0001,-0.005+0.0001	
F,ALL,FZ,308	
ALLSEL	
SOLVE	!Solve

Code B.7 Intact 3-D Plate Non-Linear Buckling Code with a Very Fine Mesh

Code	Comment
/TITLE,Very Fine Mesh	!Title
/UNITS,SI	!Determine Units
/PREP7	!Preprocessor
ET,1,SOLID186	!Element Type
MP,EX,1,2.058E11	!Define Material Data
MP,PRXY,1,0.3	
K,1,0,0,0	!Create Keypoints for Geometry
K,2,0.8,0,0	
K,3,0.8,0.8,0	
K,4,0,0.8,0	
K,5,0.4,0.4,0	
L,1,2	!Create Lines
L,2,3	
L,3,4	
L,4,1	
L,1,5	
L,2,5	
L,3,5	
L,4,5	
AL,1,5,6	!Create Triangular Areas
AL,2,6,7	
AL,3,7,8	
AL,4,5,8	
CM,GROUP1,AREA	!Group Areas
CYL4,0.4,0.4,0.1	!Create Circle
ASBA,GROUP1,5	!Generate the Hole
LCOMB,15,16,0	!Merge Lines on Hole
LCOMB,18,19,0	
LCOMB,21,22,0	
LCOMB,23,24,0	
VEXT,ALL,,,0,0,-0.01	!Extrude to Create Volume
LSEL,S,LINE,,1,,,0	!Define Outer Line Divisions
LSEL,A,LINE,,2,,,0	
LSEL,A,LINE,,3,,,0	
LSEL,A,LINE,,4,,,0	
LSEL,A,LINE,,5,,,0	
LSEL,A,LINE,,16,,,0	
LSEL,A,LINE,,26,,,0	
LSEL,A,LINE,,31,,,0	
LESIZE,ALL,,,40,,,,,1	
ALLSEL	
LSEL,S,LINE,,9,,,0	!Define Short Internal Line Divisions
LSEL,A,LINE,,10,,,0	
LSEL,A,LINE,,11,,,0	
LSEL,A,LINE,,12,,,0	
LSEL,A,LINE,,24,,,0	
LSEL,A,LINE,,25,,,0	
LSEL,A,LINE,,29,,,0	
LSEL,A,LINE,,30,,,0	
LESIZE,ALL,,,4,,,,,1	
ALLSEL	
LSEL,S,LINE,,6,,,0	!Define Inner Line Divisions and Spacing
LSEL,A,LINE,,8,,,0	
LSEL,A,LINE,,13,,,0	
LSEL,A,LINE,,14,,,0	
LSEL,A,LINE,,17,,,0	
LSEL,A,LINE,,19,,,0	
LSEL,A,LINE,,20,,,0	
LSEL,A,LINE,,27,,,0	

LESIZE,ALL,,,50,1/8,,,,,1	
ALLSEL	
LSEL,S,LINE,,7,,,0	!Define Circle Divisions
LSEL,A,LINE,,15,,,0	
LSEL,A,LINE,,18,,,0	
LSEL,A,LINE,,21,,,0	
LSEL,A,LINE,,22,,,0	
LSEL,A,LINE,,23,,,0	
LSEL,A,LINE,,28,,,0	
LSEL,A,LINE,,32,,,0	
LESIZE,ALL,,,20,,,,,1	
ALLSEL	
MSHKEY,1	!Apply Mapping Meshing
VMESH,ALL	
NSEL,S,LOC,X,0-0.0001,0+0.0001	!Define Boundary Conditions
NSEL,R,LOC,Y,0-0.0001,0.8+0.0001	
NSEL,R,LOC,Z,-0.01-0.0001,0+0.0001	
D,ALL,UX,0	
D,ALL,UY,0	
D,ALL,UZ,0	
ALLSEL	
NSEL,S,LOC,X,0.8-0.0001,0.8+0.0001	!Couple Nodes
NSEL,R,LOC,Z,-0.005-0.0001,-0.005+0.0001	
CP,NEXT,UX,ALL	
ALLSEL	
NSEL,S,LOC,X,0.8-0.0001,0.8+0.0001	!Apply Load in x Direction
NSEL,R,LOC,Y,0.4-0.0001,0.4+0.0001	
NSEL,R,LOC,Z,-0.005-0.0001,-0.005+0.0001	
F,ALL,FX,-1	
ALLSEL	
/SOLU	!Enter Solution
ANTYPE,STATIC	!Type of Analysis
PSTRES,ON	!Include Prestress Effect Calculations
SOLVE	!Solve
FINISH	!Finish First Solution
/SOLU	!Enter Solution
ANTYPE,BUCKLE	!Change Type of Analysis
BUCOPT,LANB,1	!Apply Bucking Analysis Options
SOLVE	!Solve
FINISH	!Finish Second Solution
/SOLU	!Enter Solution
EXPASS,ON	!Perform Expansion Pass
MXPAND,1	!Specify Number of Modes to Expand
SOLVE	!Solve
FINISH	!Finish Third Solve
/POST1	!Enter Post-Processor
SET,LIST	!List Eigenvalue Solution – Buckling Strength
SET,LAST	!Read Data for Desired Mode
PLDISP,2	!Plot Deflected Shape vs Original

Code B.8 3-D Plate with a Hole Eigenvalue Buckling Code with a Very Fine Mesh

/TITLE,Very Fine Mesh	!Title
/UNITS,SI	!Determine Units
/PREP7	!Preprocessor
ET,1,SOLID186	!Element Type
MP,EX,1,2.058E11	!Define Material Data
MP,PRXY,1,0.3	
K,1,0,0,0	!Create Keypoints for Geometry
K,2,0.8,0,0	
K,3,0.8,0.8,0	
K,4,0,0.8,0	
K,5,0.4,0.4,0	
L,1,2	!Create Lines
L,2,3	
L,3,4	
L,4,1	
L,1,5	
L,2,5	
L,3,5	
L,4,5	
AL,1,5,6	!Create Triangular Areas
AL,2,6,7	
AL,3,7,8	
AL,4,5,8	
CM,GROUP1,AREA	!Group Areas
CYL4,0.4,0.4,0.1	!Create Circle
ASBA,GROUP1,5	!Generate the Hole
LCOMB,15,16,0	!Merge Lines on Hole
LCOMB,18,19,0	
LCOMB,21,22,0	
LCOMB,23,24,0	
VEXT,ALL,,,0,0,-0.01	!Extrude to Create Volume
LSEL,S,LINE,,1,,,0	!Define Outer Line Divisions
LSEL,A,LINE,,2,,,0	
LSEL,A,LINE,,3,,,0	
LSEL,A,LINE,,4,,,0	
LSEL,A,LINE,,5,,,0	
LSEL,A,LINE,,16,,,0	
LSEL,A,LINE,,26,,,0	
LSEL,A,LINE,,31,,,0	
LESIZE,ALL,,,40,,,,,1	
ALLSEL	
LSEL,S,LINE,,9,,,0	!Define Short Internal Line Divisions
LSEL,A,LINE,,10,,,0	
LSEL,A,LINE,,11,,,0	
LSEL,A,LINE,,12,,,0	
LSEL,A,LINE,,24,,,0	
LSEL,A,LINE,,25,,,0	
LSEL,A,LINE,,29,,,0	
LSEL,A,LINE,,30,,,0	
LESIZE,ALL,,,4,,,,,1	
ALLSEL	
LSEL,S,LINE,,6,,,0	!Define Inner Line Divisions and Spacing
LSEL,A,LINE,,8,,,0	
LSEL,A,LINE,,13,,,0	
LSEL,A,LINE,,14,,,0	
LSEL,A,LINE,,17,,,0	
LSEL,A,LINE,,19,,,0	
LSEL,A,LINE,,20,,,0	
LSEL,A,LINE,,27,,,0	

LESIZE,ALL,,,50,1/8,,,,,1	
ALLSEL	
LSEL,S,LINE,,7,,,0	!Define Circle Divisions
LSEL,A,LINE,,15,,,0	
LSEL,A,LINE,,18,,,0	
LSEL,A,LINE,,21,,,0	
LSEL,A,LINE,,22,,,0	
LSEL,A,LINE,,23,,,0	
LSEL,A,LINE,,28,,,0	
LSEL,A,LINE,,32,,,0	
LESIZE,ALL,,,20,,,,,1	
ALLSEL	
MSHKEY,1	!Apply Mapping Meshing
VMESH,ALL	
/SOLU	!Enter Solution
ANTYPE,STATIC	!Type of Analysis
NLGEOM,ON	!Turn on Non-Linear Geometry
OUTRES,ALL,ALL	!Control Data Written to Database
NSUBST,10,10,10	!Determine Number of Sub-Steps
AUTOTS,ON	!Turn on Automatic Time Stepping
LNSRCH,ON	!Activate Line Search
NEQIT,1000	!Specify Max Number of Equilibrium Iterations
NSEL,S,LOC,X,0-0.0001,0+0.0001	!Define Boundary Conditions
NSEL,R,LOC,Y,0-0.0001,0.8+0.0001	
NSEL,R,LOC,Z,-0.01-0.0001,0+0.0001	
D,ALL,UX,0	
D,ALL,UY,0	
D,ALL,UZ,0	
ALLSEL	
NSEL,S,LOC,X,0.8-0.0001,0.8+0.0001	!Couple Nodes
NSEL,R,LOC,Z,-0.005-0.0001,-0.005+0.0001	
CP,NEXT,UX,ALL	
ALLSEL	
NSEL,S,LOC,X,0.8-0.0001,0.8+0.0001	!Apply Approx 110% of Predicted Load in x Direction
NSEL,R,LOC,Y,0.4-0.0001,0.4+0.0001	
NSEL,R,LOC,Z,-0.005-0.0001,-0.005+0.0001	
F,ALL,FX,-55750	
ALLSEL	
NSEL,S,LOC,X,0.8-0.0001,0.8+0.0001	!Apply 0.5% Load in z Direction to Initiate Buckling
NSEL,R,LOC,Y,0.4-0.0001,0.4+0.0001	
NSEL,R,LOC,Z,-0.005-0.0001,-0.005+0.0001	
F,ALL,FZ,279	
ALLSEL	
SOLVE	!Solve

Code B.9 3-D Plate with a Hole Non-Linear Buckling Code with a Very Fine Mesh

Table B.1 Intact Shell Plate with a Very Fine Mesh Raw Displacement Data

		Very Fine Mesh								
Max Load	61550									
Expected Buckling	55942	Displacement (m)								
		Point A (Top RHS Node)			Point B (Load Point Node)			Point C (Bottom RHS Node)		
Time	Load (N)	UX	UY	UZ	UX	UY	UZ	UX	UY	UZ
0	0	0	0	0	0	0	0	0	0	0
0.1	6155	-3.08E-06	4.64E-07	3.88E-04	-3.08E-06	-5.80E-16	4.23E-04	-3.08E-06	-4.64E-07	3.88E-04
0.2	12310	-6.56E-06	9.49E-07	8.88E-04	-6.56E-06	-3.09E-14	9.61E-04	-6.56E-06	-9.49E-07	8.88E-04
0.3	18465	-1.09E-05	1.47E-06	1.55E-03	-1.09E-05	-3.81E-13	1.67E-03	-1.09E-05	-1.47E-06	1.55E-03
0.4	24620	-1.69E-05	2.07E-06	2.48E-03	-1.69E-05	-4.13E-12	2.65E-03	-1.69E-05	-2.07E-06	2.48E-03
0.5	30775	-2.70E-05	2.82E-06	3.87E-03	-2.70E-05	-4.53E-11	4.09E-03	-2.70E-05	-2.82E-06	3.87E-03
0.6	36930	-4.84E-05	3.90E-06	6.14E-03	-4.84E-05	-2.53E-11	6.43E-03	-4.84E-05	-3.90E-06	6.14E-03
0.7	43085	-1.10E-04	5.80E-06	1.05E-02	-1.10E-04	-3.21E-10	1.09E-02	-1.10E-04	-5.80E-06	1.05E-02
0.8	49240	-4.19E-04	1.02E-05	2.24E-02	-4.19E-04	-1.58E-09	2.28E-02	-4.19E-04	-1.02E-05	2.24E-02
0.9	55395	-7.38E-03	2.88E-05	9.72E-02	-7.38E-03	-1.96E-08	9.74E-02	-7.38E-03	-2.89E-05	9.72E-02
1.0	61550	-0.11497	5.31E-05	0.36819	-0.11497	-3.56E-08	0.36833	-0.11497	-5.31E-05	0.36819

Table B.2 Intact Shell Plate with a Fine Mesh Raw Displacement Data

		Fine Mesh								
Max Load	61550									
Expected Buckling	55945	Displacement (m)								
		Point A (Top RHS Node)			Point B (Load Point Node)			Point C (Bottom RHS Node)		
Time	Load (N)	UX	UY	UZ	UX	UY	UZ	UX	UY	UZ
0	0	0	0	0	0	0	0	0	0	0
0.1	6155	-3.08E-06	4.64E-07	3.88E-04	-3.08E-06	-5.40E-16	4.23E-04	-3.08E-06	-4.64E-07	3.88E-04
0.2	12310	-6.56E-06	9.49E-07	8.88E-04	-6.56E-06	-3.04E-14	9.61E-04	-6.56E-06	-9.49E-07	8.88E-04
0.3	18465	-1.09E-05	1.47E-06	1.55E-03	-1.09E-05	-3.78E-13	1.67E-03	-1.09E-05	-1.47E-06	1.55E-03
0.4	24620	-1.69E-05	2.07E-06	2.48E-03	-1.69E-05	-4.11E-12	2.65E-03	-1.69E-05	-2.07E-06	2.48E-03
0.5	30775	-2.70E-05	2.82E-06	3.87E-03	-2.70E-05	-4.53E-11	4.09E-03	-2.70E-05	-2.82E-06	3.87E-03
0.6	36930	-4.83E-05	3.90E-06	6.14E-03	-4.83E-05	-2.52E-11	6.43E-03	-4.83E-05	-3.90E-06	6.14E-03
0.7	43085	-1.10E-04	5.80E-06	1.05E-02	-1.10E-04	-3.18E-10	1.09E-02	-1.10E-04	-5.80E-06	1.05E-02
0.8	49240	-4.17E-04	1.02E-05	2.23E-02	-4.17E-04	-1.51E-09	2.27E-02	-4.17E-04	-1.02E-05	2.23E-02
0.9	55395	-7.31E-03	2.88E-05	9.67E-02	-7.31E-03	-1.91E-08	9.70E-02	-7.31E-03	-2.88E-05	9.67E-02
1.0	61550	-0.11460	5.30E-05	0.36768	-0.11460	-6.76E-08	0.36781	-0.11460	-5.32E-05	0.36768

Table B.3 Intact Shell Plate with a Coarse Mesh Raw Displacement Data

		Coarse Mesh								
Max Load	61550									
Expected Buckling	55953	Displacement (m)								
		Point A (Top RHS Node)			Point B (Load Point Node)			Point C (Bottom RHS Node)		
Time	Load (N)	UX	UY	UZ	UX	UY	UZ	UX	UY	UZ
0	0	0	0	0	0	0	0	0	0	0
0.1	6155	-3.08E-06	4.64E-07	3.88E-04	-3.08E-06	-5.27E-16	4.23E-04	-3.08E-06	-4.64E-07	3.88E-04
0.2	12310	-6.56E-06	9.50E-07	8.87E-04	-6.56E-06	-2.94E-14	9.60E-04	-6.56E-06	-9.50E-07	8.87E-04
0.3	18465	-1.09E-05	1.47E-06	1.55E-03	-1.09E-05	-3.72E-13	1.67E-03	-1.09E-05	-1.47E-06	1.55E-03
0.4	24620	-1.69E-05	2.07E-06	2.48E-03	-1.69E-05	-4.08E-12	2.65E-03	-1.69E-05	-2.07E-06	2.48E-03
0.5	30775	-2.70E-05	2.82E-06	3.86E-03	-2.70E-05	-4.51E-11	4.08E-03	-2.70E-05	-2.82E-06	3.86E-03
0.6	36930	-4.82E-05	3.90E-06	6.13E-03	-4.82E-05	-2.50E-11	6.42E-03	-4.82E-05	-3.90E-06	6.13E-03
0.7	43085	-1.09E-04	5.80E-06	1.05E-02	-1.09E-04	-3.08E-10	1.09E-02	-1.09E-04	-5.80E-06	1.05E-02
0.8	49240	-4.13E-04	1.02E-05	2.22E-02	-4.13E-04	-1.36E-09	2.26E-02	-4.13E-04	-1.02E-05	2.22E-02
0.9	55395	-7.15E-03	2.87E-05	9.56E-02	-7.15E-03	-5.81E-09	9.59E-02	-7.15E-03	-2.87E-05	9.56E-02
1.0	61550	-0.11375	5.30E-05	0.36649	-0.11375	-4.49E-08	0.36663	-0.11375	-5.31E-05	0.36649

Table B.4 Intact Shell Plate with a Very Coarse Mesh Raw Displacement Data

		Very Coarse Mesh								
Max Load	61550									
Expected Buckling	55984	Displacement (m)								
		Point A (Top RHS Node)			Point B (Load Point Node)			Point C (Bottom RHS Node)		
Time	Load (N)	UX	UY	UZ	UX	UY	UZ	UX	UY	UZ
0	0	0	0	0	0	0	0	0	0	0
0.1	6155	-3.08E-06	4.64E-07	3.87E-04	-3.08E-06	-3.92E-16	4.22E-04	-3.08E-06	-4.64E-07	3.87E-04
0.2	12310	-6.56E-06	9.50E-07	8.84E-04	-6.56E-06	-2.54E-14	9.58E-04	-6.56E-06	-9.50E-07	8.84E-04
0.3	18465	-1.08E-05	1.48E-06	1.55E-03	-1.08E-05	-3.47E-13	1.66E-03	-1.08E-05	-1.48E-06	1.55E-03
0.4	24620	-1.68E-05	2.07E-06	2.47E-03	-1.68E-05	-3.93E-12	2.63E-03	-1.68E-05	-2.07E-06	2.47E-03
0.5	30775	-2.68E-05	2.82E-06	3.84E-03	-2.68E-05	-4.39E-11	4.06E-03	-2.68E-05	-2.82E-06	3.84E-03
0.6	36930	-4.77E-05	3.90E-06	6.08E-03	-4.77E-05	-2.37E-11	6.37E-03	-4.77E-05	-3.90E-06	6.08E-03
0.7	43085	-1.06E-04	5.78E-06	1.03E-02	-1.06E-04	-1.09E-09	1.07E-02	-1.06E-04	-5.78E-06	1.03E-02
0.8	49240	-3.94E-04	1.01E-05	2.17E-02	-3.94E-04	-9.09E-10	2.20E-02	-3.94E-04	-1.01E-05	2.17E-02
0.9	55395	-6.26E-03	2.80E-05	8.95E-02	-6.26E-03	-2.50E-09	8.98E-02	-6.26E-03	-2.80E-05	8.95E-02
1.0	61550	-0.10920	5.32E-05	0.36006	-0.10920	-2.26E-08	0.36020	-0.10920	-5.33E-05	0.36006

Table B.5 Plate with a Hole Shell with a Very Fine Mesh Raw Displacement Data

		Very Fine Mesh								
Max Load	55750									
Expected Buckling	50667	Displacement (m)								
		Point A (Top RH Node)			Point B (Load Point Node)			Point C (Bottom RHS Node)		
Time	Load (N)	UX	UY	UZ	UX	UY	UZ	UX	UY	UZ
0	0	0	0	0	0	0	0	0	0	0
0.1	5575	-3.22E-06	3.80E-07	3.80E-04	-3.22E-06	-2.25E-14	4.11E-04	-3.22E-06	-3.80E-07	3.80E-04
0.2	11150	-6.83E-06	7.79E-07	8.69E-04	-6.83E-06	-8.05E-13	9.34E-04	-6.83E-06	-7.79E-07	8.69E-04
0.3	16725	-1.12E-05	1.21E-06	1.52E-03	-1.12E-05	-6.01E-12	1.62E-03	-1.12E-05	-1.21E-06	1.52E-03
0.4	22300	-1.73E-05	1.70E-06	2.43E-03	-1.73E-05	-4.23E-11	2.57E-03	-1.73E-05	-1.70E-06	2.43E-03
0.5	27875	-2.73E-05	2.30E-06	3.79E-03	-2.73E-05	-5.03E-12	3.97E-03	-2.73E-05	-2.30E-06	3.79E-03
0.6	33450	-4.82E-05	3.13E-06	6.02E-03	-4.82E-05	-1.17E-10	6.25E-03	-4.82E-05	-3.13E-06	6.02E-03
0.7	39025	-1.09E-04	4.51E-06	1.04E-02	-1.09E-04	-1.22E-09	1.06E-02	-1.09E-04	-4.51E-06	1.04E-02
0.8	44600	-4.27E-04	7.27E-06	2.24E-02	-4.27E-04	-4.02E-09	2.26E-02	-4.27E-04	-7.28E-06	2.24E-02
0.9	50175	-9.81E-03	1.77E-05	0.11060	-9.81E-03	6.14E-09	0.11073	-9.81E-03	-1.77E-05	0.11060
1.0	55750	-0.10624	3.90E-05	0.35056	-0.10624	1.99E-07	0.35069	-0.10624	-3.86E-05	0.35056

Table B.6 Plate with a Hole Shell with a Fine Mesh Raw Displacement Data

		Fine Mesh								
Max Load	55750									
Expected Buckling	50667	Displacement (m)								
		Point A (Top RHS Node)			Point B (Load Point Node)			Point C (Bottom RHS Node)		
Time	Load (N)	UX	UY	UZ	UX	UY	UZ	UX	UY	UZ
0	0	0	0	0	0	0	0	0	0	0
0.1	5575	-3.22E-06	3.80E-07	3.80E-04	-3.22E-06	-2.36E-14	4.11E-04	-3.22E-06	-3.80E-07	3.80E-04
0.2	11150	-6.83E-06	7.79E-07	8.69E-04	-6.83E-06	-7.92E-13	9.34E-04	-6.83E-06	-7.79E-07	8.69E-04
0.3	16725	-1.12E-05	1.21E-06	1.52E-03	-1.12E-05	-5.93E-12	1.62E-03	-1.12E-05	-1.21E-06	1.52E-03
0.4	22300	-1.73E-05	1.70E-06	2.43E-03	-1.73E-05	-4.17E-11	2.57E-03	-1.73E-05	-1.70E-06	2.43E-03
0.5	27875	-2.73E-05	2.30E-06	3.78E-03	-2.73E-05	-4.95E-12	3.97E-03	-2.73E-05	-2.30E-06	3.78E-03
0.6	33450	-4.82E-05	3.13E-06	6.01E-03	-4.82E-05	-1.15E-10	6.24E-03	-4.82E-05	-3.13E-06	6.01E-03
0.7	39025	-1.09E-04	4.51E-06	1.04E-02	-1.09E-04	-1.19E-09	1.06E-02	-1.09E-04	-4.51E-06	1.04E-02
0.8	44600	-4.26E-04	7.25E-06	2.24E-02	-4.26E-04	-3.90E-09	2.26E-02	-4.26E-04	-7.26E-06	2.24E-02
0.9	50175	-9.78E-03	1.76E-05	0.11040	-9.78E-03	3.53E-09	0.11053	-9.78E-03	-1.76E-05	0.11040
1.0	55750	-0.10615	3.84E-05	0.35043	-0.10615	8.27E-08	0.35057	-0.10615	-3.82E-05	0.35043

Table B.7 Plate with a Hole Shell with a Coarse Mesh Raw Displacement Data

		Coarse Mesh								
Max Load	55750									
Expected Buckling	50703	Displacement (m)								
		Point A (Top RHS Node)			Point B (Load Point Node)			Point C (Bottom RHS Node)		
Time	Load (N)	UX	UY	UZ	UX	UY	UZ	UX	UY	UZ
0	0	0	0	0	0	0	0	0	0	0
0.1	5575	-3.22E-06	3.80E-07	3.80E-04	-3.22E-06	-2.35E-14	4.11E-04	-3.22E-06	-3.80E-07	3.80E-04
0.2	11150	-6.83E-06	7.78E-07	8.68E-04	-6.83E-06	-7.90E-13	9.33E-04	-6.83E-06	-7.78E-07	8.68E-04
0.3	16725	-1.12E-05	1.21E-06	1.52E-03	-1.12E-05	-5.91E-12	1.62E-03	-1.12E-05	-1.21E-06	1.52E-03
0.4	22300	-1.73E-05	1.70E-06	2.43E-03	-1.73E-05	-4.15E-11	2.57E-03	-1.73E-05	-1.70E-06	2.43E-03
0.5	27875	-2.73E-05	2.29E-06	3.78E-03	-2.73E-05	-4.88E-12	3.96E-03	-2.73E-05	-2.29E-06	3.78E-03
0.6	33450	-4.81E-05	3.12E-06	6.01E-03	-4.81E-05	-1.14E-10	6.23E-03	-4.81E-05	-3.12E-06	6.01E-03
0.7	39025	-1.08E-04	4.49E-06	1.03E-02	-1.08E-04	-1.16E-09	1.06E-02	-1.08E-04	-4.49E-06	1.03E-02
0.8	44600	-4.23E-04	7.20E-06	2.23E-02	-4.23E-04	-3.72E-09	2.25E-02	-4.23E-04	-7.21E-06	2.23E-02
0.9	50175	-9.64E-03	1.73E-05	0.10966	-9.64E-03	6.13E-09	0.10979	-9.64E-03	-1.73E-05	0.10966
1.0	55750	-0.10588	3.73E-05	0.35006	-0.10588	9.22E-08	0.35019	-0.10588	-3.71E-05	0.35006

Table B.8 Plate with a Hole Shell with a Very Coarse Mesh Raw Displacement Data

		Very Coarse Mesh								
Max Load	55750									
Expected Buckling	50831	Displacement (m)								
		Point A (Top RHS Node)			Point B (Load Point Node)			Point C (Bottom RHS Node)		
Time	Load (N)	UX	UY	UZ	UX	UY	UZ	UX	UY	UZ
0	0	0	0	0	0	0	0	0	0	0
0.1	5575	-3.22E-06	3.79E-07	3.79E-04	-3.22E-06	-2.22E-14	4.10E-04	-3.22E-06	-3.79E-07	3.79E-04
0.2	11150	-6.82E-06	7.76E-07	8.67E-04	-6.82E-06	-7.41E-13	9.30E-04	-6.82E-06	-7.76E-07	8.67E-04
0.3	16725	-1.12E-05	1.20E-06	1.52E-03	-1.12E-05	-5.52E-12	1.61E-03	-1.12E-05	-1.20E-06	1.52E-03
0.4	22300	-1.72E-05	1.69E-06	2.42E-03	-1.72E-05	-3.86E-11	2.56E-03	-1.72E-05	-1.69E-06	2.42E-03
0.5	27875	-2.71E-05	2.28E-06	3.76E-03	-2.71E-05	-2.81E-10	3.94E-03	-2.71E-05	-2.28E-06	3.76E-03
0.6	33450	-4.77E-05	3.09E-06	5.97E-03	-4.77E-05	-1.03E-10	6.19E-03	-4.77E-05	-3.09E-06	5.97E-03
0.7	39025	-1.07E-04	4.41E-06	1.02E-02	-1.07E-04	-9.76E-10	1.05E-02	-1.07E-04	-4.41E-06	1.02E-02
0.8	44600	-4.09E-04	6.94E-06	2.19E-02	-4.09E-04	-2.76E-09	2.21E-02	-4.09E-04	-6.95E-06	2.19E-02
0.9	50175	-9.07E-03	1.60E-05	0.10640	-9.07E-03	4.93E-09	0.10653	-9.07E-03	-1.60E-05	0.10640
1.0	55750	-0.10304	3.31E-05	0.34590	-0.10304	1.75E-08	0.34602	-0.10304	-3.31E-05	0.34590

Table B.9 Intact Solid Plate with a Very Fine Mesh Raw Displacement Data

		Very Fine Mesh								
Max Load	61550									
Expected Buckling	55942	Displacement (m)								
		Point A (Top RHS Centre Node)			Point B (Load Point Centre Node)			Point C (Bottom RHS Centre Node)		
Time	Load (N)	UX	UY	UZ	UX	UY	UZ	UX	UY	UZ
0	0	0	0	0	0	0	0	0	0	0
0.1	6155	-3.12E-06	4.72E-07	3.88E-04	-3.12E-06	2.68E-17	4.23E-04	-3.12E-06	-4.72E-07	3.88E-04
0.2	12310	-6.65E-06	9.65E-07	8.87E-04	-6.65E-06	8.08E-17	9.61E-04	-6.65E-06	-9.65E-07	8.87E-04
0.3	18465	-1.10E-05	1.50E-06	1.55E-03	-1.10E-05	-1.69E-15	1.67E-03	-1.10E-05	-1.50E-06	1.55E-03
0.4	24620	-1.71E-05	2.10E-06	2.48E-03	-1.71E-05	-5.86E-17	2.65E-03	-1.71E-05	-2.10E-06	2.48E-03
0.5	30775	-2.72E-05	2.85E-06	3.87E-03	-2.72E-05	7.50E-16	4.09E-03	-2.72E-05	-2.85E-06	3.87E-03
0.6	36930	-4.85E-05	3.92E-06	6.13E-03	-4.85E-05	6.83E-15	6.42E-03	-4.85E-05	-3.92E-06	6.13E-03
0.7	43085	-1.10E-04	5.81E-06	1.05E-02	-1.10E-04	-5.89E-15	1.09E-02	-1.10E-04	-5.81E-06	1.05E-02
0.8	49240	-2.06E-04	7.97E-06	1.51E-02	-2.06E-04	-2.18E-15	1.55E-02	-2.06E-04	-7.97E-06	1.51E-02
0.9	55395	-7.00E-03	2.83E-05	9.46E-02	-7.00E-03	5.30E-14	9.48E-02	-7.00E-03	-2.83E-05	9.46E-02
1.0	61550	-9.74E-02	5.25E-05	0.34201	-9.74E-02	-7.08E-13	0.34215	-9.74E-02	-5.25E-05	0.34201

Table B.10 Intact Solid Plate with a Fine Mesh Raw Displacement Data

		Fine Mesh								
Max Load	61550									
Expected Buckling	55945			Displacement (m)						
		Point A (Top RHS Centre Node)			Point B (Load Point Centre Node)			Point C (Bottom RHS Centre Node)		
Time	Load (N)	UX	UY	UZ	UX	UY	UZ	UX	UY	UZ
0	0	0	0	0	0	0	0	0	0	0
0.1	6155	-3.12E-06	4.70E-07	3.88E-04	-3.12E-06	4.08E-17	4.23E-04	-3.12E-06	-4.70E-07	3.88E-04
0.2	12310	-6.65E-06	9.62E-07	8.87E-04	-6.65E-06	3.41E-16	9.61E-04	-6.65E-06	-9.62E-07	8.87E-04
0.3	18465	-1.10E-05	1.49E-06	1.55E-03	-1.10E-05	1.35E-15	1.67E-03	-1.10E-05	-1.49E-06	1.55E-03
0.4	24620	-1.71E-05	2.09E-06	2.48E-03	-1.71E-05	-7.79E-17	2.65E-03	-1.71E-05	-2.09E-06	2.48E-03
0.5	30775	-2.72E-05	2.84E-06	3.87E-03	-2.72E-05	-7.55E-17	4.09E-03	-2.72E-05	-2.84E-06	3.87E-03
0.6	36930	-4.85E-05	3.91E-06	6.13E-03	-4.85E-05	5.77E-15	6.42E-03	-4.85E-05	-3.91E-06	6.13E-03
0.7	43085	-1.10E-04	5.79E-06	1.05E-02	-1.10E-04	2.62E-16	1.09E-02	-1.10E-04	-5.79E-06	1.05E-02
0.8	49240	-2.06E-04	7.94E-06	1.51E-02	-2.06E-04	2.82E-15	1.55E-02	-2.06E-04	-7.94E-06	1.51E-02
0.9	55395	-6.97E-03	2.82E-05	9.44E-02	-6.97E-03	1.37E-14	9.47E-02	-6.97E-03	-2.82E-05	9.44E-02
1.0	61550	-9.76E-02	5.24E-05	0.34233	-9.76E-02	1.77E-14	0.34248	-9.76E-02	-5.24E-05	0.34233

Table B.11 Intact Solid Plate with a Coarse Mesh Raw Displacement Data

		Coarse Mesh								
Max Load	61550									
Expected Buckling	55953			Displacement (m)						
		Point A (Top RHS Centre Node)			Point B (Load Point Centre Node)			Point C (Bottom RHS Centre Node)		
Time	Load (N)	UX	UY	UZ	UX	UY	UZ	UX	UY	UZ
0	0	0	0	0	0	0	0	0	0	0
0.1	6155	-3.12E-06	4.69E-07	3.88E-04	-3.12E-06	1.04E-16	4.23E-04	-3.12E-06	-4.69E-07	3.88E-04
0.2	12310	-6.64E-06	9.58E-07	8.87E-04	-6.64E-06	-3.37E-16	9.61E-04	-6.64E-06	-9.58E-07	8.87E-04
0.3	18465	-1.10E-05	1.49E-06	1.55E-03	-1.10E-05	1.11E-15	1.67E-03	-1.10E-05	-1.49E-06	1.55E-03
0.4	24620	-1.71E-05	2.09E-06	2.48E-03	-1.71E-05	3.94E-17	2.65E-03	-1.71E-05	-2.09E-06	2.48E-03
0.5	30775	-2.72E-05	2.83E-06	3.86E-03	-2.72E-05	8.86E-17	4.09E-03	-2.72E-05	-2.83E-06	3.86E-03
0.6	36930	-4.85E-05	3.89E-06	6.13E-03	-4.85E-05	3.37E-15	6.42E-03	-4.85E-05	-3.89E-06	6.13E-03
0.7	43085	-1.10E-04	5.77E-06	1.05E-02	-1.10E-04	-6.69E-15	1.09E-02	-1.10E-04	-5.77E-06	1.05E-02
0.8	49240	-4.16E-04	1.01E-05	2.23E-02	-4.16E-04	1.08E-14	2.27E-02	-4.16E-04	-1.01E-05	2.23E-02
0.9	55395	-6.98E-03	2.82E-05	9.45E-02	-6.98E-03	-5.35E-14	9.48E-02	-6.98E-03	-2.82E-05	9.45E-02
1.0	61550	-9.75E-02	5.22E-05	0.34214	-9.75E-02	2.06E-13	0.34228	-9.75E-02	-5.22E-05	0.34214

Table B.12 Intact Solid Plate with a Very Coarse Mesh Raw Displacement Data

		Very Coarse Mesh								
Max Load	61550									
Expected Buckling	55984			Displacement (m)						
		Point A (Top RHS Centre Node)			Point B (Load Point Centre Node)			Point C (Bottom RHS Centre Node)		
Time	Load (N)	UX	UY	UZ	UX	UY	UZ	UX	UY	UZ
0	0	0	0	0	0	0	0	0	0	0
0.1	6155	-3.12E-06	4.67E-07	3.87E-04	-3.12E-06	1.97E-17	4.23E-04	-3.12E-06	-4.67E-07	3.87E-04
0.2	12310	-6.64E-06	9.54E-07	8.86E-04	-6.64E-06	-1.06E-15	9.60E-04	-6.64E-06	-9.54E-07	8.86E-04
0.3	18465	-1.10E-05	1.48E-06	1.55E-03	-1.10E-05	9.70E-16	1.67E-03	-1.10E-05	-1.48E-06	1.55E-03
0.4	24620	-1.70E-05	2.08E-06	2.48E-03	-1.70E-05	-7.54E-17	2.64E-03	-1.70E-05	-2.08E-06	2.48E-03
0.5	30775	-2.72E-05	2.82E-06	3.86E-03	-2.72E-05	-1.03E-16	4.08E-03	-2.72E-05	-2.82E-06	3.86E-03
0.6	36930	-4.84E-05	3.88E-06	6.12E-03	-4.84E-05	1.17E-16	6.41E-03	-4.84E-05	-3.88E-06	6.12E-03
0.7	43085	-1.09E-04	5.76E-06	1.05E-02	-1.09E-04	1.64E-14	1.09E-02	-1.09E-04	-5.76E-06	1.05E-02
0.8	49240	-2.04E-04	7.90E-06	1.51E-02	-2.04E-04	2.79E-14	1.55E-02	-2.04E-04	-7.90E-06	1.51E-02
0.9	55395	-6.68E-03	2.79E-05	9.24E-02	-6.68E-03	1.21E-13	9.27E-02	-6.68E-03	-2.79E-05	9.24E-02
1.0	61550	-9.63E-02	5.15E-05	0.34011	-9.63E-02	8.89E-13	0.34025	-9.63E-02	-5.15E-05	0.34011

Table B.13 Solid Plate with a Hole with a Very Fine Mesh Raw Displacement Data

		Very Fine Mesh								
Max Load	55750									
Expected Buckling	50669	Displacement (m)								
		Point A (Top RHS Centre Node)			Point B (Load Point Centre Node)			Point C (Bottom RHS Centre Node)		
Time	Load (N)	UX	UY	UZ	UX	UY	UZ	UX	UY	UZ
0	0	0	0	0	0	0	0	0	0	0
0.1	5575	-3.26E-06	3.86E-07	3.81E-04	-3.26E-06	2.63E-17	4.13E-04	-3.26E-06	-3.86E-07	3.81E-04
0.2	11150	-6.92E-06	7.90E-07	8.72E-04	-6.92E-06	2.51E-17	9.37E-04	-6.92E-06	-7.90E-07	8.72E-04
0.3	16725	-1.14E-05	1.23E-06	1.52E-03	-1.14E-05	-2.15E-16	1.63E-03	-1.14E-05	-1.23E-06	1.52E-03
0.4	22300	-1.75E-05	1.72E-06	2.44E-03	-1.75E-05	2.35E-17	2.58E-03	-1.75E-05	-1.72E-06	2.44E-03
0.5	27875	-2.76E-05	2.32E-06	3.80E-03	-2.76E-05	2.30E-16	3.98E-03	-2.76E-05	-2.32E-06	3.80E-03
0.6	33450	-4.86E-05	3.16E-06	6.03E-03	-4.86E-05	-3.33E-15	6.26E-03	-4.86E-05	-3.16E-06	6.03E-03
0.7	39025	-1.10E-04	4.54E-06	1.04E-02	-1.10E-04	-1.80E-15	1.07E-02	-1.10E-04	-4.54E-06	1.04E-02
0.8	44600	-2.05E-04	6.03E-06	1.49E-02	-2.05E-04	2.62E-15	1.52E-02	-2.05E-04	-6.03E-06	1.49E-02
0.9	50175	-9.10E-03	1.73E-05	0.10655	-9.10E-03	-2.42E-14	0.10668	-9.10E-03	-1.73E-05	0.10655
1.0	55750	-9.23E-02	3.65E-05	0.32922	-9.23E-02	-6.70E-13	0.32935	-9.23E-02	-3.65E-05	0.32922

Table B.14 Solid Plate with a Hole with a Fine Mesh Raw Displacement Data

		Fine Mesh								
Max Load	55750									
Expected Buckling	50672	Displacement (m)								
		Point A (Top RHS Centre Node)			Point B (Load Point Centre Node)			Point C (Bottom RHS Centre Node)		
Time	Load (N)	UX	UY	UZ	UX	UY	UZ	UX	UY	UZ
0	0	0	0	0	0	0	0	0	0	0
0.1	5575	-3.26E-06	3.85E-07	3.81E-04	-3.26E-06	1.94E-17	4.13E-04	-3.26E-06	-3.85E-07	3.81E-04
0.2	11150	-6.92E-06	7.89E-07	8.72E-04	-6.92E-06	-1.12E-16	9.37E-04	-6.92E-06	-7.89E-07	8.72E-04
0.3	16725	-1.14E-05	1.22E-06	1.52E-03	-1.14E-05	1.91E-16	1.63E-03	-1.14E-05	-1.22E-06	1.52E-03
0.4	22300	-1.75E-05	1.72E-06	2.44E-03	-1.75E-05	-1.20E-17	2.58E-03	-1.75E-05	-1.72E-06	2.44E-03
0.5	27875	-2.76E-05	2.32E-06	3.80E-03	-2.76E-05	4.18E-17	3.98E-03	-2.76E-05	-2.32E-06	3.80E-03
0.6	33450	-4.86E-05	3.16E-06	6.02E-03	-4.86E-05	-1.14E-14	6.26E-03	-4.86E-05	-3.16E-06	6.02E-03
0.7	39025	-1.10E-04	4.54E-06	1.04E-02	-1.10E-04	9.26E-15	1.07E-02	-1.10E-04	-4.54E-06	1.04E-02
0.8	44600	-2.04E-04	6.02E-06	1.49E-02	-2.04E-04	2.62E-14	1.52E-02	-2.04E-04	-6.02E-06	1.49E-02
0.9	50175	-9.05E-03	1.72E-05	0.10623	-9.05E-03	1.75E-14	0.10637	-9.05E-03	-1.72E-05	0.10623
1.0	55750	-9.23E-02	3.63E-05	0.32924	-9.23E-02	2.00E-13	0.32937	-9.23E-02	-3.63E-05	0.32924

Table B.15 Solid Plate with a Hole with a Coarse Mesh Raw Displacement Data

		Coarse Mesh								
Max Load	55750									
Expected Buckling	50677	Displacement (m)								
		Point A (Top RHS Centre Node)			Point B (Load Point Centre Node)			Point C (Bottom RHS Centre Node)		
Time	Load (N)	UX	UY	UZ	UX	UY	UZ	UX	UY	UZ
0	0	0	0	0	0	0	0	0	0	0
0.1	5575	-3.26E-06	3.85E-07	3.81E-04	-3.26E-06	7.68E-18	4.13E-04	-3.26E-06	-3.85E-07	3.81E-04
0.2	11150	-6.92E-06	7.89E-07	8.71E-04	-6.92E-06	2.01E-16	9.37E-04	-6.92E-06	-7.89E-07	8.71E-04
0.3	16725	-1.14E-05	1.22E-06	1.52E-03	-1.14E-05	-5.69E-16	1.63E-03	-1.14E-05	-1.22E-06	1.52E-03
0.4	22300	-1.75E-05	1.72E-06	2.44E-03	-1.75E-05	-4.66E-17	2.58E-03	-1.75E-05	-1.72E-06	2.44E-03
0.5	27875	-2.76E-05	2.32E-06	3.80E-03	-2.76E-05	-3.22E-16	3.98E-03	-2.76E-05	-2.32E-06	3.80E-03
0.6	33450	-4.85E-05	3.15E-06	6.02E-03	-4.85E-05	-7.78E-15	6.25E-03	-4.85E-05	-3.15E-06	6.02E-03
0.7	39025	-1.09E-04	4.53E-06	1.04E-02	-1.09E-04	-6.57E-15	1.07E-02	-1.09E-04	-4.53E-06	1.04E-02
0.8	44600	-2.04E-04	6.01E-06	1.49E-02	-2.04E-04	1.64E-14	1.52E-02	-2.04E-04	-6.01E-06	1.49E-02
0.9	50175	-8.92E-03	1.71E-05	0.10547	-8.92E-03	3.04E-15	0.10561	-8.92E-03	-1.71E-05	0.10547
1.0	55750	-9.24E-02	3.59E-05	0.32929	-9.24E-02	-2.60E-13	0.32942	-9.24E-02	-3.59E-05	0.32929

Table B.16 Solid Plate with a Hole with a Very Coarse Mesh Raw Displacement Data

Max Load	55750	Very Coarse Mesh								
Expected Buckling	50718	Displacement (m)								
		Point A (Top RHS Centre Node)			Point B (Load Point Centre Node)			Point C (Bottom RHS Centre Node)		
Time	Load (N)	UX	UY	UZ	UX	UY	UZ	UX	UY	UZ
0	0	0	0	0	0	0	0	0	0	0
0.1	5575	-3.27E-06	3.86E-07	3.81E-04	-3.27E-06	-4.83E-18	4.13E-04	-3.27E-06	-3.86E-07	3.81E-04
0.2	11150	-6.92E-06	7.90E-07	8.71E-04	-6.92E-06	-9.52E-16	9.36E-04	-6.92E-06	-7.90E-07	8.71E-04
0.3	16725	-1.14E-05	1.23E-06	1.52E-03	-1.14E-05	-2.98E-15	1.62E-03	-1.14E-05	-1.23E-06	1.52E-03
0.4	22300	-1.75E-05	1.72E-06	2.43E-03	-1.75E-05	2.05E-17	2.57E-03	-1.75E-05	-1.72E-06	2.43E-03
0.5	27875	-2.76E-05	2.32E-06	3.79E-03	-2.76E-05	1.16E-15	3.98E-03	-2.76E-05	-2.32E-06	3.79E-03
0.6	33450	-4.85E-05	3.15E-06	6.01E-03	-4.85E-05	4.42E-15	6.24E-03	-4.85E-05	-3.15E-06	6.01E-03
0.7	39025	-1.09E-04	4.52E-06	1.04E-02	-1.09E-04	3.58E-15	1.06E-02	-1.09E-04	-4.52E-06	1.04E-02
0.8	44600	-2.03E-04	5.98E-06	1.49E-02	-2.03E-04	3.86E-15	1.52E-02	-2.03E-04	-5.98E-06	1.49E-02
0.9	50175	-8.89E-03	1.68E-05	0.10528	-8.89E-03	-9.15E-14	0.10541	-8.89E-03	-1.68E-05	0.10528
1.0	55750	-9.21E-02	3.50E-05	0.32878	-9.21E-02	1.79E-12	0.32891	-9.21E-02	-3.50E-05	0.32878

Appendix C: Additional Information from Chapter Nine

/TITLE,Eigenvalue Buckling of an Insulated 2D Shell Element with a Hole	!Title
/UNITS,SI	!Determine Units
/PREP7	!Enter Preprocessor
ET,1,SHELL181	!Element Type
MP,EX,1,2.058E11	!Define Steel Plate Material Data
MP,PRXY,1,0.3	
MP,EX,2,1	!Define Void Material Data
MP,PRXY,2,0.3	
MP,EX,3,5.1E10	!Define Mineral Wool Insulation Material Data
MP,PRXY,3,0.064	
MP,EX,4,6.9E10	!Define Aluminium Jacketing Material Data
MP,PRXY,4,0.334	
SECTYPE,1,SHELL	!Define Outer Plate Shell Section ID
SECDATA,0.01,1	
SECDATA,0.01,3	
SECDATA,0.0005,4	
SECTYPE,2,SHELL	!Define Hole Shell Section ID
SECDATA,0.01,2	
SECDATA,0.01,3	
SECDATA,0.0005,4	
K,1,0,0	!Create Keypoints
K,2,0.8,0	
K,3,0.8,0.8	
K,4,0,0.8	
K,5,0.4,0	
K,6,0.8,0.4	
K,7,0.4,0.8	
K,8,0,0.4	
K,9,0.4,0.4	
L,1,5	!Create Lines
L,1,8	
L,5,9	
L,8,9	
L,2,5	
L,2,6	
L,6,9	
L,3,6	
L,3,7	
L,7,9	
L,4,7	
L,4,8	
A,1,5,9,8	!Create Areas
A,2,6,9,5	
A,3,7,9,6	
A,4,8,9,7	
CM,GROUP1,AREA	!Group Areas
CIRCLE,9,0.1,,,360,4	!Create Hole
A,9,10,11	!Create Areas
A,9,11,12	
A,9,12,13	
A,9,13,10	
ASEL,S,AREA,,5,8	!Group Areas
CM,GROUP2,AREA	
ALLSEL	
ASBA,GROUP1,GROUP2	!Generate the Hole

K,9,0.4,0.4	!Create Hole
CIRCLE,9,0.1,,,360,4	
A,9,15,16	!Create Areas
A,9,16,17	
A,9,17,14	
A,9,14,15	
LCCAT,1,2	!Concatenate Lines for Meshing
LCCAT,5,6	
LCCAT,8,9	
LCCAT,11,12	
LSEL,S,LINE,,1,,,0	!Define Outer Line Divisions
LSEL,A,LINE,,2,,,0	
LSEL,A,LINE,,5,,,0	
LSEL,A,LINE,,6,,,0	
LSEL,A,LINE,,8,,,0	
LSEL,A,LINE,,9,,,0	
LSEL,A,LINE,,11,,,0	
LSEL,A,LINE,,12,,,0	
LESIZE,ALL,,,32,,,,,1	
ALLSEL	
LSEL,S,LINE,,21,,,0	!Define Inner Line Divisions and Spacing
LSEL,A,LINE,,22,,,0	
LSEL,A,LINE,,23,,,0	
LSEL,A,LINE,,24,,,0	
LESIZE,ALL,,,50,1/10,,,,,1	
ALLSEL	
LSEL,S,LINE,,3,,,0	!Define Circle Divisions
LSEL,A,LINE,,4,,,0	
LSEL,A,LINE,,7,,,0	
LSEL,A,LINE,,10,,,0	
LSEL,A,LINE,,13,,,0	
LSEL,A,LINE,,14,,,0	
LSEL,A,LINE,,15,,,0	
LSEL,A,LINE,,16,,,0	
LESIZE,ALL,,,32,,,,,1	
ALLSEL	
LSEL,S,LINE,,17,,,0	!Define Inner Circle Divisions
LSEL,A,LINE,,18,,,0	
LSEL,A,LINE,,19,,,0	
LSEL,A,LINE,,20,,,0	
LESIZE,ALL,,,32,,,,,,1	
ALLSEL	
NUMMRG,ALL	!Glue Areas
MSHKEY,1	!Apply Mapped Meshing
AMESH,ALL	
ASEL,S,AREA,,1,4	!Assign Section Data to Hole Area
ESLA,S	
EMODIF,ALL,SEC,2	
ALLSEL	
NSEL,S,LOC,X,0-0.0001,0+0.0001	!Define Boundary Conditions
NSEL,R,LOC,Y,0-0.0001,0.8+0.0001	
D,ALL,UX,0	
D,ALL,UY,0	
D,ALL,UZ,0	
D,ALL,ROTX,0	
D,ALL,ROTY,0	
D,ALL,ROTZ,0	
ALLSEL	
NSEL,S,LOC,X,0.8-0.0001,0.8+0.0001	!Couple Nodes

CP,NEXT,UX,ALL	
ALLSEL	
NSEL,S,LOC,X,0.8-0.0001,0.8+0.0001	!Apply Load in x Direction
NSEL,R,LOC,Y,0.4-0.0001,0.4+0.0001	
F,ALL,FX,-1	
ALLSEL	
/SOLU	!Enter Solution
ANTYPE,STATIC	!Type of Analysis
PSTRES,ON	!Include Prestress Effect Calculations
SOLVE	!Solve
FINISH	!Finish First Solve
/SOLU	!Enter Solution
ANTYPE,BUCKLE	!Change Type of Analysis
BUCOPT,LANB,1	!Apply Bucking Analysis Options
SOLVE	!Solve
FINISH	!Finish Second Solve
/SOLU	!Enter Solution
EXPASS,ON	!Perform Expansion Pass
MXPAND,1	!Specify Number of Modes to Expand
SOLVE	!Solve
/ESHAPE,1	!View Plate in 3D
FINISH	!Finish Third Solve
/POST1	!Enter Post-Processor
SET,LIST	!List Eigenvalue Solution – Buckling Strength
SET,LAST	!Read Data for Desired Mode
PLDISP,2	!Plot Deflected Shape vs Original

Code C.1 Eigenvalue Buckling of an Insulated 2D Shell Element with a Hole

Table C.1 Raw Buckling Data for Mineral Wool Insulation with an Aluminium Jacketing

Mineral Wool Insulation Thickness (m)	Aluminium Jacketing Thickness (m)	Plate with Hole Eigenvalue Buckling (N)	Plate with 3/4 Depth Pit Eigenvalue Buckling (N)	Plate with 1/2 Depth Pit Eigenvalue Buckling (N)	Plate with 1/4 Depth Pit Eigenvalue Buckling (N)	Intact Plate Eigenvalue Buckling (N)
0	0	50667	53141	53246	54135	55937
0.01	0.0005	209610	215660	216810	216900	217460
0.01	0.00075	219830	226100	227330	227430	227980
0.01	0.001	230270	236760	238070	238190	238730
0.01	0.00125	240920	247640	249040	249170	249710
0.01	0.0015	251790	258750	260230	260390	260920
0.02	0.0005	666710	682340	687600	689170	690420
0.02	0.00075	690390	706440	711910	713580	714910
0.02	0.001	714310	730790	736480	738250	739660
0.02	0.00125	738490	755400	761310	763180	764680
0.02	0.0015	762920	780260	786400	788380	789980
0.03	0.0005	1542600	1573500	1587200	1593100	1598200
0.03	0.00075	1583600	1615100	1629200	1635300	1640600
0.03	0.001	1624900	1657000	1671400	1677800	1683200
0.03	0.00125	1666400	1699100	1713900	1720500	1726200
0.03	0.0015	1708200	1741500	1756700	1763500	1769500
0.04	0.0005	2934600	2985700	3012700	3026500	3039600
0.04	0.00075	2996300	3048100	3075600	3089800	3103300
0.04	0.001	3058200	3110800	3138800	3153300	3167300
0.04	0.00125	3120400	3173700	3202300	3217200	3231600
0.04	0.0015	3183000	3237000	3266200	3281400	3296200
0.05	0.0005	4930500	5005700	5051000	5076600	5103300
0.05	0.00075	5016000	5092000	5137900	5164000	5191400
0.05	0.001	5101700	5178500	5225200	5251800	5279800
0.05	0.00125	5187700	5265300	5312700	5339800	5368500
0.05	0.0015	5274100	5352500	5400600	5428200	5457600
0.06	0.0005	7612800	7714900	7783300	7824800	7871700
0.06	0.00075	7725000	7827900	7897200	7939300	7987100
0.06	0.001	7837400	7941100	8011400	8054100	8102800
0.06	0.00125	7950200	8054700	8125800	8169200	8218900
0.06	0.0015	8063300	8168600	8240600	8284600	8335300
0.07	0.0005	11060000	11191000	11287000	11349000	11423000
0.07	0.00075	11202000	11333000	11431000	11493000	11569000
0.07	0.001	11344000	11476000	11574000	11637000	11715000
0.07	0.00125	11486000	11619000	11719000	11782000	11861000
0.07	0.0015	11629000	11762000	11863000	11928000	12007000
0.08	0.0005	15348000	15507000	15637000	15722000	15833000
0.08	0.00075	15522000	15682000	15812000	15899000	16012000
0.08	0.001	15697000	15857000	15989000	16076000	16190000
0.08	0.00125	15871000	16032000	16165000	16253000	16369000
0.08	0.0015	16046000	16208000	16342000	16431000	16549000
0.09	0.0005	20551000	20737000	20904000	21017000	21175000
0.09	0.00075	20760000	20947000	21115000	21229000	21389000
0.09	0.001	20969000	21157000	21326000	21441000	21603000
0.09	0.00125	21178000	21367000	21537000	21654000	21818000
0.09	0.0015	21388000	21577000	21749000	21866000	22032000
0.1	0.0005	26739000	26950000	27158000	27304000	27520000
0.1	0.00075	26986000	27197000	27406000	27553000	27771000
0.1	0.001	27232000	27444000	27655000	27803000	28024000
0.1	0.00125	27479000	27691000	27904000	28053000	28276000
0.1	0.0015	27726000	27939000	28153000	28303000	28529000

Table C.2 Raw Buckling Data for Mineral Wool Insulation with a Polycarbonate Jacketing

Mineral Wool Insulation Thickness (m)	Polycarbonate Jacketing Thickness (m)	Plate with Hole Eigenvalue Buckling (N)	Plate with 3/4 Depth Pit Eigenvalue Buckling (N)	Plate with 1/2 Depth Pit Eigenvalue Buckling (N)	Plate with 1/4 Depth Pit Eigenvalue Buckling (N)	Intact Plate Eigenvalue Buckling (N)
0	0	50667	53141	53246	54135	55937
0.01	0.002	192910	198630	199650	199730	200320
0.01	0.004	196990	202780	203840	203920	204510
0.01	0.006	202140	208020	209100	209180	209770
0.01	0.008	208480	214430	215550	215640	216230
0.01	0.01	216120	222150	223300	223400	223990
0.02	0.002	627140	642120	647030	648440	649560
0.02	0.004	635630	650760	655750	657190	658330
0.02	0.006	645620	660920	665980	667460	668640
0.02	0.008	657250	672710	677850	679370	680590
0.02	0.01	670610	686240	691470	693030	694290
0.03	0.002	1473500	1503500	1516600	1522200	1526800
0.03	0.004	1487500	1517700	1530900	1536500	1541200
0.03	0.006	1503300	1533800	1547100	1552800	1557600
0.03	0.008	1521200	1551900	1565400	1571200	1576100
0.03	0.01	1541300	1572200	1585800	1591700	1596700
0.04	0.002	2830200	2880200	2906300	2919500	2931900
0.04	0.004	2850600	2900800	2927100	2940400	2953000
0.04	0.006	2873200	2923800	2950800	2963700	2976400
0.04	0.008	2898300	2949200	2975800	2989400	3002300
0.04	0.01	2925900	2977100	3003900	3017600	3030700
0.05	0.002	4785500	4859500	4903500	4928400	4954000
0.05	0.004	4813200	4887500	4931800	4956800	4982600
0.05	0.006	4843600	4918200	4962700	4987800	5013900
0.05	0.008	4876700	4951600	4996400	5021700	5048000
0.05	0.01	4912800	4988000	5033100	5058500	5085100
0.06	0.002	7422200	7523000	7590000	7630400	7675700
0.06	0.004	7458100	7559200	7626500	7667100	7712700
0.06	0.006	7497000	7598500	7666100	7706900	7752800
0.06	0.008	7539100	7640900	7708800	7749900	7796100
0.06	0.01	7584400	7686500	7754800	7796100	7842700
0.07	0.002	10819000	10948000	11043000	11103000	11176000
0.07	0.004	10864000	10994000	11089000	11149000	11222000
0.07	0.006	10912000	11042000	11138000	11198000	11272000
0.07	0.008	10964000	11094000	11190000	11251000	11325000
0.07	0.01	11020000	11150000	11246000	11308000	11382000
0.08	0.002	15052000	15210000	15338000	15422000	15530000
0.08	0.004	15107000	15266000	15393000	15477000	15586000
0.08	0.006	15166000	15324000	15452000	15537000	15647000
0.08	0.008	15228000	15387000	15516000	15601000	15711000
0.08	0.01	15295000	15454000	15583000	15668000	15779000
0.09	0.002	20196000	20381000	20545000	20657000	20812000
0.09	0.004	20261000	20447000	20612000	20724000	20879000
0.09	0.006	20331000	20517000	20682000	20795000	20950000
0.09	0.008	20404000	20591000	20757000	20870000	21026000
0.09	0.01	20483000	20669000	20836000	20949000	21106000
0.1	0.002	26320000	26531000	26736000	26880000	27091000
0.1	0.004	26397000	26608000	26814000	26958000	27170000
0.1	0.006	26478000	26690000	26896000	27041000	27254000
0.1	0.008	26564000	26776000	26983000	27128000	27342000
0.1	0.01	26655000	26867000	27074000	27220000	27435000

Appendix D: Raw Data Tables for Various Insulation Systems

Table D.1 Raw Buckling Data for Calcium Silicate Insulation and Aluminium Jacketing

Calcium Silicate Insulation Thickness (m)	Aluminium Jacketing Thickness (m)	Plate with Hole Eigenvalue Buckling (N)	Plate with 3/4 Depth Pit Eigenvalue Buckling (N)	Plate with 1/2 Depth Pit Eigenvalue Buckling (N)	Plate with 1/4 Depth Pit Eigenvalue Buckling (N)	Intact Plate Eigenvalue Buckling (N)
0	0	50667	53141	53246	54135	55937
0.01	0.0005	90724	92988	93110	93439	94785
0.01	0.00075	103710	106100	106250	106510	107780
0.01	0.001	116810	119370	119560	119760	120960
0.01	0.00125	130050	132800	133040	133200	134350
0.01	0.0015	143450	146410	146700	146860	147930
0.02	0.0005	182530	185300	185600	185750	186940
0.02	0.00075	216300	219410	219810	219910	221100
0.02	0.001	250020	253500	254010	254090	255290
0.02	0.00125	283710	287590	288230	288290	289540
0.02	0.0015	317390	321700	322480	322540	323850
0.03	0.0005	350110	354040	354750	354830	356210
0.03	0.00075	413800	418270	419200	419280	420830
0.03	0.001	476980	482040	483200	483320	485060
0.03	0.00125	539740	545420	546840	547000	548980
0.03	0.0015	602100	608450	610150	610360	612620
0.04	0.0005	612450	618120	619610	619800	621910
0.04	0.00075	714460	720890	722760	723030	725600
0.04	0.001	815280	822510	824790	825180	828260
0.04	0.00125	915020	923110	925840	926360	930020
0.04	0.0015	1013800	1022800	1026000	1026700	1030900
0.05	0.0005	986960	994960	997720	998260	1001900
0.05	0.00075	1135000	1144000	1147300	1148100	1152700
0.05	0.001	1281000	1290900	1294900	1295900	1301500
0.05	0.00125	1425000	1436000	1440700	1442000	1448600
0.05	0.0015	1567200	1579300	1584800	1586400	1594200
0.06	0.0005	1489600	1500500	1505100	1506400	1512900
0.06	0.00075	1690800	1702300	1708300	1709900	1718000
0.06	0.001	1888700	1901900	1908400	1910400	1920100
0.06	0.00125	2083600	2098000	2105600	2108000	2119500
0.06	0.0015	2275800	2291500	2300100	2303000	2316300
0.07	0.0005	2135000	2149200	2156600	2159000	2169900
0.07	0.00075	2395700	2411100	2419800	2422700	2436100
0.07	0.001	2651800	2668500	2678500	2682100	2697900
0.07	0.00125	2903700	2921800	2933100	2937400	2955900
0.07	0.0015	3151700	3171200	3184000	3188900	3210200
0.08	0.0005	2936600	2954300	2965400	2969500	2987000
0.08	0.00075	3262500	3281600	3294300	3299200	3320300
0.08	0.001	3582500	3602900	3617300	3623100	3647800
0.08	0.00125	3896800	3918600	3934900	3941500	3970100
0.08	0.0015	4205800	4229100	4247200	4254900	4287400
0.09	0.0005	3906200	3927700	3943500	3949900	3976900
0.09	0.00075	4302700	4325500	4343400	4350900	4382700
0.09	0.001	4691500	4715600	4735700	4744400	4781200
0.09	0.00125	5073200	5098500	5120900	5130800	5172900
0.09	0.0015	5448100	5474700	5499500	5510700	5558200
0.1	0.0005	5054800	5079900	5101600	5111100	5150800
0.1	0.00075	5526600	5552700	5577900	5587900	5634100
0.1	0.001	5988800	6015900	6043000	6055400	6108300
0.1	0.00125	6442100	6470300	6500200	6514200	6574000
0.1	0.0015	6887100	6916400	6949200	6964700	7031800

Table D.2 Raw Buckling Data for Cellular Glass Insulation and Aluminium Jacketing

Cellular Glass Insulation Thickness (m)	Aluminium Jacketing Thickness (m)	Plate with Hole Eigenvalue Buckling (N)	Plate with 3/4 Depth Pit Eigenvalue Buckling (N)	Plate with 1/2 Depth Pit Eigenvalue Buckling (N)	Plate with 1/4 Depth Pit Eigenvalue Buckling (N)	Intact Plate Eigenvalue Buckling (N)
0	0	50667	53141	53246	54135	55937
0.01	0.0005	80267	82354	82448	82882	84392
0.01	0.00075	93295	95478	95596	95935	97373
0.01	0.001	106350	108680	108820	109090	110490
0.01	0.00125	119460	121960	122150	122360	123730
0.01	0.0015	132650	135360	135590	135760	137130
0.02	0.0005	134610	136570	136720	137020	138560
0.02	0.00075	168460	170670	170880	171100	172710
0.02	0.001	201930	204430	204720	204880	206620
0.02	0.00125	235070	237890	238280	238390	240310
0.02	0.0015	267930	271100	271600	271690	273830
0.03	0.0005	221250	223200	223450	223670	225560
0.03	0.00075	285120	287370	287750	287910	290170
0.03	0.001	347710	350300	350830	350960	353710
0.03	0.00125	409160	412110	412820	412930	416270
0.03	0.0015	469560	472880	473790	473900	477930
0.04	0.0005	344090	345950	346360	346540	349190
0.04	0.00075	446530	448620	449240	449390	452930
0.04	0.001	546280	548590	549460	549610	554250
0.04	0.00125	643550	646080	647250	647420	653330
0.04	0.0015	738550	741280	742770	742990	750340
0.05	0.0005	506670	508230	508860	509030	512990
0.05	0.00075	655580	657120	658070	658250	663880
0.05	0.001	799790	801240	802570	802790	810430
0.05	0.00125	939670	940980	942730	943030	952950
0.05	0.0015	1075500	1076600	1078900	1079300	1091700
0.06	0.0005	712230	713120	714050	714260	720230
0.06	0.00075	914860	915260	916650	916910	925660
0.06	0.001	1100100	1109900	1111800	1112200	1124200
0.06	0.00125	1295700	1297700	1300100	1300700	1316300
0.06	0.0015	1470900	1479000	1482100	1482800	1502600
0.07	0.0005	963010	963430	964740	965020	973920
0.07	0.00075	1222600	1225100	1227100	1227500	1240600
0.07	0.001	1471900	1475900	1478500	1479100	1497200
0.07	0.00125	1711400	1716700	1720000	1720800	1744500
0.07	0.0015	1944900	1948200	1952300	1953400	1983100
0.08	0.0005	1257800	1261600	1263400	1263800	1276800
0.08	0.00075	1582900	1588500	1591100	1591700	1610800
0.08	0.001	1897400	1900300	1903800	1904600	1930800
0.08	0.00125	2194500	2198400	2202700	2203900	2237900
0.08	0.0015	2477400	2483800	2489100	2490600	2533300
0.09	0.0005	1604800	1609900	1612300	1612800	1631300
0.09	0.00075	2005300	2006800	2010200	2011000	2037900
0.09	0.001	2376600	2383900	2388300	2389500	2426100
0.09	0.00125	2730400	2742800	2748200	2749800	2797200
0.09	0.0015	3068000	3085000	3091600	3093600	3152800
0.1	0.0005	2007800	2010000	2013200	2013900	2039500
0.1	0.00075	2475400	2481200	2485500	2486600	2523500
0.1	0.001	2917400	2926900	2932400	2934000	2983800
0.1	0.00125	3337100	3349600	3356300	3358300	3422500
0.1	0.0015	3746400	3751000	3759000	3761500	3841200

Table D.3 Raw Buckling Data for Expanded Perlite Insulation and Aluminium Jacketing

Expanded Perlite Insulation Thickness (m)	Aluminium Jacketing Thickness (m)	Plate with Hole Eigenvalue Buckling (N)	Plate with 3/4 Depth Pit Eigenvalue Buckling (N)	Plate with 1/2 Depth Pit Eigenvalue Buckling (N)	Plate with 1/4 Depth Pit Eigenvalue Buckling (N)	Intact Plate Eigenvalue Buckling (N)
0	0	50667	53141	53246	54135	55937
0.01	0.0005	259120	267010	268790	269010	269500
0.01	0.00075	268200	276300	278170	278420	278900
0.01	0.001	277510	285840	287790	288060	288550
0.01	0.00125	287060	295610	297650	297950	298450
0.01	0.0015	296860	305630	307760	308090	308590
0.02	0.0005	847330	867890	875660	878450	880550
0.02	0.00075	867610	888530	896500	899390	901590
0.02	0.001	888210	909490	917660	920660	922950
0.02	0.00125	909130	930770	939150	942260	944640
0.02	0.0015	930370	952370	960970	964180	966670
0.03	0.0005	1964000	2002700	2021600	2030700	2038700
0.03	0.00075	1998700	2037800	2057100	2066400	2074600
0.03	0.001	2033800	2073300	2092900	2102500	2110900
0.03	0.00125	2069200	2109300	2129200	2138900	2147500
0.03	0.0015	2105100	2145600	2165800	2175800	2184600
0.04	0.0005	3737000	3797400	3832800	3852400	3871800
0.04	0.00075	3789000	3850000	3885800	3905700	3925400
0.04	0.001	3841500	3903000	3939200	3959400	3979500
0.04	0.00125	3894500	3956400	3993000	4013600	4034100
0.04	0.0015	3947900	4010400	4047500	4068300	4089200
0.05	0.0005	6286700	6371100	6427800	6462200	6499700
0.05	0.00075	6358900	6443900	6501100	6539500	6574000
0.05	0.001	6431600	6517100	6574900	6610100	6648700
0.05	0.00125	6504900	6590900	6649300	6684800	6724000
0.05	0.0015	6578700	6665200	6724200	6760100	6799900
0.06	0.0005	9729300	9838500	9921300	9974600	10038000
0.06	0.00075	9824400	9934100	10018000	10071000	10136000
0.06	0.001	9920100	10030000	10114000	10169000	10234000
0.06	0.00125	10016000	10127000	10212000	10267000	10333000
0.06	0.0015	10113000	10225000	10310000	10365000	10432000
0.07	0.0005	14178000	14311000	14424000	14501000	14600000
0.07	0.00075	14299000	14432000	14546000	14623000	14723000
0.07	0.001	14420000	14554000	14669000	14746000	14847000
0.07	0.00125	14542000	14676000	14792000	14870000	14972000
0.07	0.0015	14665000	14799000	14916000	14994000	15097000
0.08	0.0005	19743000	19897000	20045000	20149000	20294000
0.08	0.00075	19891000	20046000	20195000	20299000	20446000
0.08	0.001	20041000	20196000	20346000	20451000	20598000
0.08	0.00125	20191000	20347000	20497000	20603000	20752000
0.08	0.0015	20342000	20498000	20650000	20756000	20906000
0.09	0.0005	26531000	26703000	26890000	27024000	27228000
0.09	0.00075	26711000	26883000	27070000	27206000	27411000
0.09	0.001	26891000	27063000	27252000	27388000	27595000
0.09	0.00125	27072000	27245000	27434000	27571000	27779000
0.09	0.0015	27254000	27427000	27617000	27755000	27965000
0.1	0.0005	34648000	34832000	35061000	35230000	35507000
0.1	0.00075	34861000	35045000	35275000	35445000	35723000
0.1	0.001	35075000	35258000	35489000	35660000	35940000
0.1	0.00125	35289000	35472000	35705000	35876000	36159000
0.1	0.0015	35504000	35687000	35921000	36093000	36378000

Table D.4 Raw Buckling Data for Fibreglass Insulation and Aluminium Jacketing

Fibreglass Insulation Thickness (m)	Aluminium Jacketing Thickness (m)	Plate with Hole Eigenvalue Buckling (N)	Plate with 3/4 Depth Pit Eigenvalue Buckling (N)	Plate with 1/2 Depth Pit Eigenvalue Buckling (N)	Plate with 1/4 Depth Pit Eigenvalue Buckling (N)	Intact Plate Eigenvalue Buckling (N)
0	0	50667	53141	53246	54135	55937
0.01	0.0005	253730	261370	263050	263250	263740
0.01	0.00075	262890	270740	272510	272730	273230
0.01	0.001	272290	280360	282220	282460	282960
0.01	0.00125	281920	290220	292170	292440	292940
0.01	0.0015	291800	300330	302370	302660	303180
0.02	0.0005	828260	848200	855640	858260	860310
0.02	0.00075	848760	869060	876710	879430	881560
0.02	0.001	869570	890240	898100	900920	903150
0.02	0.00125	890710	911750	919810	922740	925070
0.02	0.0015	912170	933580	941860	944900	947320
0.03	0.0005	1919100	1956800	1975100	1983800	1991600
0.03	0.00075	1954200	1992300	2010900	2019800	2027800
0.03	0.001	1989600	2028200	2047200	2056300	2064500
0.03	0.00125	2025500	2064500	2083800	2093100	2101600
0.03	0.0015	2061700	2101200	2120900	2130400	2139000
0.04	0.0005	3649800	3708800	3743100	3762000	3781100
0.04	0.00075	3702300	3761900	3796700	3815800	3835300
0.04	0.001	3755300	3815400	3850700	3870100	3889900
0.04	0.00125	3808800	3869400	3905100	3924900	3945100
0.04	0.0015	3862800	3923900	3960000	3980100	4000700
0.05	0.0005	6135900	6218400	6273800	6307000	6344100
0.05	0.00075	6208700	6291800	6347700	6381400	6419000
0.05	0.001	6282100	6365800	6422200	6456300	6494500
0.05	0.00125	6356100	6440200	6497300	6531800	6570500
0.05	0.0015	6430500	6515200	6572800	6607700	6647100
0.06	0.0005	9488700	9595400	9676400	9728300	9791300
0.06	0.00075	9584600	9691800	9773500	9825900	9889700
0.06	0.001	9681100	9788800	9871200	9924000	9988600
0.06	0.00125	9778100	9886400	9969400	10023000	10088000
0.06	0.0015	9875800	9984600	10068000	10122000	10188000
0.07	0.0005	13816000	13946000	14057000	14132000	14230000
0.07	0.00075	13938000	14068000	14180000	14255000	14354000
0.07	0.001	14060000	14191000	14303000	14379000	14480000
0.07	0.00125	14183000	14314000	14427000	14504000	14605000
0.07	0.0015	14306000	14438000	14552000	14629000	14732000
0.08	0.0005	19223000	19374000	19519000	19620000	19765000
0.08	0.00075	19373000	19524000	19670000	19772000	19918000
0.08	0.001	19523000	19675000	19822000	19925000	20072000
0.08	0.00125	19674000	19826000	19974000	20078000	20226000
0.08	0.0015	19826000	19978000	20127000	20231000	20381000
0.09	0.0005	25812000	25979000	26163000	26295000	26498000
0.09	0.00075	25992000	26160000	26345000	26477000	26682000
0.09	0.001	26174000	26341000	26527000	26660000	26867000
0.09	0.00125	26356000	26523000	26710000	26844000	27052000
0.09	0.0015	26539000	26706000	26894000	27029000	27239000
0.1	0.0005	33683000	33860000	34086000	34252000	34528000
0.1	0.00075	33896000	34074000	34301000	34468000	34746000
0.1	0.001	34111000	34288000	34516000	34684000	34964000
0.1	0.00125	34326000	34503000	34732000	34901000	35183000
0.1	0.0015	34542000	34719000	34950000	35119000	35403000

Table D.5 Raw Buckling Data for Syntactic Polypropylene Insulation and Aluminium Jacketing

Syntactic Polypropylene Insulation Thickness (m)	Aluminium Jacketing Thickness (m)	Plate with Hole Eigenvalue Buckling (N)	Plate with 3/4 Depth Pit Eigenvalue Buckling (N)	Plate with 1/2 Depth Pit Eigenvalue Buckling (N)	Plate with 1/4 Depth Pit Eigenvalue Buckling (N)	Intact Plate Eigenvalue Buckling (N)
0	0	50667	53141	53246	54135	55937
0.01	0.0005	81321	83414	83511	83932	85420
0.01	0.00075	94383	96578	96698	97028	98440
0.01	0.001	107490	109830	109990	110250	111610
0.01	0.00125	120680	123200	123390	123600	124930
0.01	0.0015	133970	136700	136930	137090	138410
0.02	0.0005	139410	141430	141590	141870	143360
0.02	0.00075	173420	175920	175920	176120	177660
0.02	0.001	207120	209710	210020	210160	211800
0.02	0.00125	240580	243910	243910	244020	245800
0.02	0.0015	273840	277120	277640	277730	279690
0.03	0.0005	234190	236280	236570	236760	238570
0.03	0.00075	298420	300870	301280	301420	303560
0.03	0.001	361610	364430	365010	365130	367670
0.03	0.00125	423850	427080	427850	427950	430990
0.03	0.0015	485210	488870	489850	489970	493580
0.04	0.0005	371120	373270	373740	373900	376460
0.04	0.00075	474260	476720	477430	477570	480900
0.04	0.001	575140	577940	578920	579070	583350
0.04	0.00125	673940	677090	678380	678570	683930
0.04	0.0015	770810	774310	775950	776210	782780
0.05	0.0005	555230	557250	558010	558180	562050
0.05	0.00075	705290	707470	708580	708780	714130
0.05	0.001	851400	853710	855250	855510	862590
0.05	0.00125	993860	996280	998280	998650	1007700
0.05	0.0015	1132900	1135400	1137900	1138400	1149700
0.06	0.0005	791120	792690	793860	794090	800050
0.06	0.00075	995480	996880	998550	998880	1007300
0.06	0.001	1193700	1194800	1197500	1197500	1208800
0.06	0.00125	1386200	1387000	1389900	1390500	1405000
0.06	0.0015	1573400	1573800	1577300	1578200	1596200
0.07	0.0005	1083000	1083700	1085400	1085700	1094800
0.07	0.00075	1348000	1348700	1350700	1351200	1364100
0.07	0.001	1603500	1603900	1607100	1607900	1625000
0.07	0.00125	1850200	1851100	1855100	1856200	1878100
0.07	0.0015	2090000	2090500	2095400	2096800	2124000
0.08	0.0005	1433400	1433800	1436200	1436700	1450100
0.08	0.00075	1764200	1764800	1768000	1768900	1787700
0.08	0.001	2082400	2083300	2087500	2088700	2113700
0.08	0.00125	2389500	2390200	2395600	2397100	2429000
0.08	0.0015	2685200	2686500	2692900	2695000	2734300
0.09	0.0005	1844800	1846300	1849600	1850400	1869700
0.09	0.00075	2246700	2248700	2253000	2254300	2281200
0.09	0.001	2633700	2634600	2640200	2641900	2677300
0.09	0.00125	3004900	3005400	3012300	3014500	3059300
0.09	0.0015	3360500	3362100	3370300	3373100	3428100
0.1	0.0005	2323100	2324100	2328300	2329500	2356600
0.1	0.00075	2801300	2802200	2807800	2809600	2846800
0.1	0.001	3258200	3259400	3266500	3268800	3317500
0.1	0.00125	3696300	3697300	3705900	3708900	3770100
0.1	0.0015	4115100	4117300	4127500	4131200	4205800

Table D.6 Raw Buckling Data for Calcium Silicate Insulation and Polycarbonate Jacketing

Calcium Silicate Insulation Thickness (m)	Polycarbonate Jacketing Thickness (m)	Plate with Hole Eigenvalue Buckling (N)	Plate with 3/4 Depth Pit Eigenvalue Buckling (N)	Plate with 1/2 Depth Pit Eigenvalue Buckling (N)	Plate with 1/4 Depth Pit Eigenvalue Buckling (N)	Intact Plate Eigenvalue Buckling (N)
0	0	50667	53141	53246	54135	55937
0.01	0.002	68953	71103	71270	72127	73332
0.01	0.004	74096	76092	76364	77022	78340
0.01	0.006	80377	81824	82606	83047	84051
0.01	0.008	87904	90002	90109	90978	91929
0.01	0.01	96786	98861	98984	99344	100740
0.02	0.002	124810	127170	127340	127600	128880
0.02	0.004	136720	139110	139300	139540	140800
0.02	0.006	150310	152740	152960	153180	154430
0.02	0.008	165690	168180	168430	168620	169870
0.02	0.01	182970	185520	185800	185980	187230
0.03	0.002	240030	243170	243590	243710	244920
0.03	0.004	261460	264710	265170	265280	266520
0.03	0.006	285080	288440	288960	289060	290340
0.03	0.008	311000	314480	315050	315150	316490
0.03	0.01	339300	342910	343550	343650	345050
0.04	0.002	434870	439400	440320	440430	441930
0.04	0.004	468360	473050	474070	474180	475780
0.04	0.006	504500	509370	510480	510610	512340
0.04	0.008	543400	548450	549670	549810	551680
0.04	0.01	585140	590380	594720	591890	593920
0.05	0.002	728040	734540	736370	736640	739030
0.05	0.004	775880	782610	784590	784900	787510
0.05	0.006	826820	833780	835920	836280	839130
0.05	0.008	880950	888140	890450	890860	893990
0.05	0.01	938360	945790	948280	948750	952180
0.06	0.002	1136700	1145800	1149000	1149800	1154000
0.06	0.004	1201000	1210400	1213900	1214700	1219200
0.06	0.006	1268900	1278500	1282200	1283100	1288100
0.06	0.008	1340300	1350200	1354200	1355100	1360600
0.06	0.01	1415400	1425500	1429800	1430900	1436800
0.07	0.002	1676700	1688800	1694200	1695800	1703100
0.07	0.004	1759400	1771900	1777600	1779300	1787200
0.07	0.006	1846000	1858800	1864800	1866700	1875200
0.07	0.008	1936600	1949700	1956100	1958100	1967400
0.07	0.01	2031200	2044600	2051400	2053600	2063600
0.08	0.002	2362300	2378000	2386400	2389200	2401400
0.08	0.004	2465200	2481200	2490000	2493100	2506200
0.08	0.006	2572400	2588700	2598000	2601200	2615300
0.08	0.008	2683800	2700500	2710200	2713700	2728800
0.08	0.01	2799700	2816700	2826900	2830600	2846800
0.09	0.002	3206800	3226300	3238600	3243300	3262700
0.09	0.004	3331500	3351300	3364200	3369100	3389800
0.09	0.006	3460700	3480800	3494300	3499600	3521600
0.09	0.008	3594600	3615000	3629100	3634700	3658100
0.09	0.01	3733200	3753900	3768700	3774600	3799500
0.1	0.002	4222000	4245300	4262700	4269900	4299400
0.1	0.004	4369800	4393400	4411500	4419100	4450400
0.1	0.006	4522600	4546400	4565300	4573300	4606300
0.1	0.008	4680300	4704400	4724000	4732400	4767400
0.1	0.01	4843100	4867400	4887800	4896600	4933600

Table D.7 Raw Buckling Data for Cellular Glass Insulation and Polycarbonate Jacketing

Cellular Glass Insulation Thickness (m)	Polycarbonate Jacketing Thickness (m)	Plate with Hole Eigenvalue Buckling (N)	Plate with 3/4 Depth Pit Eigenvalue Buckling (N)	Plate with 1/2 Depth Pit Eigenvalue Buckling (N)	Plate with 1/4 Depth Pit Eigenvalue Buckling (N)	Intact Plate Eigenvalue Buckling (N)
0	0	50667	53141	53246	54135	55937
0.01	0.002	58053	60238	60302	61046	62785
0.01	0.004	63353	65410	65449	66148	67832
0.01	0.006	69752	71711	71882	72388	74023
0.01	0.008	77364	79252	79370	79878	81471
0.01	0.01	86301	88113	88261	88727	90286
0.02	0.002	75660	77479	77563	78150	79792
0.02	0.004	87909	89639	89840	90248	91850
0.02	0.006	101750	103400	103560	104000	105580
0.02	0.008	117310	119000	119120	119520	121100
0.02	0.01	134690	136400	136540	136900	138490
0.03	0.002	108630	110230	110380	110800	112410
0.03	0.004	130610	132200	132320	132720	134340
0.03	0.006	154660	156250	156400	156750	158420
0.03	0.008	180890	182500	182680	182990	184750
0.03	0.01	209410	211050	211260	211540	213410
0.04	0.002	161600	163120	163270	163630	165330
0.04	0.004	196040	197550	197730	198050	199870
0.04	0.006	232950	234470	234690	234990	236970
0.04	0.008	272460	273980	274250	274520	276710
0.04	0.01	314640	316170	316490	316740	319180
0.05	0.002	239080	240530	240750	241050	243050
0.05	0.004	288560	289980	290260	290530	292790
0.05	0.006	340860	342250	342590	342840	345430
0.05	0.008	396080	397420	397830	398060	401050
0.05	0.01	454290	455560	456060	456280	459720
0.06	0.002	345340	346670	346990	347250	349830
0.06	0.004	412300	413530	413940	414180	417230
0.06	0.006	482340	483440	483950	484180	487790
0.06	0.008	555550	556490	557100	557330	561590
0.06	0.01	632000	632740	633470	633700	638700
0.07	0.002	484410	485460	485940	486180	489730
0.07	0.004	571120	571940	572540	572770	577070
0.07	0.006	661080	661630	662360	662600	667770
0.07	0.008	754390	754610	755480	755730	761890
0.07	0.01	850110	850940	851980	852250	859520
0.08	0.002	660040	660550	661250	661480	666530
0.08	0.004	768380	768680	769540	769790	775950
0.08	0.006	879490	880100	881130	881410	888840
0.08	0.008	993840	994870	996100	996410	1005300
0.08	0.01	1112700	1113100	1114500	1114900	1125300
0.09	0.002	875700	875300	876290	876550	883780
0.09	0.004	1004000	1006900	1008100	1008400	1017200
0.09	0.006	1139700	1141800	1143300	1143600	1154200
0.09	0.008	1278900	1280100	1281800	1282200	1294800
0.09	0.01	1420100	1421700	1423700	1424200	1438900
0.1	0.002	1130600	1132800	1134100	1134500	1144700
0.1	0.004	1287400	1289600	1291200	1291600	1304000
0.1	0.006	1447600	1449500	1451400	1451900	1466800
0.1	0.008	1610100	1612800	1615000	1615500	1633100
0.1	0.01	1777100	1779300	1781800	1782500	1803000

Table D.8 Raw Buckling Data for Expanded Perlite Insulation and Polycarbonate Jacketing

Expanded Perlite Insulation Thickness (m)	Polycarbonate Jacketing Thickness (m)	Plate with Hole Eigenvalue Buckling (N)	Plate with 3/4 Depth Pit Eigenvalue Buckling (N)	Plate with 1/2 Depth Pit Eigenvalue Buckling (N)	Plate with 1/4 Depth Pit Eigenvalue Buckling (N)	Intact Plate Eigenvalue Buckling (N)
0	0	50667	53141	53246	54135	55937
0.01	0.002	244410	251960	253610	253800	254280
0.01	0.004	248060	255700	257380	257580	258060
0.01	0.006	252720	260460	262170	262380	262870
0.01	0.008	258530	266350	268100	268320	268820
0.01	0.01	265610	273500	275290	275530	276030
0.02	0.002	813710	833710	841150	843780	845740
0.02	0.004	821010	841160	848670	851340	853330
0.02	0.006	829720	850030	857610	860320	862340
0.02	0.008	839980	860420	868090	870840	872910
0.02	0.01	851890	872470	880230	883020	885130
0.03	0.002	1906000	1943900	1962400	1971200	1978800
0.03	0.004	1917800	1956000	1974500	1983400	1991000
0.03	0.006	1931400	1969800	1988400	1997400	2005100
0.03	0.008	1947000	1985500	2004300	2013300	2021100
0.03	0.01	1964500	2003200	2022100	2031200	2039200
0.04	0.002	3649400	3709100	3743800	3762900	3781700
0.04	0.004	3666600	3726600	3761300	3780600	3799500
0.04	0.006	3686000	3746100	3781100	3800400	3819400
0.04	0.008	3707600	3768000	3803100	3822500	3841700
0.04	0.01	3731600	3792200	3827400	3847000	3866300
0.05	0.002	6164800	6248500	6304300	6338000	6374700
0.05	0.004	6188200	6272200	6328200	6362000	6398800
0.05	0.006	6214100	6298300	6354500	6388500	6425500
0.05	0.008	6242600	6327000	6383400	6417600	6454700
0.05	0.01	6273900	6358500	6415100	6449400	6486800
0.06	0.002	9568500	9677000	9758700	9811200	9873500
0.06	0.004	9598900	9707600	9789500	9842200	9904800
0.06	0.006	9632100	9741100	9823300	9876100	9939000
0.06	0.008	9668300	9777600	9859900	9913000	9976100
0.06	0.01	9707600	9817100	9899700	9952900	10016000
0.07	0.002	13974000	14106000	14218000	14294000	14391000
0.07	0.004	14012000	14145000	14257000	14333000	14430000
0.07	0.006	14053000	14186000	14299000	14375000	14472000
0.07	0.008	14098000	14231000	14344000	14420000	14518000
0.07	0.01	14146000	14279000	14393000	14469000	14568000
0.08	0.002	19490000	19645000	19791000	19894000	20036000
0.08	0.004	19537000	19692000	19839000	19941000	20084000
0.08	0.006	19587000	19742000	19889000	19992000	20136000
0.08	0.008	19641000	19796000	19944000	20047000	20191000
0.08	0.01	19699000	19854000	20002000	20106000	20250000
0.09	0.002	26227000	26399000	26584000	26717000	26918000
0.09	0.004	26283000	26455000	26640000	26774000	26975000
0.09	0.006	26343000	26515000	26701000	26835000	27037000
0.09	0.008	26407000	26579000	26766000	26900000	27102000
0.09	0.01	26475000	26648000	26834000	26969000	27172000
0.1	0.002	34288000	34471000	34699000	34867000	35140000
0.1	0.004	34354000	34538000	34766000	34934000	35207000
0.1	0.006	34424000	34608000	34837000	35005000	35279000
0.1	0.008	34499000	34683000	34912000	35081000	35356000
0.1	0.01	34578000	34763000	34992000	35161000	35437000

Table D.9 Raw Buckling Data for Fibreglass Insulation and Polycarbonate Jacketing

Fibreglass Insulation Thickness (m)	Polycarbonate Jacketing Thickness (m)	Plate with Hole Eigenvalue Buckling (N)	Plate with 3/4 Depth Pit Eigenvalue Buckling (N)	Plate with 1/2 Depth Pit Eigenvalue Buckling (N)	Plate with 1/4 Depth Pit Eigenvalue Buckling (N)	Intact Plate Eigenvalue Buckling (N)
0	0	50667	53141	53246	54135	55937
0.01	0.002	238880	246180	247730	247890	248390
0.01	0.004	242550	249940	251520	251690	252190
0.01	0.006	247240	254720	256330	256520	257020
0.01	0.008	253080	260640	262290	262490	263000
0.01	0.01	260180	267820	269510	269720	270240
0.02	0.002	794270	813640	820750	823200	825110
0.02	0.004	801630	821150	828330	830820	832760
0.02	0.006	810410	830080	837340	839870	841840
0.02	0.008	820730	840550	847890	850460	852470
0.02	0.01	832710	852670	860090	862710	864770
0.03	0.002	1860500	1897400	1915100	1923500	1930300
0.03	0.004	1872400	1909500	1927400	1935800	1943300
0.03	0.006	1886100	1923400	1941400	1949900	1957500
0.03	0.008	1901800	1939200	1957400	1966000	1973600
0.03	0.01	1919400	1957100	1975400	1984000	1991800
0.04	0.002	3561300	3619500	3653100	3671500	3690000
0.04	0.004	3578700	3637100	3670900	3689400	3707900
0.04	0.006	3598200	3656800	3690800	3709400	3728000
0.04	0.008	3619800	3678800	3712900	3731600	3750500
0.04	0.01	3644100	3703200	3737500	3756300	3775300
0.05	0.002	6012900	6094600	6149000	6181600	6217700
0.05	0.004	6036400	6118400	6173000	6205800	6242100
0.05	0.006	6062500	6144700	6199500	6232400	6268900
0.05	0.008	6091200	6173700	6228700	6261700	6298400
0.05	0.01	6122700	6205300	6260600	6293700	6330700
0.06	0.002	9326500	9432500	9512400	9563400	9625100
0.06	0.004	9357100	9463300	9543400	9594700	9656600
0.06	0.006	9390500	9497000	9577400	9628800	9691000
0.06	0.008	9427000	9533600	9614300	9665900	9728400
0.06	0.01	9466500	9573400	9654300	9706000	9768900
0.07	0.002	13610000	13740000	13849000	13923000	14020000
0.07	0.004	13649000	13778000	13888000	13962000	14059000
0.07	0.006	13690000	13820000	13930000	14004000	14102000
0.07	0.008	13735000	13865000	13976000	14050000	14148000
0.07	0.01	13783000	13914000	14025000	14099000	14197000
0.08	0.002	18969000	19119000	19264000	19364000	19506000
0.08	0.004	19016000	19167000	19311000	19411000	19554000
0.08	0.006	19067000	19217000	19362000	19463000	19606000
0.08	0.008	19121000	19277000	19417000	19518000	19661000
0.08	0.01	19179000	19330000	19475000	19576000	19721000
0.09	0.002	25506000	25673000	25855000	25986000	26186000
0.09	0.004	25562000	25729000	25912000	26043000	26243000
0.09	0.006	25622000	25790000	25973000	26104000	26305000
0.09	0.008	25687000	25854000	26038000	26169000	26371000
0.09	0.01	25755000	25923000	26107000	26238000	26441000
0.1	0.002	33320000	33498000	33722000	33887000	34159000
0.1	0.004	33387000	33564000	33789000	33954000	34227000
0.1	0.006	33457000	33635000	33860000	34026000	34299000
0.1	0.008	33532000	33710000	33936000	34101000	34376000
0.1	0.01	33612000	33790000	34016000	34182000	34457000

Table D.10 Raw Buckling Data for Syntactic Polypropylene Insulation and Polycarbonate Jacketing

Syntactic Polypropylene Insulation Thickness (m)	Polycarbonate Jacketing Thickness (m)	Plate with Hole Eigenvalue Buckling (N)	Plate with 3/4 Depth Pit Eigenvalue Buckling (N)	Plate with 1/2 Depth Pit Eigenvalue Buckling (N)	Plate with 1/4 Depth Pit Eigenvalue Buckling (N)	Intact Plate Eigenvalue Buckling (N)
0	0	50667	53141	53246	54135	55937
0.01	0.002	59126	61294	61326	62078	63794
0.01	0.004	64406	64558	64871	67176	68840
0.01	0.006	70795	72756	72885	73418	75033
0.01	0.008	78404	80298	80416	80913	82486
0.01	0.01	87346	88980	89319	89774	91312
0.02	0.002	80510	82324	82369	82953	84550
0.02	0.004	92699	94446	94575	95029	96591
0.02	0.006	106510	108260	108370	108780	110320
0.02	0.008	122070	123810	123940	124310	125850
0.02	0.01	139470	141230	141380	141720	143270
0.03	0.002	121620	123300	123420	123810	125370
0.03	0.004	143500	145170	145310	145660	147250
0.03	0.006	167500	169190	169360	169680	171310
0.03	0.008	193720	195460	195660	195940	197650
0.03	0.01	222280	224060	224300	224560	226360
0.04	0.002	188730	190390	190570	190880	192580
0.04	0.004	223000	224680	224900	225180	226990
0.04	0.006	259820	261540	261810	262060	264030
0.04	0.008	299310	301070	301390	301620	303780
0.04	0.01	341550	343340	343720	343940	346330
0.05	0.002	287880	289560	289850	290100	292180
0.05	0.004	337070	338760	339120	339350	341690
0.05	0.006	389220	390910	391340	391550	394210
0.05	0.008	444390	446070	446590	446800	449810
0.05	0.01	502670	504340	504950	505150	508590
0.06	0.002	424740	426370	426840	427050	429890
0.06	0.004	491240	492830	493390	493600	496900
0.06	0.006	561010	562520	563200	563410	567230
0.06	0.008	634120	635540	636340	636550	640980
0.06	0.01	710640	711940	712870	713110	718220
0.07	0.002	604620	606030	606750	606960	611070
0.07	0.004	690630	691890	692750	692980	697810
0.07	0.006	780170	781240	782250	782500	788160
0.07	0.008	873300	874130	875320	875590	882180
0.07	0.01	970090	970640	972010	972330	979940
0.08	0.002	832440	833340	834420	834680	840740
0.08	0.004	940010	940590	941850	942150	949300
0.08	0.006	1051300	1051500	1053000	1053300	1061700
0.08	0.008	1165800	1166100	1167800	1168200	1177900
0.08	0.01	1283300	1284500	1286500	1286900	1298100
0.09	0.002	1110800	1112700	1114300	1114600	1123600
0.09	0.004	1241700	1243200	1245000	1245400	1255800
0.09	0.006	1375600	1377400	1379400	1379900	1392100
0.09	0.008	1513300	1515400	1517700	1518300	1532300
0.09	0.01	1655000	1657300	1659900	1660600	1676700
0.1	0.002	1446800	1448200	1450400	1450900	1463800
0.1	0.004	1600900	1603400	1605900	1606500	1621500
0.1	0.006	1759900	1762400	1765200	1766000	1783300
0.1	0.008	1922900	1925300	1928500	1929300	1949200
0.1	0.01	2089800	2092100	2095600	2096600	2119200

Appendix E: Additional Information from Chapter Ten

/TITLE,Eigenvalue Buckling of a Intact 2D Shell Pipe	!Title
/UNITS,SI	!Determine Units
/PREP7	!Enter Preprocessor
ET,1,SHELL181	!Element Type
MP,EX,1,2E11	!Define Material Data
MP,PRXY,1,0.3	
SECTYPE,1,SHELL	!Define Shell Section ID
SECDATA,0.0254	
K,1,0.6223,0	!Create Keypoints for the Geometry
K,2,0,0.6223	
K,3,-0.6223,0	
K,4,0,-0.6223	
K,5,0.4400325499,0.4400325499	
K,6,-0.4400325499,0.4400325499	
K,7,-0.4400325499,-0.4400325499	
K,8,0.4400325499,-0.4400325499	
K,9,0.6223,0,-25.4	
LARC,1,2,5	!Create Arc Lines
LARC,2,3,6	
LARC,3,4,7	
LARC,4,1,8	
LDIV,1,,,0	!Divide Lines
LDIV,2,,,0	
LDIV,3,,,0	
LDIV,4,,,0	
NUMMRG,KP,,,,LOW	!Merge Keypoints
CM,GROUP1,LINES	!Group Lines
L,1,9	!Create Line to Extrude Along
ADRAG,GROUP1,,,,,,9	!Extrude to Create Areas
NUMMRG,KP,,,,LOW	!Merge Keypoints to Reduce Number of Lines
LSEL,S,LINE,,9,,,0	!Define Line Divisions
LSEL,A,LINE,,12,,,0	
LSEL,A,LINE,,14,,,0	
LSEL,A,LINE,,16,,,0	
LSEL,A,LINE,,18,,,0	
LSEL,A,LINE,,20,,,0	
LSEL,A,LINE,,22,,,0	
LSEL,A,LINE,,24,,,0	
LESIZE,ALL,,,200,,,,,1	
ALLSEL	
LSEL,S,LINE,,1,,,0	!Define Circle Divisions
LSEL,A,LINE,,2,,,0	
LSEL,A,LINE,,3,,,0	
LSEL,A,LINE,,4,,,0	
LSEL,A,LINE,,5,,,0	
LSEL,A,LINE,,6,,,0	
LSEL,A,LINE,,7,,,0	
LSEL,A,LINE,,8,,,0	
LSEL,A,LINE,,10,,,0	
LSEL,A,LINE,,13,,,0	
LSEL,A,LINE,,15,,,0	

LSEL,A,LINE,,17,,,0	
LSEL,A,LINE,,19,,,0	
LSEL,A,LINE,,21,,,0	
LSEL,A,LINE,,23,,,0	
LSEL,A,LINE,,25,,,0	
LESIZE,ALL,,,16,,,,1	
ALLSEL	
MSHKEY,1	!Apply Mapped Meshing
AMESH,ALL	
NSEL,S,LOC,Z,0-0.0001,0+0.0001	!Define Boundary Conditions
D,ALL,UX,0	
D,ALL,UY,0	
D,ALL,UZ,0	
D,ALL,ROTX,0	
D,ALL,ROTY,0	
D,ALL,ROTZ,0	
ALLSEL	
NSEL,S,LOC,Z,-25.4-0.0001,-25.4+0.0001	!Select Nodes
F,ALL,FZ,1/128	!Apply Load Equally over Nodes
ALLSEL	
ALLSEL	
/SOLU	!Enter Solution
ANTYPE,STATIC	!Type of Analysis
PSTRES,ON	!Include Prestress Effect Calculations
SOLVE	!Solve
FINISH	!Finish First Solve
/SOLU	!Enter Solution
ANTYPE,BUCKLE	!Change Type of Analysis
BUCOPT,LANB,1	!Apply Bucking Analysis Options
SOLVE	!Solve
FINISH	!Finish Second Solve
/SOLU	!Enter Solution
EXPASS,ON	!Perform Expansion Pass
MXPAND,1	!Specify Number of Modes to Expand
SOLVE	!Solve

Code E.1 Eigenvalue Buckling Validation of a 2D Pipe

/TITLE,Eigenvalue Buckling of a 2D Pipe with Holes	!Title
/UNITS,SI	!Determine Units
/PREP7	!Enter Preprocessor
ET,1,SHELL181	!Element Type
MP,EX,1,2E11	!Define Steel Pipe Data
MP,PRXY,1,0.3	
MP,EX,2,1	!Define Void Material Data
MP,PRXY,2,0.3	
MP,EX,3,5.1E10	!Define Mineral Wool Insulation Material Data
MP,PRXY,3,0.064	
MP,EX,4,6.9E10	!Define Aluminium Jacketing Material Data
MP,PRXY,4,0.334	
SECTYPE,1,SHELL	!Define Pipe Shell Section ID
SECDATA,0.0254,1	
SECDATA,0.01,3	
SECDATA,0.0005,4	
SECTYPE,2,SHELL	!Define Hole Shell Section ID
SECDATA,0.0254,2	
SECDATA,0.01,3	
SECDATA,0.0005,4	
K,1,0.622300,0,-12.5	!Create Keypoints for the Geometry
K,2,0,0.622300,-12.5	
K,3,-0.622300,0,-12.5	
K,4,0,-0.622300,-12.5	
K,5,0.4400325499,0.4400325499,-12.5	
K,6,-0.4400325499,0.4400325499,-12.5	
K,7,-0.4400325499,-0.4400325499,-12.5	
K,8,0.4400325499,-0.4400325499,-12.5	
K,9,0.622300,0,-12.9	
LARC,1,2,5	!Create Arc Lines
LARC,2,3,6	
LARC,3,4,7	
LARC,4,1,8	
LDIV,1,,,0	!Divide Lines
LDIV,2,,,0	
LDIV,3,,,0	
LDIV,4,,,0	
NUMMRG,KP,,,,LOW	!Merge Keypoints
CM,GROUP1,LINES	!Group Lines
L,1,9	!Create Line to Extrude Along
ADRAG,GROUP1,,,,,,9	!Extrude to Create Areas
NUMMRG,KP,,,,LOW	!Merge Keypoints to Reduce Number of Lines
LDIV,9,,,0	!Divide Lines
LDIV,12,,,0	
LDIV,14,,,0	
LDIV,16,,,0	
LDIV,18,,,0	
LDIV,20,,,0	
LDIV,22,,,0	
LDIV,24,,,0	
K,25,1.622300,0,-12.7	!Create Keypoints for Generating the Holes
KWPLAN,-1,25	!Move Workplane to New Keypoint
WPRO,,,90	!Rotate Workplane
K,26,1.622300,0,-12.8	!Create Keypoints for the Geometry
K,27,1.622300,0.1,-12.7	

K,28,1.622300,0,-12.6	
K,29,1.622300,-0.1,-12.7	
K,30,1.622300,0.07071068,-12.77071	
K,31,1.622300,0.07071068,-12.62929	
K,32,1.622300,-0.07071068,-12.62929	
K,33,1.622300,-0.07071068,-12.77071	
K,34,-1.622300,0,-12.8	
LARC,26,27,30	!Create Arc Lines
LARC,27,28,31	
LARC,28,29,32	
LARC,29,26,33	
LDIV,33,,,0	!Divide Lines
LDIV,34,,,0	
LDIV,35,,,0	
LDIV,36,,,0	
NUMMRG,KP,,,,LOW	!Merge Keypoints
LSEL,S,LINE,,33,40,,0	!Select Lines
CM,GROUP2,LINES	!Group Lines
L,26,34	!Create Line to Extrude Along
ADRAG,GROUP2,,,,,,41	!Extrude to Create Areas
ASEL,S,,,1,8	!Select Areas
CM,GROUP3,AREA	!Group Areas
ALLSEL	
ASEL,S,,,9,16	!Select Areas
CM,GROUP4,AREA	!Group Areas
ALLSEL	
ASBA,GROUP3,GROUP4	!Create Holes
LDELE,41,,,1	!Delete Line
LDIV,60,,,0	!Divide Lines in Hole
LDIV,61,,,0	
LDIV,64,,,0	
LDIV,65,,,0	
K,47,0,1,-12.7	!Create Keypoints for Generating the Holes
KWPLAN,-1,47	!Move Workplane to New Keypoint
WPRO,,90	!Rotate Workplane
K,48,0.1,1,-12.7	!Create Keypoints for the Geometry
K,49,0,1,-12.6	
K,50,-0.1,1,-12.7	
K,51,0,1,-12.8	
K,52,0.07071068,1,-12.62929	
K,53,-0.07071068,1,-12.62929	
K,54,-0.07071068,1,-12.77071	
K,55,0.07071068,1,-12.77071	
K,56, 0.1,-1,-12.7	
LARC,48,51,55	!Create Arc Lines
LARC,51,50,54	
LARC,50,49,53	
LARC,49,48,52	
LDIV,33,,,0	!Divide Lines
LDIV,34,,,0	
LDIV,35,,,0	
LDIV,36,,,0	
NUMMRG,KP,,,,LOW	!Merge Keypoints
CM,GROUP5,LINES	!Group Lines
LSEL,S,LINE,,33,40,,0	!Select Lines
CM,GROUP5,LINES	!Group Lines

L,48,56	!Create Line to Extrude Along
ADRAG,GROUP5,,,,,,41	!Extrude to Create Areas
ASEL,S,,,2	!Select Areas
ASEL,A,,,3	
ASEL,A,,,6	
ASEL,A,,,7	
ASEL,A,,,17	
ASEL,A,,,18	
ASEL,A,,,19	
ASEL,A,,,20	
ASEL,A,,,21	
ASEL,A,,,22	
ASEL,A,,,23	
ASEL,A,,,24	
CM,GROUP6,AREA	!Group Areas
ALLSEL	
ASEL,S,,,1	!Select Areas
ASEL,A,,,4	
ASEL,A,,,5	
ASEL,A,,,8	
ASEL,A,,,9	
ASEL,A,,,10	
ASEL,A,,,11	
ASEL,A,,,12	
CM,GROUP7,AREA	!Group Areas
ALLSEL	
ASBA,GROUP6,GROUP7	!Create Holes
LDELE,41,,,1	!Delete Line
LDIV,72,,,0	!Divide Lines in Hole
LDIV,73,,,0	
LDIV,76,,,0	
LDIV,77,,,0	
L,10,26	!Create Lines within Holes
L,10,27	
L,19,30	
L,19,31	
L,21,28	
L,21,29	
L,23,32	
L,23,33	
KDELE,25	!Delete Unnecessary Keypoints
KDELE,47	
WPCSYS,-1	!Return Working Plane to Active Coordinate System
WPSTYLE,,,,,,,,0	
K,55,0.5749302,0.2381439,-12.7	!Create Keypoints to Complete Inner Geometry
K,56,0.5749302,-0.2381439,-12.7	
K,57,0.2381439,-0.5749302,-12.7	
K,58,-0.2381439,-0.5749302,-12.7	
K,59,-0.5749302,-0.2381439,-12.7	
K,60,-0.5749302,0.2381439,-12.7	
K,61,-0.2381439,0.5749302,-12.7	
K,62,0.2381439,0.5749302,-12.7	
LARC,18,26,55	!Create Arc Lines to Complete inner Geometry
LARC,24,27,56	

LARC,24,33,57	
LARC,22,32,58	
LARC,22,29,59	
LARC,20,28,60	
LARC,20,31,61	
LARC,18,30,62	
LCCAT,1,12	!Concatenate Lines for Mapped Meshing
LCCAT,2,16	
LCCAT,3,20	
LCCAT,4,24	
LCCAT,5,12	
LCCAT,6,16	
LCCAT,7,20	
LCCAT,8,24	
LCCAT,10,26	
LCCAT,13,26	
LCCAT,15,28	
LCCAT,17,28	
LCCAT,19,30	
LCCAT,21,30	
LCCAT,23,32	
LCCAT,25,32	
LSEL,S,LINE,,1,,,0	!Define Long Concatenated Line Divisions
LSEL,A,LINE,,2,,,0	
LSEL,A,LINE,,3,,,0	
LSEL,A,LINE,,4,,,0	
LSEL,A,LINE,,5,,,0	
LSEL,A,LINE,,6,,,0	
LSEL,A,LINE,,7,,,0	
LSEL,A,LINE,,8,,,0	
LSEL,A,LINE,,10,,,0	
LSEL,A,LINE,,13,,,0	
LSEL,A,LINE,,15,,,0	
LSEL,A,LINE,,17,,,0	
LSEL,A,LINE,,19,,,0	
LSEL,A,LINE,,21,,,0	
LSEL,A,LINE,,23,,,0	
LSEL,A,LINE,,25,,,0	
LESIZE,ALL,,,20,,,,1	
ALLSEL	
LSEL,S,LINE,,12,,,0	!Define Short Concatenated Line Divisions
LSEL,A,LINE,,16,,,0	
LSEL,A,LINE,,20,,,0	
LSEL,A,LINE,,24,,,0	
LSEL,A,LINE,,26,,,0	
LSEL,A,LINE,,28,,,0	
LSEL,A,LINE,,30,,,0	
LSEL,A,LINE,,32,,,0	
LESIZE,ALL,,,10,,,,1	
ALLSEL	
LSEL,S,LINE,,9,,,0	!Define Hole Circumference Line Divisions
LSEL,A,LINE,,11,,,0	

LSEL,A,LINE,,14,,,0	
LSEL,A,LINE,,18,,,0	
LSEL,A,LINE,,22,,,0	
LSEL,A,LINE,,27,,,0	
LSEL,A,LINE,,29,,,0	
LSEL,A,LINE,,31,,,0	
LSEL,A,LINE,,60,,,0	
LSEL,A,LINE,,61,,,0	
LSEL,A,LINE,,64,,,0	
LSEL,A,LINE,,65,,,0	
LSEL,A,LINE,,72,,,0	
LSEL,A,LINE,,73,,,0	
LSEL,A,LINE,,76,,,0	
LSEL,A,LINE,,77,,,0	
LESIZE,ALL,,,10,,,,,1	
ALLSEL	
LSEL,S,LINE,,33,,,0	!Define Hole Internal Line Divisions
LSEL,A,LINE,,34,,,0	
LSEL,A,LINE,,35,,,0	
LSEL,A,LINE,,36,,,0	
LSEL,A,LINE,,37,,,0	
LSEL,A,LINE,,38,,,0	
LSEL,A,LINE,,39,,,0	
LSEL,A,LINE,,40,,,0	
LSEL,A,LINE,,58,,,0	
LSEL,A,LINE,,59,,,0	
LSEL,A,LINE,,62,,,0	
LSEL,A,LINE,,63,,,0	
LSEL,A,LINE,,70,,,0	
LSEL,A,LINE,,71,,,0	
LSEL,A,LINE,,74,,,0	
LSEL,A,LINE,,75,,,0	
LESIZE,ALL,,,16,,,,,1	
ALLSEL	
LSEL,S,LINE,,66,,,0	!Define Short Internal Line Divisions
LSEL,A,LINE,,67,,,0	
LSEL,A,LINE,,68,,,0	
LSEL,A,LINE,,69,,,0	
LSEL,A,LINE,,78,,,0	
LSEL,A,LINE,,79,,,0	
LSEL,A,LINE,,80,,,0	
LSEL,A,LINE,,81,,,0	
LESIZE,ALL,,,4,,,,,1	
ALLSEL	
LSEL,S,LINE,,41,,,0	!Define Long Internal Line Divisions
LSEL,A,LINE,,42,,,0	
LSEL,A,LINE,,43,,,0	
LSEL,A,LINE,,44,,,0	
LSEL,A,LINE,,45,,,0	
LSEL,A,LINE,,46,,,0	

LSEL,A,LINE,,47,,,0	
LSEL,A,LINE,,48,,,0	
LESIZE,ALL,,,16,,,,,1	
ALLSEL	
K,63,0.622300,0,0	!Create Keypoints to Complete the Geometry
K,64,0.622300,0,-25.4	
LSEL,S,LINE,,1,,,0	!Group Lines
LSEL,A,LINE,,2,,,0	
LSEL,A,LINE,,3,,,0	
LSEL,A,LINE,,4,,,0	
LSEL,A,LINE,,5,,,0	
LSEL,A,LINE,,6,,,0	
LSEL,A,LINE,,7,,,0	
LSEL,A,LINE,,8,,,0	
CM,GROUP8,LINES	
L,1,63	!Create Line to Extrude Along
ADRAG,GROUP8,,,,,,89	!Extrude to Create Areas
NUMMRG,KP,,,,LOW	!Merge Keypoints to Reduce Number of Lines
ALLSEL	
LSEL,S,LINE,,10,,,0	!Group Lines
LSEL,A,LINE,,13,,,0	
LSEL,A,LINE,,15,,,0	
LSEL,A,LINE,,17,,,0	
LSEL,A,LINE,,19,,,0	
LSEL,A,LINE,,21,,,0	
LSEL,A,LINE,,23,,,0	
LSEL,A,LINE,,25,,,0	
CM,GROUP9,LINES	
L,9,64	!Create Line to Extrude Along
ADRAG,GROUP9,,,,,,91	!Extrude to Create Areas
NUMMRG,KP,,,,LOW	!Merge Keypoints to Reduce Number of Lines
ALLSEL	
LSEL,S,LINE,,89,,,0	!Define New Long Line Divisions
LSEL,A,LINE,,91,,,0	
LSEL,A,LINE,,92,,,0	
LSEL,A,LINE,,94,,,0	
LSEL,A,LINE,,96,,,0	
LSEL,A,LINE,,98,,,0	
LSEL,A,LINE,,100,,,0	
LSEL,A,LINE,,102,,,0	
LSEL,A,LINE,,104,,,0	
LSEL,A,LINE,,108,,,0	
LSEL,A,LINE,,110,,,0	
LSEL,A,LINE,,112,,,0	
LSEL,A,LINE,,114,,,0	
LSEL,A,LINE,,116,,,0	
LSEL,A,LINE,,118,,,0	
LSEL,A,LINE,,120,,,0	
LESIZE,ALL,,,200,,,,,1	
ALLSEL	
NUMMRG,ALL	!Glue Areas
ASEL,S,,,1	!Select Areas

ASEL,A,,,2	
ASEL,A,,,3	
ASEL,A,,,4	
ASEL,A,,,5	
ASEL,A,,,6	
ASEL,A,,,7	
ASEL,A,,,8	
ASEL,A,,,9	
ASEL,A,,,10	
ASEL,A,,,11	
ASEL,A,,,12	
ASEL,A,,,29	
ASEL,A,,,30	
ASEL,A,,,31	
ASEL,A,,,32	
CM,GROUP10,AREA	!Group Areas
ALLSEL	
ASEL,S,,,13,28	!Select Areas
CM,GROUP11,AREA	!Group Areas
ALLSEL	
MSHKEY,1	!Apply Mapped Meshing to Outer Areas
AMESH,GROUP10	
MSHKEY,0	!Apply Free Meshing to Inner Areas
AMESH,GROUP11	
ASEL,S,AREA,,13,20	!Assign Section Data to Hole Area
ESLA,S	
EMODIF,ALL,SEC,2	
ALLSEL	
NSEL,S,LOC,Z,0-0.0001,0+0.0001	!Define Boundary Conditions
D,ALL,UX,0	
D,ALL,UY,0	
D,ALL,UZ,0	
D,ALL,ROTX,0	
D,ALL,ROTY,0	
D,ALL,ROTZ,0	
ALLSEL	
NSEL,S,LOC,Z,-25.4-0.0001,-25.4+0.0001	!Select Nodes
F,ALL,FZ,1/160	!Apply Load Equally over Nodes
ALLSEL	
/SOLU	!Enter Solution
ANTYPE,STATIC	!Type of Analysis
PSTRES,ON	!Include Prestress Effect Calculations
SOLVE	!Solve
FINISH	!Finish First Solve
/SOLU	!Enter Solution
ANTYPE,BUCKLE	!Change Type of Analysis
BUCOPT,LANB,1	!Apply Bucking Analysis Options
SOLVE	!Solve
FINISH	!Finish Second Solve
/SOLU	!Enter Solution
EXPASS,ON	!Perform Expansion Pass
MXPAND,1	!Specify Number of Modes to Expand
SOLVE	!Solve
FINISH	!Finish Third Solve

/POST1	!Enter Post-Processor
SET,LIST	!List Eigenvalue Solution – Buckling Strength
SET,LAST	!Read Data for Desired Mode
PLDISP,2	!Plot Deflected Shape vs Original

Code E.2 Eigenvalue Buckling of an Insulated Pipe with Holes

Table E.1 Raw Buckling Data for Mineral Wool Insulation with an Aluminium Jacketing

Mineral Wool Insulation Thickness (m)	Aluminium Jacketing Thickness (m)	Pipe with Holes Eigenvalue Buckling (N)	Pipe with 3/4 Depth Pits Eigenvalue Buckling (N)	Pipe with 1/2 Depth Pits Eigenvalue Buckling (N)	Pipe with 1/4 Depth Pits Eigenvalue Buckling (N)	Intact Pipe Eigenvalue Buckling (N)
0	0	1.4588E+07	1.4627E+07	1.4651E+07	1.4665E+07	1.4672E+07
0.01	0.0005	1.6126E+07	1.6168E+07	1.6195E+07	1.6210E+07	1.6219E+07
0.01	0.00075	1.6174E+07	1.6216E+07	1.6244E+07	1.6258E+07	1.6267E+07
0.01	0.001	1.6222E+07	1.6264E+07	1.6292E+07	1.6306E+07	1.6315E+07
0.01	0.00125	1.6269E+07	1.6311E+07	1.6339E+07	1.6354E+07	1.6363E+07
0.01	0.0015	1.6317E+07	1.6359E+07	1.6387E+07	1.6402E+07	1.6411E+07
0.02	0.0005	1.7546E+07	1.7592E+07	1.7621E+07	1.7637E+07	1.7647E+07
0.02	0.00075	1.7594E+07	1.7640E+07	1.7670E+07	1.7685E+07	1.7695E+07
0.02	0.001	1.7643E+07	1.7689E+07	1.7719E+07	1.7735E+07	1.7745E+07
0.02	0.00125	1.7691E+07	1.7737E+07	1.7767E+07	1.7783E+07	1.7793E+07
0.02	0.0015	1.7740E+07	1.7786E+07	1.7816E+07	1.7832E+07	1.7842E+07
0.03	0.0005	1.8960E+07	1.9009E+07	1.9042E+07	1.9059E+07	1.9069E+07
0.03	0.00075	1.9009E+07	1.9058E+07	1.9091E+07	1.9108E+07	1.9118E+07
0.03	0.001	1.9058E+07	1.9108E+07	1.9140E+07	1.9157E+07	1.9168E+07
0.03	0.00125	1.9106E+07	1.9156E+07	1.9188E+07	1.9205E+07	1.9216E+07
0.03	0.0015	1.9155E+07	1.9205E+07	1.9237E+07	1.9255E+07	1.9265E+07
0.04	0.0005	2.0369E+07	2.0422E+07	2.0457E+07	2.0475E+07	2.0486E+07
0.04	0.00075	2.0418E+07	2.0471E+07	2.0506E+07	2.0524E+07	2.0536E+07
0.04	0.001	2.0467E+07	2.0520E+07	2.0555E+07	2.0573E+07	2.0585E+07
0.04	0.00125	2.0516E+07	2.0569E+07	2.0604E+07	2.0623E+07	2.0634E+07
0.04	0.0015	2.0565E+07	2.0618E+07	2.0653E+07	2.0672E+07	2.0683E+07
0.05	0.0005	2.1773E+07	2.1830E+07	2.1867E+07	2.1886E+07	2.1898E+07
0.05	0.00075	2.1823E+07	2.1880E+07	2.1917E+07	2.1936E+07	2.1949E+07
0.05	0.001	2.1873E+07	2.1930E+07	2.1967E+07	2.1987E+07	2.1999E+07
0.05	0.00125	2.1922E+07	2.1979E+07	2.2016E+07	2.2036E+07	2.2048E+07
0.05	0.0015	2.1972E+07	2.2029E+07	2.2066E+07	2.2086E+07	2.2099E+07
0.06	0.0005	2.3175E+07	2.3235E+07	2.3275E+07	2.3296E+07	2.3308E+07
0.06	0.00075	2.3225E+07	2.3285E+07	2.3325E+07	2.3346E+07	2.3359E+07
0.06	0.001	2.3275E+07	2.3336E+07	2.3375E+07	2.3396E+07	2.3409E+07
0.06	0.00125	2.3325E+07	2.3386E+07	2.3425E+07	2.3446E+07	2.3459E+07
0.06	0.0015	2.3375E+07	2.3436E+07	2.3476E+07	2.3497E+07	2.3510E+07
0.07	0.0005	2.4575E+07	2.4639E+07	2.4681E+07	2.4703E+07	2.4717E+07
0.07	0.00075	2.4625E+07	2.4689E+07	2.4731E+07	2.4753E+07	2.4767E+07
0.07	0.001	2.4676E+07	2.4740E+07	2.4782E+07	2.4804E+07	2.4818E+07
0.07	0.00125	2.4726E+07	2.4790E+07	2.4832E+07	2.4855E+07	2.4868E+07
0.07	0.0015	2.4777E+07	2.4841E+07	2.4884E+07	2.4906E+07	2.4920E+07
0.08	0.0005	2.5974E+07	2.6042E+07	2.6086E+07	2.6109E+07	2.6124E+07
0.08	0.00075	2.6025E+07	2.6093E+07	2.6137E+07	2.6160E+07	2.6175E+07
0.08	0.001	2.6076E+07	2.6144E+07	2.6188E+07	2.6212E+07	2.6226E+07
0.08	0.00125	2.6126E+07	2.6194E+07	2.6238E+07	2.6262E+07	2.6276E+07
0.08	0.0015	2.6177E+07	2.6245E+07	2.6290E+07	2.6313E+07	2.6328E+07
0.09	0.0005	2.7372E+07	2.7443E+07	2.7490E+07	2.7514E+07	2.7530E+07
0.09	0.00075	2.7423E+07	2.7494E+07	2.7541E+07	2.7566E+07	2.7581E+07
0.09	0.001	2.7475E+07	2.7546E+07	2.7593E+07	2.7618E+07	2.7633E+07
0.09	0.00125	2.7526E+07	2.7598E+07	2.7644E+07	2.7669E+07	2.7684E+07
0.09	0.0015	2.7577E+07	2.7649E+07	2.7696E+07	2.7720E+07	2.7736E+07
0.1	0.0005	2.8772E+07	2.8847E+07	2.8896E+07	2.8922E+07	2.8938E+07
0.1	0.00075	2.8823E+07	2.8898E+07	2.8947E+07	2.8973E+07	2.8989E+07
0.1	0.001	2.8875E+07	2.8950E+07	2.8999E+07	2.9025E+07	2.9041E+07
0.1	0.00125	2.8926E+07	2.9001E+07	2.9050E+07	2.9076E+07	2.9093E+07
0.1	0.0015	2.8978E+07	2.9053E+07	2.9103E+07	2.9129E+07	2.9145E+07

Table E.2 Raw Buckling Data for Mineral Wool Insulation with a Polycarbonate Jacketing

Mineral Wool Insulation Thickness (m)	Polycarbonate Jacketing Thickness (m)	Pipe with Holes Eigenvalue Buckling (N)	Pipe with 3/4 Depth Pits Eigenvalue Buckling (N)	Pipe with 1/2 Depth Pits Eigenvalue Buckling (N)	Pipe with 1/4 Depth Pits Eigenvalue Buckling (N)	Intact Pipe Eigenvalue Buckling (N)
0	0	1.4588E+07	1.4627E+07	1.4651E+07	1.4665E+07	1.4672E+07
0.01	0.002	1.6003E+07	1.6045E+07	1.6071E+07	1.6086E+07	1.6095E+07
0.01	0.004	1.6044E+07	1.6092E+07	1.6119E+07	1.6134E+07	1.6143E+07
0.01	0.006	1.6099E+07	1.6140E+07	1.6167E+07	1.6182E+07	1.6191E+07
0.01	0.008	1.6145E+07	1.6187E+07	1.6214E+07	1.6229E+07	1.6238E+07
0.01	0.01	1.6192E+07	1.6235E+07	1.6262E+07	1.6277E+07	1.6286E+07
0.02	0.002	1.7412E+07	1.7458E+07	1.7486E+07	1.7502E+07	1.7512E+07
0.02	0.004	1.7457E+07	1.7503E+07	1.7531E+07	1.7547E+07	1.7557E+07
0.02	0.006	1.7516E+07	1.7562E+07	1.7590E+07	1.7606E+07	1.7616E+07
0.02	0.008	1.7566E+07	1.7613E+07	1.7641E+07	1.7657E+07	1.7667E+07
0.02	0.01	1.7618E+07	1.7665E+07	1.7693E+07	1.7709E+07	1.7719E+07
0.03	0.002	1.8815E+07	1.8865E+07	1.8895E+07	1.8913E+07	1.8924E+07
0.03	0.004	1.8864E+07	1.8914E+07	1.8944E+07	1.8962E+07	1.8973E+07
0.03	0.006	1.8927E+07	1.8977E+07	1.9007E+07	1.9026E+07	1.9037E+07
0.03	0.008	1.8982E+07	1.9032E+07	1.9063E+07	1.9081E+07	1.9092E+07
0.03	0.01	1.9038E+07	1.9088E+07	1.9119E+07	1.9137E+07	1.9148E+07
0.04	0.002	2.0214E+07	2.0267E+07	2.0300E+07	2.0318E+07	2.0330E+07
0.04	0.004	2.0267E+07	2.0320E+07	2.0353E+07	2.0371E+07	2.0383E+07
0.04	0.006	2.0334E+07	2.0388E+07	2.0421E+07	2.0439E+07	2.0451E+07
0.04	0.008	2.0393E+07	2.0447E+07	2.0480E+07	2.0498E+07	2.0510E+07
0.04	0.01	2.0453E+07	2.0507E+07	2.0540E+07	2.0559E+07	2.0571E+07
0.05	0.002	2.1607E+07	2.1664E+07	2.1699E+07	2.1719E+07	2.1731E+07
0.05	0.004	2.1663E+07	2.1720E+07	2.1755E+07	2.1775E+07	2.1787E+07
0.05	0.006	2.1736E+07	2.1793E+07	2.1828E+07	2.1848E+07	2.1860E+07
0.05	0.008	2.1799E+07	2.1856E+07	2.1891E+07	2.1912E+07	2.1924E+07
0.05	0.01	2.1863E+07	2.1921E+07	2.1956E+07	2.1976E+07	2.1988E+07
0.06	0.002	2.2998E+07	2.3059E+07	2.3096E+07	2.3118E+07	2.3130E+07
0.06	0.004	2.3058E+07	2.3119E+07	2.3156E+07	2.3178E+07	2.3190E+07
0.06	0.006	2.3135E+07	2.3196E+07	2.3233E+07	2.3256E+07	2.3268E+07
0.06	0.008	2.3202E+07	2.3263E+07	2.3301E+07	2.3323E+07	2.3335E+07
0.06	0.01	2.3270E+07	2.3332E+07	2.3370E+07	2.3392E+07	2.3404E+07
0.07	0.002	2.4388E+07	2.4452E+07	2.4491E+07	2.4514E+07	2.4528E+07
0.07	0.004	2.4451E+07	2.4516E+07	2.4555E+07	2.4578E+07	2.4592E+07
0.07	0.006	2.4533E+07	2.4598E+07	2.4637E+07	2.4660E+07	2.4674E+07
0.07	0.008	2.4604E+07	2.4669E+07	2.4708E+07	2.4731E+07	2.4746E+07
0.07	0.01	2.4677E+07	2.4742E+07	2.4781E+07	2.4804E+07	2.4819E+07
0.08	0.002	2.5776E+07	2.5844E+07	2.5885E+07	2.5910E+07	2.5924E+07
0.08	0.004	2.5843E+07	2.5911E+07	2.5952E+07	2.5977E+07	2.5991E+07
0.08	0.006	2.5929E+07	2.5998E+07	2.6039E+07	2.6064E+07	2.6078E+07
0.08	0.008	2.6005E+07	2.6073E+07	2.6115E+07	2.6140E+07	2.6154E+07
0.08	0.01	2.6081E+07	2.6150E+07	2.6192E+07	2.6217E+07	2.6231E+07
0.09	0.002	2.7163E+07	2.7235E+07	2.7279E+07	2.7304E+07	2.7319E+07
0.09	0.004	2.7234E+07	2.7306E+07	2.7350E+07	2.7375E+07	2.7390E+07
0.09	0.006	2.7325E+07	2.7397E+07	2.7441E+07	2.7467E+07	2.7482E+07
0.09	0.008	2.7404E+07	2.7477E+07	2.7521E+07	2.7546E+07	2.7561E+07
0.09	0.01	2.7485E+07	2.7558E+07	2.7602E+07	2.7627E+07	2.7643E+07
0.1	0.002	2.8553E+07	2.8627E+07	2.8674E+07	2.8701E+07	2.8717E+07
0.1	0.004	2.8627E+07	2.8701E+07	2.8748E+07	2.8776E+07	2.8792E+07
0.1	0.006	2.8723E+07	2.8797E+07	2.8845E+07	2.8872E+07	2.8888E+07
0.1	0.008	2.8806E+07	2.8881E+07	2.8928E+07	2.8956E+07	2.8972E+07
0.1	0.01	2.8891E+07	2.8966E+07	2.9014E+07	2.9041E+07	2.9057E+07

References

Allameh-Haery, H., Kisi, E., Pineda, J., Suwal, L. P., & Fiedler, T. (2017). Elastic properties of green expanded perlite particle compacts. *Powder Technology, 310*, 329-342. doi:https://doi.org/10.1016/j.powtec.2017.01.045

American Elements. (2018). Silicon Wool Properties (Theoretical). Retrieved from https://www.americanelements.com/silicon-wool-7440-21-3

ASTM International. (2017). Standard Practice for Preparing, Cleaning, and Evaluating Corrosion Test Specimens.

Beer, F. P. & Johnston, E. R. (2014). *Mechanics of Materials*. New York: McGraw-Hill Higher Education.

Berkeley Research Company. (2018). Failure Analysis Case Studies. Retrieved from http://www.berkeleyrc.com/FAcasestudies.html

Bouchonneau, N., Sauvant-Moynot, V., Grosjean, F., Choqueuse, D., Poncet, E., & Perreux, D. (2007). *Thermal Insulation Material for Subsea Pipelines: Benefits of Instrumented Full-Scale Testing To Predict the Long-Term Thermomechanical Behaviour*.

Chandrasekaran, S. & Jain, A. K. (2017). *Ocean Structures: Construction, Materials, and Operations*: CRC Press, Taylor & Francis Group.

Chemblinks Blogspot. (2018). Corrosion Forms. Retrieved from http://chemblinks.blogspot.com/2014/04/corrosion-forms.html

Daidola J, C., Parente J., Orisamolu I. R., et al. (1997). *Residual strength assessment of pitted plate panels*. Report SSC-394, Ship Structure Committee.

Devold, H. (2013). *Oil and Gas Production Handbook: An Introduction to Oil and Gas Production, Transport, Refining and Petrochemical Industry*

Dhanak, M. R. & Xiros, N. I. (2016). *Springer Handbook of Ocean Engineering*: Springer International Publishing.

Edwards, R. (2013). Aqueous Corrosion of Steel Technical Note. In (pp. 1-3): Corrosion Engineering Solutions.

El-Sherik, A. M. (2017). *Trends in Oil and Gas Corrosion Research and Technologies*. Boston: Woodhead
Publishing.

Frankel, G.S., Stockert, L., Hunkeler, F. and Boehni, H. (1987). *Metastable pitting of
stainless steel*. Corrosion, 43(7), pp.429-436.

Goodfellow. (2018). Polycarbonate Material Information. Retrieved from
Goodfellow.com/E/polycarbonate.html

Hart, D. K., Rutherford, S. E. and Wickham, A. H. (1986). *Structural reliability analysis of
stiffened panels*. Naval Architect October 1986

Integrated Publishing. (2018). Corrosion Rate. Retrieved from
http://www.tpub.com/doechem1/chem133.htm

International Energy Agency. (2018). Oil Market Report. Retrieved from
www.iea.org/oilmarketreport/omrpublic/

Katz, H. S. & Milewski, J. V. (1987). *Handbook of Reinforcement for Plastics*. New York: Van Nostrand
Reinhold Co.

King Fahd University of Petroleum & Minerals. (2018). Hydrogen Induced Cracking. Retrieved from
http://faculty.kfupm.edu.sa/ME/hussaini/Corrosion%20Engineering/04.08.01.htm

Kolmetz, K., Ajes, M.S.A. and Sari, R.M. (2016, October 2016). .

Lettich, M. J. (2005). Is there a Cure for Corrosion under Insulation?

Logan, D. L. (2012). *First Course in the Finite Element Method* (Fifth Edition ed.): Thomson.

Madenci, E. & Guven, I. (2015). *The Finite Element Method and Applications in Engineering Using
ANSYS®* (Second ed.): Springer US.

Mather, A. (2000). *Offshore Engineering: An Introduction*: Witherby.

Maverick Inspection Ltd. (2018). Hydrogen Blistering. Retrieved from
http://www.maverickinspection.com/services/remote-video-inspection/rvi-video-imagery-
gallery/storage-underground-tanks/image025/

McIntyre, P. (2003). Corrosion management for upstream oil and gas Metal dusting carburisation and nitridation. *Corrosion Engineering, Science and Technology, 38*(2), 89-96. doi:10.1179/147842203767789168

NACE International. (2005). *Standard recommended practice : preparation, installation, analysis, and interpretation of corrosion coupons in oilfield operations*. Houston, TX: NACE International.

NACE International. (2016). Control of Corrosion Under Thermal Insulation and Fireproofing Materials. In (pp. 36): NACE International.

InterNACHI. (2018). Galvanic Corrosion. Retrieved from https://www.nachi.org/galvanic-corrosion.htm

Nayyar, M. L. (2000). *Piping Handbook* (7th Edition ed.). New York, Chicago, San Francisco, Athens, London, Madrid, Mexico City, Milan, New Delhi, Singapore, Sydney, Toronto: McGraw-Hill Education.

OPEC. (2018). *OPEC Annual Statisitcal Bulletin*. Retrieved from

Oxyplast UK Ltd. (2018). Different types of corrosion. Retrieved from https://oxyplastuk.com/technical/different-types-of-corrosion/

Pace Technologies. (2018). Refractory Materials Metallographic Preparation. Retrieved from http://www.metallographic.com/Metallographic-Preparation-Procedures/Refractory-Metals-Description.htm

Paik, J. K., Lee, J. M., & Ko, M. J. (2003). Ultimate compressive strength of plate elements with pit corrosion wastage. *Proceedings of the Institution of Mechanical Engineers, Part M: Journal of Engineering for the Maritime Environment, 217*(4), 185-200. doi:10.1177/147509020321700402

Paik, J. K., Lee, J. M., & Ko, M. J. (2004). Ultimate shear strength of plate elements with pit corrosion wastage. *Thin-Walled Structures, 42*(8), 1161-1176. doi:https://doi.org/10.1016/j.tws.2004.03.024

Papavinasam, S. (2014). *Corrosion Control in the Oil and Gas Industry*. Boston: Gulf Professional Publishing.

Pojtanabuntoeng, T., Ehsani, H., Kinsella, B., & Brameld, M. (2017). *Comparison of Insulation Materials and Their Roles on Corrosion under Insulation*. Paper presented at the CORROSION 2017, New Orleans, Louisiana, USA.

Popov, B. N. (2015). *Corrosion Engineering*. Amsterdam: Elsevier.

Process Insulation. (1987). Ontario, Canada: Department of Energy, Mines and Industry.

Rajeev, P.V. Khanna, A.S., Sharma, K.S., Sharma, K.S., & Sinha, A.K. (2000). *Pitting corrosion of metals*. India: Akademia Books International.

Resource Dynamics LLC. (2018). Industry Overview. Retrieved from http://resourcedynamicsllc.com/

Roberge, P. (2000). *Handbook of Corrosion Engineering*: McGraw-Hill

SHARCNET. (2018a). SOLID185. Retrieved from https://www.sharcnet.ca/Software/Ansys/16.2.3/en-us/help/ans_elem/Hlp_E_SOLID185.html

SHARCNET. (2018b). SOLID186. Retrieved from https://www.sharcnet.ca/Software/Ansys/16.2.3/en-us/help/ans_elem/Hlp_E_SOLID186.html

Shutov, F. A. (1986, 1986). *Syntactic polymer foams.* Paper presented at the Chromatography/Foams/Copolymers, Berlin, Heidelberg.

Singh, R. (2017). *Pipeline Integrity Handbook* (Second Edition ed.): Gulf Professional Publishing.

Soares, C.G., 1988. *Uncertainty modelling in plate buckling*. Structural Safety, 5(1), pp.17-34.

Soares, C.G. and Garbatov, Y., (1999). *Reliability of maintained, corrosion protected plates subjected to non-linear corrosion and compressive loads*. Marine Structures, 12(6), 425-445

Socotherm. (2018). Wetisokote (5LPP Syntatic). Retrieved from http://www.socotherm.com/en/products/wetisokote/wetisokote_5LPPSyn.html

Southwest Research Institute. (2018). Stress Corrosion Cracking. Retrieved from https://www.swri.org/stress-corrosion-cracking

Steel Fabrication Services. (2018a). Crevice Corrosion and How to Treat it. Retrieved from https://steelfabservices.com.au/a-guide-to-crevice-corrosion-how-to-treat-it/

Steel Fabrication Services. (2018b). Pitting Corrosion and How to Treat it. Retrieved from https://steelfabservices.com.au/pitting-corrosion-how-to-treat-it/

Stochastic Simulation and Lagrangian Dynamics. (2018). What does shape function mean in finite
element formulation? Retrieved from
http://stochasticandlagrangian.blogspot.com/2011/07/what-does-shape-function-mean-in-finite.html

Substech. (2018). Pitting Corrosion. Retrieved from
http://www.substech.com/dokuwiki/lib/exe/detail.php?id=pitting_corrosion&cache=cache&media=pitting_corrosion.png

System 22 Inc. (2018). How to Avoid Hydrogen Embrittlement. Retrieved from
http://www.system22.com/hydrogen-embrittlement-in-plated-parts/

Teixeira, A. P. and Guedes Soares, C. (2008). *Ultimate Strength of Plates with Random
Fields of Corrosion*. Structure and Infrastructure Engineering. 4(5):363-370.

The Engineering Toolbox. (2018a). Poisson's Ratio. Retrieved from
https://www.engineeringtoolbox.com/poissons-ratio-d_1224.html

The Engineering Toolbox. (2018b). Young's Modulus - Tensile and Yield Strength for common Materials.
Retrieved from https://www.engineeringtoolbox.com/young-modulus-d_417.html

Turner, W. C. & Doty, S. (2007). *Energy Management Handbook* (6th Edition ed.): Wiley.

Vermelfoort, A. T. & Ng'andu, B. M. (2005, June 8 – 12, 2005). *The response of calcium silicate element
wallettes to 2d compression loading* Paper presented at the 10th Canadian Masonry
Symposium, Banff, Alberta.

Watson, D. (2005). National Insulation Standards. In. Canada: Thermal Insulation Association of Canada.

Winnik, S. (2016). *Corrosion-Under-Insulation (CUI) Guidelines* Woodhead Publishing.

World Energy Council. (2016). *World Energy Resources Report 2016*. Retrieved from

Zhang, Y., Huang, Y., Zhang, Q., & Liu, G. (2016). Ultimate strength of hull structural plate with pitting
corrosion damnification under combined loading. *Ocean Engineering, 116*, 273-285.
doi:https://doi.org/10.1016/j.oceaneng.2016.02.039